12 November 2010 | $10

Science

AAAS

EDITORIAL

890 Next-Generation Assessments
Lorrie A. Shepard

NEWS OF THE WEEK

896 Researchers Anxious and on the Defensive After Republican Gains
Ralph Hall Bids to Lead Science Panel
>> Science *Podcast*
897 Election Means Change in Climate for Efforts to Curb Emissions
898 Retiring Legislators Warn of Pitfalls Facing Science in New Congress
899 From the *Science* Policy Blog
900 Neandertal Brain Growth Shows a Head Start for Moderns
900 The Promise and Pitfalls of a Cancer Breakthrough
901 From *Science*'s Online Daily News Site
902 Earth-Observation Summit Endorses Global Data Sharing
903 Affordable 'Exomes' Fill Gaps in a Catalog of Rare Diseases

NEWS FOCUS

904 Scientific Gold Mine or Dicey Money Pit?
907 Collapse? What Collapse? Societal Change Revisited
910 Taking the Sting Out of Acid Rain

LETTERS

912 Retraction
A. Beloqui et al.
Editorial Expression of Concern
B. Alberts
Training Physicians to Communicate
G. W. Jones
Birds of Prey Remain at Risk
D. A. Bell and K. S. Smallwood
Mentors for Elementary School Teachers
S. B. Oppenheimer
913 CORRECTIONS AND CLARIFICATIONS

BOOKS *ET AL.*

914 How Did the First Stars and Galaxies Form?
A. Loeb, reviewed by J. C. Tan
915 The Double Helix and the Law of Evidence
D. H. Kaye, reviewed by C. McCartney

POLICY FORUM

916 Earth System Science for Global Sustainablility: Grand Challenges
W. V. Reid et al.

PERSPECTIVES

918 Prion-Like Behavior of Amyloid-β
J. Kim and D. M. Holtzman
>> *Report p. 980*
919 Materials Ecology: An Industrial Perspective
P. Collier and C. M. Alles
920 Irremediable Complexity?
M. W. Gray et al.
922 Fertility Goddesses as Trojan Horses
F. Govers and G. C. Angenent
>> *Report p. 968*
923 Cooperation and the Commons
B. Vollan and E. Ostrom
>> *Report p. 961*
924 Glimpsing the Critical Intermediate in Cytochrome P450 Oxidations
S. G. Sligar
>> *Research Article p. 933*
926 Retrospective: Benoît B. Mandelbrot (1924–2010)
H.-O. Peitgen

REVIEW

927 Amazonia Through Time: Andean Uplift, Climate Change, Landscape Evolution, and Biodiversity
C. Hoorn et al.

CONTENTS continued >>

page 896

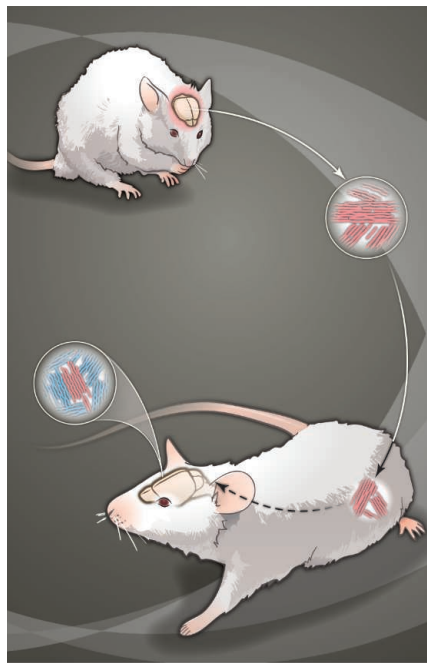

pages 918 & 980

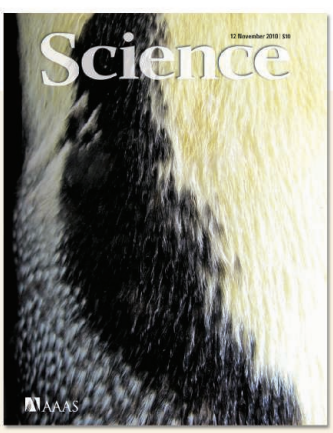

COVER

Neck region of an emperor penguin (*Aptenodytes forsteri*), the skin of which was collected in 1929 on Richard E. Byrd's first Antarctic expedition. The ~36-million-year-old feathers of a giant fossil penguin from Peru indicate that feather shape evolved early in the penguin lineage, but that adult penguin coloration has shifted from a color palette that included reddish-browns and grays. See page 954.

Photo: Julia Clarke, University of Texas at Austin

DEPARTMENTS

889 This Week in *Science*
891 Editors' Choice
892 *Science* Staff
895 Random Samples
990 New Products
991 *Science* Careers

Published by AAAS

BREVIA

932 A Wandering Mind Is an Unhappy Mind
M. A. Killingsworth and D. T. Gilbert
The iPhone Hap App reveals that wandering thoughts lead to unhappiness.
>> Science *Podcast*

RESEARCH ARTICLES

933 Cytochrome P450 Compound I: Capture, Characterization, and C-H Bond Activation Kinetics
J. Rittle and M. T. Green
The iron-bound oxygen intermediate responsible for many challenging biochemical oxidations has been thoroughly characterized.
>> *Perspective p. 924*

937 How the CCA-Adding Enzyme Selects Adenine over Cytosine at Position 76 of tRNA
B. Pan et al.
Crystal structures along the reaction pathway show that only adenine is correctly oriented for incorporation at transfer RNA position 76.

REPORTS

940 Radio-Frequency Association of Efimov Trimers
T. Lompe et al.
A bound state of three fermionic atoms in different quantum states is formed directly by laser association.

944 A Low-Magnetic-Field Soft Gamma Repeater
N. Rea et al.
A neutron star lacking a strong magnetic field can still emit short bursts of high-energy radiation.

946 Anomalous Strength Characteristics of Tilt Grain Boundaries in Graphene
R. Grantab et al.
Simulations indicate that high-angle boundaries can better accommodate strain and prevent failure in graphene.

949 Structure and Formation of the Lunar Farside Highlands
I. Garrick-Bethell et al.
A mathematical analysis of the lunar farside highlands implicates the role of tidal processes in building the lunar crust.

952 Coupling of Nitrous Oxide and Methane by Global Atmospheric Chemistry
M. J. Prather and J. Hsu
Nitrous oxide emissions affect atmospheric methane concentrations on a time scale that is 10 times longer than the methane lifetime.

954 Fossil Evidence for Evolution of the Shape and Color of Penguin Feathers
J. A. Clarke et al.
A fossil penguin shows that the wing and feather form evolved before distinctive microstructural changes in the feathers.

957 Effects of Rapid Global Warming at the Paleocene-Eocene Boundary on Neotropical Vegetation
C. Jaramillo et al.
Palynology shows that tropical forests persisted under conditions of rapid climate warming 55 million years ago.

961 Conditional Cooperation and Costly Monitoring Explain Success in Forest Commons Management
D. Rustagi et al.
Social behaviors in lab experiments that result in long-term productivity are seen in a real-world forest management program.
>> *Perspective p. 923*

965 The Role of Discharge Variation in Scaling of Drainage Area and Food Chain Length in Rivers
J. L. Sabo et al.
The lengths of river food chains are indirectly related to drainage area and directly affected by flow and discharge.

968 Conserved Molecular Components for Pollen Tube Reception and Fungal Invasion
S. A. Kessler et al.
In *Arabidopsis*, development and disease use the same pollen-tube or hyphal tip-growing strategies.
>> *Perspective p. 922*

971 Optogenetic Control of Cardiac Function
A. B. Arrenberg et al.
Optogenetics is applied to study development of the zebrafish pacemaker.

974 Kinetic Scaffolding Mediated by a Phospholipase C–β and G_q Signaling Complex
G. L. Waldo et al.
A crystal structure shows how the two components of a central signaling complex regulate each other.

980 Peripherally Applied Aβ-Containing Inoculates Induce Cerebral β-Amyloidosis
Y. S. Eisele et al.
Amyloid-containing brain extracts can "infect" susceptible Alzheimer's disease model animals.
>> *Perspective p. 918*

982 Contact Network Structure Explains the Changing Epidemiology of Pertussis
P. Rohani et al.
Age-specific social networks can influence transmission of infection and should be considered in health policy planning.

985 Essential Regulation of CNS Angiogenesis by the Orphan G Protein–Coupled Receptor GPR124
F. Kuhnert et al.
A factor is identified that determines the amount of vasculature in the brain, and, in so doing, affects brain function.

CONTENTS continued >>

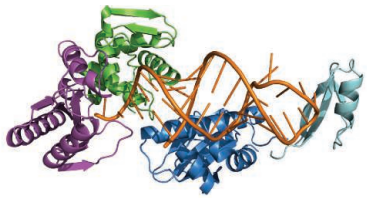

page 937

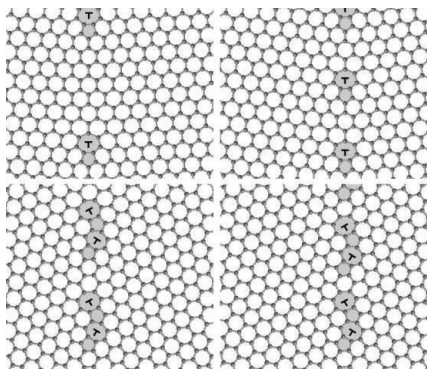

page 946

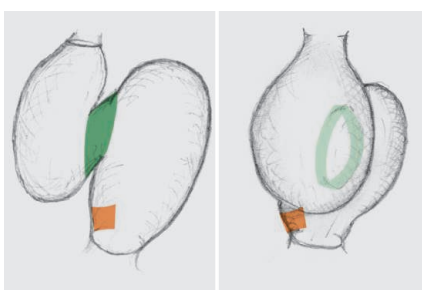

page 971

SCIENCEONLINE

SPECIAL ANNOUNCEMENT: ELECTIONS

Additional Candidates for AAAS Annual Election

The following candidates have been added to the ballot for the 2010 election of AAAS officers. Members registered in more than one section will receive ballots for elections for each section they are enrolled in. For a list of other candidates, please see AAAS News & Notes in the 29 October 2010 issue of *Science*.

AAAS will be offering the opportunity to vote either by mail or via a Web balloting system for this year's election. Detailed instructions for using the online option will be provided to all members.

General Election

Committee on Nominations: Rosina M. Bierbaum, Univ. of Michigan; Francisco J. Ayala, Univ. of California, Irvine; John E. Burris, Burroughs Wellcome Fund; May R. Berenbaum, Univ. of Illinois, Urbana-Champaign; Thomas D. Pollard, Yale Univ.; Jo Handelsman, Yale Univ.; Roger N. Beachy, U.S. Department of Agriculture; Sandra M. Faber, Univ. of California, Santa Cruz

Atmospheric and Hydrospheric Sciences

Council Delegate: Lynne D. Talley, Scripps Institution of Oceanography

Societal Impacts of Science and Engineering

Council Delegate: C. K. Gunsalus, Univ. of Illinois, Urbana-Champaign

SCIENCEXPRESS

www.sciencexpress.org

How Learning to Read Changes the Cortical Networks for Vision and Language
S. Dehaene et al.
Reading changes the mind.
10.1126/science.1194140
>> Science *Podcast*

Lynx1, a Cholinergic Brake, Limits Plasticity in Adult Visual Cortex
H. Morishita et al.
A gene identified in the mouse may show the way to improved treatments for amblyopia, a condition of indistinct vision.
10.1126/science.1195320

How Cats Lap: Water Uptake by *Felis catus*
P. M. Reis et al.
Cats use fluid inertia to generate a liquid column that they catch in their mouths before gravity destroys it.
10.1126/science.1195421

Optomechanically Induced Transparency
S. Weis et al.
Radiation pressure is used to manipulate the optical properties of an optomechanical system.
10.1126/science.1195596

A Cryptic Sulfur Cycle in Oxygen-Minimum–Zone Waters off the Chilean Coast
D. E. Canfield et al.
Bacterial sulfur reduction and oxidation accompanies nitrogen cycling where oxygen levels at depth are low.
10.1126/science.1196889

SCIENCENOW

www.sciencenow.org
Highlights From Our Daily News Coverage

New Malaria Drug Could Save Tens of Thousands
Artesunate bests quinine at saving African children from the disease.

Rethinking Galactic Architecture: Dark Matter Optional
Clusters of thousands of stars may have formed in an unexpected way.

Time for Your Skin Transfusion?
Study suggests new route for making blood cells from skin.

SCIENCESIGNALING

www.sciencesignaling.org
The Signal Transduction Knowledge Environment

EDITORIAL GUIDE: Focus Issue—Getting Excited About Glia
E. M. Adler
Complementing the 5 November *Science* special issue, this issue highlights glial cell function, development, and disease.

RESEARCH ARTICLE: Akt and Autophagy Cooperate to Promote Survival of Drug-Resistant Glioma
Q.-W. Fan et al.
Combined inhibition of PI3K, mTOR, and autophagy promotes glioma cell death.

PERSPECTIVE: Control of Breathing by "Nerve Glue"
K. Ballanyi et al.
Astrocytes sense the need to breathe.

PRESENTATION: Wnt5a Induces Simultaneous Cortical Axon Outgrowth and Repulsive Turning Through Distinct Signaling Mechanisms
L. Li et al.
Chemorepulsion and growth stimulation may cooperate to guide cortical axons.

JOURNAL CLUB: Grooming and Growing with Microglia
J. M. Antony
Microglia modulate neurobehavior.

TEACHING RESOURCE: Visualizing Calcium Signaling in Astrocytes
R. D. Fields
Astroctye signaling is apparent in movies of rat brain astrocytes cultured with fluorescent calcium indicator dyes.

SCIENCECAREERS

www.sciencecareers.org/career_magazine
Free Career Resources for Scientists

SPECIAL FOCUS ON RESEARCH INTEGRITY

Working With Industry Under a Microscope
K. Hede
Regulations seem to discourage academic scientists from partnering with industry, but such collaboration is essential to translational research.

Ghostwriters in the Medical Literature
S. Gaidos
Despite new disclosure requirements, ghostwriters remain a threat to the integrity of the scientific literature, as well as careers.

SCIENCETRANSLATIONAL MEDICINE

www.sciencetranslationalmedicine.org
Integrating Medicine and Science

COMMENTARY: Achieving a Nationwide Learning Health System
C. P. Friedman et al.
The secure re-use of patient data will speed knowledge transfer from bench to bedside.

RESEARCH ARTICLE: TLR9 Differentiates Rapidly from Slowly Progressing Forms of Idiopathic Pulmonary Fibrosis
G. Trujillo et al.
Increased expression of Toll-like receptor 9 boosts fibrosis in patients with rapidly progressing lung disease.

RESEARCH ARTICLE: Prevention of Muscle Aging by Myofiber-Associated Satellite Cell Transplantation
J. K. Hall et al.
Transplanting myofiber satellite stem cells into mouse muscle protects against age-related muscle degeneration.

SCIENCEPODCAST

www.sciencemag.org/multimedia/podcast
Free Weekly Show

Download the 12 November *Science* Podcast to hear about literacy's effects on brain function, U.S. election results, happiness by living in the moment, and more.

SCIENCEINSIDER

news.sciencemag.org/scienceinsider
Science Policy News and Analysis

SCIENCE (ISSN 0036-8075) is published weekly on Friday, except the last week in December, by the American Association for the Advancement of Science, 1200 New York Avenue, NW, Washington, DC 20005. Periodicals Mail postage (publication No. 484460) paid at Washington, DC, and additional mailing offices. Copyright © 2010 by the American Association for the Advancement of Science. The title SCIENCE is a registered trademark of the AAAS. Domestic individual membership and subscription (51 issues): $146 ($74 allocated to subscription). Domestic institutional subscription (51 issues): $910; Foreign postage extra: Mexico, Caribbean (surface mail) $55; other countries (air assist delivery) $85. First class, airmail, student, and emeritus rates on request. Canadian rates with GST available upon request, GST #1254 88122. Publications Mail Agreement Number 1069624. **Printed in the U.S.A.**

Change of address: Allow 4 weeks, giving old and new addresses and 8-digit account number. **Postmaster:** Send change of address to AAAS, P.O. Box 96178, Washington, DC 20090–6178. **Single-copy sales:** $10.00 current issue, $15.00 back issue prepaid includes surface postage; bulk rates on request. **Authorization to photocopy** material for internal or personal use under circumstances not falling within the fair use provisions of the Copyright Act is granted by AAAS to libraries and other users registered with the Copyright Clearance Center (CCC) Transactional Reporting Service, provided that $20.00 per article is paid directly to CCC, 222 Rosewood Drive, Danvers, MA 01923. The identification code for *Science* is 0036-8075. *Science* is indexed in the *Reader's Guide to Periodical Literature* and in several specialized indexes.

AAAS
ADVANCING SCIENCE, SERVING SOCIETY

Published by AAAS

Next-Generation Assessments

Lorrie A. Shepard is University Distinguished Professor and Dean of the School of Education, University of Colorado, Boulder, CO. She is the recent past president of the U.S. National Academy of Education. E-mail: lorrie.shepard@colorado.edu

SPURRED BY ITS POOR PERFORMANCE ON INTERNATIONAL TESTS, THE UNITED STATES IS NOW embarked on a new round of education standards development. Common Core State Standards have been released in English language arts and mathematics, and a draft framework for science education standards from the U.S. National Research Council provides a complex conception of scientific reasoning practices that are integrated with principled understanding of science content. These ambitious standards aim at problem-solving and knowledge application and are urgently needed, but will fail if lessons from the past go unheeded. In the United States, tests—not standards—determine what gets taught, and these tests must change dramatically.

The U.S. has a 30-year history of accountability testing in grades 3 to 10. An extensive research literature has documented the negative effects of such test-driven instruction, the most obvious being the reduction or elimination of less-tested subjects, including science and social studies. Less obvious have been the negative effects on learning in tested subjects. When students are drilled on materials that closely resemble accountability tests, test scores can rise dramatically without a commensurate gain in learning. This "test score inflation" is revealed when the apparent gains fail to replicate on independent measures that cover the same content, such as U.S. National Assessment of Educational Progress. More serious are the distorting effects on students' conceptions of what it means to know and do science and mathematics.

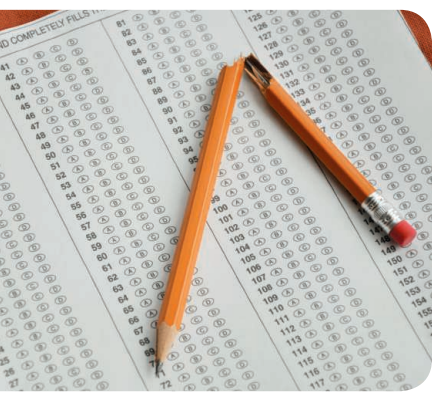

Previous reforms have tried to avoid such shortfalls. When the U.S. standards-based educational reform movement began in the early 1990s, the goal was to replace low-level, basic-skills tests with much more challenging, authentic assessments focused on problem-solving and higher-order reasoning. A start was made, but the sheer quantity of tests required by the No Child Left Behind (NCLB) Act of 2001 forced a retreat to inexpensive multiple-choice tests.

In September 2010, the U.S. Department of Education awarded Race-to-the-Top grants to two state consortia that have promised to prepare mathematics assessments that include "challenging performance tasks and innovative, computer-enhanced items that elicit complex demonstrations of learning."* These consortia were intended to permit economies of scale and enable the development of quality assessments tied to a shared curriculum, something missing in the United States but found in top-performing countries.** Unfortunately, negotiating deeper curriculum development has become unwieldy, and there is an emphasis instead on the timeliness and frequency of score reporting. Enormous care is now needed to prevent this opportunity from being undone by the efficiencies of multiple-choice testing, which currently dominates the new interim assessment systems sold to school districts to help raise scores on NCLB tests.

Fundamentally different forms of assessment are needed in the United States to directly capture more complex levels of achievement: the ability to solve nonroutine problems, to analyze data and reason from evidence, to communicate effectively both orally and in writing, and to frame and conduct scientific investigations. "Performance assessments" that require students to demonstrate their learning and reasoning are far better measuring devices and predominate in high-performing countries that the United States seeks to emulate. To explain successes on international assessments, researchers point to the importance of ongoing instruction that calls on students to apply their knowledge and the use of curriculum-embedded assessments that help students and teachers develop common understandings of scoring criteria. These ideas are already being implemented in the redesign of the U.S. Advanced Placement precollege curricula and examinations, but they are just as important in the early grades. Real demonstrations of mathematics and science mastery, not ease of scoring, must determine assessment policy.

– Lorrie A. Shepard

10.1126/science.1199897

*www.achieve.org/files/PARCC_Summary_92910.pdf. **L. Shepard, J. Hannaway, E. Baker, *Standards, Assessments, and Accountability: Education Policy White Paper* (National Academy of Education, 23 September 2009).

Downloaded from www.sciencemag.org on November 11, 2010

CREDITS: (TOP) CASEY A. CASS/UNIVERSITY OF COLORADO; (LEFT) THINKSTOCK

Published by AAAS

www.sciencemag.org

Science

1200 New York Avenue, NW
Washington, DC 20005
Editorial: 202-326-6550, FAX 202-289-7562
News: 202-326-6581, FAX 202-371-9227
Bateman House, 82-88 Hills Road
Cambridge, UK CB2 1LQ
+44 (0) 1223 326500, FAX +44 (0) 1223 326501

Subscription Services For change of address, missing issues, new orders and renewals, and payment questions: 866-434-AAAS (2227) or 202-326-6417, FAX 202-842-1065. Mailing addresses: AAAS, P.O. Box 96178, Washington, DC 20090-6178 or AAAS Member Services, 1200 New York Avenue, NW, Washington, DC 20005

Institutional Site Licenses please call 202-326-6755 for any questions or information

Reprints: Author Inquiries 800-635-7181
Commercial Inquiries 803-359-4578

Permissions 202-326-7074, FAX 202-682-0816

Member Benefits AAAS/Barnes&Noble.com bookstore www.aaas.org/bn; AAAS Online Store www.apisource.com/aaas/ code MKB6; AAAS Travels: Betchart Expeditions 800-252-4910; Apple Store www.apple.com/eppstore/aaas; Bank of America MasterCard 1-800-833-6262 priority code FAA3YU; Cold Spring Harbor Laboratory Press Publications www.cshlpress.com/affiliates/aaas.htm; GEICO Auto Insurance www.geico.com/landingpage/go51.htm?logo=17624; Hertz 800-654-2200 CDP#343457; Office Depot https://bsd.officedepot.com/portalLogin.do; Seabury & Smith Life Insurance 800-424-9883; Subaru VIP Program 202-326-6417; VIP Moving Services www.vipmayflower.com/domestic/index.html; Other Benefits: AAAS Member Services 202-326-6417 or www.aaasmember.org.

science_editors@aaas.org	(for general editorial queries)
science_letters@aaas.org	(for queries about letters)
science_reviews@aaas.org	(for returning manuscript reviews)
science_bookrevs@aaas.org	(for book review queries)

Published by the American Association for the Advancement of Science (AAAS), *Science* serves its readers as a forum for the presentation and discussion of important issues related to the advancement of science, including the presentation of minority or conflicting points of view, rather than by publishing only material on which a consensus has been reached. Accordingly, all articles published in *Science*—including editorials, news and comment, and book reviews—are signed and reflect the individual views of the authors and not official points of view adopted by AAAS or the institutions with which the authors are affiliated.

AAAS was founded in 1848 and incorporated in 1874. Its mission is to advance science, engineering, and innovation throughout the world for the benefit of all people. The goals of the association are to: enhance communication among scientists, engineers, and the public; promote and defend the integrity of science and its use; strengthen support for the science and technology enterprise; provide a voice for science on societal issues; promote the responsible use of science in public policy; strengthen and diversify the science and technology workforce; foster education in science and technology for everyone; increase public engagement with science and technology; and advance international cooperation in science.

Information for Authors
See pages 352 and 353 of the 15 January 2010 issue or access www.sciencemag.org/about/authors

EDITOR-IN-CHIEF **Bruce Alberts**
EXECUTIVE EDITOR **Monica M. Bradford**
NEWS EDITOR **Colin Norman**
MANAGING EDITOR, RESEARCH JOURNALS **Katrina L. Kelner**
DEPUTY EDITORS **R. Brooks Hanson, Barbara R. Jasny, Andrew M. Sugden**

Editorial senior editors/commentary Lisa D. Chong, Brad Wible; **senior editors** Gilbert J. Chin, Pamela J. Hines, Paula A. Kiberstis (Boston), Marc S. Lavine (Toronto), Beverly A. Purnell, L. Bryan Ray, Guy Riddihough, H. Jesse Smith, Phillip D. Szuromi (Tennessee), Valda Vinson, Jake S. Yeston; **associate editors** Kristen L. Mueller, Jelena Stajic, Sacha Vignieri, Nicholas S. Wigginton, Laura M. Zahn (San Diego); **book review editor** Sherman J. Suter; **associate letters editor** Jennifer Sills; **editorial manager** Cara Tate; **senior copy editors** Jeffrey E. Cook, Cynthia Howe, Harry Jach, Lauren Kmec, Barbara P. Ordway, Trista Wagoner; **copy editor** Chris Filiatreau; **editorial coordinators** Carolyn Kyle, Beverly Shields; **publications assistants** Ramatoulaye Diop, Joi S. Granger, Emily Guise, Jeffrey Hearn, Michael Hicks, Lisa Johnson, Scott Miller, Jerry Richardson, Jennifer A. Seibert, Brian White, Anita Wynn; **editorial assistants** Emily C. Horton, Patricia M. Moore, Miriam Weinberg; **executive assistant** Alison Crawford; **administrative support** Maryrose Madrid; **editorial fellow** Melissa R. McCartney

Editorial director, web and new media Stewart Wills; **senior web editor** Tara S. Marathe; **web editor** Robert Frederick; **web development manager** Martyn Green; **web developer** Andrew Whitesell; **intern** Sophia Cai

News deputy news editors Robert Coontz, David Grimm (Online), Eliot Marshall, Jeffrey Mervis, Leslie Roberts; **contributing editors** Elizabeth Culotta, Polly Shulman; **news writers** Yudhijit Bhattacharjee, Adrian Cho, Jennifer Couzin, Jocelyn Kaiser, Richard A. Kerr, Eli Kintisch, Greg Miller, Elizabeth Pennisi, Lauren Schenkman, Robert F. Service (Pacific NW), Erik Stokstad; **web developer** Daniel Berger; **intern** Kristen Minogue; **contributing correspondents** Jon Cohen (San Diego, CA), Daniel Ferber, Ann Gibbons, Sam Kean, Andrew Lawler, Mitch Leslie, Charles C. Mann, Virginia Morell, Gary Taubes; **copy editors** Linda B. Felaco, Melvin Gatling, Melissa Raimondi; **administrative support** Scherraine Mack; **bureaus** San Diego, CA: 760-942-3252, FAX 760-942-4979; Pacific Northwest: 503-963-1940

Production director Wendy K. Shank; **assistant manager** Rebecca Doshi; **senior specialists** Steve Forrester, Chris Redwood, Anthony Rosen; **Preflight director** David M. Tompkins; **manager** Marcus Spiegler; **specialist** Jason Hillman

Art director Yael Fitzpatrick; **associate art director** Laura Creveling; **senior illustrators** Chris Bickel, Katharine Sutliff; **illustrator** Yana Hammond; **senior art associates** Holly Bishop, Preston Huey, Nayomi Kevitiyagala; **art associates** Kay Engman, Matthew Twombly; **photo editor** Leslie Blizard

***Science* International**

Europe (science@science-int.co.uk) **editorial: international managing editor** Andrew M. Sugden; **senior editor/commentary** Julia Fahrenkamp-Uppenbrink; **senior editors** Caroline Ash, Stella M. Hurtley, Ian S. Osborne, Peter Stern; **associate editor** Maria Cruz; **locum editor** Helen Pickersgill; **editorial support** Samantha Hogg, Alice Whaley; **administrative support** John Cannell, Janet Clements, Louise Hartwell; **news: europe news editor** John Travis; **deputy news editor** Daniel Clery; **contributing correspondents** Michael Balter (Paris), John Bohannon (Vienna), Martin Enserink (Amsterdam and Paris), Gretchen Vogel (Berlin); **intern** Jennifer Carpenter

Latin America contributing correspondent Antonio Regalado

Asia Japan Office: Asca Corporation, Tomoko Furusawa, Rustic Bldg. 7F, 77 Tenjin-cho, Shinjuku-ku, Tokyo 162-0808, Japan; +81 3 6802 4616, FAX +81 3 6802 4615, inquiry@sciencemag.jp; **asia news editor** Richard Stone (Beijing: rstone@aaas.org); **contributing correspondents** Dennis Normile [Japan: +81 (0) 3 3391 0630, FAX +81 (0) 3 5936 3531; dnormile@gol.com]; Hao Xin [China: cindyhao@gmail.com]; Pallava Bagla [South Asia: +91 (0) 11 2271 2896; pbagla@vsnl.com]

EXECUTIVE PUBLISHER **Alan I. Leshner**
PUBLISHER **Beth Rosner**

Fulfillment Systems and Operations (membership@aaas.org); **director** Waylon Butler; **customer service supervisor** Pat Butler; **specialists** Latoya Casteel, LaVonda Crawford, Vicki Linton, April Marshall; **data entry supervisor** Cynthia Johnson; **specialists** Shirlene Hall, Tarrika Hill, William Jones

Business Operations and Administration director Deborah Rivera-Wienhold; **business systems and financial analysis director** Randy Yi; **manager, business analysis** Eric Knott; **manager, business operations** Jessica Tierney; **financial analysts** Priti Pamnani, Celeste Troxler; **rights and permissions: administrator** Emilie David; **associate** Elizabeth Sandler; **marketing director** Ian King; **marketing managers** Allison Pritchard, Alison Chandler, Julianne Wielga; **marketing associates** Aimee Aponte, Mary Ellen Crowley, Wendy Wise; **senior marketing executive** Jennifer Reeves; **director, site licensing** Tom Ryan; **director, corporate relations** Eileen Bernadette Moran; **publisher relations, eresources specialist** Kiki Forsythe; **senior publisher relations specialist** Catherine Holland; **publisher relations, east coast** Phillip Smith; **publisher relations, west coast** Philip Tsolakidis; **fulfillment supervisor** Iquo Edim; **fulfillment coordinator** Carrie MacDonald; **marketing manager** Christina Schlecht; **marketing associate** Laura Tutino; **electronic media: manager** Lizabeth Harman; **project manager** Trista Snyder; **assistant manager** Lisa Stanford; **senior production specialists** Ryan Atkins, Christopher Coleman, **computer specialist** Walter Jones, Kai Zhang; **production specialists** Nichele Johnston, Kimberly Oster; **director, web and new media** Will Collins

advertising director, worldwide ad sales Bill Moran
commercial editor Sean Sanders: 202-326-6430
assistant commercial editor Tianna Hicklin 202-326-6463
project director, outreach Brianna Blaser

Product (science_advertising@aaas.org); **midwest** Rick Bongiovanni: 330-405-7080, FAX 330-405-7081; **east coast/e. canada** Laurie Faraday: 508-747-9395, FAX 617-507-8189; **west coast/w. canada** Lynne Stickrod: 415-931-9782, FAX 415-520-6940; **uk/europe/asia** Roger Goncalves: TEL/FAX +41 43 243 1358; **japan** ASCA Corporation, Nanako Ide +81 (0) 3 6802 4616, FAX +81 (0) 3 6802 4615; ads@sciencemag.jp; **senior traffic associate** Deiandra Simms

worldwide associate director of *Science* Careers Tracy Holmes: +44 (0) 1223 326525, FAX +44 (0) 1223 326532

Classified (advertise@sciencecareers.org); **u.s.: midwest/west coast/south central/canada** Tina Burks: 202-326-6577; **east coast/industry** Elizabeth Early: 202-326-6578; **sales administrator:** Marci Gallun **sales coordinators** Rohan Edmonson, Shirley Young; **europe/row sales:** Susanne Kharraz, Dan Pennington, Alex Palmer; **sales assistant** Lisa Patterson; **japan** ASCA Corporation, Jie Chin +81 (0) 3 6802 4616, FAX +81 (0) 3 6802 4615; careerads@sciencemag.jp; **advertising support manager** Karen Foote: 202-326-6740; **advertising production operations manager** Deborah Tompkins; **senior production specialist/graphic designer** Amy Hardcastle; **production specialist** Yuse Lajiminmuhip; **senior traffic associate** Christine Hall

AAAS Board of Directors retiring president, chair Peter C. Agre; **president** Alice Huang; **president-elect** Nina Fedoroff; **treasurer** David E. Shaw; **chief executive officer** Alan I. Leshner; **board** Linda P. B. Katehi, Nancy Knowlton, Stephen Mayo, Cherry A. Murray, Julia M. Phillips, Sue V. Rosser, David D. Sabatini, Thomas A. Woolsey

AAAS
ADVANCING SCIENCE, SERVING SOCIETY

SENIOR EDITORIAL BOARD

John I. Brauman, *Chair, Stanford Univ.*
Richard Losick, *Harvard Univ.*
Linda Partridge, *Univ. College London*
Michael S. Turner, *University of Chicago*

BOARD OF REVIEWING EDITORS

Adriano Aguzzi, *Univ. Hospital Zürich*
Takuzo Aida, *Univ. of Tokyo.*
Sonia Altizer, *Univ. of Georgia*
David Altshuler, *Broad Institute*
Arturo Alvarez-Buylla, *Univ. of California, San Francisco*
Richard Amasino, *Univ. of Wisconsin, Madison*
Angelika Amon, *MIT*
Kathryn Anderson, *Memorial Sloan-Kettering Cancer Center*
Siv G. E. Andersson, *Uppsala Univ.*
Peter Andolfatto, *Princeton Univ.*
Meinrat O. Andreae, *Max Planck Inst., Mainz*
John A. Bargh, *Yale Univ.*
Ben Barres, *Stanford Medical School*
Marisa Bartolomei, *Univ. of Penn. School of Med.*
Jordi Bascompte, *Estación Biológica de Doñana, CSIC*
Facundo Batista, *London Research Inst.*
Ray H. Baughman, *Univ. of Texas, Dallas*
David Baum, *Univ. of Wisconsin*
Yasmine Belkaid, *NIAID, NIH*
Stephen J. Benkovic, *Penn State Univ.*
Gregory C. Beroza, *Stanford Univ.*
Ton Bisseling, *Wageningen Univ.*
Mina Bissell, *Lawrence Berkeley National Lab*
Peer Bork, *EMBL*
Robert W. Boyd, *Univ. of Rochester*
Paul M. Brakefield, *Leiden Univ.*
Christian Büchel, *Universitätsklinikum Hamburg-Eppendorf*
Joseph A. Burns, *Cornell Univ.*
William P. Butz, *Population Reference Bureau*
Mats Carlsson, *Univ. of Oslo*
Mildred Cho, *Stanford Univ.*
David Clapham, *Children's Hospital, Boston*
David Clary, *Oxford University*
J. M. Claverie, *CNRS, Marseille*
Jonathan D. Cohen, *Princeton Univ.*
Andrew Cossins, *Univ. of Liverpool*
Alan Cowman, *Walter & Eliza Hall Inst.*
Robert H. Crabtree, *Yale Univ.*
Wolfgang Cramer, *Potsdam Inst. for Climate Impact Research*
F. Fleming Crim, *Univ. of Wisconsin*
Jeff L. Dangl, *Univ. of North Carolina*
Stanislas Dehaene, *Collège de France*
Emmanouil T. Dermitzakis, *Univ. of Geneva Medical School*
Robert Desimone, *MIT*
Claude Desplan, *New York Univ.*
Ap Dijksterhuis, *Radboud Univ. of Nijmegen*
Dennis Discher, *Univ. of Pennsylvania*
Scott C. Doney, *Woods Hole Oceanographic Inst.*
Jennifer A. Doudna, *Univ. of California, Berkeley*
Julian Downward, *Cancer Research UK*
Bruce Dunn, *Univ. of California, Los Angeles*
Christopher Dye, *WHO*
Michael B. Elowitz, *Calif. Inst. of Technology*
Gerhard Ertl, *Fritz-Haber-Institut, Berlin*
Mark Estelle, *Indiana Univ.*
Barry Everitt, *Univ. of Cambridge*
Paul G. Falkowski, *Rutgers Univ.*
Ernst Fehr, *Univ. of Zurich*
Tom Fenchel, *Univ. of Copenhagen*
Alain Fischer, *INSERM*
Wulfram Gerstner, *EPFL Lausanne*
Charles Godfray, *Univ. of Oxford*
Diane Griffin, *Johns Hopkins Bloomberg School of Public Health*
Christian Haass, *Ludwig Maximilians Univ.*
Steven Hahn, *Fred Hutchinson Cancer Research Center*
Gregory J. Hannon, *Cold Spring Harbor Lab.*
Niels Hansen, *Technical Univ. of Denmark*
Dennis L. Hartmann, *Univ. of Washington*
Chris Hawkesworth, *Univ. of St Andrews*
Martin Heimann, *Max Planck Inst., Jena*
James A. Hendler, *Rensselaer Polytechnic Inst.*
Janet G. Hering, *Swiss Fed. Inst. of Aquatic Science & Technology*
Ray Hilborn, *Univ. of Washington*
Michael E. Himmel, *National Renewable Energy Lab.*
Kei Hirose, *Tokyo Inst. of Technology*
Ove Hoegh-Guldberg, *Univ. of Queensland*
David Holden, *Imperial College*
Lora Hooper, *UT Southwestern Medical Ctr at Dallas*
Ronald R. Hoy, *Cornell Univ.*
Jeffrey A. Hubbell, *EPFL Lausanne*
Steven Jacobsen, *Univ. of California, Los Angeles*
Peter Jonas, *Universität Freiburg*
Barbara B. Kahn, *Harvard Medical School*
Daniel Kahne, *Harvard Univ.*
Bernhard Keimer, *Max Planck Inst., Stuttgart*
Robert Kingston, *Harvard Medical School*
Hanna Kokko, *Univ. of Helsinki*
Alberto R. Kornblihtt, *Univ. of Buenos Aires*
Leonid Kruglyak, *Princeton Univ.*
Lee Kump, *Penn State Univ.*
Mitchell A. Lazar, *Univ. of Pennsylvania*
David Lazer, *Harvard Univ.*
Virginia Lee, *Univ. of Pennsylvania*
Olle Lindvall, *Univ. Hospital, Lund*
Marcia C. Linn, *Univ. of California, Berkeley*
John Lis, *Cornell Univ.*
Richard Losick, *Harvard Univ.*
Ke Lu, *Chinese Acad. of Sciences*
Laura Machesky, *CRUK Beatson Inst. for Cancer Research*
Andrew P. MacKenzie, *Univ. of St Andrews*
Anne Magurran, *Univ. of St Andrews*
Oscar Marin, *CSIC & Univ. Miguel Hernández*
Charles Marshall, *Univ. of California, Berkeley*
Martin M. Matzuk, *Baylor College of Medicine*
Grahma Medley, *Univ. of Warwick*
Virginia Miller, *UNC, Chapel Hill*
Yasushi Miyashita, *Univ. of Tokyo*
Richard Morris, *Univ. of Edinburgh*
Edvard Moser, *Norwegian Univ. of Science and Technology*
Sean Munro, *MRC Lab. of Molecular Biology*
Naoto Nagaosa, *Univ. of Tokyo*
James Nelson, *Stanford Univ. School of Med.*
Timothy W. Nilsen, *Case Western Reserve Univ.*
Pär Nordlund, *Karolinska Inst.*
Helga Nowotny, *European Research Advisory Board*
Stuart H. Orkin, *Dana-Farber Cancer Inst.*
Christine Ortiz, *MIT*
Elinor Ostrom, *Indiana Univ.*
Andrew Oswald, *Univ. of Warwick*
Jonathan T. Overpeck, *Univ. of Arizona*
P. David Pearson, *Univ. of California, Berkeley*
John Pendry, *Imperial College*
Reginald M. Penner, *Univ. of California, Irvine*
John H. J. Petrini, *Memorial Sloan-Kettering Cancer Center*
Simon Phillpot, *Univ. of Florida*
Philippe Poulin, *CNRS*
Colin Renfrew, *Univ. of Cambridge*
Trevor Robbins, *Univ. of Cambridge*
Barbara A. Romanowicz, *Univ. of California, Berkeley*
Jens Rostrup-Nielsen, *Haldor Topsoe*
Edward M. Rubin, *Lawrence Berkeley National Lab*
Shimon Sakaguchi, *Kyoto Univ.*
Michael J. Sanderson, *Univ. of Arizona*
Jürgen Sandkühler, *Medical Univ. of Vienna*
Randy Seeley, *Univ. of Cincinnati*
Christine Seidman, *Harvard Medical School*
Vladimir Shalaev, *Purdue Univ.*
Joseph Silk, *Univ. of Oxford*
Montgomery Slatkin, *Univ. of California, Berkeley*
Davor Solter, *Inst. of Medical Biology, Singapore*
Allan C. Spradling, *Carnegie Institution of Washington*
Jonathan Sprent, *Garvan Inst. of Medical Research*
Elsbeth Stern, *ETH Zürich*
Yoshiko Takahashi, *Nara Inst. of Science and Technology*
Jurg Tschopp, *Univ. of Lausanne*
Herbert Virgin, *Washington Univ.*
Bert Vogelstein, *Johns Hopkins Univ.*
Cynthia Volkert, *Univ. of Gottingen*
Bruce D. Walker, *Harvard Medical School*
Christopher A. Walsh, *Harvard Medical School*
David A. Wardle, *Swedish Univ. of Agric Sciences*
Colin Watts, *Univ. of Dundee*
Detlef Weigel, *Max Planck Inst., Tübingen*
Jonathan Weissman, *Univ. of California, San Francisco*
Sue Wessler, *Univ. of Georgia*
Ian A. Wilson, *The Scripps Res. Inst.*
Timothy D. Wilson, *Univ. of Virginia*
Xiaoliang Sunney Xie, *Harvard Univ.*
John R. Yates III, *The Scripps Res. Inst.*
Jan Zaanen, *Leiden Univ.*
Mayana Zatz, *University of Sao Paolo*
Jonathan Zehr, *Ocean Sciences*
Huda Zoghbi, *Baylor College of Medicine*
Maria Zuber, *MIT*

BOOK REVIEW BOARD

John Aldrich, *Duke Univ.*
David Bloom, *Harvard Univ.*
Angela Creager, *Princeton Univ.*
Richard Shweder, *Univ. of Chicago*
Ed Wasserman, *DuPont*
Lewis Wolpert, *Univ. College London*

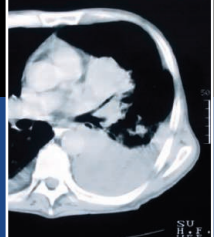

The dilemma of lung cancer screening
900

The power of exome sequencing
903

U.S. ELECTIONS

Researchers Anxious and on the Defensive After Republican Gains

More scrutiny. Less money.

U.S. scientists trying to assess the impact of last week's midterm elections on the U.S. research enterprise have begun preparing for the former in hopes of staving off the latter. At the same time, community leaders acknowledge that additional scrutiny of their work and its value to the nation is merited and that scientists need to do a better job of interacting with Congress and the public if they hope to fend off assaults on research and training budgets.

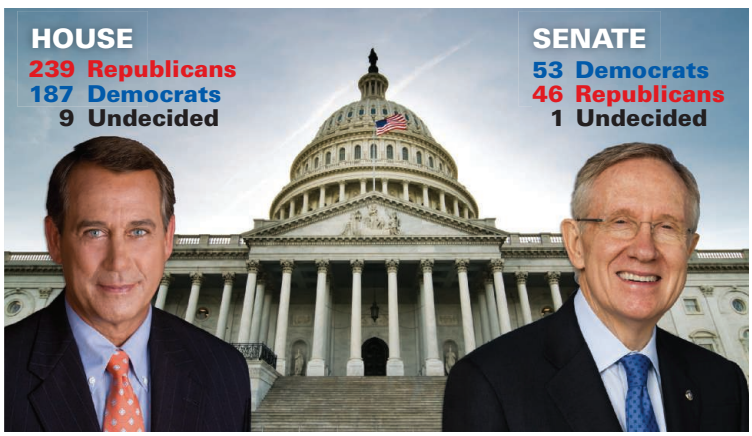

Turf war. Presumptive House Speaker John Boehner (*left*) and Senator Majority Leader Harry Reid (*right*) will square off in the next Congress.

Many researchers fear the worst after a Republican resurgence at the polls produced a 25-plus-seat majority in the House of Representatives and loosened the Democrats' grip on the Senate. The 2 November vote ended a 4-year streak of district, state, and national successes by Democrats that paved the way for unprecedented increases in federal research funding. One notable achievement was the 2007 America COMPETES Act that authorized a 7-year doubling of spending on the physical sciences at three key agencies, a promise that subsequent congresses have tried to keep. Another landmark was the $20 billion for basic research across several agencies that was part of the $787 billion stimulus package enacted shortly after President Barack Obama took office in 2009 (*Science*, 27 November 2009, p. 1176).

The 112th Congress that will convene in January could be headed down another path. Budget hawks are preparing to reduce overall federal spending, newly elected members are questioning the need to take action against rising levels of greenhouse gases, and advocates for smaller government are eying pieces of the Department of Education, the Department of Energy, and even the National Science Foundation (NSF).

Still, science lobbyists point to some bright spots amid those dark clouds. They emphasize that previous Republican Administrations and Congresses have been strong supporters of basic research, which has remained one of the few bipartisan issues in an increasingly divided political culture. They note that Obama has already said he will consider alternatives to the much maligned cap-and-trade system to lower carbon emissions (see p. 897). And they suggest that dismantling government is easier said than done. The 1994 Republican electoral wave that was buoyed by similar rhetoric failed to crest, they recall; indeed, the federal government actually grew significantly during the subsequent Administration of George W. Bush. In addition, they note, any House-passed measures are likely to face tough resistance in the Senate.

But few deny that the election has altered the landscape for science. "In terms of appropriations, it'll be harder for everybody, including academic research," says Peter McPherson, president of the Association of Public and Land-grant Universities. "I agree that we need to reduce the deficit [$1.3 trillion this year]. But it would not be good for the country if Congress didn't continue to provide strong support for university research."

The new Congress will convene without several staunch supporters of science. In the Senate, Arlen Specter (D–PA), a fierce and effective advocate for biomedical research, is departing after 30 years, following a loss in the Democratic primary earlier this year. Two huge losses to the House Science and Technology Committee are Representative Bart Gordon (D–TN), its current chair and the driving force behind an attempted reauthorization this year of the COMPETES Act, and Representative Vern Ehlers (R–MI), one of three physicists in the current Congress. Both are retiring, Gordon after 26 years and Ehlers after 17. The science committee also loses veterans representatives Brian Baird (D–WA) and Bob Inglis (R–SC). On appropriations, the subcommittee that funds NSF, NASA, and the Commerce Department's science agencies loses Representative Alan Mollohan (D–WV), its current chair. Representative Bill Foster (D–IL), the second member of the unofficial physics caucus, lost his bid last week for a second full term. [The lone remaining physicist in the House is Representative Rush Holt (D–NJ), who narrowly won reelection to a seventh term.]

"We're back to where we were in 2004," observes Michael Lubell, a lobbyist for the American Physical Society, about the ideological makeup of the new Congress. And that's not a good place to be, he says. "There will be a lot of new members who don't have much interest in the so-called elites, including scientists. The public doesn't dislike science, but it doesn't like scientists, especially if they say that they are from Stanford or Harvard and that they know what's best."

Ehlers, a college physics professor turned lawmaker and a champion of both basic research and science education, agrees with Lubell that scientists need to change their approach to public discourse. "A frequent mistake that intellectuals make is to think, 'Since I'm smart, I know everything, and that if you don't listen to me you're an idiot,'" says

Online
sciencemag.org
Podcast analysis of the election results.

Downloaded from www.sciencemag.org on November 11, 2010

CREDITS: U.S. CONGRESS; THINKSTOCK.COM

Published by AAAS

Underground physics

904

20 years of acid rain curbs

910

Ehlers. "That doesn't work. You have to have respect for your member of Congress and say, 'What can I tell you that will help you understand the gravity of the situation?' "

He also thinks that scientists need to adapt to what he says is a major change in the political landscape. "There is a new era here, and they should be getting to know the Republicans," says Ehlers. "Scientists are making a big mistake if they think that they can hunker down and just wait for Democrats to reclaim the House. Most university faculty tend to be liberal and identify with Democrats. So they need to become more open-minded and stop ridiculing Republicans and start trying to work with them. Otherwise, they won't be very effective."

Lubell suspects that many scientists will have a hard time making those adjustments. "I spoke at a national lab before the election and asked them what plans they had made for reductions in federal support and for working with people who know nothing about science," he says. "They were shocked. They didn't believe me."

And even a fresh approach may not be good enough, he warns. "I think that there are Republicans who will be receptive if you make the case that science isn't something that the private sector will fund," says Lubell. "But even then, it may come down to trying to argue against cutting science, or that Congress should use a duller ax." **–JEFFREY MERVIS**

U.S. ELECTIONS

Election Means Change in Climate for Efforts to Curb Emissions

Joe Manchin, the Democratic governor from coal-rich West Virginia, won a narrow election for a U.S. Senate seat last week, helping Democrats retain control of that body. But a memorable TV ad showing him shooting a copy of a cap-and-trade bill with a rifle sent a clear message: A core feature of the Obama Administration's approach to curbing greenhouse gas emissions is dead.

With "No on cap-and-tax" among their key talking points, Republicans who triumphed in Congress and in dozens of state capitols have vowed to block the president's plan to limit greenhouse gas emissions and reject state laws with a similar goal. And many Democrats, like Manchin, are likely to join them.

Although a California state referendum that would have effectively repealed a statewide cap-and-trade law was defeated, the Administration is already bowing to the inevitable. "Cap and trade was just one way of skinning the cat," a chastened President Barack Obama said in a press conference the day after the election. "It was a means, not an end. And I'm going to be looking for other means to address this problem." With those words, Obama signaled that he is eager to find a bipartisan approach to curbing emissions. But aggressive questioning of the fundamental tenets of climate science by many right-leaning politicians may make such an approach elusive.

Full bore. Even Democrats took shots at climate legislation.

Several postelection analyses suggested that most Democrats who lost races for the House of Representatives would have done so whether or not they voted against the cap-and-trade bill that passed the House before stalling in the Senate. But the Republican electoral wave was accompanied by an increasing willingness of candidates to ques-

Ralph Hall Bids to Lead Science Panel

In an election that saw Republicans gain control of the House of Representatives, it's perhaps fitting that the presumptive new chair of the House science committee, Representative Ralph Hall (R–TX), is a former Democrat. But the committee's traditional bipartisan culture could take a hit if Hall's first public comment on how he might run the panel is any guide.

Hall, who represents a rural district east of Dallas, came to Washington as a conservative Democrat in 1981 and switched parties in 2004, 3 years before his new party lost its House majority. A lawyer and former businessman, Hall easily won reelection last week to a 16th 2-year term. At 87, he's the oldest member of Congress but has never chaired a committee.

It may be weeks before House Republicans choose committee chairs for the 112th Congress. And Representative James Sensenbrenner (R–WI), who is in line to head the special committee on climate change that the Democrats created after taking over in 2007, could use his seniority to stake a claim on the science post if Republican leaders eliminate the climate panel.

Although Hall voted with a majority of his Republican colleagues 94% of the time in the current Congress, he'll need to convince the new leadership that he's an able and willing soldier. Perhaps with that in mind, Hall issued a statement the day after the election pledging "strong oversight over the [Obama] administration in key areas including climate change, scientific integrity, energy research and development, cybersecurity, and science education." He also mentioned his concerns about "the unprecedented growth in the federal government" in recent years and his conviction that "federal investment in R&D must empower the free market, not interfere with it."

Then he went a step further. He promised that the committee "will be a place … where all Republicans can play a role in crafting good science policy." An aide says that "Mr. Hall was not trying to exclude Democrats. … He certainly did not intend to infer that Democrats are not welcome to also play a role in crafting science policy."

In an era of increasing partisanship, however, Democrats will be looking closely to see which interpretation holds sway if and when Hall takes the gavel in January. **–J.D.M.**

CREDITS (TOP TO BOTTOM): JOE MANCHIN CAMPAIGN AD/YOUTUBE; (MONITOR) PHOTOS.COM; U.S. CONGRESS

Downloaded from www.sciencemag.org on November 11, 2010

Published by AAAS

Holding the line. An attempt to repeal cap-and-trade legislation in California was defeated.

tion whether anthropogenic greenhouse gas emissions are warming the planet. Morgan Griffith, who defeated veteran Representative Rick Boucher (D–VA), said humanmade warming was a "scientific theory … that many scientists do not even believe is happening." Dozens of House candidates—and every Republican Senate candidate—made similar public statements. "It's not only anti-science and anti–fact-based policymaking, but it's just political demagoguery," says Representative Alan Mollohan (D–WV), a senior House member who lost his seat in a Democratic primary.

Still, policymakers are looking for areas of compromise. White House spokesperson Robert Gibbs said one possible way to make progress on emissions might be to pass a national "renewable portfolio standard." Enacted in two dozen states, such a system requires utilities to obtain a significant portion of their power from nonemitting sources. Congress so far has balked at such legislation, although Senator Jeff Bingaman (D–NM), chair of the Senate Energy and Natural Resources Committee, hopes to succeed in the lame-duck session.

Economist Richard Schmalensee of the Massachusetts Institute of Technology in Cambridge, however, warns that such a standard could deliver more costly emissions reductions than a cap-and-trade scheme. He says it would limit utilities' options by forcing them to use solar or wind power, for example, instead of making their coal plants more efficient.

A new report by authors who span the political spectrum calls for rapidly doubling federal funding for the Department of Energy's Office of Science and its Energy Frontier Research Centers while quintupling the budget of the Advanced Research Projects Agency–Energy. Even so, co-author Mark Muro of the Brookings Institution admits that a big boost in federal spending on energy research—now roughly $4 billion annually—would be a "real challenge" for Congress, given the newly powerful Tea Party movement, for whom limiting spending is paramount.

Even with cap and trade dead, there will be plenty of new opportunities for rancor. The Environmental Protection Agency (EPA) is currently setting up rules to limit carbon emissions from power plants, and Obama has underscored that he is committed to that effort. But House Republicans—and many in the Senate, which Democrats still control—have vowed to risk an Obama veto by withholding funding for such efforts. "If [Obama] wants a fight on the [EPA's] budget, we'll need to take it to him," says Griffith.

The lawmakers expected to chair key House committees—such as Representative Darrell Issa (R–CA), in line to run the Oversight and Government Reform panel—have made it clear that they intend to investigate not only EPA Administrator Lisa Jackson but also the "Climategate" scandal of last year. "If the raw data's in doubt, then the idea that we have settled science doesn't exist. I want settled science," Issa told *ClimateWire*.

Representative Bob Inglis (R–SC), who lost earlier this year in a Republican primary, was one of two lawmakers who attributed his defeat to his vote in favor of cap and trade. (Boucher was the other one.) "It is a challenge," says the six-term legislator. "We've got to figure out a way to get the triple play of this American century, which is improving the national security of the United States, creating jobs, and cleaning up the air."

–ELI KINTISCH

U.S. ELECTIONS

Retiring Legislators Warn of Pitfalls Facing Science in New Congress

Two days after last week's midterm election, *Science* talked with four veteran legislators who have been staunch defenders of science and science education. Three are retiring next month: representatives Brian Baird (D–WA) and Bob Inglis (R–SC) of the House science commitee and appropriations subcommittee chair Alan Mollohan (D–WV). A fourth, Representative Sherwood Boehlert (R–NY), a former chair of the House science committee, left in 2007. Here are excerpts from that discussion, available online, with Deputy News Editor Jeffrey Mervis.

Online
sciencemag.org
Listen to the roundtable discussion online at http://podcasts.aaas.org/science_news/ScienceNews_101109_JM.mp3.

On the prospects for a spending freeze

Sherwood Boehlert: One of the most important things for scientists to do is to change the vocabulary. No longer should we be talking about investing in science or increasing R&D funding or STEM education because it's important for science. We should make this a national security issue. When a lot of the conversation is about the next Congress cutting or freezing all non–national security spending, we ought to take [science] funding and put it under the national security umbrella. Because it is a question of national security: lessening dependence on foreign oil, competitiveness, providing opportunities for our young people, creating jobs. …

Alan Mollohan: There has to be a national consensus that increased funding for science is akin to supporting economic growth and development generally.

CREDIT: © TED SOQUI/CORBIS

Downloaded from www.sciencemag.org on November 11, 2010

Published by AAAS

… We ought to be working against having a continuing resolution this year, because a CR would cost science funding in our bill [Commerce, Justice, Science] about $500 million. That would mean cuts, because we have increases in this bill over last year that would not be implemented.

On so-called negative earmarks

Brian Baird: There's a lot of talk about how [the next Congress] is going to eliminate earmarks. But my hunch is that the practice of negative earmarking [eliminating specific projects or programs] will continue and expand and that science, particularly the social sciences, may suffer from this. People will grandstand and take positions about how they're saving the public money … by taking money from an NSF- or NIH-approved grant and applying it to some "mom and apple pie" issue. And science needs to be mindful and watchful of some members, especially the newer ones, who may try to earn some cheap political points by substituting themselves for the peer-review process.

Rep. Brian Baird (D–WA)

On explaining the value of research

Bob Inglis: It's very important for scientists to explain the implications of their research, to make it more real to the people who are paying the bills. … By selling the sizzle, scientists can help rescue us from a retreat from science.

Rep. Bob Inglis (R–SC)

On the need for compromise

S.B.: When I announced my decision not to run in 2006, *The New York Times* referred to me as an endangered species because of my moderation. Now it appears that I'm almost extinct. The [Democratic] Blue Dogs have suffered, too. There has to be a role for the center in American politics. … Let's hope that after all is said and done, people will come to their senses. I'm not overly optimistic, but I'm keeping my fingers crossed.

On 17 November, the science committee will hold what may be the last Democratic-led hearing on climate change, billed as a "rational discussion" of the issue. Two members explained why.

B.B.: We're going to start with the basics: why the ocean is acidifying, why we think the climate will change. I don't think we've made the case for the basic physics and chemistry of these two phenomena and presented the evidence that it is happening. …

B.I.: I would encourage the scientists to come to these hearings with great glee, to show the data that they have discovered, and to present it in a winning way. … If they come with an attitude of defensiveness, then it will support those who say, "This is a bunch of hooey, and we don't need to spend any money on it." They should welcome the inquiry and say, "We're happy you asked. Now we're going to tell you what the data are."

On the role of U.S. businesses

B.B.: It's true that America COMPETES has been endorsed by the Chamber of Commerce and the National Association of Manufacturers, et cetera. But if you look at where their campaign contributions went, they quite literally do not put their money where their mouth is. They're happy to endorse legislation, but they don't fight vigorously to make sure [pro-science] candidates get in, nor do they insist that if a candidate is antithetical to investments in research and education, that candidate is antithetical to the interests of business and to economic and national security.

Rep. Sherry Boehlert (R–NY)

Rep. Alan Mollohan (D–WV)

On the learning curve for new members

A.M.: The reality is that most new members will be preoccupied with getting reelected and won't have the kind of responsibilities that would prompt them to get deeply involved [in the substance of a particular committee] until their second or third or fourth term. If they're on a nonscience committee, they won't become versed in the pros and cons of any particular [science] issue for a long time.

CREDITS (TOP TO BOTTOM): U.S. CONGRESS; DAVID SIMS/U.S. CONGRESS; COURTESY OF THE OFFICE OF REP. BOB INGLIS; U.S. CONGRESS

ScienceInsider

From the *Science* Policy Blog

Physicist and Representative Bill Foster (D–IL) **lost his seat in last week's election** as the Republican wave hit his conservative-leaning district, despite considerable financial support from colleagues at his district's Fermi National Accelerator Laboratory, where he worked for 22 years. "We [always knew] it would be a tough seat for a Democrat to hold," said Fermi physicist James Volk. "We're not going to elect him single-handedly out of Fermi."

Meanwhile, voter initiatives on defining "personhood" at birth and establishing the right to hunt failed at the voting booth.
http://scim.ag/congress2010

An arbitrator has ruled that Florida State University's decision to **lay off 12 tenured faculty members** last year was the result of an "arbitrary, capricious and unreasonable" process. The university promptly reinstated all 21 tenured faculty members axed in the cost-cutting move.
http://scim.ag/fsu_faculty

Officials with the **ITER fusion reactor** in Cadarache, France, are debating several controversial ways to save money. Among the proposed steps is to eliminate magnetic coils for controlling disturbances in the gas at the heart of the reactor or to skip tests on the reactor's giant containment magnets.
http://scim.ag/iter_cuts

A federal judge for the District of Columbia has rejected a legal argument used by the Bush Administration in 2008 to argue that **polar bears** are threatened, not endangered. That moves the animals one step closer to being listed as endangered under U.S. law.
http://scim.ag/polar-bear-ruling

Popular **genetic testing services** may sometimes be wrong about a customer's cancer risk, according to a new study. When test results for a small group of patients were compared with their risk calculated from family history, the results differed about half the time.
http://scim.ag/bad-tests

For more science policy news, visit **http://news.sciencemag.org/scienceinsider**.

Downloaded from www.sciencemag.org on November 11, 2010

Published by AAAS

PALEOANTHROPOLOGY

Neandertal Brain Growth Shows A Head Start for Moderns

With brains as big as ours, Neandertals were no dumb brutes. But they may not have used their brains the same way we do. In the crucial first year of life, their brains developed dramatically differently from the way ours do, according to a report in this week's issue of *Current Biology*. "Although they have the same brain size as us, Neandertals missed something that [modern] humans got in the first year of life," says study co-author Jean-Jacques Hublin of the Max Planck Institute for Evolutionary Anthropology in Leipzig, Germany.

Like chimpanzees, Neandertals apparently skip a phase during which infant *Homo sapiens* expand certain regions of the brain, when the dome of the *H. sapiens* skull rounds into its distinctive globular shape, says Hublin. This bulging in the parietal and temporal regions (at the top of the brain and above the ear) and in the cerebellum (at the base of the brain) suggests that humans are building brains that are fundamentally different from those of Neandertals, says Hublin. Paleoanthropologist Steven Leigh of the University of Illinois, Urbana-Champaign, who was not involved in the work, says, "Quite importantly, it moves us beyond examining simply the size of brains in these taxa and begins providing meaningful information on shape change."

Researchers have long recognized that adult Neandertal brains were more elongated and less globular than those of modern humans. But when do such changes appear in the life span?

To find out, Hublin, Philipp Gunz, and Simon Neubauer of Max Planck first compared CT scans of the brains of 58 humans and 60 chimps, varying in age from birth to adulthood, including seven newborns of each species. Using three-dimensional imaging and several hundred landmarks on the braincases to match them accurately despite differences in size, the team showed that humans—but not chimps—preferentially expand their parietal lobes and cerebellums and widen their temporal lobes in the first year of life, according to a report in November's *Journal of Human Evolution*. This

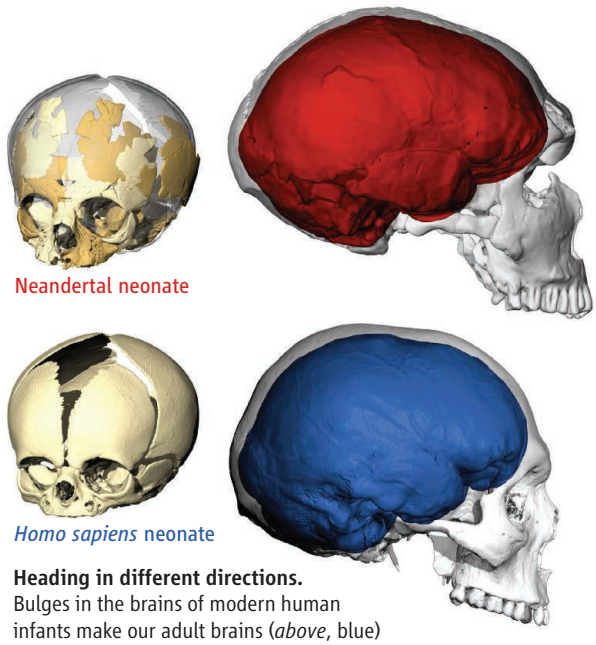

Heading in different directions. Bulges in the brains of modern human infants make our adult brains (*above*, blue) rounder than those of Neandertals adults (*top*, red).

CREDITS: (NEONATES) P. GUNZ *ET AL.*, *CURRENT BIOLOGY* **20**, 21 (9 NOVEMBER 2010); (ADULTS) PHILIPP GUNZ, MPI EVA LEIPZIG

CANCER SCREENING

The Promise and Pitfalls of a Cancer Breakthrough

Cancer research got some good news last week: A landmark clinical trial reported that screening for small tumors with advanced x-ray imaging led to a significant drop in lung cancer deaths (20% fewer) among smokers and ex-smokers, compared with screening with standard chest x-rays. Such positive results are unheard of, particularly for lung cancer, which kills 157,000 people in the United States each year. Until now, no randomized study has shown that screening for lung cancer can save lives.

But the news was double-edged. Experts quickly warned that the U.S. health care system isn't ready for what may follow. The new evidence, they said, is likely to bring a surge in demand for lung screening, which most insurers and Medicare do not pay for. In addition, perhaps a quarter of the people who decide to get screened will be burdened with false alarms and expensive follow-up tests.

Even the National Cancer Institute (NCI), which sponsored this $250 million study of a 3D imaging method known as low-dose helical computed tomography (CT), was guarded in its comments. NCI Director Harold Varmus said in a teleconference on 4 November that he saw "a potential for saving many lives," presumably through early detection and treatment. The study, called the National Lung Screening Trial (NLST), enrolled 53,454 smokers and ex-smokers between ages 55 and 74; 354 died of lung cancer in the CT screening arm compared with 442 in the chest x-ray group. But Varmus warned that the results apply only to heavy smokers and that the data must still be scrubbed, a process that will take months, before recommendations can be made.

NCI Deputy Director Douglas Lowy, also speaking at the teleconference, ticked off some "disadvantages" of CT screening. One is cost. The price of a scan, estimated at about $300 to $500 per screening, is the least of it. Big expenses ensue, Lowy said, from the high ratio of people who get positive test results but do not have lung cancer. Even if you focus strictly on those with the highest risk—this trial screened smokers and ex-smokers who had used a pack of cigarettes a day for 30 years—"20% to 50%" of the CT scans "will show abnormalities" according to recent studies, said Lowy. According to NCI, about 96% to 98% are false positives.

In NLST, about 25% of those screened with CT got a positive result requiring follow-up. Some researchers have seen higher rates. Radiologist Stephen Swensen of the Mayo Clinic in Rochester, Minnesota, says that a nonrandomized study he led in 2005 gave positive results for 69% of the screens. One difference between the Mayo and NLST studies, Swensen says, is that Mayo tracked nodules as small as 1 to 3 millimeters whereas NLST, which began in 2002, cut off positive findings below 4 mm.

One negative consequence of CT screening, Lowy said at the teleconference, is that it triggers follow-up scans, each of which increases radiation exposure. Even low-dose CT scans deliver a "significantly greater" exposure than conventional chest x-rays, said Lowy, noting that, "It remains to be determined how, or if, the radiation doses from screening … may have increased the risks for cancer during the remaining lifetime" of those screened. Clinical follow-up may also include biopsy and surgery, Lowy said,

Downloaded from www.sciencemag.org on November 11, 2010

Published by AAAS

results in the characteristic rounded dome of our skulls. Computer modeling showed how those early changes set human brains on a developmental trajectory that is different from that of chimps.

Then the team used the same imaging methods to study nine fossil Neandertals, including a newborn, a year-old baby, and three children. Because the brain does not fossilize, they studied endocasts, imprints of the brain left in the skull. They found that at birth, both Neandertal and modern human infants had elongated braincases that were similar in shape, although Neandertal faces were already larger. By age 1 or so, modern humans had grown globular brains, but Neandertal babies did not show the preferential bulging in the parietal and cerebellar regions, even though the brain grew overall. "They finally demonstrate that this stage [bulging] is absent in Neandertals," says paleoneurologist Emiliano Bruner of the National Research Centre on Human Evolution in Burgos, Spain.

In living people, those areas of the brain are linked with key functions such as the ability to integrate sensory information and to form abstract representations of the environment. The differences suggest that Neandertals didn't behave just like we do, says Hublin.

However, because there are so few fossils of Neandertal infants, the new analysis depends on endocasts of only one incomplete skull of a Neandertal newborn and of an older baby, points out anthropologist Marcia Ponce de León of the University of Zurich in Switzerland. "They do reveal a pattern," says Leigh, but "this pattern needs statistical support before we can be confident about its validity. That may not be possible with such small samples."

Hublin and Gunz acknowledge the sample-size problem but say that they also used computer growth simulations that did not rely on juvenile fossils. When they modeled the development of modern human babies without a globular growth stage, the babies' brains grew to look like those of Neandertal adults. The team recently confirmed its findings in a second, more complete Neandertal newborn. Now, they are investigating how brain development may be linked to genes that differ in Neandertals and modern humans, working with the Max Planck researchers who sequenced the Neandertal genome. "Very small differences in this crucial time in development can have serious consequences," says Gunz.

–ANN GIBBONS

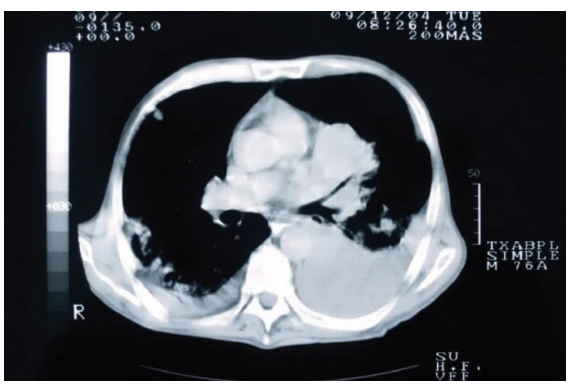

Inside view. Spiral x-ray scans yield a highly detailed view of the lungs and small nodules, most of which are benign.

CREDITS (TOP TO BOTTOM): AMY DUFFIELD; ISTOCKPHOTO.COM

"potentially risky procedures that can cause a host of complications."

G. Scott Gazelle, a radiologist and director of the Institute for Technology Assessment at Massachusetts General Hospital in Boston, has been analyzing the likely impacts of lung cancer screening for a decade. He agrees that people are going to demand it—and that "there are going to be a huge number of false positives." He was not surprised at NLST's finding of a lifesaving benefit of 20%. His group's prediction of mortality reduction through CT scans, based on "micromodeling" of actual cancers and data from previous studies, was 18% to 25%, right on target. But Gazelle says this analysis, now under review, still suggests that a national program of CT screening for lung cancer "would not be cost effective." Indeed, the costs seem likely to be three to four times those of breast cancer screening, with similar benefits.

Advocates of screening, in contrast, see the NLST results as vindicating a campaign to put advanced computer technology to work on lung cancer. The detailed images of early tumors in CT scans are "exquisite," says James Mulshine, vice president for research at Rush University Medical Center in Chicago, Illinois, and an adviser to the pro-screening advocacy group, the Lung Cancer Alliance in Washington, D.C. He thinks it should be straightforward to reduce the number of biopsies and surgeries resulting from false positives by monitoring small tumors for a time before intervening. There are 45 million smokers in the United States who might benefit from CT screening, says Mulshine. He asks: Do we provide it, or "Do we tell them, 'Tough luck'?"

–ELIOT MARSHALL

ScienceNOW

From *Science*'s Online Daily News Site

Cats' Tongues Employ Tricky Physics

Cats like to do things their own way—even, it seems, when it comes to drinking.

Dogs and other animals lap up water by curling their tongues into a cuplike shape, but high-speed cameras reveal that cats rest the tips of their tongues on the liquid's surface without penetrating it. The water adheres to the cat's tongue and is pulled upward in a column as the cat draws its tongue into its mouth—a complex maneuver that pits gravity against inertia. The technique maximizes a feline's gulp while keeping its whiskers clean, researchers report online this week in *Science*. http://scim.ag/cat-tongue

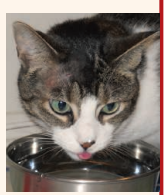

New Malaria Drug Could Save Tens of Thousands

It's not often that spontaneous applause erupts halfway through a scientific talk. But when malaria researcher Arjen Dondorp came to the crucial slide of his presentation last week at the American Society of Tropical Medicine and Hygiene's annual meeting, the audience couldn't contain itself. Dondorp's study showed that compared with an older drug called quinine, a new one called artesunate reduces the risk of death from severe malaria in African children by 23%—a finding that could save tens or even hundreds of thousands of lives annually. http://scim.ag/malaria-drug

Comet Revealed as a Giant Dog Bone

Last Thursday, the EPOXI spacecraft screamed by the icy nucleus of comet Hartley 2—the fifth comet ever imaged close up. Photos beamed back reveal that the comet looks like a dog bone. Presumably, comet Hartley 2 was once two separate bodies that came together. Or, it could have always been a single body now stretched out by its own spinning. Today, the sun's warmth is driving off primordial gases and dust, especially in bright jets seen streaming off the far end. Surprisingly, frozen carbon dioxide—dry ice—rather than water ice seems to be contributing most of the gas that's driving the dust. http://scim.ag/comet-hartley

Read the full postings, comments, and more at **http://news.sciencemag.org/sciencenow.**

Downloaded from www.sciencemag.org on November 11, 2010

Published by AAAS

REMOTE SENSING

Earth-Observation Summit Endorses Global Data Sharing

BEIJING—Last August, heavy monsoon rains submerged nearly one-fifth of Pakistan, inflicting $43 billion worth of damage. The floodwaters destroyed homes and businesses, washed away bridges and roads, ruined crops, and claimed about 1800 lives. As bad as it was, the toll could have grown in the weeks that followed if not for a novel Earth-observation system featured at a meeting here last week.

In July, before the deluge, the International Centre for Integrated Mountain Development in Kathmandu—along with NASA and the U.S. Agency for International Development—had booted up SERVIR-Himalaya, a Web-based monitoring system that pulls together satellite imagery, forecast models, and ground observations. It "showed the progression of the floods in [near] real time," says Sherburne Abbott, associate director for environment at the White House Office of Science and Technology Policy. As the disaster unfolded, analyses revealed that flooding had knocked nearly 200 tuberculosis clinics out of commission. Forewarned, aid agencies scrambled to steer patients to functioning health centers. "They knew they were going to have a real problem," Abbott says.

SERVIR is one new instrument in a veritable orchestra of Earth-observation systems intended to make reams of data available and relevant to decision-makers. At the summit last week of the Group on Earth Observations (GEO)—the organization attempting to get this ensemble performing in synchrony—initiatives were unveiled to monitor land-cover changes and forest carbon stocks. And GEO delegates embraced plans to funnel data from platforms tracking everything from biodiversity to earthquake risks into a free and open database. "What's happening is groundbreaking," says David Hayes, deputy secretary of the U.S. Department of the Interior. "This data is incredibly valuable. If you share it, your incremental contribution can yield a super benefit."

Established in 2005, GEO is an effort by 85 countries, the European Commission, and 58 international organizations to meld disparate remote-sensing tools and ground-based databases—300 databases and counting—into a seamless Global Earth Observation System of Systems (GEOSS), which is expected to come fully online in 2015. When GEO was conceived, "we understood that if you want to manage planetary problems, you have to have planetary information—which didn't exist at that stage," says Bob Scholes, a biodiversity expert at the Council for Scientific and Industrial Research in Pretoria.

GEO's progress has been remarkably swift, Scholes adds, and the project has overcome the view that data should be hoarded, not shared. "When an earlier generation of scientists collected data on the public purse, they considered it their data. The norm now is that data will quickly enter the public domain," he says. To reinforce such good behavior, "persistent identifier" tags are being developed that will note which scientists or teams contributed data to GEOSS. The U.S. Office of Management and Budget (OMB) is spurring agencies to release data via www.data.gov. "OMB is looking to measure our department's productivity in part by how much we're adding to the public's access to data," says Hayes.

NASA and the U.S. Geological Survey 2 years ago began allowing free access to their 4-decade Landsat archive, including images with a resolution of 30 meters that enable tracking of land-cover changes wrought by human activity. And riding new open-data legislation in the European Union, the European Space Agency plans to allow free access to data streams from its soon-to-be-launched Sentinel satellites, says Manuela Soares, director for environmental research at the European Commission's Research Directorate. "There's been delivery of data on a massive scale," says Gary Richards of Australia's Department of Climate Change and Energy Efficiency in Canberra.

Ground-truthing such data is a key element of SilvaCarbon, a U.S.-led scientific network announced here to help GEO improve access to Earth-observation data on forests. SilvaCarbon is expected to develop technologies to implement one of the few bright spots in international climate negotiations: REDD+, a program to reduce emissions from deforestation and enhance forest carbon stocks. Together with GEO's Global Forest Observation Initiative, SilvaCarbon "shows that we are ready to take the next big step to a robust and transparent global monitoring system for forest carbon," says Richards.

A second new effort, the Global Land-Cover Data Initiative, aims over the next 2 years to compile and publicly share a current snapshot of Earth's land-cover conditions. Landsat data provide 80% coverage; GEO partners will fork over the rest.

As GEOSS is woven from disparate data sets, there have been a few glitches in integrating the information. "We can't get all data into the free and open database at this point," says Abbott. And some resistance remains. "We still get pushback," says Scholes. "Some countries worry about how data release will affect national security." Nations fret, for instance, over satellite data they have no control over and others revealing info such as flows rates of transboundary rivers. Of course, all agree that some sensitive data, such as the precise location of the last few individuals of an endangered species, should not enter the public domain. "But these instances are now perceived as the exceptions to the rule," Scholes says. And that, he says, testifies to the profound cultural change on data sharing that GEO is helping drive. **–RICHARD STONE**

GEOSS'S TOP TARGETS

1. Precipitation
2. Soil moisture
3. Surface air temperature
4. Surface wind speed
5. Land cover
6. Surface humidity
7. Vegetation cover
8. Surface wind direction
9. NDVI*
10. Sea surface temperature

*Normalized difference vegetation index

Data fundamentals. Of 146 critical Earth observations, GEO rates these 10 as the highest priority.

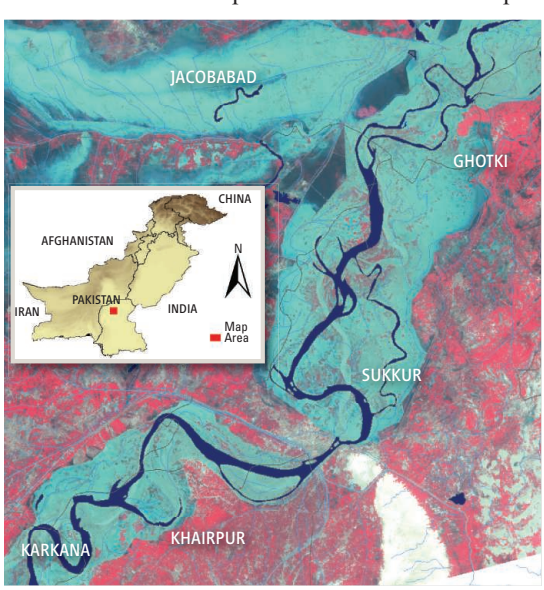

Waterlogged. This SERVIR-Himalaya analysis shows flooding along the Indus River in Pakistan's Sindh Province last August.

CREDITS (TOP TO BOTTOM): (SOURCE) GEO; ICIMOD, NASA

Downloaded from www.sciencemag.org on November 11, 2010

Published by AAAS

HUMAN GENETICS

Affordable 'Exomes' Fill Gaps in a Catalog of Rare Diseases

The couple had four healthy babies, but tragedy struck as the children became teenagers: Three began to lose their sight. Now in their 30s, two of the sisters and their only brother have lost most peripheral vision; one is legally blind from retinitis pigmentosa, the disease all three inherited. Although doctors tested them for more than 50 genetic mutations linked to the disease, they came up empty. Then late last year, geneticists at the University of Miami in Florida tried a new test, one that searched for mutations by sequencing the siblings' entire protein-coding DNA.

By July, the family had an answer: The three affected siblings had inherited two copies of a defect in a gene called *DHDDS*. It codes for an enzyme that may be involved in tacking sugar groups to the light-sensing protein rhodopsin; when researchers blocked *DHDDS* in zebrafish, the fish became partially blind. The family members, who for years worked to raise money to study inherited blindness, "were overwhelmed when they learned that we found the gene," says geneticist Stephen Züchner of the University of Miami. He presented the study this week at the American Society for Human Genetics (ASHG) meeting in Washington, D.C.

The study adds to a flurry of reports this year on new genes for Mendelian disorders: rare diseases caused by a defect in a single gene. The work takes advantage of cheap, next-generation DNA-sequencing technologies that make it possible, for a few thousand dollars, to sequence the 1% of the genome that codes for proteins, known as exons. This so-called exome sequencing has "reinvigorated the field of Mendelian disorders," says Jay Shendure of the University of Washington, Seattle, who gave an overview at the ASHG meeting. Researchers studying rare diseases are experiencing a "euphoria," says Eric Green, director of the National Human Genome Research Institute (NHGRI) in Bethesda, Maryland.

For decades, geneticists have had only one way to find the genes underlying Mendelian disorders: studying families. By analyzing inheritance patterns of genetic markers, they could pinpoint the disease gene. But this so-called linkage approach doesn't work when few affected family members can be found or the disease is extremely rare, often because the mutation was not inherited but occurred spontaneously. As a result, of the nearly 7000 known or suspected Mendelian disorders identified based on clinical features, less than half have been linked to a gene (see table).

That is changing thanks to exome sequencing. Researchers use an off-the-shelf kit to separate out the exon-coding DNA in a sample, then feed the DNA into the new sequencing machines. This yields a list of perhaps 20,000 mutations. The researchers then filter out data such as changes that don't alter amino acids in proteins or mutations commonly found in other people.

In August 2009, Shendure and colleagues reported as a proof of principle that by sequencing the exomes of four unrelated patients with the same disease, Freeman-Sheldon syndrome, they found the known underlying gene. A string of reports of new Mendelian disease mutations have followed, some in known genes but also 10 or so novel disease genes, says Shendure. These include, for example, the first gene for Kabuki syndrome, an extremely rare disorder involving deformities and retardation. (In a couple of cases, the researchers used whole-genome sequencing, which costs eight to 10 times as much as exome sequencing, but the genes could have been found with just the exome, Shendure notes.) "It's solving things that we've been looking at for a long time," says molecular geneticist Joris Veltman of Radboud University Nijmegen Medical Centre in the Netherlands, whose group has found several novel genes—and "you don't have to be a big genome institute."

Mystery solved. Exome sequencing found the mutation that led to blindness in three children in the Lidsky family of Miami. The approach is uncovering the cause of other single-gene disorders.

MENDELIAN DISORDERS

	Number
Gene known	2893
Gene unknown	1771
Suspected disorders	1977
Total	6641

Some mutations point toward treatments. Yale University geneticist Richard Lifton's team last year reported that a Turkish infant with failure to thrive who had been diagnosed with an inherited kidney disorder instead had a known defect in a gene coding for an intestinal chloride transporter, leading to chronic diarrhea; the boy was put on oral rehydration therapy. Züchner's group is exploring whether drops of the chemical made by the DHDDS enzyme can restore some sight in the blind siblings.

Other discoveries reveal new insights about human biology. For example, as reported online in *Nature* in August, Lifton's group found a gene called *WDR62*, which when mutated severely alters how the brain develops.

Exome sequencing isn't perfect, however. The kits used in most published work capture only about 75% of all 20,000 genes, although newer versions are more comprehensive. The approach also misses structural changes and noncoding DNA that can influence gene regulation. The exome could soon be eclipsed by whole-genome sequencing, which is getting ever cheaper, geneticists say.

It's an open question whether exome sequencing can ferret out rare mutations that underlie complex, common diseases. Answers may come soon: Tens of thousands of exomes from people with common diseases are now pouring out of sequencing machines, Shendure notes.

But the technique's success for Mendelian disorders is undisputed. One sign is that NHGRI plans to fund a center next year that would find the genes underlying 40 to 50 Mendelian diseases a year and coordinate samples for studying others. Medical geneticist David Rosenblatt of McGill University in Montreal, Canada, spoke out passionately at the ASHG meeting in support of such a systematic effort to find the genes behind Mendelian diseases. "We should put the pins in the map … and in the next 2 years find them all," Rosenblatt said. **–JOCELYN KAISER**

CREDITS: COURTESY OF BETTI LIDSKY; (INSET SOURCE) ONLINE MENDELIAN INHERITANCE IN MAN (6 NOVEMBER 2010)

Downloaded from www.sciencemag.org on November 11, 2010

Published by AAAS

Dig in. Preliminary excavation has begun at Homestake, funded by South Dakota.

CREDIT: BILL HARLAN/SANFORD UNDERGROUND LABORATORY

Scientific Gold Mine Or Dicey Money Pit?

Scientists say a proposed underground laboratory in South Dakota could be a world beater. But they must persuade the National Science Foundation to pay for the massive project

MINERS ONCE HAULED GOLD OUT OF THE Homestake mine in the Black Hills of South Dakota. Now particle physicists hope to find scientific treasures there. They want to convert the mine into the Deep Underground Science and Engineering Laboratory (DUSEL), the largest underground lab in the world. In it they would seek the elusive "dark matter" whose gravity binds the galaxies, a type of radioactivity that would blur the line between matter and antimatter, and protons falling apart as predicted by some particle theories.

Advocates say the $875 million project is too good an opportunity to pass up. "We're investing in a suite of experiments, and three, four, or five of them could be discovery experiments that will change the textbooks," says Kevin Lesko, a physicist at Lawrence Berkeley National Laboratory in California, who leads the DUSEL design team. But DUSEL is not a typical project for the U.S. National Science Foundation (NSF), which historically builds scientific instruments such as telescopes. Instead, DUSEL is mostly an infrastructure project to provide lab space for a host of experiments in a variety of disciplines. Moreover, the biggest experiment in it would be a gargantuan particle detector funded primarily by the Department of Energy (DOE), not NSF. Operations such as pumping water out of the mine also cost $1 million a month.

The project must win approval from the National Science Board (NSB), which sets policy for NSF, and observers say that board members will want good answers to three important questions before they sign off on the project. How would DUSEL stack up against other underground labs around the world? How will NSF and DOE coordinate efforts to ensure the project stays on track? And will DUSEL yield enough science to justify the investment? "The NSF science projects have to be enough in the forefront to make it a good sell," says Barry Barish, a physicist at the California Institute of Technology in Pasadena and a consultant to the board. "The more it looks like it's just a big hole in the ground for a DOE experiment, the less sellable it is."

The project is entering a crucial period. The preliminary design should be completed by year's end. Meanwhile, the National Academies' National Research Council has begun a study of the three main questions and should provide input to NSF by the spring. Based on the preliminary design, NSB could vote on the project as early as August. "The question is, how much of this list of issues will be settled by next summer?" Barish says.

The lowdown on labs low down

When it comes to underground labs, "the deeper the better, the bigger the better, there is no doubt," says Franz von Feilitzsch, a physicist at the Technical University of Munich in Germany. Deep under ground, scientists can escape the hail of ordinary particles from space called cosmic rays to search for more exotic things. Big labs provide room for the huge detectors needed to spot very rare phenomena.

At a lab like DUSEL, four physics studies would anchor the research program. One would search for the dark matter that cosmologists say makes up 85% of all matter. Physicists are already trying to glimpse dark-matter particles smacking into nuclei in detectors weighing tens of kilograms in various underground labs around the world. They're spurred by a concept called "supersymmetry," which predicts that every known particle has a massive "superpartner." The lightest superpartner would be a prime candidate for dark matter. Fully testing the idea may require a detector weighing a metric ton.

Physicists would also search for a type of radioactivity called "neutrinoless double beta decay" that would blur the distinction between matter and antimatter. Many a nucleus can change identity through beta decay, when a neutron in it turns into a proton and spits out an electron and an elusive antineutrino. Others change by absorbing a neutrino instead of emitting an antineutrino. In neutrinoless double beta decay, two neutrons in a nucleus such as germanium-76 or tellurium-130 would change into protons while ejecting only two electrons. That can happen only if the neutrino is its own antiparticle—so the antineutrino emitted by one neutron can absorb the other neutron because it's also an antineutrino.

The biggest experiment in DUSEL would be a detector weighing between 100,000 and 200,000 tons that would snare neutrinos fired through Earth from a distant particle accelerator. Using such setups, physicists in the United States, Europe, and Japan are already studying

Downloaded from www.sciencemag.org on November 11, 2010

Published by AAAS

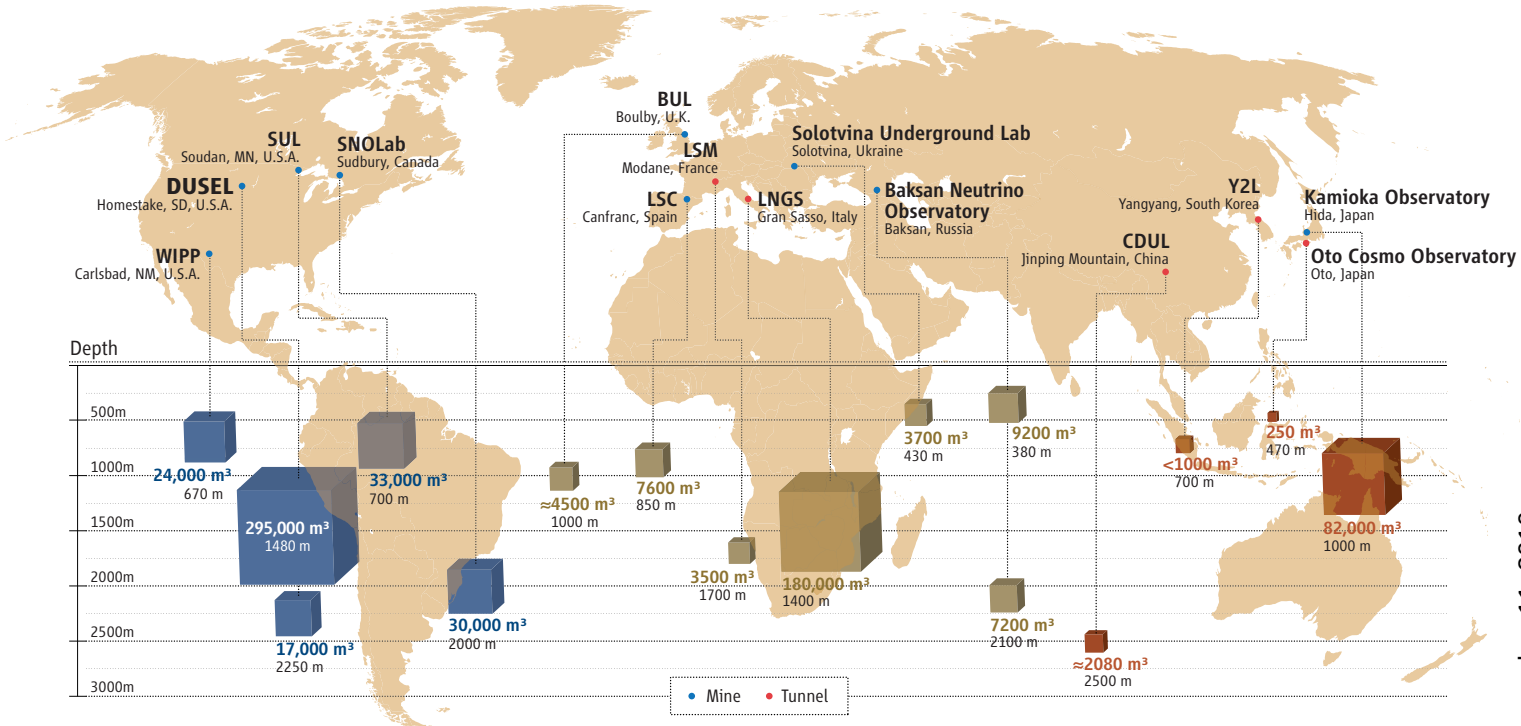

The hole story. DUSEL would provide more lab space than any other facility in the world and would be among the deepest. Volume estimates are approximate.

how the three types of neutrinos—electron, muon, and tau—change into one another as they whiz along. The Long-Baseline Neutrino Experiment (LBNE) would go further and look for an asymmetry between the behavior of neutrinos and antineutrinos, called charge-parity (CP) violation, that might explain why the universe contains so much more matter than antimatter. LBNE would cost between $660 million and $940 million.

In addition to detecting neutrinos from the sun or from supernovae, such a huge detector could also search for proton decay, the fourth key experiment. Theorists have developed "grand unified theories" that roll together the three forces that dominate particle interactions: electromagnetism, the strong force that binds the nucleus, and the weak force that causes beta decay. Those theories predict that the otherwise eternal proton should decay, albeit on a time scale so immensely long that physicists would have to study hundreds of thousands of tons of matter in a detector to spot a few decays.

DUSEL would also house experiments in microbiology, geoscience, and engineering. For example, Derek Elsworth, a geophysicist at Pennsylvania State University, University Park, has proposed heating a 10-meter-wide cubic volume of rock to see how heat affects stresses, chemistry, and fluid flow in it. The data could aid in, among other things, designing geothermal reservoirs. "You have these processes going on 2 or 3 kilometers down in geothermal structures, but you can never see them," Elsworth says. With DUSEL, "you're right there."

Leapfrogging the competitors

All of this would occur at Homestake, the deepest mine in North America. Starting in 2014, workers would carve out two labs with a total volume of 72,000 cubic meters at a depth of 1480 meters, and a third smaller lab 2255 meters down. On the upper level they would dig at least one 50-meter-tall, 260,000-cubic-meter cavity for the LBNE detector to field neutrinos beamed from Fermi National Accelerator Laboratory (Fermilab) 1300 kilometers away in Batavia, Illinois. Construction would take about 5 years, but some experiments could move in before work is completed.

A dozen mines and tunnels around the world already house underground labs (see map). None has enjoyed more success than the Kamioka Observatory in central Japan. In 1998, physicists there used the 22,500-ton Super-Kamiokande detector to prove that muon neutrinos generated in the air change type in flight. (Fewer survived the long trip through Earth than the short trip from above, proving that some changed en route.) This year they began shooting neutrinos at the detector from a lab 295 kilometers away in Tokai to measure a key parameter describing such "neutrino oscillations," a number called θ_{13}.

Italy's Gran Sasso National Laboratory is currently the largest underground lab. Lying next to a highway tunnel under the Apennine Mountains in central Italy and boasting a volume of 180,000 cubic meters, it houses, among others, two detectors to field neutrinos from the European particle physics laboratory, CERN, near Geneva, Switzerland. SNOLab in Sudbury, Canada, is the deepest big lab, with a depth of 2073 meters. Physicists there showed in 2001 that electron neutrinos from the sun also change type in transit.

But even though they have large labs, physicists in Europe and Asia say DUSEL would propel the United States to the lead in underground science. "Japan is doing really well, but I am worried that the U.S. will pull ahead of us," says Masayuki Nakahata of the University of Tokyo. In fact, overseas researchers are planning bigger labs that resemble DUSEL. But they have not yet found sites for them.

In Europe, physicists hope to build a lab with a neutrino detector weighing as much as 440,000 tons to receive a beam from CERN. They are studying seven possible sites, ranging from Canfranc, Spain, to Pyhäsalmi, Finland, says Andre Rubbia of the Swiss Federal Institute of Technology Zurich. In Japan, physicists want to build a huge lab either 20 kilometers south of Kamioka or on the island of Okinoshima, 658 kilometers west of Tokai. The site decision may have to wait 2 or 3 years for measurements of θ_{13}, says Takashi Kobayashi of Japan's accelerator lab KEK in Tsukuba. That's because CP violation can exist among neutrinos only if θ_{13} is not zero.

Experiments in existing labs could discover dark matter or neutrinoless double beta decay before those planned for DUSEL. But that would only spur more experiments requiring more lab space, physicists say.

CREDIT: M. TWOMBLY/*SCIENCE*

Downloaded from www.sciencemag.org on November 11, 2010

Published by AAAS

Some say that relatively shallow Kamioka and Gran Sasso may soon be inadequate for newer experiments requiring even lower background radiation. Munich's von Feilitzsch works on a detector called Borexino in Gran Sasso that detects low-energy neutrinos from the sun. "For this physics, Gran Sasso is not deep enough," he says. "It's done its job."

Worries closer to home

Although DUSEL may have non-U.S. researchers looking over their shoulders, U.S. scientists are afraid that cost considerations may force designers to pare down their plans in ways that would dull the lab's competitive edge. In particular, they worry that the lab's lower 2250-meter level, which is currently flooded, will be smaller than they want and may not be available right away. A 2007 "conceptual design report" envisioned three halls at that lower level with a total volume of 4500 cubic meters; current plans call for a single hall of 1700 cubic meters.

Those changes could cause some scientists to make do with existing facilities. "It's possible that by the time DUSEL is built the people who need easy access will have gone to Gran Sasso and the people who need to go deep will have gone to SNOLab and there will be no customers," says Giorgio Gratta, a physicist at Stanford University in Palo Alto, California, who is working on neutrinoless double beta decay.

Others say that the changes simply reflect a determination to build only what's necessary. Design-team leader Lesko notes that when the conceptual design report was written in 2007, designers had received no specific proposals for experiments to go into DUSEL. Now, they have more than a dozen to which they're tailoring their plans.

At the same time, some scientists fret over the balance between spending on infrastructure and funding for experiments. When Homestake was selected in 2007 over seven other potential sites, NSF officials estimated it would cost $500 million, with half of the money going to key experiments other than LBNE. That pot of money would make DUSEL the obvious place to propose a dark-matter experiment, says Blas Cabrera, a physicist at Stanford.

However, the balance between infrastructure and science has shifted, so that grant money now accounts for $175 million of the $875 million total. In part, retrofitting the old mine has proved more expensive than originally estimated. Also, Lesko says, the original cost breakdown did not include the $123 million NSF would now contribute to LBNE, to which DOE gave the initial nod earlier this year.

Nevertheless, NSF officials say that anything less than a broad science program and four key experiments would be hard to sell to the science board. "If it turned out that only one of these experiments could be done within the cost envelope, then obviously [getting approval] would be difficult," says Edward Seidel, who leads NSF's mathematical and physical sciences directorate.

Observers say concern over the balance of science and infrastructure may have led to a glitch in the president's 2011 budget request for NSF that threatened DUSEL. NSF initially asked for $38 million for DUSEL design work, but the White House Office of Management and Budget (OMB) cut that amount in half. NSF and OMB officials now seem to have agreed to support the project until NSB can evaluate it, although parties to the negotiations declined to discuss the details.

The 2011 budget is still pending before Congress, but Lesko says the design team has submitted a proposal to NSF to fund the "scope of work" to be completed in 2011. NSB consultant Barish says he's "absolutely sure" the board will approve the additional money.

Some researchers also worry about the partnership between NSF and DOE. DOE's interest in DUSEL should bolster the project, especially as LBNE anchors DOE's plans for Fermilab's future. But the two agencies have a mixed record on joint projects. One glaring failure, scientists say, was a pair of NSF experiments known as Rare Symmetry Violating Processes (RSVP) that in 2000 was approved to run at DOE's Brookhaven National Laboratory in Upton, New York. Uncertainties over whether DOE would run an accelerator long enough to complete the experiments or make NSF pay for more time led NSF to cancel the project in 2005. Researchers say the agencies didn't discuss the problem until after RSVP was approved.

To avoid such snags with DUSEL, officials from DOE and NSF are hammering out an arrangement in which one agency would take the lead for an experiment but the other would also contribute. For example, DOE would lead on neutrinoless double beta decay, and NSF would spearhead dark-matter searches. The approach would give both agencies a stake in every experiment. "It's like any marriage," says Fermilab's Robert Tschirhart. "If you have a common goal, you'll work it out."

Of course, most marriages begin with a wedding. And DUSEL scientists are hoping that it won't be too long until the science board responds to their proposal with "I do."

–ADRIAN CHO

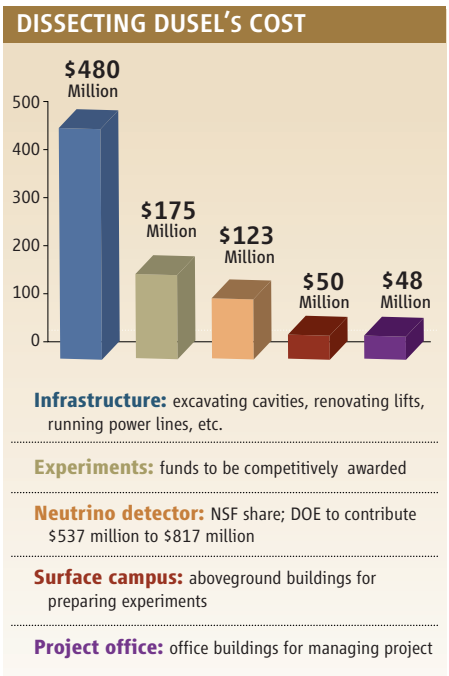

Price list. Funding for experiments, including a huge neutrino detector, accounts for 34% of DUSEL's cost.

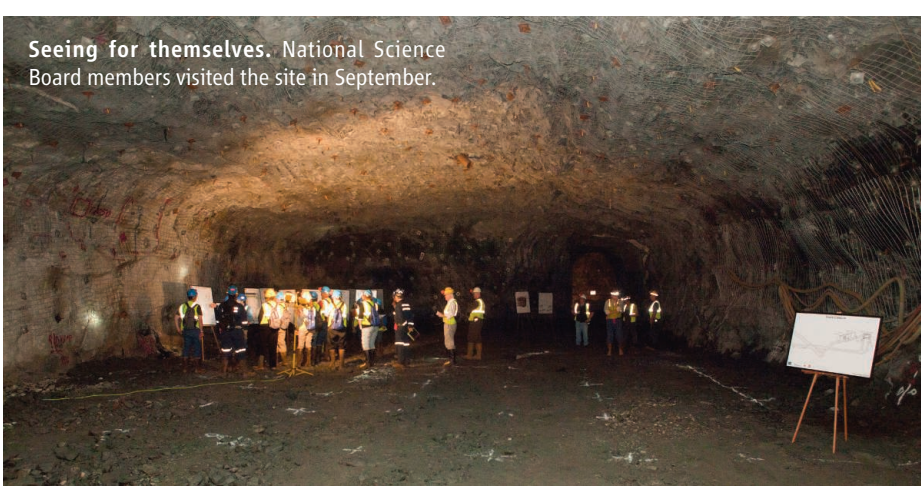

Seeing for themselves. National Science Board members visited the site in September.

CREDITS (TOP TO BOTTOM): KEVIN LESKO (SOURCE); BILL HARLAN/SANFORD UNDERGROUND LABORATORY

Downloaded from www.sciencemag.org on November 11, 2010

Published by AAAS

Barbarians at the gate. Alaric and his Visigoths sacked Rome in 410 C.E.

ARCHAEOLOGY

Collapse? What Collapse? Societal Change Revisited

Old notions about how societies fail are at odds with new data painting a more nuanced, complicated—and possibly hopeful—view of human adaptation to change

CAMBRIDGE, UNITED KINGDOM—At midnight on 24 August, 410 C.E., slaves quietly opened Rome's Salaria gate. The waiting Visigoths poured through the narrow passage, trumpets blaring and torches held high. The first sack of Rome in 8 centuries has often been cited as the moment when one of the world's largest, wealthiest, and most sophisticated empires died a violent death. For researchers struggling to understand how societies collapse, Rome's fall has served as a model and a touchstone.

And yet an eclectic group of scholars who met recently at the University of Cambridge* argues that true social collapse is actually rare. They say that new data demonstrate that classic examples of massive collapse such as the disintegration of Egypt's Old Kingdom, the end of the Classic Maya period, and the vanishing of pre-Columbian societies of the U.S. Southwest were neither sudden nor disastrous for all segments of their populations. "Collapses are perhaps more apparent than real," says Cambridge archaeologist Colin Renfrew.

Rome, for example, didn't fall in a day, as Edward Gibbon recognized in the 18th century in *The History of the Decline and Fall of the Roman Empire*. More recent work underscores the fact that the sack of Rome was just one step in a long and complex spiral of decline that affected peoples of the empire differently. For example, archaeologists in northeastern England have recently uncovered post-Roman villages that clung to the empire's ways while their neighbors swiftly abandoned the Latin language, Roman-style kitchenware, and construction practices.

Dry run. Yale's Harvey Weiss thinks climate has often spurred societal breakdowns.

"There's a bewildering diversity that is only magnified as the system falls apart," says Cambridge archaeologist Martin Millett.

This emphasis on decline and transformation rather than abrupt fall represents something of a backlash against a recent spate of claims that environmental disasters, both natural and humanmade, are the true culprits behind many ancient societal collapses. Yale University archaeologist Harvey Weiss, for example, fingered a regional drought as the reason behind the collapse of Mesopotamia's Akkadian empire in a 1993 *Science* paper. And in his 2005 book *Collapse: How Societies Choose to Fail or Succeed*, geographer Jared Diamond of the University of California, Los Angeles—who was invited to but did not attend the meeting—cites several examples of poor decision-making in fragile ecosystems that led to disaster.

Renfrew and others don't deny that disasters happen. But they say that a closer look demonstrates that complex societies are remarkably insulated from single-point failures, such as a devastating drought or disease, and show a marked resilience in coping with a host of challenges. Whereas previous studies of ancient societies typically relied on texts and ceramics, researchers can now draw on climate, linguistics, bone, and pollen data, along with better dating techniques. The result, they say, is a more nuanced understanding of the complicated and often slow-moving processes behind massive societal change. "The rarity of collapse due to the resistance of populations to environmental changes or disease is considerable," says Cambridge historian John Hatcher, who studies the Black Death; that plague ravaged medieval Europe and Asia yet did not overturn the existing social order.

The change remains the same

Societal collapse is a slippery concept that defies a strict definition. Renfrew contends that it involves the loss of central administration, disappearance of an elite, decline in settlements, and a loss of social and political complexity. Collapse implies an abrupt end rather than a long, slow devolution.

That description would seem to fit the demise of Egypt's Old Kingdom around 2200 B.C.E., after a 1000-year reign of pharaohs. As far back as the 1800s, research-

*Crisis, what Crisis? Collapses and Dark Ages in Comparative Perspective, The McDonald Institute for Archaeological Research, University of Cambridge, 24–26 September.

CREDITS (TOP TO BOTTOM): AKG-IMAGES/NEWSCOM; RICHARD H. MEADOW

Downloaded from www.sciencemag.org on November 11, 2010

Published by AAAS

ers found texts and archaeological evidence pointing to a nightmarish era of civil war, drought, famine, and anarchy. This collapse, which brought down the all-powerful kings who built the pyramids, long appeared to be a relatively sudden event that ushered in a century dubbed the First Intermediate Period. Earlier work suggested that a massive drought, the same one that may have laid the Akkadian Empire low, struck at this time and dropped the level of the Nile.

But the latest climate data from the northern Ethiopian highlands—a key source of the Nile—do not support a severe drought, says Richard Bates of the University of St. Andrews in the United Kingdom. "Likely, climate change was not as much of an impact as perhaps first thought," he says.

An increasing number of Egyptologists also now posit a more complicated and drawn-out decline—and one that ultimately had limited impact on the population. Miroslav Barta of Charles University in Prague notes that by the 25th century B.C.E., important changes in Egyptian society were already afoot. Smaller pyramids were built, nepotism within the royal families diminished, royal princesses married nonroyals, and the move from a centralized, pharaonic kingdom to a more regionalized structure was well under way. "The idea that this was sudden is nonsense," he says.

The changes were accelerated rather than caused by the drought, says Barta, citing details such as species of beetles in a 2300 B.C.E. tomb that thrive only in desert conditions. "There's a sense that the climate change was more gradual," agrees Mark Lehner, an Egyptologist based in Cambridge, Massachusetts, who works at Giza and sees drying as early as the 24th century B.C.E. "It is already happening earlier in the Old Kingdom."

For Barta, the 22nd century B.C.E. shift away from a single leader lacked the disruptive effect imagined by 19th century C.E. archaeologists and their 21st century descendants who are focused on a short and brutal drought. "There was no collapse," he insists. While the unified state disappeared and large monuments weren't built, copper continued to be imported from abroad and the concept of *maat* or kingship continued to be used at a more local level. "The peasants may never have noticed the change," he adds.

Not all scholars agree. Some hold fast to the idea of a more rapid climate-based change. "It's hard to eat when there is no food," says Weiss. But John Baines of the University of Oxford says Barta's view of a more gradual transition is "more or less a consensus these days." He adds that the changes that took place prior, during, and after the Old Kingdom's demise "were about redistribution of power and wealth more than about collapse."

Searching the jungle. UCL's Elizabeth Graham (*top*) sees continuity where others see collapse, as Mayan potters continued to make sophisticated wares (*above*) after the Classic period.

Kingdoms in the forest

Like the end of Egypt's Old Kingdom, the close of the classic Maya period around 900 C.E. has long been a poster child of collapse. Huge cities in the northern highlands were abandoned, monumental architecture ceased, and royal inscriptions halted. Foreign invasion, epidemics, social revolt, and the collapse of trade have been identified as key factors. Richardson Gill, a Texas businessman and archaeologist, argued a decade ago that the worst drought in 7000 years afflicted the Yucatán Peninsula between 800 C.E. and 1000 C.E., an idea with widespread support. Some researchers now favor a more nuanced version, in which environmental, political, and social changes combined to ravage the society.

But Elizabeth Graham, an archaeologist at University College London who works in the lowlands of Belize, says "there's not a blip" in the occupation of the Maya areas she has dug along the coast, which lie about 300 kilometers from major inland centers to the north. Graham is convinced that additional settled areas existed during and after the end of the Classic period but that archaeologists haven't found them yet, due to the uncertainties of preservation in the humid tropics and the difficulties of spotting low mounds in tropical forests.

Coastal sites like Lamanai and Tipu were admittedly smaller than the great inland cities, but Graham says there is no sign of crisis there at the end of the Classic period. Skeletons show no increase in dietary stress, populations seem constant, terraces and check dams are maintained, and sophisticated pottery continues to be crafted. The drying of the climate doesn't appear to trigger any societal rupture. Such new conclusions are "staggeringly important," says Norman Yoffee, an archaeologist at the University of Michigan, Ann Arbor, and co-editor of a 2010 book called *Questioning Collapse* that challenged many of Diamond's ideas.

Not everyone accepts that most of the Maya thrived at the end of the Classic Period, however. "It depends where you are standing," says Stephen Houston, an archaeologist at Brown University. He digs inland, in areas like northern Guatemala, where he says "there absolutely is a collapse." But he adds that "the image of people dying in the streets is a caricature of what was taking place; these cities just become not very attractive places to live," in large part because of the loss of an elite. "People voted with their feet." Houston suggests that the drought took place over a long period of time and that different parts of the Yucatán were affected differently. Even Diamond acknowledges in his writings that the Maya collapse was most intense in the highlands with its more fragile soils. Houston says that archaeologists must look more closely at how regional events may affect local areas in radically different ways.

CREDITS (TOP TO BOTTOM): KATARINA DOKTOR; LAMANAI PROJECT

Downloaded from www.sciencemag.org on November 11, 2010

Published by AAAS

Rising from the ashes?

Ancient ruins and canals prompted the founders of Arizona's future capital to name their city after the mythological sacred bird that is reborn in its own ashes every 500 years. Five centuries prior, the Hohokam had lived in the Phoenix basin, creating a complex society from 750 C.E. to 1450 C.E. with vast irrigation systems, ball courts, plazas, platform mounds, and polychrome pottery. Then the population vanished, the canals were forgotten, and even outlying areas were abandoned. The abandonment appears total.

Archaeologists have long blamed a sudden onslaught of flooding that destroyed the canals and suggested that field salinization and overpopulation contributed; some see European diseases, arriving after 1500 C.E., as the ultimate culprit. But archaeologist Randall McGuire of Binghamton University in New York state argues that the data don't support any of these theories.

He says that the lack of remains after 1450 C.E. make the disease idea untenable and that there is no evidence for the destruction of the life-giving canals. Drawing on data from the Center for Desert Archaeology in Tucson, Arizona, he instead links the Hohokam's disappearance with broader changes across the Southwest between 1250 C.E. and 1450 C.E., when the population shrank by as much as 75%. "This is not a catastrophic event but a slow process over 150 years or more," he says. "Were [the Hohokam] even aware that this was a 'collapse'?"

The data show clusters of populations gradually vanishing or migrating during the 2-century period; one cluster in northern New Mexico, by contrast, gradually increases. McGuire suggests that Southwest pueblo structures based on rival clans that kept each other in check survived, while the Hohokam, who increasingly favored a more rigid hierarchical system, eventually failed. So although a drying climate no doubt played a role in the dissolution of societies and the migration of peoples, McGuire believes that a complex combination of religious movements and elite interactions were also important factors and that they took place over a much longer period than previously imagined.

Paul Fish, an archaeologist at Arizona State University, Tempe, says that McGuire "is certainly correct in that no simple environmental, economic, or social explanation is satisfactory." But he notes that the final years of the Hohokam remain the least understood phase. "I don't believe we have the dating evidence to know how rapid the decline actually was," he adds.

Such appeals to "complex factors" have their critics. Weiss, for example, insists that "mushy 1960s multicausality collapses" in the face of hard "21st century paleoclimate data" that definitively pinpoint serious droughts. But other researchers argue that scientists have been too quick to overlook sociological explanations and turned to environmental change "as the snappy explanation" for collapse, as Poul Holm, a historian at Trinity College Dublin, puts it.

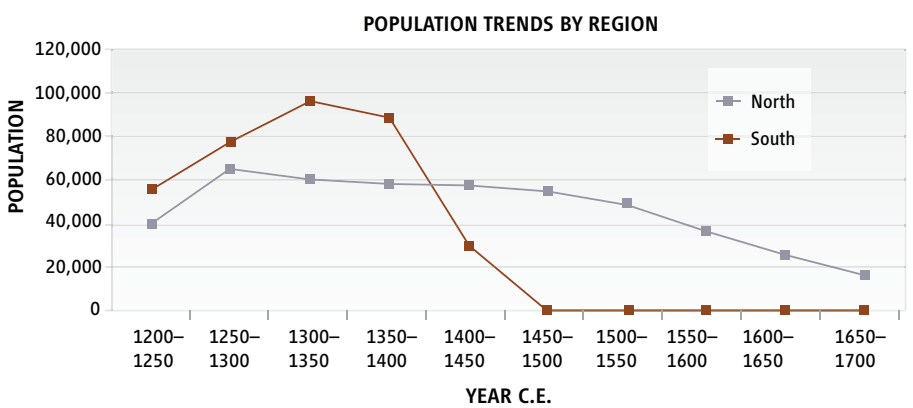

Dwindling. In their heyday, the Hohokam had impressive platforms just outside Phoenix (*top*). But population estimates from archaeological sites show a gradual dropoff in people living in the southern part of the U.S. Southwest (*above in red*), including in the Phoenix area, while the population in the north (*in black*) was more stable.

Holm decries what he sees as an industry of apocalypse that pervades religion, academia, and even Hollywood, with its blockbusters like *2012*. He argues that societies under stress have actually shown surprising resilience in overcoming crises. An old way of life may quietly continue in a revamped but world-changing form, such as the way some Imperial Roman traditions survive today in the Roman Catholic Church.

Unlike the dangers faced by many past societies, however, today's big threats—global climate change, war, peak oil, economic dislocation—are nearly all due to human choice rather than natural causes. Like Diamond, Holm sees awareness of our predicament as the key to not repeating past mistakes. "At the end of the day, trying to understand how humans cope with change is about how we think," he says. Immediate threats to individual as well as societal existence may be what humans require to change outdated thinking. We may, after all, need those barbarians at the gate.

–ANDREW LAWLER

PHOTO CREDIT: ADRIEL HEISEY

Downloaded from www.sciencemag.org on November 11, 2010

Published by AAAS

Back from the dead. Once fishless, Brooktrout Lake in the Adirondacks is rebounding from acid rain damage and has become an important study site for regional researchers.

AIR POLLUTION

Taking the Sting Out of Acid Rain

As a landmark U.S. law turns 20, success marks the acid rain control program, but the cap-and-trade market it created is in turmoil

The water in Brooktrout Lake is getting a bit murky these days. Two decades ago, visitors could see up to 16 meters down, clear to the bottom of this remote lake nestled high in the Adirondack Mountains of New York state. Today, visibility is often just 5 meters.

The cloudy water might be cause for concern in many places. But in the Adirondacks, it has sparked a cautious celebration. "The reduced visibility means there is more algae and plankton in the water—and that means life in Brooktrout Lake is starting to recover from acid rain," says biologist Clifford Siegfried of the New York State Museum in Albany, who has been studying the lake for more than 25 years. "It is a really encouraging sign." So encouraging, in fact, that some 35 years after the lake became too acidic to support fish, biologists have been able to restock it with—what else?—colorful, darting brook trout.

That feel-good fish story is making Brooktrout Lake something of an icon for a landmark air pollution control law that celebrates its 20th anniversary next week. On 15 November 1990, after a bruising, 13-year-long legislative battle, President George H. W. Bush signed a sweeping set of changes to the U.S. Clean Air Act designed to take the sting out of acid rain. Most notably, the amendments called for using a controversial new "cap-and-trade" system to slash sulfur emissions from coal-fired power plants. The acidic plumes were transforming Brooktrout Lake—and hundreds of other lakes, ponds, and streams in the eastern United States—into eerily clear, seemingly sterilized ecosystems. Skeptics from both industry and environmental groups attacked the emissions trading scheme, predicting it would be too expensive, too ineffective—or both.

How times have changed. The 1990 Clean Air Act Amendments are now widely hailed as a "win-win-win" for the environment, consumers, and industry. Cap-and-trade has helped cut sulfur pollution faster and at lower cost than many predicted and become a widely emulated model for dealing with other pollutants. The amount of acidic sulfur returning to Earth, meanwhile, has dropped by roughly 50% across the eastern United States. Many fishless lakes and streams, once written off as dead, are showing signs of renewed life.

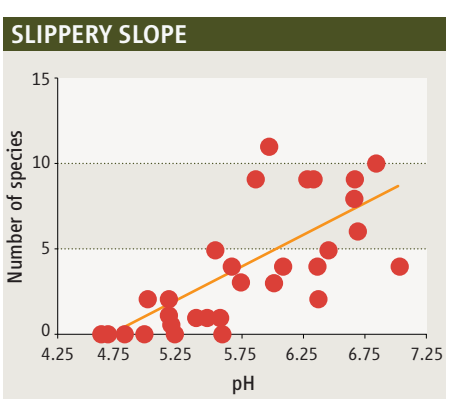

Crystal clear. Scientists studying 30 Adirondack lakes have found that more acidic waters mean less biodiversity: A one-point drop in pH can mean four fewer fish species.

Even as many prepare to toast the success of the 1990 law, however, the U.S. acid rain program is facing turmoil and uncertainty. Its once high-flying emissions-trading market has collapsed in the wake of a complex court ruling, legislative gridlock—and its own success. Industry analysts say the collapse could create a perverse incentive for utilities to ease up, at least temporarily, on cutting emissions while the government works on new rules. Researchers, meanwhile, warn that the problem isn't going away. Acid deposition continues to threaten many sensitive ecosystems, and analysts say deeper emissions cuts are needed to prevent future pollution from undoing the gains of the past 20 years. "We're at a point where we need to reevaluate how far we've come and where we need to go," says microbial ecologist Sandra Nierzwicki-Bauer of the Darrin Fresh Water Institute in Bolton Landing, New York, part of the Rensselaer Polytechnic Institute (RPI) in Troy, New York.

Ghost lakes

Today's turning point has its origins in the plight of places like Brooktrout Lake. Once a flourishing fishery, the last documented catch came in 1975. By 1984, when Siegfried first visited, Brooktrout had become one of more than 350 Adirondack lakes that had become highly acidified (a pH of about 5.5 or less) and no longer sustained fish. Soon, major media were featuring dramatic stories on these "ghost lakes," with *Sports Illustrated* declaring acid rain "a chemical leprosy … eating away at the face of the U.S." In a slew of technical papers, researchers pointed the finger at what they said was one obvious cause: a fleet of power plants in the Upper Midwest that burned massive piles of high-sulfur coal and then sent sulfur dioxide emissions wafting east on prevailing winds. "What goes up must come down," Gene Likens, a prominent ecologist at the Cary Institute of Ecosystem Studies in Millbrook, New York, told one Washington audience at the time. Likens was on the team that first documented acid rain in

CREDITS (TOP TO BOTTOM): ADAPTED FROM S. NIERZWICKI-BAUER *ET AL.*, *ENVIRONMENTAL SCIENCE AND TECHNOLOGY* (2010); CHUCK BOYLEN/DARRIN FRESH WATER INSTITUTE

Downloaded from www.sciencemag.org on November 11, 2010

Published by AAAS

the United States in the 1960s.

Neither the science nor the aphorisms, however, persuaded President Ronald Reagan and congressional leaders to act. By one scholar's count, they killed at least 50 legislative proposals to cut sulfur emissions between the late 1970s and 1988. George H. W. Bush's campaign pledge to be "the environmental president," however, opened the door to regulation. The final 1990 deal called for using flexible, free-market mechanisms to cut sulfur emissions by nearly 50% from 1980 levels by 2010. Under the plan, the government set a declining annual "cap" on emissions that included specific goals for several hundred power plants. Companies could choose the best—and cheapest—way to meet those targets, including installing new smokestack "scrubbers," shifting to lower-sulfur coal, or buying "allowances" to pollute from other companies that had met their targets.

Despite some early bumps, the system flourished. Millions of allowances traded hands, and compliance costs, which some estimated might be as high as $25 billion annually, proved to be just a few billion dollars a year. By 2009, sulfur emissions had dropped to 5.7 million tons, well below the mandated cap of 8.95 million tons and down 67% from 1980 levels. The deposition of sulfate across the eastern United States fell by about 50%, and lakes and rivers showed an increasing ability to neutralize, or "buffer," acidic precipitation.

Assessing improvements

The 1990 law also established a research program to document how life in Adirondack lakes and rivers was responding to the chemical shift. "It was pretty novel at the time to build science right into the legislation," says RPI limnologist Chuck Boylen. Starting in 1994, Boylen helped guide the Adirondack Effects Assessment Program (AEAP), a multi-institution effort funded by the U.S. Environmental Protection Agency (EPA) and New York state. For 13 years, it sent scientists out to collect data from about 30 lakes. Although federal funding for AEAP has dried up, the state recently funded more monitoring of 17 lakes, and researchers are still producing papers.

They reveal the often complex—and sometimes surprising—ways that acid rain has reshuffled aquatic food webs in sensitive waters. One trend is crystal clear, a team led by Nierzwicki-Bauer reported this past July in *Environmental Science & Technology*: More acid meant less biodiversity. The researchers came up with a grim rule of thumb: For every one-digit drop in pH (from 6 to 5, for instance, which represents a 10-fold increase in acidity), there were 2.5 fewer genera of bacteria, 1.43 fewer bacterial classes, and 3.97 fewer species of phytoplankton. A one-digit drop in pH also meant nearly two fewer crustacean species and about four fewer species of aquatic plants, rotifers, and fish. "Lots of studies had examined acid rain's impact at a chemical level," says Nierzwicki-Bauer. "We tried to quantify how it changes the biota."

One thing researchers learned is that acidity isn't necessarily destiny for a lake bacterium. A study of 18 lakes showed that, although acidification favored species able to survive in low-pH waters, these "acidophiles" didn't always take over the base of the food pyramid. Instead, apparently more generalist species were often more numerous, perhaps because factors such as water depth also play an important role in shaping bacterial communities. That AEAP study appeared in the March 2008 issue of *Applied and Environmental Microbiology*.

A LIGHTER BURDEN

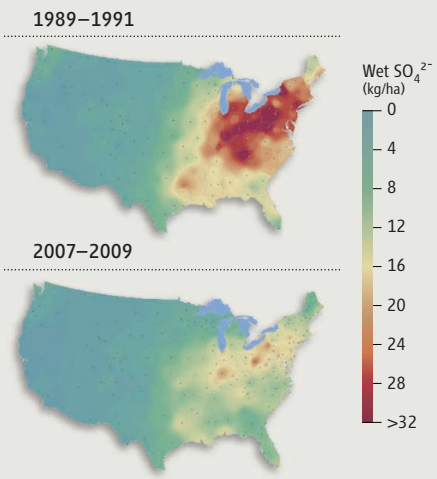

Acid test. Controls on sulfur emissions enacted in 1990 have produced a 43% drop in "wet" sulfate deposition, a key contributor to acid rain.

CREDIT: ADAPTED FROM EPA

Celebration and concern

Overall, long-term monitoring has shown that many acidified Adirondack lakes are "now on the trajectory to recovery," says Nierzwicki-Bauer, with Brooktrout Lake a prime example. Its pH, perhaps once as low as 4.6, has risen to nearly 6. By 2005, "you could really see things were starting to happen biologically," says Siegfried. "Zooplankton was increasing, larger invertebrates were coming back." In late 2005, biologist James Sutherland of the New York Department of Environmental Conservation decided the lake was healthy enough to reintroduce trout—not for anglers, but for the scientists. "The hypothesis that's being tested is that fish are essential to recovery" of the ecosystem, says Boylen. "It's one big experiment." Since then, state and academic researchers have regularly taken the 10-kilometer hike, or short helicopter ride, from the nearest road to the lake to check on how the ecosystem is changing. "I'm surprised at just how well those fish are doing," Siegfried says. "It's really a cause for celebration."

But "it's not clear that all the lakes are going to recover like Brooktrout Lake," he adds. At least 10% of the region's lakes do not have improving pH trends, according to EPA data, and about 40% aren't showing an increased capacity to resist acidification. In part, that's because acid deposition continues to leach buffering minerals from surrounding soils and affect vegetation. And water-quality improvements have slowed in the past decade, according to state studies, partly due to the complex role played by other pollutants, such as nitrogen oxides. The bottom line, concluded one recent state study, is that "unless air pollution emissions are further reduced, this recovery will likely be followed by a lengthy period of renewed acidification of lakes that were recently recovering."

Ironically, efforts to achieve those deeper cuts may end up gutting the cap-and-trade system that has become the hallmark of the 1990 law. In 2005, the second Bush Administration approved a plan known as the Clean Air Interstate Rule (CAIR) for a new round of emissions reductions. One result was that the cost of sulfur allowances more than doubled to nearly $1600 a ton, as utilities braced for expensive new controls. But now spot prices have plunged to just $5 a ton, in large part because of a 2008 court ruling that invalidated CAIR and sent it back to EPA and Congress for retooling. Last July, EPA responded with a new plan that relies less on cap-and-trade. The chaos has "essentially killed an acid rain market that was working just fine, thanks," one anonymous emissions trader noted on an online discussion board. Others have speculated that the crash could lead some utilities to turn off expensive sulfur scrubbing equipment and buy cheap allowances instead, until the new rules take effect in 2012.

So far, experts say that isn't happening. And whatever happens, Adirondack researchers hope policymakers will pay attention to what they've learned about acid rain from places like Brooktrout Lake. "Good policy has to be driven by good science," says Nierzwicki-Bauer. And in this case, the science offers cause for both hope and concern. **–DAVID MALAKOFF**

David Malakoff is a writer in Alexandria, Virginia.

Downloaded from www.sciencemag.org on November 11, 2010

Published by AAAS

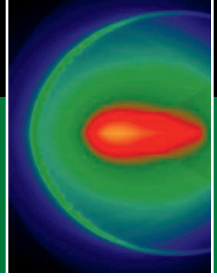

Lights on early stars
914

Amyloid transmission
918

LETTERS

edited by Jennifer Sills

Retraction

THE RESEARCH ARTICLE "REACTOME ARRAY: FORGING A LINK BETWEEN METABOLOME AND genome" (*1*) described the synthesis of some 2000 quenched fluorescent dye-metabolite compounds, and their use to create an array to obtain a global overview of the metabolic network operating in a population of cells at the time of sampling. Upon productive interaction with an enzyme in a sample, an array compound releases the dye, which fluoresces and its signal is captured. To our profound regret, peer inspection of the paper after publication revealed errors and omissions in the information provided on the chemistry underlying array compound synthesis, and the processing of array data obtained. After an investigation, the Ethics Committee of the CSIC in Madrid has recommended the withdrawal of the paper. Given the errors in the paper, and the skepticism about the array that they have generated, we retract the paper. We apologize to *Science*, our institutions, and the scientific community for any inconvenience caused by our paper and its retraction.

ANA BELOQUI,[1] MARÍA EUGENIA GUAZZARONI,[1] FLORENCIO PAZOS,[2] JOSÉ M. VIEITES,[1] MARTA GODOY,[2] OLGA V. GOLYSHINA,[3] TATYANA N. CHERNIKOVA,[3] AGNES WALICZEK,[3] RAFAEL SILVA-ROCHA,[2] YAMAL AL-RAMAHI,[1] VIOLETTA LA CONO,[4] CARMEN MENDEZ,[5] JOSÉ A. SALAS,[5] ROBERTO SOLANO,[2] MICHAIL M. YAKIMOV,[4] KENNETH N. TIMMIS,[3,6] PETER N. GOLYSHIN,[3,7,8] MANUEL FERRER[1]*

[1]CSIC, Institute of Catalysis, 28049 Madrid, Spain. [2]CSIC, Centro Nacional de Biotecnología, 28049 Madrid, Spain. [3]HZIHelmholtz Centre for Infection Research, 38124 Braunschweig, Germany. [4]Institute for Coastal Marine Environment, CNR, Messina 98122, Italy. [5]Universidad de Oviedo, 33006 Oviedo, Spain. [6]Institute of Microbiology, Carolo-Wilhelmina Technical University of Braunschweig, 38106 Braunschweig, Germany. [7]School of Biological Sciences, Bangor University, Gwynedd LL572 UW, UK. [8]Centre for Integrated Research in the Rural Environment, Aberystwyth University–Bangor University Partnership (CIRRE).

*To whom correspondence should be addressed. E-mail: mferrer@icp.csic.es

Reference

1. A. Beloqui *et al.*, *Science* **326**, 252 (2009).

Editorial Expression of Concern

RESEARCHERS INVOLVED IN GENOME-WIDE association studies have expressed technical concerns about a Report by P. Sebastiani *et al*., "Genetic signatures of exceptional longevity in humans," published in *Science* Express on 1 July 2010. In their study (*1*), Sebastiani *et al*. used a number of different genotyping platforms and neglected to perform data quality-control steps, which resulted in their reporting several false-positive single-nucleotide polymorphism (SNP) associations. In particular, one of the platforms used in their work, the Illumina 610-Quad array, has been shown in unpublished studies by other investigators to produce artifactual genotype data at a subset of SNPs.

Science and the authors are taking these concerns seriously. Since learning of these potential problems, Sebastiani *et al*. have been performing a thorough quality-control analysis on the original raw data, as well as generating new data to compare the genotype calls from the 610-Quad array and the other platforms within the same individuals. These steps aim to eliminate biases between platforms. Furthermore, they are undertaking an additional validation measure on several SNPs via the TaqMan® assay, a non–microarray-based genotyping method. After ensuring that all data are clean, they will redo the statistical and modeling analyses, which they expect to be completed in December. At that point, *Science* will reevaluate the paper, determine the extent to which the strength of its original conclusions has been altered by the revised data, and take the appropriate action.

BRUCE ALBERTS

Editor-in-Chief

Reference

1. P. Sebastiani *et al*., *Science* 10.1126/science.1190532 (2010).

Training Physicians to Communicate

BASIC SCIENCE TRAINING IS CERTAINLY CRUcial for future physicians ("Science for physicians," M. Cooke, Editorial, 24 September, p. 1573). Effective patient care requires physicians to keep pace with change in the natural sciences. However, clinical practice also requires the recognition that social sciences are equally important. Incorporating good social science involves more than establishing health values (*1*) and economics, and acknowledging diversity. Rather, physicians must understand patient autonomy and be sensitive to each patient's unique preferences and experience (*2*, *3*). Excessive focus on natural science education, including the technologies underlying "personalized" genetic medicine, could further dehumanize care. In the past decade, treatments have improved spectacularly in all oncology subdisciplines, yet patient concerns, distress, and satisfaction ratings have remained unchanged (*4*). Understanding the relevant natural science does not necessarily translate into a physician's ability to communicate with patients, nor does it guarantee informed consent. The most basic education for a physician is learning to develop a helpful and caring relationship with every patient.

GLENN W. JONES

Department of Radiation Oncology, Credit Valley Hospital, McMaster University, Mississauga, ON L5M 2N1, Canada. E-mail: gjones@cvh.on.ca

Downloaded from www.sciencemag.org on November 11, 2010

Published by AAAS

Trojan horse or fertility goddess?
922

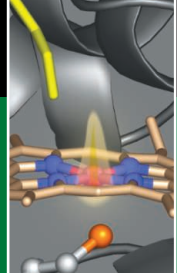

Examining enzymatic oxidations
924

References

1. M. G. M. Hunink *et al.*, *Decision-Making in Health and Medicine—Integrating Evidence and Values* (Cambridge Univ. Press, Cambridge, 2001).
2. G. W. Jones, in *Questions of Right and Wrong*, E. C. Hui, Ed. (Regent College, Vancouver, 1994), pp. 140–155.
3. D. L. Sackett, W. M. C. Rosenberg, J. A. M. Gray, R. B. Haynes, W. S. Richarson, *Br. Med. J.* **312**, 71 (1996).
4. Cancer Quality Council of Ontario, Patient Experience (http://csqi.cancercare.on.ca/dimensions/responsive/pat_exp/).

Birds of Prey Remain at Risk

E. KINTISCH'S NEWS STORY "OUT OF SITE" (special section on Scaling Up Alternative Energy, 13 August, p. 788) discusses the bird-of-prey deaths (including golden eagles) caused by wind turbines. The story implies that the problem at the Altamont Pass Wind Resource Area (APWRA) in California has been reduced by spacing turbines farther apart and removing turbines from problematic sites. These statements are misleading.

In fact, numerous mitigation measures recommended by the Scientific Review Committee as part of the Alameda County Avian Wildlife Protection Program were either never implemented or implemented in a piecemeal manner (*1*). Neither total avian fatality rates nor fatality rates of focal raptors (golden eagle, red-tailed hawk, American kestrel, and burrowing owl) at the APWRA have decreased when compared with the periods 1998 to 2002 and 2005 to 2009. Some fatality rates may have actually increased between the comparison periods (*2*). For the period from 2005 to 2007, an estimated 65 golden eagles were killed annually at the APWRA (*3*). Given that little has been done to implement substantial mitigation measures, such high fatality rates for golden eagles, as for other species, will likely continue.

To reduce bird deaths in the APWRA, we must either (i) abandon the site altogether for wind energy production or (ii) replace existing infrastructure with fewer, larger wind turbines, and choose their locations by using map-based technologies that incorporate mortality studies and species-specific avian flight behavior (*4*) or avian land-use patterns (*5*). Even then, no single siting plan can take into account the patterns of all avian species. What works for birds might not work for bats.

DOUGLAS A. BELL[1]* AND K. SHAWN SMALLWOOD[2]

[1]Wildlife Department, East Bay Regional Park District, Oakland, CA 94605, USA. [2]Davis, CA 95616, USA.

*To whom correspondence should be addressed. E-mail: dbell@ebparks.org

References

1. K. S. Smallwood, *Environ. Energy Law Pol. J.* **2**, 229 (2008).
2. K. S. Smallwood, "Fatality rates in the Altamont Pass Wind Resource Area 1998-2009" (Altamont Scientific Review Committee Report P145, 2010); www.altamontsrc.org/alt_doc/p145_smallwood_fatality_monitoring_results_12_31_09.pdf.
3. K. S. Smallwood, B. Karas, *J. Wildlife Manage.* **73**, 1062 (2009).
4. K. S. Smallwood, L. Neher, "Siting repowered wind turbines to minimize raptor collisions at the Tres Vaqueros Wind Project, Contra Costa County, California" (Altamont Scientific Review Committee Report P162, 2010); www.altamontsrc.org/alt_doc/p162_smallwood_and_neher_tres_vaqueros_repowering_siting.pdf.
5. K. S. Smallwood, L. Neher, D. A. Bell, *Energies* **2**, 915 (2009).

CREDIT: TIM MESSICK/ISTOCKPHOTO.COM

Mentors for Elementary School Teachers

IN HIS NEWS OF THE WEEK STORY "A WAY to heal science education, but is there the political will?" (24 September, p. 1582), J. Mervis quotes from the President's Council of Advisors on Science and Technology (PCAST) report, stating that "too many American students conclude early in their education that STEM [science, technology, engineering, and math] subjects are boring, too difficult, or unwelcoming, leaving them ill-prepared to meet the challenges that will face their generation, their country, and the world" (*1*). The PCAST report proposes some solutions but overlooks one possibility.

The answer lies in elementary school, where children form their first opinions about STEM. How can they develop a passion for STEM when many elementary school teachers themselves hate or fear these subjects?

I propose that all elementary school teachers be provided with real-world STEM research experiences from scientist mentors. One case study showed that after a 6-week research experience, elementary school teacher attitudes changed from "my students will not become scientists" to "my students are scientists" (*2*). Quality research experiences for elementary school teachers will help solve the national crisis cited in the PCAST report (*1*).

STEVEN B. OPPENHEIMER

Center for Cancer and Developmental Biology, California State University Northridge, Northridge, CA 91330–8303, USA. E-mail: steven.oppenheimer@csun.edu

References

1. President's Council of Advisors on Science and Technology, "Prepare and inspire: K-12 education in science, technology, engineering, and math (STEM) for America's future" (PCAST, 2010); www.whitehouse.gov/sites/default/files/microsites/ostp/pcast-stemed-report.pdf.
2. P. Dixon, R. A. Wilke, *J. Elem. Sci. Educ.* **19**, 25 (2007).

CORRECTIONS AND CLARIFICATIONS

Policy Forum: "Remeasuring aging" by W. C. Sanderson and S. Scherbov (10 September, p. 1287). At the start of the second paragraph on the second page, the year was incorrect. The text should read as follows: "In our forecasts for the United States, in 2023, the number of expected years of disability above age 65 is 4.1."

Reports: "Females use multiple mating and genetically loaded sperm competition to target compatible genes" by S. R. Pryke *et al.* (20 August, p. 964). The legend for Fig. 1C was incorrect. It should read "eight of nine broods contained extra-pair offspring when the social male was incompatible and the extra-pair male was compatible."

Perspectives: "An outlook on microalgal biofuels" by R. H. Wijffels and M. J. Barbosa (13 August, p. 796). The text attributed the following parameter to C. de Fraiture, M. Giordano, Y. Liao, *Water Pol.* **10** (suppl. 1), 67 (2008): "For the production of 1 liter of biofuel from fuel crops, approximately 10,000 liters of water are needed." In fact, the de Fraiture paper states: "It takes on average roughly 2,500 l[iters] of crop evapotranspiration and 820 l[iters] of irrigation water withdrawn to produce one liter of biofuel. But regional variation is large."

Letters to the Editor

Letters (~300 words) discuss material published in *Science* in the previous 3 months or issues of general interest. They can be submitted through the Web (www.submit2science.org) or by regular mail (1200 New York Ave., NW, Washington, DC 20005, USA). Letters are not acknowledged upon receipt, nor are authors generally consulted before publication. Whether published in full or in part, letters are subject to editing for clarity and space.

Downloaded from www.sciencemag.org on November 11, 2010

Published by AAAS

ASTRONOMY

Stars in the Beginning

Jonathan C. Tan

Abraham Loeb has a warning for those seeking a career in theoretical cosmology: If you devote yourself to trying to understand the global properties of the universe and its underlying physics, you risk becoming obsolete once data are so precise that further refinement is pointless. And if you study the complex processes by which stars, galaxies, and black holes form from cosmological initial conditions, you are likely to spend an entire career without ever reaching an elegant resolution of the problem. You may, however, decide to ignore these risks after being taken to the common frontiers of cosmology and astrophysics in the engaging, fast-paced *How Did the First Stars and Galaxies Form?* Loeb's infectious excitement stirs desire to join him in these endeavors.

The first stars were the result of an unavoidable meeting between the simplicity of cosmology and the complexity of astrophysics. Their initial conditions are thought to be tiny overdensities of matter laid down in the inflationary epoch moments after the Big Bang. After a few hundred thousand years, the fluctuations were still miniscule (just one part in a hundred thousand), as revealed in the cosmic microwave background. That crucial observation sets a firm foundation for theoretical models of the subsequent growth of structure via gravitational instability. Growing clumps of cold dark matter collapsed, later trapping cooling baryonic matter (mostly hydrogen and helium) in their deepening potential wells. The baryons themselves became gravitationally unstable, concentrating to higher and higher densities, pressures, and temperatures that eventually (about 100 million years after the Big Bang) allowed nuclear fusion of hydrogen to provide energy and pressure to halt the collapse. These first stars then illuminated, reionized, and spread heavy elements through the universe. They may have evolved into—or at least set the conditions for the formation of—the first black holes. They were the opening act for the formation and evolution of all complex structures, a cosmic saga of galaxies, stars, planets, and (ultimately) life. Although attractive, this scenario, based on theoretical and numerical studies of structure formation, remains difficult to test observationally because the first stars are, literally, near the edge of the observable universe.

How Did the First Stars and Galaxies Form?

by Abraham Loeb

Princeton University Press, Princeton, NJ, 2010. 209 pp. $75, £52. ISBN 9780691145150. Paper, $24.95, £16.95. ISBN 9780691145167. Frontiers in Physics.

Loeb (Harvard University) tells this tale from the perspective of a theoretical cosmologist who has made important contributions to our understanding of all these stages. Writing at a level suitable for advanced undergraduates, he introduces the concepts required to understand our modern view of cosmology. He focuses on structure formation and predictions of the frequency and mass of collapsed dark matter halos, the nurseries of the earliest stars and galaxies. Loeb develops this formalism to predict observational signatures of cosmic reionization, given assumptions about how these halos are populated with ionizing sources, such as stars and accreting black holes.

As the author points out, the actual process of star formation and its outcome involve large degrees of uncertainty. He describes the results from numerical simulations that have followed collapse to near stellar densities. However, these are still a long way from, for example, predicting the mass of the first stars, which is so critical to their detectability and their influence on subsequent galaxy evolution.

Loeb presents a scenario to explain how supermassive black holes (millions to billions of times the mass of the Sun), which are seen in the centers of most nearby galaxies, could have formed in the environments of the first stars and galaxies. A few examples of these black holes have been seen as quasars in the early (less-than-one-billion-year-old) universe, which likely requires initial seed masses to be much greater than the circa 100 solar masses expected of the earliest stars. Loeb suggests that such massive seeds could have formed in halos that only experience cooling by atomic processes, which would likely require an intense surrounding ultraviolet radiation field to destroy H_2 molecules. However, some have argued that such strong radiation fields can, if they generate ionization fronts that compress gas to high densities, promote molecule formation (*1*). The astrophysical complexities associated with the interplay among radiation, hydrodynamics, astrochemistry, gravity, and potentially even dark matter annihilation (*2*) are such that the mechanism of supermassive black hole formation and its relation to the earliest stars remain quite uncertain. Perhaps these great uncertainties motivated Loeb's apt choice of cover illustration (a large question mark).

The very first stars and galaxies are impossible to observe directly with current astronomical telescopes. Indeed, their detection is one of the main drivers of the next generation of facilities, including the James Webb Space Telescope, large (about 30-m-diameter) ground-based telescopes, the Atacama Large Millimeter Array, and low-frequency radio telescopes that hope to trace the cosmic web of atomic hydrogen before and after reionization. Loeb gives an excellent summary of the prospects of the last of these: although challenging,

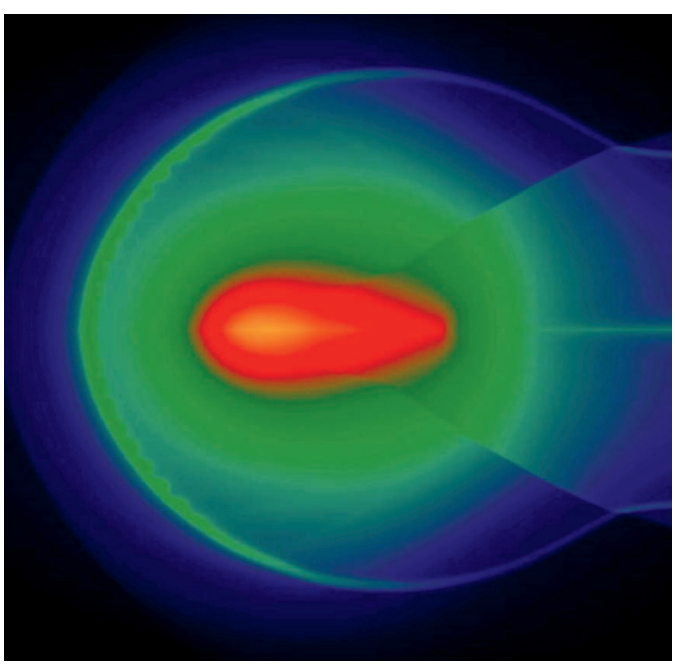

Shock start. Density of primordial hydrogen and helium gas in a dark matter halo being impacted by ionizing radiation from the left, which drives shocks, generates instabilities, and may trigger star formation [from simulations of (*1*)].

CREDIT: COURTESY DAN WHALEN

The reviewer is at the Department of Astronomy, Post Office Box 112055, University of Florida, Gainesville, FL 32611, USA. E-mail: jt@astro.ufl.edu

Downloaded from www.sciencemag.org on November 11, 2010

Published by AAAS

this technique has the potential to give us the most detailed view of the initial conditions of our universe. It will also tell us when and how early galaxies reionized the universe.

Perhaps inevitably, some current topics in this fast-moving research field receive only limited coverage. Whereas Loeb describes the detectability of the direct radiation from early sources, he omits mention of the integrated background light from these sources and the statistics of its fluctuations. There have been a number of claims of detections of these effects, including a recent study with the AKARI satellite (*3*). Some astronomers hope to find nucleosynthetic fingerprints of the first supernovae from the abundance patterns of elements dusted in the atmospheres of old, very metal poor galactic stars (*4*), and this complementary approach of cosmic archaeology deserves more discussion. Despite such omissions, readers will find *How Did the First Stars and Galaxies Form*? a lucid introduction to an exciting research field that is set to flourish in the next decades.

References

1. D. Whalen *et al., Astrophys. J.* **679**, 925 (2008).
2. D. Spolyar *et al., Phys. Rev. Lett.* **100**, 051101 (2008).
3. T. Matsumoto *et al.,* http://arxiv.org/abs/1010.0491v1 (2010).
4. T. C. Beers, N. Christlieb, *Annu. Rev. Astron. Astrophys.* **43**, 531 (2005).

10.1126/science.1197651

SCIENCE AND THE LAW

Power and Pitfalls of DNA Profiling

Carole McCartney

Despite the first use of DNA profiling in a criminal investigation back in 1985, until very recently a search of any respectable library catalog for books on forensic DNA would have returned the unsatisfactory "no matching results." Fast-forward to 2010, and there are now, *inter alia*, scientific texts on forensic genetic testing, historical treatments, sociological and sociolegal examinations, and guides for scientifically illiterate lawyers. In *The Double Helix and the Law of Evidence*, David Kaye considers all of these angles. He describes the book as "part history, part legal analysis, part popular science, and part applied statistics."

The Double Helix and the Law of Evidence
by David H. Kaye
Harvard University Press, Cambridge, MA, 2010. 348 pp. $45, £33.95, €40.50. ISBN 9780674035881.

The author intends the book to be the first of a pair on forensic DNA profiling. Nevertheless, this first text is itself quite comprehensive. Kaye (a law professor at Pennsylvania State University) begins his account in "pre-DNA" times, with a detailed discussion of the use of genetic markers (popularly known as blood grouping). After exploring early forensic uses of DNA data, he takes the reader diligently through the "DNA wars" to arrive at current developments and scientific advances. Along the way, Kaye chronicles the "scientific egos, journalistic hype, lawyerly maneuvering, and judicial doctrine and disposition," ensuring that the reader is never left for long in the depths of scientific or statistical exposition. The scope of Kaye's analysis, his insightful and meticulous eye for detail, the coverage of both law and science (not forgetting the math), and the spicing with human tales of crimes and academic rivalries combine to ensure the book will interest a medley of readers.

As Kaye points out in his introduction, the power of DNA technology is now beyond dispute. However, media portrayals of this power are often inaccurate, while those professionals tasked with employing the technology may not possess a competent understanding of its actual strengths and limitations. The book could go a long way toward correcting these failures, were it to become essential reading for reporters, criminal investigators, legal professionals, and, ultimately, the public—who are most often characterized as demanding the increased use of DNA evidence by law enforcement. Further, Kaye's account may help forensic scientists who do not work with DNA to better understand the trials and tribulations that were weathered by forensic DNA profiling on the "far from smooth" road to legal acceptance. With DNA hailed as the gold standard of forensic science, Kaye presents a lesson that bears learning by those disciplines or techniques currently struggling to sustain their integrity as a science and gain, or maintain, legal acceptance. DNA profiling did not become the gold standard overnight, and even gold can be tarnished if mistreated or mishandled.

Forensic DNA profiling offers a perhaps perfect example of a scientific technology that has captured the public imagination. Its value in criminal investigations can scarcely be overplayed, and its use in exonerating the innocent will continue to have far wider consequences than the (albeit vital) freeing of the innocent—leading to improvements across the criminal justice process. Its enthusiastic embracement by filmmakers and television producers needs no rehearsal here or by Kaye, who steers clear of indulging in the hype that has surrounded DNA profiling. He does, however, defend it as a profoundly valuable tool for investigators, if used with diligence: "industrial-strength quality control is not too much to demand." Yet in order to benefit from the power of DNA, the criminal justice system must be able to harness it.

Throughout the book, Kaye highlights idiosyncrasies of DNA that mean that the potential for misunderstanding and misuse are always present. For example, juries can give DNA undue weight, an issue that needs to be better understood before it can be overcome—and overcome it must be if flawed analyses of DNA data are not to lead to wrongful convictions. This is a systemic issue: "the system might have failed, as it too often does, because of the inadequacies of its participants." One of the root causes of such inadequacies lies in the lack of dialogue among legal, science, and criminal-justice professionals. Language receives much of the blame for this failure to exchange ideas, as scientists, lawyers, and law enforcement officials each have their own vernacular. The work of Kaye goes some way to demonstrate that the barriers to communication can be breached. Doing so may require some initially discomfiting forays into other disciplines, departures from comfort zones, and patience, but it is essential.

If we are to realize the full forensic potential of DNA to improve detection rates, convict the guilty, and exculpate the innocent, then everyone involved in the use of DNA profiling needs a proper appreciation of the technology's history, strengths, and weaknesses. This is what *The Double Helix and the Law of Evidence* provides. I look forward to the next installment and hope that Kaye turns his attention to a global consideration of the forensic use of DNA (taking in more than just the United States). For the present, may the book get the wide readership it deserves.

10.1126/science.1196972

The reviewer is at the School of Law, University of Leeds, Leeds LS2 9JT, UK, and Bond University, Queensland 4229, Australia. E-mail: lawcim@leeds.ac.uk

Downloaded from www.sciencemag.org on November 11, 2010

Published by AAAS

ENVIRONMENT AND DEVELOPMENT

Earth System Science for Global Sustainability: Grand Challenges

Progress in understanding and addressing both global environmental change and sustainable development requires better integration of social science research.

W. V. Reid,[1]* D. Chen,[2] L. Goldfarb,[2] H. Hackmann,[3] Y. T. Lee,[2] K. Mokhele,[4] E. Ostrom,[5] K. Raivio,[2] J. Rockström,[6] H. J. Schellnhuber,[7] A. Whyte[8]

Tremendous progress has been made in understanding the functioning of the Earth system and, in particular, the impact of human actions (*1*). Although this knowledge can inform management of specific features of our world in transition, societies need knowledge that will allow them to simultaneously reduce global environmental risks while also meeting economic development goals. For example, how can we advance science and technology, change human behavior, and influence political will to enable societies to meet targets for reductions in greenhouse gas emissions to avoid dangerous climate change? At the same time, how can we meet needs for food, water, improved health and human security, and enhanced energy security? Can this be done while also meeting the United Nations Millennium Development Goals of eradicating extreme poverty and hunger and ensuring ecosystem integrity?

Answering these questions will require reorientation toward new research that better allows science and society to address the needs of decision-makers and citizens at global, regional, national, and local scales (*2*). We will have to meet a twofold challenge: (i) develop strategies to respond to ongoing global change while meeting development goals and (ii) deepen knowledge of the functioning of the Earth system and its critical thresholds (*3*). Promoting sustainable development requires research on a wide range of social, economic, cultural, institutional, and environmental issues (*4*). Given that sustainable development is no longer possible without addressing interactions with global change dynamics (*5*), we focus here on an important dimension of this larger sustainability agenda: the need to broaden and deepen Earth system research to encompass the intersection of global environmental change and sustainable development.

[1]David and Lucile Packard Foundation, Los Altos, CA 94022, USA. [2]International Council for Science (ICSU), 75116 Paris, France. [3]International Social Science Council (ISSC), 75732 Paris, France. [4]National Research Foundation of South Africa, Pretoria, 0001, South Africa. [5]Indiana University, Bloomington, IN 47408, USA. [6]Stockholm Environment Institute, SE-106 91 Stockholm, Sweden. [7]Potsdam Institute for Climate Impact Research, 14473 Potsdam, Germany. [8]Environment and Natural Resources, International Development Research Centre, Ottawa K1G 3H9, Canada.

*Author for correspondence: wreid@packard.org

Grand Challenges

A great deal of collaborative international research on global environmental change is coordinated through four Global Environmental Change Research Programmes (*6*) and the Earth System Science Partnership. In light of the need for an overarching set of solution-focused and integrated research priorities for these institutions, the International Council for Science (ICSU) and the International Social Science Council (ISSC) carried out a consultative process to rethink the focus and framework of Earth system research (*7*, *8*). Efforts were made to obtain balanced input from developed and developing country experts, young and senior scientists, social and natural sciences, and both researchers and those using the findings of research. This process resulted in five "Grand Challenges" (listed below in italics), a consensus list of the highest priorities for Earth system science that would remove critical barriers impeding progress toward sustainable development (*9*). The challenges meet four criteria: (i) scientific importance, (ii) need for global coordination, (iii) relevance to decision-makers, and (iv) leverage (i.e., would help address multiple problems). For each grand challenge, several important research questions are identified as answerable within a decade.

Improve the usefulness of forecasts of future environmental conditions and their consequences for people. We need to develop what amounts to an enhanced Earth system simulator to improve our ability to anticipate impacts of a given set of human actions or conditions on global and regional climate and on biological, geochemical, and hydrological systems on seasonal to decadal time scales. Most current efforts to build state-of-the-art whole-Earth system models depart from sophisticated geophysical kernels (coupled atmosphere-ocean models based on exact dynamical equations like Navier-Stokes) that are to be complemented by equally powerful tools (once they become available) representing other parts of the planetary makeup. But, for instance, there is no marine-biosphere model available that will match the standards of the fluid-dynamics–based simulators of the atmosphere within the next 5 years, and the situation seems to be even worse when it comes to simulation of economic, social, and cultural processes. Thus, alternative approaches need to be explored, such as distributed simulators, where available models for all relevant Earth system compartments are virtually assembled from institutions around the world, even if those sectoral models differ heavily in predictive power, or an ensembles approach, where a given Earth system module would be represented by an entire set of credible realizations.

Research is also needed to assess the potential impact of environmental changes on regional economic conditions, food security, water supplies, health, biodiversity, and energy security. Furthermore, research is needed to understand how people are likely to respond to such changes in different sociogeographic and cultural contexts, in particular in poor and vulnerable communities.

Develop, enhance, and integrate observation systems to manage global and regional environmental change. Although investments are being made to build and coordinate more effective observation systems (e.g., the Global Earth Observation System of Systems), current systems fall short of addressing the grand challenges and meeting decision-makers' needs for forecasts and other research products. Economic and social science data, for example, are often gathered and reported at scales that are incompatible for analyzing interlinkages between social and natural systems. The paucity of empirical data on changes in social-environmental systems undermines the ability of decision-makers and the public to establish appropriate responses to emerging threats and address the needs of vulnerable groups. To design cost-effective systems that meet these needs, important scientific questions need to be addressed: What do we need to observe, at what scales, in coupled social environmental systems in order to respond to, adapt to, and influence global change?

Determine how to anticipate, avoid, and

Downloaded from www.sciencemag.org on November 11, 2010

Published by AAAS

manage disruptive global environmental change. Human interference will likely trigger highly nonlinear changes in the global environment that will tend to alter the very character of the life-support system in question and be largely irreversible on human time scales. In turn, disruptive changes in social systems can result from such events, as well as from more gradual environmental changes. For example, a relatively gradual decline in annual precipitation or soil fertility could lead to an abrupt change in the social system as residents abandon unproductive lands and become environmental refugees. Social and economic policies and institutions are rarely designed for abrupt nonlinear social and environmental change. Understanding the underlying nonlinear dynamics will require integration of environmental and complexity sciences, two fields that have developed largely separately. To confine global change to tolerable ranges, having a low risk of dangerous thresholds or "tipping points," we will have to identify and track system conditions with respect to key planetary boundaries (e.g., critical levels of ocean acidification) (*10*). To confine the impacts of unavoidable excursions of the system into dangerous ranges, we will have to enhance resilience to change. Such research may explore whether there are also "positive" social tipping points, that is, pioneering action that can tip economic or social dynamics into sustainable regimes.

Determine institutional, economic, and behavioral changes to enable effective steps toward global sustainability. Global change exposes gaps in social institutions for managing emerging problems. Modern systems of governance are much more effective in addressing national and local problems over time scales of years to decades than in addressing global problems that will affect future generations more strongly than current generations. Addressing problems of global change will require a step change in research on fundamental questions of governance, economic systems, and the assumptions, beliefs, and values underlying human behavior. This must involve close integration of social and biophysical sciences. We must understand how more effective environmental governance can be established at a time of weakening confidence in traditional forms of governance. It is insufficient to identify necessary reforms in policies and institutions; research must explore how to catalyze adoption of those reforms.

Encourage innovation (and mechanisms for evaluation) in technological, policy, and social responses to achieve global sustainability. We need to improve our understanding about how to strengthen incentives for technology, policy, and institutional innovation to respond to global environmental change. For example, there is need for transformative changes in the world's energy system, including efforts at an international level (e.g., establishing a global cap-and-trade system or a global tax on carbon). Insights into how best to attain such international policies can be drawn from innovations at local and regional levels, which are important laboratories for assessing how diverse carbon policies affect economic and social development at multiple scales. Just as countries seek to harmonize public sector research, economic incentives for emerging industries, and public policies to stimulate growth of new competitive industries, a mix of incentives will be needed to generate ideas and technologies to address global change in the context of sustainable development. In particular, we need focused efforts, coupled with careful assessment, on such issues as the potentials and risks of geoengineering strategies (including exploration of local to global institutional arrangements needed to oversee them) and options to meet competing demands for scarce land and water over the next half-century.

A Call to Action

These grand challenges provide an overarching research framework to mobilize the international scientific community around a focused decade of research to support sustainable development in the context of global environmental change. This will require new research capacity, including efforts to attract young scientists, particularly in developing countries. Research dominated by the natural sciences must transition toward research involving the full range of sciences and humanities. A more balanced mix of disciplinary and interdisciplinary research is needed that actively involves stakeholders and decision-makers.

These needs will be challenging to address. There is no simple mechanism to fund "global" research. And because research at the intersection of Earth system science and sustainable development has not attracted great attention from either natural or social scientists, it will take time to build this research community. The disciplinary-dominated structure of academia runs counter to the need to address interdisciplinary aspects of these grand challenges.

But, building on ongoing efforts to promote the broader field of "sustainability science," there is a growing effort by Earth system science researchers and research funders to overcome these barriers (*11*–*13*). For example, discussions are now under way with the Belmont Forum (*13*), a group of leading global-change funding agencies, to design an overarching approach that would (i) coordinate and focus international scientific research to address the grand challenges; (ii) deliver at global and regional scales the knowledge that societies need to effectively respond to global environmental change while meeting economic and social goals; and (iii) engage a new generation of researchers in the social, economic, natural, health, and engineering sciences in the necessary research. An innovative international partnership between researchers, operational agencies, research funders, and users is fundamental to this approach. Ultimately, a coordinated international funding approach is needed to ensure strategic codesign and implementation of the research.

Roughly 30 years ago, establishment of the first global environmental change research programs represented a revolutionary response by the scientific community to coordinate research across countries and continents to understand the functioning of the Earth system. In a similar spirit, we call on the scientific community to continue improving our understanding of the Earth system and human impacts, but also to deliver knowledge that will enable human development in a world facing rapid global change.

References and Notes

1. H. J. Schellnhuber, D. Sahagian, *Global Change Newsl.* **49**, 20 (2002).
2. W. C. Clark, H. J. Schellnhuber, P. J. Crutzen, in *Earth System Analysis for Sustainability*, H. J. Schellnhuber *et al.*, Eds. (MIT Press, Cambridge, MA, 2004), pp. 1–28.
3. The Earth system is the physical, chemical, biological, and social components, processes, and interactions that together determine the state and dynamics of Earth, including its biota and human occupants.
4. R. W. Kates *et al.*, *Science* **292**, 641 (2001).
5. B. Walker *et al.*, *Science* **325**, 1345 (2009).
6. These are the World Climate Research Programme, International Geosphere-Biosphere Programme, International Human Dimensions Programme on Global Environmental Change, and DIVERSITAS.
7. W. V. Reid, C. Bréchignac, Y. T. Lee, *Science* **325**, 245 (2009).
8. For process details, see www.icsu-visioning.org/the-visioning-process.
9. For challenge details, see www.icsu-visioning.org.
10. J. Rockström *et al.*, *Nature* **461**, 472 (2009).
11. B. L. Turner, 2nd *et al.*, *Proc. Natl. Acad. Sci. U.S.A.* **100**, 8074 (2003).
12. E. Ostrom, *Science* **325**, 419 (2009).
13. ICSU analyzed global change research capacity needs on behalf of research donors; www.icsu.org/2_resourcecentre/ICSU_Belmont_report.

14. H.H., K.M., E.O., K.R., W.V.R., J.R., H.J.S., and A.W. were appointed by ICSU to guide the visioning process. We thank the more than 1000 individuals from 85 countries who contributed to the initial online consultation, participants in the September 2009 research priorities workshop, and the more than 200 individuals and 46 institutions that reviewed the draft of the grand challenges report.

10.1126/science.1196263

Downloaded from www.sciencemag.org on November 11, 2010

Published by AAAS

MEDICINE

Prion-Like Behavior of Amyloid-β

Can Alzheimer's disease arise through pathogenic transmission of a protein aggregate?

Jungsu Kim and David M. Holtzman

Can certain neurodegenerative diseases be transmitted between humans by an infectious agent? The discovery that protein particles called prions can enter healthy mammals, including humans, and trigger a cascade of endogenous protein misfolding associated with bovine spongiform encephalopathy ("mad cow disease") and Creutzfeldt-Jakob disease, certainly demonstrates this in prion diseases. Remarkably, neuronal proteins such as tau, α-synuclein, and polyglutamine aggregates, which are causally implicated in the neurodegenerative disorders Alzheimer's disease, Parkinson's disease, and Huntington's disease, respectively, can be released from donor cells and taken up by neighboring acceptor cells. Moreover, treatment with exogenous misfolded neuronal proteins, such as tau, can trigger the misfolding and aggregation of their properly folded endogenous counterparts in host cells and animals (*1*). Besides prions, there is yet no evidence that other neurodegenerative diseases associated with protein misfolding are transmissible between humans by an infectious agent. But on page 980 in this issue, Eisele *et al*. (*2*) report that peripherally injected (outside the brain) mouse brain lysates containing aggregates of amyloid-β (Aβ)—the peptide that induces the formation of debilitating brain plaques in Alzheimer's disease—causes plaque-associated pathological changes in the brains of recipient mice. This has implications for a pathogenic mechanism reminiscent of prion transmission.

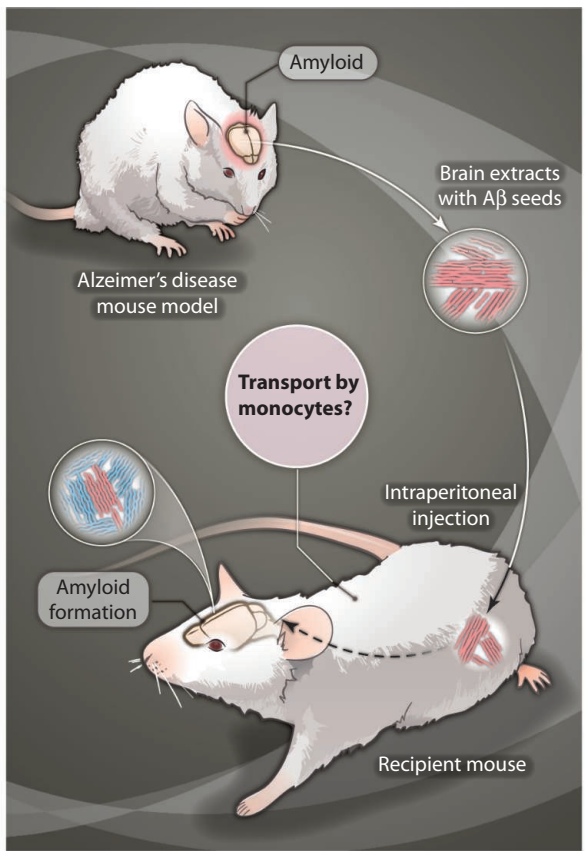

Amyloid transmission. Injection of mouse brain extract containing Aβ seeds (similar to those found in the Alzheimer's disease brain) into the peritoneal cavity of mice (that are genetically engineered to develop amyloid plaques) accelerates Aβ deposition in the host brain. The transport mechanism from peripheral tissue to the brain is unclear.

Alzheimer's disease is characterized clinically by progressive cognitive decline, and pathologically by the formation of Aβ-containing amyloid plaques and tau-containing neurofibrillary tangles (*3*). Aβ aggregation is characterized by a slow nucleation phase in which it undergoes a series of association steps to form small seeds, and a growth phase in which the seeds rapidly grow to form larger fibrils and ultimately, plaques (*4*). Plaque formation can be facilitated by preformed seeds. Indeed, the formation of amyloid plaques can be induced in vivo by injecting brain extracts containing such seeds (from patients with Alzheimer's disease) into mice that are genetically engineered to be predisposed to developing brain amyloidosis (*5*). This suggested that a factor in the brain extract triggers amyloid formation in vivo, but it was not clear whether the factor is solely Aβ or whether other factors are required. However, the amyloid-inducing activity of brain extracts was abolished by protein denaturation and specific immunodepletion of Aβ (*6*). Yet systemic administration of Aβ-containing brain lysates, either orally or by intravenous, intraocular, or intranasal injection, failed to induce cerebral Aβ amyloidosis in mice (*7*).

Surprisingly, Eisele *et al*. show that intraperitoneal injection of mice with mouse brain extracts containing Aβ aggregates leads to earlier-onset amyloid deposition and other pathological alterations in recipient mice (5 months after exposure) (see the figure). Aβ aggregates were predominantly associated with cerebral blood vessels, and amyloidosis was associated with local gliosis (proliferation of glia in damaged areas) and hyperphosphorylation of tau protein, the major component of neurofibrillary tangles. Thus, cerebral amyloidosis can be induced in a susceptible host by Aβ-containing material delivered outside the brain. It is unclear why the previous attempts with intravenous injection failed to trigger Aβ deposition. It is possible that other modes of administration could induce amyloidosis if the incubation time of the injected seed is sufficiently long and if the seed has a proper conformation.

The transmission mechanism by which the peripherally injected amyloid-inducing factor penetrates into the brain is also not clear. The authors propose that macrophages and monocytes in the peritoneal cavity could take up Aβ-containing material, enter the general circulation, migrate into the cerebral perivascular space, and deliver seeds for amyloidosis. Another possibility might be that some Aβ-containing material gets rapidly into the brain across the blood-brain barrier without entering circulating cells.

Still, Eisele *et al*. do not provide direct evidence that peripherally injected Aβ (independent of other Aβ-associated cofactors) in the brain extracts is necessary and sufficient to trigger cerebral amyloid deposition. Induction of amyloid formation in vivo with synthetic Aβ has been unsuccessful so far, leading to the hypothesis that an amyloid-enhancing factor or a particular conformation of Aβ aggregates is required to trigger Aβ deposition in vivo (*6*). Similarly, numerous attempts to trigger prion diseases with synthetic prion proteins alone have not been successful (*8*). A recent study demonstrated the critical role of lipid molecules and RNAs as cofactors in producing recombinant infectious prions (*9*).

Department of Neurology, Hope Center for Neurological Disorders, Knight Alzheimer's Disease Research Center, Washington University School of Medicine, St. Louis, MO 63110, USA. E-mail: holtzman@neuro.wustl.edu

Downloaded from www.sciencemag.org on November 11, 2010

CREDIT: Y. HAMMOND/SCIENCE

Published by AAAS

It is possible that cerebral Aβ amyloidosis also requires brain-specific endogenous amyloid-enhancing factors. Plaque-associated proteins and lipids, such as apolipoprotein E, proteoglycan, and ganglioside, might serve as cofactors and facilitate Aβ aggregation (*10*). The chemical and physical features of the amyloid-inducing factor remain to be determined.

The cell-to-cell passage of misfolded proteins opens up the possibility of new treatment strategies for their associated disorder, such as antibodies or small molecules that block transmission of the protein. However, such transmission imposes a cautionary caveat for stem cell–based therapy. Conveyance of misfolded protein into the transplanted stem cells might limit therapeutic benefits.

References

1. B. Frost, M. I. Diamond, *Nat. Rev. Neurosci.* **11**, 155 (2010).
2. Y. S. Eisele *et al.*, *Science* **330**, 980 (2010).
3. J. Hardy, D. J. Selkoe, *Science* **297**, 353 (2002).
4. J. D. Harper, P. T. Lansbury Jr., *Annu. Rev. Biochem.* **66**, 385 (1997).
5. M. D. Kane *et al.*, *J. Neurosci.* **20**, 3606 (2000).
6. M. Meyer-Luehmann *et al.*, *Science* **313**, 1781 (2006).
7. Y. S. Eisele *et al.*, *Proc. Natl. Acad. Sci. U.S.A.* **106**, 12926 (2009).
8. G. Legname *et al.*, *Science* **305**, 673 (2004).
9. F. Wang, X. Wang, C. G. Yuan, J. Ma, *Science* **327**, 1132 (2010).
10. J. Kim, J. M. Basak, D. M. Holtzman, *Neuron* **63**, 287 (2009).

10.1126/science.1198314

MATERIALS SCIENCE

Materials Ecology: An Industrial Perspective

Careful process design that considers material use and reuse over the entire product life cycle is important for a sustainable industry.

Paul Collier[1] and Carina Maria Alles[2]

There are many reasons for the current drive for more sustainable industrial processes, including a desire for enhanced societal value, lower-energy demand, less waste, and more effective products. Much of this drive comes from a new generation of industry CEOs who are committed to sustainability (*1*). Sustainability naturally includes a view on what to do with products at the end of their lives, and the best modern products are designed to make recycling easier. However, there is much that is not deemed to be worth recycling and goes into landfill (*2*). Population increase and changes in consumption patterns combined with the inefficient use of materials push us toward a crisis point. To achieve stable long-term growth, something will have to change—and perhaps a new approach based on the materials themselves can help.

Industrial ecology is now a thriving sector of engineering design and practice and has become a welcome part of modern industrial life (*3*, *4*). It derives from a high-level systems study of the energy and material flows through industrial processes. The aim is to improve sustainability by closing loops and recycling materials. "Materials ecology," a less well known concept, was examined at a recent Frontiers of Engineering event (*5*). Several of the ideas presented below crystallized during the series of talks and ensuing panel discussion. This term has been used before, principally to describe metals and minerals (*6*); however, before our modern age such philosophies were surprisingly widespread (*7*).

Materials ecology is a subset of industrial ecology and offers a materials-centered view of manufacturing processes rather than a systems view. Materials ecology is about the interconnectivity of materials and the relative cost of loop closure with respect to other materials and the environment. Loop closure refers to a process for converting a product at the end of its life into a new material and is related to the term "cradle to cradle" (*8*). By necessity, it operates at smaller scales but is intimately meshed with industrial ecology at larger scales (see the figure).

In industrial ecology, a general approach might be to examine a particular industrial system—for example, for producing a refrigerator—and to test inputs and outputs (covering all raw materials, waste products, desired products, pollutants, energy required, and heat generated) against sustainability criteria. For each new product, this is repeated, recalculating inputs and outputs each time. A materials ecology viewpoint would complement this approach by allowing us to make connections between the same material used in different processes. For example, polyethylene terephthalate is used in many products, such as fibers and bottles. The materials ecology approach would focus on this individual material and consider it as the center of a network analysis diagram with connections to all the products that can be made from it. At each link, all material and energy inputs and outputs are evaluated in terms of the closed-loop use of the material (i.e., including recycles) and classi-

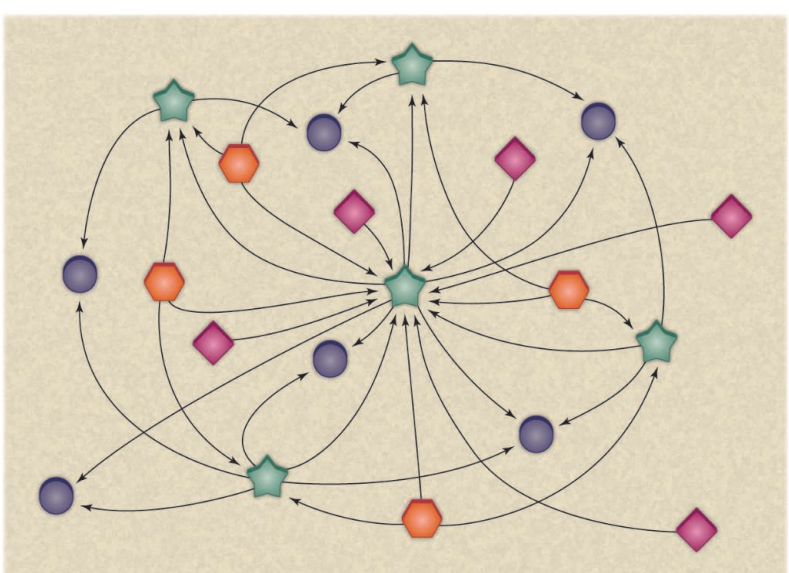

In the loop. Schematic representation of manufacturing networks.

[1]Johnson Matthey Technology Centre, Blount's Court Road, Sonning Common, Reading, RG4 9NH, UK. [2]DuPont Engineering Research and Technology, DuPont Building D5085, 1007 Market Street, Wilmington, DE 19898, USA. E-mail: collipj@matthey.com, carina.alles@usa.dupont.com

CREDIT: ADAPTED FROM WWW.EMERALDINSIGHT.COM/CONTENT_IMAGES/FIG102401706040001.PNG

Downloaded from www.sciencemag.org on November 11, 2010

Published by AAAS

fied as an environmental payment or credit. It may be possible to extend this and include other environmental impact parameters, such as water demand, environmental toxicity, and pollutants.

Categories of material rather than individual ones could also be the focus. For example, if we are interested in polymer fibers for clothing, then all of the materials capable of forming fibers could be compared in terms of their potential for closed-loop processing, to allow us either to select between them or to look for improvements on the current material.

A further interpretation of materials ecology puts emphasis on avoiding end-of-life situations where a material cannot be reused or recycled, or the energy required to do so is prohibitively high. Are there ways to validate this concept? Perhaps one way is to view the amount of energy required to place a material in a closed loop and consume it as a starting material for another industrial process. This could be in terms of the energy required for a conversion. For example, carbon dioxide's Gibbs free energy of formation is very high. This means that a lot of energy input is required to convert CO_2 into a useful product in a closed-loop system. In a materials ecology network analysis diagram, CO_2 will appear as an island with a relative high cost of closed-loop processing.

In the worst cases, products are treated as dead-ends, because complex products, particularly with many constituent materials, are not really designed for reuse. Materials ecology is about the evolution of a new generation of products that can easily be reused elsewhere at the end of their lives. For example, a modern automobile is a very complex product requiring many thousands of parts. At the end of its life, the car is dismantled and much of it is recycled, especially the metals. Some components are less effectively recycled and go to landfill. However, there is a growing trend in some industries to reuse polymer waste rather than landfill it, and materials ecology embraces this potentially lower-energy option. The modern term "upcycling" is actually an old tradition: In rural communities, objects are endlessly reused and adapted for new uses as they age. This was actually practiced by the father of mass production, Henry Ford. Almost 100 years ago, Ford shipped model "A" trucks in wooden crates from the Ford factory; the crates were then used as the floorboards for the vehicle when sold.

The current obsession with "elementalism," that is, striving to return all objects as close to the pure element state as possible, regardless of the environmental cost, is going to look rather odd in the future. New industrial processes will be required to take in objects and "reshape" them for new uses rather than crush and melt them down into pure elemental streams

The key success parameters of the new industrial landscape are no longer based solely on profit margin, but now include environmental, social, and ethical measures. This will only increase in the future, and the most successful materials will be the ones that thrive in this more complex framework of materials ecology.

References and Notes

1. T. Ellis, *The New Pioneers: Sustainable Business Success Through Social Innovation and Social Entrepreneurship* (Wiley, Hoboken, NJ, 2010).
2. M. Hill, *Understanding Environmental Pollution* (Cambridge Univ. Press, Cambridge, 2010).
3. T. E. Graedel, B. R. Allenby, *Industrial Ecology* (Prentice Hall, Upper Saddle River, NJ, ed. 2, 2002).
4. R. Ayres, L. Ayres, Eds., *A Handbook of Industrial Ecology* (Elgar, Cheltenham, 2002).
5. U.S. National Academy of Engineering and Royal Academy of Engineering, Frontiers in Engineering, EU-US Symposium, Cambridge, UK, 31 August to 3 September 2010; www.raeng.org.uk/international/activities/frontiers_engineering_symposium.htm.
6. M. A. Reuter *et al.*, *The Metrics of Material and Metal Ecology: Harmonizing the Resource, Technology and Environmental Cycles (Developments in Mineral Processing)* (Elsevier Science, Amsterdam, 2005).
7. P. Desrochers, K. Lam, *Electronic J. Sustainable Dev.* **1**, 1 (2007).
8. W. McDonough, M. Braungart, *Cradle to Cradle: Remaking the Way We Make Things* (North Point Press, New York, ed. 1, 2002).

9. We thank the speakers at the Materials Ecology session of (*5*): S. Suh, K. Hellgardt, J.-S. Thomas, and W.-P. Schmidt, as well as the event organizers: the U. S. National Academy of Engineering and The Royal Academy of Engineering (on behalf of the umbrella organization of European engineering academies, Euro-CASE). P.C. also thanks S. Axon.

10.1126/science.1197478

CELL BIOLOGY

Irremediable Complexity?

Michael W. Gray,[1] Julius Lukeš,[2] John M. Archibald,[1] Patrick J. Keeling,[3] W. Ford Doolittle[1]

Complex cellular machines may have evolved through a ratchet-like process called constructive neutral evolution.

Many of the cell's macromolecular machines appear gratuitously complex, comprising more components than their basic functions seem to demand. How can we make sense of this complexity in the light of evolution? One possibility is a neutral ratchet-like process described more than a decade ago (*1*), subsequently called constructive neutral evolution (*2*). This model provides an explanatory counterpoint to the selectionist or adaptationist views that pervade molecular biology (*3*).

Seemingly gratuitous complexity is illustrated by RNA processing systems such as splicing and editing. The most complicated macromolecular machine in the cell may be the eukaryotic spliceosome (*4*), which removes noncoding regions (introns) from precursor messenger RNA (mRNA) in a process called splicing. The spliceosome uses five small nuclear RNAs and hundreds of proteins to do the same job that some catalytic introns (called ribozymes) can do alone. The mitochondrial RNA editing system of trypanosomes, in which hundreds of guide RNAs and several large protein complexes insert and delete uridine residues to restore mRNAs to their "ancestral" state, is similarly complex (*5*). Even the multicomponent contemporary ribosome, which translates mRNA into protein, boasts far more constituent parts than most imagine its purely ribozymatic ancestor would have required.

When faced with such complexity, the favored (adaptationist) explanation would surely be selection for improved basic function. For example, ribosomal complexity is not generally regarded as gratuitous, but rather the result of evolutionary accretion of proteins that made this machine progressively faster, more stable, and more efficient at translation (*6*). For the addition of some of these proteins, selection probably did drive increased complexity, but there is no basis to assume that this explains all, or even most, of the increased complexity of these machines.

As an alternative to such adaptationist thinking, Lynch invoked fixation of neutral or slightly deleterious features as a general and unavoidable source of complexity in

[1]Department of Biochemistry and Molecular Biology, Dalhousie University, Halifax, Nova Scotia B3H 1X5, Canada. [2]Institute of Parasitology, Czech Academy of Sciences and Faculty of Sciences, University of South Bohemia, 37005 České Budějovice, Czech Republic. [3]Department of Botany, University of British Columbia, Vancouver, British Columbia V6T 1Z4, Canada. E-mail: ford@dal.ca

Downloaded from www.sciencemag.org on November 11, 2010

Published by AAAS

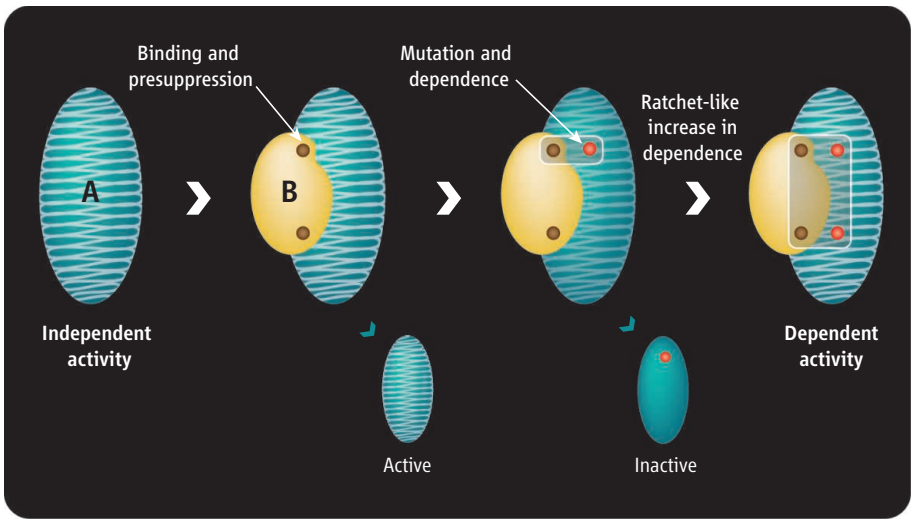

Becoming interdependent. Cellular component A fortuitously interacts with B, which allows (presuppresses) mutations that would otherwise inactivate A. Subsequent mutations render reversion to independence unlikely.

taxa with small populations (*3*, *7*). Such nonselective processes could account for the origins and spread of transposons (mobile DNA elements), introns, and other contributors to the high DNA content of many eukaryotes, which typically have small populations relative to prokaryotes. Neutrally fixed complexity could be neutrally "unfixed" (through random reversion), but ratchet-like (one-directional) tendencies might prevent this. For example, a genome once infected with an active but harmless transposon will not likely regain its simpler, pristine condition without selection for reduced element number. At the organismal level, Maynard Smith and Szathmary proposed that a ratchet mechanism called contingent irreversibility might render previously independent evolutionary units interdependent for "accidental reasons that have little to do with the selective forces that led to the evolution of the higher entity in the first place" (*8*). An example is the mutual loss of autonomy by the symbionts that became mitochondria or plastids and the cells that harbored them.

At the subcellular level, similar forces may also be at work, a simple example of which is found in the *Neurospora* mitochondrion (*9*). The *Neurospora* mitochondrial genome encodes several introns, some of which can self-splice, but others require a tyrosyl tRNA synthetase (TyrRS) to splice. This interaction is typically interpreted as having arisen "to compensate for structural defects acquired" by the intron sequences (*10*). But this order of events puts the cart before the horse: Introns bearing such defects would be at an immediate selective disadvantage and would not likely be fixed in populations before the TyrRS binding evolved to suppress their deleterious effects. If the order of events is reversed, then there would be no deleterious intermediate. Specifically, if the binding interaction arose first—fortuitously or for some reason unrelated to splicing—its existence could allow the accumulation of mutations in the intron that would have inactivated splicing, were the protein not bound. Because the compensatory or suppressive activity of the protein is imagined to exist fortuitously before any intron mutation, this might be called "presuppression," and the acquisition of protein dependence by the intron could be selectively neutral (or even slightly disadvantageous), and yet also inevitable, in finite populations.

An idealized general model of such a chain of events (see the figure) illustrates how the two components (such as an intron and TyrRS) might revert to independence, but are more likely to "ratchet" toward greater dependency over time. An initial mutation creates a dependent state, and only reversion at this site is likely to break the dependency. By contrast, mutations at any other site have the potential to create further dependencies. Random mutations are therefore unlikely to restore one component to its original state of independence from the other. If there are more ways for dependence to increase than decrease, an increase is unavoidable. Thus, constructive neutral evolution is a directional force that drives increasing complexity without positive (and in small populations, against mildly negative) selection. Negative selection is involved, but only as the stabilizing force that keeps this directionality from reversing.

Both the order of events and the potential for a ratchet-like increase in complexity are often overlooked when explaining complex systems, in particular when intricate features are interpreted as having arisen as corrections or countermeasures. RNA editing has been rationalized as a form of repair (*11*), whereas the nuclear-cytosolic compartmentalization that defines eukaryotes has been hypothesized to have arisen to compensate for the baleful effect of introns on translation (*12*). Although compensation for defects caused by "selfish" (self-propagating) DNA elements may seem intuitive, it is problematic to propose that, on the way to evolving compensatory machinery, an intermediate state had to exist that was less fit than its ancestors and sisters. Why would such an intermediate not just die out in competition before its rescue by compensatory complexity yet to be invented? A more workable model is that the compensating mechanism was already present (possibly serving unrelated functions).

Although this model is easiest to illustrate using molecular systems of peripheral importance or limited distribution (such as splicing or RNA editing), there is no reason why it might not contribute to the generation of any cellular complexity (the ribosome; mitochondrial respiratory complexes; light-harvesting antennae in photosynthetic organisms; RNA and DNA polymerases and their initiation, elongation, and termination complexes; protein import, folding, and degradation apparatuses; the cytoskeleton and its motors). Much of the bewildering intricacy of cells could consist of originally fortuitous molecular interactions that have become more or less fixed by constructive neutral evolution. Indeed, although complexity in biology is generally regarded as evidence of "fine tuning" or "sophistication," large biological conglomerates might be better interpreted as the consequences of runaway bureaucracy—as biological parallels of nonsensically complex Rube Goldberg machines that are overengineered to perform a single task (*13*).

References

1. P. S. Covello, M. W. Gray, *Trends Genet.* **9**, 265 (1993).
2. A. Stoltzfus, *J. Mol. Evol.* **49**, 169 (1999).
3. M. Lynch, *Proc. Natl. Acad. Sci. U.S.A.* **104** (suppl. 1), 8597 (2007).
4. T. W. Nilsen, *Bioessays* **25**, 1147 (2003).
5. J. Lukeš, H. Hashimi, A. Zíková, *Curr. Genet.* **48**, 277 (2005).
6. G. E. Fox, *Cold Spring Harb. Perspect. Biol.* **2**, a003483 (2010).
7. M. Lynch, *The Origins of Genome Architecture* (Sinauer, Sunderland, MA, 2007).
8. J. Maynard Smith, E. Szathmary, *The Major Transitions in Evolution* (Oxford Univ. Press, Oxford, 1995).
9. R. A. Akins, A. M. Lambowitz, *Cell* **50**, 331 (1987).
10. P. J. Paukstelis, *Proc. Natl. Acad. Sci. U.S.A.* **105**, 6010 (2008).
11. D. Speijer, *IUBMB Life* **58**, 91 (2006).
12. W. Martin, E. V. Koonin, *Nature* **440**, 41 (2006).
13. A. Sancar, *Nat. Struct. Mol. Biol.* **15**, 23 (2008).

10.1126/science.1198594

Downloaded from www.sciencemag.org on November 11, 2010

Published by AAAS

PLANT SCIENCE

Fertility Goddesses as Trojan Horses

In flowering plants, fertilization and fungal infection depend on the same type of receptor proteins.

Francine Govers[1,4] and Gerco C. Angenent[2,3,4]

Tip growth is similar in many features in plants and fungi. The tube-like structures that emerge from both plant pollen grains and fungal spores, for instance, exhibit "polarized" cell growth that enables rapid elongation. It is not surprising that, before the 19th century, researchers believed that emerging pollen tubes were invading fungal parasites. On page 968 of this issue, Kessler *et al*. (*1*) show that this similarity extends beyond looks: Both pollen tubes and fungi exploit similar receptor proteins that function either as goddesses of fertility that enable fertilization—or as Trojan horses that enable pathogenic fungi to invade plant tissues.

In nature, plants are constantly exposed to potential pathogens, but most stay healthy. They are equipped with effective mechanisms for keeping pathogens out, including physical barriers and immune responses that activate upon pathogen recognition. In most cases, plant resistance is mediated by receptors that are triggered by compounds secreted by the pathogen (called effectors). Hence, resistance mostly acts as a dominant trait. One well-known exception is a recessively inherited resistance to powdery mildew, a common fungal disease that causes severe losses in a wide range of crops. Molecular cloning of the first "mildew locus of resistance o" (*mlo*) in barley (*2*) revealed that the MLO protein must be present in a plant for successful infection by powdery mildew. This Trojan horse is a seven-transmembrane (7-TM) receptor protein that acts both as a defense modulator and a docking molecule for the fungus (*3*).

In experiments with mutant *Arabidopsis*, Kessler *et al*. show that a similar MLO docking receptor plays an important role in the fertilization of flowering plants, and that another fertility protein is involved in pathogen invasion. In flowering plants, the first barrier encountered during fertilization is the stigma, the landing platform for the pollen. Here, the pollen, which encloses two sperm cells, germinates. The pollen tube grows toward the ovule and penetrates one of the two synergid cells at one end of the embryo sac. The tube then bursts, releasing the sperm cells; one sperm cell fuses with the adjacent egg cell to form a zygote (*4*). As in fungal infection, successful docking is a prerequisite for fertilization, and Kessler *et al*. show that it relies on a 7-TM receptor protein in the MLO family, NORTIA (NTA). Moreover, they show that another female fertility component, the receptor-like kinase FERONIA (FER), is required for host cell invasion by fungi. FER is one of 17 known CrRLK1L-type kinases in *Arabidopsis* (*5*). Like MLO, FER violates the rule that resistance is dominant, and it is the first known receptor-like kinase that functions as a susceptibility factor for fungal plant pathogens.

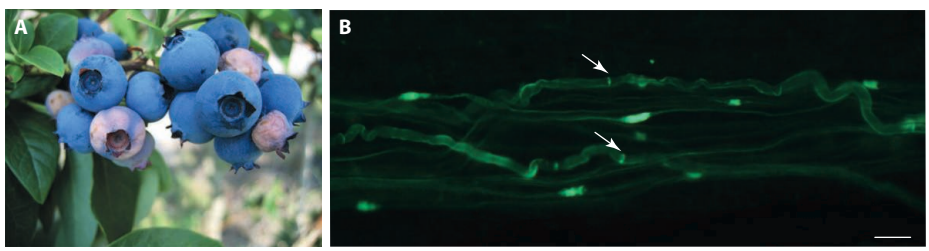

Mummy mimic. Pollen mimicry is a mechanism exploited by some pathogenic fungi to mislead their hosts (*9*). (**A**) "Mummy berries" are shriveled blueberries resulting from infection by *Monilinia vaccinii-corymbosi* during flowering. (**B**) Germ tubes with septa (arrows) emerging from fungal spores invade the style and behave as pollen tubes (with bright callose deposits) (*11*). Mummy berry is the most common blueberry disease in North America.

In the *Arabidopsis* mutants *nta* and *fer*, named after the Etruscan fertility goddesses Nortia and Feronia, fertility is impaired due to a communication failure between the pollen tube and the embryo sac. The pollen tube enters a synergid cell, but instead of bursting, it continues to grow within the cell (*1*, *6*). The mutant phenotype was observed only when *nta* and *fer* mutations were located in the genome of the female parent; this suggests that the communication deficiency is in the receptive synergid cells. Indeed, FER turned out to be located in the filiform apparatus, a specialized membrane-rich structure in synergid cells found at the end where pollen tubes enter (*4*). Kessler *et al*. showed that NTA is a membrane-associated protein that colocalizes with FER in the filiform apparatus. Before pollination, NTA, but not FER, is randomly distributed in the synergids. After pollination, NTA moves to the site of pollen tube entry, apparently under the direct or indirect control of FER.

This redistribution is strikingly similar to that observed for MLO in barley upon infection with powdery mildew (*7*). At sites where the fungus attempts to penetrate the leaf epidermis, membranes accumulate that recruit and collect compounds involved in penetration resistance, in structures reminiscent of lipid "rafts." MLO suppresses this defense by modulating proteins, such as syntaxins, that are involved in vesicle transport. As a result, the presence of MLO allows the fungus to invade epidermal cells and to establish feeding structures known as haustoria. So far, the role of FER in redistributing MLO to the invasion site has not been addressed.

The fact that the filiform apparatus in synergid cells and the lipid rafts in pathogen-challenged leaves are polarly localized (occur on one side of cells), and recruit MLO proteins, raises a question: Are NTA-associated vesicles in synergids transporting cargo necessary for communication with the pollen tube? Cargo candidates are two recently identified cysteine-rich proteins that act as pollen tube attractants and are required for pollen tube rupture (*8*). These proteins are similar to NTA in that they accumulate in the filiform apparatus. Moreover, they resemble defensins, plant proteins that inhibit fungal growth and act as components of the plant

[1]Laboratory of Phytopathology, Wageningen University, 1-6708 PB Wageningen, Netherlands. [2]Laboratory of Molecular Biology, Wageningen University, 1-6708 PB Wageningen, Netherlands. [3]Business Unit Bioscience, Plant Research International, 16-6700 AA Wageningen, Netherlands. [4]Centre for BioSystems Genomics (CBSG), 98-6700 AB Wageningen, Netherlands. E-mail: francine.govers@wur.nl

PHOTO CREDIT: MUMMY BERRIES, COURTESY OF W. O. CLINE/NCSU PLANT PATHOLOGY DEPARTMENT

Downloaded from www.sciencemag.org on November 11, 2010

Published by AAAS

innate immune system.

Kessler *et al*.'s findings may also have implications for a little-studied phenomenon known as pollen mimicry. Although powdery mildew fungi rarely colonize flowers or gain contact with the ovule, other fungi—including smuts, ergot, and head blight on cereal crops (*9*, *10*)—specifically infect flowers. Some fungi mimic pollen by using the same route as pollen to gain access to the host's ovules (*11*); spores land on the stigma and germ tubes penetrate the style (see the figure).

Overall, the most striking observation by Kessler *et al*. is that two seemingly distinct processes, i.e., pathogen invasion and sperm cell release, are controlled by the same factors. What do these two processes have in common? As in sex, a successful plant-pathogen interaction requires compatible partners. Apparently, tube-like structures of either plant or fungal origin release signals that, directly or indirectly, activate plant cells to allow invasion. Because FER is responsible for redistribution of NTA upon pollination, it is likely that FER is the receptor that senses the signal, and not NTA or MLO. This implies that the same receptor-like kinase can initiate a signaling cascade in two different types of receptive cells, i.e., leaf and synergid cells, and that the penetrating structure (pollen tube or pathogen) provides the ligand that interacts with FER.

In recent years, genome sequencing and high-throughput functional analyses of pathogen effectors have boosted the discovery rate of ligands (effectors) that interact with defense receptors (*12*, *13*). The similarities between the goddesses of fertility and the Trojan horses described by Kessler *et al*. suggest that the ligands produced by powdery mildews and pollen have several features in common, and it would be worth using similar, high-throughput approaches to identify the ligands of FER. Once the ligands are known, the next challenge will be to exploit them for improving seed production without promoting fungal infection.

References

1. S. A. Kessler *et al*., *Science* **330**, 968 (2010).
2. R. Büschges *et al*., *Cell* **88**, 695 (1997).
3. R. Panstruga, *Biochem. Soc. Trans.* **33**, 389 (2005).
4. S. McCormick, *Science* **317**, 606 (2007).
5. K. Hématy, H. Höfte, *Curr. Opin. Plant Biol.* **11**, 321 (2008).
6. N. Huck, J. M. Moore, M. Federer, U. Grossniklaus, *Development* **130**, 2149 (2003).
7. R. A. Bhat, M. Miklis, E. Schmelzer, P. Schulze-Lefert, R. Panstruga, *Proc. Natl. Acad. Sci. U.S.A.* **102**, 3135 (2005).
8. S. Okuda *et al*., *Nature* **458**, 357 (2009).
9. H. K. Ngugi, H. Scherm, *Annu. Rev. Phytopathol.* **44**, 261 (2006).
10. P. Tudzynski, J. Scheffer, *Mol. Plant Pathol.* **5**, 377 (2004).
11. H. K. Ngugi, H. Scherm, *Physiol. Mol. Plant Pathol.* **64**, 113 (2004).
12. J. G. Ellis, M. Rafiqi, P. Gan, A. Chakrabarti, P. N. Dodds, *Curr. Opin. Plant Biol.* **12**, 399 (2009).
13. V. G. Vleeshouwers *et al*., *PLoS ONE* **3**, e2875 (2008).

10.1126/science.1198347

SOCIAL SCIENCE

Cooperation and the Commons

In Ethiopia, groups with a higher propensity to cooperate avoid the tragedy of the commons.

Björn Vollan[1] and Elinor Ostrom[2]

Sustainably managing common natural resources, such as fisheries, water, and forests, is essential for our long-term survival. Many analysts have assumed, however, that people will maximize short-term self-benefits—for example, by cutting as much firewood as they can sell—and warned that this behavior will inevitably produce a "tragedy of the commons" (*1*), such as a stripped forest that no longer produces wood for anyone. But in laboratory simulations of such social dilemmas, the outcome is not always tragedy. Instead, a basic finding is that humans do not universally maximize short-term self-benefits, and can cooperate to produce shared, long-term benefits (*2, 3*). Similar findings have come from field studies of commonly managed resources (*6*–*7*). It has been challenging, however, to directly relate laboratory findings to resource conditions in the field, and identify the conditions that enhance cooperation. On page 961 of this issue, Rustagi *et al*. (*8*) help fill this gap. In an innovative study of Ethiopia's Oromo people, they use economic experiments and forest growth data to show that groups that had a higher proportion of "conditional cooperators" were more likely to invest in forest patrols aimed at enforcing firewood collection rules—and had more productive forests. They also show that other factors, including a group's distance to markets and the quality of its leadership, influenced the success of cooperative management.

Researchers have translated social dilemmas into economic games in which the players—typically college students in the United States or Europe—can earn real money, depending on whether they and others "invest" in a common good, or become "free riders" who benefit without paying their fair share. Cardenas (*9*) was the first to translate a game carried out with students using computers in a lab (*5*) into a pen-and-paper version that was played by actual users of local forests in Colombia. This field effort essentially replicated the lab findings, but the levels of cooperative behavior observed were more variable. Other field experiments examined how people who relied on forests, fisheries, and grazing lands responded to experimental designs that enabled them to impose sanctions on free riders, including varying monetary penalties (*10*, *11*). Several examined whether rules established by an external authority—such as a government—"crowded out" a group's motivation to cooperate (*12*, *13*).

In Ethiopia's Bale Mountains, Rustagi *et al*. took these experiments a step fur-

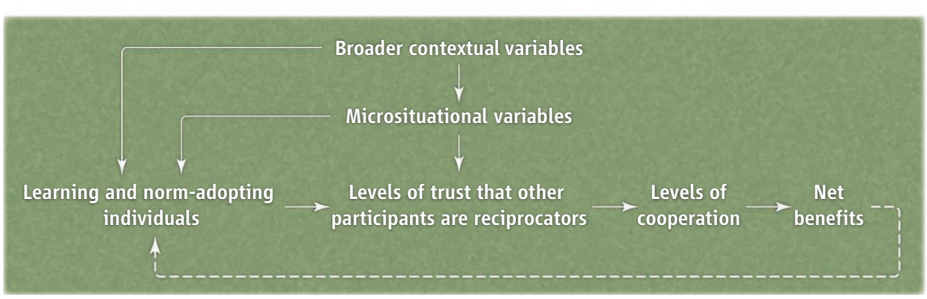

Trust me. "Microsituational" and broader contextual variables can influence levels of trust and cooperation in managing common resources such as forests. [Adapted from (*18*)]

[1]Department of Economics, University of Mannheim, L7, 3-5, D-68131 Mannheim, Germany. [2]Indiana University, Bloomington, IN 47408, USA, and Arizona State University, Tempe, AZ 85287, USA. E-mail: bjoern.vollan@uni-mannheim.de; ostrom@indiana.edu

CREDIT: ADAPTED FROM (18) PERMISSION OF PRINCETON UNIVERSITY PRESS

Downloaded from www.sciencemag.org on November 11, 2010

Published by AAAS

ther. There, high livestock density poses a major threat to forests, because the animals browse on young trees. To address this and other problems, officials launched a forest management program that gave Bale Oromo groups common ownership of woodlands, and responsibility for maintaining forest cover. To explore the role of cooperation in the success of these efforts, Rustagi *et al*. first set up "field labs" in a number of villages, and invited residents to play games designed to measure their propensity to cooperate (conditional on others' cooperation). They also conducted surveys that gathered socioeconomic data and information about resource monitoring efforts. Finally, they compared the game results and the survey data from 49 groups to measurements of potential crop trees, an indicator of forest productivity. Overall, they found that the groups with the larger shares of conditionally cooperative members were more likely to be successful in managing their forest commons. They also invested more in "costly" enforcement of cooperation (participating in forest patrols, which promote cooperation by sanctioning free riders).

By establishing this link between the levels of cooperation observed in field labs with local forest conditions, Rustagi *et al*. have increased the confidence that scholars can have in the external validity of results from previous experiments carried out all over the world, with student and nonstudent subjects. In addition, by adding to findings showing diverse levels of cooperation in social dilemmas, rather than no cooperation, they support the growing acceptance of a behavioral theory of human action (*14*): Individuals facing dilemmas, who learn from experience and adopt a norm of conditional cooperation, achieve levels of cooperation that increase over time—if a sufficient number of conditional cooperators are present. If a group is composed of a substantial number of free riders, however, cooperation levels fall over time.

One way of interpreting Rustagi *et al*.'s findings is that learning and norm-adopting individuals are attracted to certain situations, and then are affected by the behavior of other actors facing the same situation (see the figure). Initially, this leads to some degree of cooperation (e.g., acceptance of rules of the forest group, monitoring other users, and helping to maintain their forest). If enough individuals initially cooperate, they slowly obtain benefits from the forest, and levels of cooperation grow. Alternatively, initial cooperation rates can be low, and then can continue to decline over time.

Rustagi *et al*. identify a number of well-known variables that can influence cooperation, including the size of the forest group, its leadership, and the heterogeneity of the group. Other, broader, variables include village elevation and market access, with villages closer to markets for wood products more likely to invest in cooperative management. Other field studies have found that prior experience in cooperative management increases the likelihood of groups successfully managing a resource.

Rustagi *et al*. also found that the share of conditional cooperators in a group is affected by clan affiliation and the leader, who needs to have sufficient prestige to change the norms of the group. Other recent evidence from field experiments shows that resource users responded prosocially to environmental appeals made by park rangers (*15*). More details of cultural effects on cooperation are provided by Prediger *et al*. (*16*), who use a socioecological framework (*17*) to identify main differences between two populations before performing field experiments. They show that historical events that interfere with self-governance, as well as subtle ecological differences, can affect the propensity to cooperate.

More research is needed to explain the factors that produce variation in cooperation. Using multiple methods (*18*) to identify the relevant "microsituational" and broader contextual variables, and using robust econometric methods to link these variables with differences in behavior and real-world outcomes, will constitute a major step in advancing a behavioral theory of human action.

References

1. G. Hardin, *Science* **162**, 1243 (1968).
2. E. Fehr, S. Gächter, *Am. Econ. Rev.* **90**, 980 (2000).
3. E. Ostrom, R. Gardner, J. Walker, *Rules, Games, and Common-Pool Resources* (Univ. of Michigan Press, Ann Arbor, 1994).
4. National Research Council, *Conference on Common Property Resource Management* (National Academies Press, Washington, DC, 1986).
5. National Research Council, *The Drama of the Commons* (National Academies Press, Washington, DC, 2002).
6. J.-M. Baland, J.-P. Platteau, *Halting Degradation of Natural Resources* (Clarendon, Oxford, 2005).
7. E. Ostrom, *Governing the Commons* (Cambridge Univ. Press, New York, 1990).
8. D. Rustagi, S. Engel, M. Kosfeld, *Science* **330**, 961 (2010).
9. J.-C. Cardenas, *Environ. Dev. Sustain.* **2**, 305 (2000).
10. J.-C. Cardenas, *For. Policy Econ.* **6**, 229 (2004).
11. M. A. Velez, J. J. Murphy, J. K. Stranlund, *Econ. Inq.* **48**, 254 (2010).
12. J.-C. Cardenas, J. K. Stranlund, C. E. Willis, *World Dev.* **28**, 1719 (2000).
13. B. Vollan, *Ecol. Econ.* **67**, 560 (2008).
14. C. F. Camerer, *Behavioral Game Theory* (Princeton Univ. Press, Princeton, NJ, 2003).
15. R. Moreno-Sánchez, J. H. Maldonado, *Ecol. Econ.* **69**, 2557 (2010).
16. S. Prediger, B. Vollan, M. Frölich, *Ecol. Econ.* (2010).
17. E. Ostrom, *Science* **325**, 419 (2009).
18. A. Poteete, M. Janssen, E. Ostrom, *Working Together* (Princeton Univ. Press, Princeton, NJ, 2010).

10.1126/science.1198349

CHEMISTRY

Glimpsing the Critical Intermediate in Cytochrome P450 Oxidations

Stephen G. Sligar

The key intermediate in the oxidation of carbon-hydrogen bonds by cytochrome P450 has been characterized.

Almost all living organisms make use of atmospheric oxygen (O_2) for respiration. Another critical role of oxygen is in the partial oxidation of organic compounds, which can remove toxins or create compounds for specialized tasks such as signaling. The enzymes that accomplish this task, the oxygenases, were discovered by Hayaishi in 1955. Among them are the dioxygenases, which insert both of the O atoms into one or more substrates, and the monooxygenases, which incorporate only one of the O atoms into a substrate and reduce the other to water. The cytochrome P450 monooxygenases (P450s) (*1*), crucial to metabolism, can catalyze a most difficult transformation: the oxidation of aliphatic carbon-hydrogen bonds. The structure of a key intermediate in this reaction, a heme iron bearing a single oxygen atom, has eluded chemists for three decades. On page 933 of this issue, Rittle and Green (*2*) used Mössbauer and electron paramagnetic resonance spectroscopy, in concert with optical absorption spectroscopy, to characterize this hot oxidant in P450 catalysis as an Fe(IV)-oxo-porphyrin cation radical.

Department of Biochemistry, University of Illinois, Urbana, IL 61801, USA. E-mail: s-sligar@illinois.edu

Downloaded from www.sciencemag.org on November 11, 2010

Published by AAAS

The P450 heme-containing enzymes were discovered five decades ago; their optical spectroscopic signature—strong absorption at wavelengths of ~450 nm—stood out even in the crude tissue preparations studied at that time. The P450s are now known to be one of the largest superfamilies of proteins, with more than 14,000 genes identified in diverse organisms from all life forms (*3*). They serve two broad functional roles. In catabolic pathways, they initiate the breakdown of environmental compounds, either for use as food or as a means of detoxification. They also serve as the critical steps in the synthesis of secondary metabolites that are often used in signaling. In humans, these roles are represented by the liver and kidney enzymes involved in drug metabolism and in the biosynthesis of steroid hormones in the ovaries, testes, and adrenals. Thus, the P450s have received considerable attention from pharmacologists, toxicologists, biochemists, and chemists since their discovery.

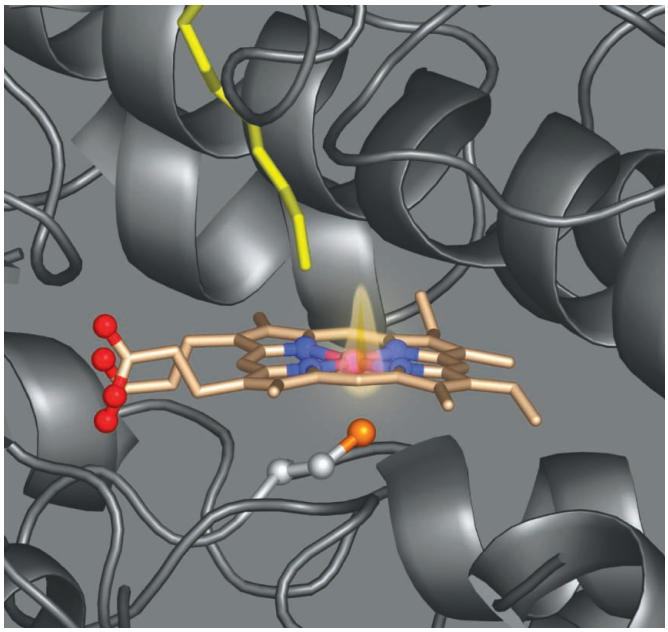

Ready to oxidize. The cytochrome P450 enzymes can oxidize normally unreactive carbon-hydrogen bonds. Their heme iron site binds atmospheric dioxygen (O_2), catalytically breaking the O-O bond and reducing one O atom to form water; the other O atom (shown schematically as the oxidizing flame in the P450 active site) is incorporated into product. In this radical species, this key intermediate resembles "compound I" first seen in peroxidases.

The active site of the P450 protein contains a heme prosthetic group, the same entity as found in the oxygen transport and storage proteins hemoglobin and myoglobin. Like these common heme proteins, P450s bind atmospheric O_2 when the heme iron is reduced. Although the globins and P450s share a common reactivity with O_2 to form an end-on O_2-iron bound state, the distinctive chemical reactivity of the P450s arises from their ability to accept two electrons from a redox partner and catalytically break the O-O bond. The extra reducing equivalents produce a single water molecule. The remaining oxygen atom oxidizes the carbon-hydrogen bond of a substrate.

This difficult chemical transformation raises several questions: What is the electronic structure of the remaining oxygen atom bound to heme, and how is the difficult task of transferring it to a substrate molecule catalyzed? There must be an extremely "hot flame" at the heme active site to be able to oxidize unactivated hydrocarbons (see the figure).

A major breakthrough in understanding P450 chemistry was made by Groves and coworkers in the mid-1970s (*4*, *5*). By determining the stereochemistry of oxygenated products and the kinetic isotope effect, they inferred a stepwise process whereby a P450 heme intermediate containing a single oxygen atom initiated a hydrogen abstraction event. This reaction generated a transient substrate radical that would then recombine quickly to form the oxidized product. This two-step mechanism suggested that the reactive intermediate in P450 catalysis was an iron-oxygen adduct similar to that of the so-called "compound I" intermediate found in the peroxidase class of enzymes. Peroxidases also cycle through various heme iron–oxygen states but with the use of hydrogen peroxide, a reduced form of O_2. Detailed studies of peroxidases, most notably by Debrunner and colleagues (*6*–*8*), defined the electronic structure of this compound I intermediate.

Could this compound I state be the P450 "flame," and would it be possible to form it by adding peroxide or peracid to the ferric enzyme? Many investigators, beginning in the mid-1970s, used rapid reaction methods to try to generate the compound I state by this approach, yet only fleeting glimpses were observed (*9*). A breakthrough in mechanistic investigations of P450 monooxygenases was the crystallographic determination of the ferrous oxygenated intermediate of cytochrome P450 (*10*). It was hoped that a stabilized compound I would be seen via reduction by the x-ray beam at 100 K, but again only a hint of this critical intermediate was seen.

Using the logic that enzymes from organisms that normally function at elevated temperatures may have altered reaction rates that would favor observing this intermediate, our laboratory was able to observe an optical signature that suggested compound I formation in the thermophilic P450 CYP119 (*11*). However, only a relatively small fraction of the heme protein could be caught in this state, perhaps because of the presence of an endogenous substrate at the active site that quickly reacted with the hot oxidant. The optical absorption spectrum of this intermediate, while indicative of a compound I state, was not sufficient proof of its detailed electronic structure or reactivity.

By careful purification of the P450 CYP119 protein, Rittle and Green were able to isolate the compound I state in high yield. They characterized its electronic structure by a variety of spectroscopic tools and found that the P450 compound I was analogous to that previously seen in the peroxidases. These authors not only explain how the protein structure controls the detailed electronic structure of this iron-oxygen adduct, but also demonstrate the chemical competence and large kinetic isotope effect of this P450 state in converting substrates to oxygenated products.

Now that compound I has been definitively observed in the cytochrome P450s, and its immense reactivity in oxidizing carbon substrates quantified, many doors are opened that will lead to an understanding of how the structure of metalloproteins controls the reactivity of O_2. These enzymes are important targets for therapeutic intervention. Understanding the chemical process by which a recalcitrant substrate can be functionalized would also provide key insight into harnessing these biotransformations.

References

1. S. G. Sligar, *Essays Biochem.* **34**, 71 (1999).
2. J. Rittle, M. T. Green, *Science* **330**, 933 (2010).
3. http://drnelson.uthsc.edu/cytochromeP450.html
4. J. T. Groves, G. A. McClusky, *J. Am. Chem. Soc.* **98**, 859 (1976).
5. J. T. Groves, *J. Chem. Educ.* **62**, 928 (1985).
6. C. E. Schulz *et al.*, *FEBS Lett.* **103**, 102 (1979).
7. C. E. Schulz, R. Rutter, J. T. Sage, P. G. Debrunner, L. P. Hager, *Biochemistry* **23**, 4743 (1984).
8. R. Rutter *et al.*, *Biochem. Mol. Biol. Int.* **23**, 6809 (1984).
9. T. Egawa, H. Shimada, Y. Ishimura, *Biochem. Biophys. Res. Commun.* **201**, 1464 (1994).
10. I. Schlichting *et al.*, *Science* **287**, 1615 (2000).
11. D. G. Kellner, S. C. Hung, K. E. Weiss, S. G. Sligar, *J. Biol. Chem.* **277**, 9641 (2002).

10.1126/science.1197881

GRAPHIC COURTESY OF ILIA DENISOV

Downloaded from www.sciencemag.org on November 11, 2010

Published by AAAS

RETROSPECTIVE

Benoît B. Mandelbrot (1924–2010)

Heinz-Otto Peitgen

A mathematician's revelation about visual irregularities in nature spawned the field of fractal geometry, now widely used to interpret patterns in diverse fields.

Fractal geometry was created by Benoît B. Mandelbrot nearly 40 years ago, and with the 1982 publication of his seminal book, "The Fractal Geometry of Nature," its application took off, opening our eyes to patterns in nature on all scales and across diverse disciplines. On 14 October, he died of cancer in Cambridge, Massachusetts. He fundamentally and irrevocably changed our view of the world and left us a tool that will continue to unveil nature's most peculiar commonalities that might otherwise be left aside as insignificant.

Mandelbrot was born in 1924 in Warsaw, Poland. With the rise of Nazism, his family left for France in 1936, where he pursued an education in mathematics and earned a doctorate at the University of Paris in 1952. His career path took him to prominent establishments: the California Institute of Technology, the Institute for Advanced Study in Princeton, the Centre National de la Recherche Scientifique in Paris, IBM Research in New York, Harvard University, the Massachusetts Institute of Technology, and to Yale University (where he retired in 2005).

Whereas the Renaissance saw geometry in the forefront, much of the 19th and 20th century sought an algebraic representation of nearly all mathematical fields. As a result, the patterns and forms that real nature presents were increasingly neglected. Geometry in the ordinary sense was left to school children, and even school mathematics departed from geometry in favor of an algebraic and abstract underpinning of curricula. Mandelbrot always felt this view was narrow and inappropriate for understanding nature. After decades of a mathematical trend to abandon visual representation of phenomena, which was spurred by French mathematicians (the so-called Bourbaki group) in the mid-1930s, Mandelbrot gave the eye a central role again.

His whole career became one long and ardent pursuit of the concept of "roughness"—the roughness of clusters in the physics of disorder, of turbulent flows, of exotic noises, of chaotic dynamical systems, of distributions of galaxies, of coastlines, of stock-price charts, and of mathematical constructions. Some describe Mandelbrot as one who chose the role of a maverick in the mainstream sciences. Quite to the contrary, his uncompromising devotion to analyze and understand the "rough" reality of nature isolated him from the mainstream. In his view, the common "smooth" representations of natural processes were entirely inappropriate and far from the essence of nature: "Clouds are not spheres and mountains are not cones." Alone, he shaped a program of geometry based on fractals, a term he coined to refer to mathematical shapes with irregular contours, just as seen in nature. The notion of self-similarity is key in fractal geometry: geometric shapes that break into parts, each a small-scale model of the whole.

His mathematical sources were deeply rooted in the entire history of mathematics, notably the work of Felix Hausdorff and Paul Lévy, and the "Mandelbrot set" that bears his name would likely not have been discovered without his peculiar contact with some forgotten jewels of mathematics produced at the turn of the 19th century by Gaston Julia and Pierre Fatou. He told me that his uncle, Szolem Mandelbrojt, had almost forced him to study their papers as the best introduction to good mathematics. In fact, his uncle, a traditional mathematician, student of Jacques Hadamard, and member of the Collège de France, sought to eradicate Benoît's preference for a geometric approach to mathematics. Fortunately, Mandelbrot's advocacy for geometry was without compromise.

The mathematical genre of Julia and Fatou has experienced a great revival through Mandelbrot, and their topic—iteration—became a guiding principle for his own discovery and work. Whereas classical geometry and many of its modern algebraic and other extensions encode objects from closed elementary formulas to differential equations, Mandelbrot made us aware of a mathematical universe yet to be harvested—the world of iterative processes. Within this framework, he developed the tools that appear ideally suited for the rough nature of the world. And "world" is meant literally, because his footprints are left in the theory of finance, linguistics, biology, medicine, chemistry, physics, earth science, cosmology, computer science, astronomy, many of the engineering disciplines, and of course, mathematics.

The Mandelbrot set provides perhaps the most striking example of a mathematical object whose properties would remain undiscovered without the guiding power of the human eye used by an able mathematician. For example, the key for understanding the myriads of patterns that sprout at the boundary of the Mandelbrot set is governed by a peculiar mathematical coding scheme within the field lines of its potential. Mandelbrot earned not only the credit for its discovery but also for expressing provocative mathematical conjectures about its properties. For instance, he proposed that the boundary of the Mandelbrot set, which exhibits all the marvelous and seemingly complex images that turned it into a cult object, has a fractal dimension of only two.

Now that Mandelbrot's work can be considered to belong to mainstream mathematics and the sciences, it is important to remember that there was once strong resistance and skepticism. I have often asked myself where Mandelbrot found the source of his strength, determination, and endurance in those decades when he was practically isolated in his own mathematical world. He used to claim that his geometrical view and associated gifts guided him and that he did not feel isolated at all. I would add that his pristine character as someone who sought the truth in life and nature led him as well. Moreover, I remember Benoît as a universal scientist and very conscious citizen of the world, knowledgeable and sharp in all branches of the sciences and beyond: the arts, politics, and history. It will take further generations to grasp the full significance and impact of his insight far beyond the borders of mathematics.

His personal history left him as someone who was fortunate to escape the darkest periods of mankind. He chose to remain forever suspicious toward any form of establishment and mainstream.

Department of Mathematics and Biomedical Sciences, University of Bremen and Florida Atlantic University, Fraunhofer MEVIS, D-28359 Bremen, Germany. E-mail: peitgen@mevis.de

10.1126/science.1199471

CREDIT: RAMA/WIKIPEDIA

Downloaded from www.sciencemag.org on November 11, 2010

Published by AAAS

Science
AAAS

Amazonia Through Time: Andean Uplift, Climate Change, Landscape Evolution, and Biodiversity
C. Hoorn, *et al.*
Science **330**, 927 (2010);
DOI: 10.1126/science.1194585

This copy is for your personal, non-commercial use only.

If you wish to distribute this article to others, you can order high-quality copies for your colleagues, clients, or customers by clicking here.

Permission to republish or repurpose articles or portions of articles can be obtained by following the guidelines here.

The following resources related to this article are available online at www.sciencemag.org (this information is current as of November 11, 2010):

Updated information and services, including high-resolution figures, can be found in the online version of this article at:
http://www.sciencemag.org/cgi/content/full/330/6006/927

Supporting Online Material can be found at:
http://www.sciencemag.org/cgi/content/full/330/6006/927/DC1

This article **cites 57 articles**, 18 of which can be accessed for free:
http://www.sciencemag.org/cgi/content/full/330/6006/927#otherarticles

This article appears in the following **subject collections**:
Evolution
http://www.sciencemag.org/cgi/collection/evolution

Downloaded from www.sciencemag.org on November 11, 2010

Science (print ISSN 0036-8075; online ISSN 1095-9203) is published weekly, except the last week in December, by the American Association for the Advancement of Science, 1200 New York Avenue NW, Washington, DC 20005. Copyright 2010 by the American Association for the Advancement of Science; all rights reserved. The title *Science* is a registered trademark of AAAS.

Amazonia Through Time: Andean Uplift, Climate Change, Landscape Evolution, and Biodiversity

C. Hoorn,[1]* F. P. Wesselingh,[2] H. ter Steege,[3] M. A. Bermudez,[4] A. Mora,[5] J. Sevink,[1] I. Sanmartín,[6] A. Sanchez-Meseguer,[6] C. L. Anderson,[6] J. P. Figueiredo,[7] C. Jaramillo,[8] D. Riff,[9] F. R. Negri,[10] H. Hooghiemstra,[1] J. Lundberg,[11] T. Stadler,[12] T. Särkinen,[13] A. Antonelli[14]*†

The Amazonian rainforest is arguably the most species-rich terrestrial ecosystem in the world, yet the timing of the origin and evolutionary causes of this diversity are a matter of debate. We review the geologic and phylogenetic evidence from Amazonia and compare it with uplift records from the Andes. This uplift and its effect on regional climate fundamentally changed the Amazonian landscape by reconfiguring drainage patterns and creating a vast influx of sediments into the basin. On this "Andean" substrate, a region-wide edaphic mosaic developed that became extremely rich in species, particularly in Western Amazonia. We show that Andean uplift was crucial for the evolution of Amazonian landscapes and ecosystems, and that current biodiversity patterns are rooted deep in the pre-Quaternary.

Pleistocene forest remnants ("refugia") were long held to be responsible for Amazonian diversity (*1*). In the 1990s the centers of diversity, postulated as prime evidence for the refuge theory, were shown to be sampling artifacts (*2*). Over time, the theory was abandoned and an older origin for the Amazonian diversity was proposed (*3*). Perhaps more important, regional diversification events, as inferred from the fossil record and molecular phylogenetic studies, mostly predate the Pleistocene (*4*, *5*). Although the mechanisms of diversification remain elusive and speciation may occur with barriers (*6*) and even without clear barriers (*7*), it is now generally acknowledged that the development of Amazonian biota has been a long and complex process (*3*, *8*).

At the global scale, the Neogene (the 20 million years that preceded the Pleistocene) was a defining period during which much of the present geography and biotic composition was formed (*9*). The process of species diversification is strongly linked to tectonism and climate, both in the terrestrial (*10*, *11*) and marine realms (*12*). The dynamic geologic history of South America should thus be very relevant for understanding the origins of the present diversity.

Recent advances in the fields of Andean and Amazonian geology and phylogenetics have proceeded in parallel. The geosciences community provided new data on mountain building in the Andes and on the timing and types of biotic and paleoenvironmental changes in lowland Amazonia. Climatologists modeled the atmospheric patterns that resulted from the formation of the Andean orographic barrier. At the same time, new molecular analyses based on DNA sequence variation of living organisms shed further light on the sequence and approximate timing of diversifications.

These new data made it clear that the Cenozoic uplift history of the Andes and its effect on regional climate (*13*, *14*) has had a large impact on the landscape evolution in entire northern South America, including Amazonia (*15*, *16*). Although links between the Andean orogeny and neotropical diversification have long been suggested (*17*), only recently have researchers started to explore dated phylogenetic trees [e.g., (*18*, *19*)], in combination with more realistic, complex geological scenarios (*8*, *20*).

Here, we review the timing and extent of mountain building in northern South America and compare it with geologic evidence from sedimentary basins in Amazonia. We explore the origins of Amazonian ecosystems and biodiversity with the use of a combination of geologic (including paleontologic) and ecologic data sets as well as dated molecular phylogenies. Through schematic representation of these findings, we summarize the geologic evolution of this area, outline the age structure of its biodiversity, and provide a guideline for future integrated geologic, biogeographic, and conservation studies.

Amazonia Prior to Andean Influence: An Ancient, River-Dominated Landscape

The area known today as Amazonia was once part of a much larger "pan-Amazonian" region, which, before the late Miocene [until 10 million years ago (Ma)], included the area of the present Amazon, Orinoco, and Magdalena drainage basins (Fig. 1A). At times this region extended to the south, into the northern Paraná region (*21*). We call this vast area pan-Amazonia because we know from the fossil record that a diverse fauna existed, elements of which are now restricted to Amazonia.

Most of Amazonia's geologic history was centered on the Amazon Craton, the hard rock core in the eastern part of South America, but this situation changed during the course of the Cenozoic. Following continental breakup (135 to 100 Ma), both the growing Atlantic Ocean and plate tectonic adjustments along the Pacific margin (*22*) caused deformation within the Amazon Craton, and later the formation of the Andes (figs. S1 to S4) (*23*). Archives of this regional history are stored within a series of north-south–trending foreland basins along the Andes, in the east-west–trending intracratonic basins, and in the Amazon submarine fan in the Atlantic (*24*–*26*).

Testimony to the post-breakup changes on the craton are alluvial and braided river deposits of Cretaceous age that accumulated in the east-west–stretching sedimentary basins. These drainage systems were captured in a "reversed" trunk river with westward flow (*27*), quite dissimilar from the present Amazon River. The drainage divide was initially situated in eastern Amazonia, but during Paleogene times (~65 to 23 Ma) it migrated westward (*25*, *28*), giving way to the precursor of the modern lower Amazon River (Fig. 1, A and B). Toward the end of the Paleogene, the continental divide was located in Central Amazonia and separated east- and west-flowing Amazonian rivers (*24*).

During the Paleogene, the western and northwestern parts of the pan-Amazonian lowlands were characterized by alternating fluvial conditions and marginal marine embayments (*26*). Fossils show that a diverse mammalian fauna including rodents, marsupials, ungulates, and xenarthrans existed in the central-western part of pan-Amazonia [e.g., (*29*)]. Paleogene fossils also reveal diversification of a variety of freshwater catfishes, characins, and cichlids now prominent in Amazonian waters

[1]Paleoecology and Landscape Ecology, Institute for Biodiversity and Ecosystem Dynamics (IBED), University of Amsterdam, Science Park 904, 1098 XH Amsterdam, Netherlands. [2]Nederlands Centrum voor Biodiversiteit Naturalis, P.O. Box 9517, 2300 RA Leiden, Netherlands. [3]Institute of Environmental Biology, Department of Biology, Faculty of Science, Utrecht University, Padualaan 8, 3584 CH Utrecht, Netherlands. [4]Laboratorios de Termocronología y Geomatemáticas, Escuela de Geología, Minas y Geofísica. Facultad de Ingeniería, Universidad Central de Venezuela, Postal Code 1053, Caracas, Venezuela. [5]ECOPETROL, Instituto Colombiano del Petroleo, Piedecuesta, Santander, Colombia. [6]Real Jardin Botanico, CSIC, Plaza de Murillo 2, 28014 Madrid, Spain. [7]Petroleo Brasileiro SA (Petrobras), Av. Republica do Chile, 330, 14o Andar, CEP 20.031-170, Rio de Janeiro, Brazil. [8]Smithsonian Tropical Research Institute, Box 0843-03092, Balboa, Republic of Panama. [9]Instituto de Biologia, Universidade Federal de Uberlândia, Campus Umuarama, Bloco 2D-sala 28, Rua Ceará s/n, Bairro Umuarama, Uberlândia, CEP 38400-902, Minas Gerais, Brazil. [10]Laboratório de Paleontologia, Campus Floresta, Universidade Federal do Acre, Estrada do Canela Fina, Km 12, Cruzeiro do Sul, Acre, CEP 69980-000, AC, Brazil. [11]Department of Ichthyology, Academy of Natural Sciences, 1900 Benjamin Franklin Parkway, Philadelphia, PA 19103, USA. [12]Institute of Integrative Biology, ETH Zürich, Universitätsstrasse 16, 8092 Zürich, Switzerland. [13]Department of Plant Sciences, University of Oxford, South Parks Road, Oxford OX1 3RB, UK. [14]Institute of Systematic Botany, University of Zürich, Zollikerstrasse 107, CH 8008 Zürich, Switzerland.

*To whom correspondence should be addressed. E-mail: carina.hoorn@milne.cc (C.H.); alexandre.antonelli@vgregion.se (A.A.)

†Present address: Gothenburg Botanical Garden, Carl Skottsbergs Gata 22A, 413 19 Göteborg, Sweden, and Department of Plant and Environmental Sciences, University of Gothenburg, Carl Skottsbergs Gata 22B, 413 19 Göteborg, Sweden.

Downloaded from www.sciencemag.org on November 11, 2010

(*21*, *30*). Typical South American mammals such as the xenarthrans (sloths, armadillos, and anteaters), as well as podocnemidid turtles and plant groups such as *Nothofagus*, *Araucaria*, *Gunnera*, and Winteraceae, may have colonized South America through the southern "Gondwanan" connection with Antarctica and Australia, which lasted until the Late Eocene (*31*–*33*). But the role of dispersal versus vicariance in shaping disjunct distributions in the southern hemisphere is intensely debated. Despite continental isolation to the north lasting until the Pliocene, waves of immigrants (e.g., bats and plant families such as Malpighiaceae, Fabaceae, Annonaceae, and Rubiaceae) arrived from the boreotropical regions while caviomorph rodents and platyrrhine primates possibly crossed the Atlantic from Africa (Fig. 2A).

Andean Uplift, a Major Driver for Change in the Amazonian Landscape and Biota

Uplift in the Central and Northern Andes was a partially synchronous process caused by plate tectonic readjustments [(*23*); see also references in (*16*)]. Plate subduction along the Pacific margin caused uplift in the Central Andes during the Paleogene [65 to 34 Ma; see references in (*14*, *16*)]. Posterior plate breakup in the Pacific (~23 Ma) and subsequent collision of the new plates with the South American and Caribbean plates resulted in intensified mountain building in the Northern Andes (figs. S1 to S4) (*16*). Mountain building first peaked in this region by the late Oligocene to early Miocene (~23 Ma), at an age

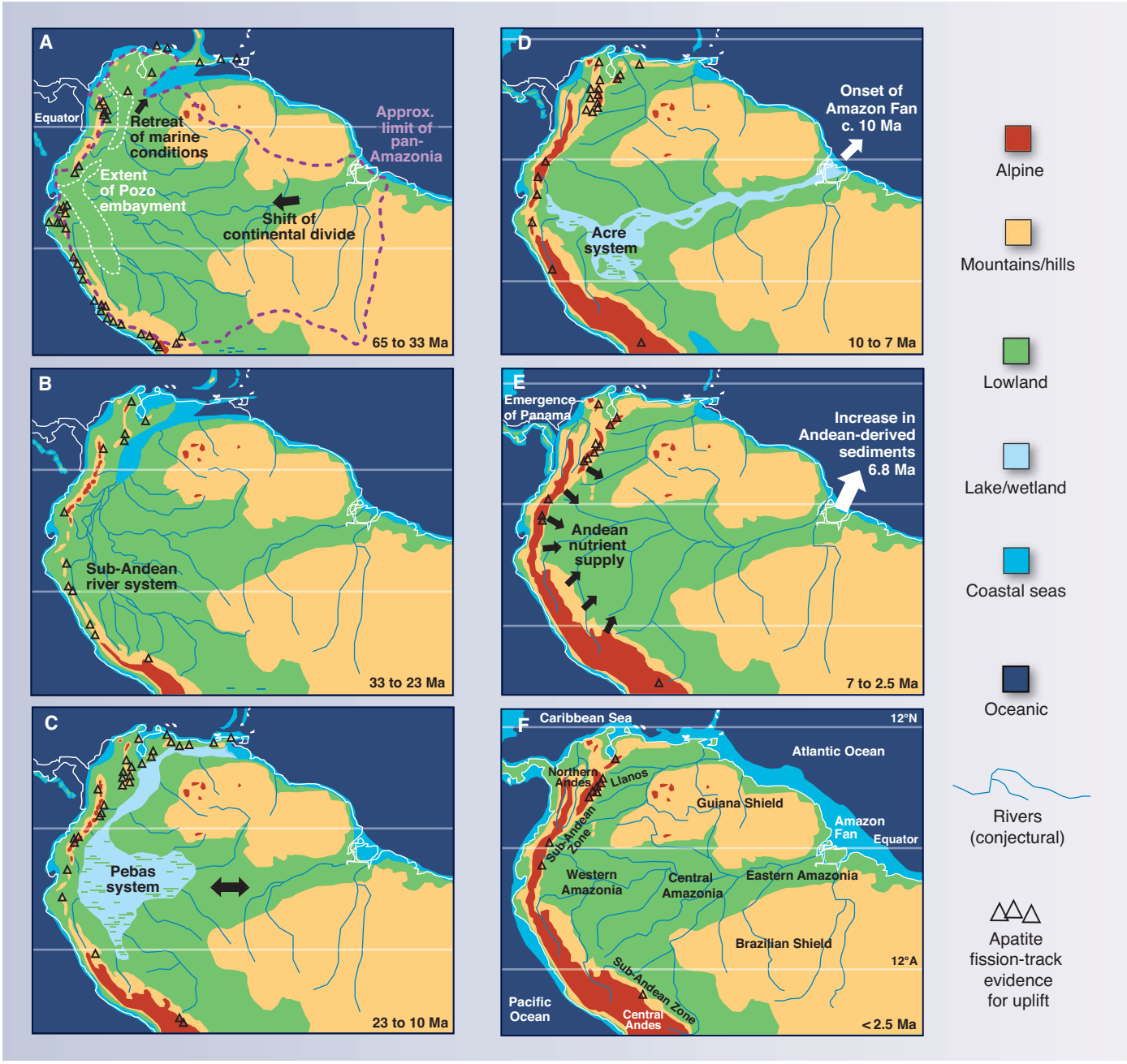

Fig. 1. Paleogeographic maps of the transition from "cratonic" (**A** and **B**) to "Andean"-dominated landscapes (**C** to **F**). (A) Amazonia once extended over most of northern South America. Breakup of the Pacific plates changed the geography and the Andes started uplifting. (B) The Andes continued to rise with the main drainage toward the northwest. (C) Mountain building in the Central and Northern Andes (~12 Ma) and wetland progradation into Western Amazonia. (D) Uplift of the Northern Andes restricted "pan-Amazonia" and facilitated allopatric speciation and extirpation [e.g., (*21*)]. (E) The megawetland disappeared and *terra firme* rainforests expanded; closing of Panama Isthmus and start of GABI. (F) Quaternary. Note that South America migrated northward during the course of the Paleogene.

Downloaded from www.sciencemag.org on November 11, 2010

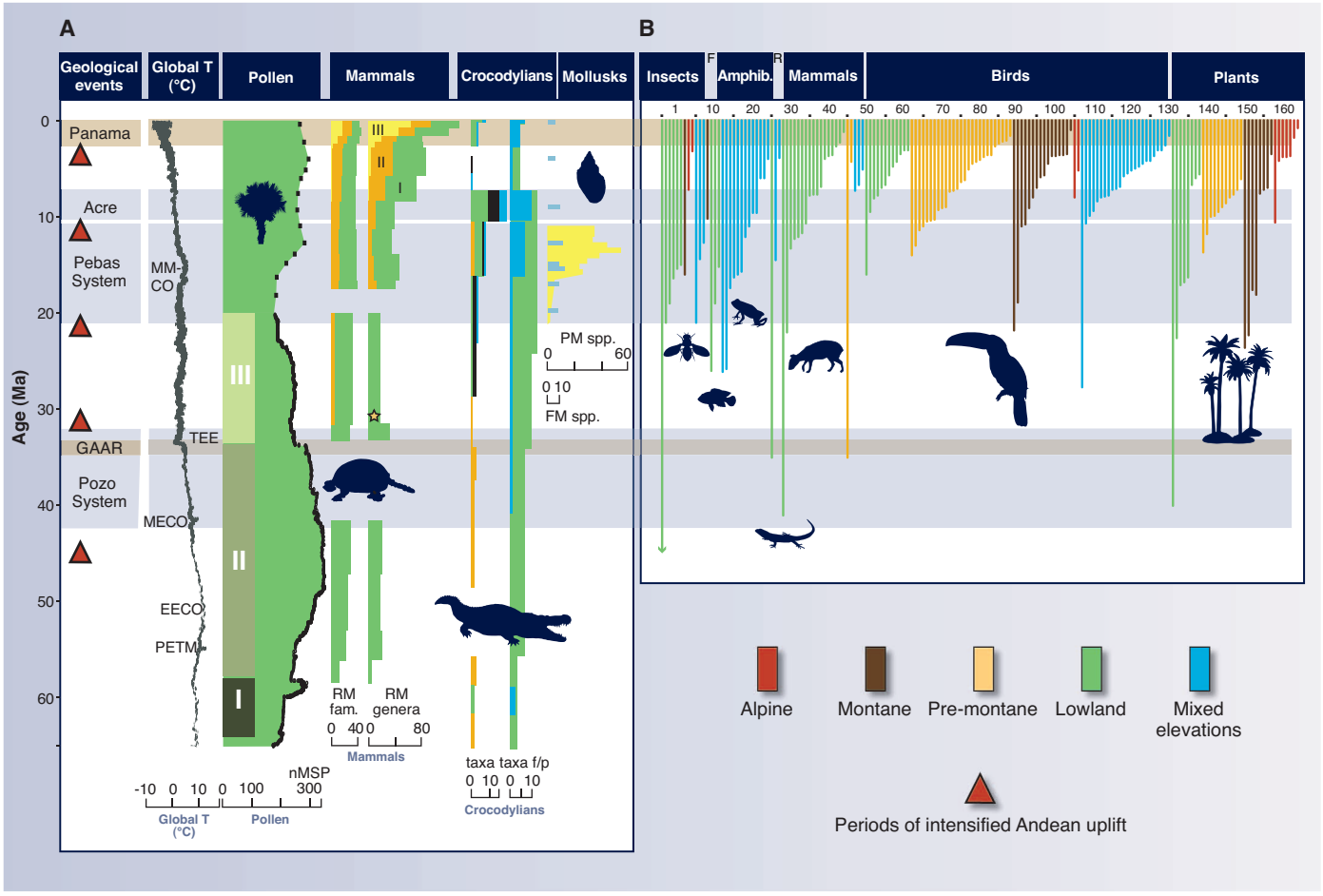

Fig. 2. Biotic changes in Amazonia through time (*23*). (**A**) The Cenozoic fossil record of the tropical lowlands reveals the timing of biotic turnover. Paleogene floral diversity (from pollen records) increased with high temperature, but in the Neogene it was unrelated and remained relatively high even under cooler conditions. Mollusks and crocodiles diversified with the onset of the Miocene megawetlands and declined with its demise. The fossil record, as is shown for the caimanine crocodiles (blue in the right column), is nonetheless incomplete when compared to minimum expected numbers of species (green in the right column) derived from phylogenetic reconstructions (*23*). Late Neogene mammal diversification was particularly strong among North American derived taxa. MMCO, Middle Miocene Climate Optimum; PETM, Paleocene-Eocene Thermal Maximum; MECO, Middle Eocene Climate Optimum; EECO, Early Eocene Climate Optimum; TEE, Terminal Eocene Event; GAAR, Greater Antilles-Aves Ridge; nMSP, number of pollen morphospecies; RM, running mean; f/p, from the fossil record or as based on caimanine phylogeny; FM, fluvial mollusk; PM, Pebasian endemic mollusk species. Crocodylians: Left column, number of species from fossil record; right column, number of caimanine species from fossil record versus number of lineages (orange, non-eusuchian crocodyliforms; green, Caimaninae; black, Gavialoidea; blue, Crocodylidae). Global temperature curve is based on (*68*). Abbreviations are further explained in (*23*). (**B**) Diversification of modern lineages revealed from molecular phylogenies. The lines illustrate the approximate timing of diversification for genera of animals and plants in northern South America, in relation to the elevation zone they inhabit (lowland, 0 to 500 m; premontane, 500 to 1500 m; montane, 1500 to 3000 m; alpine, 3000 to 4800 m). Nearly all living genera in northern South America have a pre-Quaternary origin, but ages of taxa differ between major elevation zones. Several highland genera are fairly young; lowland genera are a mixture of young and old lineages. Numbers above individual lines refer to table S1, where additional details are given.

that coincides with the diversification of the first modern montane plant and animal genera (Fig. 2B). However, the most intense peaks of Andean mountain building followed during the late middle Miocene (~12 Ma, Fig. 1C) and early Pliocene (~4.5 Ma, Fig. 1E and figs. S3 to S5) (*16*). Plate reorganization ultimately resulted in closing of the Panama Isthmus during the Pliocene (at ~3.5 Ma) (*34*) and led to the Great American Biotic Interchange (see below).

Mountain building in the Andes generated tectonic load and renewed accommodation space in the adjacent foreland basins. As mountain building progressed and a critical elevation (~2000 m; figs. S3 to S5) was surpassed, rainfall increased along the eastern flank. This coupling of tectonic and climatic processes resulted in further uplift, erosion, and water and sediment supply (*13*, *14*, *35*) and is in accordance with changes in the depositional record of the Andean foreland and Amazonia (fig. S5). However, the Andean sediment flux that engulfed lowland Amazonia (*36*) was not continuous; intramontane basins and perimontane basins may have captured influx for periods of millions of years, resulting in pulses of deposition eastward.

Parallel to intensified uplift in the Andes, a large wetland of shallow lakes and swamps developed in Western Amazonia (Fig. 1C) (*37*). These new aquatic environments of the "Pebas" system were colonized by rapidly radiating endemic invertebrate faunas composed of mollusks and ostracods (*38*). This was also the stage for a diverse reptile fauna including gharials, caimans, and turtles (Fig. 2A). One of the most remarkable representatives of this now-extinct fauna was *Purussaurus,* the largest known caiman, which reached ~12 m in length (*39*).

The wetland fragmented the preexisting rainforests, yet a diverse forest that already bore resemblance to the modern forest (in terms of plant family composition) remained at the margins of this new aquatic system (*15*, *40*). Although lower than in the Paleogene, plant diversity (as indicated by pollen types) peaked at 13 Ma, near the end of

Downloaded from www.sciencemag.org on November 11, 2010

the Middle Miocene Climatic Optimum (Fig. 2A). Geochemical evidence from mollusk shells further indicates that a modern type of monsoonal climate was already present and provided a seasonal water influx into the wetland system (*41*). Terrestrial taxa such as xenarthrans, *Gonatodes* geckos, and leaf beetles, as well as cichlid fish in the aquatic environments, lived and diversified in the wetlands (Fig. 2B and table S1).

Taxa of marine ancestry in the Miocene (*42*) or earlier (*43*), such as potamotrygonid stingrays, thrived in the Amazonian freshwater wetlands. Periods with somewhat elevated salinities are also indicated by benthic foraminifera, barnacles, (marginal) marine mollusks, and the geochemical signature in the mollusk shells (*44*). These marine invertebrates, however, were Neogene arrivals and disappeared with the withdrawal of marginal marine conditions. Other indicators of marine influence in the wetlands were dinoflagellates, pollen from mangrove trees, and marine ichnofossils. Biogeographic reconstructions based on phylogenies also fit this scenario (*8*, *20*, *42*). Despite such evidence, the extent of marine influence in Amazonia is still debated (*45*).

By the end of the middle Miocene (~12 Ma), faster and more widespread Andean mountain building prompted peak topographic growth. This created deep canyon incision and erosion in the Central and Northern Andes, especially in the Eastern Cordilleras and in the Venezuelan Andes (figs. S1 to S4) (*16*, *46*), where alluvial megafans developed (*47*, *48*). It also coincided with raised sedimentation rates in the Andean foreland basins that eventually became overfilled. At ~10 Ma, coinciding with global sea level drop and climate cooling, Andean sediments reached the Atlantic coast through the Amazon drainage system, and the Amazon River became fully established at ~7 Ma (*24*, *49*).

Meanwhile, the Western Amazonian wetland changed from a lacustrine to a fluvial or fluviotidal system (Fig. 1D) (*37*, *45*, *50*), which resembled the present-day Pantanal in southern Amazonia (*45*). This so-called "Acre" system harbored a very rich aquatic vertebrate fauna that included mega-sized gharials, caimanines, and side-neck turtles (*39*), which eventually declined with the disappearance of megawetlands in Western Amazonia at ~7 Ma (Fig. 2A) (*21*, *38*, *39*). Most of the endemic mollusk fauna was unable to adapt to the initial fluvial conditions and was strongly reduced around 10 Ma (*38*). The floodplains of this system were dominated by grasses (*51*) and were inhabited by a more diverse xenarthran fauna than at present (*52*).

Preliminary palynological evidence indicates a ~10 to 15% increase of plant diversity between ~7 and 5 Ma, shortly after the wetlands were replaced by forested habitats (Fig. 2A). Molecular studies of tree genera such as *Guatteria* (Annonaceae, ~250 species) and *Inga* (Fabaceae, ~300 species) show a similar trend of rapid diversification following the demise of Amazonian wetlands (*53*, *54*). This suggests that the establishment of terrestrial conditions in Western Amazonia may have been an important prerequisite for the diversification of the current biota of this region. However, the actual triggers of speciation in these and other cases may have been much more complex, involving factors such as soil adaptation and plant-herbivore interactions (*55*).

Western Amazonia from then on bore the key geographic features of the landscape as we know it today (Fig. 1, E and F). It had changed from a drowning, negative relief into a positive relief incised by an increasingly entrenched river system with high sediment load. By the late Miocene, good swimmers such as proboscideans had crossed the relatively small seaway that remained between Central and South America and were at the forefront of a major immigration wave (*56*, *57*).

The final scenes of this history are characterized by further Andean uplift (Fig. 1F), closure of the Panama Isthmus (~3.5 Ma), the Quaternary ice ages (2.5 to 0.01 Ma), and restriction of megafans in the foreland basin zone. This, together with neotectonic processes in Amazonian lowlands (*28*), caused uplift of the Neogene deposits, development of widespread river terrace systems, and readjustments of river patterns, and led to the mosaic-type landscape of the present (*58*). The accelerated uplift phases during the last 10 Ma fostered spectacular radiations of highland plants such as lupines (*59*), as well as tanagers, bumblebees, and some rodents (Fig. 2B and table S1). This was also a time of extensive migration, when both Amazonia and the new montane habitats in the Andes were colonized by taxa of North American descent during the Great American Biotic Interchange (GABI) (*56*).

The GABI caused decline in the number of endemic South American mammal families during the Pliocene and especially the Quaternary. However, the overall generic diversity of South American mammal taxa remained stable, and the total number of genera increased by the strong diversification of taxa derived from North American immigrants (*56*) (Fig. 2A). Molecular studies suggest that many bird lineages also took part in the GABI (*60*, *61*). By contrast, plants have been more capable of overseas dispersal, and many lineages crossed the Panama Isthmus before its final closure (*62*), whereas others probably reached South America directly from Africa (*63*). These results, based on molecular and fossil studies, suggest that immigrants from other landmasses have played an important role in the historic assembly of the Amazonian biota (*64*).

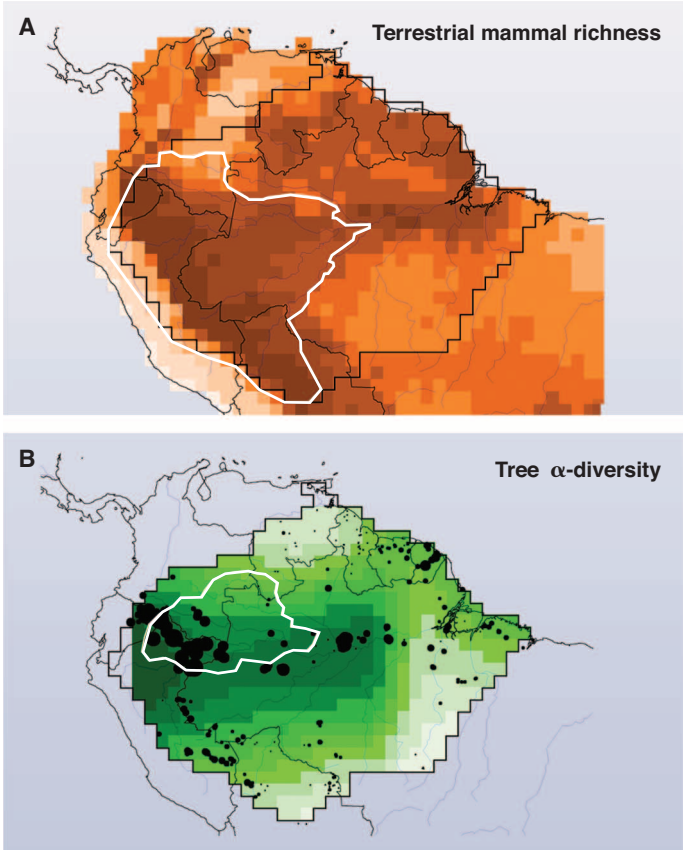

Fig. 3. Present Amazonian diversity patterns. See figs. S6 and S7 for depictions of the close relationship among Amazonian geology, soils, climate, and diversity. (**A**) Terrestrial mammal richness (range: lightest color, 2 to 10 species; darkest, 89 to 109 species) (*69*); white polygon denotes relatively rich soils (fig. S6C). (**B**) Tree α-diversity (*66*). Black dots: local tree α-diversity on 1-ha plots (n = 752); Fisher's α ranges from 3.6 to 300; green shades: loess spatial interpolation of 1-ha values (6 to 117); white polygon: area of least severe water shortage (see fig. S6D).

Can Geologic History Help Us Understand Present Biodiversity in Amazonia?

A comparison of present biodiversity patterns with geologic and edaphic units shows that the highest concentrations of terrestrial mammal and amphibian richness are found on Western Amazonian soils that developed on the Neogene (Andean) sediments (Fig. 3A and figs. S6 and S7). These soils show much higher variation in levels of nutrients and are in stark contrast to generally nutrient-poor soils on the craton in Eastern Amazonia (*65*). Forest productivity and forest dy-

Downloaded from www.sciencemag.org on November 11, 2010

namics are also higher on these soils (fig. S8), which suggests that bedrock composition, diversity, and ecosystem productivity are interrelated (*66*).

Water geochemistry, sediment composition, and fertility of floodplains further confirm the disproportionate richness in nutrients of the Andean system versus the relative nutrient poverty in the "cratonic" aquatic system (*67*). It seems paradoxical that the old Amazon Craton, which had the opportunity to accumulate taxa for a much longer period than the young areas in Western Amazonia, has fewer species, genera, and families.

Nutrients and habitat heterogeneity are paramount in Amazonian diversity, but they are not the only ingredient. Tree α-diversity (i.e., the diversity measured on 1-ha plots) peaks in the wetter, less seasonal part of Western Amazonia (Fig. 3B), which suggests a role for climate in sustaining (and perhaps also driving) diversity (*66*). By contrast, the highest levels of mammal diversity appear little affected by rainfall seasonality, from aseasonal Ecuador down to highly seasonal Bolivia (Fig. 3A and fig. S6D); this suggests that additional factors such as productivity need to be considered.

Although the transition from a "cratonic" to an "Andean"-dominated system was a fundamental change in the evolution of Amazonian landscapes and species composition, all data suggest that this switch was a complex, stepwise process. Species accumulation was driven by more than one single, overarching mechanism, and Amazonian biodiversity was certainly not a by-product of just Pleistocene ice ages, but resulted from a much more extended period of evolution. However, after the draining of the wetlands (late Miocene), diversification in Western Amazonia must have been particularly rapid, as the diversity of this area greatly outnumbers the diversity in the cratonic areas.

Many outstanding research questions concerning Amazonia remain. Understanding the mechanisms that underlie the assembly and evolution of Amazonian biodiversity continues to be a major challenge that will require hitherto unrealized interdisciplinary scientific collaboration. Evolutionary studies linked to molecular phylogenies and fossil assemblages should focus on Neogene records and on species-rich but poorly sampled areas. Future research should be concentrated on the interface between the Cenozoic and cratonic areas, and on the transition zone between the Andes and Western (lowland) Amazonia (fig. S6). This area, together with the southern fringe of Amazonia, has become rapidly occupied by humans but nonetheless remains scientifically poorly known.

References and Notes

1. J. Haffer, *Science* **165**, 131 (1969).
2. B. W. Nelson, C. A. C. Ferreira, M. F. da Silva, M. L. Kawasaki, *Nature* **345**, 714 (1990).
3. M. B. Bush, *J. Biogeogr.* **21**, 5 (1994).
4. C. Jaramillo, M. J. Rueda, G. Mora, *Science* **311**, 1893 (2006).
5. V. Rull, *Mol. Ecol.* **17**, 2722 (2008).
6. F. E. Hayes, J. A. N. Sewlal, *J. Biogeogr.* **31**, 1809 (2004).
7. M. A. M. de Aguiar, M. Baranger, E. M. Baptestini, L. Kaufman, Y. Bar-Yam, *Nature* **460**, 384 (2009).
8. J. C. Santos *et al.*, *PLoS Biol.* **460**, e1000056 (2009).
9. P. E. Potter, P. Szatmari, *Earth Sci. Rev.* **96**, 279 (2009).
10. M. J. Kohn, T. J. Fremd, *Geology* **36**, 783 (2008).
11. J. A. Finarelli, C. Badgley, *Proc. Biol. Sci.* **277**, 2721 (2010).
12. W. Renema *et al.*, *Science* **321**, 654 (2008).
13. N. Insel, C. J. Poulsen, T. A. Ehlers, *Clim. Dyn.* (2009).
14. C. J. Poulsen, T. A. Ehlers, N. Insel, *Science* **328**, 490 (2010); 10.1126/science.1185078.
15. C. Hoorn, *Palaeogeogr. Palaeoclimatol. Palaeoecol.* **105**, 267 (1993).
16. A. Mora *et al.*, in *Amazonia, Landscape and Species Evolution*, C. Hoorn, F. P. Wesselingh, Eds. (Wiley, Oxford, 2010), pp. 38–60.
17. A. H. Gentry, *Ann. Mo. Bot. Gard.* **69**, 557 (1982).
18. J. S. Albert, N. R. Lovejoy, W. G. R. Crampton, *J. S. Am. Earth Sci.* **21**, 14 (2006).
19. R. T. Brumfield, S. V. Edwards, *Evolution* **61**, 346 (2007).
20. A. Antonelli, J. A. A. Nylander, C. Persson, I. Sanmartín, *Proc. Natl. Acad. Sci. U.S.A.* **106**, 9749 (2009).
21. J. G. Lundberg *et al.*, in *Phylogeny and Classification of Neotropical Fishes*, M. Malabarba, R. E. Reis, R. P. Vari, Z. M. Lucena, C. A. S. Lucena, Eds. (Edipucrs, Porto Alegre, Brazil, 1998), pp. 13–48.
22. B. L. Isacks, *J. Geophys. Res.* **93**, 3211 (1988).
23. See supporting material on *Science* Online.
24. J. Figueiredo, C. Hoorn, P. van der Ven, E. Soares, *Geology* **37**, 619 (2009).
25. J. R. Wanderley-Filho, J. F. Eiras, P. R. da Cruz-Cunha, P. H. van der Ven, in *Amazonia, Landscape and Species Evolution*, C. Hoorn, F. P. Wesselingh, Eds. (Wiley, Oxford, 2010), pp. 29–37.
26. M. Roddaz *et al.*, in *Amazonia, Landscape and Species Evolution*, C. Hoorn, F. P. Wesselingh, Eds. (Wiley, Oxford, 2010), pp. 61–88.
27. R. W. Mapes, thesis, University of North Carolina at Chapel Hill (2009).
28. J. B. Sena Costa, R. Léa Bemerguy, Y. Hasui, M. da Silva Borges, *J. S. Am. Earth Sci.* **14**, 335 (2001).
29. K. E. Campbell Jr., Ed., *The Paleogene Mammalian Fauna of Santa Rosa, Amazonian Peru* (Natural History Museum of Los Angeles County, Los Angeles, 2004).
30. M. C. Malabarba, L. R. Malabarba, C. Del Papa, *J. Vertebr. Paleontol.* **30**, 341 (2010).
31. S. F. Vizcaíno, G. J. Scillato-Yané, *Antarct. Sci.* **7**, 407 (1995).
32. I. Sanmartín, F. Ronquist, *Syst. Biol.* **53**, 216 (2004).
33. B. P. Noonan, P. T. Chippindale, *Am. Nat.* **168**, 730 (2006).
34. A. G. Coates *et al.*, *Geol. Soc. Am. Bull.* **104**, 814 (1992).
35. M. R. Strecker *et al.*, *Geology* **37**, 643 (2009).
36. R. Aalto, T. Dunne, J.-L. Guyot, *J. Geol.* **114**, 85 (2006).
37. C. Hoorn, F. P. Wesselingh, J. Hovikoski, J. Guerrero, in *Amazonia, Landscape and Species Evolution*, C. Hoorn, F. P. Wesselingh, Eds. (Wiley, Oxford, 2010), pp. 123–142.
38. F. P. Wesselingh, J. Salo, *Scr. Geol.* **133**, 439 (2006).
39. D. Riff, P. S. R. Romano, G. R. Oliveira, O. A. Aguilera, in *Amazonia, Landscape and Species Evolution*, C. Hoorn, F. P. Wesselingh, Eds. (Wiley, Oxford, 2010), pp. 259–280.
40. D. Pons, D. De Franceschi, *Bull. Geosci.* **82**, 343 (2007).
41. R. J. G. Kaandorp *et al.*, *Palaeogeogr. Palaeoclimatol. Palaeoecol.* **221**, 1 (2005).
42. N. R. Lovejoy, J. S. Albert, W. G. R. Crampton, *J. S. Am. Earth Sci.* **21**, 5 (2006).
43. M. R. De Carvalho, J. G. Maisey, L. Grande, *Bull. Am. Mus. Nat. Hist.* **284**, 1 (2004).
44. H. B. Vonhof *et al.*, *Geol. Soc. Am. Bull.* **115**, 983 (2003).
45. E. M. Latrubesse *et al.*, *Earth Sci. Rev.* **99**, 99 (2010).
46. M. Bermúdez *et al.*, *Tectonics* **29**, TC5009 (2010).
47. B. K. Horton, P. G. DeCelles, *Basin Res.* **13**, 43 (2001).
48. C. E. Uba, M. R. Strecker, A. K. Schmitt, *Geology* **35**, 979 (2007).
49. J. Figueiredo, C. Hoorn, P. van der Ven, E. Soares, *Geology* **38**, e213 (2010).
50. J. Hovikoski *et al.*, *Geol. Soc. Am. Bull.* **119**, 1506 (2007).
51. S. A. F. da Silva-Caminha, C. A. Jaramillo, M. L. Absy, *Palaeontogr. Abt. B* **283**, 1 (2010).
52. F. R. Negri, thesis, Pontifícia Universidade Católica do Rio Grande do Sul (2004).
53. R. H. J. Erkens, L. W. Chatrou, J. W. Maas, T. van der Niet, V. Savolainen, *Mol. Phylogenet. Evol.* **44**, 399 (2007).
54. J. E. Richardson, R. T. Pennington, T. D. Pennington, P. M. Hollingsworth, *Science* **293**, 2242 (2001).
55. P. V. A. Fine, D. C. Daly, G. Villa Muñoz, I. Mesones, K. M. Cameron, *Evolution* **59**, 1464 (2005).
56. L. G. Marshall, R. L. Cifelli, *Palaeovertebrata* **19**, 169 (1990).
57. B. J. MacFadden, *Trends Ecol. Evol.* **21**, 157 (2006).
58. T. Toivonen, S. Mäki, R. Kalliola, *J. Biogeogr.* **34**, 1374 (2007).
59. C. Hughes, R. Eastwood, *Proc. Natl. Acad. Sci. U.S.A.* **103**, 10334 (2006).
60. B. T. Smith, J. Klicka, *Ecography* **33**, 333 (2010).
61. J. T. Weir, E. Bermingham, D. Schluter, *Proc. Natl. Acad. Sci. U.S.A.* **106**, 21737 (2009).
62. S. Cody, J. E. Richardson, V. Rull, C. Ellis, R. T. Pennington, *Ecography* **33**, 326 (2010).
63. S. Renner, *Int. J. Plant Sci.* **165** (suppl. 4), S23 (2004).
64. R. T. Pennington, C. W. Dick, *Philos. Trans. R. Soc. Ser. B* **359**, 1611 (2004).
65. C. A. Quesada *et al.*, *Biogeosci. Discuss.* **6**, 3923 (2009).
66. H. ter Steege, Amazon Tree Diversity Network, RAINFOR (Amazon Forest Inventory Network), in *Amazonia: Landscape and Species Evolution*, C. Hoorn, F. Wesselingh, Eds. (Wiley, Oxford, 2010), pp. 349–359.
67. M. E. McClain, R. J. Naiman, *Bioscience* **58**, 325 (2008).
68. J. C. Zachos, G. R. Dickens, R. E. Zeebe, *Nature* **451**, 279 (2008).
69. M. F. Tognelli, D. A. Kelt, *Ecography* **27**, 427 (2004).

70. We thank all colleagues who shared their data; M. F. Tognelli for mammal richness data; and B. P. Kohn, M. Bernet, P. van der Beek, R. T. Pennington, S. B. Kroonenberg, B. Bookhagen, C. Uba, and three anonymous reviewers for constructive comments on the manuscript. Supported by the Osk. Huttunen Foundation, the Ella and Georg Ehrnrooth Fund, and the Helsingin Sanomain Saatio (T.S.) and by the Academy of Sciences of Finland (F.P.W.).

Supporting Online Material

www.sciencemag.org/cgi/content/full/330/6006/927/DC1
Materials and Methods
Figs. S1 to S8
Tables S1 to S3
References

10.1126/science.1194585

Downloaded from www.sciencemag.org on November 11, 2010

A Wandering Mind Is an Unhappy Mind

Matthew A. Killingsworth* and Daniel T. Gilbert

Unlike other animals, human beings spend a lot of time thinking about what is not going on around them, contemplating events that happened in the past, might happen in the future, or will never happen at all. Indeed, "stimulus-independent thought" or "mind wandering" appears to be the brain's default mode of operation (*1*–*3*). Although this ability is a remarkable evolutionary achievement that allows people to learn, reason, and plan, it may have an emotional cost. Many philosophical and religious traditions teach that happiness is to be found by living in the moment, and practitioners are trained to resist mind wandering and "to be here now." These traditions suggest that a wandering mind is an unhappy mind. Are they right?

Laboratory experiments have revealed a great deal about the cognitive and neural bases of mind wandering (*3*–*7*), but little about its emotional consequences in everyday life. The most reliable method for investigating real-world emotion is experience sampling, which involves contacting people as they engage in their everyday activities and asking them to report their thoughts, feelings, and actions at that moment. Unfortunately, collecting real-time reports from large numbers of people as they go about their daily lives is so cumbersome and expensive that experience sampling has rarely been used to investigate the relationship between mind wandering and happiness and has always been limited to very small samples (*8*, *9*).

We solved this problem by developing a Web application for the iPhone (Apple Incorporated, Cupertino, California), which we used to create an unusually large database of real-time reports of thoughts, feelings, and actions of a broad range of people as they went about their daily activities. The application contacts participants through their iPhones at random moments during their waking hours, presents them with questions, and records their answers to a database at www.trackyourhappiness.org. The database currently contains nearly a quarter of a million samples from about 5000 people from 83 different countries who range in age from 18 to 88 and who collectively represent every one of 86 major occupational categories.

To find out how often people's minds wander, what topics they wander to, and how those wanderings affect their happiness, we analyzed samples from 2250 adults (58.8% male, 73.9% residing in the United States, mean age of 34 years) who were randomly assigned to answer a happiness question ("How are you feeling right now?") answered on a continuous sliding scale from very bad (0) to very good (100), an activity question ("What are you doing right now?") answered by endorsing one or more of 22 activities adapted from the day reconstruction method (*10*, *11*), and a mind-wandering question ("Are you thinking about something other than what you're currently doing?") answered with one of four options: no; yes, something pleasant; yes, something neutral; or yes, something unpleasant. Our analyses revealed three facts.

First, people's minds wandered frequently, regardless of what they were doing. Mind wandering occurred in 46.9% of the samples and in at least 30% of the samples taken during every activity except making love. The frequency of mind wandering in our real-world sample was considerably higher than is typically seen in laboratory experiments. Surprisingly, the nature of people's activities had only a modest impact on whether their minds wandered and had almost no impact on the pleasantness of the topics to which their minds wandered (*12*).

Second, multilevel regression revealed that people were less happy when their minds were wandering than when they were not [slope (b) = –8.79, $P < 0.001$], and this was true during all activities, including the least enjoyable. Although people's minds were more likely to wander to pleasant topics (42.5% of samples) than to unpleasant topics (26.5% of samples) or neutral topics (31% of samples), people were no happier when thinking about pleasant topics than about their current activity (b = –0.52, not significant) and were considerably unhappier when thinking about neutral topics (b = –7.2, $P < 0.001$) or unpleasant topics (b = –23.9, $P < 0.001$) than about their current activity (Fig. 1, bottom). Although negative moods are known to cause mind wandering (*13*), time-lag analyses strongly suggested that mind wandering in our sample was generally the cause, and not merely the consequence, of unhappiness (*12*).

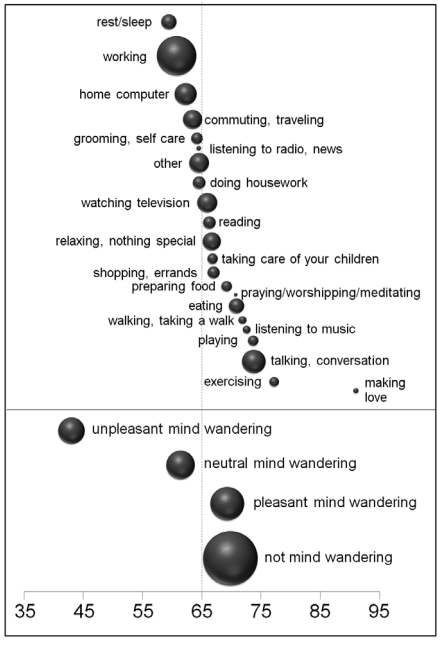

Fig. 1. Mean happiness reported during each activity (**top**) and while mind wandering to unpleasant topics, neutral topics, pleasant topics or not mind wandering (**bottom**). Dashed line indicates mean of happiness across all samples. Bubble area indicates the frequency of occurrence. The largest bubble ("not mind wandering") corresponds to 53.1% of the samples, and the smallest bubble ("praying/worshipping/meditating") corresponds to 0.1% of the samples.

Third, what people were thinking was a better predictor of their happiness than was what they were doing. The nature of people's activities explained 4.6% of the within-person variance in happiness and 3.2% of the between-person variance in happiness, but mind wandering explained 10.8% of within-person variance in happiness and 17.7% of between-person variance in happiness. The variance explained by mind wandering was largely independent of the variance explained by the nature of activities, suggesting that the two were independent influences on happiness.

In conclusion, a human mind is a wandering mind, and a wandering mind is an unhappy mind. The ability to think about what is not happening is a cognitive achievement that comes at an emotional cost.

References and Notes

1. M. E. Raichle *et al.*, *Proc. Natl. Acad. Sci. U.S.A.* **98**, 676 (2001).
2. K. Christoff, A. M. Gordon, J. Smallwood, R. Smith, J. W. Schooler, *Proc. Natl. Acad. Sci. U.S.A.* **106**, 8719 (2009).
3. R. L. Buckner, J. R. Andrews-Hanna, D. L. Schacter, *Ann. N. Y. Acad. Sci.* **1124**, 1 (2008).
4. J. Smallwood, J. W. Schooler, *Psychol. Bull.* **132**, 946 (2006).
5. M. F. Mason *et al.*, *Science* **315**, 393 (2007).
6. J. Smallwood, E. Beach, J. W. Schooler, T. C. Handy, *J. Cogn. Neurosci.* **20**, 458 (2008).
7. R. L. Buckner, D. C. Carroll, *Trends Cogn. Sci.* **11**, 49 (2007).
8. J. C. McVay, M. J. Kane, T. R. Kwapil, *Psychon. Bull. Rev.* **16**, 857 (2009).
9. M. J. Kane *et al.*, *Psychol. Sci.* **18**, 614 (2007).
10. D. Kahneman, A. B. Krueger, D. A. Schkade, N. Schwarz, A. A. Stone, *Science* **306**, 1776 (2004).
11. A. B. Krueger, D. A. Schkade, *J. Public Econ.* **92**, 1833 (2008).
12. Materials and methods are available as supporting material on *Science* Online.
13. J. Smallwood, A. Fitzgerald, L. K. Miles, L. H. Phillips, *Emotion* **9**, 271 (2009).
14. We thank V. Pitiyanuvath for engineering www.trackyourhappiness.org and R. Hackman, A. Jenkins, W. Mendes, A. Oswald, and T. Wilson for helpful comments.

Supporting Online Material

www.sciencemag.org/cgi/content/full/330/6006/932/DC1
Materials and Methods
Table S1
References

18 May 2010; accepted 29 September 2010
10.1126/science.1192439

Harvard University, Cambridge, MA 02138, USA.

*To whom correspondence should be addressed. E-mail: mkilling@fas.harvard.edu

Downloaded from www.sciencemag.org on November 11, 2010

Cytochrome P450 Compound I: Capture, Characterization, and C-H Bond Activation Kinetics

Jonathan Rittle and Michael T. Green*

Cytochrome P450 enzymes are responsible for the phase I metabolism of approximately 75% of known pharmaceuticals. P450s perform this and other important biological functions through the controlled activation of C-H bonds. Here, we report the spectroscopic and kinetic characterization of the long-sought principal intermediate involved in this process, P450 compound I (P450-I), which we prepared in approximately 75% yield by reacting ferric CYP119 with *m*-chloroperbenzoic acid. The Mössbauer spectrum of CYP119-I is similar to that of chloroperoxidase compound I, although its electron paramagnetic resonance spectrum reflects an increase in $|J|/D$, the ratio of the exchange coupling to the zero-field splitting. CYP119-I hydroxylates the unactivated C-H bonds of lauric acid [D(C-H) ~ 100 kilocalories per mole], with an apparent second-order rate constant of $k_{app} = 1.1 \times 10^7$ per molar per second at 4°C. Direct measurements put a lower limit of $k \geq 210$ per second on the rate constant for bound substrate oxidation, whereas analyses involving kinetic isotope effects predict a value in excess of 1400 per second.

Cytochrome P450s are thiolate-ligated heme enzymes that use dioxygen and the formal equivalents of molecular hydrogen ($2H^+$ and $2e^-$) to functionalize a wide range of biologically active compounds (*1*, *2*). Interest in these systems stems not only from their obvious medical and biological importance but also from a desire to harness their synthetic potential. P450s hydroxylate unactivated C-H bonds (*3*–*5*), which are ubiquitous and rather unreactive in organic molecules (*6*, *7*). A major goal of bioinorganic chemistry has been the elucidation of factors that determine P450s' ability to activate inert C-H bonds (*8*–*12*). Central to these efforts have been attempts to obtain electronic and structural characterizations of the highly reactive intermediate, termed compound I, that is thought to be responsible for these demanding oxidations (*5*, *12*–*19*).

P450 compound I (P450-I) is postulated to be an iron(IV)oxo (or ferryl) species with an additional oxidizing equivalent delocalized over the porphyrin and thiolate ligands. This species has for the most part eluded spectroscopic detection. It is not seen under normal turnover conditions but has been generated transiently in stopped-flow reactions (via the peroxide shunt pathway) (*2*). In each case, this reactive intermediate was prepared in low yield, and the reported ultraviolet (UV)/visible spectrum was extracted from the data set by using mathematical techniques (global analysis) (*2*, *20*–*22*).

Insights into the electronic and geometric structures of P450-I have come from theoretical calculations and comparisons with the enzyme chloroperoxidase (CPO). This thiolate-ligated heme-protein has served as an important (but limited) model system for the study of P450 chemistry. CPO compound I (CPO-I) is stable enough to be prepared in high yield, and detailed electronic and structural characterizations of CPO-I have been reported (*23*–*28*). However, it is clear that substantial differences exist between this species and the more reactive P450-I. CPO-I does not oxidize unactivated hydrocarbons, and it only sluggishly hydroxylates benzylic hydrogens [D(C-H) ~ 89 kcal/mol] (*29*). Evidence suggests that this difference in reactivity cannot be explained in terms of substrate access alone (*30*, *31*). The aliphatic termini of fatty acids [D(C-H) ~ 100 kcal/mol] readily access the active site of CPO-I, yet no reaction is observed.

P450-I does not accumulate during turnover, and no kinetic studies have yet fully confirmed generation of the species and subsequently tracked its reaction with substrate (*21*, *32*–*34*). The inability of researchers to "see compound I in action" has led some to question its competence as a hydroxylating species and its role in

Department of Chemistry, Pennsylvania State University, University Park, PA 16802, USA.

*To whom correspondence should be addressed. E-mail: mtg10@psu.edu

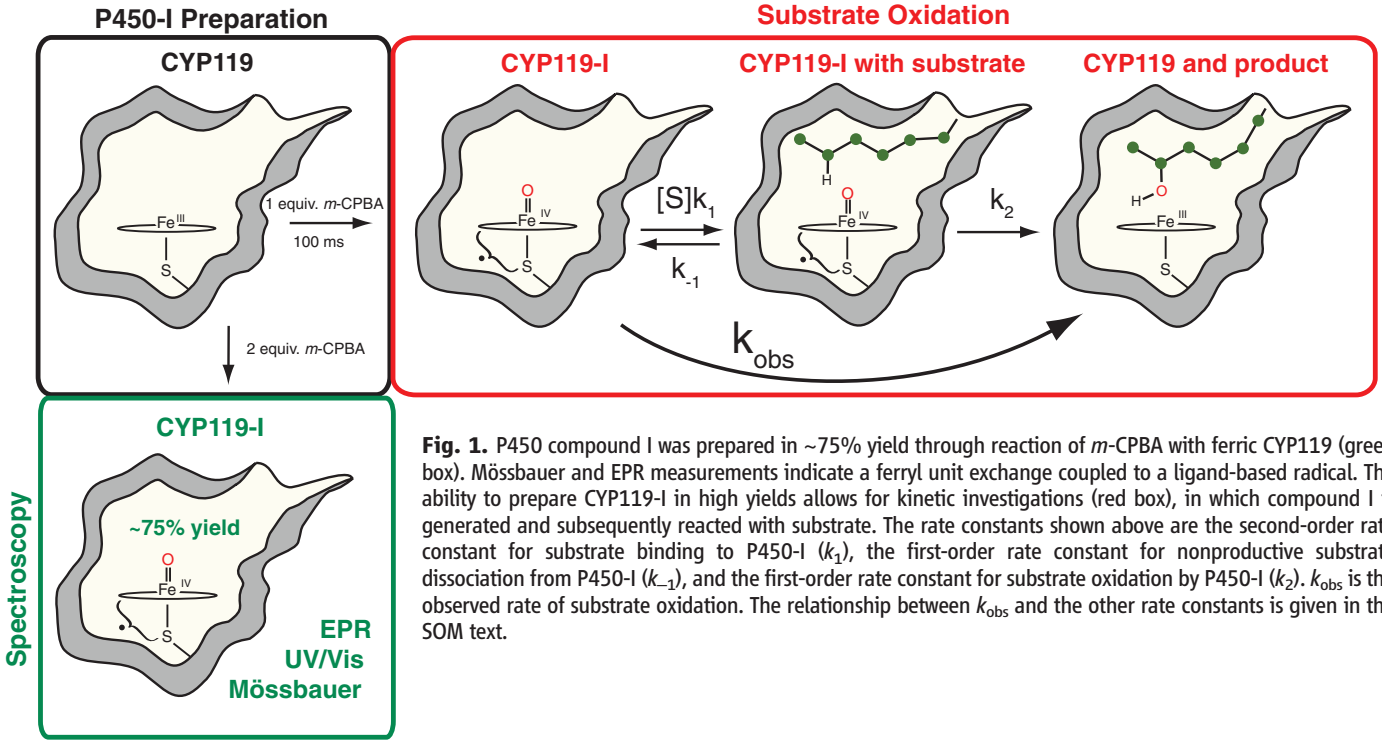

Fig. 1. P450 compound I was prepared in ~75% yield through reaction of *m*-CPBA with ferric CYP119 (green box). Mössbauer and EPR measurements indicate a ferryl unit exchange coupled to a ligand-based radical. The ability to prepare CYP119-I in high yields allows for kinetic investigations (red box), in which compound I is generated and subsequently reacted with substrate. The rate constants shown above are the second-order rate constant for substrate binding to P450-I (k_1), the first-order rate constant for nonproductive substrate dissociation from P450-I (k_{-1}), and the first-order rate constant for substrate oxidation by P450-I (k_2). k_{obs} is the observed rate of substrate oxidation. The relationship between k_{obs} and the other rate constants is given in the SOM text.

Downloaded from www.sciencemag.org on November 11, 2010

P450 chemistry. Perferryl [iron(V)oxo] and ferric hydroperoxo complexes have been suggested as alternative hydroxylating agents (*2*, *4*, *34*–*36*). The perferryl species has been proposed to be the immediate product of oxygen activation, but evidence for its existence is lacking. The hydroperoxo complex has been prepared and characterized. However, experiments have ruled out its involvement in the hydroxylation step (*14*).

Our understanding of C-H bond activation in P450s has stagnated for want of a system in which P450-I could be prepared in high yield. Here, we report a breakthrough on this front (Fig. 1). We have found that highly purified preparations of CYP119, the thermophillic P450 from *Sulfolobus acidocaldarius* (*37*–*39*), allow the generation of compound I in unprecedented yields. In what follows, we detail the spectroscopic and kinetic characterization of CYP119-I.

Spectroscopic characterization of P450 compound I. When a 20 μM ferric enzyme solution (buffered to pH 7) was mixed (1:1) with a 40 μM *m*-chloroperbenzoic acid (*m*-CPBA) solution, we observed approximately 70% conversion to P450-I 35 ms after mixing (Fig. 2) (*40*). Multiple isosbestic points in the stopped-flow data set from 0 to 35 ms indicate the presence of only two UV/visible absorbing species: ferric enzyme and compound I. The dashed line in Fig. 2 gives the spectrum of CYP119-I. Because the 0-to-35-ms data set comprises only two absorbing species, the CYP119-I spectrum can be obtained with difference techniques or through the use of target testing (*41*). The spectrum of CYP119-I shown in Fig. 2 is in good agreement with the UV/visible spectrum reported previously by Kellner *et al.* (*21*).

Although a number of researchers have been able to observe P450-I in stopped-flow reactions (*20*–*22*), none have been able to prepare the intermediate using rapid freeze-quench techniques. This has been a rather puzzling aspect of P450 chemistry. The intermediate has been observed on time scales that are amenable to freeze-quenching. Yet all attempts to prepare P450-I with this technique have failed. The reason such efforts have gone unrewarded is not clear, but many have concluded that the intermediate is simply too reactive to be trapped. To determine whether unwanted side reactions (at the millimolar concentrations used in freeze-quench reactions) could be a detriment to compound I formation, high-concentration stopped-flow experiments were performed (fig. S2). These experiments, which revealed no substantial change in the compound I decay rate, suggested that CYP119-I could be prepared at millimolar concentrations by use of freeze-quench techniques.

With hopes of preparing CYP119-I samples for further spectroscopic characterizations, we performed freeze-quench experiments. Ferric CYP119 (3 mM) was mixed (2:1) with a 12 mM solution of *m*-CPBA, and the aqueous reaction mixture was sprayed into liquid ethane (89 K) 3.5 ms after mixing. Liquid ethane was subsequently removed under vacuum in an isopentane bath (~120 K), after which the samples were packed under liquid nitrogen.

Mössbauer measurements on the freeze-quenched samples confirmed the formation of P450-I in ~75% yield. The spectra shown in Fig. 3 were obtained by subtracting the spectrum of ferric CYP119 (25%) from the raw data [fig. S3 and supporting online material (SOM) text]. Spectrum A/B was obtained with a 54-mT field applied parallel/perpendicular to the γ-beam. These spectra were fit simultaneously (solid lines) assuming an effective $S = 1/2$ representation (SOM text). The parameters obtained from these fits are listed (along with the values obtained for CPO-I) in Table 1. The Mössbauer parameters and spectra of the CYP119 intermediate are similar to those reported for CPO-I (*23*). This similarity facilitates assignment of the CYP119 intermediate: It is best described as having an iron(IV)oxo unit exchange coupled to a ligand-based radical—the elusive P450 compound I.

Although CPO-I and CYP119-I have similar UV/visible and Mössbauer spectra, their electron paramagnetic resonance (EPR) signatures are different (Fig. 4). EPR measurements of freeze-quenched samples reveal the presence of CYP119-I, ferric CYP119, and at least two additional paramagnetic species. The spectra of these additional species (presumably protein-based radicals, although *m*-chlorobenzoic acid radicals have not been ruled out) overlap the CYP119-I spectrum but are easily differentiated by their temperature and power dependence (fig. S4). Like CPO-I, CYP119-I is fast-relaxing, and EPR signals associated with the intermediate can be observed only below ~25 K (*23*). As a result, the spectrum of CYP119-I can be extracted from measurements at low temperature and high power. Under the appropriate conditions, the signals of the other paramagnetic species can be fully saturated, and the spectrum of CYP119-I can be obtained by difference. The spectrum of CYP119-I shown in Fig. 4 was obtained by taking the difference of spectra obtained at 7.5 K using 203-mW and 128-mW microwave power (fig. S4).

The electronic structure of P450 compound I is best described as an $S = 1$ iron(IV)oxo unit exchange coupled with an $S = 1/2$ ligand-based radical. This exchange coupling (J) produces doublet and quartet states, which are mixed by the strong zero-field splitting (D) of the ferryl moiety. These interactions split the system into three-Kramers doublets, only the lowest of which is populated and EPR-active. As a result, the system may be modeled in an effective $S = 1/2$ representation (*23*). The g values of this effective representation can be shown to be functions of the ferryl g values and the ratio of J/D (SOM text and eq. S3). Fits of the CYP119-I data yield $g^{eff} = (1.86, 1.96, 2.00)$. These values are indicative of antiferromagnetic coupling and $|J|/D = 1.3$ (*42*). Similar procedures for CPO-I yield $g^{eff} = (1.61, 1.72, 2.00)$ and $|J|/D = 1.02$—values in good agreement with those reported by Rutter *et al.* (*23*). The increased $|J|/D$ in CYP119-I pushes $g_{\perp}^{eff}$ to lower fields, altering the shape of the spectrum relative to CPO-I. This effect is illustrated with simulated absorption spectra in Fig. 4C. The factors resulting in the increased $|J|/D$ in CYP119-I are not known. We have reported that axial-ligand

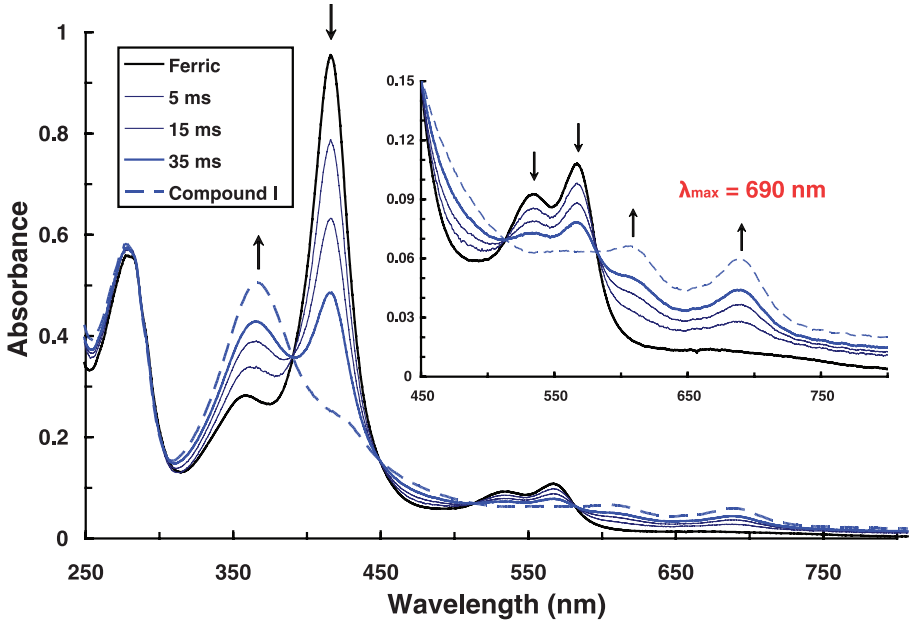

Fig. 2. UV/visible spectra obtained from the stopped-flow mixing (1:1) of 20 μM ferric CYP119 with 40 μM *m*-CPBA at 4°C. The blue traces correspond to spectra taken 5, 15, and 35 ms after mixing. Maximum yield of P450-I was ~70% at 35 ms. At later times, isosbestic points were lost, and a portion of the protein was degraded from the use of excess *m*-CPBA as judged by the final Reinheitszahl ($R_z = Abs_{416\ nm}/Abs_{280\ nm}$) ($R_z$) of 1.31 (fig. S1). All spectral changes were completed within 2.5 s. Dashed line indicates the spectrum of CYP119 compound I obtained by difference techniques (*41*).

Downloaded from www.sciencemag.org on November 11, 2010

spin density favors antiferromagnetic coupling (*43*). A larger value of $|J|$ could be the hallmark of increased sulfur spin density or a shortened Fe-S bond. It is unclear how these factors would affect the zero-field splitting.

Kinetic characterization of P450 compound I. The natural substrate of CYP119 is unknown, but previous work has shown that CYP119 oxidizes long-chain fatty acids (*44*). CYP119 binds these C_{10}- to C_{20}-sized saturated hydrocarbons with micromolar affinity and hydroxylates them at the ω- through ω-3 positions (*44*, *45*). The reaction with lauric acid (C_{12}) is the best characterized, kinetically. Under turnover conditions, CYP119 hydroxylates lauric acid at a rate of $k_{cat} = 11\ min^{-1}$ (*45*). One expects direct oxidation by compound I to be many orders of magnitude faster.

To investigate the rate at which compound I hydroxylates unactivated hydrocarbons, reactions of CYP119-I with hexanoic, octanoic, and dodecanoic acids (C_6, C_8, C_{12}), their perdeuterated forms, and camphor (the natural substrate of $P450_{cam}$) were studied at 4°C under pseudo first-order conditions by using stopped-flow techniques. In a typical kinetic experiment, CYP119 was premixed with one equivalent of *m*-CPBA and aged until exponential decay of compound I was apparent (100 ms). This solution, typically consisting of 35 to 40% compound I, was then mixed with a solution containing the desired substrate. This process allowed for the reaction of ~2.5 μM CYP119-I with varying substrate concentrations. Progress of the reaction was monitored by following the return of ferric enzyme (416 nm) or the decay of compound I (690 nm). Kinetic traces showed good single-exponential behavior for more than six half-lives (figs. S8 to S11). Fits of these traces provided observed rate constants, k_{obs}. Plots of k_{obs} versus substrate concentration were linear and provided apparent second-order rate constants, k_{app}, for the oxidation of substrate by CYP119-I (Fig. 5, Table 2, and SOM text). The ability of CYP119 to hydroxylate substrates using *m*-CPBA was verified with gas chromatography–mass spectrometry (GC-MS) (fig. S5).

The apparent second-order rate constants for substrate oxidation by CYP119-I are listed in Table 2. The rate constant for the oxidation of lauric acid is a remarkably efficient $k_{app} = 1.1 \times 10^7\ M^{-1}s^{-1}$. In the presence of 20 μM lauric acid, the observed rate of compound I decay is $220\ s^{-1}$.

The kinetic parameters listed in Table 2 reveal an interesting trend in fatty acid oxidation. The apparent second-order rate constant for substrate oxidation is a function of chain length. On going from C_6 to C_{12}, k_{app} increases by ~10^3. Plots of ln (k_{app}) versus chain length suggest a linear free-energy relationship—possibly derived from the free energy of binding. The perdeuterated substrates show an even larger (~10^4) increase in rate constant. As a result, the isotope effects obtained from these rate constants ($KIE_{obs} = {}^{H}k_{app}/{}^{D}k_{app}$) also show variation, but the trend is reversed: The observed kinetic isotope effects (KIEs) decrease with chain length. The variation in KIE can be understood in terms of the mechanism shown in Fig. 1.

Under nonsaturating conditions, the KIEs for strongly bound substrates are masked. The full unmasked values can be obtained only when nonproductive substrate dissociation is rapid as compared with substrate oxidation (SOM text). The observed KIEs are determined by the relative magnitudes of k_{-1} and k_2. For highly reactive intermediates and strong substrate binding (${}^{H}k_2$, ${}^{D}k_2 >> k_{-1}$), substrate association is rate limiting, $k_{obs} = [S]k_1$. Under these conditions, $k_{app} = k_1$ and an isotope effect of $KIE_{obs} = 1.0$ is predicted (for example, lauric acid). With decreasing substrate affinity ($C_6 < C_8 << C_{12}$), k_{-1} increases relative to k_2, and KIE_{obs} grows from the limiting value of 1.0 toward the full unmasked value of ${}^{H}k_2/{}^{D}k_2$. This latter value is obtained only when substrate binding is in rapid equilibrium ($k_{-1} >> {}^{H}k_2$, ${}^{D}k_2$). Under these conditions, $k_{app} = K_e k_2$, where $K_e = k_1/k_{-1}$ is the equilibrium constant.

The preceding analysis provides the second-order rate constant for lauric acid association, $k_1 = k_{app} = 1.1 \times 10^7\ M^{-1}s^{-1}$. Assuming a dissociation constant (K_d) similar to that of ferric enzyme ($K_d = 1\ \mu M$), one obtains a value of $k_{-1} \sim 10\ s^{-1}$ for the rate of nonproductive lauric acid dissociation, whereas the largest measured value of k_{obs} provides a lower limit for the rate of lauric acid oxidation, $k_2 > 210\ s^{-1}$. These values are consistent with the conditions required (${}^{H}k_2$, ${}^{D}k_2 >> k_{-1}$) for an observed isotope effect of $KIE_{obs} = 1.0$.

P450 hydroxylations are subject to large intrinsic isotope effects, and the observation of unmasked KIEs ≥ 10 is typical (*3*, *4*). These KIEs, which indicate substantial hydrogen tunneling, are larger than the value obtained from semiclassical arguments, $KIE_{SC} \sim 7$ (*46*). As a result, we may use KIE_{SC} to provide a lower limit for the rate of bound lauric acid oxidation (${}^{H}k_2$). Assuming KIE ≥ 7, one obtains ${}^{H}k_2 \geq 1400\ s^{-1}$.

This report confirms not only the existence but the catalytic competence of P450-I. CYP119-I

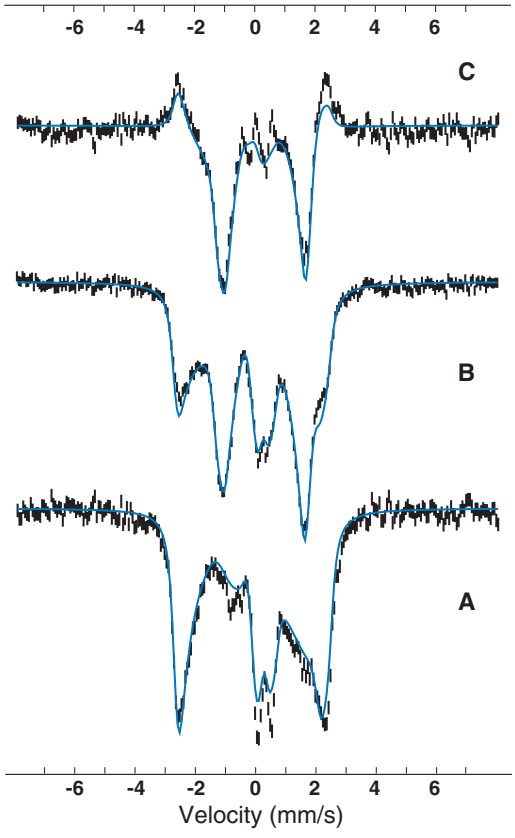

Fig. 3. Mössbauer spectra of CYP119 compound I at a temperature of 4.2 K, obtained by subtracting the spectrum of ferric CYP119 (25%) from the raw data (fig. S3 and SOM text). A 54-mT field was applied parallel to the γ-beam for spectrum A and perpendicular to the γ-beam for B. Spectrum C is the A-B difference spectrum. Solid lines are best fits of the data. Spectra A and B were fit simultaneously, assuming an effective $S = 1/2$ representation (SOM text, fitting details). Fit parameters are listed in Table 1. CYP119-I samples were prepared by mixing (2:1) ferric CYP119 (3 mM, $R_z \geq 1.65$, in 100 mM Kphos buffer, pH 7.0) with a solution of *m*-CPBA (12 mM, in 20:80 acetonitrile:water).

Table 1. Mössbauer and EPR parameters for P450-I and CPO-I. The relationship between the effective *g* values, *J*/*D*, and the ferryl *g* values can be found in (*40*). See (*42*) for a discussion of the ferryl *g* values. The intrinsic ferryl hyperfine couplings were obtained by fitting the Mössbauer data in the coupled representation.

	δ (mm/s)	ΔE_Q (mm/s)	Effective $S = 1/2$ representation							Ferryl values						
			g_x	g_y	g_z	A_x (T)	A_y (T)	A_z (T)	*J*/*D*	g_x	g_y	g_z	A_x (T)	A_y (T)	A_z (T)
CPO-I	0.13	0.96	1.72	1.61	2.00	−31	−30	−2	1.02	2.27	2.19	2.00	−24	−22	−2
CYP119-I	0.11	0.90	1.96	1.86	2.00	−28	−32	−3	1.30	2.27	2.20	2.00	−20	−23	−3

Downloaded from www.sciencemag.org on November 11, 2010

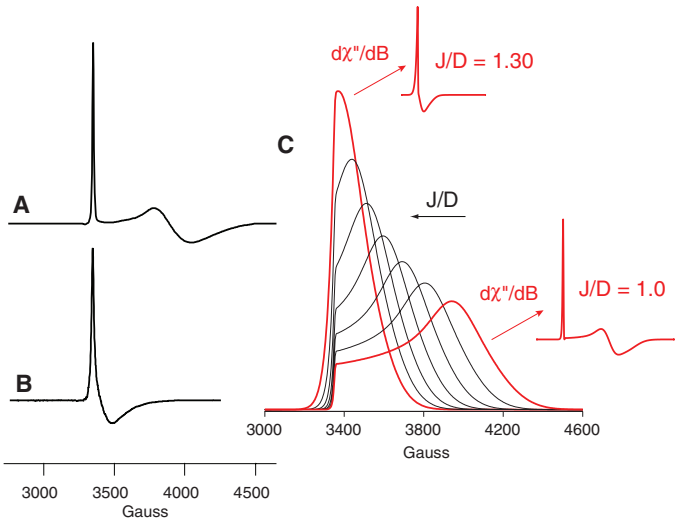

Fig. 4. (**A**) EPR spectrum of CPO-I at a temperature of 8 K taken with 203-mW microwave power. (**B**) EPR spectrum of CYP119-I at a temperature of 7.5 K. The CYP119-I spectrum was obtained from the difference of spectra taken with 203-mW and 128-mW microwave power (fig. S4). At these high powers, signals associated with other paramagnetic species are fully saturated, whereas the CYP119-I signal continues to grow with increasing power. Fits of the CPO-I and CYP119-I EPR spectra can be found in (*40*). (**C**) Effect of *J*/*D* on the EPR spectrum is best illustrated through a comparison of simulated absorption spectra. The simulations were performed with the ferryl *g* values listed in Table 1. *J*/*D* changes from 1.0 to 1.3 across the series (0.05 increments). The derivative of the *J*/*D* = 1.0 simulation resembles the CPO-I spectrum shown in (A). The derivative of the *J*/*D* = 1.30 spectrum resembles the CYP119-I spectrum shown in (B).

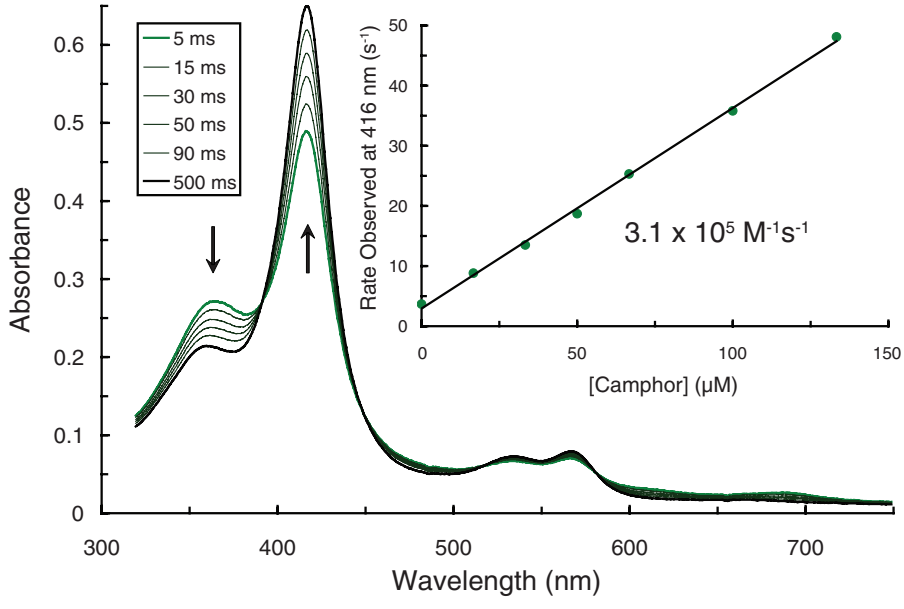

Fig. 5. UV/visible spectra taken during the reaction of CYP119-I with 50 μM camphor at 4°C. In a typical kinetic experiment, 20 μM CYP119 (100 mM Kphos pH 7.0) was premixed with one equivalent of *m*-CPBA and aged until exponential decay of compound I was apparent (100 ms). This solution, which typically consisted of 35 to 40% compound-I, was then mixed with a solution containing the desired substrate (100 mM Kphos pH 7.0). This process allowed for the reaction of ~2.5 μM CYP119-I, with varying concentrations of substrate. The UV/visible traces were taken at the times listed after the final mix. Singular value decomposition analysis indicated that only two UV/visible absorbing species were present in the reaction. (Inset) Observed CYP119-I decay rate versus camphor concentration.

Table 2. Apparent second-order rate constants at 4°C, observed isotope effect, and substrate concentration range for CYP119-I oxidations.

Substrate	$^{H}k_{app}$ (M^{-1} s^{-1})	$^{D}k_{app}$ (M^{-1} s^{-1})	KIE_{obs}	[^{H}S]/[^{D}S]
Camphor	3.5 (±0.1) × 10^5	—	—	0 to 266 μM/–
Hexanoic acid	4.4 (±0.6) × 10^4	3.5 (±0.8) × 10^3	12.5	0 to 5 mM/0 to 12 mM
Octanoic acid	4.5 (±0.3) × 10^5	8.6 (±0.5) × 10^4	5.3	0 to 533 μM/0 to 1.3 mM
Dodecanoic (lauric) acid	1.1 (±0.1) × 10^7	1.1 (±0.3) × 10^7	1.0	0 to 17 μM/0 to 17 μM

is capable of oxidizing unactivated hydrocarbons with an apparent second-order rate constant of k_{app} = 1.1 × 10^7 $M^{-1}s^{-1}$. The large intrinsic KIE (≥12.5) observed in the direct oxidation of substrate is consistent with values obtained from intramolecular competition studies (*3*, *4*). Its magnitude supports a mechanism in which compound I abstracts hydrogen from substrate, forming an iron(IV)hydroxide that rapidly recombines with substrate to yield hydroxylated product: the rebound mechanism as postulated by Groves.

References and Notes

1. P. R. O. de Montellano, Ed., *Cytochrome P450: Structure, Mechanism, and Biochemistry* (Kluwer Academic/Plenum, New York, ed. 3, 2005).
2. I. G. Denisov, T. M. Makris, S. G. Sligar, I. Schlichting, *Chem. Rev.* **105**, 2253 (2005).
3. J. T. Groves, G. A. McClusky, R. E. White, M. J. Coon, *Biochem. Biophys. Res. Commun.* **81**, 154 (1978).
4. P. R. Ortiz de Montellano, *Chem. Rev.* **110**, 932 (2010).
5. T. M. Makris, K. von Koenig, I. Schlichting, S. G. Sligar, *J. Inorg. Biochem.* **100**, 507 (2006).
6. H. M. L. Davies, J. R. Manning, *Nature* **451**, 417 (2008).
7. K. Godula, D. Sames, *Science* **312**, 67 (2006).
8. B. M. Hoffman, *Proc. Natl. Acad. Sci. U.S.A.* **100**, 3575 (2003).
9. J. T. Groves, *Proc. Natl. Acad. Sci. U.S.A.* **100**, 3569 (2003).
10. L. Que Jr., Y. Watanabe, *Science* **292**, 651 (2001).
11. K. D. Karlin, *Nature* **463**, 168 (2010).
12. S. G. Sligar, T. M. Makris, I. G. Denisov, *Biochem. Biophys. Res. Commun.* **338**, 346 (2005).
13. I. Schlichting *et al.*, *Science* **287**, 1615 (2000).
14. R. Davydov *et al.*, *J. Am. Chem. Soc.* **123**, 1403 (2001).
15. V. Schünemann, C. Jung, J. Terner, A. X. Trautwein, R. Weiss, *J. Inorg. Biochem.* **91**, 586 (2002).
16. I. G. Denisov *et al.*, *J. Inorg. Biochem.* **87**, 215 (2001).
17. I. G. Denisov, T. M. Makris, S. G. Sligar, *J. Biol. Chem.* **276**, 11648 (2001).
18. R. Davydov *et al.*, *J. Am. Chem. Soc.* **127**, 1403 (2005).
19. S. H. Kim *et al.*, *Dalton Trans.* **21**, 3464 (2005).
20. T. Egawa, H. Shimada, Y. Ishimura, *Biochem. Biophys. Res. Commun.* **201**, 1464 (1994).
21. D. G. Kellner, S. C. Hung, K. E. Weiss, S. G. Sligar, *J. Biol. Chem.* **277**, 9641 (2002).
22. T. Spolitak, J. H. Dawson, D. P. Ballou, *J. Biol. Chem.* **280**, 20300 (2005).
23. R. Rutter *et al.*, *Biochemistry* **23**, 6809 (1984).
24. M. T. Green, J. H. Dawson, H. B. Gray, *Science* **304**, 1653 (2004).
25. K. L. Stone, R. K. Behan, M. T. Green, *Proc. Natl. Acad. Sci. U.S.A.* **102**, 16563 (2005).
26. T. Egawa *et al.*, *FEBS Lett.* **305**, 206 (1992).
27. S. H. Kim, R. Perera, L. P. Hager, J. H. Dawson, B. M. Hoffman, *J. Am. Chem. Soc.* **128**, 5598 (2006).
28. K. L. Stone, R. K. Behan, M. T. Green, *Proc. Natl. Acad. Sci. U.S.A.* **103**, 12307 (2006).
29. F. van Rantwijk, R. A. Sheldon, *Curr. Opin. Biotechnol.* **11**, 554 (2000).
30. A. Zaks, D. R. Dodds, *J. Am. Chem. Soc.* **117**, 10419 (1995).
31. R. Zhang, N. Nagraj, D. S. Lansakara-P, L. P. Hager, M. Newcomb, *Org. Lett.* **8**, 2731 (2006).
32. Recent reports have advocated the use of peroxynitrite and laser flash photolysis (LFP) to generate a species that has been assigned as CYP119-I (*34*). However, critical flaws in the preparation of this species have been noted (*33*). The UV/visible spectrum of the LFP-generated species bears no resemblance to the UV/visible spectrum of CYP119-I described in this or other work (*21*). The spectrum of the LFP-generated species resembles that of ferric enzyme. The LFP-generated species is reported to oxidize lauric acid at a rate of 0.8 s^{-1}. This is at least 2000 times slower than CYP119-I. No spectroscopic characterizations of the LFP-generated species other than UV/visible have been reported. We have recently suggested that the LFP-generated intermediate is not compound I (*41*).
33. R. K. Behan, L. M. Hoffart, K. L. Stone, C. Krebs, M. T. Green, *J. Am. Chem. Soc.* **129**, 5855 (2007).

Downloaded from www.sciencemag.org on November 11, 2010

34. Q. Wang, X. Sheng, J. H. Horner, M. Newcomb, *J. Am. Chem. Soc.* **131**, 10629 (2009).
35. R. E. P. Chandrasena, K. P. Vatsis, M. J. Coon, P. F. Hollenberg, M. Newcomb, *J. Am. Chem. Soc.* **126**, 115 (2004).
36. M. Newcomb *et al.*, *J. Am. Chem. Soc.* **125**, 6064 (2003).
37. R. L. Wright, K. Harris, B. Solow, R. H. White, P. J. Kennelly, *FEBS Lett.* **384**, 235 (1996).
38. M. A. McLean, S. A. Maves, K. E. Weiss, S. Krepich, S. G. Sligar, *Biochem. Biophys. Res. Commun.* **252**, 166 (1998).
39. K. S. Rabe, K. Kiko, C. M. Niemeyer, *ChemBioChem* **9**, 420 (2008).
40. Materials and methods are available as supporting material on *Science* Online.
41. J. Rittle, J. M. Younker, M. T. Green, *Inorg. Chem.* **48**, 3610 (2010).
42. Although it is clear from our fitting—as well as the spectra displayed in Fig. 4—that $|J|/D$ in CYP119-I has increased substantially relative to its value in CPO-I, the magnitude of the increase is not definite. The actual value of J/D depends critically on the choice of ferryl g values, for which only estimates are available. In our analysis, we have obtained ferryl g values by fitting CPO-I under the assumption that $|J|/D = 1.02$, as originally reported by Rutter *et al.* (*23*). This procedure provided the ferryl g values listed for CPO-I in Table 1, which were then used as input for the fitting of CYP119-I. The ferryl g values obtained for both species are reasonably similar to the CPO-I values ($g_\perp = 2.28$ and $g_\parallel = 1.94$) used by Rutter *et al.*, who modeled but did not fit their CPO-I data. Our ferryl g values result in a 27% increase in $|J|/D$ relative to CPO, whereas the values of Rutter *et al.* result in an increase of 24%. Recently, it was suggested that $g_\perp = 2.0$ may be more appropriate for the ferryl moiety (*27*). If this report is accurate, it would suggest that the ratio of $|J|/D$ in CYP119-I is almost twice as large as the value observed for CPO-I.
43. M. T. Green, *J. Am. Chem. Soc.* **123**, 9218 (2001).
44. L. S. Koo, C. E. Immoos, M. S. Cohen, P. J. Farmer, P. R. Ortiz de Montellano, *J. Am. Chem. Soc.* **124**, 5684 (2002).
45. Y. R. Lim *et al.*, *J. Microbiol. Biotechnol.* **20**, 574 (2010).
46. J. P. Klinman, in *Quantum Tunnelling in Enzyme-Catalysed Reactions*, R. K. Allemann, N. S. Scrutton, Eds. (The Royal Society of Chemistry, Cambridge, 2009), pp. 132–157.
47. This work was supported by NSF. We thank T. Grove and J. C. Calixto Moreno for assistance with GC-MS and C. Krest for help with preliminary EPR experiments. The CYP119 plasmid was graciously provided by P. R. Ortiz de Montellano.

Supporting Online Material

www.sciencemag.org/cgi/content/full/330/6006/933/DC1
Materials and Methods
Figs. S1 to S12
Table S1
References

9 June 2010; accepted 16 September 2010
10.1126/science.1193478

How the CCA-Adding Enzyme Selects Adenine over Cytosine at Position 76 of tRNA

Baocheng Pan,[1] Yong Xiong,[1] Thomas A. Steitz[1,2,3]*

CCA-adding enzymes [ATP(CTP):tRNA nucleotidyltransferases] add CCA onto the 3′ end of transfer RNA (tRNA) precursors without using a nucleic acid template. Although the mechanism by which cytosine (C) is selected at position 75 of tRNA has been established, the mechanism by which adenine (A) is selected at position 76 remains elusive. Here, we report five cocrystal structures of the enzyme complexed with both a tRNA mimic and nucleoside triphosphates under catalytically active conditions. These structures suggest that adenosine 5′-monophosphate is incorporated onto the A76 position of the tRNA via a carboxylate-assisted, one–metal-ion mechanism with aspartate 110 functioning as a general base. The discrimination against incorporation of cytidine 5′-triphosphate (CTP) at position 76 arises from improper placement of the α phosphate of the incoming CTP, which results from the interaction of C with arginine 224 and prevents the nucleophilic attack by the 3′ hydroxyl group of cytidine75.

CCA-adding enzymes are nucleotidyltransferases that catalyze the posttranscriptional addition of CCA onto the 3′ terminus of immature tRNAs without using a nucleic acid template (*1*). They are essential in all three kingdoms of life and are divided into two classes based on their sequences. The enzymes from Archaea belong to class I, whereas those from eubacteria and eukaryotes belong to class II (*2*). These two classes of enzymes may have quite different catalytic mechanisms.

During the past several years, crystal structures of CCA-adding enzymes and their tRNA complexes from Archaea (*3*–*7*), bacteria (*8*, *9*), and humans (*10*) have been determined. These structures show that both families have only one site for binding either cytidine 5′-triphosphate (CTP) or adenosine 5′-triphosphate (ATP). Though the crystal structures shed light on how class I CCA-adding enzymes achieve their specificity for addition of the second C at position 75 without the use of a nucleic acid template (*11*), the question of how A, rather than C, is added at position 76 remains controversial. Based on the crystal structures of ternary complexes prepared by diffusing nucleotides into preexisting crystals of an RNA-protein binary complex, two different models have been suggested. One proposal from studies of class I enzymes is that the specificity is conferred by the size and shape of the nucleotide-binding pocket that is determined by the movement of the flexible head domain (*5*). In contrast, another set of crystal structures of class I enzymes led to the conclusion that the discrimination is dictated by a single, flexible amino acid side chain (Arg^{224}) of the enzyme for addition of A76 (*6*).

To understand the structural basis of a biological process, structures of the entire assembly captured at each step in the process are necessary (*12*). The greatest challenge is to control the catalytic reaction of the nucleotide incorporation so that crystals of the whole assembly can be obtained at each step. The initial assembly is the ternary complex of the polymerase, the RNA primer, and the nucleotide triphosphate (NTP) substrate. Capturing this complex requires stopping its catalytic activity with strategies such as mutation of key amino acid residues (*13*), nonhydrolyzable NTP

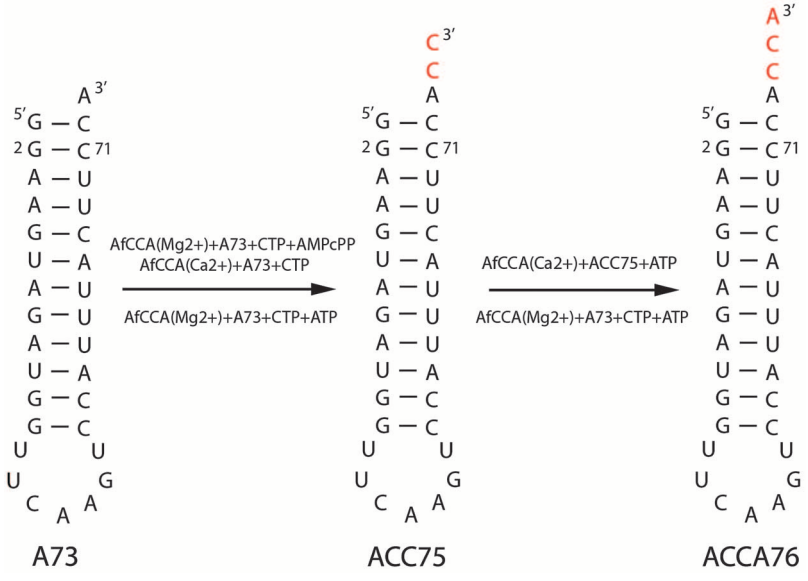

Fig. 1. Schematic diagram showing the tRNA mimics A73 and ACC75 that we used in the present study. The products of the reaction are shown on the right-hand side of the ternary complexes, with the nucleotides incorporated in the 3′ end of tRNA shown in red.

[1]Department of Molecular Biophysics and Biochemistry, Yale University, New Haven, CT 06520, USA. [2]Department of Chemistry, Yale University, New Haven, CT 06520, USA. [3]Howard Hughes Medical Institute, New Haven, CT 06520, USA.

*To whom correspondence should be addressed. E-mail: thomas.steitz@yale.edu

Downloaded from www.sciencemag.org on November 11, 2010

analogs (*14*–*16*), or a polynucleotide primer that is incapable of nucleotide incorporation (*17*, *18*). Though these approaches have successfully yielded structures, they also have major limitations. For instance, the structural information may be altered by the modifications that are used to inactivate the complex, and the complex may not be trapped in the correct conformation. Further, structures of the initial ground state of the catalytic process may not allow correct extrapolation to the subsequent intermediate states. Therefore, illuminating the correct mechanism of polymerization could be facilitated by accurate and detailed structural information from catalytically active complexes.

We have determined the cocrystal structures of five ternary complexes of the archaeal CCA-adding enzyme from *Archaeoglobus fulgidus* (abbreviated AfCCA) that illuminate the mechanism and specificity by which the enzyme incorporates A, and not C, at position 76 of tRNA. The divalent metal ions in the buffer were either Mg^{2+}, Ca^{2+}, or Mn^{2+}. The reaction equilibrium of nucleotide addition can be altered by the use of different divalent metal ions, and we took the advantage of this to trap the different steps in the reaction (*19*). The RNA primers were nucleotide hairpin mimics of *Mycoplasma pneumoniae* $tRNA^{Ile}$ composed of the TΨC stem loop and the acceptor stem whose 3′ ends were at the positions of 73 (called A73) or 75 (called ACC75) (Fig. 1), which have been demonstrated to be good substrates for the addition of CCA (*20*). The specific combinations of reactants and divalent metal ions cocrystallized were: [1] AfCCA(Mg^{2+})+A73+[CTP+AMPcPP] (preinsertion complex), in which AMPcPP (α,β-methylene ATP) is the nonreactive ATP analog (and AMP is adenosine 5′ monophosphate); [2] AfCCA(Mn^{2+})+ACC75+ATP (initial complex); [3] AfCCA(Mg^{2+})+A73+[CTP+ATP] (intermediate complex); [4] AfCCA(Ca^{2+})+ACC75+ATP (product complex); and [5] AfCCA(Ca^{2+})+A73+CTP (CTP complex).

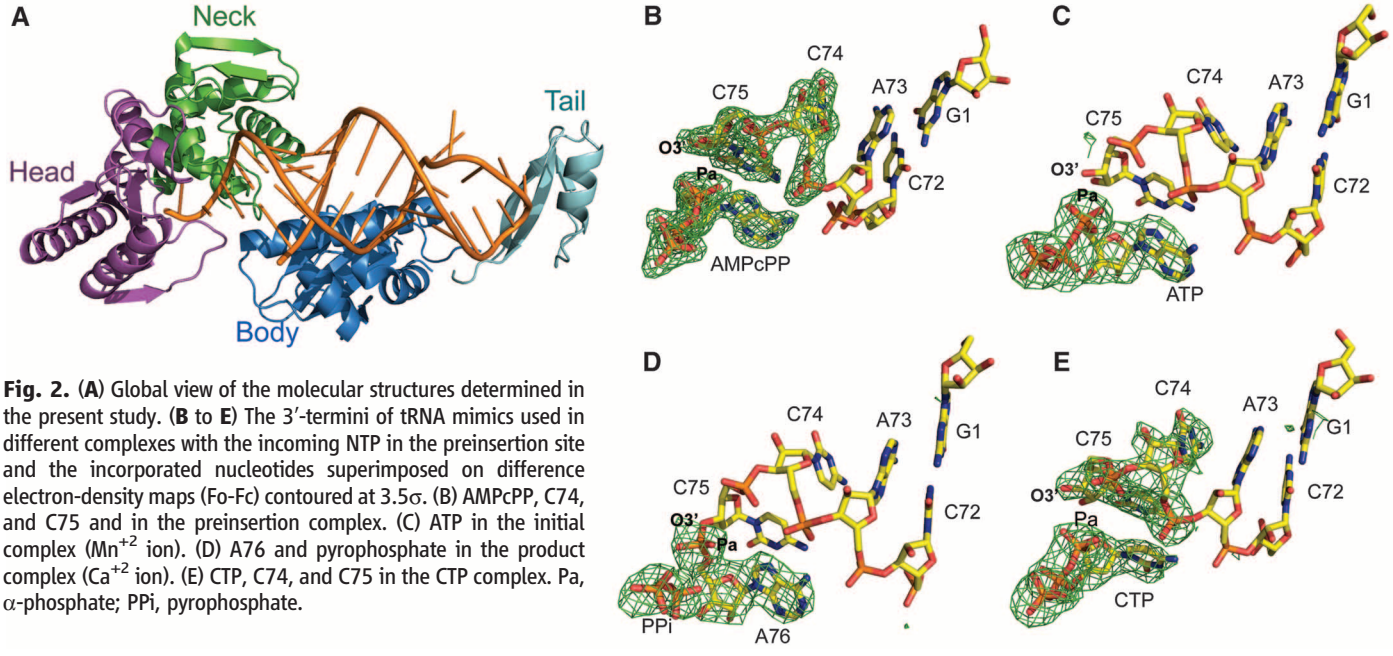

Fig. 2. (**A**) Global view of the molecular structures determined in the present study. (**B** to **E**) The 3′-termini of tRNA mimics used in different complexes with the incoming NTP in the preinsertion site and the incorporated nucleotides superimposed on difference electron-density maps (Fo-Fc) contoured at 3.5σ. (B) AMPcPP, C74, and C75 and in the preinsertion complex. (C) ATP in the initial complex (Mn^{+2} ion). (D) A76 and pyrophosphate in the product complex (Ca^{+2} ion). (E) CTP, C74, and C75 in the CTP complex. Pa, α-phosphate; PPi, pyrophosphate.

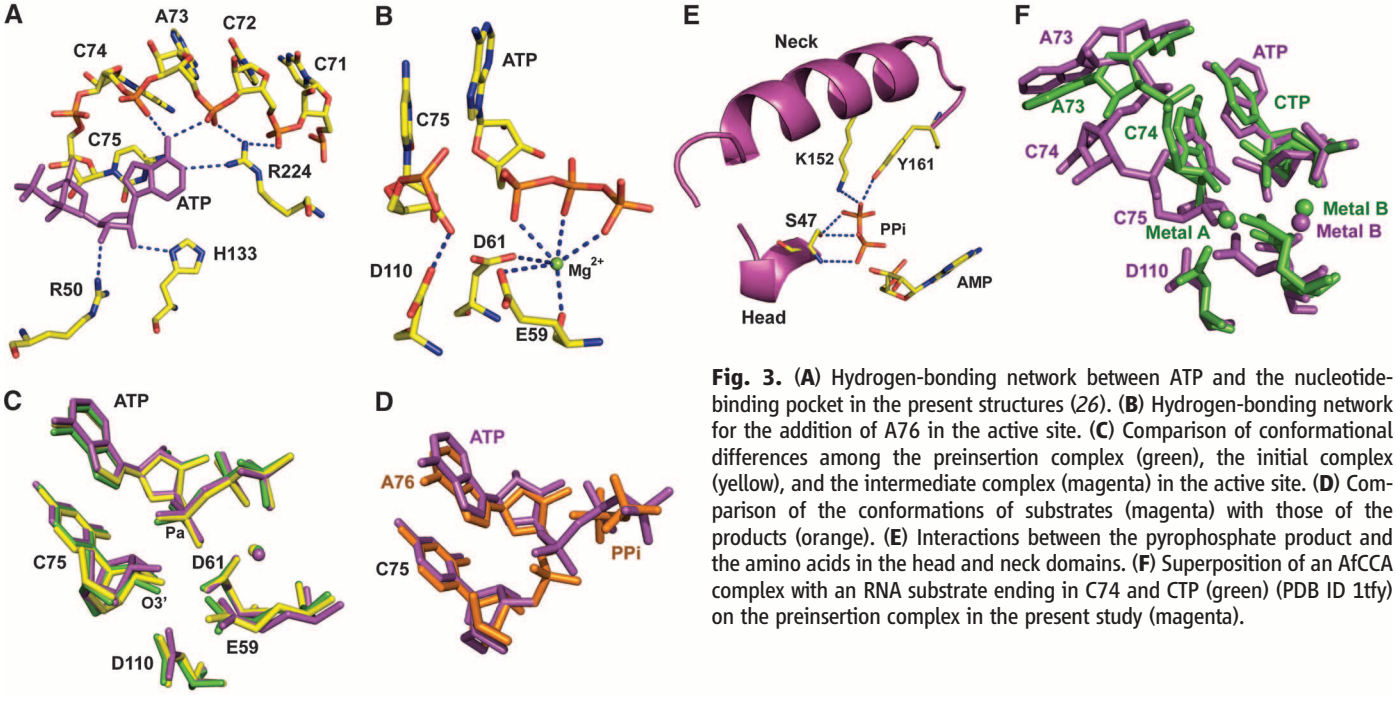

Fig. 3. (**A**) Hydrogen-bonding network between ATP and the nucleotide-binding pocket in the present structures (*26*). (**B**) Hydrogen-bonding network for the addition of A76 in the active site. (**C**) Comparison of conformational differences among the preinsertion complex (green), the initial complex (yellow), and the intermediate complex (magenta) in the active site. (**D**) Comparison of the conformations of substrates (magenta) with those of the products (orange). (**E**) Interactions between the pyrophosphate product and the amino acids in the head and neck domains. (**F**) Superposition of an AfCCA complex with an RNA substrate ending in C74 and CTP (green) (PDB ID 1tfy) on the preinsertion complex in the present study (magenta).

Downloaded from www.sciencemag.org on November 11, 2010

The crystal structures of complexes [1], [3], and [5] show that the RNA primer A73 has been extended to ACC75 in all three complexes during crystallization (Fig. 2). In the intermediate complex AfCCA(Mg^{2+})+A73+[CTP+ATP], ~50% of ATP remains in a preinsertion site without being incorporated, and the other 50% is incorporated into the primer ACC75 to form the product ACCA76 and pyrophosphate (fig. S1). In the structures of complexes [1] and [5], the reaction stalls after the incorporation of C75 with all of the nonreactive AMPcPP or noncognate substrate CTP in the preinsertion site (Fig. 2, B and E). The activity of complex [5] is different from the poly(C) polymerase activity observed in the CCA-adding enzymes from *Escherichia coli*, *Sulfolobus shibatae*, and *Methanococcus jannaschii* (*21*), which may result from the different conditions that we used in the crystallographic and biochemical studies. Similarly, the primer ACC75 has been extended to ACCA76 in the product complex AfCCA(Ca^{2+})+ACC75+[ATP] (Fig. 2D). However, somewhat surprisingly, the ATP stays in the preinsertion site in the initial complex AfCCA(Mn^{2+})+ACC75+[ATP] without incorporation (Fig. 2C).

The preinsertion complex AfCCA(Mg^{2+})+A73+[CTP+AMPcPP] cannot incorporate A76 because AMPcPP is unreactive. This structure reveals the essential network of interactions in the active site before catalysis begins. AMPcPP forms hydrogen-bonding interactions in the nucleotide-binding pocket with Arg^{224}, His^{133}, and Arg^{50} of the enzyme and with the phosphates of A73 and C74 of the RNA primer (Fig. 3A). In addition, Nη2 of Arg^{224} forms hydrogen bonds to the phosphate groups of C72 and A73, and its Nε hydrogen bonds to the O1P of C72. Similar interactions between ATP and the enzyme have been observed in the initial, intermediate, and product complexes, as well as in the previous structural studies of the A-adding step (*5*, *6*).

A metal ion that is coordinated to the triphosphate moiety of ATP (metal ion B) is observed in the active site of all of the structures reported here, except for that of the product complex. In the preinsertion complex, the metal ion (Mg^{2+}) is coordinated by the triphosphate moiety of AMPcPP and the two carboxylates of Glu^{59} and Asp^{61} (Fig. 3B). A third carboxylate, Asp^{110}, forms a strong hydrogen bond with the 3′ OH of the primer terminal C75. In the product complex in which AMP has been incorporated into the RNA primer, the pyrophosphate rotates ~180° away from the active site relative to the phosphate moiety of AMPcPP in the preinsertion complex and loses its interaction with metal ion B. Nonetheless, the pyrophosphate maintains essentially the same hydrogen-bonding interactions with the head and neck domains of the enzyme (Fig. 3E).

The superposition of the structures of the preinsertion, initial, and intermediate complexes shows the process of ATP incorporation (Fig. 3C). The distance between the primer terminal O3′ of C75 and the Pα of ATP decreases, and the angle formed by the O3′, the Pα, and the bridging oxygen atom between Pα and Pβ (O3′-Pα-O3A) increases from 155° toward 180° from the preinsertion state to the reaction intermediate state, illustrating the process of a nucleophilic attack of the O3′ on the Pα. In the intermediate complex, where both the reactants and the products coexist, the primer terminal O3′ atom remains in the same position, whereas the AMP moves toward the O3′ atom to form the O3′-Pα bond (Fig. 3D). A similar movement of the nucleotide substrate has been observed in the structures of ternary substrate [Protein Data Bank identification number (PDB ID): 1S76] and product (PDB ID: 1S77) complexes of T7 RNA polymerase (*14*).

Only one metal ion is observed in the active sites of the three A-adding complexes, which is consistent with previous structures (*5*, *6*). This metal ion corresponds to metal ion B of the classic two–metal-ion mechanism, which functions to coordinate and stabilize the leaving pyrophosphate group (*22*). The position of the 3′ terminal nucleotide C75 in the nucleotide-binding pocket sterically excludes the metal ion A from binding to the active site and facilitates the addition of A76. After the incorporation of C75 by a two–metal-ion mechanism (*5*), the acceptor stem of the tRNA does not translocate as first observed biochemically (*23*), but rather the previous primer terminal nucleotide, C74, is repositioned from its helical stacking position to a bulged position to allow the new primer terminal C75 nucleotide to now occupy the same priming-site position. The bulged out C74 lies in a nucleotide-binding pocket of limited size, which positions the 3′ OH of C75 more than 3 Å closer to the catalytic carboxylates than the 3′ OH of C74 in the previous addition step. Consequently, the O3′ of C75 occupies the metal ion position (Fig. 3F). The carboxylate side chain of Asp^{110} forms a new hydrogen bond with the O3′ of C75, whereas the other two catalytic carboxylates, Glu^{59} and Asp^{61}, coordinate metal ion B (Fig. 3B).

This model suggests that class I CCA-adding enzymes catalyze the addition of A76 by a carboxylate-assisted, one–metal-ion mechanism rather than a two–metal-ion mechanism. In the classic two–metal-ion mechanism, metal ion A facilitates the nucleophilic attack of the primer terminal 3′ OH on the α-phosphate of the incoming nucleotide by lowing its pK_a (where K_a is the acid dissociation constant), whereas metal ion B assists the leaving of the pyrophosphate group (*22*). The absence of metal ion A raises the question of what activates the nucleophilic attack of the 3′ OH to form the O3′-Pα bond. On the basis of the strong H-bond between Asp^{110} and the 3′-hydroxyl group of C75, we suggest that the third carboxylate residue in the active site, Asp^{110}, could function as a general base. Consistent with this proposal, biochemical studies have shown that mutation of Asp^{110} impairs addition of A76 but does not affect the addition of either C74 or

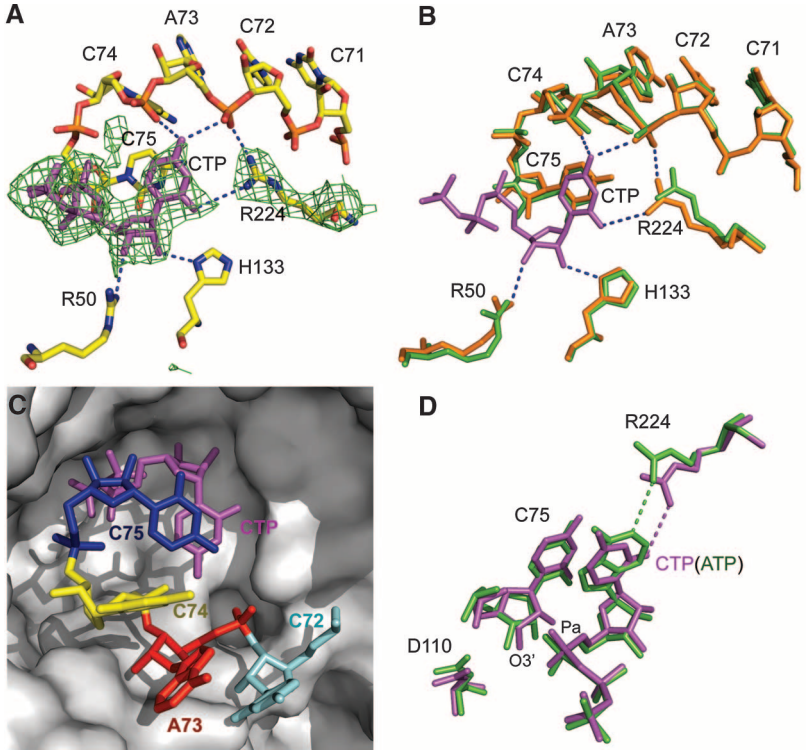

Fig. 4. (**A**) Hydrogen-bonding network in the nucleotide-binding pocket in the CTP complex with CTP and Arg^{224} superimposed on a difference electron-density map (Fo-Fc) contoured at 3.5σ. (**B**) Superposition of the CTP complex (orange) onto a binary complex of AfCCA and an RNA substrate ending in C75 (PDB ID 2dr9) (green). (**C**) The size of the binding pocket in the CTP complex with the enzyme shown in the surface representation. (**D**) Conformational differences between the CTP complex (magenta) and the preinsertion complex (green) in the nucleotide-binding pocket.

Downloaded from www.sciencemag.org on November 11, 2010

C75 (*24*, *25*). Thus, the one–metal-ion mechanism requires all three carboxylates: two that function in binding metal ion A and a third required for A76 addition only.

The structure of the ternary CTP complex, AfCCA(Ca^{2+})+A73+[CTP], showed that, in position 76, the CTP base makes the same hydrogen-bonding interaction with Arg^{224} as the base of ATP does in the preinsertion complex (Fig. 4A), which requires the movement of CTP toward Arg^{224} (Fig. 4D). Superposition onto the previously reported binary enzyme + tRNA complex AfCCA+ACC75 (*6*) shows that, in the CTP complex, the key amino acids in the binding pocket, Arg^{224}, His^{133} and Arg^{50}, move toward the incoming CTP, which fits snugly in the pocket (Fig. 4, B and C). In addition, oxygen atoms of the phosphate groups of A73 and C74 move toward CTP to engage in stronger hydrogen-bonding interactions with N4 of CTP. Such "induced fit" behavior of the binding pocket shows the effects of the incoming nucleosides on catalytic activity of nucleotidyltransferases.

The ability of the CCA-adding enzyme to insert ATP and not CTP at position 76 is a result of its properly positioning the α phosphate of ATP, but not that of CTP, in the active site for a nucleophilic attack by the 3′ OH of C75. CTP at position 76 has the same hydrogen-bonding interaction network as does ATP in the preinsertion complex. Because CTP is smaller, these interactions cause it to be located closer to Arg^{224} and cause Arg^{224} to move closer to CTP (Fig. 4D). As a result, the distance between the α-phosphate of the CTP and the 3′ oxygen atom O of C75 is 4.5 Å, which is too far for a reaction to occur. Furthermore, the 3′ terminal primer nucleotide C75 moves upward relative to the base of CTP, presumably to produce a better base-stacking interaction. This change moves the primer terminal 3′ OH out of interaction range with the catalytic carboxylate of Asp^{110} (Fig. 4D). Thus, the nucleophilic attack of O3′ of C75 on the α-phosphate of CTP is prevented.

Our results differ from those of a previous study in which CTP or ATP was soaked into the crystals of the binary complex, drawing the conclusion that Arg^{224} remains in the same configuration for the addition of nucleotide 76 onto ACC75, regardless of whether ATP or CTP is soaked into the crystal, and the base of CTP is positioned too far from Arg^{224} to interact with the guanidinium group (*6*). It could be that crystal-lattice constraints prevented the structural changes that we observe. Consistent with this, the soaking experiments did not result in extension of AC74 or ACC75 (*6*).

The present study resolves the disagreement between the two mechanisms that have been proposed for how the class I CCA-adding enzymes discriminate between CTP and ATP at the final addition step (*5*, *6*). The discrimination was first attributed to the size and shape changes of the nucleotide-binding pocket, caused by the movement of the head domain of the enzyme (*5*). However, in a subsequent study, the Arg^{224} residue was proposed to be the principal determinant of the discrimination between A and C incorporation at position 76 (*6*). In this model, the enzyme conformation did not change so that the smaller CTP could not react with Arg^{224}. Based on the five cocrystal structures, we show that the flexible side chain of Arg^{224} repositions in response to an incoming nucleotide base to hydrogen bond with the Watson-Crick edge of either C or A. The discrimination against incorporation of C arises, not from its lack of interaction with A224, but because the protein's flexibility to accommodate these interactions results in the improper geometry of CTP in the active site.

References and Notes

1. M. P. Deutscher, *The Enzymes* **15**, 183 (1982).
2. D. Yue, N. Maizels, A. M. Weiner, *RNA* **2**, 895 (1996).
3. Y. Xiong, F. Li, J. Wang, A. M. Weiner, T. A. Steitz, *Mol. Cell* **12**, 1165 (2003).
4. M. Okabe *et al.*, *EMBO J.* **22**, 5918 (2003).
5. Y. Xiong, T. A. Steitz, *Nature* **430**, 640 (2004).
6. K. Tomita, R. Ishitani, S. Fukai, O. Nureki, *Nature* **443**, 956 (2006).
7. Y. Toh *et al.*, *EMBO J.* **27**, 1944 (2008).
8. F. Li *et al.*, *Cell* **111**, 815 (2002).
9. K. Tomita *et al.*, *Nature* **430**, 700 (2004).
10. M. A. Augustin *et al.*, *J. Mol. Biol.* **328**, 985 (2003).
11. Y. Xiong, T. A. Steitz, *Curr. Opin. Struct. Biol.* **16**, 12 (2006).
12. T. A. Steitz, *Structure* **15**, 1523 (2007).
13. P. B. Balbo, A. Bohm, *Structure* **15**, 1117 (2007).
14. Y. W. Yin, T. A. Steitz, *Cell* **116**, 393 (2004).
15. D. Temiakov *et al.*, *Cell* **116**, 381 (2004).
16. D. G. Vassylyev *et al.*, *Nature* **448**, 163 (2007).
17. S. Doublié, S. Tabor, A. M. Long, C. C. Richardson, T. Ellenberger, *Nature* **391**, 251 (1998).
18. A. J. Berman *et al.*, *EMBO J.* **26**, 3494 (2007).
19. Materials and methods are available as supporting material on *Science* Online.
20. H. D. Cho, Y. Chen, G. Varani, A. M. Weiner, *J. Biol. Chem.* **281**, 9801 (2006).
21. M. Seth, D. L. Thurlow, Y. M. Hou, *Biochem* **41**, 4521 (2002).
22. T. A. Steitz, *Nature* **391**, 231 (1998).
23. P. Y. Shi, N. Maizels, A. M. Weiner, *EMBO J.* **17**, 3197 (1998).
24. D. Yue, A. M. Weiner, N. Maizels, *J. Biol. Chem.* **273**, 29693 (1998).
25. H. D. Cho, C. L. Verlinde, A. M. Weiner, *J. Biol. Chem.* **280**, 9555 (2005).
26. Single-letter abbreviations for the amino acid residues are as follows: A, Ala; C, Cys; D, Asp; E, Glu; F, Phe; G, Gly; H, His; I, Ile; K, Lys; L, Leu; M, Met; N, Asn; P, Pro; Q, Gln; R, Arg; S, Ser; T, Thr; V, Val; W, Trp; and Y, Tyr.

27. We thank the staff at the Advanced Photon Source beamline ID19 and at the National Synchrotron Light Source beamline X25. We also thank the staff of the Center for Structural Biology core facility at Yale University. This work was supported by NIH grant GM57510 (to T.A.S.). The coordinates and structure factors for the five structures have been deposited in the Research Collaboratory for Structural Bioinformatics Protein Data Bank with accession numbers 3OVA, 3OV7, 3OVB, 3OUY, and 3OVS for preinsertion, initial, intermediate, product, and CTP complexes, respectively.

Supporting Online Material

www.sciencemag.org/cgi/content/full/330/6006/937/DC1
Materials and Methods
Fig. S1
Table S1
References

12 July 2010; accepted 23 September 2010
10.1126/science.1194985

Downloaded from www.sciencemag.org on November 11, 2010

REPORTS

Radio-Frequency Association of Efimov Trimers

Thomas Lompe,[1,2,3]* Timo B. Ottenstein,[1,2,3] Friedhelm Serwane,[1,2,3] Andre N. Wenz,[1,2] Gerhard Zürn,[1,2] Selim Jochim[1,2,3]

The quantum mechanical three-body problem is one of the fundamental challenges of few-body physics. When the two-body interactions become resonant, an infinite series of universal three-body bound states is predicted to occur, whose properties are determined by the strength of the two-body interactions. We used radio-frequency fields to associate Efimov trimers consisting of three distinguishable fermions. The measurements of their binding energy are consistent with theoretical predictions that include nonuniversal corrections.

Under certain conditions, the long-range behavior of a physical system can be described without detailed knowledge of its short-range properties; few-body systems with resonant interactions are a prime example of this concept of universality (*1*). Ultracold gases, where resonant scattering may be achieved by tuning the interactions with the use of Feshbach resonances (*2*), have been used extensively to test the predictions of universal theory.

If the parameter describing the interactions, the s-wave scattering length a, is much larger than the characteristic length scale r_0 of the interaction potential, the few-body physics in such ultracold gases is predicted to become universal. For two particles with a large positive scattering

[1]Physikalisches Institut, Ruprecht-Karls-Universität Heidelberg, 69120 Heidelberg, Germany. [2]Max-Planck-Institut für Kernphysik, Saupfercheckweg 1, 69117 Heidelberg, Germany. [3]ExtreMe Matter Institute EMMI, GSI Helmholtzzentrum für Schwerionenforschung, 64291 Darmstadt, Germany.

*To whom correspondence should be addressed. E-mail: thomas.lompe@mpi-hd.mpg.de

length, there is a weakly bound universal dimer state whose binding energy scales as $1/a^2$. For three particles with large interparticle interactions, there is a series of weakly bound trimer states, which are called Efimov trimers (*3*). For negative scattering lengths, these trimer states become bound at critical values of the interaction strength, which are spaced by a universal scaling factor. For diverging interaction strength, this results in an infinite series of Efimov states. Their absolute position depends on short-range three-body physics, which can be described by a single three-body parameter. For positive scattering lengths, the trimer states disappear when they cross the atom-dimer threshold; that is, their binding energy becomes degenerate with the binding energy of a dimer state (fig. S1). These crossings of trimer states with the continuum threshold can be observed experimentally as resonant enhancements of the rate constants for inelastic three-atom and atom-dimer collisions, respectively. This made it possible to obtain the first convincing evidence for the existence of Efimov trimers by tuning the interparticle interaction in an ultracold atomic gas using a Feshbach resonance, which enabled the observation of signatures of Efimov trimers in the rate of inelastic three-body collisions (*4*). Since then, this technique has been used with great success, but it is limited to observations of the crossings of Efimov states with the continuum (*5*–*17*).

The predictions of universal theory can be tested by observing multiple crossings of trimer states with the continuum in a single system. Some experiments are consistent with these predictions (*11*, *13*), whereas others see larger deviations (*9*) or even a systematic shift across a Feshbach resonance (*12*).

We studied Efimov physics in a conceptually different manner by directly measuring the binding energy of an Efimov state as a function of interaction strength. Our experiments use an ultracold Fermi gas consisting of fermionic ^{6}Li atoms in the three energetically lowest Zeeman substates. We label these states $|1\rangle$, $|2\rangle$, and $|3\rangle$ (*6*). Because of Pauli blocking, only atoms in different states interact with each other at ultracold temperatures. These interactions are described by three different interparticle scattering lengths a_{12}, a_{23}, and a_{13} for the respective combinations of atoms in different states (*18*) (Fig. 1A). For each of these combinations, there is a broad Feshbach resonance leading to three different weakly bound dimer states, which we label $|12\rangle$, $|23\rangle$, and $|13\rangle$ (Fig. 1B). If the corresponding scattering length is much larger than the characteristic radius $r_0 \approx 60\ a_0$ of the ^{6}Li interaction potential (where a_0 is Bohr's radius), the dimer binding energy E_{ij} is given by the universal relation $E_{ij} = \hbar^2/ma_{ij}^2$, where m is the mass of a ^{6}Li atom, $\hbar$ is Planck's constant divided by 2π, and the indices $i, j = 1, 2, 3$ indicate the state of the atoms. Because the Feshbach resonances for the three combinations overlap, all scattering lengths can be tuned to large values simultaneously, leading to the appearance of Efimov states. However, as the different scattering lengths do not diverge at the same magnetic field, the series of trimer states is finite. There are two Efimov trimer states in this system (*19*) whose crossings with the continuum have already been located by observing enhanced

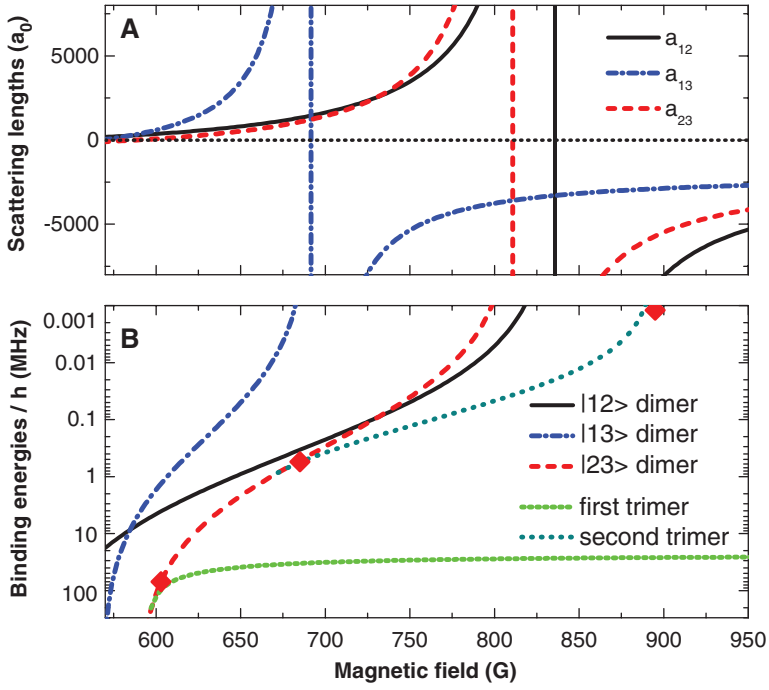

Fig. 1. (**A**) Values of the three different two-body scattering lengths for magnetic fields between 570 and 950 G, given in units of Bohr's radius a_0 (*18*). (**B**) Binding energy of the dimer and trimer states according to universal theory, calculated using the three-body parameter determined from the crossing at $B = 895$ G (*19*). The measured positions of the crossings of the trimer states with the continuum are marked by red diamonds (*10*, *14*, *15*).

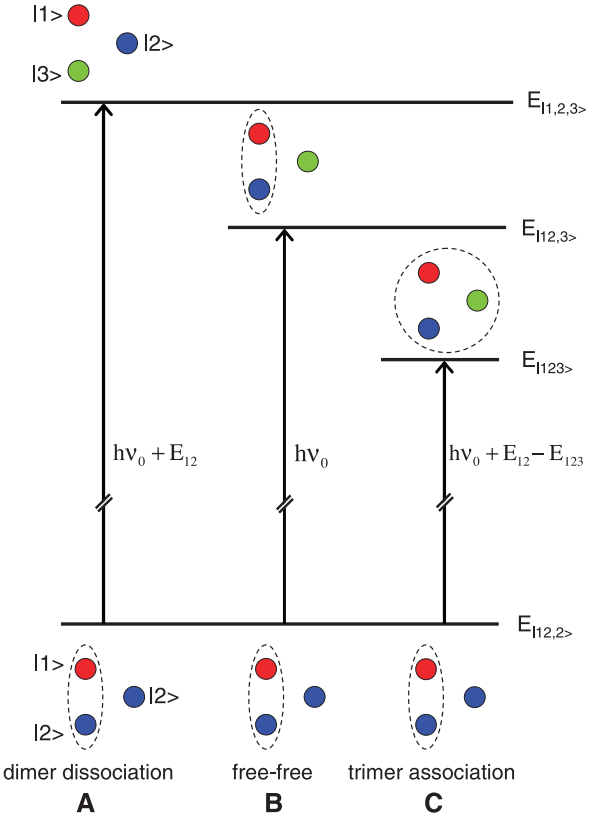

Fig. 2. (**A** to **C**) Relevant transitions and energy levels for the radio-frequency (rf) association of trimers. The initial system has the energy $E_{|12,2\rangle}$ of a free atom in state $|2\rangle$ and a $|12\rangle$ dimer. The frequency ν_0 of the bare transition drives the unbound atoms from state $|2\rangle$ to state $|3\rangle$, leading to a $|3\rangle$-$|12\rangle$ atom-dimer mixture (B). By choosing the appropriate detuning from the bare atomic transition, we can either dissociate the dimer, leading to three unbound atoms in states $|1\rangle$, $|2\rangle$, and $|3\rangle$ (A), or associate a dimer and an atom into a trimer (C).

Downloaded from www.sciencemag.org on November 11, 2010

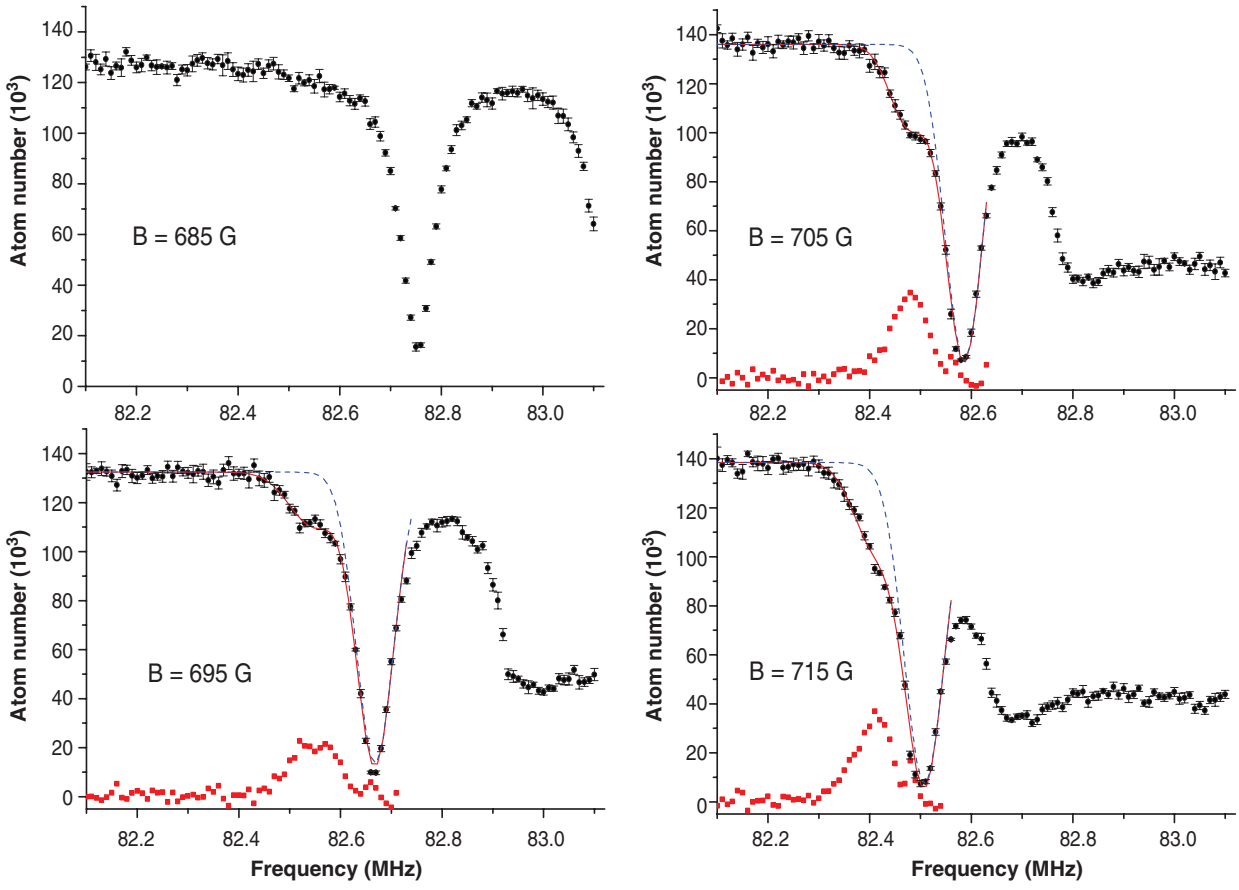

Fig. 3. Number of atoms in state $|2\rangle$ remaining after the rf pulse as a function of frequency for four different magnetic fields (black circles). Each data point is the average of five to eight individual measurements; error bars denote SEM. The central dip results from driving the bare atomic transition, and the dip to the right is a consequence of the dissociation of dimers. The trimer association manifests itself as a smaller feature sitting on the left flank of the central dip. The red lines are a fit of two overlapping Gaussians to the data. The dashed blue line shows the Gaussian fitted to the central dip. The difference between this fit and the data, which shows the signal from the trimer association, is plotted as red squares.

inelastic collision rates (*6*, *7*, *10*, *14*, *15*) (Fig. 1B). From these measurements, the binding energies of these trimer states according to universal theory have been calculated (*15*, *19*), where (*15*) also included finite range corrections to the two-body interactions.

To directly measure the binding energy of one of these Efimov states, we used radio-frequency (rf) spectroscopy, a technique that has been extensively used to study weakly bound dimer states (*18*, *20*). This technique is based on the use of rf fields to drive transitions between different internal states of the atoms, where in both the initial and final state the atoms can be either free or bound in a molecule. The difference in binding energy between the initial and final state can be measured as a shift of the transition frequency from the bare atomic transition.

The most straightforward way to perform rf spectroscopy of a bound state is to dissociate the molecule into free atoms. In this case, the rf transition is simply shifted by the binding energy of the molecule. However, because Efimov trimers are highly unstable—with lifetimes expected to range from a few nanoseconds to tens of microseconds (*19*)—it is impossible to prepare macroscopic samples of trimers in current experiments, and dissociation spectroscopy is not technically feasible. This can be overcome by using rf fields to associate trimers from free atoms or from atoms and dimers, but obtaining observable association rates is challenging for several reasons.

Let us first consider the initial states available for the association. Starting from one atom in state $|1\rangle$ and two atoms in state $|2\rangle$, one can use an rf transition to drive the atoms in state $|2\rangle$ to state $|3\rangle$. However, this is a coherent process that affects both atoms in state $|2\rangle$ in the same way, so they remain identical particles. Thus, this process cannot lead to the formation of trimers. Instead we can bind two of the atoms into a weakly bound $|12\rangle$ dimer, which breaks the symmetry between the two atoms in state $|2\rangle$, because for one of them the rf transition is now shifted by the binding energy of the dimer (*21*).

Next, the wave function overlap of the initial and final state must be considered. Close to the crossing of the trimer state with the atom-dimer threshold, the size of the dimer and the trimer are on the order of the scattering lengths. Hence, the spatial wave function of a dimer and an atom has a finite overlap with the spatial wave function of the trimer when the atom approaches the dimer to a distance on the order of the scattering length. Therefore, the association rate depends critically on the phase-space density of the initial atom-dimer mixture. If we were to use a degenerate gas, it would spatially separate into a molecular Bose-Einstein condensate of dimers and an outer shell of unbound fermionic atoms (*22*), which would reduce the spatial overlap between atoms and dimers in the trap. Therefore, we must use a thermal mixture ($T \approx 1$ μK; $T/T_F \approx 0.7$, where T_F is the Fermi temperature of the unpaired atoms) of atoms in state $|2\rangle$ and $|12\rangle$ dimers, which limits the efficiency of the association. A similar limitation has already been observed in the rf association of weakly bound dimers (*23*). Finally, the short lifetime of the Efimov trimer leads to a suppression of trimer formation analogous to the quantum Zeno effect. This can in principle be avoided by driving the rf transition with a Rabi frequency that is large relative to the decay rate of the trimer. However, this is not feasible with our current experimental setup, which further reduces the association rate.

From these considerations, it follows that the trimer state with the most favorable conditions for

Downloaded from www.sciencemag.org on November 11, 2010

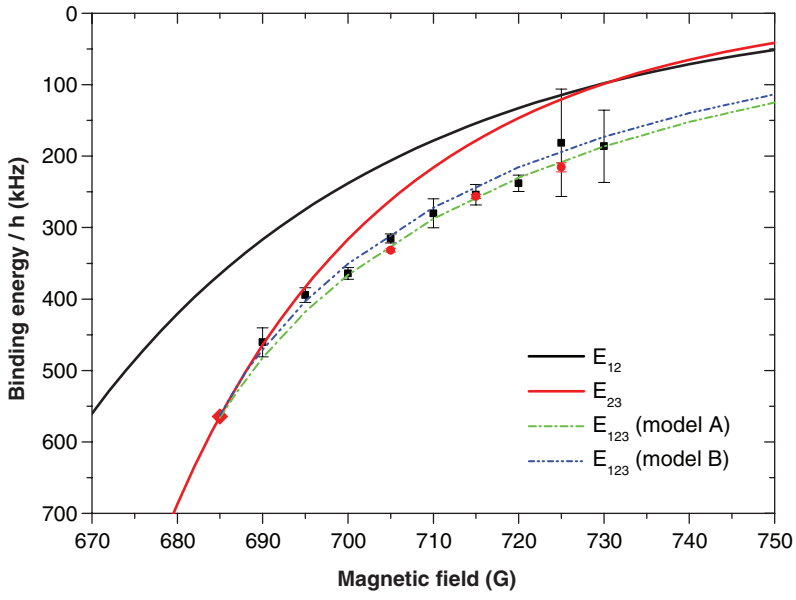

Fig. 4. Binding energy of the second Efimov trimer in ^{6}Li measured using a |2⟩-|12⟩ (black squares) or |2⟩-|23⟩ (red dots) mixture as the initial system. The error bars are derived from the 2σ confidence bounds of the fit to the rf spectra. Additionally, there are systematic uncertainties caused by the broadened line shapes and temperature effects (see supporting online material). The solid lines give the binding energies of the |12⟩ and |23⟩ dimers including nonuniversal corrections (*15*). The red diamond marks the position of the observed crossing of the trimer state with the |1⟩-|23⟩ atom-dimer threshold (*14*, *15*). The dashed lines show the binding energy of the trimer according to calculations from (*15*).

rf association in our system is the second trimer state, as it is larger in size and has a longer lifetime (*19*). This state crosses into the |1⟩-|23⟩ atom-dimer continuum at B = 685 G (Fig. 1B). To measure its binding energy, we prepared mixtures of atoms in state |2⟩ and |12⟩ dimers at magnetic fields between 670 and 740 G and applied rf fields at frequencies around the |2⟩-|3⟩ transition.

At the frequency ν_0 that corresponds to the bare atomic transition, the free atoms are driven from state |2⟩ to state |3⟩ while the dimer remains unaffected (Fig. 2B). If the RF is blue-detuned by the binding energy E_{12} of the dimers, the dimers are dissociated (Fig. 2A). The trimer is associated at the frequency $\nu = \nu_0 - (E_{123}/h) + (E_{12}/h)$, where E_{123} is the binding energy of the Efimov trimer with respect to the |1⟩-|2⟩-|3⟩ continuum. Therefore, the association is red-shifted from the bare transition by the difference between the dimer and trimer binding energies (Fig. 2C). In each of these cases, we observe a loss of atoms from the trap, either through decay in inelastic |3⟩-|12⟩ or |1⟩-|2⟩-|3⟩ collisions or through the decay of the associated trimers. If the rf is not resonant for either of these processes, the atom number is not affected. Sample spectra for different magnetic fields are shown in Fig. 3.

Because of the limited wave function overlap of the initial and final state and the quantum Zeno suppression of the association, we apply strong rf pulses with a duration of 35 to 50 ms and a Rabi frequency of $\Omega \approx 2\pi \times 7$ kHz to associate enough trimers to obtain an observable decrease in the atom number. Collisions lead to decoherence and thus a strong broadening of the bare transition. However, as the association is offset from the free-free transition by $(E_{123} - E_{12})/h$, the association features can still be observed (Fig. 3). For magnetic fields below the crossing of the trimer and the |1⟩-|23⟩ atom-dimer threshold at 685 G, there is no trimer state and consequently we observe no association peak. At B = 695 G, the association signal is clearly visible. For higher magnetic fields, $E_{123} - E_{12}$ becomes smaller, and the association peak moves closer to the free-free transition. Because we do not have a better model for the line shapes of the broadened transitions, we fit the spectra with two overlapping Gaussians to determine the position of the association dips. From these we calculate the binding energy of the trimer using the values of the binding energy of the |12⟩ dimer known from previous experiments (*18*). The resulting binding energies of the trimer are plotted in Fig. 4. To confirm that the results were independent of the initial system and the transition used, we performed the same measurement starting from a |2⟩-|23⟩ mixture at magnetic fields between 705 and 725 G and driving the |1⟩-|2⟩ transition (fig. S2). The two sets of measurements agree within experimental uncertainties (Fig. 4).

The measured binding energy of the trimer increases with decreasing scattering lengths while the difference to the binding energy of the |23⟩ dimer decreases, as expected from the universal scenario. At B = 690 G, the dimer and trimer binding energies are the same within our experimental resolution, and for $B \leq 685$ G, the trimer association feature vanishes. This coincides with the previously observed enhancement of inelastic atom-dimer collisions at 685 ± 2 G (*14*), which confirms the interpretation of such loss resonances as signatures of a crossing of a trimer state with the continuum.

We also compared our data to the predictions from a theoretical model by Nakajima *et al.* that uses the observed crossings of the trimer states as inputs to calculate the trimer binding energies (*15*). This model includes finite range corrections to the two-body interactions known from previous experiments (*18*). To exclude a dependence of their results on the specific model, Nakajima *et al.* used two different parameterizations of the nonuniversal corrections (A and B) that yielded essentially identical results. Within the systematic uncertainties due to temperature effects and the broadened line shapes, our data are in good agreement with their predictions. Additionally, their model includes an energy dependence of the three-body parameter. However, in the magnetic field region of interest, the difference to a model with a constant three-body parameter derived from the atom-dimer resonance at 685 G is too small to be resolved with our current resolution (*15*, *24*).

By increasing the resolution of the measurements and reducing the systematic uncertainties, it should be possible to use the techniques developed in this work to do precision tests of few-body physics and to directly determine the lifetime of Efimov trimers from the width of the association peaks. Driving the rf transition with a Rabi frequency larger than the decay rate of the trimers should allow coherent population of the trimer state, as was done for universal dimers (*23*). This would be a major step toward the preparation of macroscopic samples of Efimov trimers.

References and Notes

1. E. Braaten, H. W. Hammer, *Phys. Rep.* **428**, 259 (2006).
2. C. Chin, R. Grimm, P. Julienne, E. Tiesinga, *Rev. Mod. Phys.* **82**, 1225 (2010).
3. V. Efimov, *Sov. J. Nucl. Phys.* **12**, 589 (1971); originally: *Yad. Fiz.* **12**, 1080 (1970).
4. T. Kraemer *et al.*, *Nature* **440**, 315 (2006).
5. S. Knoop *et al.*, *Nat. Phys.* **5**, 227 (2009).
6. T. B. Ottenstein, T. Lompe, M. Kohnen, A. N. Wenz, S. Jochim, *Phys. Rev. Lett.* **101**, 203202 (2008).
7. J. H. Huckans, J. R. Williams, E. L. Hazlett, R. W. Stites, K. M. O'Hara, *Phys. Rev. Lett.* **102**, 165302 (2009).
8. G. Barontini *et al.*, *Phys. Rev. Lett.* **103**, 043201 (2009).
9. M. Zaccanti *et al.*, *Nat. Phys.* **5**, 586 (2009).
10. J. R. Williams *et al.*, *Phys. Rev. Lett.* **103**, 130404 (2009).
11. N. Gross, Z. Shotan, S. Kokkelmans, L. Khaykovich, *Phys. Rev. Lett.* **103**, 163202 (2009).
12. S. E. Pollack, D. Dries, R. G. Hulet, *Science* **326**, 1683 (2009).

Downloaded from www.sciencemag.org on November 11, 2010

13. N. Gross, Z. Shotan, S. Kokkelmans, L. Khaykovich, *Phys. Rev. Lett.* **105**, 103203 (2010).
14. T. Lompe *et al.*, *Phys. Rev. Lett.* **105**, 103201 (2010).
15. S. Nakajima, M. Horikoshi, T. Mukaiyama, P. Naidon, M. Ueda, *Phys. Rev. Lett.* **105**, 023201 (2010).
16. J. von Stecher, J. P. D'Incao, C. H. Greene, *Nat. Phys.* **5**, 417 (2009).
17. F. Ferlaino *et al.*, *Phys. Rev. Lett.* **102**, 140401 (2009).
18. M. Bartenstein *et al.*, *Phys. Rev. Lett.* **94**, 103201 (2005).
19. E. Braaten, H. W. Hammer, D. Kang, L. Platter, *Phys. Rev. A* **81**, 013605 (2010).
20. C. A. Regal, C. Ticknor, J. L. Bohn, D. S. Jin, *Nature* **424**, 47 (2003).
21. The lifetime of this atom-dimer mixture is on the order of several seconds; as for two-component Fermi gases, inelastic processes are suppressed by Pauli blocking. In bosonic systems, such mixtures decay much more quickly and this scheme is probably inapplicable.
22. Y. Shin, M. W. Zwierlein, C. H. Schunck, A. Schirotzek, W. Ketterle, *Phys. Rev. Lett.* **97**, 030401 (2006).
23. C. Klempt *et al.*, *Phys. Rev. A* **78**, 061602 (2008).
24. P. Naidon, M. Ueda, http://arxiv.org/abs/1008.2260 (2010).
25. We thank E. Braaten, J. P. D'Incao, and H. W. Hammer for inspiring discussions; P. Naidon for providing his data on the trimer binding energies; and J. Ullrich and his group for their support. Supported by the IMPRS-QD (G.Z. and A.N.W.), the Helmholtz Alliance HA216/EMMI, and the Heidelberg Center for Quantum Dynamics.

Supporting Online Material

www.sciencemag.org/cgi/content/full/330/6006/940/DC1
Materials and Methods
Figs. S1 and S2

2 June 2010; accepted 8 October 2010
10.1126/science.1193148

A Low-Magnetic-Field Soft Gamma Repeater

N. Rea,[1]* P. Esposito,[2] R. Turolla,[3,4] G. L. Israel,[5] S. Zane,[4] L. Stella,[5] S. Mereghetti,[6] A. Tiengo,[6] D. Götz,[7] E. Göğüş,[8] C. Kouveliotou[9]

Soft gamma repeaters (SGRs) and anomalous x-ray pulsars form a rapidly increasing group of x-ray sources exhibiting sporadic emission of short bursts. They are believed to be magnetars, that is, neutron stars powered by extreme magnetic fields, $B \sim 10^{14}$ to 10^{15} gauss. We report on a soft gamma repeater with low magnetic field, SGR 0418+5729, recently detected after it emitted bursts similar to those of magnetars. X-ray observations show that its dipolar magnetic field cannot be greater than 7.5×10^{12} gauss, well in the range of ordinary radio pulsars, implying that a high surface dipolar magnetic field is not necessarily required for magnetar-like activity. The magnetar population may thus include objects with a wider range of *B*-field strengths, ages, and evolutionary stages than observed so far.

Magnetized, isolated rotating neutron stars are often detected as pulsating sources in the radio and x-ray bands, hence the name pulsars. Pulsars slow down with time as their rotational energy is lost via magnetic dipole radiation. The surface dipolar magnetic field (B) of a pulsar can be estimated using its spin period, P, and spin-down rate, $\dot{P}$, as follows:

$$B = (3Ic^3 P\dot{P}/8\pi^2 R^6)^{1/2} \sim 3.2 \times 10^{19}(P\dot{P})^{1/2}\mathrm{G} \quad (1)$$

where P is in seconds and $\dot{P}$ is in seconds/seconds; we assumed $R \sim 10^6$ cm and $I \sim 10^{45}$ g cm^2, which are the neutron star radius and moment of inertia, respectively.

Although this expression was developed to estimate the magnetic fields of radio pulsars, usually ~10^{12} gauss (G), it has been traditionally used also for magnetars, where the derived values of B reach ~10^{15} G (*1*). To date, only ~16 of these ultramagnetized neutron stars have been observed (*2*, *3*); their population includes soft gamma repeaters (SGRs) and anomalous x-ray pulsars (AXPs). All known magnetars are x-ray pulsars with luminosities of $L_X \sim 10^{32}$ to 10^{36} erg s^{-1}, usually much higher than the rate at which the star loses its rotational energy through spin-down. Their high luminosities together with the lack of evidence for accretion from a stellar companion (*4*, *5*) led to the conclusion that the energy reservoir fueling the SGR/AXP activity is their extreme magnetic field (*6*, *7*). Observationally, magnetars are characterized by stochastic outbursts (lasting from days to years) during which they emit very short x-ray and γ-ray bursts; they have rotational periods in a narrow range (2 to 12 s) and, compared with other isolated neutron stars, large period derivatives of ~10^{-13} to 10^{-10} s s^{-1}. Their large dipolar B fields and relatively young characteristic ages (t_c) are estimated to be more than ~5×10^{13} G, and $t_c = P/2\dot{P} \sim 0.2$ thousand years to 0.2 million years [see (*2*) for a review].

In addition to the canonical SGRs and AXPs, two other sources are known to show magnetar-like activity: PSR J1846–0258 (*8*, *9*) and PSR 1622–4950 (*10*). The former is a 0.3 s, allegedly rotation-powered, x-ray pulsar, with a magnetic field of $B \sim 4.8 \times 10^{13}$ G (in the lower end of the magnetar range), from which a typical magnetar outburst and short x-ray bursts were detected. In the latter, flaring radio emission with a rather flat spectrum [similar to those observed in the two transient radio magnetars (*11*, *12*)] was detected from a 4.3-s radio pulsar with a magnetic field in the magnetar range ($B \sim 3 \times 10^{14}$ G).

In all sources with magnetar-like activity, the dipolar field spans 5×10^{13} G $< B < 2 \times 10^{15}$ G, which is ~10 to 1000 times the average value in radio pulsars and higher than the electron quantum field, $B_Q = m_e^2 c^3/e\hbar \sim 4.4 \times 10^{13}$ G. The existence of radio pulsars with $B > B_Q$ and showing only normal behavior (*13*) is an indication that a magnetic field larger than the quantum electron field alone may not be a sufficient condition for the onset of magnetar-like activity. In contrast, so far the opposite always held: Magnetar-like activity was observed only in sources with dipolar magnetic fields stronger than B_Q.

SGR 0418+5729 was discovered on 5 June 2009 when the Fermi Gamma-ray Burst Monitor (GBM) observed two magnetar-like bursts (*14*).

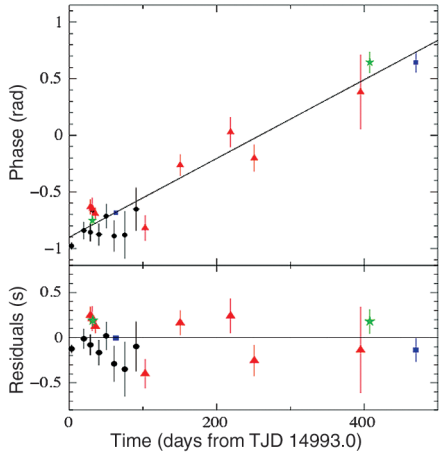

Fig. 1. (**Top**) Rotation phase versus time for the coherent timing solution for SGR 0418+5729 obtained using data taken with Rossi X-ray Timing Explorer (black circles), Swift (red triangles), XMM-Newton (blue squares), and Chandra (green stars). The solid line shows the best-fitting linear function (χ^2 = 1.8 for 18 degrees of freedom; root mean square ~3%). (**Bottom**) Fit residuals.

[1]Institut de Ciéncies de l'Espai, Consejo Superior de Investigaciones Científicas, Institut d'Estudis Espacials de Catalunya, Facultat de Ciéncies, Campus UAB, Torre C5-parell, 2a planta, 08193 Bellaterra (Barcelona), Spain. [2]Istituto Nazionale di Astrofisica (INAF), Osservatorio Astronomico di Capodimonte, Località Poggio dei Pini, Strada 54, I-09012 Capoterra, Italy. [3]Dipartimento di Fisica, Università di Padova, Via Francesco Marzolo 8, I-35131 Padova, Italy. [4]Mullard Space Science Laboratory, University College London, Holmbury St. Mary, Dorking, Surrey RH5 6NT, UK. [5]INAF, Osservatorio Astronomico di Roma, Via Frascati 33, I-00040 Monteporzio Catone, Italy. [6]INAF, Istituto di Astrofisica Spaziale e Fisica Cosmica di Milano, Via Edoardo Bassini 15, I-20133 Milano, Italy. [7]Astrophysique Instrumentation et Modélisation, Commissariat à l'Énergie Atomique et aux Énergies Alternatives, Direction des Sciences de la Matière, CNRS, Université Paris Diderot, Institut de Recherche sur les Lois Fondamentales de l'Univers, Service d'Astrophysique, Saclay, F-91191 Gif-sur-Yvette, France. [8]Sabancı University, Orhanlı-Tuzla, 34956 Istanbul, Turkey. [9]NASA Marshall Space Flight Center, Huntsville, AL 35812, USA.

*To whom correspondence should be addressed. E-mail: rea@ieec.uab.es

Downloaded from www.sciencemag.org on November 11, 2010

Follow-up observations with several x-ray satellites show that it has x-ray pulsations at ~9.1 s, well within the range of periods of magnetar sources (*15*, *16*). Further studies show that SGR 0418+5729 exhibits all the typical characteristics of a magnetar: (i) emission of short x-ray bursts, (ii) enhanced persistent flux, (iii) slow pulsations with a variable pulse profile, and (iv) an x-ray spectrum characterized by a thermal plus nonthermal component, which softened as the outburst decayed.

What made this source distinctly different was the failure of detecting a period derivative in the first 160 days after the outburst onset, despite frequent observational coverage. Several x-ray satellites (*16*) monitored the source almost weekly since its detection. This extensive observational campaign allowed the determination of an accurate ephemeris for the pulsar rotational period, but no sign of a spin-down was detected. In the first 160 days after the outburst onset, the upper limit on the period derivative was 10^{-13} s s^{-1} (90% confidence level), which, according to Eq. 1, translates into a surface dipolar magnetic field $B < 3 \times 10^{13}$ G (*16*). This limit is quite low for a magnetar source, but not abnormally so, given the detection of a comparable magnetic field in the magnetar-like PSR J1846–0258 (*8*), or the case of AXP 1E 2259+586 with $B \sim 6 \times 10^{13}$ G (*17*).

SGR 0418+5729 could not be monitored for a while after the first 160 days, because the Sun became too close to its position in the sky. On 9 July 2010, soon after it became observable again, we started an extensive monitoring of the source with the Swift, Chandra, and X-ray Multimirror Misson–Newton (XMM-Newton) x-ray satellites (table S1). In particular, on 23 July 2010, we detected it with the Advanced Charge-Coupled Device Imaging Spectrometer (ACIS) onboard Chandra at a flux of $(1.2 \pm 0.1) \times 10^{-13}$ erg s^{-1} cm^{-2} (0.5 to 10 keV), more than one order of magnitude fainter than in the previous available observation (*16*). The spectrum is well fit by an absorbed blackbody with a line-of-sight absorption $N_H = (1.5 \pm 1.0) \times 10^{21}$ cm^{-2} and $kT = 0.67 \pm 0.11$ keV (all quoted errors are at 90% confidence level). Pulsations were also clearly detected at the known magnetar period. On 24 September 2010, we observed SGR 0418+5729 with the European Photon Imaging Camera (EPIC) onboard XMM-Newton, which detected it at a comparable flux, and could measure again the rotational period of the neutron star. We used our new Swift, Chandra, and XMM-Newton observations, together with several other observations (table S1) and phase-connected all the source data from 5 June 2009 until 24 September 2010 (Fig. 1 and Supporting Online Material). We found a best-fit period of 9.07838827(4) s referred to TJD (Truncated Julian Day) 14993.0 and to the solar system barycenter. The phase evolution of SGR 0418+5729 is well described by a linear relation $\varphi = \varphi_0 + 2\pi(t - t_0)/P$, and a quadratic term $-2\pi\dot{P}(t - t_0)^2/2P^2$ (which reflects the presence of a spin-down) is not statistically required. This implies an upper limit on the period derivative of SGR 0418+5729 of $\dot{P} < 6.0 \times 10^{-15}$ s s^{-1} (90% confidence level). This value is the smallest of all known SGRs/AXPs, of the two magnetar-like pulsars PSR J1846–0258 and PSR 1622–4950, and of the x-ray dim isolated neutron stars (XDINSs) (*18*) for which a measure of $\dot{P}$ is available (Fig. 2). The corresponding limit on the surface dipolar magnetic field of SGR 0418+5729 is $B < 7.5 \times 10^{12}$ G, making it the magnetar with the lowest surface dipolar magnetic field yet. The upper limit on the period derivative implies a characteristic age of the source $t_c > 24$ million years.

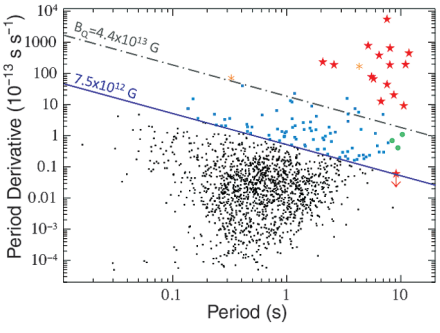

Fig. 2. *P*–$\dot{P}$ diagram for all known isolated pulsars [data are from (*29*, *30*)]. $\dot{P}$ is in units of 10^{-13} s s^{-1}. Black squares represent normal radio pulsars, light-blue squares are normal radio pulsars with a magnetic field larger than 7.5×10^{12} G (our limit for SGR 0418+5729), red stars are the magnetars, orange asterisks are the magnetar-like pulsars PSR J1846–0258 and PSR 1622–4950, and green circles are the XDINSs. The blue solid line marks the 90% upper limit for the dipolar magnetic field of SGR 0418+5729. The value of the electron quantum magnetic field is also reported (dash-dotted gray line).

Although the characteristic age is known to overestimate the true age of a neutron star in which magnetic field decay occurred (*19*), as is likely the case of SGR 0418+5729, the rather high Galactic latitude ($b = 5.1$ deg) and its position on the *P*–$\dot{P}$ plane [close to the death line for radio pulsars, below which the radio emission is supposed to be halted (*20*, *21*)], suggest that this system is quite a lot older than the other SGRs/AXPs.

The existence of magnetar-like sources with low values of *B* has several consequences. Among isolated pulsars, which are presumably rotation-powered, ~18% have a dipolar magnetic field higher than the upper limit we derived for SGR 0418+5729 (Fig. 2). The discovery of PSR 1622–4950 (*10*), on the other hand, suggests that magnetar-like behavior may manifest itself mostly in the radio band. In this framework, our result indicates that a large number of apparently normal pulsars might turn on as magnetars at any time, regardless of whether the surface dipole magnetic field is above the quantum limit. As a direct consequence, magnetar-like activity may occur in pulsars with a very wide range of magnetic fields, and it may fill a continuum in the *P*–$\dot{P}$ diagram (Fig. 2).

So far, we have been considering the relationship between the surface dipolar magnetic field and magnetar-like activity. However, it is likely that the magnetar activity is driven by the magnetic energy stored in the internal toroidal field (*6*, *22*); this component cannot be measured directly. If the magnetar model as it is currently understood is indeed valid, despite its low surface dipolar field, SGR 0418+5729 is expected to harbor a sufficiently intense internal toroidal component B_{tor} in order to be able to undergo outbursts and emit bursts. This large internal field can stress the crust and ultimately deforms and cracks the star surface layers, periodically allowing magnetic helicity to be transferred to the external field, thus causing the (repeated) short x-ray bursts and the overall magnetar-like activity (*6*, *23*, *24*).

As with other magnetars, B_{tor} can be estimated assuming that the magnetic energy stored in the internal toroidal field powers the quiescent emission of SGR 0418+5729 during its entire lifetime, $B_{tor}^2 \sim 6 L_X t_c / R_{NS}^3$ (*6*). Assuming a source distance of 2 kpc (*14*, *16*), and that the current luminosity $L_X \sim 6.2 \times 10^{31}$ erg s^{-1} (the lowest measured so far for this source) corresponds to the quiescent luminosity, we obtain $B_{tor} \sim 5 \times 10^{14}$ G for a neutron star radius of $R_{NS} = 10^6$ cm and a source characteristic age of $t_c \sim 24$ million years. A value of the same order is obtained if the ratio of the toroidal to poloidal field strength is ~50, as in the magneto-thermal evolution scenario (*25*, *26*). In this picture, SGR 0418+5729 may possess a high enough internal magnetic field to overcome the crustal yield and give rise to magnetar-like activity despite its low surface dipolar magnetic field. However, should the actual measurement of the surface dipolar *B* field of SGR 0418+5729 turn out to be much smaller than the present upper limit, it may be necessary to rethink some of the ingredients at the basis of the magnetar scenario.

SGR 0418+5729 may represent the tip of the iceberg of a large population of old and low-dipolar-field magnetars that are dissipating the last bits of their internal magnetic energy (*27*). Indeed, a large fraction of the radio pulsar population may have magnetar-like internal fields not reflected in their normal dipolar component.

References and Notes

1. We note that the surface dipolar magnetic field of magnetars has been estimated also with several other methods (*6*, *22*, *28*); these give values consistent with those derived from the formula in Eq. 1.
2. S. Mereghetti, *Astron. Astrophys. Rev.* **15**, 225 (2008).
3. See www.physics.mcgill.ca/~pulsar/magnetar/main.html for an updated catalog of SGRs and AXPs.
4. S. Mereghetti, G. L. Israel, L. Stella, *Mon. Not. R. Astron. Soc.* **296**, 689 (1998).
5. R. Dib, V. M. Kaspi, F. P. Gavriil, *Astrophys. J.* **666**, 1152 (2007).
6. C. Thompson, R. C. Duncan, *Mon. Not. R. Astron. Soc.* **275**, 255 (1995).
7. C. Thompson, R. C. Duncan, *Astrophys. J.* **473**, 322 (1996).
8. F. P. Gavriil *et al.*, *Science* **319**, 1802 (2008).
9. H. S. Kumar, S. Safi-Harb, *Astrophys. J.* **678**, L43 (2008).

Downloaded from www.sciencemag.org on November 11, 2010

10. L. Levin *et al.*, *Astrophys. J.* **721**, L33 (2010).
11. F. Camilo *et al.*, *Nature* **442**, 892 (2006).
12. F. Camilo, S. M. Ransom, J. P. Halpern, J. Reynolds, *Astrophys. J.* **666**, L93 (2007).
13. V. M. Kaspi, *Proc. Natl. Acad. Sci. U.S.A.* **107**, 7147 (2010).
14. A. J. van der Horst *et al.*, *Astrophys. J.* **711**, L1 (2010).
15. E. Göğüş, P. Woods, C. Kouveliotou, *Astron. Telegram*, 2076 (2009); www.astronomerstelegram.org/?read=2076.
16. P. Esposito *et al.*, *Mon. Not. R. Astron. Soc.* **405**, 1787 (2010).
17. F. P. Gavriil, V. M. Kaspi, *Astrophys. J.* **567**, 1067 (2002).
18. R. Turolla, in *Neutron Stars and Pulsars*, W. Becker, Ed. (Springer, Berlin, 2009), pp. 141–164.
19. M. Colpi, U. Geppert, D. Page, *Astrophys. J.* **529**, L29 (2000).
20. A. F. Cheng, M. A. Ruderman, *Astrophys. J.* **235**, 576 (1980).
21. B. Zhang, A. K. Harding, A. G. Muslimov, *Astrophys. J.* **531**, L135 (2000).
22. C. Thompson, R. C. Duncan, *Astrophys. J.* **561**, 980 (2001).
23. C. Thompson, M. Lyutikov, S. R. Kulkarni, *Astrophys. J.* **574**, 332 (2002).
24. A. M. Beloborodov, *Astrophys. J.* **703**, 1044 (2009).
25. J. Pons, J. A. Miralles, U. Geppert, *Astron. Astrophys.* **496**, 207 (2009).
26. The internal field strength required to produce crustal cracking should be typically in excess of 10^{14} G (*6*).
27. If fast-spinning young pulsars were among these, the resulting magnetically induced ellipticity would lead to powerful emission of periodic gravitational waves.
28. M. Vietri, L. Stella, G. L. Israel, *Astrophys. J.* **661**, 1089 (2007).
29. R. N. Manchester, G. B. Hobbs, A. Teoh, M. Hobbs, *Astron. J.* **129**, 1993 (2005).
30. The online Australia Telescope National Facility Pulsar Catalogue is available at www.atnf.csiro.au/research/pulsar/psrcat.
31. N.R. is supported by a Ramón y Cajal fellowship through Consejo Superior de Investigaciones Cientfícas and by grants AYA2009-07391 and SGR2009-811. N.R. thanks D. F. Torres for useful discussions. P.E. acknowledges financial support from the Autonomous Region of Sardinia through a research grant under the program PO Sardegna FSE 2007-2013, L.R. 7/2007 "Promoting scientific research and innovation technology in Sardinia." D.G. acknowledges the Centre National d'Études Spatiales for financial support. The work of R.T., G.L.I., L.S., S.M., and A.T. is partially supported by INAF Agenzia Spaziale Italiana through grant AAE I/088/06/0. We are grateful to H. Tananbaum, N. Gehrels, and N. Schartel for granting us Chandra, Swift, and XMM-Newton time, respectively, for this research.

Supporting Online Material

www.sciencemag.org/cgi/content/full/science.1196088/DC1
SOM Text
Table S1
References

4 August 2010; accepted 7 October 2010
Published online 14 October 2010;
10.1126/science.1196088
Include this information when citing this paper.

Anomalous Strength Characteristics of Tilt Grain Boundaries in Graphene

Rassin Grantab,[1] Vivek B. Shenoy,[1]* Rodney S. Ruoff[2]*

Graphene in its pristine form is one of the strongest materials tested, but defects influence its strength. Using atomistic calculations, we find that, counter to standard reasoning, graphene sheets with large-angle tilt boundaries that have a high density of defects are as strong as the pristine material and, unexpectedly, are much stronger than those with low-angle boundaries having fewer defects. We show that this trend is not explained by continuum fracture models but can be understood by considering the critical bonds in the strained seven-membered carbon rings that lead to failure; the large-angle boundaries are stronger because they are able to better accommodate these strained rings. Our results provide guidelines for designing growth methods to obtain sheets with strengths close to that of pristine graphene.

Graphene is one of the thinnest materials ever synthesized, yet it is one of the strongest ever measured (*1*, *2*), and it exhibits exceptional electronic, thermal, and optical properties (*1*, *3*); however, growing large-area, single-layer graphene sheets remains a major challenge. Recently, a chemical vapor deposition (CVD) technique has been devised that exploits the low solubility of carbon in metals such as nickel (*4*, *5*) and copper (*6*, *7*) in order to grow graphene on metal foils. A consequence of this technique is that the large-area graphene sheets contain grain boundaries, because each grain in the metallic foil serves as a nucleation site for individual grains of graphene (*6*).

Tilt grain boundaries in graphite had first been observed in scanning tunneling microscopy (STM) experiments by Albrecht *et al.* (*8*), and since then several groups have performed similar microscopy studies (*9*–*14*). More recently, Hashimoto *et al.* (*15*) have observed individual dislocations in graphene using transmission electron microscopy (TEM), and the structure, as well as the electronic, magnetic, and dynamical properties of grain boundaries in graphene have been investigated by a number of other research teams (*16*–*18*). With all this previous work established, a natural question to ask is how these grain boundaries influence the mechanical properties of graphene. Given the fact that graphene is one of the stiffest (modulus ~ 1 TPa) and strongest (strength ~ 100 GPa) materials, in order to use CVD-synthesized graphene sheets in nano-electromechanical systems (NEMS), in sensors, and as pressure barriers, it is important to know how the grain boundaries influence these fundamental mechanical properties.

Although a number of studies have been carried out on the mechanics of dislocations and defects in carbon nanotubes (*19*–*21*) and graphene (*22*), the mechanical properties of hydrogen-functionalized graphene (*23*), and the fracture and failure of graphene and carbon nanotubes with multiple vacancies (*24*) and Stone-Wales defects (*24*–*26*), the effect of grain boundaries on the mechanical properties of graphene has been largely neglected. To address this outstanding problem, we have

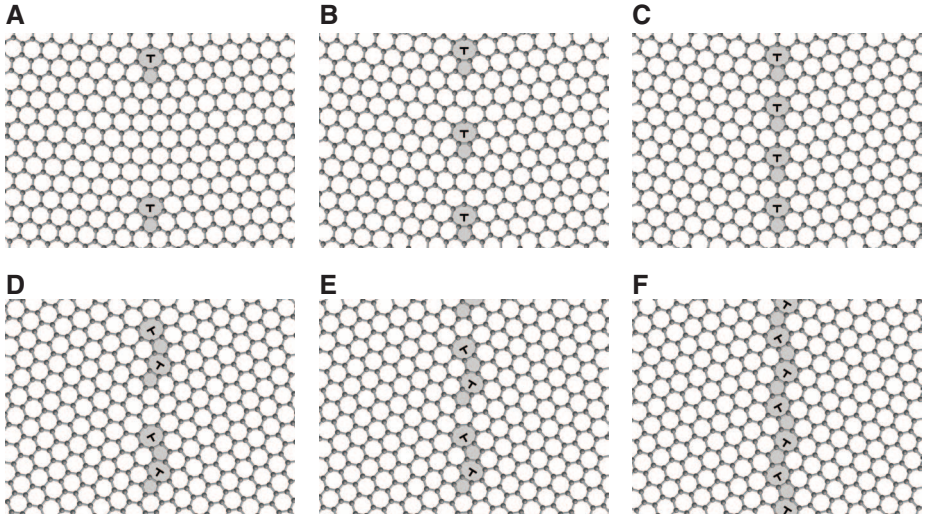

Fig. 1. The structures of grain boundaries in (**A** to **C**) zigzag-oriented and (**D** to **F**) armchair-oriented graphene sheets with varying mismatch angles.

[1]School of Engineering, Brown University, Providence, RI 02906, USA. [2]Department of Mechanical Engineering and the Texas Materials Institute, University of Texas, Austin, TX 78712, USA.

*To whom correspondence should be addressed: vivek_shenoy@brown.edu (V.B.S.); r.ruoff@mail.utexas.edu (R.S.R.)

Downloaded from www.sciencemag.org on November 11, 2010

performed molecular dynamics (MD) and density functional theory (DFT) calculations using the packages Large-Scale Atomic/Molecular Massively Parallel Simulator (LAMMPS) and Vienna Ab-Initio Simulation Package (VASP), respectively. The full details of the computational methods are included in the supporting online material (SOM).

The structures of tilt grain boundaries in zigzag- and armchair-oriented graphene are shown in Fig. 1 for various grain boundary angles (the angles represent the total mismatch angles between the left and right grains). For the zigzag orientation, the grain boundaries consist of repeating five- and seven-membered ring pairs (5-7 pairs) that are separated by several hexagonal rings (hex rings). As the grain boundary angle increases, the number of hex rings separating the 5-7 defects decreases, with the ultimate limit occurring at 21.7° when only a single hex ring separates the periodic 5-7 defects. Therefore, more severe grain boundary angles are composed of higher defect densities. The repeating defect pairs can also be thought of as an array of edge dislocations with horizontal Burgers vectors where the five-membered rings represent the extra plane of atoms, as shown in Fig. 1.

For the armchair orientation, the repeating defect consists of two diagonally opposed 5-7 pairs that are separated by several hex rings. As was the case for the zigzag orientation, larger grain boundary angles consist of higher defect densities; however, for the armchair-oriented graphene, the most severely misoriented boundary (28.7°) consists of repeating 5-7 pairs without any intermediate hex rings. Viewing the grain boundary in terms of dislocations, the two diagonally opposed, repeating 5-7 pairs represent two partial edge dislocations, as shown in Fig. 1. The vertical components of the Burgers vectors of the two partial dislocations nullify one another, leaving the grain boundary vertically oriented (for a vertical boundary, the net Burgers vector must be purely horizontal).

The stress-strain curves for zigzag- and armchair-oriented graphene sheets pulled perpendicular to the grain boundaries are shown in Fig. 2, and those of the sheets deformed parallel to the boundaries are shown in fig. S1. In general, grain boundaries may be oriented at an angle relative to the tensile axes; to study the effect of this variation, we consider the extreme cases, that is, the grain boundaries oriented perpendicular to and along the loading axes. In both cases, the variation of the failure strength with angle is larger when the sheets are pulled perpendicular to the boundaries than when they are pulled parallel to the boundaries. From these plots, it can be seen that as the grain boundary angle, and hence the defect density, increase, the ultimate failure strength and strain at failure increase. These results are very unexpected and are completely contrary to the natural intuition that as the number of defects increases, the strength of a material decreases.

To see whether the nonintuitive results can be understood on the basis of continuum mechanics concepts, we consider a fracture-mechanics–based approach in which we model the seven-membered rings along the grain boundary as an infinite array of Griffith cracks. This is a reasonable continuum-level analog of the seven-membered rings, because these rings are larger than the hex rings and so they can be represented as a crack or a void within the material. This assumption is also consistent with the fact that failure in the graphene sheets always begins at the seven-membered rings. We therefore consider an infinite array of Griffith cracks (the crack tips aligned along the boundary), each of length $2a$ and separated by a length $2h$ from one another. The common method that is used to determine whether a crack advances upon application of a remote stress, σ_∞, is to compute the stress-intensity factor, K_I. If K_I exceeds K_{IC} (the experimentally measured fracture toughness for a given material), then crack propagation will ensue. The stress-intensity factor for the arrangement of cracks outlined above can be computed using standard fracture mechanics techniques (*27*) and is given by the following equation:

$$K_I = \sigma_\infty \sqrt{(2h)\tan\left(\frac{\pi a}{2h}\right)} \qquad (1)$$

A plot of the nondimensional stress-intensity factor, $K_I/\sigma_\infty\sqrt{a}$, versus normalized crack-spacing, h/a, is presented in Fig. 3. As the intercrack spacing, $2h$, decreases, the stress-intensity factor, K_I, increases due to the interaction of the stress fields of adjacent cracks. Based on the plot in Fig. 3, graphene sheets should be weaker as the defect distribution becomes more dense. Clearly, this fracture mechanics analogy fails to explain our results, so the explanation we seek does not lie within continuum mechanics techniques but on the atomic-level details of bond rupture and failure. We therefore focus on the sequence of atomic-scale events that leads to tensile failure.

Figure 4 shows the first signs of failure within the zigzag- and armchair-oriented graphene sheets during deformation perpendicular to the boundaries. What is striking is that the first bonds to break (the encircled bonds) are always the same ones for all three grain boundary angles. The location of the critical bonds is dependent on the orientation of the graphene (zigzag or armchair) and the loading direction (perpendicular or parallel to the grain boundary); for each specific combination of orientation and loading direction, the critical bonds are the same for all three grain boundary angles. Once these bonds have been broken, complete failure of the sheets proceeds rapidly along the grain boundaries. There is, however, an exception in the case of the 28.7° armchair graphene, which actually fails away from the boundary, within the highlighted region in Fig. 4F.

The first signs of failure for the zigzag- and armchair-oriented graphene sheets pulled parallel to the grain boundaries are shown in fig. S2. As was the case previously, we observe that for each of the three grain boundary angles, the same bonds in the seven-membered rings (the encircled bonds) are the first to break, although it should be reiterated that the critical bonds for this loading direction are different from those of the sheets that were pulled perpendicular to the boundaries. An exception arises again for the 28.7° armchair graphene, which fails away from the boundary.

Having identified the critical bonds, we now focus on the initial strains in these bonds as a function of the grain boundary angle and uncover clues toward understanding the anomalous strength

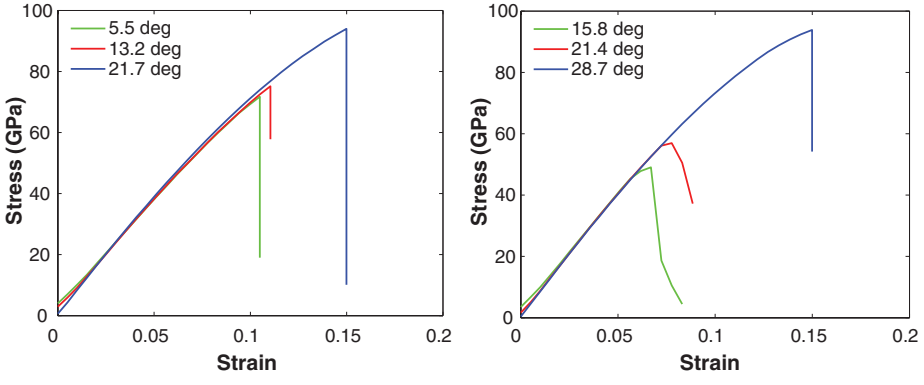

Fig. 2. The stress-strain curves of (**left**) zigzag-oriented and (**right**) armchair-oriented graphene sheets pulled perpendicular to the grain boundaries.

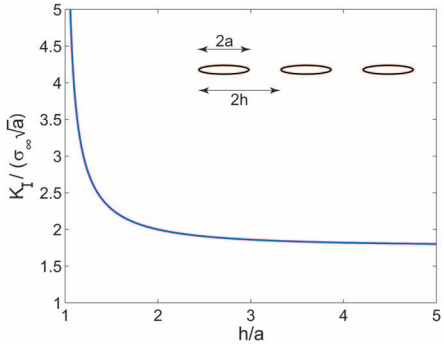

Fig. 3. Nondimensional stress-intensity factor versus normalized crack-spacing.

Downloaded from www.sciencemag.org on November 11, 2010

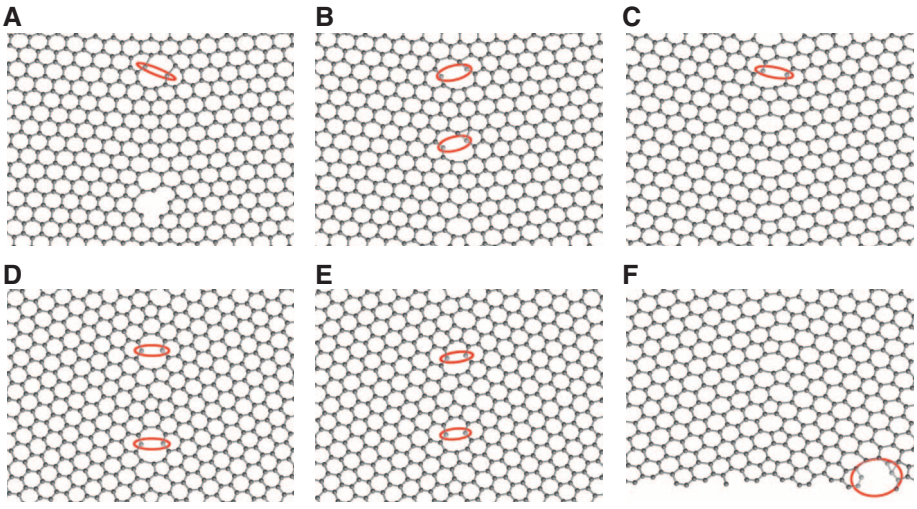

Fig. 4. The initial stages of failure in (**A** to **C**) zigzag-oriented and (**D** to **F**) armchair-oriented graphene sheets pulled perpendicular to the grain boundaries.

of tilt grain boundaries in graphene. As the grain boundary angle increases, the initial lengths of the critical bonds decrease toward the sp^2 carbon-carbon bond length in pristine graphene. Before any applied deformation, for loading perpendicular to the boundary, the strain in the critical bonds of the zigzag-oriented graphene sheets with grain boundary angles of 5.5°, 13.2°, and 21.7° are 12.2%, 10.3%, and 5.4%, respectively. Our DFT simulations validate these results and the general trend, with calculated strains of 9.5%, 8.7%, and 5.4% as the grain boundary angle increases. Naturally, as the prestrain in the material decreases, the strain at failure and ultimate strength will increase. It is the level of preexisting strain within the critical bonds of the seven-membered rings that accounts for the counterintuitive results we have observed in our simulations.

In the undeformed state, the critical bonds in armchair graphene pulled perpendicular to the boundary are strained by a factor of 23.4%, 9.3%, and 1.7% for the 15.8°, 21.4°, and 28.7° boundary angles, respectively. Once again, we observe the trend of decreasing initial strain with increasing grain boundary angle. Interestingly, the graphene sheet with a 28.7° grain boundary angle begins to fail away from the boundary at the location highlighted in Fig. 4F. This is because, in this case, the bond lengths in the seven-membered rings are very close to those of pure graphene (the previously mentioned strain of 1.7% being the largest among the seven bonds), and two of the bonds are actually initially shorter than those of pure graphene. Reexamination of the stress-strain curve corresponding to this grain boundary angle and pulling direction (shown in Fig. 2, right) indicates a strain at failure of 15.5% and an ultimate strength of 95 GPa, values that are approaching the strength of pure armchair graphene. Based on these results, we can conclude that grain boundaries with a mismatch angle of 28.7° do not affect the strength of armchair-oriented graphene sheets appreciably, whereas those with lower separation angles weaken them considerably.

The initial strains in the critical bonds for zigzag graphene pulled parallel to the boundary are 2.1%, 1.7%, and 0.7% for the 5.5°, 13.2°, and 21.7° grain boundary angles, respectively. The strains calculated through DFT are slightly higher at 3.2%, 2.2%, and 1.7%; however, the trend matches that of the MD simulations perfectly. Although the level of initial strain is lower for these critical bonds than those discussed for the perpendicular deformation direction, the general trend of decreasing strain with increasing grain boundary angle is the same and is consistent with the stress-strain results.

For armchair graphene pulled parallel to the boundary, the critical bonds in the 15.8° and 21.4° are strained by factors of 5.4% and 4.0%, respectively; the 28.7° sheets begin to fail away from the boundary (within the highlighted region in fig. S2F), because for the most severe grain boundary angle, this bond is actually the same length as those in pure graphene. Thus, we have shown that the general trend of decreasing initial strain with increasing grain boundary angle is perfectly consistent for zigzag- and armchair-oriented graphene sheets and that the initial bond lengths fully explain the counterintuitive results observed in our MD simulations.

We used MD and DFT calculations to study the mechanical strength of grain boundaries in zigzag- and armchair-oriented graphene sheets. For both orientations, we have found that the strain at failure and ultimate strength of graphene increases with grain boundary angle. We have looked in detail at the atomic-scale bond-breaking processes that lead to failure and have identified the critical bonds that determine the ultimate strength of the grain boundaries. Based on these analyses, it is clear that the initial strain in these bonds determines the failure strength: the higher the strain, the lower the strength. Higher grain boundary angles can better accommodate the seven-membered ring defects that make up the grain boundaries; therefore, the initial strain in the critical bonds decreases with increasing angle. Fracture mechanics methods were unable to predict the trends from our simulations because the influence of strained atomic bonds is inherently absent from continuum techniques.

References and Notes

1. A. K. Geim, *Science* **324**, 1530 (2009).
2. C. Lee, X. Wei, J. W. Kysar, J. Hone, *Science* **321**, 385 (2008).
3. A. K. Geim, K. S. Novoselov, *Nat. Mater.* **6**, 183 (2007).
4. Q. Yu *et al.*, *Appl. Phys. Lett.* **93**, 113103 (2008).
5. K. S. Kim *et al.*, *Nature* **457**, 706 (2009).
6. X. Li *et al.*, *Science* **324**, 1312 (2009).
7. M. P. Levendorf, C. S. Ruiz-Vargas, S. Garg, J. Park, *Nano Lett.* **9**, 4479 (2009).
8. T. Albrecht, H. Mizes, J. Nogami, S. Park, C. Quate, *Appl. Phys. Lett.* **52**, 362 (1988).
9. J. Osing, I. Shvets, *Surf. Sci.* **417**, 145 (1998).
10. P. Simonis *et al.*, *Surf. Sci.* **511**, 319 (2002).
11. Y. Gan, W. Chu, L. Qiao, *Surf. Sci.* **539**, 120 (2003).
12. W.-T. Pong, J. Bendall, C. Durkan, *Surf. Sci.* **601**, 498 (2007).
13. J. Cervenka, C. F. J. Flipse, *Phys. Rev. B* **79**, 195429 (2009).
14. H. S. Wong, C. Durkan, N. Chandrasekhar, *ACS Nano* **3**, 3455 (2009).
15. A. Hashimoto, K. Suenaga, A. Gloter, K. Urita, S. Iijima, *Nature* **430**, 870 (2004).
16. O. V. Yazyev, S. G. Louie, *Phys. Rev. B* **81**, 195420 (2010).
17. S. Malola, H. Hakkinen, P. Koskinen, *Phys. Rev. B* **81**, 165447 (2010).
18. J. Cervenka, M. I. Katsnelson, C. F. J. Flipse, *Nat. Phys.* **5**, 840 (2009).
19. Z. Li, P. Dharap, P. Sharma, S. Nagarajaiah, B. Yakobson, *J. Appl. Phys.* **97**, 074303 (2005).
20. J. Y. Huang, F. Ding, B. I. Yakobson, *Phys. Rev. Lett.* **100**, 035503 (2008).
21. S. Zhang *et al.*, *Phys. Rev. B* **71**, 115403 (2005).
22. X. Zhang, K. Jiao, P. Sharma, B. I. Yakobson, *J. Mech. Phys. Solids* **54**, 2304 (2006).
23. Q. X. Pei, Y. W. Zhang, V. B. Shenoy, *Carbon* **48**, 898 (2010).
24. J. R. Xiao, J. Staniszewski, J. W. Gillespie Jr., *Compos. Struct.* **88**, 602 (2009).
25. J. R. Xiao, J. Staniszewski, J. W. Gillespie Jr., *Mater. Sci. Eng. A* **527**, 715 (2010).
26. Q. Lu, B. Bhattacharya, *Nanotechnology* **16**, 555 (2005).
27. K. Broberg, *Cracks and Fracture* (Academic Press, San Diego, 1999).
28. R.G. and V.B.S. gratefully acknowledge research support from NSF and the Nanoelectronics Research Initiative through Brown University's Materials Research Science and Engineering Center program and from NSF through grants CMMI-0825771 and CMMI-0855853. The computational support for this work was provided by grant TG-DMR090098 from the TeraGrid Advanced Support Program and the Center for Computation and Visualization at Brown University.

Supporting Online Material

www.sciencemag.org/cgi/content/full/330/6006/946/DC1
Materials and Methods
Figs. S1 and S2
References

24 August 2010; accepted 5 October 2010
10.1126/science.1196893

Downloaded from www.sciencemag.org on November 11, 2010

Structure and Formation of the Lunar Farside Highlands

Ian Garrick-Bethell,[1]*† Francis Nimmo,[2] Mark A. Wieczorek[3]

The formation of the lunar farside highlands has long been an open problem in lunar science. We show that much of the topography and crustal thickness in this terrain can be described by a degree-2 harmonic. No other portion of the Moon exhibits comparable degree-2 structure. The quantified structure of the farside highlands unites them with the nearside and suggests a relation between lunar crustal structure, nearside volcanism, and heat-producing elements. The farside topography cannot be explained by a frozen-in tidal bulge. However, the farside crustal thickness and the topography it produces may have been caused by spatial variations in tidal heating when the ancient crust was decoupled from the mantle by a liquid magma ocean, similar to Europa's present ice shell.

Since the Apollo 15 laser altimeter experiment, it has been widely known that the topography of the lunar farside highlands is the highest on the Moon (*1*). This elevated region makes up a large part of the Feldspathic Highlands Terrane (FHT), the largest of the Moon's three major geologic provinces (*2*). Because the farside highlands may be a relict of very early thermal processes (*2*, *3*), understanding their structure and formation may help constrain models of global lunar evolution and magma-ocean processes in general (*4*). Theories for the formation of the farside highlands include South Pole–Aitken (SP-A) basin ejecta deposits (*5*), asymmetric nearside/farside cratering (*6*), magma-ocean convective asymmetries (*7*), and asymmetric crustal growth (*3*). However, there has been no quantitative description of the farside highlands to date; therefore, models that describe their formation are poorly constrained.

Here, we analyze global topography (*8*) and gravity data sets (*9*) to better describe the lunar farside highlands. We fit the mean topography from five swaths of terrain centered in the farside highlands to a degree-2 Legendre polynomial P_2 [Fig. 1, supporting online material (SOM), fig. S2] in north, northeast, and east directions (Fig. 1A, black portion of topography profile, 0° to between 95° and 105° of arc). We used a variety of swath centers because of the uncertainty in the exact terrain center. The fit to P_2 is excellent in all cases (correlation coefficient $R^2 > 0.93$), and two additional observations allow us to confirm that the terrain is indeed described by P_2. First, for swaths 1 to 3, the fits accurately predict the topography encountered in the western, southwestern, and southeastern portions of the swaths for at least 55° of arc (~1700 km, leftmost blue section of topography profiles; figs. S2 and S8). Second, the entire northern-, northeastern-, and eastern-directed decrease in topography on the lunar farside takes place over ~90° of arc, as expected from a P_2 function. A global search revealed that no other region of the Moon exhibits comparable degree-2 structure (figs. S4 to S7), including all of the nearside, despite the Moon's well-known high degree-2 topography and gravity spherical harmonic coefficients.

We have also applied the same swath fitting analysis described above to a crustal-thickness model derived from topography (*8*) and gravity data (*9*) (SOM). We find that all of the same trends in topography are also observed in crustal thickness (Fig. 1, C and D), indicating that the farside highlands topography is largely due to crustal-thickness variations, as inferred previously (*1*). Using the average values of the fitted regions in swaths 1 to 5, the maximum crustal thickness is 76 km, and the minimum is 40 km (amplitude of ~36 km).

The maximum amplitude and center of the terrain described by a P_2 function is near 0° ± 5°N, 215° ± 5°E, close to the direction of the center-of-mass/center-of-figure offset at 8°N, 203°E (*10*). Overall, the region fit by P_2 comprises ~24% of the lunar surface, and, for convenience, we refer to it here as the DTT (degree-2 terrain).

Two observations suggest that ejecta from the neighboring SP-A basin had a minimal effect on the DTT and farside highlands and that SP-A postdates their formation. First, the DTT topography obeys a P_2 function that is centered external to and northeast of the basin, and there are no models for ejecta production that would explain such an unusual distribution. The lack of an extensive ejecta deposit for SP-A is consistent with anomalously low excavated volumes for this and the next two largest lunar basins (*11*). Second, a comparison of swaths 4 and 5, which extend into SP-A's depression, with swaths 1 to 3, suggests that SP-A is superimposed on a longer wavelength P_2 shape in the south and southwest. Therefore, because of the great antiquity of SP-A, the P_2 shape of the DTT is probably the Moon's most primordial feature, in agreement with (*12*).

The DTT extends for ~40° of arc into the lunar nearside, crossing mare units in Oceanus Procellarum and parts of Mare Frigoris (Fig. 1), thereby linking two traditionally separate geologic units: the farside FHT and the Procellarum KREEP Terrane (PKT) (*2*). Profiles of crustal thickness and topography along the borders of both units are relatively constant (SOM, fig. S17). This continuity and constancy of border data suggest a related early geologic history for both provinces and that the borders of Oceanus Procellarum and Mare Frigoris are related to long-wavelength crustal structure (Fig. 1D). The DTT structure is also undisturbed across the rim of the putative Procellarum impact basin that has been suggested to produce a number of nearside-farside differences (*13*). Therefore, either the Procellarum basin formed well before complete crust formation, or it never formed. Finally, if the DTT center was once nearer to 0°N, 180°E, as implied by the tidal-heating calculations developed below, it would imply the Moon's minimum moment of inertia axis has shifted only ~35° since crust formation.

The DTT must have formed very early in lunar thermal evolution, because its crust is nearly compensated, as indicated by the regional lack of strong positive free-air gravity anomalies (*9*) (SOM). In order for such compensation to have taken place, the Moon must have still been very hot, probably <100 million years (My) after accretion (*14*), when a subsurface magma ocean was likely present (*15*, *16*).

The DTT follows a P_2 function like that expected from a tidal process, but it cannot have been formed entirely by freezing in an ancient tidal bulge (*17*), because such a bulge would not cause crustal-thickness variations. In addition, a hydrostatic tide of 6.4-km amplitude (mean of swaths 1 to 5) exists at a semimajor axis of ~12 Earth radii (R_E). The Moon evolved to this location only ~10^6 years after accretion (SOM) and was certainly too hot and its lithosphere too thin to retain such a bulge.

Predominantly degree-2 crustal-thickness variations similar to those in the DTT may arise in tidally heated satellites with subsurface liquid oceans, such as Europa (*18*–*20*) and Titan (*21*). The subsurface ocean decouples the crust from the mantle and leads to high tidal dissipation in the crust's warm base. This dissipation serves as a heat source within the crust, such that the crust will be thinner relative to its thickness without dissipation (*18*). Because dissipation is greatest at the poles and least at the equatorial 0° and 180° longitudes, the crust becomes thinner and thicker in those locations, respectively, for low-obliquity orbits. Like Europa, the Moon also once possessed an ocean beneath its crust.

We calculated the tidal heating in a floating anorthositic lunar crust (*19*) with a temperature-dependent viscosity (*22*) (SOM). We assumed

[1]Department of Geological Sciences, Brown University, Providence, RI 02912, USA. [2]Department of Earth and Planetary Sciences, University of California, Santa Cruz, 1156 High Street, Santa Cruz, CA 95064, USA. [3]Institut de Physique du Globe de Paris - Sorbonne Paris Cité, Paris, France.

*To whom correspondence should be addressed. E-mail: igarrick@ucsc.edu

†Present address: Department of Earth and Planetary Sciences, University of California, Santa Cruz, 1156 High Street, Santa Cruz, CA 95064, USA.

Downloaded from www.sciencemag.org on November 11, 2010

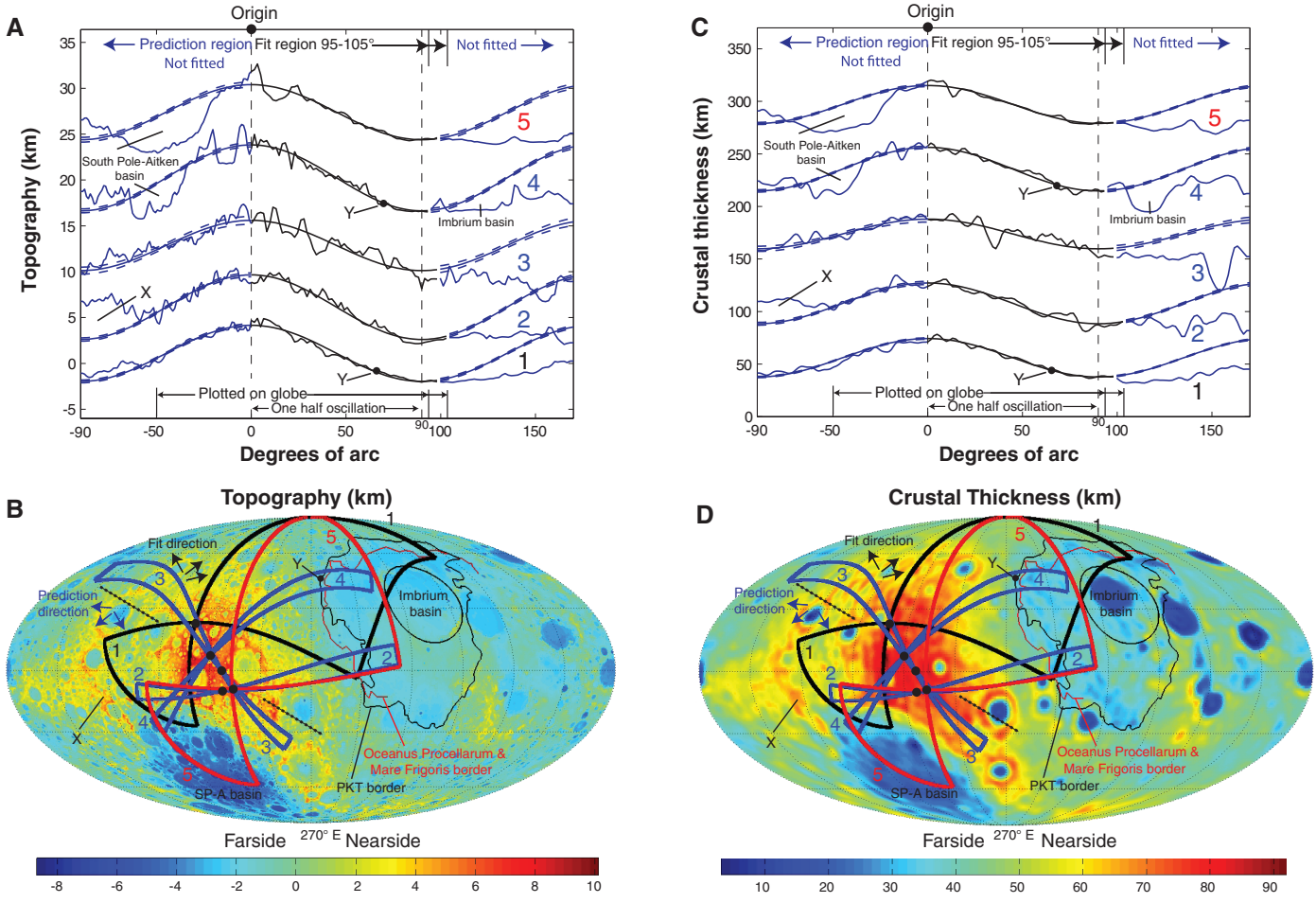

Fig. 1. The degree-2 structure of the lunar farside highlands. (**A**) Mean topography inside the five great-circle swaths shown in (B), fitted to a P_2 function in the black region, and vertically offset for clarity. Data and fitted P_2 function beyond the fit region are illustrated in blue with 95% confidence intervals (dashed lines). Vertical axis applies to swath 1 only, but scale is constant throughout. X, region described by a possible degree-4 harmonic (see text and Fig. 2A); Y, point on the PKT border and central to swaths 1 and 4. (**B**) Portions of swaths from (A) plotted over topography data (*8*). Swaths 1 (black) and 5 (red) are averages over large regions. The PKT boundary is based on the 3.5–parts per million thorium contour (*2*). Points X and Y from (A) are shown. Black and blue arrows indicate fit and prediction directions, respectively. (**C**) and (**D**) Same as (A) and (B), but for crustal thickness.

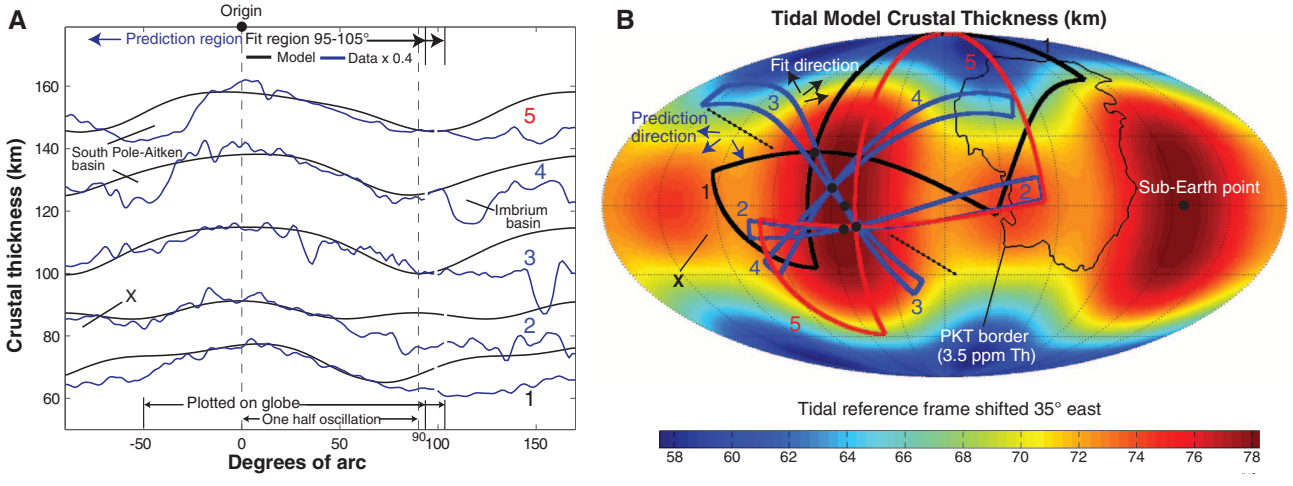

Fig. 2. Lunar crustal thickness compared with a tidal-dissipation model. (**A**) Mean profiles of lunar crustal-thickness swaths derived from tidal dissipation at $a = 20\ R_E$, $e = 0.02$, $T_b = 1175$°C, and $q_o = 27$ mW/m^2 (black lines), along with the profiles from Fig. 1C (multiplied by 0.4, blue lines, arbitrarily offset). Swath dimensions are the same as in Fig. 1. Vertical axis applies to model swath 1 only, but scale is constant throughout. Fit directions are indicated, but no fits were performed in this figure. (**B**) Map of crustal thickness used for (A). Model data in both (A) and (B) have been shifted 35° east, because the DTT center is ~35° east of the theoretical maximum crustal thickness at 0°N, 180°E. Compare with Fig. 1, C and D; see also fig. S10.

Downloaded from www.sciencemag.org on November 11, 2010

synchronous rotation and that the crust is in conductive thermal equilibrium with tidal heating and an additional basal heat flux (q_o) from mantle cooling and radiogenic heat. Important parameters are the eccentricity (e), semimajor axis (a), and magma-ocean temperature (T_b). We calculate that, 100 My after accretion, there was an approximate mean basal heat flux of ~27 mW/m^2: ~20 mW/m^2 from radiogenic magma-ocean liquids and ~7 mW/m^2 from mantle cooling (SOM).

We find that crustal-thickness differences of 21 km (mean = 65 km, minimum = 50 km, maximum = 71 km) can be generated for $e = 0.02$, $a = 20\ R_E$, $T_b = 1175$°C, and $q_o = 27$ mW/m^2 (Fig. 2). The mean thickness is slightly higher than the present estimate of ~45 km, but it is lower than present farside values. The value of a corresponds to up to tens of million years of lunar evolution, during which the crust may have grown by tens of kilometers (SOM), relatively consistent with the calculated thickness, given our uncertainty in early orbital evolution. Further, the value of e is not inconsistent with our knowledge of the early lunar eccentricity (SOM). The value of T_b is reasonable based on the temperature of late-stage crystallization products [for instance, KREEP basalt liquidus of ~1185°C (*23*); pyroxene-ilmenite cumulate solidus of ~1125°C (*24*)] (SOM).

The net crustal-thickness difference arising from dissipation depends on numerous orbital and thermal parameters that are difficult to constrain precisely (*25*). Higher differences may result from a basal partially molten zone (*26*) (SOM), a different rheology, higher e, or higher T_b. For example, the use of the above parameters (with $T_b = 1225$°C and $q_o = 30$ mW/m^2) yields a crustal-thickness amplitude of 44 km (mean thickness = 39 km), which is close to the observed values. Such a temperature may be too hot for late-stage magma-ocean liquids

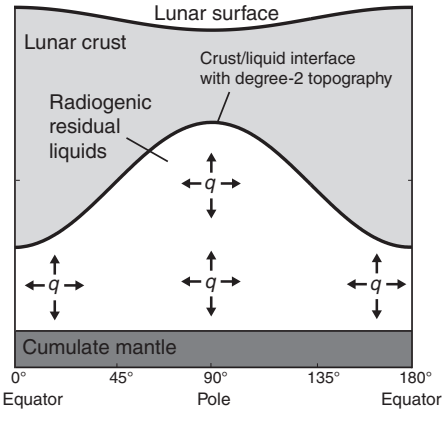

Fig. 3. Degree-2 basal topography on the crust also causes degree-2 variations in magma-ocean thickness, such that higher total heat production will be found beneath regions of thinner crust, possibly influencing crustal crystallization. q, volumetric heat production. Image not shown to scale.

(SOM), but it illustrates the effect of increased dissipation.

Despite these uncertainties in crustal amplitude, the detailed crustal-thickness pattern is very similar for all models in which dissipation is strong, and it can, therefore, be used to test our predictions (Fig. 2, SOM, fig. S12). The crustal-thickness patterns in swaths 3 to 5 are in good agreement with amplitude-scaled tidal model data (*27*), over the regions plotted on the globe in Fig. 2B, except for the effect of SP-A. Swath 1 has good agreement over ~90° of arc, but is poorer elsewhere. Swath 2 has good agreement from –90° to +50° and also predicts the terrain labeled "X" in Fig. 1. Generally, the lack of agreement is due to the superposition of a weak pole-to-equator surface temperature effect and degree-4 harmonic on the model's stronger degree-2 pattern (SOM). Note that swath 2 shows evidence of the predicted degree-4 harmonic at site X. The case for $T_b = 1225$°C gives even better agreement in shape without any rescaling of the actual crustal thickness (fig. S10).

Though there is disagreement between model and observations in some locations, the model shows clear evidence for a degree-2 pattern that dominates higher-order effects (SOM). Physically, the imperfect agreement may be due to subsequent thermal processes that altered the distribution of crustal thickness near the PKT and elsewhere (*28*). Alternatively, polar wander about the axis through the primordial sub and anti-Earth points (*29*) could have averaged out harmonics other than the dominant degree-2 harmonic. In addition, lower crustal flow may have preferentially removed the higher-order degree-4 thickness variations (SOM). Most importantly, however, whereas other large-scale geophysical processes (such as convection and Rayleigh-Taylor instabilities) can be described mathematically in spherical harmonics, there is no simple reason that they must manifest themselves geologically with a predominantly P_2 shape (SOM), in contrast to the tidal-dissipation mechanism discussed here. Therefore, early tidal dissipation is presently the strongest candidate for the formation of the DTT.

A consequence of tidally driven crustal-thickness variations is that the subsurface magma ocean will be thicker and thinner in regions of thinner and thicker crust, respectively, assuming negligible mantle topography (Fig. 3). Because magma-ocean liquids are enriched in radiogenic elements (*4*), regions of thinner crust will have higher subsurface heat production than regions of thicker crust. Depending on the ocean depth and vigor of convective heat redistribution, this variable heat production may further influence crustal crystallization (SOM) (*3*) and global ocean convection patterns.

A tidally driven crust-building mechanism would have likely once had global symmetry. A second region of thickened crust would have been centered antipodal to the DTT at present day (0°N, 35°E), and the present PKT would have been approximately between them (Fig. 2B). In the 4.4 billion years after the magma-ocean epoch, many geologic processes may have altered and diminished the evidence for this crust-building process on the other ~76% of the Moon, such as large impact basins, long wavelength thermal-compositional events (*28*), and volcanism. However, the relict of that epoch identified here has linked two previously disparate sections of the Moon and implicates the role of ancient tidal processes in defining the present-day structure of the lunar crust.

References and Notes

1. W. M. S. Kaula, G. Schubert, R. E. Lingenfelter, W. L. Sjogren, W. R. Wollenhaupt, *Proc. Lunar Sci. Conf.* **5**, 3049 (1974).
2. B. L. Jolliff, J. J. Gillis, L. A. Haskin, R. L. Korotev, M. A. Wieczorek, *J. Geophys. Res.* **105**, 4197 (2000).
3. J. T. Wasson, P. H. Warren, *Icarus* **44**, 752 (1980).
4. C. K. Shearer *et al.*, *Rev. Mineral. Geochem.* **60**, 365 (2006).
5. M. T. Zuber, D. E. Smith, F. G. Lemoine, G. A. Neumann, *Science* **266**, 1839 (1994).
6. J. A. Wood, *Moon* **8**, 73 (1973).
7. D. E. Loper, C. L. Werner, *J. Geophys. Res.* **107**, 5046 (2002).
8. D. E. Smith *et al.*, *Geophys. Res. Lett.* **37**, L18204 (2010).
9. N. Namiki *et al.*, *Science* **323**, 900 (2009).
10. D. E. Smith, M. T. Zuber, G. A. Neumann, F. G. Lemoine, *J. Geophys. Res.* **102**, 1591 (1997).
11. M. A. Wieczorek, R. J. Phillips, *Icarus* **139**, 246 (1999).
12. I. Garrick-Bethell, M. T. Zuber, *Icarus* **204**, 399 (2009).
13. D. E. Wilhelms, *The Geologic History of the Moon*. *U.S. Geological Survey (USGS) Professional Paper 1348* (USGS, Denver, CO, 1987).
14. S. Zhong, M. T. Zuber, *J. Geophys. Res.* **105**, 4153 (2000).
15. S. C. Solomon, J. Longhi, *Proc. Lunar Sci. Conf.* **8**, 583 (1977).
16. A. Nemchin *et al.*, *Nat. Geosci.* **2**, 133 (2009).
17. H. Jeffreys, *The Earth* (Cambridge Univ. Press, Cambridge, 1976).
18. G. W. Ojakangas, D. Stevenson, *Icarus* **81**, 220 (1989).
19. F. Nimmo, P. C. Thomas, R. T. Pappalardo, W. B. Moore, *Icarus* **191**, 183 (2007).
20. G. Tobie, A. Mocquet, C. Sotin, *Icarus* **177**, 534 (2005).
21. F. Nimmo, B. G. Bills, *Icarus* **208**, 896 (2010).
22. E. Rybacki, G. Dresen, *J. Geophys. Res.* **105**, 26017 (2000).
23. P. C. Hess, M. J. Rutherford, H. W. Campbell, *Proc. Lunar Sci. Conf.* **9**, 705 (1978).
24. J. A. Van Orman, T. L. Grove, *Meteorit. Planet. Sci.* **35**, 783 (2000).
25. Crustal-thickness differences may also be lowered as the remaining liquids under the crust crystallize (SOM section 8).
26. E. M. Parmentier, Y. Liang, in *41st Lunar and Planetary Science Conference (LPSC)*, *Abstract 1824* (LPSC, The Woodlands, TX, 1 to 5 March 2010).
27. We have multiplied the actual crustal thickness by 0.4 to better match the thickness amplitudes in the two cases.
28. E. M. Parmentier, S. Zhong, M. T. Zuber, *Earth Planet. Sci. Lett.* **201**, 473 (2002).
29. G. W. Ojakangas, D. J. Stevenson, *Icarus* **81**, 242 (1989).

30. We thank E. M. Parmentier, G. Hirth, L. Elkins-Tanton, M. T. Zuber, J. Andrews-Hanna, G. A. Glatzmaier, P. C. Hess, and M. J. Rutherford for helpful discussions. This work was made possible by a Brown University postdoctoral research assistantship to I.G.-B.

Supporting Online Material

www.sciencemag.org/cgi/content/full/330/6006/949/DC1
SOM Text
Figs. S1 to S17
Tables S1 to S5
References

8 June 2010; accepted 7 October 2010
10.1126/science.1193424

Downloaded from www.sciencemag.org on November 11, 2010

Coupling of Nitrous Oxide and Methane by Global Atmospheric Chemistry

Michael J. Prather and Juno Hsu

Nitrous oxide (N_2O) and methane (CH_4) are chemically reactive greenhouse gases with well-documented atmospheric concentration increases that are attributable to anthropogenic activities. We quantified the link between N_2O and CH_4 emissions through the coupled chemistries of the stratosphere and troposphere. Specifically, we simulated the coupled perturbations of increased N_2O abundance, leading to stratospheric ozone (O_3) depletion, altered solar ultraviolet radiation, altered stratosphere-to-troposphere O_3 flux, increased tropospheric hydroxyl radical concentration, and finally lower concentrations of CH_4. The ratio of CH_4 per N_2O change, −36% by mole fraction, offsets a fraction of the greenhouse effect attributable to N_2O emissions. These CH_4 decreases are tied to the 108-year chemical mode of N_2O, which is nine times longer than the residence time of direct CH_4 emissions.

Methane (CH_4) has environmental impacts beyond those of a direct greenhouse gas, through atmospheric chemistry that enhances the abundance of tropospheric ozone (O_3) and decreases that of hydroxyl radicals (OH) and hence the atmospheric lifetime of many other pollutants (*1*, *2*). Likewise, nitrous oxide (N_2O) is a known O_3-depleting substance (*3*, *4*). Both CH_4 and N_2O interact directly in the chemistry of stratospheric O_3, where global CH_4 concentration increases drive proportional but much smaller N_2O increases (*5*). The pathway of how N_2O affects global CH_4 is more complex, involving the coupling of stratospheric O_3 depletion with global tropospheric chemistry through OH, and consequently the lifetime of CH_4.

This chemical coupling of the stratosphere and troposphere alters one's expectations about the amplitude and persistence of anthropogenic perturbations. Here we describe four multidecade numerical simulation experiments—one control and three perturbations runs—which have been designed to find such coupling between N_2O and CH_4 through analysis of long-lived chemical modes. We define modes as the perturbation patterns in the abundances of all chemical species resulting from, for example, the addition of one species (i.e., eigenvectors of the linearized system). In atmospheric chemistry, the most important modes are the long-lived, slowly decaying ones associated with N_2O and CH_4, because these have the largest environmental impacts.

The University of California Irvine's three-dimensional chemistry-transport model incorporates algorithms for both stratospheric and tropospheric chemistry (*5*–*7*). The meteorology and trace gas emissions in this study are representative of conditions in the year 2005 (*7*). For our control run, the CH_4 and N_2O emissions are prescribed to achieve steady-state abundances of 1775 and 320 parts per billion (ppb), respectively. The annual budgets for N_2O, CH_4, and carbon monoxide (CO) from year 80 of this run are summarized in Table 1. Surface N_2O emissions of 13 Tg of N/year are matched by stratospheric loss. There are small terms (~1%) in the budget accounting for stratospheric production ($N + NO_2$) and tropospheric loss [$O(^1D) + N_2O$]. The budget lifetime of N_2O is 118 years. Surface CH_4 emissions of 643 Tg/year are balanced by tropospheric (95%) and stratospheric (5%) loss, giving a budget lifetime of 7.8 years, which is within the range of models reported in (*8*) (Table 1). Surface CO emissions of 1050 Tg/year are augmented by 2070 Tg/year from photochemical production in the atmosphere.

The chemical modes, using an annually repeating meteorology, are five-dimensional (species, time of year, and three spatial dimensions) quantities, as shown in previous studies (*5*, *9*, *10*). Here we focus on the global burden on 1 January, thus ignoring the spatial and seasonal variations shown in (*9*). Modes are calculated from the difference between a perturbation and the control simulation. The same initialization and 80-year control simulation (C1) is used in all cases. The N_2O perturbation (simulation C2) introduces a pulse of 10 Tg of N from N_2O in the lowest four model layers on top of the initial conditions; the CO perturbation (simulation C3) introduces 100 Tg of CO; and the CH_4 perturbation (simulation C4) introduces 10 Tg of CH_4. In the perturbation-minus-control differences, the shorter-lived modes (those associated with other chemical species, interhemispheric mixing, and stratosphere-troposphere exchange) decay within a few years, leaving behind a combination of the N_2O-driven mode 1 (108 years) and the CH_4-driven mode 2 (12.5 years).

The pulse of N_2O alone (C2 – C1) induces perturbations in almost all species as shown in Fig. 1A. The relative perturbations in total atmospheric burden (in kilograms) eventually lock into the pattern of the 108-year mode 1: positive perturbations (solid lines) for N_2O, odd nitrogen species (NOy), and upper tropospheric O_3; and negative (dashed lines) for CH_4, CO, total O_3, and lower tropospheric O_3. The relative amplitudes, in terms of percent of the steady-state control C1, are shown in Fig. 2. For the long-lived gases N_2O and CH_4, these have only slight variations with altitude, but for O_3, the pattern changes sign and varies greatly with latitude.

The CO pulse (C3 – C1) is shown in Fig. 1B. Results are plotted beginning 1 year after the pulse, when the initial 10^{11} kg of CO and its related perturbation of tropospheric O_3 have mostly decayed. The CH_4 perturbation, caused by the CO-driven decrease in OH, is established by year 1 and decays with the mode 2 time of 12.5 years, which is longer than the budget lifetime of 7.8 years. Perturbations of CO and total O_3 also occur in mode 2 and are apparent for at least the first 60 years. The N_2O perturbation is predominantly in mode 1 and is caused by increased CH_4 in the stratosphere [see the stratospheric chemistry modes in (*5*)]. Following the chemical perturbations by the difference between two runs, C3 – C1, becomes difficult when the amplitudes in modes 1 and 2 become comparable as they do near the end of the simulation in Fig. 1B. The control C1 does not begin in an exact steady state and thus has a drift that is also a combination of the two modes, with the transition in O_3 and CO amplitudes from 2 to 1 occurring near year 50. This interference of the modes causes the derived amplitudes of CO and O_3 to diverge from a simple decay curve (e-fold), plus some noise in the subtraction (thin lines in Fig. 1B). This transition does not affect Fig. 1A, where the amplitudes in the longer-lived mode 1 are much larger.

In these perturbations, modes 1 and 2 can be separated and then traced back to a value at time zero, knowing that exponential decay is fixed globally for each mode. These time-zero amplitudes are reported in Table 2 for the three perturbations and the primary species of interest here (N_2O, NOy, CH_4, total O_3, and tropospheric O_3). Chemical modes, like eigenvectors, are scalable patterns; and thus in Table 2, mode 1 perturbations can be characterized by the total mass of N_2O, and mode 2 perturbations by that of CH_4. The pulse of 10 Tg of N from N_2O (C2) leads to a mode 1 amplitude of 10.2 Tg of N. Loss of this surface pulse is minimal in the first year as it mixes slowly into the region of stratospheric

Table 1. Annual mean chemical budget terms (in teragrams/year) and budget lifetimes. Surface emissions, production (prod), and loss are in teragrams/year except for N_2O, which are in teragrams of N/year. Terms are split into stratosphere (strat) and troposphere (trop). CO surface deposition is included in trop loss. CH_4 surface deposition is not included, and it would have shortened the CH_4 lifetime to 7.44 years, which is still within the standard deviation of models in (*8*), 8.7 ± 1.3 years.

Species	Surface	Trop prod	Trop loss	Strat prod	Strat loss	Lifetime (years)
N_2O	+13.0	0	−0.14	+0.14	−13.1	118.3
CH_4	+643	0	−611	0	−32	7.8
CO	+1050	+2070	−2955	0	−165	0.33

Department of Earth System Science, University of California, Irvine, CA 92697–3100, USA.

Downloaded from www.sciencemag.org on November 11, 2010

destruction. Thus, the avoided loss, about 0.2 Tg of N, adds to the amplitude of mode 1, amplifying the integrated radiative forcing from the N_2O pulse. Such an increase of about 2% should be applied to all greenhouse gases with stratospheric loss, such as chlorofluorocarbons, but not to those with tropospheric loss, such as hydrofluorocarbons. In a similar but opposite vein, the pulse of 10 Tg of CH_4 (C4) has an amplitude of only 9.85 Tg in mode 2, because the most rapid loss occurs in the lower atmosphere where it is emitted. The N_2O pulse (C2) produces a CH_4 amplitude of –2.1 Tg in mode 1 and +2.8 Tg in mode 2. This pulse must also excite other, short-lived modes (not seen here) with a net CH_4 amplitude of –0.7 Tg, because the initial CH_4 perturbation is zero. The overall negative perturbation of CH_4 appears within the first year, and within two decades, the CH_4 perturbation parallels that of N_2O in mode 1.

This study looks at the coupled chemistry of stratosphere and troposphere, and thus we examine the mode patterns in Fig. 2 to trace causality, beginning with a surface increase in N_2O of 10% (32 ppb). The increase in N_2O directly causes an increase in NOy, which depletes O_3 by about 2% in the middle stratosphere (a height of 25 to 40 km). The decrease in O_3 allows greater penetration of solar ultraviolet (UV) into the middle stratosphere, enhancing the destruction of N_2O. Thus, the relative perturbation of N_2O declines from +10% to about +8.5% above 35 km. The relative increase in NOy is about the same as that in its source (N_2O) below 30 km, but rapidly falls off aloft where the quadratic photochemical loss of NOy buffers its abundance. The maximum decrease of –1.2% in the overhead O_3 column occurs at about 22 km and varies with latitude. Lower overhead O_3 inventories allow more UV into the lower stratosphere and upper troposphere, where enhanced photolysis of O_2 (*11*) increases O_3 by as much as +1.3%. The stratosphere-to-troposphere flux of O_3 [~500 Tg/year in this simulation (*12*, *13*)] increases by +0.9%, caused by O_3 increases in the mid-latitude lower stratosphere. The O_3 column near the surface is reduced by –0.45%, and thus reductions in lower tropospheric O_3 concentrations of about –0.2% are driven by increased UV and more rapid photochemical O_3 loss under moist conditions [$O(^1D) + H_2O$, $HO_2 + O_3$]. The global burden of CH_4 is decreased by –0.65% because of greater tropospheric OH abundances, caused by enhanced UV from the smaller O_3 column. Like N_2O, the relative perturbation of CH_4 declines further to –1.5% by 50 km because of the enhanced UV and loss in the middle stratosphere.

The use of chemical modes to deconstruct such perturbations allows for better understanding and predictions. Here we go beyond a one-dimensional (1D) representation of the N_2O chemical modes (*14*) by following the perturbations into 3D tropospheric chemistry. A relatively large reduction in CH_4 concentration (–3.6 ppb) is tied to an increase in N_2O (+10 ppb) that decays with a 108-year time scale. Thus, N_2O's climate impact through radiative forcing is diminished: (i) –8.4% because the decay of a pulse is faster than the e-fold of the steady-state lifetime used previously (*15*), and (ii) a further –4.5% to account for the decrease in the concentration of CH_4. For CH_4, the chemical feedbacks are opposite, lengthening the time scale of perturbations and increasing the greenhouse impact by about +40% (*16*–*18*).

Using the mode 1 coupling across species, one can readily compute that the N_2O concentration increase since preindustrial times, from 270 to 320 ppb, has caused a 2–Dobson unit (DU) (0.7%) decrease in total O_3 abundance, as compared with the 3.5% decrease since 1980 that is attributable primarily to halocarbons (*19*). The corresponding mode 1 offset in CH_4 since preindustrial times, –18 ppb, is small relative to the overall CH_4 concentration increase of 1000 ppb.

The agreed-on atmospheric residence time for CH_4 used to weight emissions in international treaties is based on the mode 2 time scale, currently estimated as 12 years (*20*). Our derived mode 2 time scale of 12.5 years is well within the uncertainty, but the ratio of residence to budget lifetime in our model is 1.6, at the upper end of the model range in that assessment. Our model thus predicts much stronger chemical feedbacks from CH_4 perturbations. The increase in global tropospheric O_3 per unit of increase in CH_4 is part of the mode 2 pattern calculated here, and the ratio in more traditional units, 3.1 DU per ppm, is similar to other model results [for example, 3.7 for (*2*) and 2.4 for (*1*)]. The CO-CH_4 coupling here, 7.4 Tg of CH_4 generated from 100 Tg of CO, is consistent with the indirect global warming potential of CO emissions (*18*).

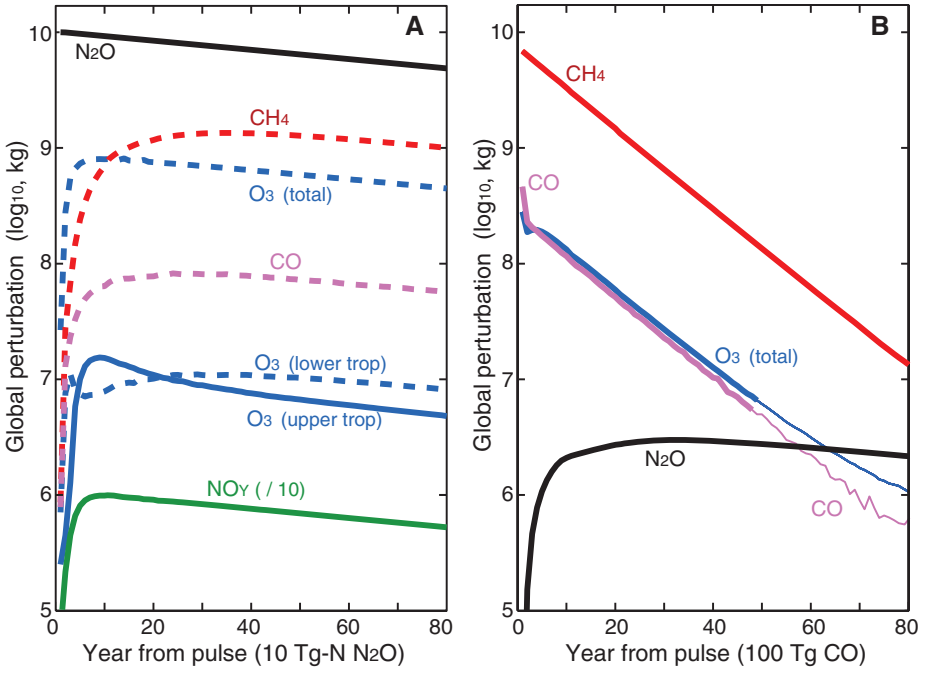

Fig. 1. Decay of atmospheric chemical perturbations caused by an initial pulse of (**A**) 10 Tg of N from N_2O and (**B**) 100 Tg of CO (1 Tg = 10^9 kg). Perturbations represent the total atmospheric burden of key species. Positive perturbations are indicated by solid lines; negative ones by dashed lines. The asymptotic behavior in (A) is chemical mode 1 with a decay time of 108 years. (B) shows both mode 2 (12.5 years) and mode 1 (N_2O only) decays. Values are plotted every 1 January, beginning 1 year after the initial pulse. The thin extension lines in (B) for O_3 (total) and CO indicate difficulties in separating the modes in both control C1 and perturbation C3.

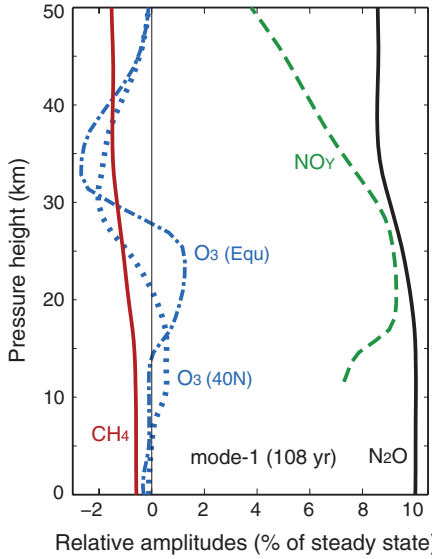

Fig. 2. Altitude profiles of the pattern of key species in mode 1 on 1 January. For N_2O, NOy, and CH_4, each profile is a global mean, but for O_3 the profiles are sampled at the equator and 40°N latitude. The amplitudes are shown as relative to the steady-state profiles and are scaled to 10% in N_2O at the surface.

Downloaded from www.sciencemag.org on November 11, 2010

Table 2. Chemical modes and amplitudes excited by pulses of N_2O, CO, and CH_4. The modes are identified with perturbation minus control (P − C) simulations. Amplitudes (*A*) are in globally integrated teragrams of N for N_2O and NOy and in teragrams for other species. The amplitudes of these modes are characterized by the amounts of N_2O (mode 1) and CH_4 (mode 2), shown in bold. Relatively small amplitudes are not shown (–).

P − C	Initial pulse	Mode (time)	*A* N_2O	*A* NOy	*A* CH_4	*A* O_3	*A* trop O_3
C2 − C1	10 Tg of N from N_2O	1 (108.4 years)	**+10.2**	+0.011	−2.1	−0.93	−0.01
		2 (12.5 years)	−0.002	–	**+2.8**	+0.11	0.03
C3 − C1	100 Tg of CO	1 (108.4 years)	**+0.0045**	–	–	–	–
		2 (12.5 years)	−0.005	−0.00003	**+7.4**	+0.30	+0.09
C4 − C1	10 Tg of CH_4	1 (108.4 years)	**+0.006**	–	–	–	–
		2 (12.5 years)	−0.007	-0.00004	**+9.85**	+0.40	+0.12

This N_2O-CH_4 coupling will shift with climate change over the 21st century. For example, the upper stratosphere cools as CO_2 increases, and this temperature change alters the N_2O-NOy-O_3 chemistry, reducing the impact of N_2O on O_3 (*21*). The importance of N_2O as an ozone-depleting substance (*22*) will thus be reduced, weakening the coupling described here but still maintaining the negative greenhouse feedback effect of CH_4 on N_2O emissions.

References and Notes

1. A. M. Fiore, J. J. West, L. W. Horowitz, V. Naik, M. D. Schwarzkopf, *J. Geophys. Res.* **113**, D08307 (2008).
2. M. Prather *et al.*, in *Climate Change 2001: The Scientific Basis. Third Assessment Report of the Intergovernmental Panel on Climate Change*, J. T. Houghton *et al.*, Eds. (Cambridge Univ. Press, Cambridge, 2001), pp. 239–287.
3. M. B. McElroy, J. C. McConnell, *J. Atmos. Sci.* **28**, 1095 (1971).
4. World Meteorological Organization (WMO), *Atmospheric Ozone 1985: Assessment of Our Understanding of the Processes Controlling Its Present Distribution and Change*, R. T. Watson *et al.*, Eds. (Global Ozone Research and Monitoring Project Report No. 16, WMO, Geneva, 1985).
5. J. Hsu, M. J. Prather, *Geophys. Res. Lett.* **37**, L07805 (2010).
6. Q. Tang, M. J. Prather, *Atmos. Chem. Phys.* **10**, 9681 (2010).
7. Materials and methods are available as supporting material on *Science* Online.
8. D. S. Stevenson *et al.*, *J. Geophys. Res.* **111**, D08301 (2006).
9. O. Wild, M. J. Prather, *J. Geophys. Res.* **105**, 24647 (2000).
10. R. G. Derwent, W. J. Collins, C. E. Johnson, D. S. Stevenson, *Clim. Change* **49**, 463 (2001).
11. M. J. Prather, *Geophys. Res. Lett.* **36**, L03811 (2009).
12. J. Hsu, M. J. Prather, O. Wild, *J. Geophys. Res.* **110**, D19305 (2005).
13. J. Hsu, M. J. Prather, *J. Geophys. Res.* **114**, D06102 (2009).
14. M. J. Prather, *Science* **279**, 1339 (1998).
15. D. L. Albritton, R. G. Derwent, I. S. A. Isaksen, M. Lal, D. J. Wuebbles, in *Climate Change 1994, Intergovernmental Panel on Climate Change*, J. T. Houghton *et al.*, Eds. (Cambridge Univ. Press, Cambridge, 1995), pp. 204–231.
16. M. J. Prather, *Geophys. Res. Lett.* **21**, 801 (1994).
17. M. Prather *et al.*, in *Climate Change 1994, Intergovernmental Panel on Climate Change*, J. T. Houghton *et al.*, Eds. (Cambridge Univ. Press, Cambridge, 1995), pp. 73–126.
18. P. Forster *et al.*, in *Climate Change 2007: The Physical Science Basis. Fourth Assessment Report of the Intergovernmental Panel on Climate Change*, S. Solomon *et al.*, Eds. (Cambridge Univ. Press, Cambridge, 2007), pp. 129–234.
19. WMO, *Scientific Assessment of Ozone Depletion: 2006*, C. A. Ennis, Ed. (WMO, Geneva, 2006).
20. K. L. Denman *et al.*, in *Climate Change 2007: The Physical Science Basis. Fourth Assessment Report of the Intergovernmental Panel on Climate Change*, S. Solomon *et al.*, Eds. (Cambridge Univ. Press, Cambridge, 2007), pp. 499–587.
21. J. E. Rosenfield, A. R. Douglass, *Geophys. Res. Lett.* **25**, 4381 (1998).
22. A. R. Ravishankara, J. S. Daniel, R. W. Portmann, *Science* **326**, 123 (2009).

23. This research was supported by NSF's Atmospheric Chemistry program (grant ATM-0550234) and NASA's Modeling, Analysis, and Prediction/Global Modeling Initiative program (grants NNG06GB84G and NNX09AJ47G).

Supporting Online Material

www.sciencemag.org/cgi/content/full/330/6006/952/DC1
Methods
References

9 August 2010; accepted 8 October 2010
10.1126/science.1196285

Fossil Evidence for Evolution of the Shape and Color of Penguin Feathers

Julia A. Clarke,[1]* Daniel T. Ksepka,[2,3] Rodolfo Salas-Gismondi,[4] Ali J. Altamirano,[4] Matthew D. Shawkey,[5] Liliana D'Alba,[5] Jakob Vinther,[6] Thomas J. DeVries,[7] Patrice Baby[8,9]

Penguin feathers are highly modified in form and function, but there have been no fossils to inform their evolution. A giant penguin with feathers was recovered from the late Eocene (~36 million years ago) of Peru. The fossil reveals that key feathering features, including undifferentiated primary wing feathers and broad body contour feather shafts, evolved early in the penguin lineage. Analyses of fossilized color-imparting melanosomes reveal that their dimensions were similar to those of non-penguin avian taxa and that the feathering may have been predominantly gray and reddish-brown. In contrast, the dark black-brown color of extant penguin feathers is generated by large, ellipsoidal melanosomes previously unknown for birds. The nanostructure of penguin feathers was thus modified after earlier macrostructural modifications of feather shape linked to aquatic flight.

During wing-propelled diving, penguins generate propulsive forces in a fluid environment ~800 times more dense and ~70 times more viscous than air (*1*). Recent fossil discoveries have yielded information on the sequence of early osteological changes in penguins accompanying the evolution of aquatic flight (*2*–*5*), but these specimens have not included feathers. Living penguin melanosome morphologies have not been described, although the melanin they contain is generally known to provide both color and wear-resistance to bird feathers (*6*–*8*). Here, we describe a giant fossil penguin with feathers recording preserved melanosome morphologies (*9*) and discuss the pattern and timing of major events in the evolution of penguin integument.

Systematic paleontology: Aves Linnaeus 1758 *sensu* Gauthier 1986. Sphenisciformes Sharpe 1891 *sensu* Clarke *et al.* 2003. *Inkayacu paracasensis* new gen. and sp. **Etymology:** *Inkayacu*—the Quechua, "Inka" for emperor and "yacu" for water; *paracasensis* for the Reserva Nacional de Paracas, Peru, the type locality. **Holotype**: MUSM 1444, a nearly complete skeleton with wing feathering, body contour feathers, and pedal scales (Figs. 1 to 3) (*10*). **Locality and horizon:** Upper Eocene of Yumaque Point, Paracas Reserve, Peru (*10*). **Diagnosis:** *Inkayacu paracasensis* is diagnosed by the following combination of characters (autapomorphies within Sphenisciformes demarcated by an asterisk): paired grooves meeting at midline on dorsal surface of premaxilla* (Fig. 1, GR), articular surfaces of otic and squamosal head of quadrate contacting one another,* furcula with blade-like hypocleidium,* conspicuous n. coracobrachialis sulcus developed on the humerus (Fig. 1, CNS), femur with widened and sharply distally tapering medial condyle* and tab-like process projecting from posterior intramuscular ridge at midshaft* (Fig. 1, MC and T), and weak proximal projection of cnemial crests of tibiotarsus (Fig. 1, CNE). See (*10*) for additional diagnosis, figures, and description.

[1]Department of Geological Sciences, University of Texas at Austin, Austin, TX 78712, USA. [2]Department of Marine, Earth, and Atmospheric Sciences, North Carolina State University, Raleigh, NC 27695–8208, USA. [3]Department of Paleontology, North Carolina Museum of Natural Sciences, Raleigh, NC 27601–1029, USA. [4]Departamento de Paleontología de Vertebrados, Museo de Historia Natural–Universidad Nacional Mayor de San Marcos (UNMSM), Lima 14, Perú. [5]Integrated Bioscience Program, University of Akron, Akron, OH 44325, USA. [6]Department of Geology and Geophysics, Yale University, New Haven, CT 06511, USA. [7]Burke Museum of Natural History and Culture, University of Washington, Seattle, WA 98195, USA. [8]Laboratoire des Mécanismes et Transferts en Géologie, Institut de Recherche pour de Développement, 14 Avenue Edouard Belin, F-31400 Toulouse, France. [9]Université de Toulouse, F-31400 Toulouse, France.

*To whom correspondence should be addressed: julia_clarke@jsg.utexas.edu

Downloaded from www.sciencemag.org on November 11, 2010

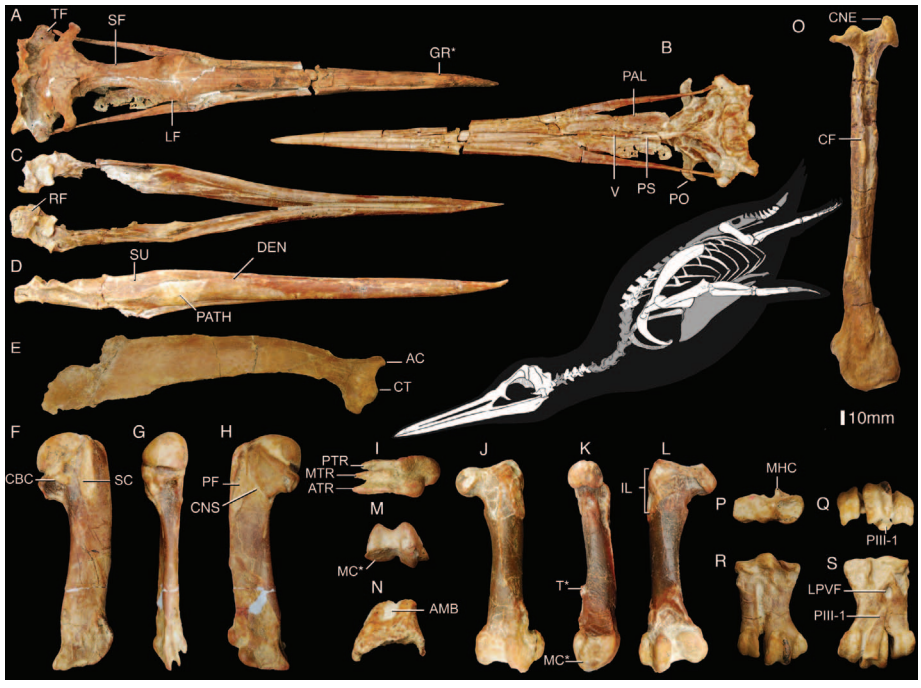

Fig. 1. Reconstruction of *Inkayacu paracasensis* in oblique anterior view showing recovered elements in white and photographs of the holotype specimen (MUSM 1444): skull and mandible in (**A** and **C**) dorsal, (**B**) ventral, and (**D**) lateral views; scapula in (**E**) lateral view and humerus in (**F**) posterior, (**G**) ventral, (**H**) anterior, and (**I**) distal views; femur in (**J**) dorsal, (**K**) medial, (**L**) ventral, and (**M**) distal views; patella in (**N**) anterior view; tibiotarsus in (**O**) lateral view; and tarsometatarsus in (**P**) proximal, (**Q**) distal, (**R**) anterior, and (**S**) plantar views. AC, acromion; AMB, pathway of m. ambiens tendon; ATR, anterior trochlear process; CBC, m. coracobrachialis caudalis insertion; CF, fibular crest; CNE, cnemial crests; CNS, coracobrachialis nerve sulcus; CT, coracoid tuberosity; DEN, dentary; GR, groove on premaxilla; IL, m. iliofemoralis and iliotrochantericus insertions; LF, lacrimal facet; LPVF, lateral proximal vascular foramen; MHC, medial hypotarsal crest; MC, medial condyle; MTR, middle trochlear process; PIII-1, manual phalanx III-1; PAL, palatine; PATH, pathology; PF, pectoralis fossa; PO, postorbital process; PS, parasphenoid rostrum; PTR, posterior trochlear process; SC, m. supracoracoideus insertion; SF, salt gland fossa; SU, surangular; T, tab-like process; TF, temporal fossa; V, vomer. Asterisks demarcate autapomorphies referenced in the diagnosis (*10*).

The holotype skeleton of *Inkayacu paracasensis* is disarticulated, with the exception of regions with extensive soft tissue impressions [distal left flipper (Fig. 2) and distal left pes (*10*)]. The fossil represents an animal with an estimated swimming length of 1.5 m. It has a hyper-elongate beak with a grooved tip and relatively gracile wing bones as compared with those of other giant penguins [such as *Icadyptes* (*11*)]. Conservative estimates of body mass for *Inkayacu* (~54.6 to 59.7 kg) are approximately twice the average mass of the Emperor Penguin (*12*); it is among the largest described fossil penguins (*10*).

Isolated contour feathers exhibit the broadened rachis of extant penguins. They grade from a light-colored (pale gray) base to a dark gray-black distal end (Fig. 3), where the rachis narrows and a cluster of distally directed, clumped darker barbs are developed at the tip. This coloration pattern is observed in penguins and other birds, resulting from increasing melanization toward the tip (*13*). Preserved portions of contour feathers and estimates from rachis diameter are consistent with a maximum length of approximately 3 cm, which is within the range of extant penguin body contour feathers (*10*) but notably shorter than contour feathers from several smaller-bodied extant high-latitude species (*10*). As in extant penguins, these feathers are pennaceous over most of their length; barbs are relatively evenly spaced, although barbule structure is not visible.

Preserved feathering along the left distal wing is exposed in dorsal view (Fig. 2) and appears to be close to life position with only slight peri-depositional posterior movement of the distal carpometacarpus. At the leading edge, texturing of a thin layer of gray matrix records the tips of tiny, closely packed covert feathers with melanosomes (Fig. 2, A to C). This darker layer continues over most of the carpometacarpus and distal radius. Where it split from the dorsal carpometacarpal surface, the underlying, light-colored matrix is textured with small regularly distributed raised knobs (Fig. 2A). Thin, paired impressions in this pale matrix preserve melanosomes (Fig. 2, D and E) that we interpret as melanized bases of the short,

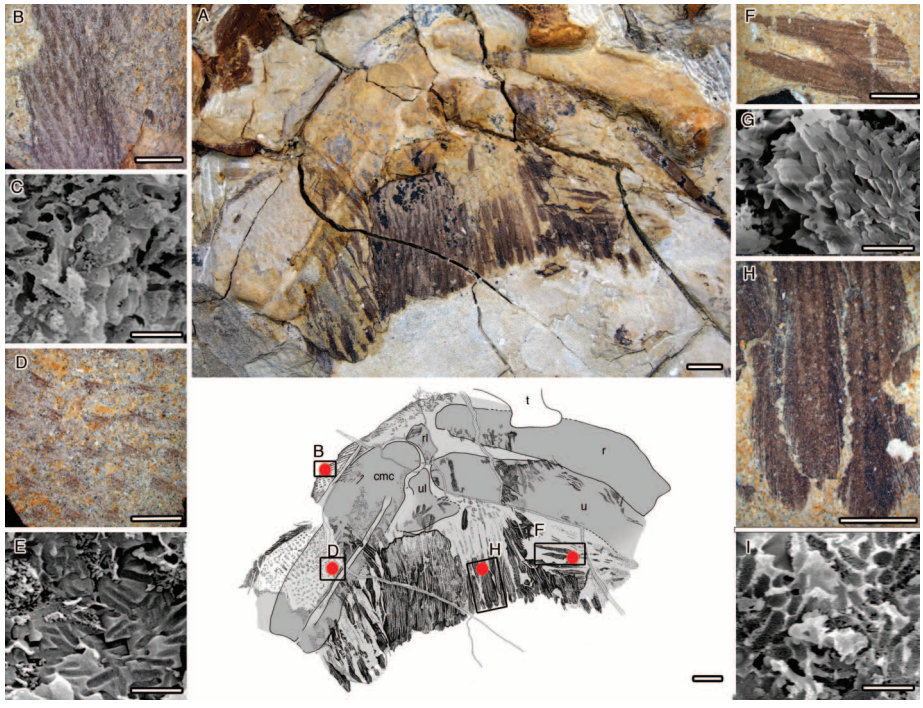

Fig. 2. The wing feathering of *Inkayacu paracasensis*. (**A**) Photograph and line drawing of the left wing (scale bar, 1 cm) showing location of insets and samples (circles) taken for scanning electron microscopy (SEM). (**B**) Close-up of the counterpart showing the surface of imbricated short covert feathers from the leading edge of the wing and (**C**) SEM of melanosomes in (B). (**D**) Close-up of the counterpart to the surface of the carpometacarpus with preserved melanized bases of covert feathers and (**E**) SEM of melanosomes from feather bases in (D) (melanosomes were not observed in surrounding matrix). (**F**) Close-up of tertiaries and (**G**) SEM of melanosomes in (F). (**H**) Secondaries and (**I**) SEM of melanosomes from (H). Scale bar for SEM images, 1 μm, and for insets, 3 mm. mc, carpometacarpus; r, radius; rl, radiale; t, tibiotarsus; u, ulna; ul, ulnare.

Downloaded from www.sciencemag.org on November 11, 2010

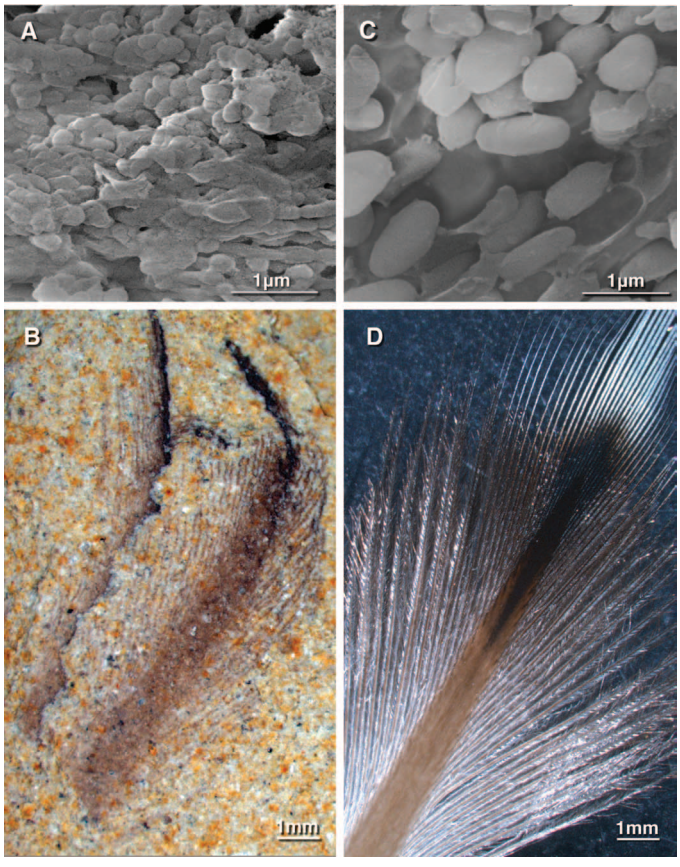

Fig. 3. Comparison of melanosome proportions and body contour feather morphology in (**A** and **B**) *Inkayacu paracasensis* and (**C** and **D**) representative extant penguins. (A) SEM of melanosomes preserved in the tip of (B) body contour feathers of *I. paracasensis*; (C) SEM of large, ellipsoidal melanosomes (shown, *Eudyptula minor*) from (D) similarly shaped body contour feathers (shown, *Aptenodytes forsteri*) in the penguin crown clade.

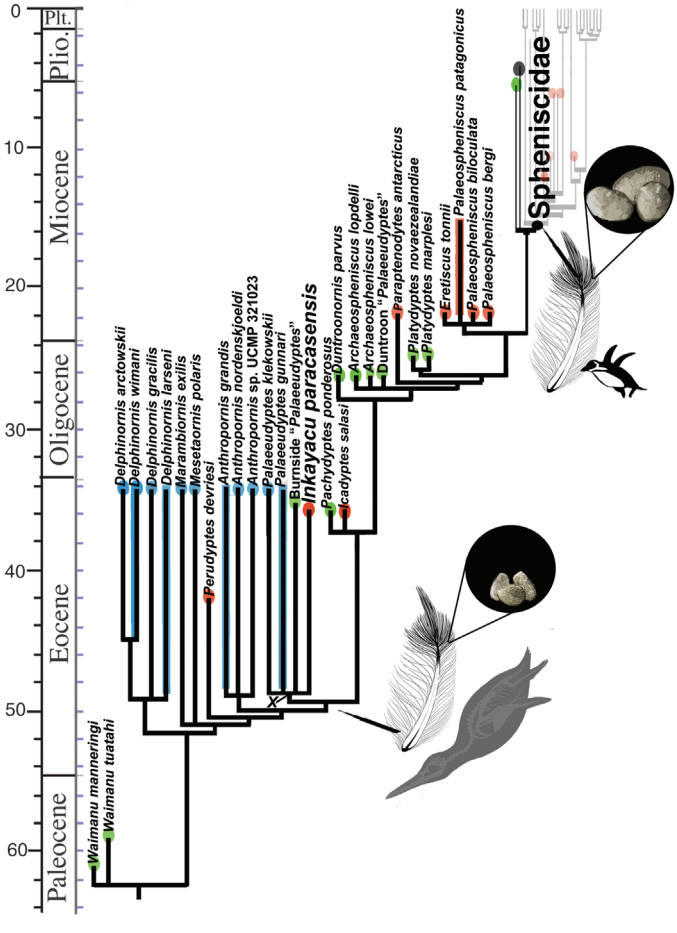

Fig. 4. Phylogenetic placement of *Inkayacu paracasensis* in a strict consensus cladogram of 45 most-parsimonious trees (MPTs) [Crown clade collapsed; see (*10*) for details of analysis]. Placement in a clade of Eocene giant penguins (X) implies an origin for the modified wing feathering, undifferentiated remiges, and broad rachis of body contour feathers (**insets**) no later than the early Eocene (*10*). Enlarged melanosomes are phylogenetically supported at minimum as a novelty of the penguin crown clade (**insets**). Stratigraphic distributions from (*5*). Fossil distributions are Antarctica, blue; New Zealand, green; Africa, dark gray; and South America, red.

darker-tipped covert feathers. Similarly, extant penguin coverts that exhibit dark tips are commonly white proximally but bear melanin stripes where the feathers enters the skin. The absence of melanosomes in the light matrix surrounding these marks in the fossil is consistent with similarly white proximal feathers (*9*) in *Inkayacu*. Presence of intact lesser covert feather bases and tips (in part and counterpart) represents a dimensionality rare in feather preservation.

Dorsal lesser-wing covert feathers partially overlie the distal wing bones (Fig. 2). Layers of elongate under-wing coverts pass ventral to the ulnare and carpometacarpus. The morphology and dark tonality of the feathers originating from the carpometacarpus and ulna, which comprise the trailing edge of the wing, are identical (Fig. 2, A and H). The homology of any one stacked layer of these feathers with the primaries and secondaries (remiges) of other birds is uncertain, but if one layer is considered to represent the remiges, at least one layer of coverts subequal in length must be present. All of these feathers show a broadened rachis and are relatively larger than in any extant penguin. The centers of rachises are light with darker edges. Many barbs are visible in distal feathers, and fewer are decipherable at midshaft. Seven incomplete feathers preserved in the matrix overlying the secondaries appear to be associated with the distal humerus.

All preserved feather types in *Inkayacu* record melanosomes (Figs. 2 and 3) (*10*) of dimensions within the range for avian taxa other than extant penguins (*10*). Although the length of extant penguin melanosomes was similar to other eumelanosomes, (mean of ~900 nm), their width (mean of ~440 nm) was far greater than all other Aves sampled (mean of ~300 nm) and in some cases approached their length (table S3). We thus analyzed them as a separate class in a discriminant analysis (*10*). We used four properties of melanosome morphology and distribution—long-axis variation, short-axis skew, aspect ratio, and density—to estimate the color predicted from the fossil feather samples (*10*). All six *Inkayacu* samples were assigned a gray or reddish-brown color with high probability, and none clustered with extant penguin samples.

The *Inkayacu* specimen provides evidence for an Eocene giant penguin clade (Fig. 4, Clade X) with a wide Southern Ocean distribution and for a third early-stem penguin dispersal to low latitudes (*11*). Phylogenetic analysis of a combined data set (*10*) finds the new species allied with three early- to late-Eocene species from New Zealand and Antarctica (*10*). The most recent common ancestor of *Inkayacu* and living penguins (Spheniscidae) is thus inferred to be present by the early Eocene and to have shared the lack of differentiation between stacked remiges and greater coverts, densely packed, squamiform lesser coverts, and broad flattened contour feather rachises seen in extant penguins. Early modifications in the wing feathering seen in *Inkayacu* created a narrow streamlined flipper and changed the hydrodynamic properties of the body feathers. Broad flat contour

Downloaded from www.sciencemag.org on November 11, 2010

feather rachises create less turbulent flow (*12*), which is an effect hypothesized to explain a lower observed drag coefficient than predicted from streamlined penguin body shape alone (*14*). They also facilitate reduction of intraplumage air (*15*). Most of the insulating properties of extant penguin contour feathers derive from their plumulaceous afterfeathers (*16*), which are not preserved or not present in *Inkayacu*.

Inkayacu shows that the large, subround melanosomes of extant penguin feathers were absent early in penguin evolution. At minimum, an increase in melanosome size and a decrease in their aspect ratio occurred after the early Eocene divergence of the clade that includes *Inkayacu* (Fig. 4, Clade X) and before the origin of extant penguins (Spheniscidae) by the late Miocene (*5*). The specific proportions of extant penguin melanosomes, the packing of these melanosomes into clusters within the barbs and rachis (*10*), and yellow, pterin-like pigmentation (*17*) are so far only known in the penguin crown clade.

Shifts in penguin plumage coloration indicated by the fossil may be linked to differences in ecology, thermoregulatory demands (*18*), or the more recent, predominantly Neogene, diversification of their primary mammalian predators (*19*, *20*). However, they do not explain the aberrant melanosome morphology associated with extant penguin brown-black color. Indeed, rather than selection for color, these changes may represent an unanticipated response to the hydrodynamic demands of underwater propulsion. Low aspect ratio, large size, and clustered melanosome distribution (*10*) may affect melanin packing and feather material properties. Melanin confers resistance to fracture (*6*, *21*, *22*), which is important to materials like feathers subjected to cyclical loading (*22*). Selective pressures for the color and material properties of penguin feathers could thus have led to nanoscale changes in melanosome morphology.

References and Notes

1. M. Denny, *Air and Water* (Princeton Univ. Press, Princeton, NJ, 1993).
2. R. E. Fordyce, C. M. Jones, in *Penguin Biology*, L. S. Davis, J. T. Darby, Eds. (Academic Press, San Diego, CA, 1990), pp. 419–226.
3. K. E. Slack *et al.*, *Mol. Biol. Evol.* **23**, 1144 (2006).
4. P. Jadwiszczak, *Polar Res.* **30**, 3 (2009).
5. D. T. Ksepka, J. A. Clarke, *Bull. Am. Mus. Nat. Hist.* **337**, 1 (2010).
6. E. H. Burtt Jr., *Ornithol. Monogr.* **38**, 1 (1986).
7. K. J. McGraw, in *Bird Coloration, vol.1, Mechanisms and Measurements*, G. E. Hill, K. J. McGraw (Harvard Univ. Press, Boston, 2006), pp. 243–294.
8. B. Stonehouse, *The Biology of Penguins* (Macmillan, London, 1975).
9. J. Vinther, D. E. G. Briggs, R. O. Prum, V. Saranathan, *Biol. Lett.* **4**, 522 (2008).
10. Materials and methods are available as supporting material on *Science* Online.
11. J. A. Clarke *et al.*, *Proc. Natl. Acad. Sci. U.S.A.* **104**, 11545 (2007).
12. B. Stonehouse, *Adv. Ecol. Res* **4**, 131 (1967).
13. W. L. N. Tickell, *Waterbirds* **26**, 1 (2003).
14. J. Lovvorn, G. A. Liggins, M. H. Borstad, S. M. Calisal, J. Mikkelsen, *J. Exp. Biol.* **204**, 1547 (2001).
15. R. P. Wilson, K. Hustler, P. G. Ryan, A. E. Burger, E. C. Noldeke, *Am. Nat.* **140**, 179 (1992).
16. C. Dawson, J. F. V. Vincent, G. Jeronimidis, G. Rice, P. Forshaw, *J. Theor. Biol.* **199**, 291 (1999).
17. K. J. McGraw *et al.*, *Pigment Cell Res.* **20**, 301 (2007).
18. H. M. Rowland, *Philos. Trans. R. Soc. London Ser. B Biol. Sci.* **364**, 519 (2009).
19. A. Berta, in *Encyclopedia of Marine Mammals, Second Edition*, W. Perrin, B. Würsing, J. G. M. Thewissen, Eds. (Academic Press, San Diego, CA, 2009), pp. 861–868.
20. U. Arnason *et al.*, *Mol. Phylogenet. Evol.* **41**, 345 (2006).
21. A. A. Voitkevich, *The Feathers and Plumage of Birds* (October House, New York, 1966).
22. R. H. Bonser, P. P. Purslow, *J. Exp. Biol.* **198**, 1029 (1995).

23. K. Browne helped produce the figures; W. Aguirre, P. Brinkman, and V. Schneider prepared the fossil. K. Middleton and M. Stucchi provided discussion. P. Unitt, K. Zyskowski, B. Wang, J. Tejada, J. Reyes, E. Díaz, and Z. Jiang provided professional assistance. The research was funded by the National Science Foundation (DEB-0949897 and DEB-0949899), the National Geographic Society Expeditions Council, the Air Force Office of Scientific Research (FA9550-09-1-0159), and University of Akron startup funds. MUSM 1444 is permanently deposited at the Museo de Historia Natural–UNMSM, Lima, Peru.

Supporting Online Material

www.sciencemag.org/cgi/content/full/science.1193604/DC1
Materials and Methods
SOM Text
Figs. S1 to S9
Tables S1 to S8
References
Phylogenetic Data Set

10 June 2010; accepted 10 September 2010
Published online 30 September 2010;
10.1126/science.1193604
Include this information when citing this paper.

Downloaded from www.sciencemag.org on November 11, 2010

Effects of Rapid Global Warming at the Paleocene-Eocene Boundary on Neotropical Vegetation

Carlos Jaramillo,[1]* Diana Ochoa,[1,2] Lineth Contreras,[3,1,4] Mark Pagani,[5] Humberto Carvajal-Ortiz,[6,1] Lisa M. Pratt,[6] Srinath Krishnan,[5] Agustin Cardona,[1] Millerlandy Romero,[1] Luis Quiroz,[1,7] Guillermo Rodriguez,[3,8] Milton J. Rueda,[9,3] Felipe de la Parra,[3] Sara Morón,[1,10] Walton Green,[1] German Bayona,[11,1] Camilo Montes,[1,11] Oscar Quintero,[12] Rafael Ramirez,[13] Germán Mora,[14] Stefan Schouten,[15] Hermann Bermudez,[16] Rosa Navarrete,[17] Francisco Parra,[18] Mauricio Alvarán,[16] Jose Osorno,[19] James L. Crowley,[20] Victor Valencia,[21] Jeff Vervoort[22]

Temperatures in tropical regions are estimated to have increased by 3° to 5°C, compared with Late Paleocene values, during the Paleocene-Eocene Thermal Maximum (PETM, 56.3 million years ago) event. We investigated the tropical forest response to this rapid warming by evaluating the palynological record of three stratigraphic sections in eastern Colombia and western Venezuela. We observed a rapid and distinct increase in plant diversity and origination rates, with a set of new taxa, mostly angiosperms, added to the existing stock of low-diversity Paleocene flora. There is no evidence for enhanced aridity in the northern Neotropics. The tropical rainforest was able to persist under elevated temperatures and high levels of atmospheric carbon dioxide, in contrast to speculations that tropical ecosystems were severely compromised by heat stress.

The Late Paleocene-Eocene Thermal Maximum [PETM, 56.3 million years ago (Ma)], lasting only ~100,000 to 200,000 years, was one of the most abrupt global warming events of the past 65 million years (*1*–*3*). The PETM is associated with a large negative carbon isotope excursion recorded in carbonate and organic materials, reflecting a massive release of ^{13}C-depleted carbon (*4*, *5*), an ~5°C increase in mean global temperature in ~10,000 to 20,000 years (*1*), a rapid and transient northward migration of plants in North America (*6*), and a mammalian turnover in North America and Europe (*7*).

Efforts to understand the impact of climate change on terrestrial environments have focused on mid- to high-latitude localities, but little is known of tropical ecosystems during the PETM. Tropical temperature change is poorly constrained, but, given the magnitude of temperature change elsewhere, tropical ecosystems are thought to have suffered extensively because mean temperatures are surmised to have exceeded the ecosystems' heat tolerance (*8*).

For this study, three tropical terrestrial PETM sites from Colombia and Venezuela were analyzed for pollen and spore content and stable carbon isotopic composition of organic materials (Fig. 1) (*9*). The analysis included 317 pollen samples, 1104 morphospecies, and 37,952 individual occurrences together with 489 carbon isotopes samples, 21 plant biomarker samples, and one radiometric age (*9*). Localities Mar 2X (core), Riecito Mache (outcrop), and Gonzales (outcrop and well) contain sediments that accumulated in fluvial to coastal plain settings. Biostratigraphy and carbon isotope stratigraphy, using bulk δ^{13}C and plant wax *n*-alkanes, confirm the position of the PETM at the three sites (Figs. 2 and 3) (*9*), which is not associated with any formation boundary or major lithological or depositional environment change. The location of the

PETM is further confirmed by a U-Pb radiometric dating of a felsic volcanic tuff found within the PETM in Riecito Mache section (Fig. 3) (*9*).

Plant standing diversity, inferred from pollen assemblages at Mar 2X (Fig. 2D) and Riecito Mache (Fig. 3C), shows a low diversity during the Late Paleocene, followed by a significant increase during the PETM. Low-diversity Paleocene floras and an increase in Early Eocene diversity had been previously observed in tropical South America (*10*, *11*), but the timing of the onset of the diversity changes was not resolved. Within-sample diversity in Mar 2X (*9*) shows a pattern similar to that for standing diversity. Paleocene samples (mean = 23.5) have fewer species than the PETM (mean = 35.9, $P < 0.00449$, df = 23.9), rarefied to a grain count of 150 (maintained even at a 100-grain count, Fig. 2C), whereas no significant difference is observed between the PETM and the Eocene (mean = 38.9, $P < 0.33$, df = 12.04). Similar diversity patterns characterize Gonzales (Fig. 3C), but within-sample diversity could not be calculated for Riecito Mache (*9*). The Simpson index, which measures the probability that two individuals taken at random will not belong to the same species, also reveals a similar pattern. In Mar 2X, the Simpson index is higher for the PETM (mean = 0.90) than for the Paleocene (mean = 0.76, $P < 0.0008$, df = 30.4), whereas the PETM and the Eocene (mean = 0.89) show no difference ($P < 0.44$, df = 54.8). A higher Simpson index for the PETM indicates that it has more species per sample than the Paleocene (as indicated by the higher within-sample diversity) and more evenly distributed species abundances. A similar pattern is recorded for Gonzales, but the Simpson index is slightly higher for the Eocene. In contrast, the Simpson index of the PETM at Riecito Mache was only slightly higher than the Paleocene, but the difference is not significant (*9*).

Taxa were divided into three groups, those for which extinction occurs in the Late Paleocene (P taxa), those whose origination occurs in the Early Eocene, including the PETM (E taxa), and those that are found in both the Paleocene and the Eocene (PE taxa). At the Mar 2X locality, standing diversity is lower for P taxa (13.6) than for E taxa (85.7; $P < 0.001$, df = 91.6) (Fig. 2E). Paleocene samples have a slightly higher standing diversity of PE taxa than Eocene samples (157.6 on the Paleocene side versus 135.8 on the Eocene side; $P < 0.001$, df = 58.542). When relative abundances are compared, the relation is similar, with P taxa less abundant in the Paleocene flora (4.6% of the assemblage) than E taxa in the Eocene flora (23.8% of the assemblage; $P < 0.001$, df = 107.9). The Paleocene flora at Mar 2X is composed largely of taxa that persisted into the Early Eocene, a pattern also evident in both Riecito Mache and Gonzales (Fig. 3D). Thus, our results demonstrate that the increase in tropical floral diversity during the PETM and Early Eocene resulted from the addition of a large set of new species, mostly angiosperms, to the existing, low-diversity floras that were holdovers from the Paleocene.

We assessed changes in floral composition by using a detrended correspondence analysis (DCA) and agglomerative clustering (*9*). The DCA shows a gradual change in flora during the PETM in the three studied sites (Figs. 2B and 3B) that is confirmed by the clustering analysis (*9*) (fig. S13), indicating that there was a significant change in the overall plant assemblage across the PETM. Even though we still do not know the affinities of ~85% of the flora, we were able to compare the remaining 15% (*9*). Diversity remained unchanged from the Paleocene into the Early Eocene for many families, including Polypodiaceae (ferns), Podocarpaceae (gymnosperms), Onagraceae, Ctenolophonaceae, Annonaceae, Moraceae, Rhizophoraceae, and Ulmaceae. However, diversity decreased in Proteaceae and increased in Arecaceae (palms), Bombacoideae, Fabaceae, Araceae, Poaceae, and Convolvulaceae. New families also appeared (i) during the uppermost Paleocene, including Myrtaceae, Sapotaceae, and Passifloraceae; (ii) within the PETM, including Sterculioideae, Euphorbiaceae, and Pellicieraceae; and (iii) during the Early Eocene, including Olacaceae and Ericaceae. Most of these originations, such as Sapotaceae, Passifloraceae, Ericaceae, Sterculioideae, Euphorbiaceae, and Pellicieraceae, represent the oldest pollen records for each family in the neotropics (*12*). Relative abundances show a similar pattern (Fig. 2).

The rate of extinction increased slightly during the PETM at a rate comparable to that during intervals within the Early Eocene (Fig. 4), with the gradual extinction of a small proportion (~5%) of Paleocene flora. However, extinction does not appear different from the background extinction rates of the entire sequence (Fig. 4). In contrast, per capita rate of origination increased significantly within the PETM interval (Fig. 4). Although the rates of origination continued to be high into the Early Eocene (*10*), the increase in rate began within the PETM.

Overall diversity and composition analysis suggest that the onset of the PETM is concomitant with an increase in diversity produced by the addition of many taxa (with some representing new families) to the stock of preexisting Paleocene taxa. This change in diversity was permanent and not transient, as documented for temperate North America (*6*). Interestingly, phylogenetic molecular studies of extant ephypitic ferns (which are mostly restricted to tropical rainforest canopies) and orchids indicate a major radiation at the onset of the Eocene (*13*, *14*).

Temperature and precipitation are important factors affecting plant communities. Estimates of PETM mean annual temperature (MAT) from tropical latitudes are scarce. By using both published literature and TEX_{86} values from a nearby marine core [P2 core (Fig. 1 and fig. S14) (*9*)], we estimate that tropical temperatures during the PETM increased by ~3°C in the northern Neotropics and that mean temperatures were between 31° and 34°C (±2°C) during the peak of global

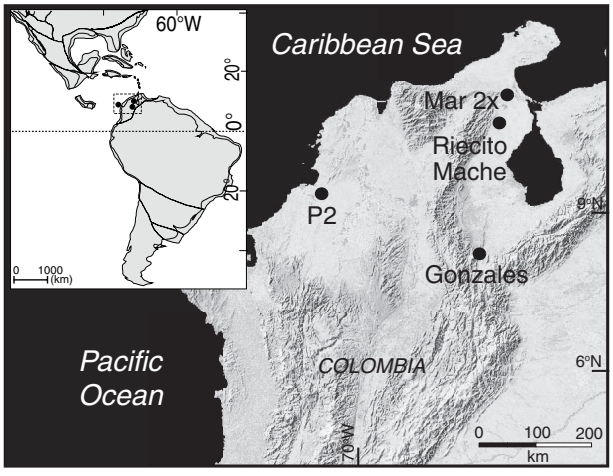

Fig. 1. Geographical location of the studied sections. Inset shows the Late Paleocene paleogeographic location of the studied sections [paleogeographic map after (*27*)]. Note that the northern Andes had not been uplifted yet, and most of Central America was still underwater.

[1]Smithsonian Tropical Research Institute, Box 0843-03092, Balboa, Ancon Republic of Panama. [2]Department of Biological Sciences, East Tennessee State University, Johnson City, TN 37614–14850, USA. [3]Colombian Petroleum Institute, Km 7 Via Piedecuesta, Bucaramanga, Colombia. [4]Institute of Geosciences, Goethe University Frankfurt, Altenhöferallee 1, D-60438 Frankfurt am Main, Germany. [5]Department of Geology and Geophysics, Yale University, New Haven, CT 06520, USA. [6]Department of Geological Sciences, Indiana University, Bloomington, IN 47405, USA. [7]Department of Geology, University of Saskatchewan, 114 Science Place, Saskatoon SK, Canada. [8]Department of Geological Sciences and Engineering, Missouri University of Science and Technology, Rolla, MO 65409–0140, USA. [9]Paleoflora Limitada, Calle 9 No. 9-09, Zapatoca, Colombia. [10]Department of Geology, University of Minnesota, Minneapolis, MN 55455–0231, USA. [11]Corporación Geológica Ares, Calle 57 N.24-11 ofic. 202, Bogotá, Colombia. [12]Petróleos de Venezuela S.A. (PDVSA) Exploración, Nucleoteca La Concepción, Maracaibo, Venezuela. [13]PDVSA Exploración, Edificio Guaraguao Puerto de la Cruz, Venezuela. [14]Goucher College, 1021 Dulaney Valley Road, Baltimore, MD 21204, USA. [15]Royal Netherlands Institute for Sea Research (NIOZ), Department of Marine Organic Biogeochemistry, Post Office Box 59, 1790 AB, Den Burg, Texel, Netherlands. [16]Department of Geological Sciences, University of Caldas, Manizales, Colombia. [17]Paleosedes, Tv 27 No. 57-49 Bogota, Colombia. [18]Université Paul Sabatier, CU Ponsan Bellevue, Rue Maurice Becanne, 31078 Tolulouse CX 04, France. [19]Agencia Nacional de Hidrocarburos, Bogotá, Colombia. [20]Department of Geosciences, Boise State University, Boise, ID 83725–1535, USA. [21]Valencia Geoservices, Tucson, AZ 85712, USA. [22]School of Earth and Environmental Sciences, Washington State University, Pullman, WA 99164–2812, USA.

*To whom correspondence should be addressed. E-mail: jaramilloc@si.edu

Downloaded from www.sciencemag.org on November 11, 2010

warmth [see (*9*) for a detailed explanation]. To reconstruct regional hydrology, we classified plant families according to the rainfall preferences using Gentry's neotropical plant data set (*15*) into dry- versus wet-preferred habitats (*9*) (table S9). Both Paleocene and Eocene are dominated by families indicating wet habitats, with no significant difference across the Paleocene-Eocene (Paleocene = 64%, Eocene = 61%, $P < 0.49$, df = 32.5), and low abundance of dry elements (e.g., Poaceae) that represents <2% of the assemblage (Paleocene = 0.7%, Eocene = 2%), all suggesting that no increase in aridity occurred across the PETM. This conclusion is further supported by stable carbon and hydrogen isotope (D/H) compositions of higher-plant–derived *n*-alkanes at site Mar 2X. A negative carbon isotope excursion (CIE) is evident in all *n*-alkanes measured and ranges between 2 and 3 per mil (‰), roughly matching bulk organic $^{13}C/^{12}C$ ($\delta^{13}C$) trends (Fig. 1 and fig S11) (*9*). At the onset of the PETM, *n*-alkane D/H compositions become more D-depleted (~35‰) and do not return to pre-PETM values within the measured section (*9*) (fig. S12). Changes in the D/H composition of plant lipids are related to changes in biosynthetic fractionation (related to a plant's specific water-use efficiency), meteoric water D/H composition, amount of precipitation, and moisture recycling in forest ecosystems. Given the setting of these sites and the observed increase in tropical rainforest diversity, the negative shift in the hydrogen isotope value (δD) of *n*-alkanes likely reflects the predominance of D-depleted precipitation related to increased precipitation during rainout events (e.g., amount effects).

If we assume that our compound-specific $\delta^{13}C$ record captures the maximum extent of the CIE within the body of the PETM, a much smaller CIE is observed at Mar 2X relative to the ~4.6‰ excursion recorded globally (*16*). In addition to the atmospheric carbon isotopic composition, environmental parameters in tropical rainforests that influence *n*-alkane $\delta^{13}C$ values include water stress (*17*), ecosystem changes (related to changes in net isotope fractionation) (*16*), and canopy effects (*18*). It is possible that the smaller CIE recorded in this study resulted from ecosystem turnover and the prevalence of flora with higher water-use efficiencies. Alternatively, temporal changes in the carbon isotopic composition could be attributable to changes in mean annual precipitation (MAP), given that relations between total carbon isotope fractionation during carbon fixation and MAP have been observed today (*16*). A smaller CIE could imply that MAP decreased in the tropics, an interpretation unsupported by floral assemblages or by the δD record, which displays a negative shift (~–35‰) during the onset of the PETM. However, we cannot exclude the possibility that changes in moisture recycling also influenced the D/H record. Indeed, it is difficult to explain the totality of the carbon isotope record in light of our understanding of the PETM elsewhere. For example, carbon isotope compositions return to pre-event values by the end of the PETM, albeit slightly more negative as observed globally. However, the recovery phase at our localities is not accompanied by changes in vegetation, inconsistent with our assumption that ecosystem

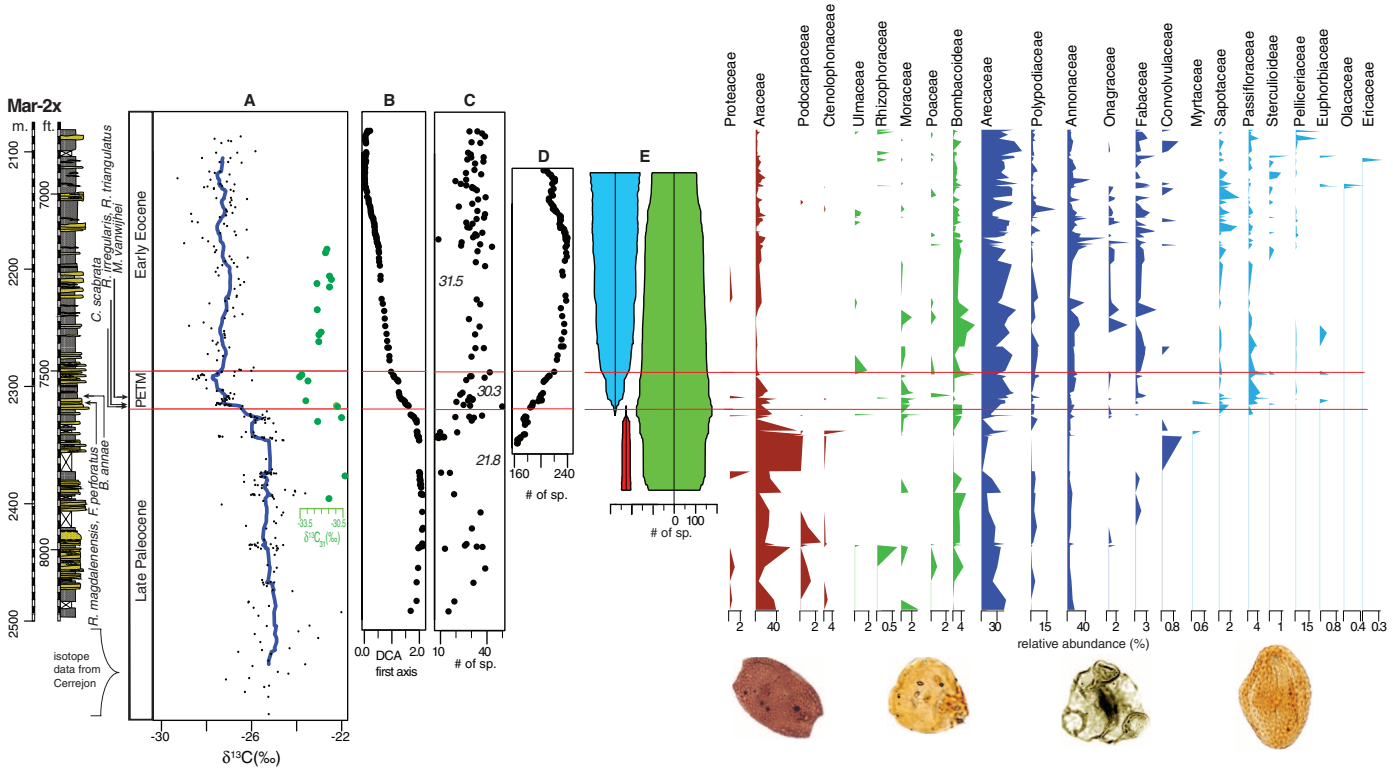

Fig. 2. Changes in palynofloral diversity and composition across the PETM in the Mar 2X core. The lithological description of the core and key biostratigraphic events are shown to the left. (**A**) $\delta^{13}C$ values of bulk organic matter across the PETM. Isotope data from the lowest part of the section was previously published (*28*). Blue line corresponds to a 20-point running mean of bulk data. (Inset) $\delta^{13}C$ values of the C_{31} *n*-alkanes (*n*-C_{31}) showing a pattern similar to those of *n*-C_{25}, *n*-C_{27}, and *n*-C_{29} (fig. S11). (**B**). First axis of a DCA, which explains 34.9% of the total variance in species composition along the stratigraphic profile. Paleocene palynofloras are distinct from Eocene palynofloras, with a gradual transition during the PETM. (**C**) Within-sample (rarefied) diversity at a count of 100 grains. The Paleocene (mean = 21.8) is less diverse than the PETM (30.3), and the PETM and Eocene (31.5) are very similar. (**D**) Pollen and spore standing diversity using the range-through method and eliminating edge effect and single-occurrence species. Note increase in diversity at the onset of the PETM. (**E**) Eocene-restricted taxa (blue) are more diverse than Paleocene-restricted taxa (red), whereas diversity of taxa that cross the Paleocene into the Eocene (green) does not change. Increase in diversity at the onset of the PETM is due to a large addition of taxa to the preexisting Paleocene flora. Family relative abundances are shown to the right of the figure. Families that are more abundant in the Paleocene are shown in purple; families that do not change in abundance across the Paleocene/Eocene transition, green; families that are more abundant in the Eocene, dark blue; and families that originate at the latest Paleocene, PETM, or Early Eocene, light blue. Images in the lower left correspond to distinct taxa of the sequence: *Retidiporites magdalenensis* (Proteaceae), *Momipites africanus* (Moraceae), *Corsinipollenites undulatus* (Onagraceae), and *Rhoipites guianensis* (Sterculioideae).

Downloaded from www.sciencemag.org on November 11, 2010

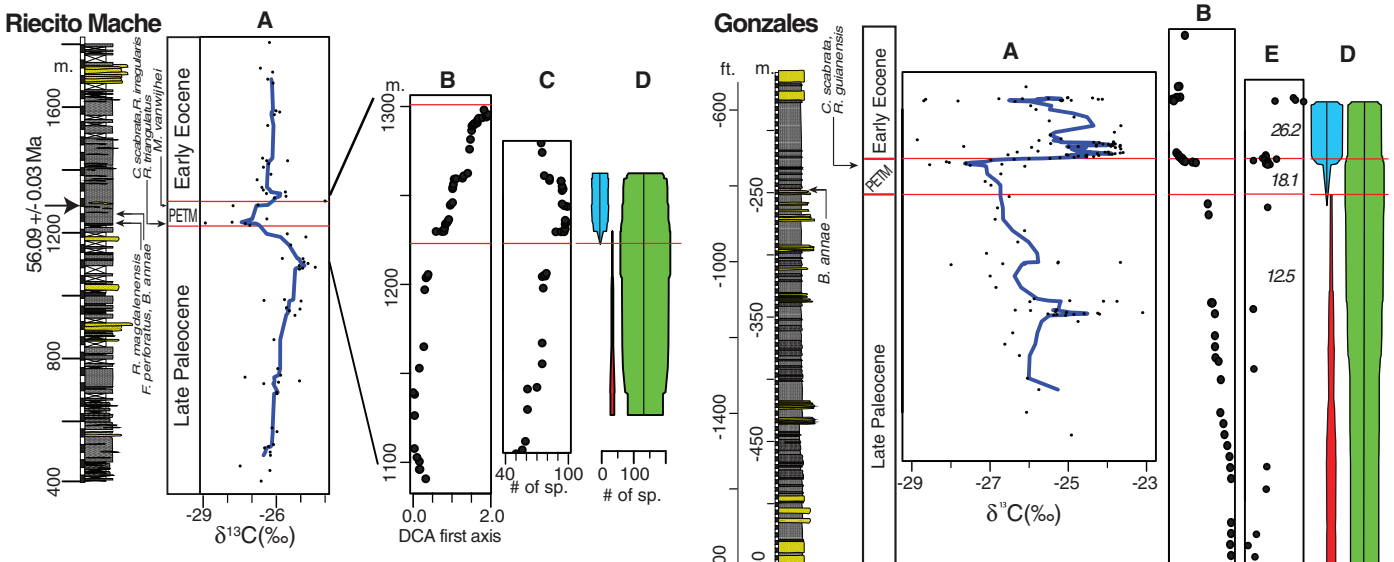

Fig. 3. Changes in palynofloral diversity and composition across the PETM at Riecito Mache and Gonzales. Lithological description of the section, key biostratigraphic events, and a radiometric age of a volcanic tuff dated by the U-Pb zircon radiometric method are shown to the left. (**A**) $\delta^{13}C$ values of bulk organic matter across the PETM. Blue line corresponds to a 7-point running mean of bulk data. (**B**) First axis of a DCA, which explains 22.2% (Riecito Mache) and 34.6% (Gonzales) of the total variance in species composition along the stratigraphic profile. (**C**) Pollen and spore standing diversity using the range-through method and eliminating edge effect and single-occurrence species. Note the increase in diversity at the onset of the PETM. (**D**) PETM-restricted taxa (blue) are more diverse than Paleocene-restricted taxa (red), whereas diversity of taxa that cross from the Paleocene into the PETM (green) does not change. Increase in diversity at the onset of the PETM is due to a large addition of taxa to the preexisting Paleocene flora. (**E**) Within-sample (rarefied) diversity at a count of 100 grains. The PETM (mean = 18.1) is more diverse than the Paleocene (12.5) and less diverse than the Eocene (26.2).

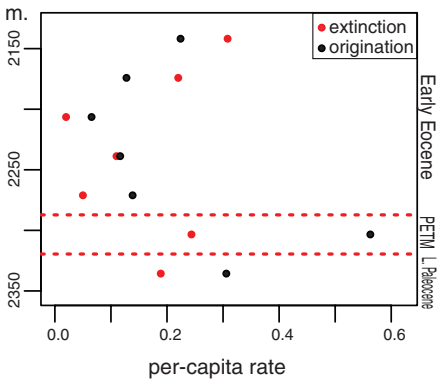

Fig. 4. Per capita rates of origination and extinction per 200,000 years (the time span of the PETM) in Mar 2X. The per capita extinction rate (red) shows a slight increase in extinction during the PETM that is comparable to other intervals in the Eocene. The per capita origination rate (black) shows a spike in origination during the PETM.

turnover was the cause for the relatively ^{13}C-enriched CIE. More likely, a smaller CIE from this study could simply be the result of incomplete recovery of the PETM maxima.

Today, most tropical rainforests are found at MAT below 27.5°C. Many have argued that tropical communities live near their climatic optimum (*19*) and that higher temperatures could be deleterious to the health of tropical ecosystems (*8*, *19*–*23*). Indeed, tropical warming during the PETM is surmised to have produced intolerable conditions for tropical ecosystems (*8*, *21*), although 31° to 34°C is still within the maximum tolerance of leaf temperature of some tropical plants (*24*). We recognize that further studies toward the center of the South American continent need to be performed in order to understand the effects of warming in more continental tropical settings. However, at our sites in northern South America, tropical forests were maintained during the warmth of the PETM (~31° to 34°C). Greenhouse experiments have shown that high levels of CO_2 together with high levels of soil moisture improve the performance of plants under high temperatures (*25*), and it is possible that higher Paleogene CO_2 levels (*26*) contributed to their success. Higher precipitation amounts could have been as important as high CO_2. Precipitation reconstruction from a nearby Late Paleocene site, Cerrejon, indicate high precipitation regimes: about 3.2 m of rain per year (*11*). Our data, including a –35% shift in leaf-wax δD values, no increase in plant abundance of dry indicators (e.g., Poaceae), absence of a large plant extinction, high plant diversity, and high abundance of families typical of wet tropical rainforests (such as Annonaceae, Passifloraceae, Sapotaceae, Araceae, and Arecaceae), suggest that precipitation in the northern Neotropics during the PETM was either similar to Paleocene levels (3.2 m/year) or higher. Indeed, it is possible that rainforest families in general, which have been present in the Neotropics since the Paleocene (*11*), have the genetic variability to cope with high temperatures, CO_2, and rainfall (*25*).

References and Notes

1. J. C. Zachos *et al.*, *Science* **302**, 1551 (2003); 10.1126/science.1090110.
2. T. Westerhold, U. Röhl, H. K. McCarren, J. C. Zachos, *Earth Planet. Sci. Lett.* **287**, 412 (2009).
3. J. P. Kennett, L. D. Stott, *Nature* **353**, 225 (1991).
4. M. Pagani, K. Caldeira, D. Archer, J. C. Zachos, *Science* **314**, 1556 (2006).
5. R. E. Zeebe, J. C. Zachos, G. R. Dickens, *Nat. Geosci.* **2**, 576 (2009).
6. S. L. Wing *et al.*, *Science* **310**, 993 (2005).
7. W. C. Clyde, P. D. Gingerich, *Geology* **26**, 1011 (1998).
8. M. Huber, *Science* **321**, 353 (2008).
9. Materials and methods are available as supporting material on *Science* Online.
10. C. Jaramillo, M. J. Rueda, G. Mora, *Science* **311**, 1893 (2006).
11. S. L. Wing *et al.*, *Proc. Natl. Acad. Sci. U.S.A.* **106**, 18627 (2009).
12. J. Muller, *Bot. Rev.* **47**, 1 (1981).
13. S. R. Ramírez, B. Gravendeel, R. B. Singer, C. R. Marshall, N. E. Pierce, *Nature* **448**, 1042 (2007).
14. E. Schuettpelz, K. M. Pryer, *Proc. Natl. Acad. Sci. U.S.A.* **106**, 11200 (2009).
15. S. W. Punyasena, G. Eshel, J. C. McElwain, *J. Biogeogr.* **35**, 117 (2008).
16. A. F. Diefendorf, K. E. Mueller, S. L. Wing, P. L. Koch, K. H. Freeman, *Proc. Natl. Acad. Sci. U.S.A.* **107**, 5738 (2010).
17. G. D. Farquhar, J. R. Ehleringer, K. T. Hubick, *Annu. Rev. Plant Physiol. Plant Mol. Biol.* **40**, 503 (1989).
18. N. J. van der Merwe, E. Medina, *J. Archaeol. Sci.* **18**, 249 (1991).
19. N. Stoskopf, *Understanding Crop Production* (Prentice-Hall, Upper Saddle River, NJ, 1981).
20. S. L. Bassow, K. D. McConnaughay, F. A. Bazzaz, *Ecol. Appl.* **4**, 593 (1994).
21. M. Huber, *Nature* **457**, 669 (2009).
22. S. L. Lewis, Y. Malhi, O. L. Phillips, *Philos. Trans. R. Soc. B* **359**, 437 (2004).
23. J. J. Tewksbury, R. B. Huey, C. A. Deutsch, *Science* **320**, 1296 (2008).

Downloaded from www.sciencemag.org on November 11, 2010

24. G. H. Krause *et al.*, *Funct. Plant Biol.* **37**, 890 (2010).
25. J. Lloyd, G. D. Farquhar, *Philos. Trans. R. Soc. London Ser. B* **363**, 1811 (2008).
26. D. L. Royer, *Proc. Natl. Acad. Sci. U.S.A.* **107**, 517 (2010).
27. C. R. Scotese, *Paleogeographic Atlas. Earth System History Geographic Information System, Version 02b* (PALEOMAP Project, Arlington, TX, 2001).
28. C. Jaramillo *et al.*, *Palynology* **31**, 153 (2007).
29. Supported by Banco de la República, National Geographic, Smithsonian Women's Club, Instituto de Colombiano de Petroleo (ICP)–Ecopetrol SA, and Smithsonian. M.P. was supported by NSF EAR-0628358 and ATM-0902882. S.S. was supported by a VISI grant from Netherlands Organisation for Scientific Research. Thanks to PDVSA for access to Mar 2X and the Instituto de Patrimonío Cultural of Venezuela for allowing us to sample in Riecito Mache. Thanks to Agencia Nacional de Hidrocarburos, A. Pardo, J. Sanchez, C. Guerrero, M. Carvalho, and the Colombian Armed Forces for logistic support. Thanks to the biostratigraphic team at ICP. Patrice Brenac did preliminary palynological analysis of Gonzales. N. Atkins provided editing support. A. Mets (NIOZ) is thanked for analytical assistance. K. Winter, H. Muller-Landau, J. Wright, and S. Punyasena and three anonymous reviewers provided comments on the manuscript. Special thanks to M. I. Barreto for continuous support and sources of ideas.

Supporting Online Material

www.sciencemag.org/cgi/content/full/330/6006/957/DC1
Material and Methods
Figs. S1 to S14
Tables S1 to S10

16 June 2010; accepted 1 October 2010
10.1126/science.1193833

Conditional Cooperation and Costly Monitoring Explain Success in Forest Commons Management

Devesh Rustagi,[1]* Stefanie Engel,[1] Michael Kosfeld[2]*

Recent evidence suggests that prosocial behaviors like conditional cooperation and costly norm enforcement can stabilize large-scale cooperation for commons management. However, field evidence on the extent to which variation in these behaviors among actual commons users accounts for natural commons outcomes is altogether missing. Here, we combine experimental measures of conditional cooperation and survey measures on costly monitoring among 49 forest user groups in Ethiopia with measures of natural forest commons outcomes to show that (i) groups vary in conditional cooperator share, (ii) groups with larger conditional cooperator share are more successful in forest commons management, and (iii) costly monitoring is a key instrument with which conditional cooperators enforce cooperation. Our findings are consistent with models of gene-culture coevolution on human cooperation and provide external validity to laboratory experiments on social dilemmas.

Maintaining large-scale cooperation for the provision of public goods and the management of common property is fraught with the infamous cooperation dilemma in which free riders enjoy group benefits without bearing the cost of their provision. The conventional analysis, based on the assumption of self-regarding individuals, predicts zero cooperation under these conditions (*1*, *2*). Yet extensive field evidence underlines that many groups are able to manage their commons, albeit with varying degrees of success (*3*, *4*). This marked deviation from the conventional hypothesis as well as the variation in management success necessitates a coherent theory of human collective behavior that explains well the observed variation in cooperation outcomes. In addition to structural factors like resource characteristics, group size, and socioeconomic heterogeneity (*3*–*5*), recent findings suggest that social behaviors, such as the norm of conditional cooperation (individual cooperation being conditional on the cooperation of others) together with the costly enforcement of this norm, may play an important role in stabilizing large-scale cooperation (*6*–*8*).

Much of the evidence for conditional cooperation comes from behavioral laboratory experiments with student participants showing that individuals display a considerable heterogeneity in their behavioral disposition to cooperate. Although a large proportion of participants reveal conditionally cooperative behavior, a nontrivial share meets the conventional assumption by behaving as free riders (*9*–*14*). Because conditional cooperators do not cooperate if many group members ride for free, the composition of a group becomes decisive for the prospects of maintaining cooperation. Whereas voluntary cooperation may be achieved in groups with larger share of conditional cooperators (*15*, *16*), in heterogeneous groups costly norm enforcement is needed to attain cooperation (*6*, *17*–*21*). Evidence shows that many individuals, in particular those with a high propensity to cooperate, are willing to enforce cooperation even at a personal cost (*17*, *22*–*26*) and that this has a positive effect on group members' contribution (*17*, *19*, *27*, *28*).

The large body of evidence for conditional cooperation and costly norm enforcement is compelling. However, unless the relations between these behaviors and the way they affect outcomes of commons management are investigated in a concrete field setting, where one can account for context-specific information regarding relevant structural factors, their ultimate impact for commons management is hard to evaluate (*29*–*31*). Although previous studies have conducted behavioral experiments with diverse populations including commons users (*26*, *32*–*36*) and have tentatively documented the importance of local enforcement in the field (*21*, *37*), reliable evidence on the extent to which variation in conditional cooperation and costly norm enforcement among commons users affects natural commons outcomes is altogether missing.

We combined data on natural outcomes of commons management with experimental measures of conditional cooperation among 679 individuals from 49 commons user groups to investigate whether groups with larger share of conditional cooperators achieve better outcomes (*38*). We also measured costly enforcement through survey data on monitoring, an important input for the detection and punishment of free riding in our context, to analyze the extent to which monitoring plays a role in sustaining commons outcomes by conditional cooperators. In doing so, we aimed to underline the conditions under which local enforcement of commons management is predicted to work.

Our research strategy was to carry out these investigations in a field setting where individuals in a group face a natural commons dilemma and use costly enforcement mechanisms to overcome this dilemma and where there exists a reliable measure of cooperation outcomes in commons management. We conducted our study in the context of a major forest commons management program launched to save local forests and livelihoods in the Bale region of Ethiopia. Under the program, groups of the Bale Oromo people were given secure tenure rights to use and manage their forests as common property resources (*39*). In return, these groups are required to maintain their forest cover, for which they are allowed to implement local rules regarding forest use, for instance, the amount of fuelwood a member is allowed to harvest for self-consumption and sale. While managing their forest as a common property, group members confront cooperation dilemmas, because each member is better off when every member in the group cooperates by adhering to internal rules; however, violating the rules leads to higher payoffs, for instance, from the sale of extra fuelwood, implying that individual members might have little incentive to cooperate. To overcome this first-order dilemma, members have the option to engage in costly monitoring, which involves conducting patrols through the forest. Such patrols not only deter

[1]Institute for Environmental Decisions, Eidgenössische Technische Hochschule (ETH) Zurich, Universitätsstrasse 22, CH-8092 Zurich, Switzerland. [2]Faculty of Economics and Business Administration, Johann Wolfgang Goethe University Frankfurt, Grüneburgplatz 1, D-60323 Frankfurt am Main, Germany.

*To whom correspondence should be addressed. E-mail: devesh.rustagi@env.ethz.ch (D.R.); kosfeld@econ.uni-frankfurt.de (M.K.)

Downloaded from www.sciencemag.org on November 11, 2010

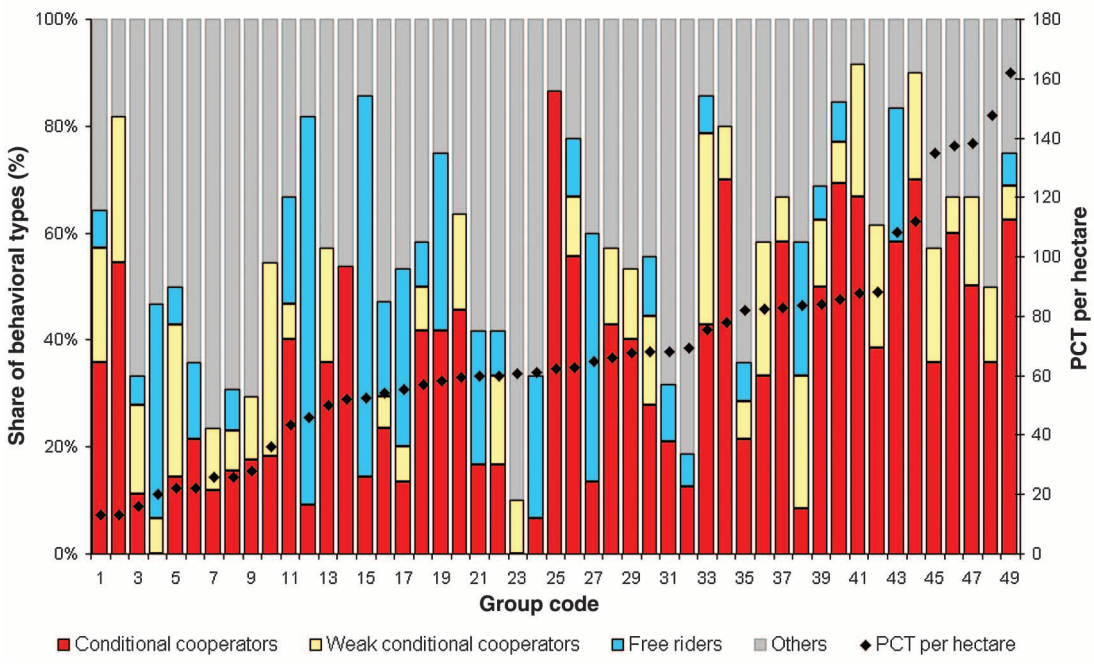

Fig. 1. Forest management outcome as measured in potential crop trees (PCT) per hectare and the relative shares of the main behavioral types in a group. The groups are sorted by PCT. Each bar represents a group engaged in the management of forest commons identified by its numerical code. There is large variation in the forest management outcome (min = 13, max = 161.9, SD = 35.2) and in the share of conditional cooperators (min = 0%, max = 86.7%, SD = 21.5%) and free riders (min = 0%, max = 72.7%, SD = 17.2%) across groups.

free riding in itself but also generate information needed for the punishment of free riders, which is determined by an executive committee on the group level chaired by the group leader. Because forest patrols cost members time and effort but generate group benefits, they are associated with a second-order cooperation dilemma.

Data collected by the program office on the outcome of commons management for each group using mensuration data on potential crop trees (PCT) [supporting online material (SOM) text] exhibit tremendous variation (Fig. 1). Because inventory studies conducted before the launch of the program indicated no major variation in PCT (*40*), the large variation in current outcomes suggests that groups achieve different degrees of success in overcoming cooperation dilemmas in managing their commons. We hypothesize that groups with larger share of conditional cooperators are more likely to be successful at managing their commons and that they achieve this by using costly monitoring as a mechanism.

To test our hypothesis, we measuref conditional cooperation among commons users by using a public goods game as a stylized model of the cooperation dilemma associated with commons management. We followed the experimental protocol of (*10*), which controls for individuals' beliefs about the cooperation of others. Controlling for beliefs is important because by the very definition conditional cooperators will not cooperate if they believe that others will not cooperate. It is thus not possible, for example, to infer the absence of conditional cooperators from a group in which little cooperation is observed. Our experimental protocol enabled us to circumvent this problem, providing an explicit measure of conditional cooperation.

Table 1. Criteria for identifying behavioral types and their share in our sample. We follow (*10*) and use Spearman's ρ between a participant's and a partner player's contribution to elicit a participant's behavioral type. We classify a player as conditional cooperator if the Spearman's ρ is positive and significant at $P \leq 0.001$, weak conditional cooperator if the Spearman's ρ is positive and significant at $0.001 < P < 0.05$, free rider if a player consistently contributes zero independent of the partner player's contribution or contributes at most the smallest positive amount in only one of the seven decisions, altruist if a player consistently contributes the entire endowment regardless of the partner's contribution, and hump-shaped if the contribution increases up to a point with the partner's contribution and then decreases (based on visual examination).

Behavioral type	*N*	%	Mean Spearman ρ
Conditional cooperator	231	34.02	0.99
Weak conditional cooperator	79	11.63	0.86
Free rider	78	11.49	–0.08
Hump-shaped	20	2.95	–0.04
Altruist	15	2.21	0.00
Other	256	37.70	0.15
All players	679	100.00	0.48

In the public goods game, two players from the same user group were randomly paired in a one-shot and anonymous interaction. Each of the two players received six bills of one Ethiopian Birr (the equivalent of a day's wage) and had to decide on his contribution to a public good, which was then multiplied by 1.5 and distributed equally among the two players irrespective of players' individual contributions. The game constitutes a cooperation dilemma because players together are best off if both contribute their entire endowment to the public good; however, because the individual cost of contributing one Birr to the public good is one but the return is only 0.75, each player's earning is maximized by contributing zero to the public good independent of the other player's contribution.

Players took two decisions in the experiment: an unconditional and a conditional decision. In the first decision, both players decided simultaneously on their contribution to the public good and stated the expected contribution of the partner player. The second decision was sequential in which players were visualized one by one each of the seven possible contribution decisions of their partner player and asked to state their own contribution to the public good for each of the other player's contributions. At the end of the experiment, a die was rolled to determine the player for whom the first decision was taken; this was matched with the second decision of the other player to deter-

Downloaded from www.sciencemag.org on November 11, 2010

Table 2. Forest management outcome, conditional cooperation, and structural variables. The dependent variable is forest management outcome, measured in PCT per hectare. The independent variables are conditional cooperator shares, market distance, and time. Additional controls include elevation, group size, share of female members, and heterogeneity in livestock ownership. Ordinary least squares (OLS) estimates with robust standard errors in parentheses. ***$P < 0.01$.

	Dependent variable: Forest management outcome	
Variables	1	2
Conditional cooperator share		52.085*** (13.117)
Market distance	−22.779*** (4.355)	−20.568*** (4.057)
Time	36.479*** (6.409)	32.185*** (6.004)
Constant	105.325*** (21.719)	81.438*** (19.186)
Additional controls	Yes	Yes
Adjusted r^2	0.58	0.67
Observations	49	49

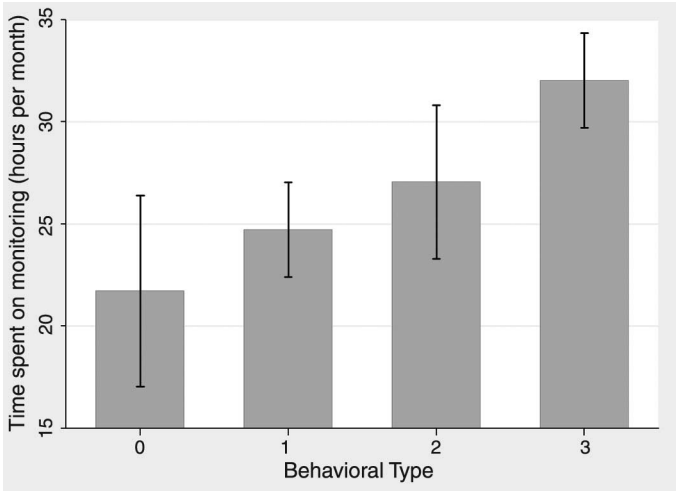

Fig. 2. Average time spent on monitoring by behavioral types. Behavioral types are as follows: 0, free rider; 1, other types; 2, weak conditional cooperator; 3, conditional cooperator. Mean ± SEM per type.

mine payoffs (*38*). Because players in the second decision could make their contribution contingent on the contribution of the other player, the experiment allowed for a clean identification of conditional cooperation as well as other types of behavior. A player is a conditional cooperator if his contribution increases with the contribution of the other player; a player who contributes zero independent of what the other player contributes is a free rider.

The exact criteria used to identify behavioral types together with their relative shares in our total sample are listed in Table 1. Thirty-four percent of the participants behaved as conditional cooperators and contributed more to the public good the more the other player contributed, such that the average correlation between self and partner player is high and highly significant [mean Spearman's rank correlation (ρ) = 0.99, $P \leq 0.001$]. Another 12% behaved as so-called weak conditional cooperators (mean Spearman's $\rho = 0.86$, $P < 0.05$). Free riders formed the second important type of behavior (11%); they either contributed zero to the public good regardless of the other player's contribution or at most one Birr in one of the seven possible decisions and zero in the remaining six decisions. The observed shares in our data fall within the range documented by previous laboratory experiments with student participants (*10*–*13*).

The distribution of the main behavioral types within and across the different forest user groups is illustrated in Fig. 1. Groups vary in their share of behavioral types, particularly in the share of conditional cooperators and free riders. In groups with more conditional cooperators, free rider shares are smaller (Spearman's $\rho = -0.45$, $P = 0.001$), suggesting that behavioral norms differ across groups. A plausible explanation may come from cultural transmission dynamics, which are able to generate within-group uniformity and between-group differences in behavioral norms (*41*, *42*) (SOM text).

Forest user groups with larger shares of conditional cooperators exhibit better outcomes on average, whereas groups with larger free rider shares exhibit on average worse outcomes (Fig. 1). We estimated the impact of conditional cooperation on forest management outcome by means of a linear regression of the forest management outcome (PCT) on the share of conditional cooperators in the respective group, controlling for relevant structural factors such as elevation, group size, female shares, heterogeneity in livestock ownership, market distance, and time (Table 2). Our assumption regarding the direction of causality has its basis in established theoretical works (*7*) and laboratory experimental evidence (*11*, *15*, *16*). Results from further statistical analyses of our data, including instrumental variables regression, corroborate this assumption (SOM text).

Model 1 (Table 2) considers the effect of structural variables in the linear regression alone, showing that the farther a group is located from the market, the lower is its forest management outcome ($P = 0.000$). Responses in the household as well as community surveys revealed that better market access allows members to earn cash income by selling forest products. As a result, groups that are closer to the market take stronger interest in forest management activities. Further, the time dummy has a strongly positive effect on the forest management outcome ($P = 0.000$), indicating that groups established earlier have better outcomes. We postulate that this effect is due to the time it takes young trees to grow to affect forest outcomes (SOM text). None of the other control variables in the regression have a robust significant effect on forest management outcome (SOM text).

Model 2 shows the effect of conditional cooperation on forest management outcome controlling for the structural variables. A larger share of conditional cooperators in a forest user group has a significantly positive effect on the forest management outcome ($P = 0.000$). Ceteris paribus, a 10% increase in the share of conditional cooperators increases forest management outcome on average by five PCT per hectare. In terms of elasticity at the mean, a 1% increase in the share of conditional cooperators increases the number of trees by 0.27%. In comparison, an increase in market distance by 1 hour of walking time reduces the forest management outcome on average by 21 PCT per hectare. In terms of elasticity at the mean, a 1% increase in the market distance decreases PCT by 0.73%. Further, groups that were established about 3 years earlier have on average 32 more PCT per hectare, ceteris paribus. Our results are robust even when we considered weak and strong conditional cooperators jointly (table S17), used weighted least squares regression to account for differences in sample size (table S13), used different proxies to measure socioeconomic structural factors (table S14 and S15), or controlled for demographic variables, such as age, education, and family size (table S16). We also interacted conditional cooperators with market distance and time but found no interaction effects on the outcome. Overall, conditional cooperators account for 9% of the variation in the forest management outcome. We got analogous results when we categorized groups by their share of free riders. As expected, larger free rider shares have a significantly negative effect on the forest management outcome ($P = 0.000$). Ceteris paribus, a 10% increase in the share of free riders leads to an average drop in forest management outcome by almost seven PCT per hectare (table S18).

In part, the positive correlation between the share of conditional cooperators and forest management outcome is likely to be due to conditional cooperators contributing more to the conservation of the forest. For example, in the unconditional decision in our experiment, conditional cooperators contributed 40% of their endowment to the

Downloaded from www.sciencemag.org on November 11, 2010

Table 3. Costly monitoring, conditional cooperation, and structural variables. The dependent variable is the average time a group member spends monitoring the forest, measured in hours per month. The independent variables are the share of conditional cooperators in a group, market distance, and time. Additional controls include monitoring difficulty, group size, share of female members, and heterogeneity in livestock ownership. OLS estimates with robust standard errors in parentheses. ***$P < 0.01$, **$P < 0.05$.

	Dependent variable: Time spent on monitoring	
Variables	1	2
Conditional cooperator share		23.782*** (8.700)
Market distance	−5.972*** (1.518)	−4.951*** (1.543)
Time	11.428*** (3.814)	9.079** (3.477)
Constant	49.467*** (16.464)	42.092** (15.553)
Additional controls	Yes	Yes
Adjusted r^2	0.31	0.42
Observations	45	45

public good compared with 15% by free riders [Kruskal-Wallis test, χ^2 (3) = 67.40, P = 0.000]. However, theory and empirical evidence suggest that conditional cooperators will not be able to sustain cooperation alone in the presence of less cooperative types unless enforcement mechanisms, such as costly monitoring and punishment, are available and used. Our experimental data confirm this. Conditional cooperators contributed significantly less to the public good if they believed that the other player contributed less (Spearman's ρ = 0.36, P = 0.000) or if there were more free riders in their group (Spearman's ρ = −0.46, P = 0.001).

Thus, forest management can only be successful if groups with larger shares of conditional cooperators also invest more in the enforcement of cooperation, a prediction that is confirmed by our data. In the field setting, forest patrols conducted by group members were the main enforcement activity allowing for the detection and punishment of free riders. Models of cultural evolution (*18*) and experimental evidence (*17*, *24*, *25*) suggest that conditional cooperators are more likely to monitor in relation to other behavioral types. We tested this by using survey data on monitoring behavior collected independently at both an individual and a community level. At the individual level, we found that, among the behavioral types, conditional cooperators indeed monitor the most, spending on average 32 hours per month on monitoring (Fig. 2); this is 1.5 times more than what free riders invested in monitoring [Kruskal-Wallis test, χ^2 (3) = 25.04, P = 0.000]. The result is corroborated by a regression analysis on the group level (Table 3) showing that groups with larger share of conditional cooperators invest on average more time monitoring their forest (P = 0.010). Ceteris paribus, a 10% increase in the share of conditional cooperators increases the time spent on monitoring by 2.5 hours on average. In terms of elasticity at the mean, a 1% increase in the share of conditional cooperators increases time spent monitoring by 0.28%. A similar result is obtained when we measure monitoring behavior by aggregating individual responses in the household questionnaire at the group level (table S20). Analogously, a larger share of free riders in a group has a significantly negative effect on monitoring (tables S19 and S20). In sum, better forest management outcomes are not only a result of conditional cooperators being more likely to abide by the local rules of the group but also being more willing to enforce these rules at a personal cost.

Our findings establish that, in addition to structural factors, behavioral motives such as the norm of conditional cooperation are an important element behind forest users' achievement in managing their commons. The results identify key complementarities between experimental measures of conditional cooperation, field outcomes on commons management, and survey measures on costly monitoring. Together, these results not only provide external validity to laboratory experiments (*30*) but also advance the frontiers of previous work on commons management. Our findings entail a number of implications for real-world common property regimes. In line with previous research, the data show that voluntary cooperation in commons management is not a pipe dream but an empirical fact. However, voluntary cooperation is fragile because the individual willingness to cooperate depends on the cooperation of others. This gives rise to important social interaction effects and implies that expectations individuals hold about the cooperation of others play a critical role. Conditional cooperators who see (or expect) others defect will exhibit very different behavior than conditional cooperators who see (or expect) others cooperate. Common property management can take this into account by designing institutions that provide incentives for purely self-regarding individuals to cooperate and at the same time foster the norm of conditional cooperation (*43*). Punishment institutions that sanction free riding and coordinate expectations on cooperation are one possible solution. In these institutions, local enforcement may play an important part (*20*, *21*), but this depends on the behavioral type composition of a group. As our data confirm, conditional cooperators play a key role in this regard: Not only do they contribute more to the first-order public good, but they are also more willing to contribute to the second-order public good, that is, to enforce first-order cooperation.

Overall, our study contributes to the accumulating evidence suggesting that an effective solution to commons problems is not based on panaceas (*44*) and incentives for self-regarding individuals alone but explicitly takes into account the complex interplay of behavioral norms and, more generally, the "ecology" of different interacting types (*11*, *16*). Policies aimed at conserving the commons may integrate the results of behavioral economic research and not only focus on the importance of structural factors but also consider the intrinsic and heterogeneous motivations of users of the commons to cooperate voluntarily.

Lastly, our results are also important for the evolution of group beneficial behaviors. The findings that groups vary in their share of conditional cooperators as well as other behavioral types and that there is a positive covariation between conditional cooperation and costly monitoring at both individual and group levels are in line with models of gene-cultural coevolution (*18*, *45*). These models predict that, in groups where costly enforcement is prevalent, cooperation is expected to be higher; this costly enforcement together with cultural transmission mechanisms is expected to lead to the emergence of stable between-group differences on which cultural group selection might then operate, ultimately paving the way for the spread of group beneficial behaviors in the population.

References and Notes

1. M. Olson, *The Logic of Collective Action: Public Goods and the Theory of Groups* (Harvard Univ. Press, Cambridge, MA, 1965).
2. G. Hardin, *Science* **162**, 1243 (1968).
3. E. Ostrom, *Governing the Commons: The Evolution of Institutions for Collective Action* (Cambridge Univ. Press, New York, 1990).
4. J. M. Baland, J. P. Platteau, *Halting Degradation of Natural Resources* (Food and Agricultural Organization of the United Nations and Oxford Univ. Press, Oxford, 1996).
5. A. Agrawal, *World Dev.* **29**, 1649 (2001).
6. E. Ostrom, J. Burger, C. B. Field, R. B. Norgaard, D. Policansky, *Science* **284**, 278 (1999).
7. A. Falk, E. Fehr, U. Fischbacher, in *The Drama of the Commons*, E. Ostrom *et al*., Eds. (National Academy Press, Washington, DC, 2002), pp. 157–192.
8. E. Fehr, U. Fischbacher, *Nature* **425**, 785 (2003).
9. C. Keser, F. Van Winden, *Scand. J. Econ.* **102**, 23 (2000).
10. U. Fischbacher, S. Gächter, E. Fehr, *Econ. Lett.* **71**, 397 (2001).
11. R. Kurzban, D. Houser, *Proc. Natl. Acad. Sci. U.S.A.* **102**, 1803 (2005).
12. M. G. Kocher, T. Cherry, S. Kroll, R. J. Netzer, M. Sutter, *Econ. Lett.* **101**, 175 (2008).
13. B. Herrmann, C. Thöni, *Exp. Econ.* **12**, 87 (2009).
14. U. Fischbacher, S. Gächter, *Am. Econ. Rev.* **100**, 541 (2010).
15. A. Gunnthorsdottir, D. Houser, K. McCabe, *J. Econ. Behav. Organ.* **62**, 304 (2007).
16. U. Ones, L. Putterman, *J. Econ. Behav. Organ.* **62**, 495 (2007).
17. E. Fehr, S. Gächter, *Nature* **415**, 137 (2002).
18. R. Boyd, H. Gintis, S. Bowles, P. J. Richerson, *Proc. Natl. Acad. Sci. U.S.A.* **100**, 3531 (2003).
19. O. Gürerk, B. Irlenbusch, B. Rockenbach, *Science* **312**, 108 (2006).
20. A. Chhatre, A. Agrawal, *Proc. Natl. Acad. Sci. U.S.A.* **105**, 13286 (2008).
21. C. C. Gibson, J. T. Williams, E. Ostrom, *World Dev.* **33**, 273 (2005).
22. T. Yamagishi, *J. Pers. Soc. Psychol.* **51**, 110 (1986).
23. E. Ostrom, J. Walker, R. Gardner, *Am. Polit. Sci. Rev.* **86**, 404 (1992).

Downloaded from www.sciencemag.org on November 11, 2010

24. M. E. Price, L. Cosmides, J. Tooby, *Evol. Hum. Behav.* **23**, 203 (2002).
25. A. Falk, E. Fehr, U. Fischbacher, *Econometrica* **73**, 2017 (2005).
26. J. Henrich *et al.*, *Science* **312**, 1767 (2006).
27. S. Gächter, E. Renner, M. Sefton, *Science* **322**, 1510 (2008).
28. D. G. Rand, A. Dreber, T. Ellingsen, D. Fudenberg, M. A. Nowak, *Science* **325**, 1272 (2009).
29. S. D. Levitt, J. A. List, *Science* **319**, 909 (2008).
30. A. Falk, J. J. Heckman, *Science* **326**, 535 (2009).
31. J. Henrich, S. J. Heine, A. Norenzayan, *Behav. Brain Sci.* **33**, 61 (2010).
32. J. C. Cardenas, *Environ. Dev. Sustain.* **2**, 305 (2000).
33. J. C. Cardenas, *J. Dev. Econ.* **70**, 263 (2003).
34. J. Henrich *et al.*, *Behav. Brain Sci.* **28**, 795 (2005).
35. M. Gurven, J. Winking, *Am. Anthropol.* **110**, 179 (2008).
36. J. Henrich *et al.*, *Science* **327**, 1480 (2010).
37. A. Agrawal, A. Chhatre, *World Dev.* **34**, 149 (2006).
38. Materials and methods are available as supporting material on *Science* Online.
39. G. Amente, thesis, Albert Ludwigs University, Freiburg, Germany (2005).
40. J. Trainer, "Forest inventory of indigenous forest of pilot area peasant associations: Denaba, Bura, Burachele-Adele" (Integrated Forest Management Project, Addis Ababa, Ethiopia, 1996).
41. J. Henrich, R. Boyd, *Evol. Hum. Behav.* **19**, 215 (1998).
42. J. Henrich, F. J. Gil-White, *Evol. Hum. Behav.* **22**, 165 (2001).
43. S. Bowles, *Science* **320**, 1605 (2008).
44. E. Ostrom, *Proc. Natl. Acad. Sci. U.S.A.* **104**, 15181 (2007).
45. J. Henrich, R. Boyd, *J. Theor. Biol.* **208**, 79 (2001).
46. We especially thank the communities that participated in our research and our research assistants. This study was financially supported by the North-South Centre at ETH Zurich, the German Federal Ministry of Education and Research (BMBF) (BioTEAM 01LM0201), and the German Federal Ministry of Economic Cooperation and Development (BMZ) via the Centre for Development Research, Bonn. We also acknowledge in-kind support from the German Organization for Technical Cooperation (GTZ) and the Oromia State Forest Enterprises Supervising Agency.

Supporting Online Material

www.sciencemag.org/cgi/content/full/330/6006/961/DC1
Materials and Methods
SOM Text
Fig. S1
Tables S1 to S20
References and Notes

11 June 2010; accepted 20 September 2010
10.1126/science.1193649

The Role of Discharge Variation in Scaling of Drainage Area and Food Chain Length in Rivers

John L. Sabo,[1]* Jacques C. Finlay,[2] Theodore Kennedy,[3] David M. Post[4]

Food chain length (FCL) is a fundamental component of food web structure. Studies in a variety of ecosystems suggest that FCL is determined by energy supply, environmental stability, and/or ecosystem size, but the nature of the relationship between environmental stability and FCL, and the mechanism linking ecosystem size to FCL, remain unclear. Here we show that FCL increases with drainage area and decreases with hydrologic variability and intermittency across 36 North American rivers. Our analysis further suggests that hydrologic variability is the mechanism underlying the correlation between ecosystem size and FCL in rivers. Ecosystem size lengthens river food chains by integrating and attenuating discharge variation through stream networks, thereby enhancing environmental stability in larger river systems.

Food chain length (FCL) is a key measure of the vertical structure of food webs (*1*, *2*) that determines energy flow through ecosystems (*3*), carbon exchange between freshwater ecosystems and the atmosphere (*4*), and nutrient cycling (*5*). FCL is also important to human health, influencing the bioaccumulation of contaminants in top predators consumed by humans (*6*). Ecological theory suggests that FCL should increase with energy supply (*7*, *8*), the available energy pool (*9*), and environmental stability (*8*). In contrast, empirical studies have revealed weak effects of energy supply (*10*–*12*) and contradictory reports of negative, positive, or null effects of environmental variation on FCL (*10*, *12*). Recent studies show a strong effect of ecosystem size on FCL in lakes and on oceanic islands (*11*, *13*), but the mechanisms underlying this relationship remain unclear (*12*, *14*).

In river ecosystems, climate change and human appropriation of fresh water are altering discharge variability and the frequency of intermittency across the globe (*15*). These hydrologic alterations have implications for the structure of river food webs. FCL in rivers may vary with the stability of the environment [for example., $\propto$ 1/(flow variation)], ecosystem size (such as drainage area), and energy supply. All three are correlated because the magnitude of high flows, channel geometry, and the relative supply of aquatic and terrestrial energy sources (such as algae and leaf litter from riparian trees, respectively) vary with drainage area (*16*–*18*). Thus, flow variation and other putative controls of FCL may scale with drainage area and mechanistically link ecosystem size to FCL. To date, no single study has addressed the simultaneous effects of energy supply, environmental variation, and ecosystem size—and correlations among these drivers—on the length of food chains in rivers or any other ecosystem.

We tested the role of ecosystem size, environmental stability, and energy supply on FCL in 36 rivers in North America. We define FCL as the maximum trophic position of stream-dwelling consumers measured via a stable isotope approach, which can accommodate omnivory and non-integer values of FCL (*19*). Our analysis expands on previous work on FCL in three ways. First, our study sites include a comprehensive range of values for all putative controls of FCL (*20*): a variation of >6 orders of magnitude in ecosystem size [drainage area (A_d) = 0.35 to 10^6 km^2], a variation of >3 orders of magnitude in energy supply [gross primary production (GPP) = 0.06 to 18.9 g of O_2 m^{-2} day^{-1}], and high-flow variation [σ_{HF} (*21*) = 0.03 to 12.9]. Our study sites also include both perennial and intermittent rivers, providing us with an opportunity to quantify how river drying affects riverine food web structure. Second, we used a hybrid of spectral and extreme event statistics to quantify environmental variation [($\propto$ 1/(environmental stability)], which provides a quantitative measure of discharge variation with reference to long-term discharge patterns (*21*). Third, we used path analysis to quantify and compare the path coefficients of drainage area→FCL and drainage area→flow variation→FCL relationships. In doing this, we asked whether ecosystem size has direct effects on FCL, or whether these effects are indirect and mediated via scaling between drainage area and flow variability (*22*).

We found that FCL increased with ecosystem size and decreased with σ_{HF} but was unrelated to energy supply (Fig. 1), which is consistent with previous findings (*23*–*25*). Ecosystem size had similar effects on FCL when measured as drainage area or cross-sectional area (fig. S1). Food chain length ranged from ~3 (predator) to nearly 5 (tertiary predator), matching the largest range of variation in FCL of any ecosystem (*10*, *11*). Top predators in 32 streams were fish, and these taxa were sufficiently large to be piscivorous in 29 sites (table S1). In intermittent streams, the top predator was consistently an invertebrate or an insectivorous fish.

Our results suggest that the strong effect of ecosystem size on FCL arises in part from a relationship between drainage area and flow variation and strong control of FCL by high- and low-flow events. σ_{HF} scaled with drainage area (Fig. 2A), but the power of the scaling relationship was significantly less steep and the mean σ_{HF} value was significantly higher in intermittent than in perennial rivers. Significant negative powers in both cases indicate that flow variation declines with drainage area. Attenuation of discharge variation results from spatial averaging in larger basins of asynchronous precipitation and high flows occurring in upstream portions of the drainage network. FCL increased

[1]Faculty of Ecology, Evolution, and Environmental Sciences, School of Life Sciences, Arizona State University, Post Office Box 874501, Tempe, AZ 85287–4501, USA. [2]Department of Ecology, Evolution and Behavior, University of Minnesota, 1987 Upper Buford Circle, St. Paul, MN 55108, USA. [3]Southwest Biological Science Center, U.S. Geological Survey, 2255 North Gemini Drive, Flagstaff, AZ 86001, USA. [4]Department of Ecology and Evolutionary Biology, Yale University, Post Office Box 208106, 165 Prospect Street, New Haven, CT 06520–8106, USA.

*To whom correspondence should be addressed. E-mail: John.L.Sabo@asu.edu

Downloaded from www.sciencemag.org on November 11, 2010

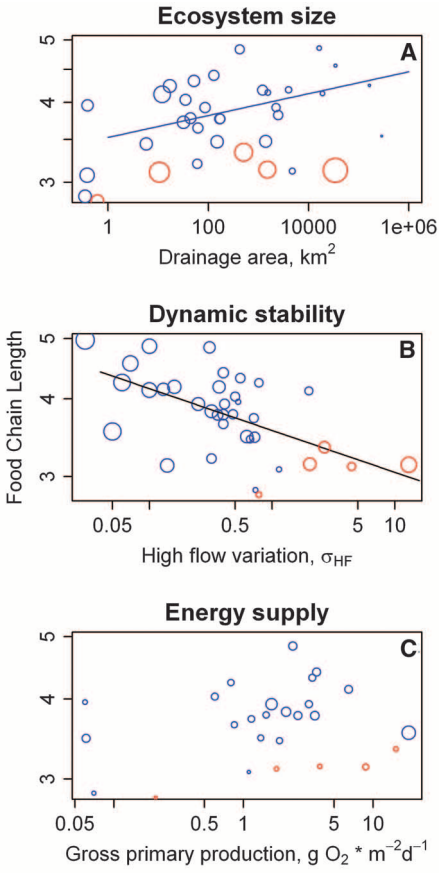

Fig. 1. Test of the effect of ecosystem size, environmental variation, and energy supply on FCL. (**A**) Relationship between drainage area (A_d in km^2) and maximum realized FCL (*20*) for streams with perennial (blue circles) and intermittent (red circles) flow. Data are shown on a double log plot. Circle diameter is proportional to σ_{HF}. A univariate mixed-effects linear model was used for the entire data set: $F = 10.58$, df = 1,29, $P < 0.005$, $R^2_{LR} = 0.48$ R^2_{LR}, coefficient of determination estimated via the likelihood ratio, LR. Regression parameters for FCL versus A_d did not differ between perennial and intermittent streams. (**B**) Relationship between σ_{HF} (*21*) and maximum realized FCL. Data are shown on a double log plot, with color as in (A). Circle diameter is proportional to drainage area. Mixed effects linear model: $F = 16.75$, df = 1, 29, $P < 0.001$, $R^2_{LR} = 0.44$. (**C**) Nonsignificant relationship between energy supply (GPP) and maximum realized FCL. Circle diameter is proportional to cross-sectional area. Mixed-effects linear model: $F = 1.37$, df = 1,20, $P > 0.25$.

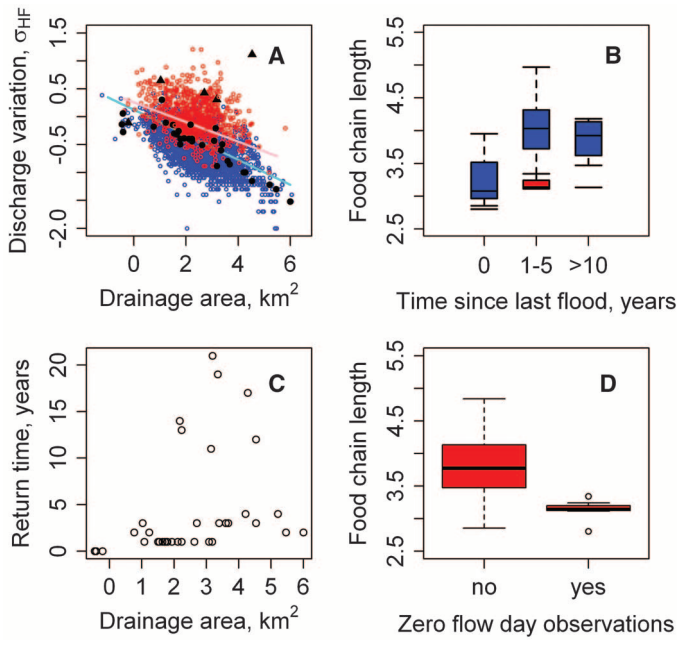

Fig. 2. Hydrologic mechanisms linking ecosystem size to FCL. (**A**) Scaling of σ_{HF} with A_d. Solid black circles and triangles are perennial and intermittent streams, respectively, from our FCL data set ($n = 31$ and 5, respectively). Blue and red open circles are supplementary data for the relationship between A_d and σ_{HF} from 3687 perennial and 866 intermittent rivers from the U.S. Geological Survey National Water Information System (NWIS) database (*20*). Cyan and pink lines are best-fit relationships between drainage area and discharge variation for NWIS data from linear mixed-effects models. Slopes for NWIS data are significantly different in a linear mixed-effects model, with an interaction term between zero flows and drainage area: $F = 50.1$, df = 1,4614, $P < 0.001$. Mean values of σ_{HF} are significantly higher in intermittent streams (linear mixed-effects model: $F = 3483.91$, df = 1,4616, $P < 0.001$). Scaling parameters (and standard errors) from model fits of the power function $\sigma_{HF} = cA_d^n$, are $c = 0.12$ (0.03), 0.25 (0.15), and $n = -0.22$ (0.004), −0.175 (0.012); for perennial and intermittent streams, respectively. The scaling relationships were significant for both stream types (linear mixed-effects model: $F = 3028.28$, df = 1,3665, $P < 0.001$, $R^2_{LR} = 0.55$; $F = 129.2$, df = 1, 865, $P < 0.001$, $R^2_{LR} = 0.33$; for perennial and intermittent streams, respectively). (**B**) Effects of high-flow return time on food chain length in perennial (blue, $n = 31$) and intermittent (red, $n = 5$) systems. Return times on the abscissa are estimated as the number of years since the last anomalous high-flow event (that is, the most recent, average daily discharge observation $>2\sigma_{HF}$). Times are binned as recent (0 years), near-recent (1 to 5 years), and long (10 or >10 years). Return times of 6 to 9 years were not observed in our data set. The effect of return times of anomalous high flows on FCL was significant in perennial rivers ($F = 4.1$, df = 2,22, $P < 0.05$; linear mixed-effects model, with return time and drainage area as fixed effects and basin as a single random effect). FCL was significantly different between recent and near-recent return time categories ($F = 6.97$, df = 1,17, sequential Bonferroni $P < 0.02$) but not for any other pairwise comparisons. The sample size was too low to test the significance of a similar asymptotic relationship between the return time of anomalous high flows and FCL in intermittent rivers. The plot shows the median (dark horizontal line), inner-quartile (box), and 95% (error bars) range of data. (**C**) Relationship between drainage area and return time of anomalous high flows ($n = 36$). The linear mixed-effects model was not significant. (**D**) Categorical effects of the occurrence of zero-flow days (*x* axis) on maximum realized FCL (*y* axis) for streams of similar size ($A_d = 10^{-1}$ to 10^5 km^2). FCL is significantly lower in intermittent streams (linear mixed-effects model: $F = 14.5$, df = 1,29, $P < 0.001$). Two seasonally intermittent streams from the SF Eel River basin without flow gages, but observed to dry during the period of observation for this study, were added to the intermediate flow type category to bolster sample size ($n = 20$, $n = 7$ for streams without and with zero flows, respectively). The plot shows the median (dark horizontal line), inner-quartile (box), and 95% range (error bars) of data and outliers (open circles).

with increasing return times of anomalous high flows (Fig. 2B), and this effect was independent of ecosystem size (Fig. 2C). The relationship between return times and FCL was asymptotic: significantly lower in systems with recent high flows (in the same year) than in systems with events occurring 1 to 5 years before FCL estimation. The shape of the relationship between high-flow return time and FCL did not differ significantly between perennial and intermittent streams, suggesting a similar effect on FCL in spite of significantly lower FCL overall in intermittent rivers. Low-flow events also constitute a form of environmental variation in rivers. Zero flows reduced FCL regardless of ecosystem size (Fig. 2D). The presence of even a single zero-flow event within the 20-year antecedent record reduced FCL by ~2/3 of a trophic level. Not all intermittent streams in our analysis were small or from arid biomes (table S1). Thus, our analyses were not confounded by covariation with other factors that could potentially influence FCL.

Finally, we used path analysis to quantify the relationships between ecosystem size, environmental stability, and FCL (Fig. 3). We applied the same path model to our full data set, including both perennial and intermittent streams and a subset that included only perennial rivers. We hypothesized that the total effect of ecosystem size (A_d) on FCL was dominated by the indirect path linking A_d to FCL via hydrologic variability ($A_d \rightarrow \sigma_{HF} \rightarrow$FCL) and that the direct effect of A_d on FCL was relatively small. For the full data set, path coefficients for the effects of A_d on σ_{HF} and σ_{HF} on FCL were both significant and negative (Fig. 3A). For the perennial subset, the path coefficient for the effect of A_d on σ_{HF} was larger and less variable than in the full data set (Fig. 3B), but the effect of σ_{HF} on FCL was not significant. Path coefficients for the direct effect of A_d on FCL were not significant for either data set; however, the total (direct and indirect) effects of A_d were significant in both analyses. The indirect path

Downloaded from www.sciencemag.org on November 11, 2010

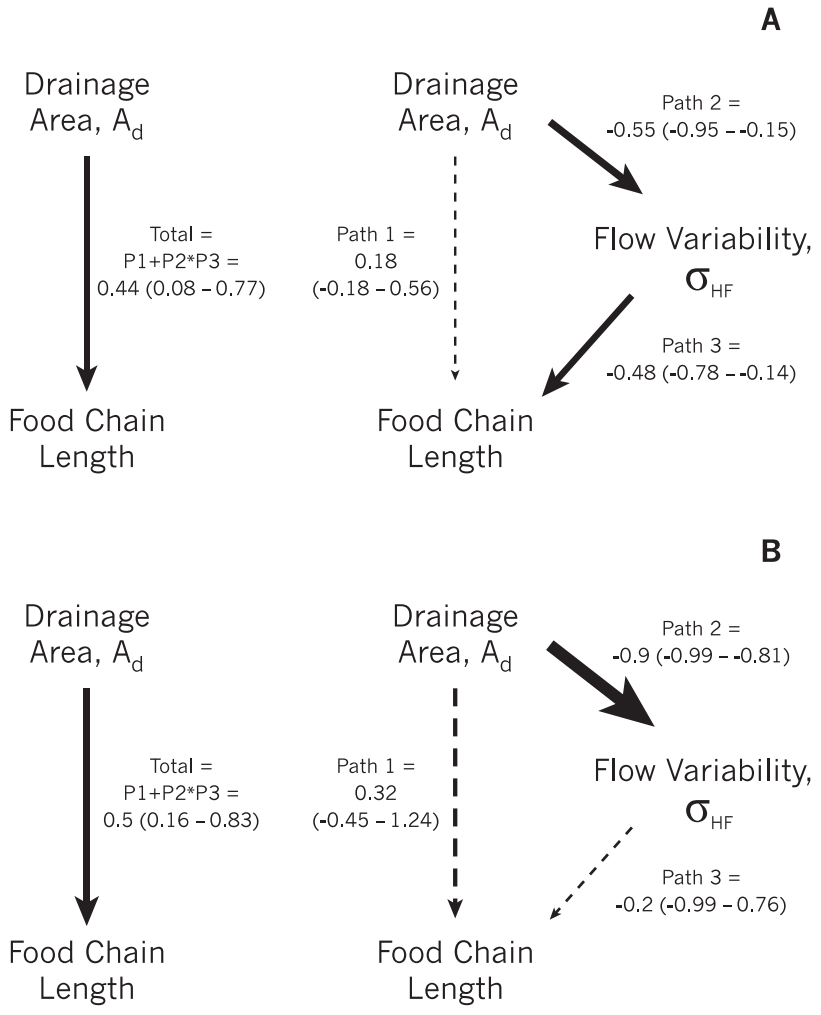

Fig. 3. Path analysis of relationships between ecosystem size (or drainage area), dynamic stability [$\propto$ 1/(flow variability)], and FCL. (**A**) Analysis of the entire data set and of perennial and intermittent streams combined. (**B**) Analysis of a subset of perennial streams. Numbers are path coefficients (mean ± bootstrapped 95% confidence limits).

($A_d \rightarrow \sigma_{HF} \rightarrow$FCL) made up >33% of the total effect of A_d on FCL in perennial streams and >60% of this total effect in all streams.

Flow variation is paramount in determining community structure (*26*, *27*) and trophic dynamics (*28*, *29*) in streams, but its effect on FCL is less clear. Previous work suggests that high flows can either lengthen or shorten food chains (*12*, *23*–*25*). Similarly, droughts increase, decrease, or have no significant effects on FCL (*12*, *30*, *31*). The idea that FCL increases with ecosystem size has support from different ecosystems, including streams (*10*–*13*), but the mechanism(s) underlying this relationship remain elusive. Our path analysis suggests that hydrologic variability is one mechanism potentially linking ecosystem size to FCL in rivers. This conclusion is strengthened by two additional lines of evidence. First, the return time of high-flow events has significant effects on FCL that were independent of drainage area. Second, σ_{HF} is consistently higher in intermittent rivers across a wide range of drainage areas. Thus, anomalous high flows occur with higher frequency in intermittent streams, independent of their size. This property, along with reduced habitat volume during periods of drying, further reduces FCL in intermittent rivers.

Our results have important implications for predicting how river food webs will respond to human- and climate-related changes in hydrology (*32*–*34*). Intermittency can have devastating effects on animal populations via reductions in habitat volume and enhanced σ_{HF}. We found that the top predators were piscivorous fish in perennial rivers, but in even the largest intermittent stream, the top predators were invertebrates or small-bodied fish. Thus, river drying will probably decrease FCL through the loss of large-bodied fishes. More broadly, our results suggest that further human- and climate-related changes in hydrology will have pronounced effects on the structure of river food webs.

References and Notes

1. C. Elton, *Animal Ecology* (Sidgwick and Jackson, London, 1927).
2. D. M. Post, G. Takimoto, *Oikos* **116**, 775 (2007).
3. N. G. Hairston Jr., N. G. Hairston Sr., *Am. Nat.* **142**, 379 (1993).
4. D. E. Schindler, S. R. Carpenter, J. J. Cole, J. F. Kitchell, M. L. Pace, *Science* **277**, 248 (1997).
5. P. B. McIntyre, L. E. Jones, A. S. Flecker, M. J. Vanni, *Proc. Natl. Acad. Sci. U.S.A.* **104**, 4461 (2007).
6. K. A. Kidd, D. W. Schindler, D. C. G. Muir, W. L. Lockhart, R. H. Hesslein, *Science* **269**, 240 (1995).
7. G. E. Hutchinson, *Am. Nat.* **93**, 145 (1959).
8. S. L. Pimm, *Food Webs* (Chapman and Hall, London, 1982).
9. T. W. Schoener, *Ecology* **70**, 1559 (1989).
10. D. M. Post, *Trends Ecol. Evol.* **17**, 269 (2002).
11. D. M. Post, M. L. Pace, N. G. Hairston Jr., *Nature* **405**, 1047 (2000).
12. J. L. Sabo, J. C. Finlay, D. M. Post, *Year Ecol. Conserv. Biol. 2009* **1162**, 187 (2009).
13. G. Takimoto, D. A. Spiller, D. M. Post, *Ecology* **89**, 3001 (2008).
14. D. M. Post, M. W. Doyle, J. L. Sabo, J. C. Finlay, *Geomorphology* **89**, 111 (2007).
15. R. Jackson *et al.*, *Ecol. Appl.* **11**, 1027 (2001).
16. D. K. Knighton, *Fluvial Forms and Processes* (Oxford Univ. Press, New York, 1998).
17. L. B. Leopold, T. Maddock Jr., *U.S. Geol. Surv. Prof. Pap. 252* (1953).
18. R. L. Vannote, G. W. Minshall, K. W. Cummins, J. R. Sedell, C. E. Cushing, *Can. J. Fish. Aquat. Sci.* **37**, 130 (1980).
19. D. M. Post, *Ecology* **83**, 703 (2002).
20. See supporting material on *Science* Online.
21. J. L. Sabo, D. M. Post, *Ecol. Monogr.* **78**, 19 (2008).
22. J. F. Guégan, S. Lek, T. Oberdorff, *Nature* **391**, 382 (1998).
23. P. A. McHugh, A. R. McIntosh, P. G. Jellyman, *Ecol. Lett.* **13**, 881 (2010).
24. C. R. Townsend *et al.*, *Ecol. Lett.* **1**, 200 (1998).
25. R. M. Thompson, C. R. Townsend, *Oikos* **108**, 137 (2005).
26. S. G. Fisher, L. J. Gray, N. B. Grimm, D. E. Busch, *Ecol. Monogr.* **52**, 93 (1982).
27. G. D. Grossman, P. B. Moyle, J. O. Whitaker Jr., *Am. Nat.* **120**, 423 (1982).
28. M. E. Power, M. S. Parker, W. E. Dietrich, *Ecol. Monogr.* **78**, 263 (2008).
29. J. T. Wootton, M. S. Parker, M. E. Power, *Science* **273**, 1558 (1996).
30. G. P. Closs, P. S. Lake, *Ecol. Monogr.* **64**, 1 (1994).
31. A. W. Walters, D. M. Post, *Ecology* **89**, 3261 (2008).
32. T. P. Barnett, D. W. Pierce, *Water Resour. Res.* **44**, W03201 (2008).
33. IPCC, Ed., *Climate Change, 2007: Synthesis Report* (Intergovernmental Panel on Climate Change, Geneva, 2007).
34. S. Liang, S. Ge, L. Wan, J. Zhang, *Water Resour. Res.* **46**, W02505 (2010).

35. The authors thank S. Beck, M. Bernot, M. Booth, M. Caron, O. Champoux, C. Crenshaw, D. Cunjak, D. Caissie, R. Doucett, S. J. Fisher, N. B. Grimm, R. O. Hall, T. K. Harms, B. Hungate, K. Luttermoser, W. McDowell, G. Morin, P. Mulholland, R. J. Naiman, J. Regetz, E. Rosi-Marshall, R. Sponseller, C. U. Soykan, and L. Thompson; the Minnesota Department of Natural Resources for fish samples; the STROUD New York Watersheds Project for access to study sites and metabolism data; the Los Angeles Department of Water and Power, the Coweeta Long-Term Ecological Research (LTER) project, the H. J. Andrews LTER project, Oak Ridge National Laboratory, Environment Canada, and the U.S. Forest Service for flow data. This work was supported by grants from NSF, including DEB-0315990 to J.C.F., DEB-0316679 to D.M.P., and DEB-0317137 and DEB-0635088 to J.L.S.. The work was also supported by a Sabbatical Fellowship to J.L.S. at the National Center for Ecological Analysis and Synthesis, a center funded by NSF (grant EF-0553768); the University of California, Santa Barbara; and the State of California. Any use of trade, product, or firm names is for descriptive purposes only and does not imply endorsement by the U.S. government.

Supporting Online Material

www.sciencemag.org/cgi/content/full/science.1196005/DC1
Materials and Methods
Figs. S1 to S3
Tables S1 to S3
References

3 August 2010; accepted 21 September 2010
Published online 14 October 2010;
10.1126/science.1196005
Include this information when citing this paper.

Downloaded from www.sciencemag.org on November 11, 2010

Conserved Molecular Components for Pollen Tube Reception and Fungal Invasion

Sharon A. Kessler,[1] Hiroko Shimosato-Asano,[1]* Nana F. Keinath,[2]† Samuel E. Wuest,[1]‡ Gwyneth Ingram,[3]§ Ralph Panstruga,[2] Ueli Grossniklaus[1]||

During sexual reproduction in flowering plants such as *Arabidopsis*, a tip-growing pollen tube (PT) is guided to the synergid cells of the female gametophyte, where it bursts and releases the two sperm. Here we show that PT reception and powdery mildew (PM) infection, which involves communication between a tip-growing hypha and a plant epidermal cell, share molecular components. NORTIA (NTA), a member of the MLO family originally discovered in the context of PM resistance, and FERONIA (FER), a receptor-like kinase, both control PT reception in synergids. Homozygous *fer* mutants also display PM resistance, revealing a new function for *FER* and suggesting that conserved components, such as FER and distinct MLO proteins, are involved in both PT reception and PM infection.

Successful pollination and fertilization depend on interactions between the male gametophyte (pollen) and female tissues (*1*). Pollen lands on a stigma and hydrates, and the pollen tubes (PTs) grow toward the ovary, where they exit the transmitting tissue and one PT is attracted to each ovule. Until Amici discovered in the 19th century that PTs enter the ovule through the micropyle and play a role in reproduction (*2*), these tip-growing cells were considered parasites. The final stage of maternal control over male gamete delivery is the arrival of the PT at the female gametophyte (embryo sac) and the release of the two sperm to effect double fertilization, which forms the zygote and the endosperm. In angiosperms, the synergids control the final steps of PT guidance and reception (*3*). They excrete PT attractants such as the LURE polypeptides (*4*), and, upon PT arrival at the micropyle, the receptive synergid starts to degenerate (*5*) and signals the PT to stop its growth and rupture to release the sperm (*6*, *7*). Over 100 years have passed since the discovery of double fertilization (*3*), but we still know little about the underlying molecular mechanisms behind the female control of PT behavior.

In *Arabidopsis*, the FERONIA (FER) CrRLK1L-type receptor-like kinase (RLK) controls PT reception. It is localized to the filiform apparatus, a membrane-rich region at the micropylar end of the synergids (*8*). In *fer* (which is allelic to *sirène*) mutants, PTs enter the synergid cell but continue to grow instead of bursting to release the sperm (*6*–*8*). In our search for additional components of this signaling pathway, we identified *nortia* (*nta*), which like *fer* was named after an Etruscan goddess of fertility (*9*). Like *fer*, *nta* is a female gametophytic mutant and displays reduced fertility and PT overgrowth in the synergids (Fig. 1, A to D). Consequently, in reciprocal crosses with wild-type individuals, the *nta* phenotype is detected only when the mutant is used as the female (fig. S1). In contrast to *fer/FER* mutants, which have close to 50% unfertilized ovules because of a failure in PT reception and are rarely transmitted through the female gametophyte (*6*–*8*), *nta* mutant alleles are transmitted normally through male gametophytes and at frequencies of 60 to 80% through female gametophytes (table S1), allowing for the isolation of homozygous mutants. *nta-1/nta-1* individuals have 22% (n = 1506 ovules) unfertilized ovules with PT overgrowth, compared to 4% (n = 1076) unfertilized ovules (without PT attraction) in the wild type.This indicates that *nta* embryo sacs differentiate normally, as evidenced by examination of egg- and synergid-specific β-glucuronidase (GUS) markers and microscopic examination of *nta* mutant embryo sacs (fig. S2).

Map-based cloning identified the *NTA* gene as *At2g17430*, or *AtMLO7*, a member of the plant-specific Mildew resistance locus o (MLO) family of proteins originally discovered to be required for powdery mildew (PM) susceptibility in barley (*10*). MLO proteins are predicted to have a signal peptide, seven transmembrane domains, and a calmodulin-binding domain in the C-terminal intracellular domain (Fig. 1, E and F). The *nta-1* allele has a 20–base pair deletion at the exon 13/intron 13 boundary, leading to failed splicing and the introduction of an early STOP codon, predicted to truncate the protein to 436 rather than the expected 543 amino acids. Two additional *nta* alleles with transfer DNA insertions in the first exon (*nta-2*) and the last exon (*nta-3*) had the same PT overgrowth phenotype as *nta-1* at similar frequencies (fig. S3), indicating that the correct gene had been identified and that the low expressivity of the *nta* phenotype was not caused by expression of a truncated protein. Genetic redundancy could play a role in the weak phenotype seen in *nta* mutants. The *Arabidopsis* genome has 15 members of the *MLO* gene family (*11*), and double or triple mutants in some of these

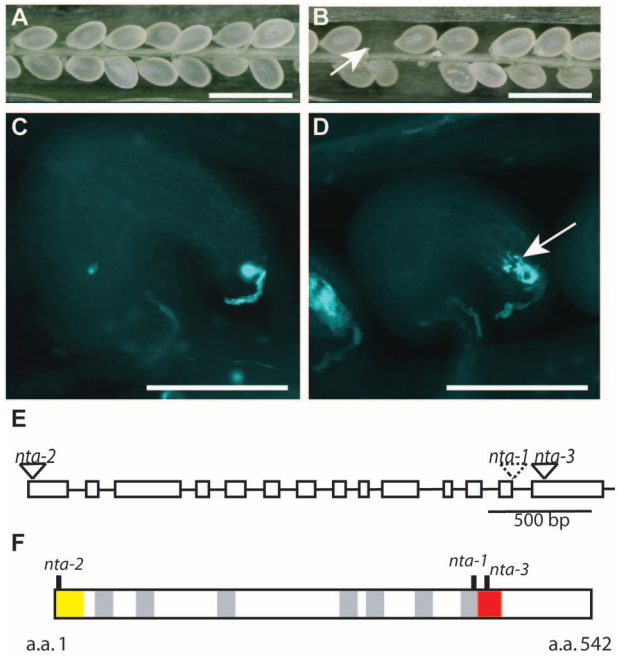

Fig. 1. NTA is an MLO protein involved in PT reception at the female gametophyte. (**A**) Wild-type silique with fertilized ovules developing into seeds. (**B**) *nta/nta* silique with unfertilized (shrunken white ovules, arrow) and fertilized ovules. (**C** and **D**) Aniline blue staining of callose in PT cell walls at 2 days after pollination. (C) Fertilized wild-type ovule with normal PT reception. (D) Unfertilized *nta/nta* ovule with PT overgrowth (arrow). (**E**) Gene structure of NTA with exons (boxes) and introns (lines). Mutations are indicated by inverted triangles: Insertions are dashed and deletions are solid. bp, base pair. (**F**) Predicted domains in the NTA protein (yellow, signal peptide; gray, transmembrane domains; red, calmodulin-binding domain). Black bars indicate insertion and deletion sites. a.a., amino acid. Scale bars in (A) and (B), 1 mm; in (C) and (D), 100 μm.

[1]Institute of Plant Biology and Zürich Basel Plant Science Center, University of Zürich, Zollikerstrasse 107, CH-8008 Zürich, Switzerland. [2]Max Planck Institute for Plant Breeding Research, Department of Plant-Microbe Interactions, Carl-von-Linné-Weg 10, 50829 Köln, Germany. [3]Institute of Molecular Plant Sciences, University of Edinburgh, Edinburgh EH9 3JR, UK.

*Present address: Graduate School of Biological Sciences, Nara Institute of Science and Technology, Ikoma, Nara 630-0192, Japan.

†Present address: Heidelberg Institute for Plant Sciences, Universität Heidelberg, Im Neuenheimer Feld 230, 69120 Heidelberg, Germany.

‡Present address: Smurfit Institute of Genetics, Trinity College Dublin, Dublin 2, Ireland.

§Present address: Laboratoire de Reproduction et Développement des Plantes, 46 Allée d'Italie, 69364 Lyon Cedex 07, France.

||To whom correspondence should be addressed. E-mail: grossnik@botinst.uzh.ch

Downloaded from www.sciencemag.org on November 11, 2010

genes have stronger phenotypes than single mutants (*12*, *13*). In addition to *NTA*, transcripts of phylogenetically related *AtMLO8* and *AtMLO10* are expressed in synergids (*14*), but mutants in these genes have no PT overgrowth phenotypes (table S2).

The expression pattern of *NTA* was examined with translational fusions of the *NTA* genomic sequence to genes encoding GUS and green fluorescent protein (GFP) under control of the native *NTA* 5′-regulatory sequences. In stable *NTA-GUS* transformants, expression was detected only in the synergids (Fig. 2A). A previous study on the expression of *Arabidopsis MLO* genes had detected *NTA* only in pollen, based on a promoter::GUS fusion lacking the introns and coding sequence of *NTA* (*11*). Using reverse transcription polymerase chain reaction on immature flowers, we detected *NTA* transcript in pistils and immature anthers (up to stage 12), but not in mature pollen (fig. S4), suggesting that not all of the elements regulating *NTA* expression are present in the promoter. The *NTA-GFP* fusion construct complemented the *nta* phenotype in 37 independent transformants (table S3), indicating that the fusion protein is fully functional. The NTA protein has multiple predicted transmembrane domains and is expected to localize to the plasma membrane. Transient expression of an NTA-GFP fusion protein under the constitutive 35*S* promoter showed NTA-GFP fluorescence at the plasma membrane in onion cells (fig. S5). However, in stable *Arabidopsis* transformants with the native *NTA* promoter, NTA-GFP fluorescence was detected in a punctate pattern throughout the cytoplasm of both synergids in unfertilized, mature female gametophytes, possibly reflecting its association with endomembrane compartments (Fig. 2, B and C, and fig. S5, E and F). Limited pollinations were performed to compare NTA-GFP localization in ovules with and without PTs at 5 to 7 hours after pollination, which is the time when PT reception occurs. NTA-GFP became polarly localized to the basal half of the synergids upon PT arrival at the micropyle (Fig. 2, D to F). The redistribution of NTA-GFP to the filiform apparatus upon PT arrival indicates that relocalization of NTA may be important for signaling during PT reception.

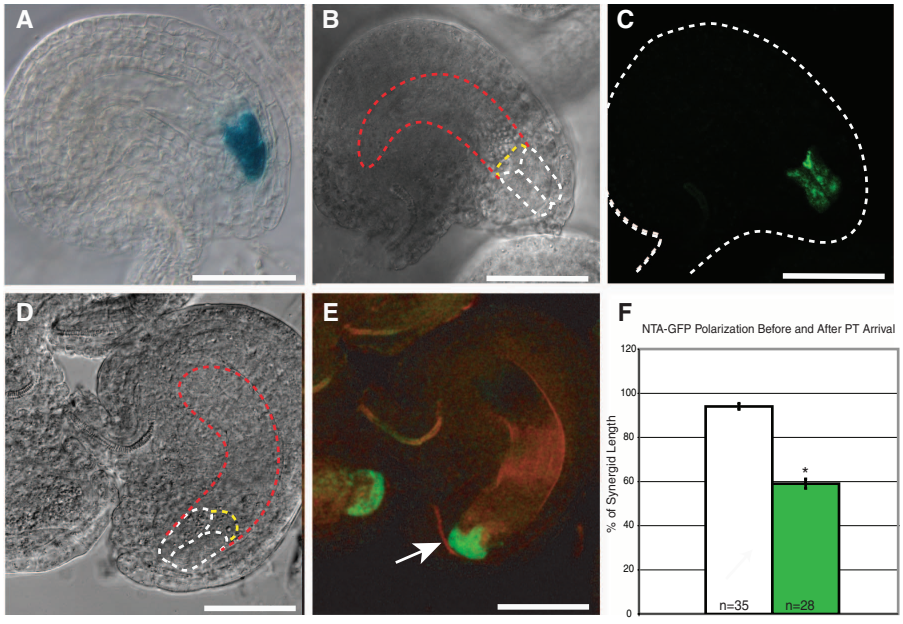

Fig. 2. NTA is expressed in the synergids of the female gametophyte and becomes polarly localized upon arrival of the PT. (**A**) Expression of *pNTA::NTA-GUS* is detected only in synergids (blue signal). (**B**) Differential interference contrast (DIC) image of the female gametophyte (white, synergids; yellow, egg cell; red, central cell). (**C**) NTA-GFP (green signal) is found throughout the synergids in unfertilized ovules. (**D**) DIC image of an ovule with a PT arriving. (**E**) NTA-GFP (green signal) is redistributed to the micropylar end of the synergids at PT arrival (red signal, arrow). (**F**) Percentage of synergid length occupied by NTA-GFP signal before and after PT arrival (white bar, no PT; green bar, after PT arrival). Scale bars, 50 μm.

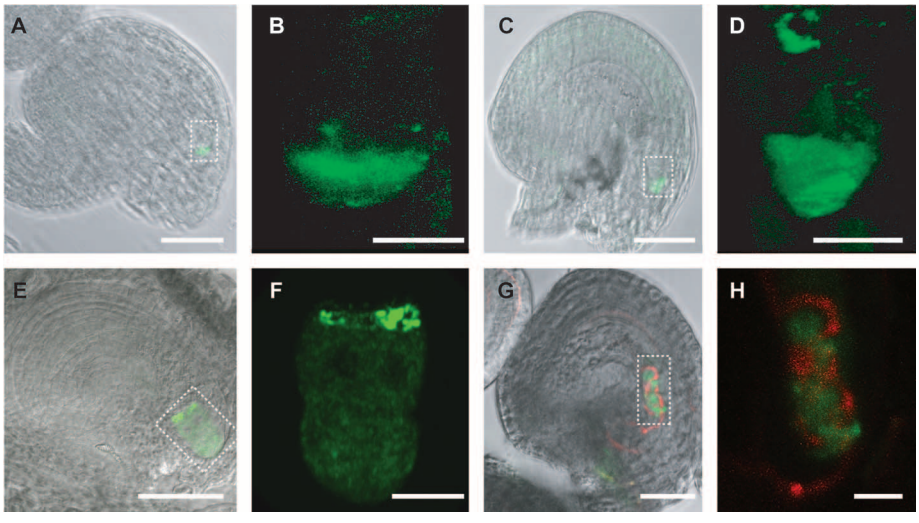

Fig. 3. NTA has no effect on FER localization, but FER controls polar localization of NTA at PT arrival. (A), (C), (E), and (G) Overlayed DIC and fluorescent marker images of FER-GFP and NTA-GFP localization. (B), (D), (F), and (H) Synergids from the boxed regions of ovules shown in (A) to (C). (**A** and **B**) FER-GFP (green signal) is localized at the filiform apparatus at the micropylar end of the synergids in wild-type ovules. (**C** and **D**) Normal localization of FER-GFP at the micropylar end of an *nta* ovule. (**E** and **F**) NTA-GFP (green signal) in *fer* ovules shows normal localization throughout the synergids before fertilization. (**G** and **H**) NTA-GFP is not polarly localized in a mutant *fer* embryo sac with PT overgrowth (red signal). Scale bars in (A), (C), (E), and (G), 30 μm; in (B), (D), (F), and (H), 10 μm.

Because mutations in *NTA* and *FER* have similar phenotypes and they are both expressed in synergids, we wondered if their expression and/or localization patterns are interdependent. Expression of a functional pFER::FER-GFP fusion protein was examined in *nta-1* homozygous versus wild-type plants. In both cases, FER-GFP was localized to the filiform apparatus (Fig. 3, A to D), indicating that NTA is not involved in the polar localization of FER. Likewise, a pNTA::NTA-GFP fusion protein showed the same distribution in all ovules of *fer/FER* plants before pollination, indicating that the *fer* mutation does not affect NTA-GFP expression and localization in mature, unfertilized embryo sacs (Fig. 3, E and F). However, in contrast to the polar localization of NTA-GFP seen in the wild type upon PT arrival (Fig. 2, D to F), in *fer* mutant embryo sacs, NTA-GFP did not become polarly localized (Fig. 3, G to H). This indicates that the *FER* pathway plays a role in controlling the redistribution of NTA protein upon PT arrival.

The identification of *NTA* as a member of the *MLO* gene family provides an interesting link between PT reception and fungal invasion. PT reception and fungal invasion of plant cells share some common features. First, both fungal hyphae and PTs show tip growth and must communicate with and penetrate into another cell. Second, polar localization of MLO proteins is correlated with

Downloaded from www.sciencemag.org on November 11, 2010

the entry processes of both fungal hyphae (*15*) and PTs. Finally, the control of PT behavior by synergids is an angiosperm innovation (*16*), and PM has not been reported to infect plants outside of the angiosperm lineage (*17*).

The first member of the *MLO* gene family described in plants was the barley (*Hordeum vulgare*) *HvMlo* gene, involved in PM resistance (*10*). In contrast to resistance (*R*) gene–mediated resistance, in which a pathogen avirulence factor is recognized by a plant *R* protein, which triggers an immune response in a gene-for-gene manner (*18*), *mlo*-based PM resistance is due to mutation of a "susceptibility" gene (*10*, *19*). During fungal invasion, *Hv*MLO and other membrane-associated proteins colocalize at the site of fungal infection (*15*), creating a pathogen-triggered membrane microdomain that might be related to exosomal transport processes. Recessive mutations in the *Arabidopsis HvMlo* ortholog *AtMLO2* (but not in *AtMLO7*/*NTA*) (*12*) also lead to partial PM resistance that is enhanced in double and triple mutants with *AtMLO6* and/or *AtMLO12*, indicating that the function of MLO proteins in PM invasion is ancient and has been conserved since the monocot/dicot divergence, estimated at around 200 million years ago (*20*).

Because MLO proteins are involved in both PT reception and PM invasion, we wondered if another component of the PT reception mechanism, the FER RLK, is also involved in PM invasion of plant cells. Unlike *NTA*, whose expression is restricted to the synergids, *FER* is expressed not only in the filiform apparatus but in all plant tissues except mature pollen (*8*). In addition to its role in PT reception (*8*), FER has recently been reported to cooperate with two other CrRLK1Ls—THESEUS (THE) and HERCULES RECEPTOR KINASE 1 (HERK1)—to control cell elongation (*21*). Indeed, *fer/fer* plants are smaller than wild-type siblings but have normal floral development except for an almost complete failure of PT reception, with very few seeds developing in each silique (fig. S6).

PM infection begins when a fungal spore lands on an epidermal cell. Subsequently, the spore hydrates, germinates, and penetrates the plant cell wall to establish a feeding structure (haustorium) within the host cell. The vegetative life cycle of the fungus is completed by the release of asexual spores from the conidiophores, which can spread the infection (*22*). *fer/fer* plants were tested for susceptibility to infection by the PM *Golovinomyces* (syn. *Erysiphe*) *orontii*, which is virulent on *Arabidopsis* accession Landsberg *erecta* (L*er*), by measuring the incidence of entry of PM spores and the production of conidiophores per PM colony. When compared to wild-type plants, *fer/fer* mutant plants were resistant to PM infection, with somewhat lower entry rates and significantly fewer conidiophores produced per fungal colony (Fig. 4 and fig. S7). This phenotype was rescued in a transgenic line with a functional FER-GFP fusion protein expressed in the *fer/fer* background (Fig. 4). Thus, like *MLO*, a wild-type copy of *FER* seems to be necessary for PM susceptibility. The *fer*-mediated PM resistance is not caused by a general resistance to pathogens, because *fer* plants have normal susceptibility to the oomycete *Hyaloperonospora arabidopsidis* and the ascomycete *Colletotrichum higginsianum* (fig. S8).

fer and *mlo* mutants share several phenotypic similarities suggesting that *FER* and various *MLO* genes function together to control PM invasion and PT reception. In *fer* and *nta* mutants, PTs exhibit normal entry into the receptive synergid but do not complete their "invasion" process, failing to burst and release the sperm. Likewise, the PM resistance phenotype in *fer* plants is predominantly manifested at the post-invasive stage: Host cell entry is not affected as severely as the establishment of successful colonies that produce conidiophores (Fig. 4G and fig. S7), a phenotype reminiscent of the *Atmlo2* resistance phenotype (*12*). Disease resistance in plants is often mediated through up-regulation of hormone signaling pathways, followed by a hypersensitive response (HR), in which cells undergo cell death (*18*, *23*). *mlo* mutants in barley and *Arabidopsis* exhibit stochastic cell death of mesophyll cells accompanied by increased production of H_2O_2 in the absence of any pathogen (*12*, *24*). Unchallenged *fer* leaves have a similar phenotype of spontaneous cell death and H_2O_2 production (fig. S9). Salicylic acid signaling does not seem to be affected in *fer* mutants; however, the ethylene/jasmonic acid defense pathways could be involved in both *mlo*- and *fer*-mediated resistance (supporting online text and fig. S10).

The mechanism for *mlo*-mediated resistance remains unclear, but MLO proteins seem to modulate SNARE-dependent and vesicle transport–associated processes at the plasma membrane (*15*, *25*). Thus, MLO could be involved in delivering cargo such as regulatory proteins to the plasma membrane. A similar mechanism can be proposed for the control of PT behavior by FER and NTA. FER would sense the arrival of the PT and initiate a signal transduction cascade leading to relocalization of NTA-containing vesicles to the filiform apparatus. Recently, the maize defensin ZmES4, required for PT rupture, was shown to relocalize to the filiform apparatus at PT arrival (*26*). A homologous *Arabidopsis* defensin would be a candidate for cargo being delivered to the filiform apparatus in response to a FER/NTA-mediated signal.

Because *FER* is ubiquitously expressed in all plant tissues except for mature pollen (*8*), whereas the 15 *AtMLO* genes are expressed in different tissues and in response to various stimuli (*11*, *13*), FER might cooperate with diverse members of

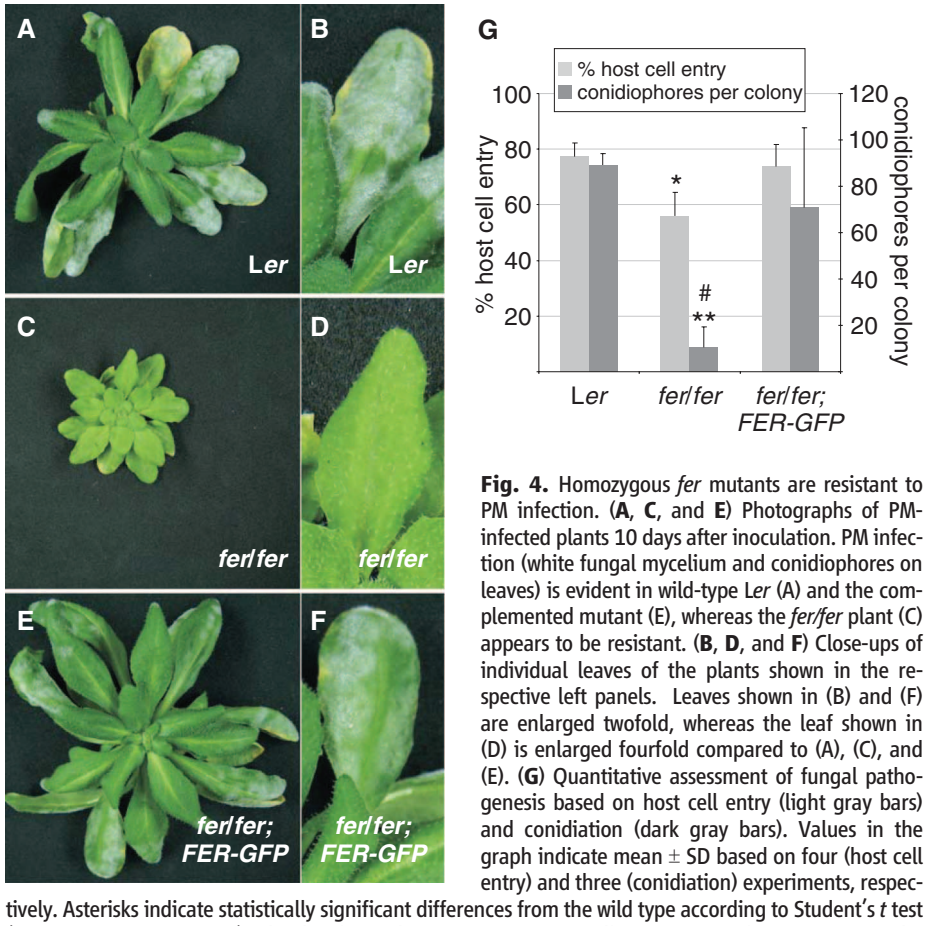

Fig. 4. Homozygous *fer* mutants are resistant to PM infection. (**A**, **C**, and **E**) Photographs of PM-infected plants 10 days after inoculation. PM infection (white fungal mycelium and conidiophores on leaves) is evident in wild-type L*er* (A) and the complemented mutant (E), whereas the *fer/fer* plant (C) appears to be resistant. (**B**, **D**, and **F**) Close-ups of individual leaves of the plants shown in the respective left panels. Leaves shown in (B) and (F) are enlarged twofold, whereas the leaf shown in (D) is enlarged fourfold compared to (A), (C), and (E). (**G**) Quantitative assessment of fungal pathogenesis based on host cell entry (light gray bars) and conidiation (dark gray bars). Values in the graph indicate mean ± SD based on four (host cell entry) and three (conidiation) experiments, respectively. Asterisks indicate statistically significant differences from the wild type according to Student's *t* test (*$P < 0.05$, **$P < 0.01$); the hatch mark signifies a statistically significant difference from the complementation line ($P < 0.05$).

Downloaded from www.sciencemag.org on November 11, 2010

the MLO family in a tissue-specific manner. The ancestral function of FER and MLO proteins is an open question, but the presence of genes with high sequence-relatedness to *FER* and *MLO* in bryophytes (*27*, *28*) suggests that these proteins were either originally implicated in processes distinct from PT reception and PM susceptibility, or that their cooperativity developed later in the course of evolution. As both proteins are required for compatible interactions with either PTs or fungal hyphae, their original role may have been in mediating susceptibility to symbiotic organisms such as mycorrhizal fungi, an interaction that was important for land plant evolution but no longer occurs with *Arabidopsis*. Because *FER* is necessary for successful fertilization, deleterious mutations that would also lead to PM resistance would be selected against. Other players in PT reception (*29*, *30*) may also be involved in PM infection, or, alternatively, different accessory molecules may be used in conjunction with FER and the MLOs in distinct response pathways.

Successful seed production and durable resistance to pathogens are two of the most important agronomic traits sought after today. The work presented here has unveiled unforeseen similarities between these processes at the molecular level. As we continue to unravel the signal transduction processes involved in intercellular communication during PT reception, we may also gain important insights into PM resistance mechanisms and vice versa.

References and Notes

1. E. M. Lord, S. D. Russell, *Annu. Rev. Cell Dev. Biol.* **18**, 81 (2002).
2. J. B. Amici, *Annales des Sciences Naturelles*, 193 (1847).
3. T. Dresselhaus, *Curr. Opin. Plant Biol.* **9**, 41 (2006).
4. S. Okuda *et al.*, *Nature* **458**, 357 (2009).
5. L. Sandaklie-Nikolova, R. Palanivelu, E. J. King, G. P. Copenhaver, G. N. Drews, *Plant Physiol.* **144**, 1753 (2007).
6. N. Huck, J. M. Moore, M. Federer, U. Grossniklaus, *Development* **130**, 2149 (2003).
7. N. Rotman *et al.*, *Curr. Biol.* **13**, 432 (2003).
8. J. M. Escobar-Restrepo *et al.*, *Science* **317**, 656 (2007).
9. T. Livius, *Ab Urbe Condita, Liber VII, 3.7* (~29 B.C.).
10. R. Büschges *et al.*, *Cell* **88**, 695 (1997).
11. Z. Chen *et al.*, *Plant Mol. Biol.* **60**, 583 (2006).
12. C. Consonni *et al.*, *Nat. Genet.* **38**, 716 (2006).
13. Z. Chen *et al.*, *Plant Cell* **21**, 1972 (2009).
14. S. E. Wuest *et al.*, *Curr. Biol.* **20**, 506 (2010).
15. R. A. Bhat, M. Miklis, E. Schmelzer, P. Schulze-Lefert, R. Panstruga, *Proc. Natl. Acad. Sci. U.S.A.* **102**, 3135 (2005).
16. T. Higashiyama, *J. Plant Res.* **115**, 149 (2002).
17. K. Amano, *Host Range and Geographical Distribution of the Powdery Mildew Fungi* (Japan Scientific Societies Press, Tokyo, 1986).
18. J. D. Jones, J. L. Dangl, *Nature* **444**, 323 (2006).
19. P. Piffanelli *et al.*, *Nature* **430**, 887 (2004).
20. K. H. Wolfe, M. Gouy, Y. W. Yang, P. M. Sharp, W. H. Li, *Proc. Natl. Acad. Sci. U.S.A.* **86**, 6201 (1989).
21. H. Guo *et al.*, *Proc. Natl. Acad. Sci. U.S.A.* **106**, 7648 (2009).
22. R. J. O'Connell, R. Panstruga, *New Phytol.* **171**, 699 (2006).
23. R. Bari, J. D. Jones, *Plant Mol. Biol.* **69**, 473 (2009).
24. P. Piffanelli *et al.*, *Plant Physiol.* **129**, 1076 (2002).
25. R. Panstruga, *Biochem. Soc. Trans.* **33**, 389 (2005).
26. S. Amien *et al.*, *PLoS Biol.* **8**, e1000388 (2010).
27. A. Devoto *et al.*, *J. Mol. Evol.* **56**, 77 (2003).
28. M. D. Lehti-Shiu, C. Zou, K. Hanada, S. H. Shiu, *Plant Physiol.* **150**, 12 (2009).
29. A. Capron *et al.*, *Plant Cell* **20**, 3038 (2008).
30. A. Boisson-Dernier, S. Frietsch, T. H. Kim, M. B. Dizon, J. I. Schroeder, *Curr. Biol.* **18**, 63 (2008).

31. We thank A. Boisson-Dernier for providing *pLat52:DsRED* and for critical reading of this manuscript; S. Schauer for providing plasmids; A. Reinstädler for technical assistance with pathogen assays; and J. M. Escobar-Restrepo, H. Lindner, M. Bayer, C. Jäger-Baroux, S. Pien, V. Gagliardini, and members of the Grossniklaus lab for helpful discussions. This work was supported by the University of Zürich, the Max Planck Society, fellowships of the Human Frontiers in Science Program (to S.A.K.), the Forschungskredit of the University of Zürich (to H.S.-A.), the International Max Planck Research School (to N.F.K.), the Royal Society of London (to G.I.), and grants from the Deutsche Forschungsgemeinschaft (SFB670 to R.P.) and the Swiss National Science Foundation (to U.G.).

Supporting Online Material

www.sciencemag.org/cgi/content/full/330/6006/968/DC1
Materials and Methods
SOM Text
Figs. S1 to S11
Tables S1 to S3
References

16 July 2010; accepted 15 September 2010
10.1126/science.1195211

Optogenetic Control of Cardiac Function

Aristides B. Arrenberg,[1,3] Didier Y. R. Stainier,[2]* Herwig Baier,[1] Jan Huisken[2,4]

The cardiac pacemaker controls the rhythmicity of heart contractions and can be substituted by a battery-operated device as a last resort. We created a genetically encoded, optically controlled pacemaker by expressing halorhodopsin and channelrhodopsin in zebrafish cardiomyocytes. Using patterned illumination in a selective plane illumination microscope, we located the pacemaker and simulated tachycardia, bradycardia, atrioventricular blocks, and cardiac arrest. The pacemaker converges to the sinoatrial region during development and comprises fewer than a dozen cells by the time the heart loops. Perturbation of the activity of these cells was entirely reversible, demonstrating the resilience of the endogenous pacemaker. Our studies combine optogenetics and light-sheet microscopy to reveal the emergence of organ function during development.

In mammals, the heart rate is controlled by a specialized group of cells in the sinoatrial (SA) node, which act as the primary pacemaker. Together with cells in the atrioventricular (AV) node (secondary pacemaker) and specialized cells in the ventricular walls, they constitute the cardiac conduction system (CCS) (*1*, *2*). In nonmammalian vertebrates, a CCS with properties similar to those of the mammalian CCS has been inferred from imaging of voltage signals (*3*, *4*) or Ca^{2+} transients (*5*); the origin of the conduction wave was located in a region apparently homologous to the SA node. However, the exact role of this presumptive pacemaker and the consequences of its inactivation remain unclear.

We combined optical tools and transgenic expression of light-gated ion channels (*6*–*8*) in zebrafish (*9*–*13*) to locate and control cardiac pacemaker cells. Halorhodopsin (NpHR) (*6*) and channelrhodopsin-2 H134R (ChR2) (*6*, *14*) enable temporally precise (tens of milliseconds) and spatially confined (single cells) control. The light-gated pump NpHR-mCherry was expressed in zebrafish cardiomyocytes by means of the Gal4/UAS system (*13*, *15*) (fig. S1A). The protein was locally activated with light patterns generated with a digital micromirror device (fig. S2), which enables synchronous, uniform illumination of arbitrary shapes, unlike laser scanning (*16*) or fiber optic (*13*) techniques. High-speed video recordings of the heart were generated with a multidirectional selective plane illumination microscope (mSPIM) (*17*–*19*) (Fig. 1A and fig. S3).

Illuminating the entire zebrafish heart at 3 days post-fertilization (dpf) with orange light instantaneously blocked contractions (Fig. 1B and movie S1), indicating that the strong hyperpolarization induced by the activated chloride pump NpHR perturbed the well-balanced interplay of ion channels in cardiomyocytes (fig. S1B) and prevented depolarizations. The heart recovered to its original beat rate instantaneously after cessation of illumination [in zebrafish, blood circulation is dispensable for survival up to 6 dpf (*20*)].

We observed that the sinoatrial region was more susceptible to NpHR manipulation than the working myocardium in the atrium and ventricle, most likely because the current densities across the cell membranes of CCS cells are smaller by a factor of >10 (*21*, *22*). To locate the pacemakers in a nonbiased way, we sequentially illuminated small, overlapping regions with constant intensity (Fig. 1C and movie S2). Maps showing the heart rate for every illuminated area were generated (Fig. 1D and fig. S4) to identify regions in which NpHR activation induced cardiac arrest or

[1]Department of Physiology, University of California, San Francisco, CA 94158, USA. [2]Department of Biochemistry and Biophysics and Cardiovascular Research Institute, University of California, San Francisco, CA 94158, USA. [3]Institute of Biology 1, University of Freiburg, 79104 Freiburg, Germany. [4]Max Planck Institute of Molecular Cell Biology and Genetics, 01307 Dresden, Germany.

*To whom correspondence should be addressed. E-mail: didier.stainier@ucsf.edu

Downloaded from www.sciencemag.org on November 11, 2010

ventricular arrhythmia. Pattern generation, data recording, and video analysis were automated and computer-controlled to enable fast and reproducible analysis of a large number of hearts (*23*).

To follow the maturation of the CCS over embryonic and larval development, we generated heart rate maps for five stages (1 dpf to 5 dpf; n = 3 to 15 hearts analyzed, mean 7.4 per stage) from different angles. In 1-dpf animals, the heart stopped beating when a large region at the venous pole of the heart was illuminated at medium light intensities (Fig. 2A). At higher light intensities, it was possible to block the heartbeat by illuminating different smaller patches of the venous pole (fig. S5A). This observation indicates that strong electrical coupling seemed to be present and suggests that at this stage the cells required to initiate the heartbeat (pacemaker cells) cover a large area at the venous pole.

In 2-dpf animals, the pacemaker region was more confined to the sinoatrial ring (SAR; Fig. 2B and fig. S5B). Although no consistent bias was found, individual hearts were more easily arrested by illuminating the right part of the SAR (right-biased: 8 hearts, left-biased: 5 hearts). Illumination of large areas adjacent to the pacemaker region did not arrest the heart (movies S3 to S5), indicating that the silencing effect did not spread farther than one or two cell diameters outside the illuminated area.

The atrioventricular canal (AVC) is formed at 2 dpf (*24*). At this stage, AV blocks were induced with high illumination intensities at the AVC; from 3 to 5 dpf, lower light intensities were sufficient to block ventricular systoles. No bias was detected around the AVC perimeter, which suggests that all AVC cells contribute equally to the conduction of the beat from the atrium to the ventricle. It has been shown that upon ablation of the primary pacemaker, downstream pacemakers such as the AV node can take over to maintain heartbeat (*25*). In our experiments, beating was always blocked when the SAR was silenced; this result implies that pacemaker currents outside the SAR are not strong enough to drive the larval heart immediately after SAR silencing.

The pacemaker region became further defined at 3 dpf (Fig. 2C and fig. S5C). The cells required to initiate the heartbeat were confined to the dorsal right quadrant of the SAR in 10 of the 13 hearts investigated, as revealed by mapping the heart from different angles. A refinement of the pacemaker area during development has also been reported in other species, where it narrows to a small region as it migrates from the atria to the right sinus primordium (*3*). In amniotes, the pacemaker is generally situated on the right side, which matches our findings in zebrafish. Furthermore, the center of the region appeared to be located about 10 μm (one or two cell diameters) farther anterior than the neck of the SAR (Fig. 2D). Interestingly, the cells that make up the lips of the sinus adjacent to the SAR appear to have an intrinsic pacemaking capability and poor coupling to the SAR, because they continued to contract in the arrested heart (movie S6), and photosilencing their contractions did not arrest the heart. The number of cells required for beating varied between animals. The size of the illuminated area generally corresponded to 10 to 30 cells, but some hearts could be arrested by illuminating very few cells (3 cells, movies S7 and S8). At 4 and 5 dpf, the pacemaker cells remained at the same relative position (Fig. 2, D and E, and fig. S5, D and E).

The zebrafish heart can be manipulated very precisely to rapidly switch between a healthy and a diseased state. We generated prominent cardiac pathologies such as AV blocks, tachycardia, and bradycardia. When illuminating the AVC (Fig. 3A), we induced different AV blocks by varying the light intensity. At high intensities, 3:1 or 4:1 AV blocks could be induced (Fig. 3, B and C); medium intensities caused 2:1 AV blocks (movie S9). Notably, the 2:1 AV block was stable over a

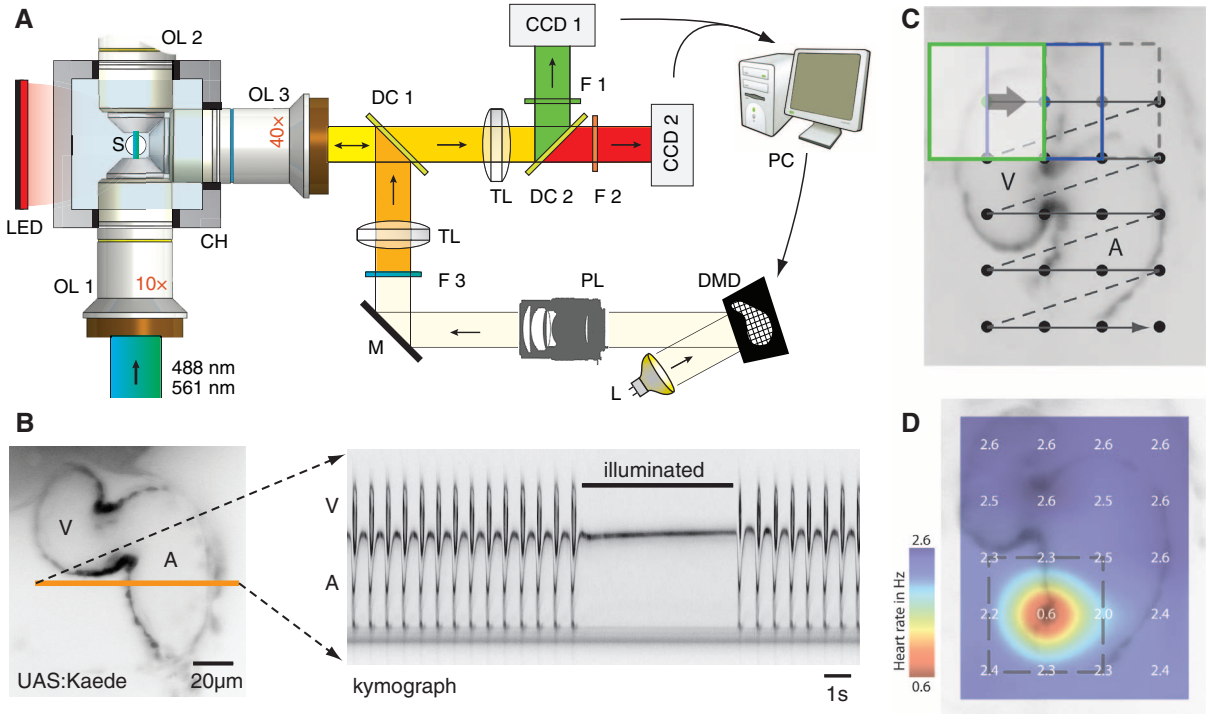

Fig. 1. Automated mapping of the cardiac pacemaker using patterned illumination in an mSPIM. (**A**) Microscope layout. A sheet of laser light (488 nm or 561 nm) illuminates the embedded fish (S) through objective lens OL1 or OL2. A computer-generated pattern is reflected off the digital micromirror device (DMD) and imaged onto the sample (S) through the detection lens OL3. See fig. S3 for details. LED, light-emitting diode (transmission); CH, chamber; DC, dichroic mirror; TL, tube lens; F, filter; M, mirror; PL, photographic lens; L, light bulb; CCD, charge-coupled device (camera). (**B**) A 3-dpf zebrafish heart expressing NpHR-mCherry stopped beating when illuminated with orange light and recovered instantaneously afterward. A high-speed video of an optical section was obtained by low-intensity light-sheet illumination. The kymograph shows the motion of the heart wall along the highlighted line. V, ventricle; A, atrium. The animal was transgenic for *Et(E1b:Gal4-VP16)s1101t*, *Tg(UAS:NpHR-mCherry)s1989t*, and *Tg(UAS:Kaede)s1999t*. Dark coloration corresponds to high Kaede fluorescence (inverted image). See movie S1. (**C**) The whole heart was sequentially illuminated with overlapping squares (see movie S2). (**D**) False-color image of the observed atrial heart rate after illumination of 20 sampled areas (ventral view, with head pointing upward). In this 3-dpf fish, the pacemaker cells are located in the dorsal-right side of the inflow ring.

Downloaded from www.sciencemag.org on November 11, 2010

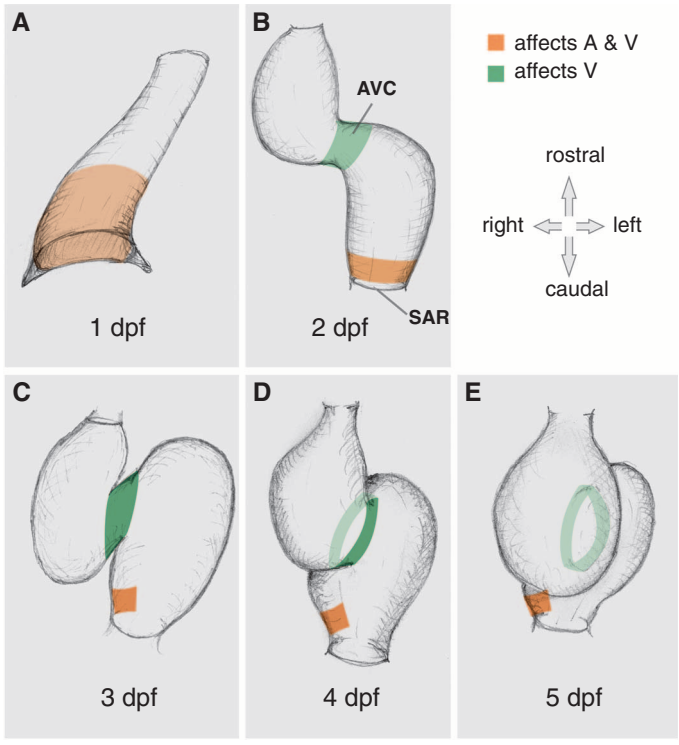

Fig. 2. Localization of the areas sensitive to hyperpolarization at the inflow and atrioventricular canal (AVC) regions of 1- to 5-dpf hearts. (**A** to **E**) Schematic drawings of the pacemaker (red) and AVC (green) regions for the developmental stages indicated SAR, sinoatrial region.

range of intensities (55 to 95% maximal light intensity; see vertical lines in Fig. 3C) and for prolonged periods of time (50 s; Fig. 3C). The induction of different AV blocks was reproducible in many different hearts (Fig. 3D), although the required light intensity varied between hearts, probably because of the varying expression levels of NpHR. In some hearts, a complete block of ventricular beats could be produced with high light intensities (movie S9).

Periodic photoactivation of the SAR with ChR2 (Fig. 3E) was used to control the heart rate in 4-dpf animals within the frequency range 2.7 to 4.7 Hz (Fig. 3F; heart rate before perturbation was 3.3 Hz). Above 4.7 Hz, atrial contractions started to skip pulses and became variable, suggesting that the heart rate cannot be sustained at such high frequency. Interestingly, our method enabled a reduction in heart rate, a modulation that was not reported in a recent study using a different laser-based stimulation technique (*26*).

In vertebrate hearts, the conduction direction is determined by the beating rates of primary (faster) and downstream (slower) pacemakers. Retrograde excitation has been reported in the zebrafish heart (*27*), and we were interested to know whether it could be forced to beat regularly in the retrograde

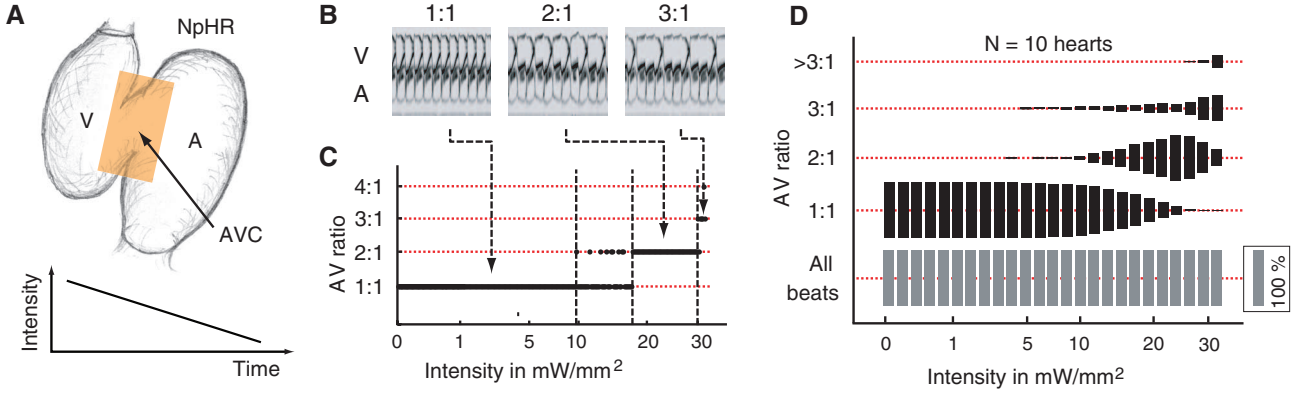

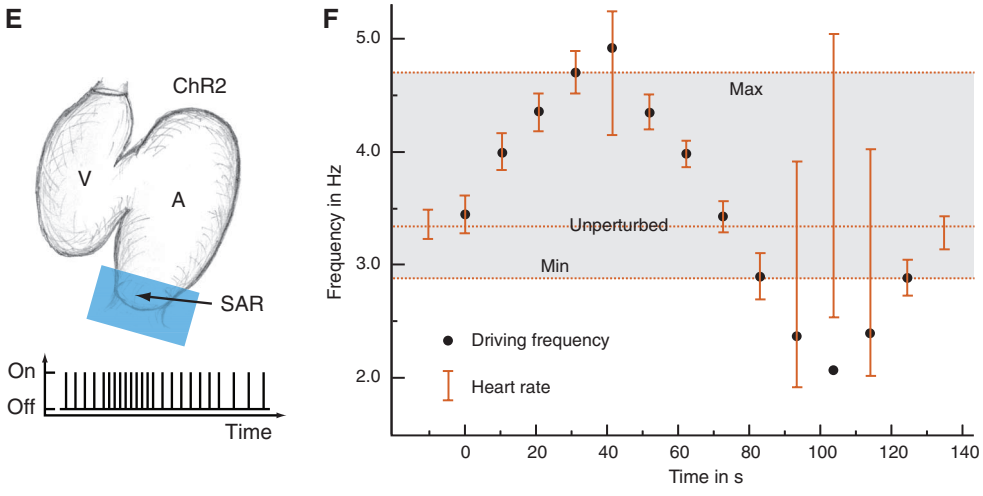

Fig. 3. Optically induced atrioventricular arrhythmia, tachycardia, and bradycardia. (**A** to **D**) Ventricular blocks of different severity are induced by illuminating the AVC with well-defined intensities. (A) Schematic of the spatial and temporal pattern of illumination. The atrioventricular ring in NpHR-expressing hearts was illuminated with slowly decreasing intensity. (B) Kymograph and (C) AV ratio for different illumination intensities. High intensities induced a 3:1 block, medium intensities a 2:1 block. (D) Summary for 10 different hearts. See movie S9. (**E**) Schematic of the region and temporal pattern of illumination. The sinoatrial ring in ChR2 expressing hearts was illuminated with short pulses with varying frequency. (**F**) The heart rate (brown bars) relative to the driving frequency (black dots) during the course of the experiment. The heart rate followed the driving frequency within the indicated dynamic range (between Min and Max). Error bars represent SD. See movie S10. A, atrium; V, ventricle; AVC, atrioventricular canal; SAR, sinoatrial ring.

Downloaded from www.sciencemag.org on November 11, 2010

direction. We applied light pulses to a ventricular region close to the bulbus to rhythmically activate ChR2 and found that cardiac conduction could be reversed (movie S11 and fig. S6) for at least 30 consecutive heartbeats.

Our results show that a surprisingly small number of pacemaker cells is indispensable for heartbeat initiation. This makes the embryonic heart very vulnerable, as no compensating mechanism seems to be in place on the time scales observed. Moreover, we have shown that this area can be optically targeted; our photostimulation methods allowed us to optically control heart rate, reverse cardiac conduction, and induce disease-like states in a reversible manner. This work opens a new avenue for controlling hemodynamic forces during studies on epigenetic factors of heart formation (*28*) and blood vessel development (*29*).

References and Notes

1. T. Mikawa, R. Hurtado, *Semin. Cell Dev. Biol.* **18**, 90 (2007).
2. M. R. Jongbloed, E. A. Mahtab, N. A. Blom, M. J. Schalij, A. C. Gittenberger-de Groot, *ScientificWorldJournal* **8**, 239 (2008).
3. K. Kamino, A. Hirota, S. Fujii, *Nature* **290**, 595 (1981).
4. D. Sedmera *et al.*, *Am. J. Physiol. Heart Circ. Physiol.* **284**, H1152 (2003).
5. N. C. Chi *et al.*, *PLoS Biol.* **6**, e109 (2008).
6. F. Zhang *et al.*, *Nature* **446**, 633 (2007).
7. M. Scanziani, M. Häusser, *Nature* **461**, 930 (2009).
8. L. Luo, E. M. Callaway, K. Svoboda, *Neuron* **57**, 634 (2008).
9. A. D. Douglass, S. Kraves, K. Deisseroth, A. F. Schier, F. Engert, *Curr. Biol.* **18**, 1133 (2008).
10. S. Szobota *et al.*, *Neuron* **54**, 535 (2007).
11. C. Wyart *et al.*, *Nature* **461**, 407 (2009).
12. H. Baier, E. K. Scott, *Curr. Opin. Neurobiol.* **19**, 553 (2009).
13. A. B. Arrenberg, F. Del Bene, H. Baier, *Proc. Natl. Acad. Sci. U.S.A.* **106**, 17968 (2009).
14. G. Nagel *et al.*, *Proc. Natl. Acad. Sci. U.S.A.* **100**, 13940 (2003).
15. E. K. Scott *et al.*, *Nat. Methods* **4**, 323 (2007).
16. O. G. Ayling, T. C. Harrison, J. D. Boyd, A. Goroshkov, T. H. Murphy, *Nat. Methods* **6**, 219 (2009).
17. J. Huisken, J. Swoger, F. Del Bene, J. Wittbrodt, E. H. Stelzer, *Science* **305**, 1007 (2004).
18. P. J. Scherz, J. Huisken, P. Sahai-Hernandez, D. Y. Stainier, *Development* **135**, 1179 (2008).
19. J. Huisken, D. Y. Stainier, *Opt. Lett.* **32**, 2608 (2007).
20. A. J. Sehnert *et al.*, *Nat. Genet.* **31**, 106 (2002).
21. R. Wilders, *Conf. Proc. IEEE Eng. Med. Biol. Soc.* **2007**, 152 (2007).
22. A. Nygren *et al.*, *Circ. Res.* **82**, 63 (1998).
23. See supporting material on *Science* Online.
24. D. Beis *et al.*, *Development* **132**, 4193 (2005).
25. D. Scherf, *Z. Gesamte Exp. Med.* **57**, 188 (1927).
26. M. W. Jenkins *et al.*, *Nat. Photonics* **4**, 623 (2010).
27. D. J. Milan, A. C. Giokas, F. C. Serluca, R. T. Peterson, C. A. MacRae, *Development* **133**, 1125 (2006).
28. J. R. Hove *et al.*, *Nature* **421**, 172 (2003).
29. C. Hahn, M. A. Schwartz, *Nat. Rev. Mol. Cell Biol.* **10**, 53 (2009).

30. We thank T. Mikawa, R. Shaw, and A. Müssigbrodt for feedback and comments on the manuscript. Supported by NIH grant HL54737 (D.Y.R.S.), the Packard Foundation (D.Y.R.S.), NIH grant R01 NS053358 (H.B.), a Sandler Opportunity Award, the Byers Award for Basic Science (H.B.), and the NIH Nanomedicine Development Center "Optical Control of Biological Functions" (H.B.). J.H. was supported by a Human Frontier Science Program (HFSP) cross-disciplinary fellowship. A.B.A. was supported by a Boehringer Ingelheim Fonds (B.I.F.) and a Krevans fellowship. The optogenetic idea, transgenic lines, and original observation originated in H.B.'s lab; follow-up experiments were carried out in D.Y.R.S.'s lab as an equal collaboration between A.B.A. and J.H. All authors worked on the manuscript, which was drafted by A.B.A. and J.H.

Supporting Online Material

www.sciencemag.org/cgi/content/full/330/6006/971/DC1
Materials and Methods
Figs. S1 to S7
Movies S1 to S11

2 August 2010; accepted 1 October 2010
10.1126/science.1195929

Kinetic Scaffolding Mediated by a Phospholipase C–β and G_q Signaling Complex

Gary L. Waldo,[1] Tiffany K. Ricks,[1] Stephanie N. Hicks,[1] Matthew L. Cheever,[1] Takeharu Kawano,[2] Kazuhito Tsuboi,[2] Xiaoyue Wang,[3] Craig Montell,[3] Tohru Kozasa,[2,4] John Sondek,[1,5,6] T. Kendall Harden[1,6]*

Transmembrane signals initiated by a broad range of extracellular stimuli converge on nodes that regulate phospholipase C (PLC)–dependent inositol lipid hydrolysis for signal propagation. We describe how heterotrimeric guanine nucleotide–binding proteins (G proteins) activate PLC-βs and in turn are deactivated by these downstream effectors. The 2.7-angstrom structure of PLC-β3 bound to activated $G\alpha_q$ reveals a conserved module found within PLC-βs and other effectors optimized for rapid engagement of activated G proteins. The active site of PLC-β3 in the complex is occluded by an intramolecular plug that is likely removed upon G protein–dependent anchoring and orientation of the lipase at membrane surfaces. A second domain of PLC-β3 subsequently accelerates guanosine triphosphate hydrolysis by $G\alpha_q$, causing the complex to dissociate and terminate signal propagation. Mutations within this domain dramatically delay signal termination in vitro and in vivo. Consequently, this work suggests a dynamic catch-and-release mechanism used to sharpen spatiotemporal signals mediated by diverse sensory inputs.

Phospholipase C (PLC) catalyzes the hydrolysis of phosphatidylinositol 4,5-bisphosphate [PtdIns(4,5)P_2] to the second messengers inositol 1,4,5-trisphosphate [Ins(1,4,5)P_3] and diacylglycerol in an essential step for the physiological action of many hormones, neurotransmitters, growth factors, and other extracellular stimuli (*1*–*3*). These cascades use signaling complexes consisting of Gα subunits of the G_q family ($G\alpha_q$, 11, 14, and 16) of heterotrimeric guanine nucleotide–binding proteins (G proteins) and PLC-β isozymes (β1-4) (*4*–*6*). Agonist-stimulated receptors increase exchange of guanosine triphosphate (GTP) for guanosine diphosphate (GDP) on $G\alpha_q$, GTP-bound $G\alpha_q$ engages and activates PLC-β, and PLC-β increases up to three orders of magnitude the rate of hydrolysis of GTP by its activating G protein (*7*–*9*). Coordination from upstream and downstream inputs sharpens time frame, amplitude, and on-off cycling of these signaling nodes. Although kinetic analyses revealed much about the dynamics of $G\alpha_q$/PLC-β signaling complexes (*10*–*12*), how PLC-βs simultaneously act as effectors and GTPase activating proteins (GAPs) has remained unknown. Here, we describe the structure of PLC-β3 in an activated complex with $G\alpha_q$, which together with supporting biochemical and physiological analyses reveals its mechanism of transmembrane signaling.

The three-dimensional structure of an AlF_4^--dependent complex of $G\alpha_q$ bound to PLC-β3 was solved by molecular replacement using PLC-β2 [Protein Data Bank (PDB) code 2FJU] and $G\alpha_q$ (PDB 2BCJ) as search models and refined at 2.7-Å resolution (table S1). PLC-β3 engages $G\alpha_q$ through three distinct regions (Fig. 1, A and B). First, an extended loop between the third and fourth EF hands of PLC-β3 directly buttresses switch residues critical for GTP hydrolysis by $G\alpha_q$. Second, the region of PLC-β3 that connects the catalytic TIM barrel and the C2 domain interacts with both switches 1 and 2 of $G\alpha_q$. Third, a segment composed of a helix-turn-helix at the C terminus of the C2 domain resides primarily within a shallow declivity on the surface of $G\alpha_q$ formed by switch 2 and α3. Other effectors are known to engage this region within Gα subunits (Fig. 1C). GTP hydrolysis by Gα subunits is independently accelerated by a large family of regulator of G protein signaling (RGS) proteins (*8*, *13*, *14*), and PLC-β3 interacts with a surface on $G\alpha_q$ that overlaps almost completely with portions of Gα subunits needed for engagement of RGS proteins (Fig. 1C). Consistent with a biologically relevant interface (*15*), the complex

[1]Department of Pharmacology, University of North Carolina School of Medicine, Chapel Hill, NC 27599, USA. [2]Department of Pharmacology, University of Illinois, Chicago, IL 60612, USA. [3]Departments of Biological Chemistry and Neuroscience, Center for Sensory Biology, Johns Hopkins University School of Medicine, Baltimore, MD 21205, USA. [4]Laboratory for Systems Biology and Medicine, Research Center for Advanced Science and Technology, University of Tokyo, Tokyo 153-8904, Japan. [5]Department of Biochemistry, University of North Carolina School of Medicine, Chapel Hill, NC 27599, USA. [6]Lineberger Cancer Center, University of North Carolina School of Medicine, Chapel Hill, NC 27599, USA.

*To whom correspondence should be addressed. E-mail: tkh@med.unc.edu

Downloaded from www.sciencemag.org on November 11, 2010

of PLC-β3 and $G\alpha_q$ buries ~3200 Å^2 of solvent-exposed surface area.

Activated $G\alpha_q$ does not impinge on the active site of PLC-β3 and indeed is at least 40 Å from the calcium ion cofactor needed for PtdIns(4,5)P_2 catalysis. Comparison of the structure of PLC-β3 in complex with $G\alpha_q$ to previous structures (*16*, *17*) of PLC-β2 indicates that lipase activation does not involve $G\alpha_q$-dependent propagation of a conformational change to the active site of the lipase (fig. S1A). Indeed, the active site of PLC-β3 is occluded by a portion of its X/Y linker (Fig. 1B): a poorly conserved loop that separates the two halves of the catalytic TIM barrel in all PLC isozymes. Our previous structural analyses illustrated that this region similarly occludes the active site of PLC-β2, and deletion of the negatively charged X/Y linker in PLC-β2, as well as in PLC-ε and -δ1, resulted in marked activation (*17*). Similarly, deletion of the highly negatively charged X/Y linker of PLC-β3 caused a large increase in lipase activity (fig. S1B), indicating that PLC-β3 also is robustly autoinhibited by its X/Y linker. Presumably, this region of PLC-β3 is forced out of the active site by steric and electrostatic repulsion mediated by the surface of the plasma membrane coupled to the engagement of $G\alpha_q$ (Fig. 1D). A similar mechanism was proposed previously for activation of PLC-β2 by Rac1, which binds entirely through the PH domain of PLC-β2 at substantial distance from the active site of the lipase (*16*). Consequently, $G\alpha_q$, Rac1, and likely other activators such as Gβγ activate PLC isozymes by anchoring and orienting them at substrate membranes to release autoinhibition by the X/Y linker and promote access of PtdIns(4,5)P_2 to the lipase active site.

PLC-β isozymes are effectors of $G\alpha_q$ as well as GAPs that enhance the intrinsic GTPase activity of the engaging Gα subunits. The structure of activated $G\alpha_q$ bound to PLC-β3 explains the integration of these reciprocal functions.

The catalytic core of the 13 mammalian PLC isozymes includes a pleckstrin homology (PH) domain, a set of four EF hands, a catalytic TIM barrel, and a C2 domain (*18*) (Fig. 1A). The canonical Gα effector-binding region of $G\alpha_q$, located between α3 and switch 2, is occupied by a helix-turn-helix (Hα1/Hα2) that immediately follows the C2 domain of PLC-β3 (Fig. 2A). PLC-δ isozymes terminate immediately after their C2 domain, which is the last common domain found in all PLC isozymes (*18*). Thus, grafting of Hα1/Hα2 onto the C terminus of the C2 domain of PLC-β3 provides a large binding surface that makes numerous contacts with $G\alpha_q$ (~1750 Å^2 of solvent accessible surface area buried). Only PLC-β isozymes are activated by $G\alpha_q$, and the highly conserved Hα1/Hα2 motif is found in all PLC-βs (Fig. 2B) but not in other PLC isozymes. PLC-βs also contain a long C-terminal region that extends about 300 residues past the Hα1/Hα2 module. This long C-terminal extension previously was thought to be important for interaction with $G\alpha_q$. However, absence of this region did not affect high affinity binding

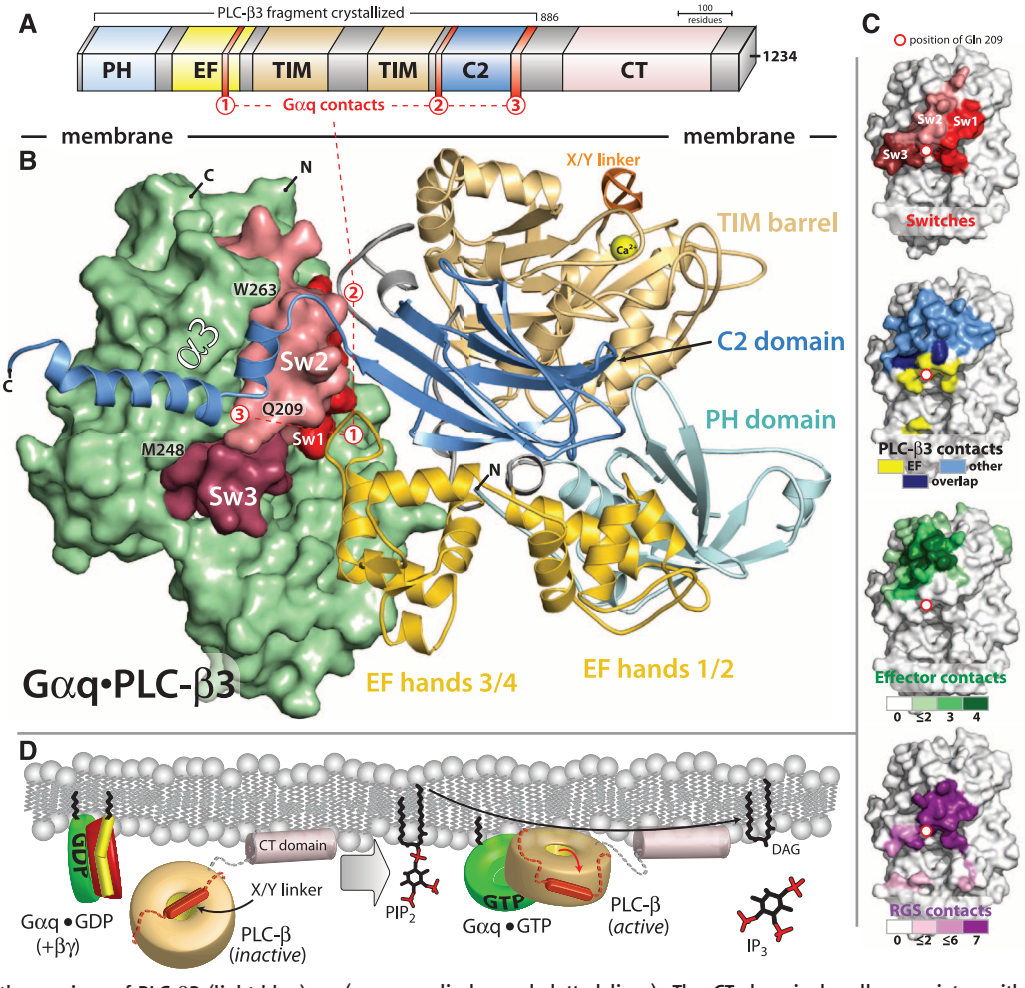

Fig. 1. Structure of $G\alpha_q$•PLC-β3. (**A**) Domain architecture of PLC-β3 drawn to scale and consisting of a N-terminal PH domain, a series of four EF hands, a catalytic TIM barrel, a C2 domain, and a carboxy-terminal (CT) domain. The CT domain is not necessary for $G\alpha_q$ binding (fig. S2), and, therefore, PLC-β3 truncated at residue 886 was used to facilitate crystallization. Three distinct regions of PLC-β3 that interact with G_q are indicated by red numerals. (**B**) Overall structure of the AlF_4^--dependent complex of $G\alpha_q$•PLC-β3 as viewed from the plane of the membrane. PLC-β3 is depicted as a ribbon cartoon with domains colored as in (A). Activated $G\alpha_q$ is depicted as a green surface with nucleotide-dependent switches (Sw1 to Sw3) in shades of red. Hα1/Hα2 (red 3) at the end of the C2 domain of PLC-β3 lies within the canonical effector-binding region of $G\alpha_q$ formed by α3 starting at M248 (*21*), the subsequent loop containing W263, and switch 2 containing Q209. The X/Y linker (orange) connects the two halves of the catalytic TIM barrel, and an ordered portion of the linker occludes the active site of the lipase highlighted by the Ca^{2+} (yellow ball) cofactor. (**C**) Surfaces of $G\alpha_q$ highlighting switches (top) in comparison to regions (lower images) of Gα subunits that interact with PLC-β3, other effectors, and RGS proteins. Interactions involving the EF3/4 loop are yellow except for overlap (dark blue) involving other regions of PLC-β3 (light blue). Gα subunits use a common interface (green) to engage four distinct effectors, and a different interface engages seven distinct RGS proteins (dark purple). Details of the analyses are supplied in (*41*). (**D**) Model for activation of PLC-β3 by GTP-activated $G\alpha_q$. $G\alpha_q$ (green) bound to GDP is sequestered by Gβγ (red and yellow) and does not interact with PLC-β, depicted as a gold toroid except for its CT domain (light pink) and X/Y linker (orange cylinder and dotted lines). The CT domain basally associates with membranes, whereas the X/Y linker blocks the lipase active site. Upon activation of heterotrimeric G_q, $G\alpha_q$-GTP dissociates from Gβγ and interacts with the main portion of PLC-β. Complex formation anchors and orients the lipase active site at membranes, leading to repulsion of the X/Y linker and freeing the active site for hydrolysis of PtdIns(4,5)P_2 into diacylglycerol (DAG) and Ins(1,4,5)P_3 (IP_3).

Downloaded from www.sciencemag.org on November 11, 2010

of PLC-β3 to $G\alpha_q$ [dissociation constant (K_d) ~ 200 nM; fig. S2], and it is not present in the PLC-β3 construct used for structure determination. The C-terminal domain is important for membrane association, but whether it has additional function(s) in the signaling complex remains unclear.

Pro^{862} of PLC-β3 lies within the turn between Hα1 and Hα2, makes extensive contacts with multiple residues of $G\alpha_q$, and forms the center of a $G\alpha_q$-binding interface (Fig. 2A). The side chain of the preceding Asn^{861} supports this turn by forming a hydrogen bond with the backbone amide of Lys^{864}. This Asn-Pro couplet is preserved in three of the four PLC-β isozymes (it is Asp-Pro in PLC-β4) and presumably defines the turn because of helix capping and breaking propensities of Asn/Asp and Pro, respectively. The turn is bracketed by Leu^{859}, which inserts into a hydrophobic pocket formed by residues in α3 and switch 2, and by Ile^{863}, which interacts with tandem glutamates in α3. Tyr^{855} in Hα1 and Asp^{870} in Hα2 also support the binding interface at the periphery. The binding of $G\alpha_q$ to Hα1/Hα2 of PLC-β3 recapitulates almost entirely the interaction of $G\alpha_q$ with several guanine nucleotide exchange factors (GEFs) for Rho, including p63RhoGEF, Trio, and Kalirin, which use a helix-turn-helix grafted onto the end of a DH/PH cassette to bind the α3/Sw2 declivity of $G\alpha_q$ (*19*, *20*) (Fig. 2C). PLC-β3 and p63RhoGEF use identical residues in their primary interfaces with $G\alpha_q$, and other effectors also engage this region of Gα subunits in similar fashion (Fig. 2C).

The role of Hα1/Hα2 residues in $G\alpha_q$-mediated activation was examined by mutational analyses. Whereas expression of $G\alpha_q$ or PLC-β3 alone in COS-7 cells had no effect, their coexpression resulted in a large increase in inositol lipid hydrolysis (fig. S3A). In contrast, coexpression of PLC-β3 with mutation $L^{859}\rightarrow E^{859}$ (*21*) [PLC-β3(L859E)] with $G\alpha_q$ had no effect over a broad range of conditions (fig. S3B). Gβγ independently activates PLC-β3, and coexpression of either PLC-β3 or PLC-β3(L859E) with $G\beta_1\gamma_2$ resulted in similar levels of activation (fig. S3C). Mutation of the analogous residue (Leu^{810}) in PLC-β1 also completely abrogated $G\alpha_q$-dependent stimulation (fig. S3D).

The contribution of residues across Hα1/Hα2 of PLC-β3 was examined (Fig. 2D and fig. S4). In each case, the relative sensitivity of the PLC-β3 mutant to activation by $G\alpha_q$ versus $G\beta_1\gamma_2$ was compared under conditions where maximal response to each activator was observed. Whereas single substitutions throughout Hα1/Hα2 did not affect Gβγ-stimulated activity (fig. S4), certain of these mutations (Y855A, L859A, N861A, P862A, and I863A) resulted in substantial or complete loss of the capacity of $G\alpha_q$ to promote PLC-β3–dependent increases in inositol phosphate accumulation (Fig. 2D).

The binding and lipase activities of PLC-β3 mutants also were tested by using purified proteins (fig. S5). PLC-β3, PLC-β3(L859E), and

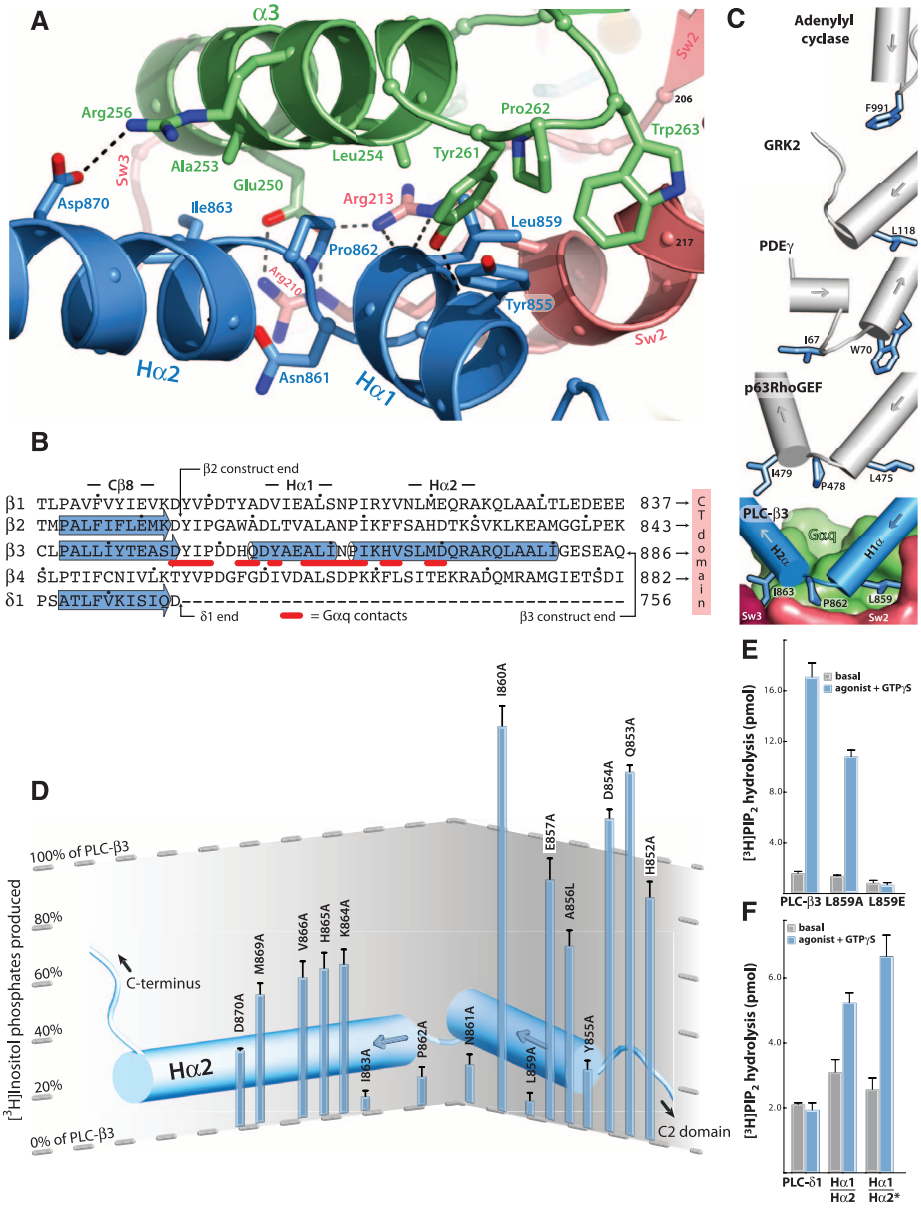

Fig. 2. Structure of the effector binding interface of $G\alpha_q$•PLC-β3. (**A**) Ribbon diagram of the interface between the Hα1/Hα2 region of PLC-β3 (blue) and the effector binding pocket of $G\alpha_q$ located between α3 (green) and Sw2 (pink). Interfacial residues (sticks) are labeled; hydrogen bonds are indicated by dashed lines. (**B**) Comparison of PLC sequences (*21*) at the end of the C2 domain (Cβ8) encompassing Hα1/Hα2. α helices (cylinders) and β sheets (arrows) were assigned by using crystal structures of PLC-β3 as reported here (PDB 3OHM), PLC-β2 (2ZKM), and PLC-δ1 (1DJX). C termini are indicated for full-length PLC-δ1 as well as the crystallized fragments of PLC-β2 and -β3. Residues in PLC-β3 that interact with $G\alpha_q$ are underlined in red. Dots indicate every 10th residue. (**C**) Comparison of effectors bound to Gα subunits. The major effector binding surface of $G\alpha_q$ (green with switches in red) engages Hα1/Hα2 (blue cylinders) of PLC-β3 through indicated residues (sticks) surrounding Pro^{862}. Structurally analogous α helices (gray cylinders) and residues (blue sticks) in other effectors are highlighted after superimposition of bound Gα subunits (not shown). PDE-γ, cyclic GMP phosphodiesterase-γ. (**D**) Mutational analyses of Hα1/Hα2. PLC-β3 mutants harboring the indicated single substitutions were assessed for capacity to be activated upon cotransfection with $G\alpha_q$ in COS-7 cells as measured by [^{3}H]inositol phosphate production. Further experimental details are described in figs. S3, A to C, and S4. (**E**) Requirement of Hα1/Hα2 for activation of PLC-β3 by $G\alpha_q$ assessed with purified proteins. [^{3}H]PtdIns(4,5)P_2-containing phospholipid vesicles reconstituted with purified $P2Y_1$ receptor, $G\alpha_q$, and $G\beta_1\gamma_2$ were used to assess the capacity of wild-type or PLC-β3 mutants (300 nM) to hydrolyze PtdIns(4,5)P_2 in the absence (basal) or presence of a $P2Y_1$ receptor agonist (2MeSADP, 1 μM) plus 100 nM GTPγS (agonist + GTPγS). Data are mean ± SEM from four independent experiments. (**F**) Grafting Hα1/Hα2 onto PLC-δ1 confers responsiveness to $G\alpha_q$. Activities of purified proteins were compared as in (E). Residues 847 to 886 of PLC-β3 were added to the end of PLC-δ1 to create PLC-δ1(Hα1/Hα2); starred variant consists of PLC-δ1(Hα1/Hα2) with additional substitutions (D610R and N612D) of PLC-δ1 to analogous PLC-β3 residues (see domain architectures in fig. S7A).

Downloaded from www.sciencemag.org on November 11, 2010

PLC-β3(L859A) exhibited similar basal lipase activities (fig. S5A) and were similarly activated by $G\beta_1\gamma_2$ (fig. S5B). However, the binding affinity of PLC-β3(L859A) for $G\alpha_q$ in the presence of AlF_4^- was sevenfold lower than PLC-β3, and no AlF_4^--dependent binding of PLC-β3(L859E) was observed (fig. S5C). Activities of PLC-β3 isozymes mutated in Hα1/Hα2 also differed markedly in a signaling complex reconstituted with purified $P2Y_1$ receptor, heterotrimeric G_q, and PLC-β3. The $P2Y_1$ receptor agonist, 2MeSADP, promoted robust activation of PLC-β3, but PLC-β3(L859E) was completely refractory to activation and intermediate activation was observed with PLC-β3(L859A) (Fig. 2E).

Alanine-scanning mutagenesis previously identified two small segments (residues 243 to 245 and 256 to 257) of $G\alpha_q$ necessary for elevated production of inositol phosphates (*22*). These regions contribute to interactions with Hα1/Hα2 (fig. S6A). Additional alanine substitutions were made in $G\alpha_q$, and, of those $G\alpha_q$ mutants that expressed as stable trypsin-resistant proteins, most exhibited a predictable loss in capacity to activate PLC-β3 (fig. S6B).

The loop between the end of the TIM barrel and the beginning of the C2 domain comprises a second distinct segment of PLC-β3 that makes extensive contacts with active $G\alpha_q$, including switches 1 and 2 (Fig. 3A). This interface includes a series of interdigitated pairs of charged residues, specifically (in PLC-β3/$G\alpha_q$) Asp^{709}/Arg^{202}, Lys^{710}/Glu^{191}, and Asp^{721}/Lys^{41}; these in turn are supported by additional charged residues (Glu^{703} and Arg^{707}) of PLC-β3. Alanine substitution of several of these residues in PLC-β3 compromised the capacity of $G\alpha_q$, but not $G\beta_1\gamma_2$, to activate PLC in COS-7 cells (Fig. 3B).

Residues adjacent to both borders of the C2 domain (Val^{724} and Tyr^{847}) converge to envelop His^{218} of $G\alpha_q$, which is wedged between the aforementioned interface and the start of Hα1/Hα2 to anchor two of the three major interfaces within the $G\alpha_q$•PLC-β3 complex (Fig. 3A). Mutation of His^{218} results in loss of capacity of $G\alpha_q$ to activate PLC-β3 (fig. S6B).

PLC-δ isozymes are not regulated by $G\alpha_q$, presumably because of lack of both Hα1/Hα2 and the $G\alpha_q$-interacting residues found in PLC-β isozymes between the TIM barrel and the C2 domain. Thus, we hypothesized that G protein–dependent regulation could be engineered into PLC-δ1 (fig. S7A). Surface plasmon resonance (SPR) analyses revealed that, whereas PLC-δ1 did not exhibit AlF_4^--dependent binding to $G\alpha_q$, introduction of the Hα1/Hα2 segment of PLC-β3 into PLC-δ1 conferred binding (fig. S7B). Moreover, receptor- and guanine nucleotide–stimulated lipase activity was observed with the chimeric isozymes but not PLC-δ1 (Fig. 2F), and the median effective concentration (EC_{50}) of GTPγS for activation of PLC-δ1(Hα1/Hα2) by GTPγS was 50 nM (fig. S7C). Thus, Hα1/Hα2 is a small, linear module used for functional engagement of $G\alpha_q$.

An extended loop between EF hands 3 and 4 of PLC-β3 interacts with the GTP-binding region of $G\alpha_q$ (Fig. 4A). This loop is highly conserved in all PLC-β isozymes, is not found in PLC-δ1 (Fig. 4B) or other PLC isozymes, and interacts with the active site of $G\alpha_q$. Asn^{260} of the EF3/4 loop promotes GTP hydrolysis by interaction with the side chain of Gln^{209} of $G\alpha_q$ (Fig. 4C), which rearranges during GTP hydrolysis to stabilize the transition state mimicked by GDP•AlF_4^-•H_20. Asn^{260} also interacts with Glu^{212} to stabilize switch 1 for GTP hydrolysis. The interactions of Asn^{260} of PLC-β3 with $G\alpha_q$ are recapitulated by a functionally equivalent asparagine in RGS9 (*23*) (Fig. 4C) and other RGS proteins (*24*, *25*).

Asn^{260} is positioned at the active site of $G\alpha_q$ as part of a tight turn (residue 260 to 264) of PLC-β3 that is stabilized by Glu^{261} and underpinned by an extensive series of hydrogen bonds principally mediated by Asp^{256} and Arg^{255} and Arg^{258} (Fig. 4A). These residues are highly conserved in all PLC-βs, as are Asn^{251} and Leu^{267}, which appear crucial in stabilizing the ends of the loop (Fig. 4B). The EF3/4 loop as well as other portions of EF hands 3 and 4 are disordered in the crystal structure of PLC-β2 (Fig. 4D). A likely scenario is that $G\alpha_q$ initially engages the EF3/4 loop of PLC-β3 to nucleate the underlying hydrogen bonding network and promote cooperative ordering of EF hands 3 and 4.

To directly examine the role of the EF3/4 region of PLC-β3 in mediating inactivation of its activating G protein, we quantified GTP hydrolysis by $G\alpha_q$ in the presence of purified PLC-β3 mutants (fig. S8A) by using phospholipid vesicles reconstituted with the $P2Y_1$ receptor and heterotrimeric G_q. In the presence of receptor agonist, PLC-β3 promoted up to 100-fold stimulation of GTP hydrolysis (Fig. 5A and fig. S8B), and activation occurred with an EC_{50} ~ 3 nM (table S2). A chimeric PLC-β3 replacing the EF3/4 loop with the analogous region of PLC-δ1 was severely crip-

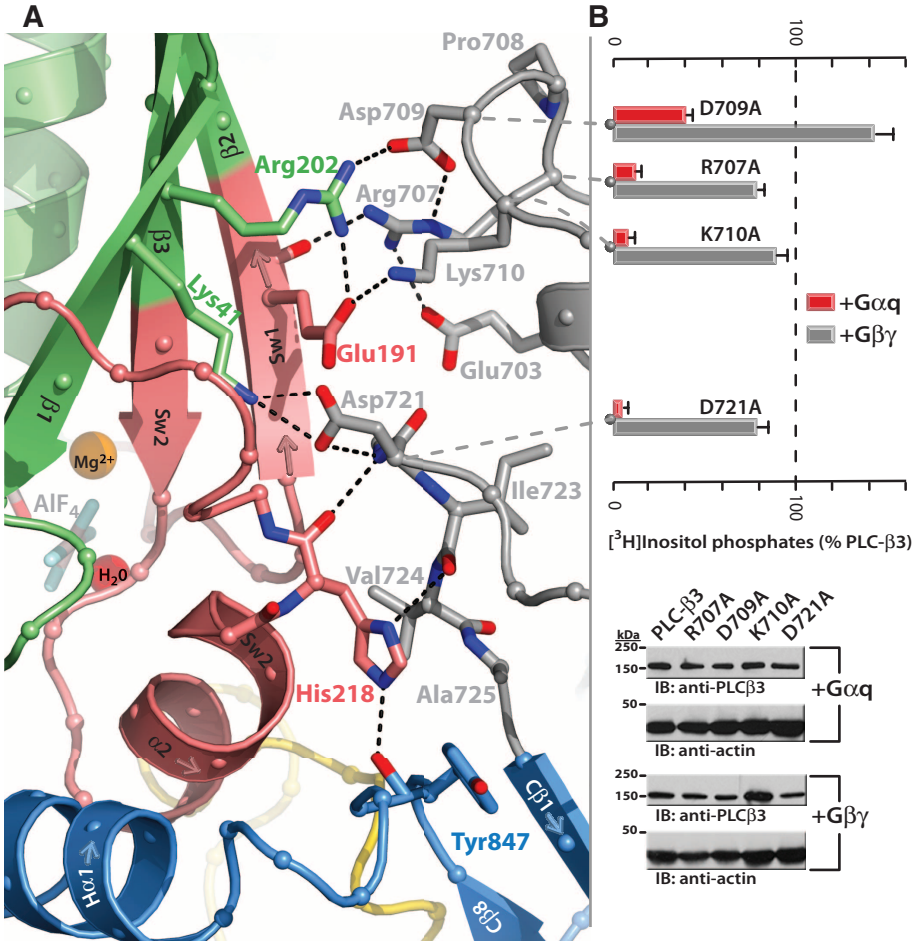

Fig. 3. Secondary $G\alpha_q$•PLC-β3 interface. (**A**) Ribbon diagram highlighting residues (gray) preceding the C2 domain (light blue) of PLC-β3 that interact with Sw1 and 2 (pink) of activated $G\alpha_q$ (green). AlF_4^- (gray cross-stick), Mg^{2+} (orange ball), and the catalytic water (red ball) within the nucleotide-binding pocket also are shown. (**B**) Mutational analysis of the $G\alpha_q$•PLC-β3 binding interface. (Top) Activation of the indicated mutants of PLC-β3 in the presence of cotransfected $G\alpha_q$ (red) or $G\beta_1\gamma_2$ (gray) was determined by quantification of [^{3}H]inositol phosphate accumulation in COS-7 cells. Data are mean ± SEM from four independent experiments. (Bottom) Relative expression of PLC-β3 and mutant forms was quantified under each transfection condition by using a PLC-β3–specific antibody. Actin immunoblots (IB) included as loading controls.

Downloaded from www.sciencemag.org on November 11, 2010

pled in its capacity to accelerate GTP hydrolysis by $G\alpha_q$ (Fig. 5A). Similarly, substitution of Asn^{260} dramatically reduced the capacity of PLC-β3 to promote GTP hydrolysis, whereas substitution of Val^{262} had negligible effect. Importantly, basal and Gβγ-stimulated lipase activities of these purified mutants were unaffected (fig. S8, A and C). The EC_{50} values of mutant and wild-type PLC-β3 for stimulation of GTP hydrolysis also were similar (table S2). In contrast, substitution of Leu^{859} to Ala^{859} within Hα1/Hα2, which reduced the binding affinity of the complex by ~sevenfold (fig S5C), also increased the EC_{50} for stimulation of GTP hydrolysis by ~10-fold (table S2). Thus, the EF3/4 loop of PLC-β3 is crucial for stimulation of GTP hydrolysis by $G\alpha_q$ but contributes minimally to forming the signaling complex.

Loss of capacity of PLC-β3 to promote GTP hydrolysis by $G\alpha_q$ should decrease its capacity to turn off subsequent to $G\alpha_q$-mediated activation. This idea was first tested in vitro with use of purified proteins. Addition of a $P2Y_1$ receptor antagonist (fig. S8, B and D) to an agonist preactivated signaling complex of the $P2Y_1$ receptor, heterotrimeric $G\alpha_q$, and wild-type PLC-β3 resulted in a rapid decline of lipase activity to levels similar to those observed in the absence of agonist (Fig. 5B). In contrast, little reversal of lipase activity occurred upon addition of $P2Y_1$ receptor antagonist to a similarly preactivated complex containing PLC-β3(δEF) (Fig. 5B).

Rhodopsin-initiated phototransduction in *Drosophila melanogaster* is mediated by $G\alpha_q$-dependent activation of PLC-β (*26*). To examine the role of the EF3/4 loop of PLC-β in a physiological system, we replaced wild-type PLC-β (NORPA) in *Drosophila* with a version mutated to alanine in the conserved Asn (N262) demonstrated above to be required for PLC-β-promoted GTP hydrolysis by $G\alpha_q$. Flies expressing wild-type NORPA or $NORPA^{N262A}$ exhibited similar amplitudes of the light-induced photoresponse (Fig. 5C). In contrast, whereas termination of light resulted in rapid termination of photoresponse in wild-type flies, we observed a marked defect in recovery with $norpA^{N262A}$.

PLC-β3 is a tumor suppressor, and its disruption in humans contributes to lymphomas and other myeloid malignancies (*27*, *28*). Similarly, $G\alpha_q$ is an oncogene, and its constitutive activation drives ~50% of all uveal melanomas (*29*). Signaling through the $G\alpha_q$/PLC-β axis is important for regulation of cell proliferation, and other disruptions in this node can be expected to contribute to cancer. In this regard, homozygous substitution of Arg^{254} within the EF3/4 loops of PLC-β4 was found in a pancreatic tumor during genome-wide profiling (*30*). The equivalent substitution in PLC-β3 resulted in a decrease in capacity to accelerate GTP hydrolysis by $G\alpha_q$ (Fig. 5D and fig. S8E).

The high-resolution structure of $G\alpha_q$•PLC-β highlights a dynamic interplay between regions of the complex needed to coordinate rapid activation and inactivation of this signaling node required for highly responsive, low-noise signal transduction. We propose that a conformationally flexible Hα1/Hα2 samples a relatively large volume to maximize probability of encounter-

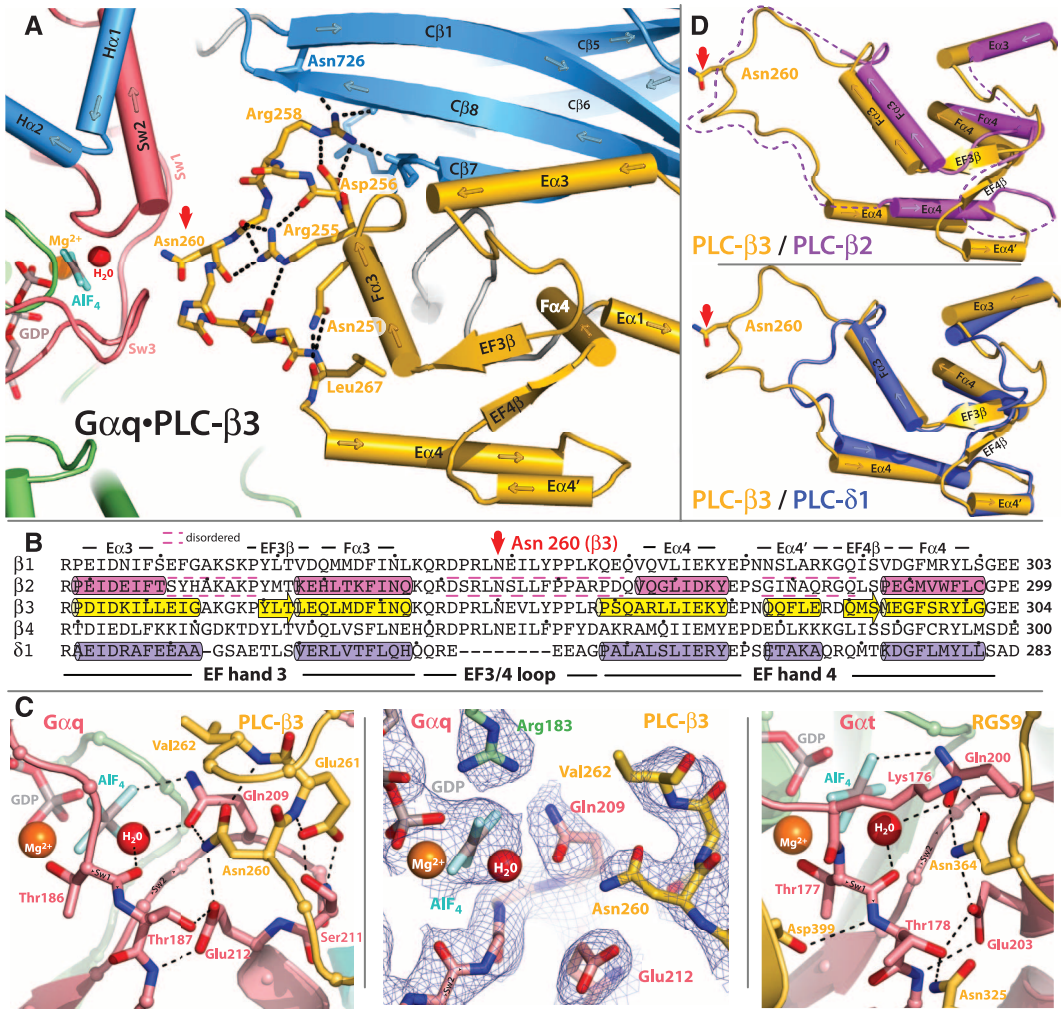

Fig. 4. Interaction of the EF3/4 loop of PLC-β3 with switch residues critical for GTP hydrolysis by $G\alpha_q$. (**A**) Ribbon and cylinder diagram highlighting conserved interactions within EF hands 3 and 4 (yellow) of PLC-β3 needed for the optimal positioning of Asn^{260} (red arrow) within the guanine nucleotide binding pocket of $G\alpha_q$. Sw1 to Sw3 are pink; other portions of $G\alpha_q$ are green. The C2 domain and adjacent Hα1/Hα2 of PLC-β3 are light blue; key PLC-β3 residues (sticks) and hydrogen bonds (dotted lines) that support Asn^{260} (red arrow) are highlighted. The guanine nucleotide binding pocket contains GDP and AlF_4^- (sticks) as well as the Mg^{2+} cofactor (orange ball) and catalytic water (red ball). (**B**) Sequence alignment comparing EF hands 3 and 4 of PLC-βs with equivalent region of PLC-δ1. α helices (cylinders) and β sheets (arrows) assigned from crystal structures (PLC-β3, 3OHM; PLC-β2, 2ZKM; δ1, 1DJX); dashed lines bracket disordered regions. The asparagine (Asn^{260} in PLC-β3) that is positioned for promotion of GTP hydrolysis by $G\alpha_q$ is indicated by a red arrow. The colors correspond to those of the structures depicted in (D) below. Dots indicate every 10th residue. (**C**) Comparison of the GTP-binding sites of $G\alpha_q$•PLC-β3 and $G\alpha_t$•RGS9. Left image depicts portions of the EF3/4 loop (yellow) of PLC-β3 contacting Sw1 and 2 (light red) of $G\alpha_q$. Other portions of $G\alpha_q$ are shown as in (A). Middle image highlights electron density (composite simulated annealing omit map contoured at 1.2 σ) centered on Asn^{260} of $G\alpha_q$•PLC-β3. Right image depicts analogous portions of RGS9 (yellow) bound to $G\alpha_t$ as revealed in the crystal structure determined by Slep *et al.* (*23*). (**D**) Ribbon and cylinder diagrams comparing EF hands 3 and 4 of PLC-β3 (yellow) with PLC-β2 (top, magenta) and PLC-δ1 (bottom, purple). Asn^{260} highlighted with red arrow, and dotted lines indicate disordered portions of PLC-β2.

Downloaded from www.sciencemag.org on November 11, 2010

ing $G\alpha_q$, and transient interactions with $G\alpha_q$ guide the final folding of Hα1/Hα2. The process of coupling folding with binding to increase the rate of formation of the final encounter complex has been described for other protein complexes (*31*, *32*) and is referred to as fly-casting. A subset of Dbl-family RhoGEFs typified by p63RhoGEF also apparently use fly-casting to engage $G\alpha_q$ (*19*, *20*). In particular, p63RhoGEF uses a helix-turn-helix immediately adjacent to a conserved PH domain to engage G_q in a fashion that is recapitulated almost identically in $G\alpha_q$•PLC-β. Thus, an independent module is grafted onto PLC-βs and RhoGEFs to confer binding to $G\alpha_q$. The Hα1/Hα2 module in PLC-βs is encoded by a single exon, which suggests that these signaling proteins acquired capacity to bind $G\alpha_q$ through intergenic exon shuffling.

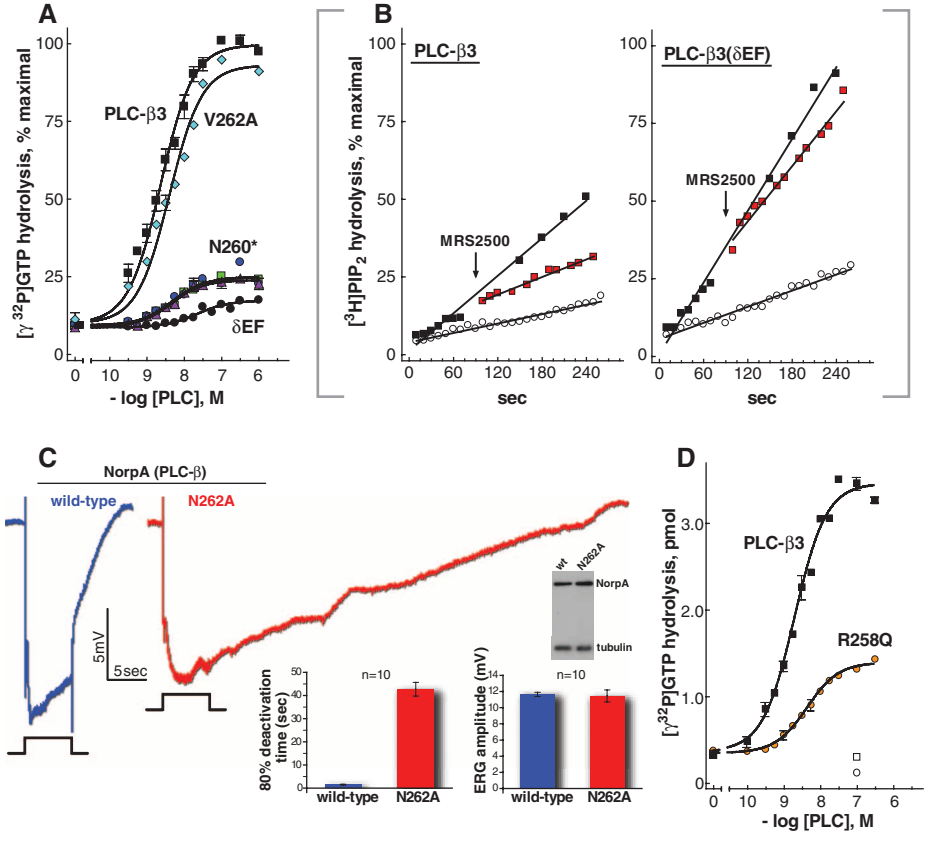

Fig. 5. Contribution of the EF hand region to GAP activity of PLC-β3. (**A**) The GAP activity of purified wild-type PLC-β3 is compared with that of mutant PLC-β3 isozymes. Steady-state GTP hydrolysis was quantified with phospholipid vesicles reconstituted with purified $P2Y_1$ receptor, $G\alpha_q$, and $G\beta_1\gamma_2$. Assays were in the presence of the $P2Y_1$ receptor agonist 2MeSADP (3 μM) and the indicated concentrations of purified PLC-β3; PLC-β3(δEF); PLC-β3(V262A); or PLC-β3(N260A), PLC-β3(N260G), or PLC-β3(N260S) [all designated as PLC-β3(N260*)] as described in (*41*). Data are plotted as percent of maximal response obtained with PLC-β3. Data are mean ± SEM of three experiments. (**B**) Deficiency in termination of $G\alpha_q$-stimulated PLC activity of a GAP-deficient mutant of PLC-β3. PLC activity was quantified with $[^3H]$PtdIns(4,5)P_2-containing phospholipid vesicles reconstituted with purified $P2Y_1$ receptor, $G\alpha_q$, and $G\beta_1\gamma_2$. Vesicles were incubated with 300 nM PLC-β3 or PLC-β3(δEF) in the absence (open circles) or presence of the $P2Y_1$ receptor agonist 2MeSADP (300 nM; black squares) and either 30 μM GTP or 100 nM GTPγS for 90 s before addition of $P2Y_1$ receptor antagonist MRS2500 (50 μM; red squares) or vehicle. Incubations were continued for an additional 165 s. Data are plotted as percent of the maximal response observed with either PLC-β3 or PLC-β3(δEF) in the presence of agonist plus GTPγS. (**C**) Delayed termination of the photoresponse in *Drosophila* expressing a GAP-deficient mutant of PLC-β. Electroretinograms from flies harboring wild-type PLC-β (NORPA, blue) or a mutant form ($NORPA^{N262A}$, red) deficient in capacity to accelerate the GTPase activity of $G\alpha_q$. Flies ~1 day posteclosion were dark-adapted for 2 min before exposure to 5-s pulses of orange light indicated by the event marker below each electroretinogram. At right are plotted deactivation rates and maximal amplitudes for the average of ten individual electroretinograms. Error bars indicate SEM. Expression of the *norpA* transgenes was confirmed by immunoblot (gel) of head extracts prepared from flies ~1 day posteclosion. (**D**) GAP activity of a mutant of PLC-β found in pancreatic cancer. PLC-β3 was mutated at a position (R258) (*21*) equivalent to a homozygous substitution identified in PLC-β4 during genome-wide profiling of pancreatic cancers (*30*). GAP activity of PLC-β3(R258Q) was compared with that of PLC-β3 as described in (A) above. Data are mean ± SEM of three experiments.

Engagement of PLC-β by $G\alpha_q$ is intimately coupled to inactivation of the complex. A primordial PLC-δ acquired an extended loop between EF hands 3 and 4 (Fig. 4D) that directly engages the switch regions of $G\alpha_q$ to stabilize the transition state for GTP hydrolysis. This EF3/4 loop and Hα1/Hα2 are linked evolutionarily, because both motifs are found in the two PLC-β isozymes of *Caenorhabditis elegans*. Indeed, they are not found separately in any PLC-β and therefore are the defining motifs of members of the PLC-β family. Taken together, we propose that $G\alpha_q$ is "caught" by a flycast from Hα1/Hα2 and is "released" by EF3/4 loop-mediated stimulation of GTP hydrolysis, which results in a conformational change in Sw2 and abrogation of the binding sites for both the EF3/4 loop and the Hα1/Hα2 segment. We also note that p115RhoGEF binds to $G\alpha_{13}$ and promotes GTP hydrolysis through two different domains (*33*).

Rapid cycling of effector engagement and GTP hydrolysis favors the maintenance of heterotrimeric G_q/effector complexes necessary for signal acuity in a process generally referred to as kinetic scaffolding (*9*, *10*, *34*, *35*). Phototransduction requires high signal amplification in rapid cycles of activation/deactivation in a signaling system organized for suppression of noise and therefore provides an excellent model for comparison of signaling mediated by PLC-βs and other effectors. Although $G\alpha_q$-promoted activation of PLC-β mediates phototransduction in some metazoans such as fruit flies, mammalian rod and cone phototransduction involves $G\alpha_t$-mediated activation of cyclic guanosine monophosphate (GMP) phosphodiesterase (PDE) (*36*). This PDE is not a GAP, and acceleration of GTP hydrolysis evolved in a separate protein, RGS9, which nonetheless stabilizes the switch regions of $G\alpha_t$ in much the way the EF3/4 loop of PLC-β stabilizes $G\alpha_q$ (*23*) (Fig. 4C). The binding of PDE to the effector pocket of $G\alpha_t$ allosterically increases binding of RGS9 (*23*, *37*). G protein–coupled receptor kinase 2 (GRK2) and, to a lesser extent, p63RhoGEF enhance the GAP activity of RGS4 in a complex with $G\alpha_q$ (*38*). This allostery is inherent in the catch-and-release mechanism used by PLC-βs. Ablation of GAP function of PLC-β markedly prolongs deactivation of phototransduction in *Drosophila* (Fig. 5C), and disruption of RGS9 in mice (*39*) and mutation of RGS9 in human disease (*40*) produce analogous phenotypes.

References and Notes

1. M. J. Berridge, R. F. Irvine, *Nature* **312**, 315 (1984).
2. R. H. Michell, *Biochim. Biophys. Acta* **415**, 81 (1975).
3. Y. Nishizuka, *Science* **258**, 607 (1992).
4. A. V. Smrcka, J. R. Hepler, K. O. Brown, P. C. Sternweis, *Science* **251**, 804 (1991).
5. S. J. Taylor, H. Z. Chae, S. G. Rhee, J. H. Exton, *Nature* **350**, 516 (1991).
6. G. L. Waldo, J. L. Boyer, A. J. Morris, T. K. Harden, *J. Biol. Chem.* **266**, 14217 (1991).
7. W. D. Singer, H. A. Brown, P. C. Sternweis, *Annu. Rev. Biochem.* **66**, 475 (1997).
8. E. M. Ross, T. M. Wilkie, *Annu. Rev. Biochem.* **69**, 795 (2000).
9. E. M. Ross, *Curr. Biol.* **18**, R777 (2008).

Downloaded from www.sciencemag.org on November 11, 2010

10. G. H. Biddlecome, G. Berstein, E. M. Ross, *J. Biol. Chem.* **271**, 7999 (1996).
11. S. Mukhopadhyay, E. M. Ross, *Proc. Natl. Acad. Sci. U.S.A.* **96**, 9539 (1999).
12. M. Turcotte, W. Tang, E. M. Ross, *PLoS Comput. Biol.* **4**, e1000148 (2008).
13. R. R. Neubig, D. P. Siderovski, *Nat. Rev. Drug Discov.* **1**, 187 (2002).
14. H. G. Dohlman, J. Thorner, *J. Biol. Chem.* **272**, 3871 (1997).
15. P. Chakrabarti, J. Janin, *Proteins* **47**, 334 (2002).
16. M. R. Jezyk *et al.*, *Nat. Struct. Mol. Biol.* **13**, 1135 (2006).
17. S. N. Hicks *et al.*, *Mol. Cell* **31**, 383 (2008).
18. T. K. Harden, J. Sondek, *Annu. Rev. Pharmacol. Toxicol.* **46**, 355 (2006).
19. R. J. Rojas *et al.*, *J. Biol. Chem.* **282**, 29201 (2007).
20. S. Lutz *et al.*, *Science* **318**, 1923 (2007).
21. Single-letter abbreviations for the amino acid residues are as follows: A, Ala; C, Cys; D, Asp; E, Glu; F, Phe; G, Gly; H, His; I, Ile; K, Lys; L, Leu; M, Met; N, Asn; P, Pro; Q, Gln; R, Arg; S, Ser; T, Thr; V, Val; W, Trp; and Y, Tyr.
22. G. Venkatakrishnan, J. H. Exton, *J. Biol. Chem.* **271**, 5066 (1996).
23. K. C. Slep *et al.*, *Nature* **409**, 1071 (2001).
24. K. C. Slep *et al.*, *Proc. Natl. Acad. Sci. U.S.A.* **105**, 6243 (2008).
25. J. J. G. Tesmer, D. M. Berman, A. G. Gilman, S. R. Sprang, *Cell* **89**, 251 (1997).
26. T. Wang, C. Montell, *Pfugers Arch.* **454**, 821 (2007).
27. C. G. Mullighan *et al.*, *Nature* **446**, 758 (2007).
28. W. Xiao *et al.*, *Cancer Cell* **16**, 161 (2009).
29. C. D. Van Raamsdonk *et al.*, *Nature* **457**, 599 (2009).
30. S. Jones *et al.*, *Science* **321**, 1801 (2008); 10.1126/science.1164368.
31. B. A. Shoemaker, J. J. Portman, P. G. Wolynes, *Proc. Natl. Acad. Sci. U.S.A.* **97**, 8868 (2000).
32. K. Sugase, H. J. Dyson, P. E. Wright, *Nature* **447**, 1021 (2007).
33. Z. Chen, W. D. Singer, P. C. Sternweis, S. R. Sprang, *Nat. Struct. Mol. Biol.* **12**, 191 (2005).
34. C. A. Doupnik, N. Davidson, H. A. Lester, P. Kofuji, *Proc. Natl. Acad. Sci. U.S.A.* **94**, 10461 (1997).
35. H. Zhong *et al.*, *J. Biol. Chem.* **278**, 7278 (2003).
36. V. Y. Arshavsky, T. D. Lamb, E. N. Pugh Jr., *Annu. Rev. Physiol.* **64**, 153 (2002).
37. N. P. Skiba, J. A. Hopp, V. Y. Arshavsky, *J. Biol. Chem.* **275**, 32716 (2000).
38. A. Shankaranarayanan *et al.*, *J. Biol. Chem.* **283**, 34923 (2008).
39. C. K. Chen *et al.*, *Nature* **403**, 557 (2000).
40. K. M. Nishiguchi *et al.*, *Nature* **427**, 75 (2004).
41. Materials and methods are available as supporting material on *Science* Online.
42. This research was supported by NIH grants GM38213 and GM57391 (J.S. and T.K.H.), GM61454 and GM074001 (T.K.), and EY010852 (C.M.). T.K.R. was supported by a Ruth L. Kirschstein National Service Award F31 Predoctoral Fellowship and a United Negro College Fund Merck Graduate Science Research Dissertation Fellowship. K.T. was supported by a Postdoctoral Fellowship for Research Abroad from the Japan Society for the Promotion of Science. We acknowledge the outstanding help with structural analyses by B. Temple, L. Betts, J. Vanhooke, T. Charpentier, V. Arshavsky, and M. Kosloff; with analysis of linker-deleted PLC-β3 by N. Vincent Jordan; with SPR analyses by A. Kimple; with [γ^{32}P]GTP purification by E. Lazarowski and the insightful comments on the manuscript by H. Dohlman, R. Nicholas, E. Ross, and K. Slep. Coordinates and structure factors for $G\alpha_q$•PLC-β3 have been deposited under the PDB accession code 3OHM.

Supporting Online Material

www.sciencemag.org/cgi/content/full/science.1193438/DC1
Materials and Methods
SOM Text
Figs. S1 to S8
Tables S1 to S2
References

8 June 2010; accepted 14 September 2010
Published online 21 October 2010;
10.1126/science.1193438
Include this information when citing this paper.

Peripherally Applied Aβ-Containing Inoculates Induce Cerebral β-Amyloidosis

Yvonne S. Eisele,[1,2] Ulrike Obermüller,[1,2] Götz Heilbronner,[1,2,3] Frank Baumann,[1,2] Stephan A. Kaeser,[1,2] Hartwig Wolburg,[4] Lary C. Walker,[5] Matthias Staufenbiel,[6] Mathias Heikenwalder,[7] Mathias Jucker[1,2]*

The intracerebral injection of β-amyloid–containing brain extracts can induce cerebral β-amyloidosis and associated pathologies in susceptible hosts. We found that intraperitoneal inoculation with β-amyloid–rich extracts induced β-amyloidosis in the brains of β-amyloid precursor protein transgenic mice after prolonged incubation times.

Intracerebral inoculation with minute amounts of brain extract containing misfolded β-amyloid (Aβ) from patients with Alzheimer's disease or from amyloid-bearing β-amyloid precursor protein (APP) transgenic (tg) mice induces cerebral β-amyloidosis and related pathologies in APP tg mice in a time- and concentration-dependent manner (*1*). However, oral, intravenous, intraocular, or intranasal inoculations have failed to induce cerebral β-amyloidosis in APP tg hosts (*2*). These findings suggest that Aβ-containing brain material in direct contact with the brain can induce cerebral β-amyloidosis, but that, unlike prions, either the inducing agent is not readily conveyed from peripheral sites to the brain or a higher concentration or longer incubation period is required for peripherally delivered Aβ seeds.

Intraperitoneal administration of prion-rich material is more efficient at transmitting prion disease than is oral administration (*3*, *4*). To test whether intraperitoneal inoculation of Aβ-rich material might similarly trigger Aβ misfolding and deposition in the brain, we administered two intraperitoneal injections (100 μl each, 1 week apart) of Aβ-laden (10 to 20 ng/μl) brain extract from aged APP23 tg mice (Tg extract) to a cohort of young (2-month-old) female APP23 tg mice (*5*). After a 7-month incubation period, cerebral β-amyloidosis was robustly induced in all intraperitoneally inoculated mice compared with untreated littermate controls (Fig. 1). To confirm this finding, we inoculated a second cohort of 2-month-old female APP23 mice with a different batch of Tg brain extract in another laboratory (cohort 2, Tübingen, versus cohort 1, Basel). After 6 to 7 months, mice injected intraperitoneally with the Tg extract exhibited robust cerebral β-amyloidosis, whereas intraperitoneal inoculation with phosphate-buffered saline (PBS) or brain extract from age-matched, non-tg wild-type mice (Wt extract) was ineffective (Fig. 1).

Induced β-amyloidosis was strongest in the anterior and entorhinal cortices, with additional deposition in the hippocampus, resembling the regional development of endogenous β-amyloidosis in aged APP23 mice (*6*). However, whereas normal aged APP23 mice manifest mostly parenchymal deposits, the induced β-amyloid in intraperitoneally seeded mice was predominantly associated with blood vessels [cerebral β-amyloid angiopathy (Aβ-CAA)], often with massive spreading into the neighboring brain parenchyma (Fig. 1). The presence of Aβ was confirmed by immunoblotting, and amyloid fibrils were evident ultrastructurally; in addition, the induced β-amyloidosis was linked to gliosis, hyperphosphorylated tau, and other associated pathologies (Fig. 2), reminiscent of the cerebral β-amyloid deposition in aged APP23 mice (*6*, *7*).

To compare the efficiency and time course of intraperitoneal versus intracerebral inoculation, 2-month-old female APP23 mice were inoculated either intraperitoneally (2 × 100 μl) or intracerebrally (2.5 μl into the hippocampus) with Tg extract, and then analyzed 4 months later. No cerebral β-amyloid induction was found in any of the four intraperitoneally inoculated mice, whereas all six intracerebrally inoculated mice revealed β-amyloid induction identical to that previously reported (*1*, *2*). From this observation, together with previous time course and 1:20 dilution experiments for intracerebral inoculations (*1*), we estimate that intraperitoneal inoculations with 1000 times as much Aβ take 2 to 5 months longer to induce cerebral β-amyloidosis than do intracerebral inoculations.

The replication of peripherally applied prions and their translocation into the central nervous

[1]Department of Cellular Neurology, Hertie-Institute for Clinical Brain Research, University of Tübingen, D-72076 Tübingen, Germany. [2]DZNE–German Center for Neurodegenerative Diseases, D-72076 Tübingen, Germany. [3]Graduate School for Cellular and Molecular Neuroscience, University of Tübingen, D-72074 Tübingen, Germany. [4]Department of Pathology, University of Tübingen, D-72076 Tübingen, Germany. [5]Yerkes National Primate Research Center and Department of Neurology, Emory University, Atlanta, GA 30322, USA. [6]Novartis Institutes for Biomedical Research, Neuroscience Discovery, CH-4056 Basel, Switzerland. [7]Department of Pathology, Institute for Neuropathology, University Hospital, CH-8091 Zürich, Switzerland.

*To whom correspondence should be addressed. E-mail: mathias.jucker@uni-tuebingen.de

Downloaded from www.sciencemag.org on November 11, 2010

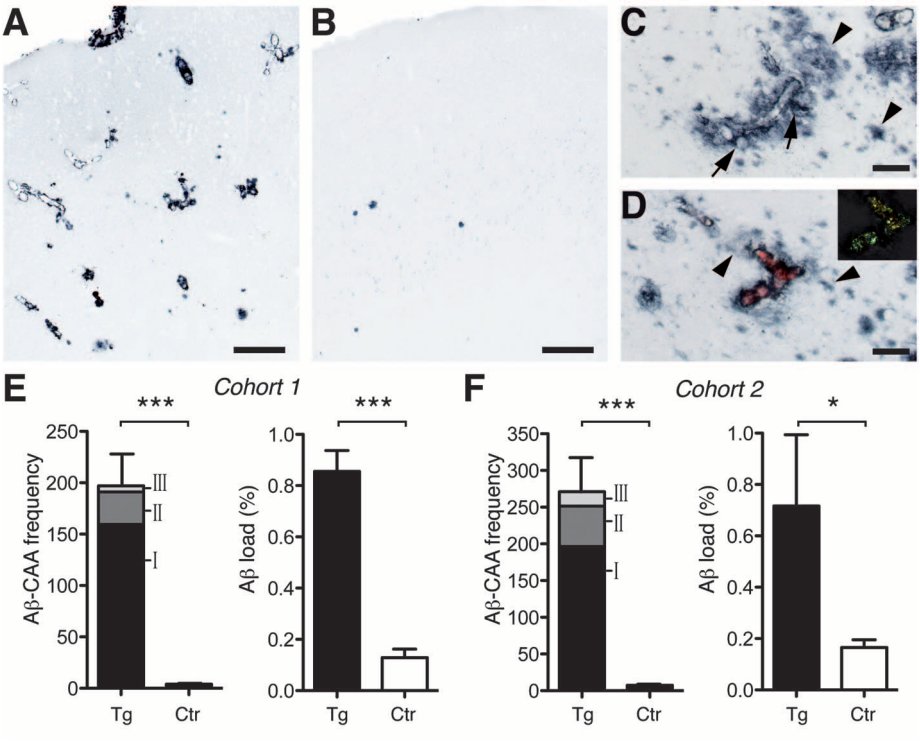

Fig. 1. Induced Aβ deposition. (**A** and **B**) Aβ-immunostained frontal cortex of APP23 mice inoculated intraperitoneally with Tg extract (A) or Wt extract (B). (**C** and **D**) Most induced β-amyloid was vascular (Aβ-CAA), with Aβ-immunoreactivity extending into the brain parenchyma (arrows). Amyloid-laden vessels were congophilic [red in (D); birefringent under cross-polarized light in inset)] and often were surrounded by diffuse, Congo red–negative Aβ deposits (arrowheads). (**E** and **F**) Analysis of the entire neocortex for Aβ-CAA frequency [indicated are all three (I to III) CAA severity grades (*5*)] and for total Aβ load in Tg extract–inoculated mice compared with control (Ctr) mice. Cohort 1 consisted of six Tg extract–inoculated mice versus seven untreated control mice. Aβ-CAA: $t(11) = 6.78$ (all severity grades combined), $^{***}P < 0.0001$; Aβ load: $t(11) = 8.79$, $^{***}P < 0.0001$. Cohort 2 consisted of five Tg extract–inoculated mice versus five Wt extract–inoculated mice and four PBS-injected mice. These latter two (control) groups did not differ significantly and were combined for analysis. Aβ-CAA: $t(12) = 7.79$, $^{***}P < 0.0001$; Aβ load $t(12) = 2.71$, $^{*}P < 0.05$. The occasional parenchymal Aβ-deposits in control mice are normal for 9-month-old APP23 mice. Error bars, means ± SEM. Scale bars: [(A) and (B)] 200 μm; [(C) and (D)] 50 μm.

system depend on hematopoietic and stromal immune cells, in combination with sympathetic innervation of abdominal lymphoid organs (*8*). Both activation of the immune system and chronic inflammation promote prion replication (*9*, *10*). To assess the immune response to Aβ-rich brain extracts, additional APP23 mice were given single intraperitoneal injections of 200 μl Tg or Wt extract and sacrificed 1 hour, 1 week, or 1 month after injection (*5*). An acute immune activation to the injected brain material was indicated by transient increases in plasma chemokines and cytokines [interleukin-6 (IL-6), IL-10, tumor necrosis factor–α, monocyte chemotactic protein–1, and macrophage inflammatory protein–1β] in both Tg and Wt extract–inoculated mice after 1 hour, with IL-6 still mildly elevated in Tg extract–injected mice 1 week after inoculation (fig. S1). However, no signs of chronic inflammation in various peripheral organs (e.g., liver, pancreas, kidney, and lung) or plasma titers of antibodies to Aβ were found in any mice investigated at 1 or 7 months after seeding (*5*). Moreover, no β-amyloid deposition was found in any of the peripheral tissues at any time point studied.

Thus, like prion disease, cerebral β-amyloidosis can be seeded in the brain by homologous protein aggregates delivered into the peritoneal cavity, although the intraperitoneal route required more time and was less efficient than was direct injection into the brain (*1*, *2*). The amyloid-inducing factor in the Tg extract is probably a species of misfolded Aβ that is generated in its most effective form or composition in vivo (*1*). Because the expression of tg (human) APP is restricted to the nervous system in APP23 mice (*7*), in this model it is likely that the seed carried to the brain was

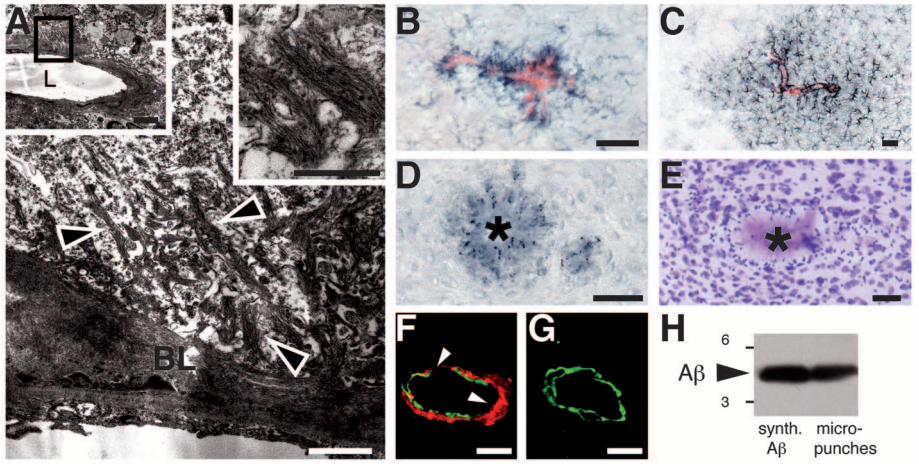

Fig. 2. Induced Aβ deposition was linked to multiple associated pathologies. (**A**) Ultrastructural analysis showed amyloid deposition within the vascular basal lamina (BL), with typical amyloid fibrils (arrowheads) extending into the brain parenchyma. Insets are low- and high-magnification views of the examined vessel (L, lumen) and the typical nonbranching amyloid fibrils. (**B** to **E**) Vascular amyloid [stained by Congo Red in (B) and (C)] and parenchymal plaques were surrounded by hypertrophic, Iba1-positive microglia (B), Glial fibrillary acidic protein (GFAP)–positive astrocytes (C), hyperphosphorylated tau-positive neurites [(D); asterisk indicates amyloid core], but a paucity of proximate neurons [cresyl-violet stain (E)]. (**F** and **G**) Vessels with CAA types II and III showed smooth muscle cell loss at the site of amyloid deposition (arrowheads; confocal image, maximum projection of 5 μm *z*-stack: red, Aβ; green, smooth muscle actin). A normal vessel (G) has a complete ring of smooth muscle cells. (**H**) Immunoblotting of micropunches of Aβ-immunoreactive material revealed the expected Aβ band. Synthetic Aβ40/42 is shown as control. Markers, 3 and 6 kD. Scale bars: (A) 1 μm (insets, 5 and 0.5 μm); [(B) to (E)] 50 μm; [(F) and (G)] 10 μm.

the injected material itself, rather than Aβ aggregates that were first amplified in peripheral tissues.

There is now persuasive evidence that the aggregation of Aβ is a key pathogenic feature of Alzheimer's disease and Aβ-CAA (*11*–*14*), although the majority of these cases are initiated by unknown causes. The possibility that mechanisms exist allowing for the transport of Aβ aggregates (and possibly other seeds) from the periphery to the brain justifies further studies to better understand the cellular and molecular origin of these diseases and to clarify the basis of infectious versus noninfectious proteopathies (*15*, *16*).

Downloaded from www.sciencemag.org on November 11, 2010

References and Notes

1. M. Meyer-Lühmann *et al.*, *Science* **313**, 1781 (2006).
2. Y. S. Eisele *et al.*, *Proc. Natl. Acad. Sci. U.S.A.* **106**, 12926 (2009).
3. S. B. Prusiner, *Prion Biology and Diseases* (Cold Spring Harbor Laboratory Press, Cold Spring Harbor, NY, ed. 2, 2004).
4. R. H. Kimberlin, C. A. Walker, *J. Comp. Pathol.* **88**, 39 (1978).
5. Materials and methods are available as supporting material on *Science* Online.
6. C. Sturchler-Pierrat *et al.*, *Proc. Natl. Acad. Sci. U.S.A.* **94**, 13287 (1997).
7. M. E. Calhoun *et al.*, *Proc. Natl. Acad. Sci. U.S.A.* **96**, 14088 (1999).
8. A. Aguzzi, C. Sigurdson, M. Heikenwälder, *Annu. Rev. Pathol. Mech. Dis.* **3**, 11 (2008).
9. M. Heikenwalder *et al.*, *Science* **307**, 1107 (2005).
10. J. Bremer *et al.*, *PLoS ONE* **4**, e7160 (2009).
11. J. Hardy, D. J. Selkoe, *Science* **297**, 353 (2002).
12. M. Storandt, M. A. Mintun, D. Head, J. C. Morris, *Arch. Neurol.* **66**, 1476 (2009).
13. J. C. Morris *et al.*, *Arch. Neurol.* **66**, 1469 (2009).
14. S. X. Zhang-Nunes *et al.*, *Brain Pathol.* **16**, 30 (2006).
15. L. C. Walker, H. Levine 3rd, M. P. Mattson, M. Jucker, *Trends Neurosci.* **29**, 438 (2006).
16. A. Aguzzi, L. Rajendran, *Neuron* **64**, 783 (2009).

17. We thank M.-J. Runser, L. Jacobson (Basel), F. Langer, J. Coomaraswamy, S. Grathwohl, N. Varvel, T. Hamaguchi, C. Schäfer, A. Bosch, G. Frommer-Kästle, U. Scheurlen (Tübingen) for experimental help and A. Aguzzi (Zürich) for insightful comments. This work was supported by the Competence Network on Degenerative Dementias (BMBF-01GI0705), the Bundesministerium für Bildung und Forschung as part of ERA-Net NEURON (MIPROTRAN), the Center for Integrative Neuroscience (Deutsche Forschungsgemeinschaft), and NIH RR-00165.

Supporting Online Material

www.sciencemag.org/cgi/content/full/science.1194516/DC1
Materials and Methods
Fig. S1
References

1 July 2010; accepted 24 September 2010
Published online 21 October 2010;
10.1126/science.1194516
Include this information when citing this paper.

Contact Network Structure Explains the Changing Epidemiology of Pertussis

Pejman Rohani,[1,2,4]*† Xue Zhong,[1,2]† Aaron A. King[1,3,4]

The epidemiology of whooping cough (pertussis) remains enigmatic. A leading cause of infant mortality globally, its resurgence in several developed nations—despite the availability and use of vaccines for many decades—has caused alarm. We combined data from a singular natural experiment and a detailed contact network study to show that age-specific contact patterns alone can explain shifts in prevalence and age-stratified incidence in the vaccine era. The practical implications of our results are notable: Ignoring age-structured contacts is likely to result in misinterpretation of epidemiological data and potentially costly policy missteps.

Understanding the epidemiology of pertussis (whooping cough) has become a public health priority (*1*). This is partly because of the continued toll exacted in developing countries, where pertussis is estimated to account for more than 295,000 infant and childhood deaths per year (*2*), and partly because, despite high vaccine uptake levels for decades, a number of developed countries have reported a resurgence in the incidence of pertussis over the past decade (*1*, *3*, *4*). Most recent research effort has focused on hypotheses that have emphasized genetics (*5*), antigenic divergence as a result of vaccination (*6*), immunology and waning protection especially after immunization (*7*, *8*), improvements in diagnostic methodology and surveillance systems (*4*), and variability in vaccine uptake (*9*) and efficacy (*3*, *10*). In pertussis, as in all other directly transmitted infections, the structure of the contact network can play an important role, yet has not been quantitatively characterized.

Here, we examine the epidemiological dynamics of pertussis using age-stratified annual incidence data from Sweden. As shown in Fig. 1A, after almost three decades of vaccination, the whole-cell (wP) pertussis vaccine was withdrawn from the Swedish childhood immunization program in 1979, after concerns over safety and efficacy (*11*–*13*). There ensued a 17-year hiatus in pertussis vaccination, ending with the introduction of the acellular (aP) vaccine in 1996. Throughout this period, the Swedish Institute for Infectious Disease Control collected incidence data stratified by age (*13*) (Fig. 1, B and C). We combined these data with contact network information from the European POLYMOD study (*14*) via an age-structured model with the principal aim of assessing the role of age-specific contacts in pertussis epidemiology.

The data presented in Fig. 1, B and C, reveal shifts in the age-specific incidence of pertussis after the introduction of the aP vaccine; these shifts are similar to those reported elsewhere (*15*). Despite annual variation in prevalence, there was little variability in the distribution of cases among different age groups from 1986 to 1996. More than 95% of cases were found in children aged 10 and younger, with the largest fraction of cases among 1- to 5-year-olds (Fig. 1B). The onset of immunization in 1996 led to a decline in pertussis cases in preschool children and an increase in all other age groups, especially infants (younger than 1 year), who account for almost 25% of cases in the recent vaccine era. At the same time, there have been changes in both the distribution and magnitude of incidence: Immunization coincides with a factor of 10 reduction in the number of reported cases, consistent with strong herd immunity effects (*13*) and an increase in the mean age at infection (from 4.1 to 10.1 years). The shift in age distribution has been observed elsewhere and has been attributed to changes in the epidemiology of pertussis (*15*, *16*), loss of immunity, or aspects of case diagnosis and reporting fidelity (*4*). Here we show that the observed shifts in incidence and age distribution of pertussis cases can be more simply explained as a direct consequence of vaccination once correct age-specific social mixing is taken into consideration. This remains true even in the absence of the aforementioned epidemiological and immunological complexities, as we show here.

We first derive an expression relating infection prevalence to the age-specific risk of infection. If the hazard of infection in age class i is denoted by λ_i, then

$$\lambda_i = \sum_j q\, c_{ij} \frac{I_j}{N_j}$$

where I_j is the number of infectives, and N_j the population size, of age class j; c_{ij} is the rate of contacts between age classes i and j; and q is the probability of infection given contact. In earlier models, the "who acquires infection from whom" (WAIFW) matrix, $\beta_{ij} = qc_{ij}$, has been parameterized under ad hoc assumptions on the matrix structure (*17*–*19*). Key epidemiological determinants, including the basic reproduction ratio R_0, are known to be highly sensitive to these assumptions (*20*–*22*). We estimated the contact matrix c_{ij} using self-reported contact data from a large-scale study (*14*) that revealed the actual age-specific pattern of contacts in a number of European countries. By combining the Sweden incidence data I_i (scaled to account for infectious period and reporting fidelity), known population sizes N_i, and the contact network structure c_{ij} (Fig. 2D), we obtain an estimate of the number of risky contacts, $K_i = \sum_j c_{ij} I_j / N_j$ (Fig. 2B). We can test this model by directly comparing the model-predicted number of risky contacts

[1]Department of Ecology and Evolutionary Biology, University of Michigan, Ann Arbor, MI 48109, USA. [2]Center for the Study of Complex Systems, University of Michigan, Ann Arbor, MI 48109, USA. [3]Department of Mathematics, University of Michigan, Ann Arbor, MI 48109, USA. [4]Fogarty International Center, National Institutes of Health, Bethesda, MD 20892, USA.

*To whom correspondence should be addressed. E-mail: rohani@umich.edu
†These authors contributed equally to this work.

Downloaded from www.sciencemag.org on November 11, 2010

to the empirically determined age-specific force of infection, λ_i (Fig. 2A) (*20*). Specifically, our model predicts that λ_i/K_i should equal the constant q. Therefore, to the extent that λ_i/K_i is independent of i, the assumed contact structure provides a complete explanation of the data. As Fig. 2C shows, λ_i/K_i varies surprisingly little across ages. The variation is smooth, with fluctuations likely to be due to age-specific biases in the contact data and age-specific variation in detectability, susceptibility, and nature of contacts as related to transmission. By making additional assumptions regarding the dependence of the above effects on age, we might achieve a deceptively high degree of model-data agreement, at the expense of robustness. In the absence of independent data quantifying the extent of these effects and in keeping with our central goal of assaying the impact of contact structure, we instead make the parsimonious assumption that λ_i/K_i and reporting probability are inde-

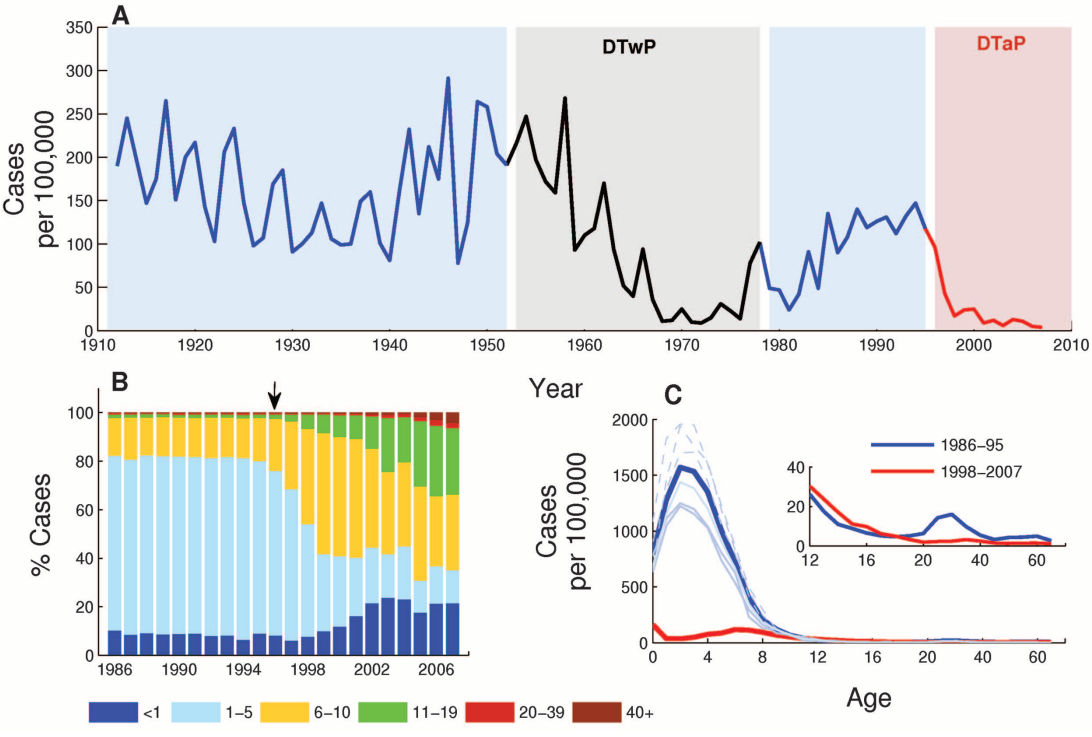

Fig. 1. Pertussis in Sweden. (**A**) Long-term incidence data from four distinct eras: prevaccination era 1910 to 1952 (shaded light blue); vaccination era with whole-cell pertussis vaccines, ending in 1979 (shaded gray); vaccine-free era (shaded light blue); and the resumption of nationwide vaccination in January 1996 with acellular pertussis (aP) vaccines (shaded pink). aP vaccine coverage instantly exceeded 98% of infants with a schedule of doses at 3, 5, and 12 months. (**B**) Case percentage among age groups: infants (<1 year), preschool children (aged 1 to 5 years), primary-school children (aged 6 to 10), adolescents (aged 11 to 19), young adults (aged 20 to 39), and older than 40. The onset of aP vaccination is marked with the arrow. (**C**) Age-specific incidence of pertussis. We present the mean in the 10 years preceding (thick dark blue line) and after (thick red line) the resumption of vaccination. For the vaccine-free era, we also plot incidence data for epidemic (thin dashed lines) and nonepidemic (thin solid lines). The disease burden among young children (aged <6 years) has been reduced by 90% after vaccination. The inset shows shifts in incidence among adolescents and adults after the 1996 resumption of vaccination. [Redrawn from data in table 3 in (*13*)]

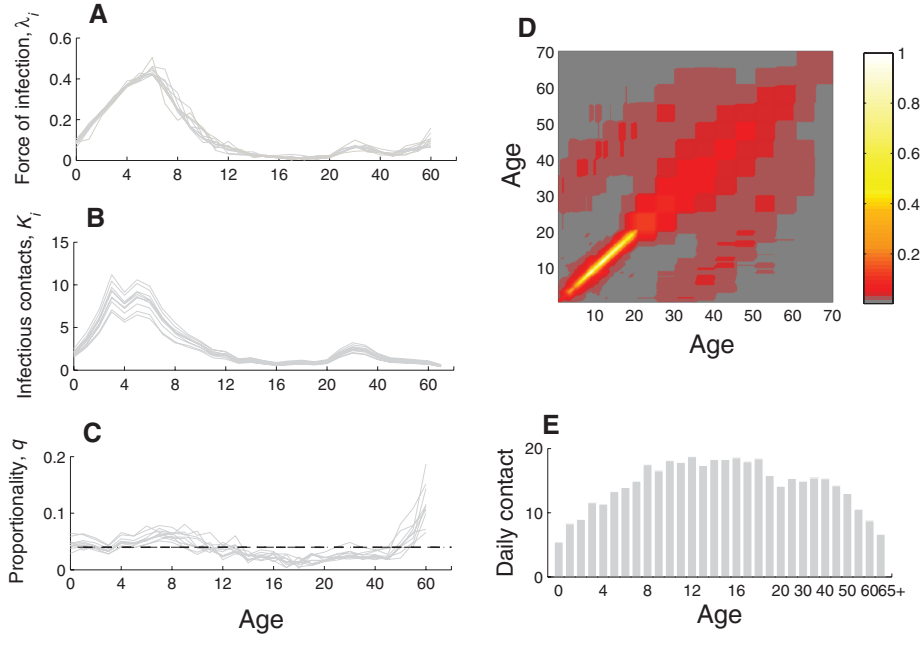

Fig. 2. (**A**) Age-specific force of infection, λ_i, for pertussis in Sweden from 1986 to 1895, calculated according to Anderson and May (*20*, *21*): $\lambda_i = -[1/(\Delta a)]\ln[(1 - p_i)/(1 - p_{i-1})]$, where Δa is the width of the age class and p_i is the proportion of cases by age class i. The force of infection initially increases with age, peaking in the 6-year-old age class followed by a decline to a plateau during adolescence, with a small subsequent peak among 30- to 40-year-olds. (**B**) Age-specific rate of risky contacts, K_i. Determined by annual disease prevalence (I_i/N_i, corrected for 10% assumed reporting probability) and the assumed matrix of population contacts. Upon an in-danger contact, a susceptible is exposed to infection. (**C**) Age-specific probability of transmission given risky contact, q, which is markedly constant, around a value of 0.04 (dashed line). In fig. S6, we show that this estimate is robust to realistic age-specific notification biases. (**D**) The normalized age-specific contact rates (c_{ij}) as estimated by averaging the data across all eight countries and correcting for reciprocity: $c_{ij} = m_{ji}/w_j$, where m_{ij} is the contact rate and w_j is the proportion of the population in age class j. The intensity of contacts is scaled to vary from 0 to 1. As shown in the SOM, our results are not sensitive to the pooling of data across the eight countries in the Mossong *et al.* (*14*) study. (**E**) Number of daily contacts per person.

Downloaded from www.sciencemag.org on November 11, 2010

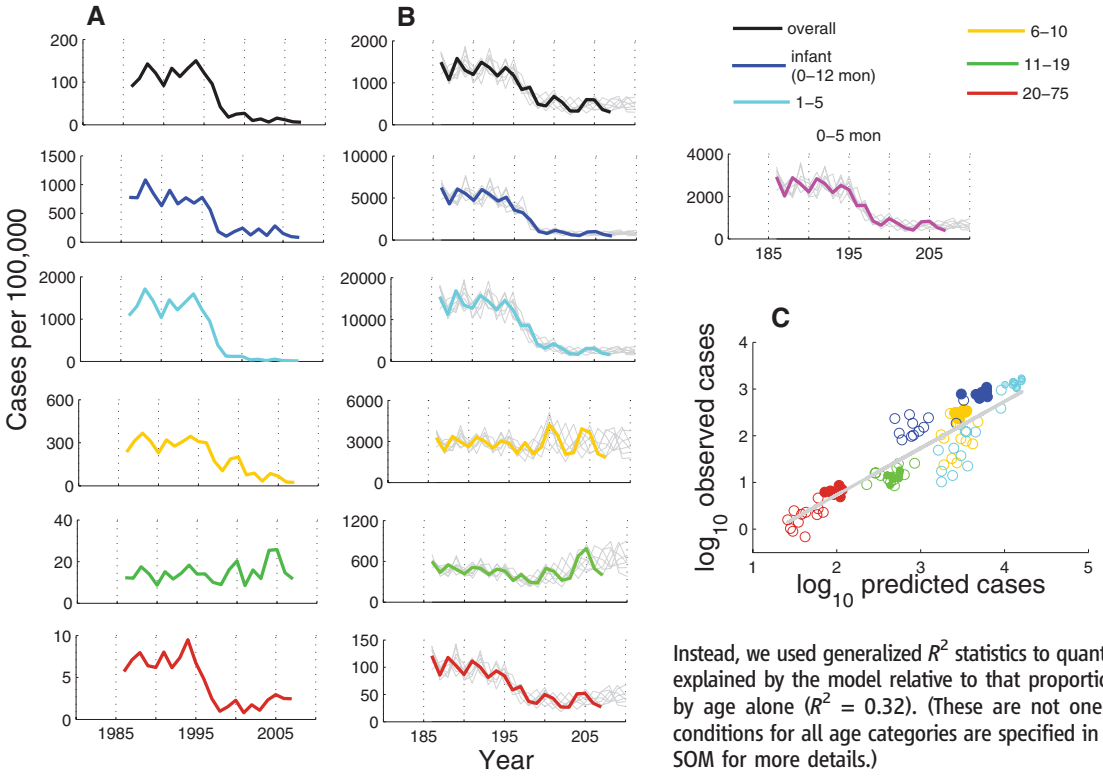

Fig. 3. (**A**) Age-specific pertussis incidence in Sweden from 1986 to 2007, compared with (**B**) model simulations. Ten stochastic realizations are presented (gray lines), with one highlighted for comparison (color bold lines). The *y*-axis scales differ between panels in (A) and (B). This is most readily attributable to age-specific reporting bias (*32*), as we discuss in the SOM. (**C**) Quantitative comparison between model simulation and data (log-log scale); the line shows regression with a slope of 1. Color of symbols according to age group, with filled (open) circles representing incidence in the prevaccine (vaccine) era. Due to the correlation among ages and between years, standard linear regression statistics are not appropriate here. Instead, we used generalized R^2 statistics to quantify the proportion of the variance explained by the model relative to that proportion of the variance not explained by age alone (R^2 = 0.32). (These are not one-step-ahead predictions; starting conditions for all age categories are specified in year 0. See the section S6 in the SOM for more details.)

pendent of age. As we next show, this yields a model that explains the disease dynamics well. In figs. S5 and S6, we demonstrate that our parameterization is only weakly sensitive to the relaxation of these assumptions.

We parameterized a stochastic seasonally forced SEIR model of transmission dynamics (*18*), using the contact matrix derived above and demographic and immunization data from Sweden [see Supporting Online Material (SOM)]. In Fig. 3, we present the comparison of the incidence data (column A) with our model output (column B), broken down by age. Despite the simplicity of our model, we find quantitative agreement between model predictions and data (Fig. 3C). Overall, the model captures the sudden decline in incidence observed in the infant, toddler, and adult classes in the recent vaccine era. The model also demonstrates that in the short term, pediatric immunization has little or no impact on pertussis in the adolescent groups and predicts an upturn in cases among teenagers, which in other settings has been attributed to changes in pertussis epidemiology due to waning of vaccine- or infection-induced immunity, but is here revealed to be a consequence of the age-structured transmission dynamics.

The most pronounced discrepancy between model and data occurs in the 6- to 10-year age class. Specifically, according to the contact network data, 6- to 10-year-olds should be epidemiologically similar to teenagers, but the incidence data portray them as intermediate between toddlers and teenagers.

These findings have policy implications; several national health agencies currently recommend the administration of pertussis boosters for ages 11 and up, based on the presumed epidemiological impact of adolescent and adult infections (*23*, *24*). Specifically, the observation that pertussis infection in many adolescents and adults can be asymptomatic (*25*, *26*) has led to the suggestion that circulation of the bacterium in the population is driven by infections among older age groups (*23*, *27*). Our simple model reproduces most of the features of the data, despite its assumption that secondary and later infections have no epidemiological impact at all. If this assumption is even approximately correct, then the policy of administering even very frequent adult boosters may be ineffective. To see this, we titrate the effectiveness of adolescent and adult booster campaigns on reducing pertussis burden (Fig. 4). We assume that in addition to the routine immunization of infants, boosters are administered to a proportion of the population every 5 years. We then calculate the reduction in the cumulative number of cases over a 10-year period compared with a no-booster scenario. Our findings are emphatic: Even if half the population aged 11 and above receive boosters every 5 years, the reduction in pertussis burden is modest in the short term, ranging from 5 to 10% (Fig. 4). The reduction is most modest among infants (fig. S13, C and D), the age group at greatest risk of mor-

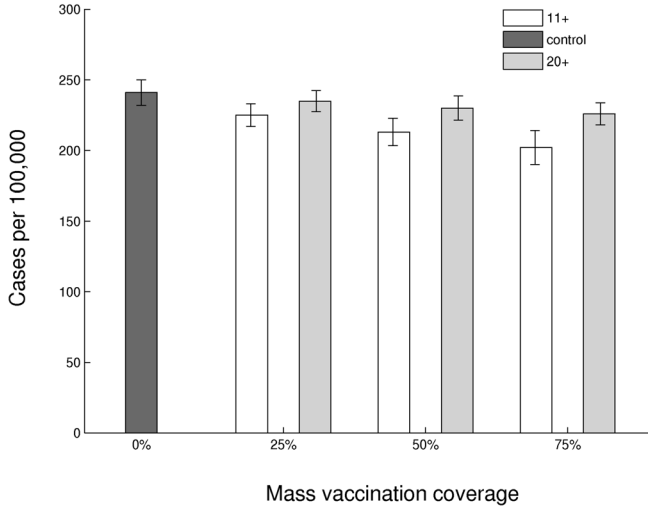

Fig. 4. Modeling the impact of adolescent and adult booster vaccination. Simulations were run for 196 years, at which point pediatric immunization was introduced, as reported for Sweden (*13*). Then, starting at year 210, boosters were administered to 25, 50, or 75% of individuals aged 11 and over (white bars) or aged 20 and over (light gray bars) every 5 years over the next decade. Total cumulative incidence (assuming 10% reporting) over the 10-year period was compared to the scenario without booster vaccination (dark gray bar). In the SOM, we show the robustness of these results to changes in the mean duration of immunity.

Downloaded from www.sciencemag.org on November 11, 2010

tality or severe complications after pertussis infection. In the extreme (and logistically unfeasable) situation where 75% of the 11 and older population are immunized at 5-yearly intervals, incidence reduction approaches only 15%. These results raise important questions about the epidemiological effectiveness and financial prudence of booster programs for adolescents and adults.

Our model ignores the myriad complexities that have been proposed as explanations for recent pertussis epidemiology. Critically, it ignores loss of immunity. This assumption is reasonable and has its basis in empirical evidence. Equivalent parameterization of an SIRS model that assumes temporary immunity reveals q—the probability of infection given contact—to be age dependent and to decay exponentially beyond ages 4 to 5 (fig. S5). Hence, the age-specific Sweden data provide strong support for the stated minimal transmission impact of repeat asymptomatic infections (*28*), which has been inferred from aggregate epidemiological data in other countries (*8*, *29*, *30*). It remains to be seen whether the explanatory power of our simple yet predictive model will substantially increase with the inclusion of additional complexities, be they age-dependent effects (e.g., differential transmissibility, susceptibility, and observability) or refinements of the contact network (e.g., household and spatial structuring).

Since the pioneering work of Fine and Clarkson, the impact of pertussis vaccines has been the subject of much debate (*31*). The focus of contention has been whether vaccination protects against transmission or merely disease. Our analysis strongly points to the former: The pronounced drop in incidence in the infant, toddler, and adult groups after infant immunization is indicative of reduced pertussis circulation and increased herd immunity (*13*). Our findings also point toward a minimal transmission role for adults, due to the strong assortativity of contacts among the young (Fig. 2D). Hence, we conclude that adults are not the missing piece of the puzzle they have been made out to be (*23*). Our results suggest that contact structure is the pivotal element for understanding the epidemiology of pertussis and, it is likely, other directly transmitted infectious diseases.

References and Notes

1. L. P. Celentano, M. Massari, D. Paramatti, S. Salmaso, A. E. Tozzi; EUVAC-NET Group, *Pediatr. Infect. Dis. J.* **24**, 761 (2005).
2. N. S. Crowcroft, C. Stein, P. Duclos, M. Birmingham, *Lancet Infect. Dis.* **3**, 413 (2003).
3. N. S. Crowcroft, R. G. Pebody, *Lancet* **367**, 1926 (2006).
4. J. D. Cherry, *Pediatrics* **112**, 405 (2003).
5. H. O. Hallander, A. Advani, D. Donnelly, L. Gustafsson, R.-M. Carlsson, *J. Clin. Microbiol.* **43**, 2856 (2005).
6. F. R. Mooi, I. H. van Loo, A. J. King, *Emerg. Infect. Dis.* **7** (suppl.), 526 (2001).
7. T. Tan, E. Trindade, D. Skowronski, *Pediatr. Infect. Dis. J.* **24** (suppl.), S10 (2005).
8. H. J. Wearing, P. Rohani, *PLoS Pathog.* **5**, e1000647 (2009).
9. S. B. Omer *et al.*, *JAMA* **296**, 1757 (2006).
10. B. Ntezayabo, G. De Serres, B. Duval, *Pediatr. Infect. Dis. J.* **22**, 22 (2003).
11. V. Romanus, R. Jonsell, S. O. Bergquist, *Pediatr. Infect. Dis. J.* **6**, 364 (1987).
12. E. J. Gangarosa *et al.*, *Lancet* **351**, 356 (1998).
13. R.-M. Carlsson, B. Trollfors, *Vaccine* **27**, 5709 (2009).
14. J. Mossong *et al.*, *PLoS Med.* **5**, e74 (2008).
15. D. M. Skowronski *et al.*, *J. Infect. Dis.* **185**, 1448 (2002).
16. D. Güris *et al.*, *Clin. Infect. Dis.* **28**, 1230 (1999).
17. D. Schenzle, *IMA J. Math. Appl. Med. Biol.* **1**, 169 (1984).
18. R. Anderson, R. May, *Infectious Diseases of Humans: Dynamics and Control* (Oxford Univ. Press, Oxford, 1991).
19. M. Keeling, P. Rohani, *Modelling Infectious Diseases* (Princeton Univ. Press, Princeton, NJ, 2008).
20. R. M. Anderson, R. M. May, *J. Hyg. (London)* **94**, 365 (1985).
21. W. J. Edmunds, N. J. Gay, M. Kretzschmar, R. G. Pebody, H. Wachmann; ESEN Project. European Sero-epidemiology Network, *Epidemiol. Infect.* **125**, 635 (2000).
22. J. Wallinga, J. C. M. Heijne, M. Kretzschmar, *PLoS Med.* **2**, e316 (2005).
23. J. D. Cherry, L. J. Baraff, E. Hewlett, *West. J. Med.* **150**, 319 (1989).
24. K. Kretsinger *et al.*, *MMWR Recomm. Rep.* **55** (RR-17), 1 (2006).
25. J. D. Nelson, *Am. J. Dis. Child.* **132**, 371 (1978).
26. J. G. Deville *et al.*, *Clin. Infect. Dis.* **21**, 639 (1995).
27. C. H. von König, S. Halperin, M. Riffelmann, N. Guiso, *Lancet Infect. Dis.* **2**, 744 (2002).
28. J. Schellekens, C. H. von König, P. Gardner, *Pediatr. Infect. Dis. J.* **24** (suppl.), S19 (2005).
29. H. Broutin, P. Rohani, J.-F. Guégan, B. T. Grenfell, F. Simondon, *Vaccine* **22**, 594 (2004).
30. H. Broutin, C. Viboud, B. T. Grenfell, M. A. Miller, P. Rohani, *Proc. Biol. Sci.* **277**, 3239 (2010).
31. P. E. Fine, J. A. Clarkson, *Lancet* **1**, 666 (1982).
32. T. Eidlitz-Markus, M. Mimouni, A. Zeharia, *Clin. Pediatr. (Phila.)* **46**, 718 (2007).

33. We thank three anonymous reviewers for comments. P.R. and A.A.K. are supported by the Research and Policy in Infectious Disease Dynamics program of the Science and Technology Directorate, Department of Homeland Security, and the Fogarty International Center, National Institutes of Health. P.R. was also supported by the Vaccine Modeling Initiative of the Bill & Melinda Gates Foundation.

Supporting Online Material

www.sciencemag.org/cgi/content/full/330/6006/982/DC1
Methods
Figs. S1 to S14
References

23 June 2010; accepted 11 October 2010
10.1126/science.1194134

Essential Regulation of CNS Angiogenesis by the Orphan G Protein–Coupled Receptor GPR124

Frank Kuhnert,[1]* Michael R. Mancuso,[1] Amir Shamloo,[2] Hsiao-Ting Wang,[1] Vir Choksi,[3] Mareike Florek,[4] Hua Su,[5] Marcus Fruttiger,[6] William L. Young,[7] Sarah C. Heilshorn,[8] Calvin J. Kuo[1]†

The orphan G protein–coupled receptor (GPCR) GPR124/tumor endothelial marker 5 is highly expressed in central nervous system (CNS) endothelium. Here, we show that complete null or endothelial-specific GPR124 deletion resulted in embryonic lethality from CNS-specific angiogenesis arrest in forebrain and neural tube. Conversely, GPR124 overexpression throughout all adult vascular beds produced CNS-specific hyperproliferative vascular malformations. In vivo, GPR124 functioned cell-autonomously in endothelium to regulate sprouting, migration, and developmental expression of the blood-brain barrier marker Glut1, whereas in vitro, GPR124 mediated Cdc42-dependent directional migration to forebrain-derived, vascular endothelial growth factor–independent cues. Our results demonstrate CNS-specific angiogenesis regulation by an endothelial receptor and illuminate functions of the poorly understood adhesion GPCR subfamily. Further, the functional tropism of GPR124 marks this receptor as a therapeutic target for CNS-related vascular pathologies.

Organ-specific vascular beds form through angiogenesis, followed by substantial anatomic and molecular differentiation to support various physiologic requirements (*1*, *2*). The central nervous system (CNS) vasculature is highly specialized, with a blood-brain barrier (BBB), extensive pericyte coverage, reciprocal interactions with neurons and glia, and function as a neural stem cell niche (*3*–*5*). In the developing CNS, the perineural vascular plexus (PNVP) surrounds the ventral neural tube at embryonic day 7.5 (E7.5) to E8.5. By E11.5, angiogenic endothelial sprouts invade the neuroepithelium from the pial surface to periventricular areas and branch, generating the periventricular vascular plexus

[1]Department of Medicine, Hematology Division, Stanford University, Stanford, CA 94305, USA. [2]Department of Mechanical Engineering, Stanford University, Stanford, CA 94305, USA. [3]Department of Bioengineering, Stanford University, Stanford, CA 94305, USA. [4]Division of Blood and Marrow Transplantation, Stanford University, Stanford, CA 94305, USA. [5]Center for Cerebrovascular Research, Department of Anesthesia and Perioperative Care, University of California San Francisco (UCSF), San Francisco, CA 94110, USA. [6]UCL Institute of Ophthalmology, University College London, London EC1V 9EL, UK. [7]Center for Cerebrovascular Research, Department of Anesthesia and Perioperative Care, Department of Neurological Surgery, Department of Neurology, University of California, San Francisco, San Francisco, CA 94110 USA. [8]Department of Materials Science and Engineering, Stanford University, Stanford, CA 94305, USA.

*Present address: Regeneron Pharmaceuticals, Tarrytown, NY 10591, USA.
†To whom correspondence should be addressed. E-mail: cjkuo@stanford.edu

Downloaded from www.sciencemag.org on November 11, 2010

(PVVP) (*6*, *7*). This angiogenic invasion has been proposed to occur concomitantly with barriergenesis, the acquisition of BBB properties (*8*, *9*). Heretofore, endothelial receptors mediating CNS-specific angiogenesis have not been described.

We investigated GPR124 or tumor endothelial marker 5 (TEM5), which is an orphan G protein–coupled receptor (GPCR) with a large ectodomain belonging to the adhesion GPCR subfamily (fig. S1A) (*10*). GPR124 (TEM5) was initially identified as differentially expressed in tumor vasculature (*11*, *12*) and in genomic analysis of GPCR loci (*13*). During mouse embryogenesis, GPR124 was expressed in both endothelial cells and pericytes, most prominently in brain and neural tube (fig. S1, B to L), and to lesser degrees in non-CNS embryonic organs, including the liver, heart, and kidney (fig S2). GPR124 was also expressed in embryonic epithelium of lung and esophagus and in mesenchyme (fig. S2). In contrast, adult GPR124 expression was exclusively vascular in tissues examined, with endothelial expression in CNS including the brain and retina (fig. S3) and more widespread pericyte expression in the brain and organs, including the kidney, pancreas, and corpus luteum (fig. S4).

To examine the function of this orphan receptor, we generated a GPR124 lacZ knock-in null allele, which displayed a vascular embryonic expression pattern upon β-galactosidase staining of heterozygous embryos at E10.5 (figs. S5 and S6). No viable adult GPR124$^{-/-}$ (GPR124$^{lacZ/lacZ}$) mice were obtained (fig. S7). Beginning at E11, GPR124$^{-/-}$ embryos exhibited completely penetrant, progressive CNS hemorrhage originating in forebrain telencephalon and ventral neural tube (Fig. 1, A to D, and figs. S7 and S8), with resultant embryonic lethality from E15.5 onward (fig. S7). Paralleling sites of hemorrhage, GPR124$^{-/-}$ embryos at E11.5 displayed selective CNS-specific vascular patterning defects, with markedly reduced angiogenic sprouting into the forebrain telencephalon and thickening of the underlying PNVP, rendering the telencephalon virtually avascular (Fig. 1, E to H). By E14.5, this culminated in formation of basally localized glomeruloid malformations and resultant distally unvascularized telencephalon in GPR124$^{-/-}$ embryos. In contrast, wild-type mice showed efficient migration of endothelial cells to the subventricular zone (SVZ) (Fig. 1, M to R). Similar striking angiogenic deficits with characteristic hemorrhagic glomeruloid malformations were also seen in GPR124$^{-/-}$ ventral neural tube and forebrain ganglionic eminences (Fig. 1, I to L). GPR124 deletion did not impair angiogenic sprouting into the embryonic diencephalon, mid- and hindbrain, or the vascularization of nonneural tissues (Fig. 1, E to F and M to N, and figs. S9 and S10). Electron microscopy (EM) of GPR124$^{-/-}$ CNS vascular malformations revealed numerous packed endothelial cells with scant cytoplasm, enveloped

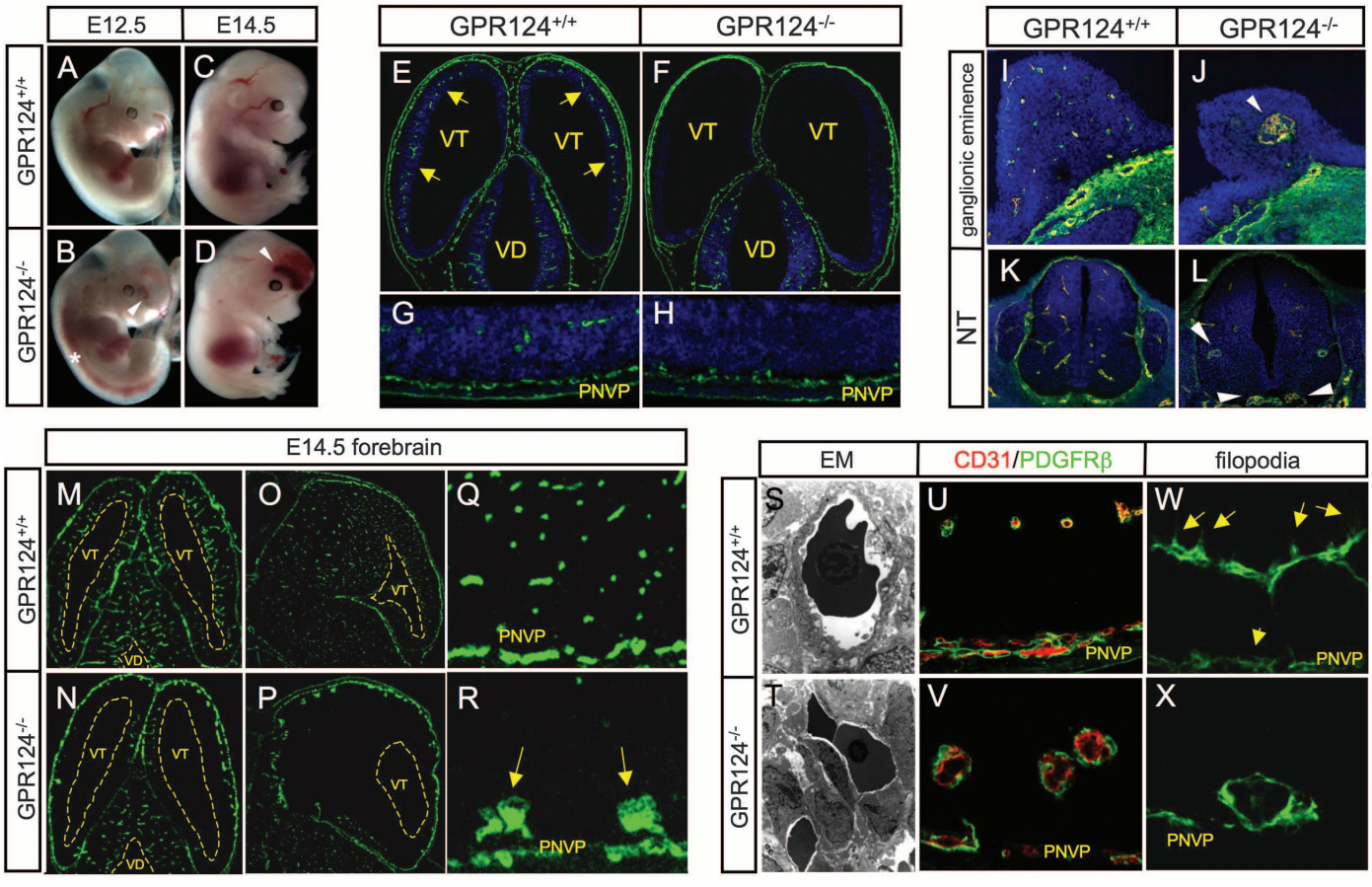

Fig. 1. CNS vascular patterning defects in GPR124$^{-/-}$ embryos. (**A** to **D**) GPR124$^{-/-}$ embryos manifested progressive hemorrhage confined to forebrain telencephalon (arrowheads) and neural tube (asterisk). (**E** and **G**) Wild-type E11.5 embryos exhibited efficient sprouting angiogenesis (arrows) from the PNVP into the telencephalon, which was (**F** to **H**) completely ablated in GPR124$^{-/-}$ embryos that exhibited PNVP thickening only. Green indicates CD31 immunofluorescence (IF). (**I** to **L**) Large, glomeruloid vascular malformations (arrowheads) and absence of a vascular network were observed in E11.5 GPR124$^{-/-}$ forebrain ganglionic eminences and ventral neural tube (CD31 IF). (**M** to **R**) By E14.5, GPR124$^{-/-}$ telencephalon was essentially devoid of a mature capillary network, with glomeruloid malformations abutting the pia/PNVP, whereas the diencephalon was unaffected [(M) to (N), transverse; (O) to (P), sagittal; vascular malformations (arrows); (Q) and (R), CD31 IF]. (**S** to **X**) Glomeruloid malformations were irregular, multilayer endothelial aggregates versus single-layer capillaries in controls [(S) and (T), EM 4300×], with normal peripheral PDGFRβ^{+} pericyte investment [(U) and (V)] but lacked ventricularly directed endothelial filopodia (arrows) [(W) and (X), CD31 IF]. VD, ventricle diencephalons; VT, ventricle telencephalon; blue, 4′,6′-diamidino-2-phenylindole.

Downloaded from www.sciencemag.org on November 11, 2010

by PDGFRβ^{+} pericytes (Fig. 1, S to V). Further, GPR124$^{-/-}$ endothelium showed markedly reduced-to-absent filopodial extensions that when present extended laterally rather than toward the ventricles as in wild type (Fig. 1, W to X). Proliferation, apoptosis, and vascular endothelial growth factor (VEGF) receptor expression were grossly unaltered in GPR124$^{-/-}$ vascular malformations (fig. S11). We conclude that GPR124 displays a pronounced functional tropism for the CNS and is essential for developmental angiogenic sprouting into forebrain and neural tube.

Mice in which Wnt7/β-catenin had been knocked out (Wnt7/β-catenin knockout mice) with CNS angiogenesis deficits exhibit defective developmental expression of the BBB-specific glucose transporter Glut1, suggesting that acquisition of BBB markers may be coupled to developmental brain angiogenesis (*8*, *9*). Glut1 expression was similarly absent in GPR124$^{-/-}$ endothelium in forebrain upon immunofluorescence and quantitative polymerase chain reaction (PCR) analysis of purified primary forebrain GPR124$^{-/-}$ endothelial cells (ECs) (Fig. 2, A to E); expression in mid- and hindbrain was unaffected. Compensatory neuroepithelial Glut-1 up-regulation was present (Fig. 2,

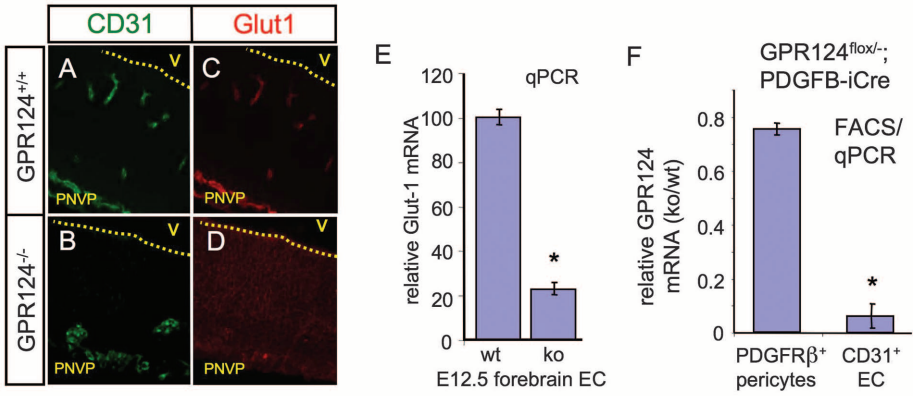

Fig. 2. GPR124 functions cell-autonomously in endothelium. (**A** to **D**) Expression of Glut1 is lost in GPR124$^{-/-}$ CNS endothelium, with compensatory Glut1 up-regulation in neuroepithelium (E12.5). Glut1 is strongly down-regulated in FACS-isolated, GPR124$^{-/-}$ telencephalic endothelium. (**E**) Quantitative PCR, $n = 9$ determinations, E12.5. Selective deletion of GPR124 in FACS-isolated forebrain CD31^{+} endothelium but not PDGFRβ+ pericytes. (**F**) Quantitative PCR, $n = 6$ determinations, E 12.5. (**G** to **L**) E12.5 GPR124$^{flox/-}$;PDGFB-iCre embryos exhibit forebrain hemorrhaging, formation of PNVP-associated glomeruloid vascular malformations, and endothelial Glut1 down-regulation, recapitulating the global GPR124 deletion phenotype. Error bars are ± 1 SD.

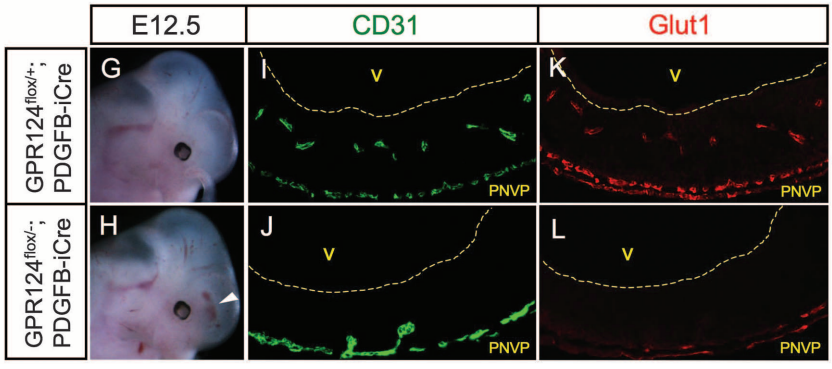

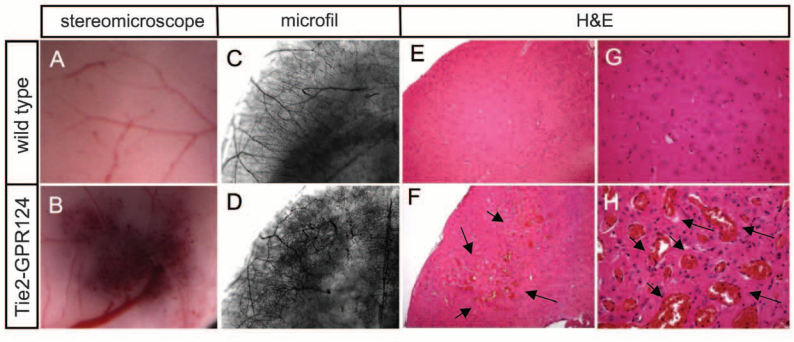

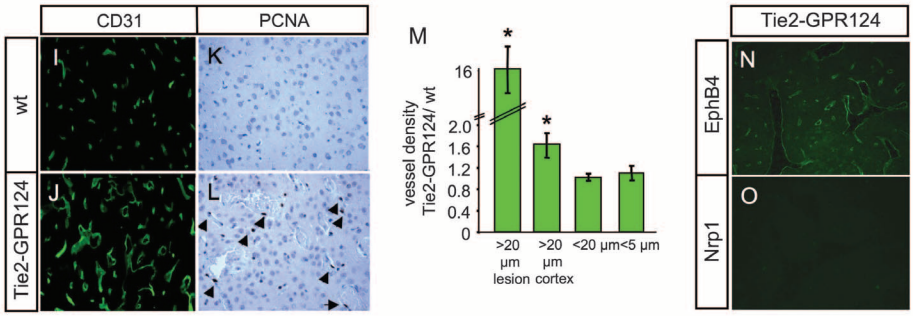

Fig. 3. CNS vascular malformations in adult (12 months old) Tie2-GPR124 transgenic animals. (**A** to **D**) Focally increased red blood cell accumulation in Tie2-GPR124 cerebral cortex [(A) and (B)] corresponded to increased vascular density and tortuous, enlarged vessels upon microfil vascular casting [(C) and (D)]. (**E** to **H**) Hematoxylin and eosin staining of a hypervascular area (arrows) in Tie2-GPR124 cortex [(E) and (F) 100×] revealed dramatically enlarged, engorged thin-walled vessels with intervening neural tissue reminiscent of venous angiomas [(G) and (H) 400×]. (**I** to **M**) Tie2-GPR124 transgenics exhibited increased CD31^{+} microvessel density and markedly enlarged [(I), (J), and (M)] and hyperproliferative vascular malformations versus wild-type controls [(K) and (L); arrowheads denote PCNA^{+} cells]. Tie2-GPR124 CNS vascular malformations expressed the venous marker EphB4 but not the arterial receptor Nrp1 (**N** and **O**). Error bars are ± 1 SD.

Downloaded from www.sciencemag.org on November 11, 2010

C and D), as also seen in Wnt7/β-catenin knockout mice (*8*, *9*).

To demonstrate endothelial cell-autonomous function of GPR124 in regulating CNS angiogenesis, we generated a floxed exon 1 GPR124 allele ($GPR124^{flox}$) and crossed to PDGFB-iCre mice so as to allow endothelial CreER-mediated deletion (*14*). Accordingly, E12.5 $GPR124^{flox/-}$;PDGFB-iCre embryos demonstrated selective GPR124 deletion in endothelium but not pericytes through fluorescence-activated cell sorting (FACS) and quantitative PCR (Fig. 2F). $GPR124^{flox/-}$;PDGFB-iCre mice fully recapitulated the GPR124 null phenotype with forebrain hemorrhage, CNS angiogenic arrest, basally localized glomeruloid malformations, and loss of endothelial Glut1 expression (Fig. 2, G to L). Identical results were obtained with an independent vascular deletion strategy in $GPR124^{flox/-}$;Tie2-Cre mice (fig. S12). These results indicate that GPR124 functions cell-autonomously in CNS endothelium, with Glut1 as a developmentally regulated downstream locus.

To analyze gain-of-function phenotypic outcomes, we generated transgenic mice overexpressing GPR124 cDNA from the Tie2 promoter/long-enhancer active in embryonic and adult endothelium (*15*). Tie2-GPR124 transgenic mice were viable and fertile. The mutant mice exhibited enhanced brain vascular GPR124 immunofluorescence versus nontransgenic littermates and displayed ectopic GPR124 expression throughout the microvasculature of adult organs that do not normally express GPR124, such as the heart and liver (fig. S13). Despite widespread GPR124 overexpression, Tie2-GPR124 animals displayed a progressive brain-specific vascular phenotype characterized by enlarging oligo-focal areas of hypervascularity that were predominantly cortical (>90%, with ~10% in the cerebellum) and presented with ~70% penetrance by 12 months of age, paralleling the forebrain telencephalon distribution of $GPR124^{-/-}$ malformations (Fig. 3, A to H and M); non-CNS organs were unaffected (fig. S14). These lesions consisted of tangled, thin-walled, CD31-positive, grossly dilated hyperproliferative capillaries with associated $PDGFR\beta^{+}$ pericytes (Fig. 3, I to L, and fig. S15). The vascular malformations exhibited intervening neural tissue reminiscent of venous angiomas and expressed the venous marker EphB4 but not the arterial marker Nrp1 (Fig. 3, N and O). Calcifications were frequently associated (fig. S15E), and transgenic mice occasionally exhibited neurologic symptoms, such as ataxia. Thus, both the Tie2-GPR124–overexpressing mice and

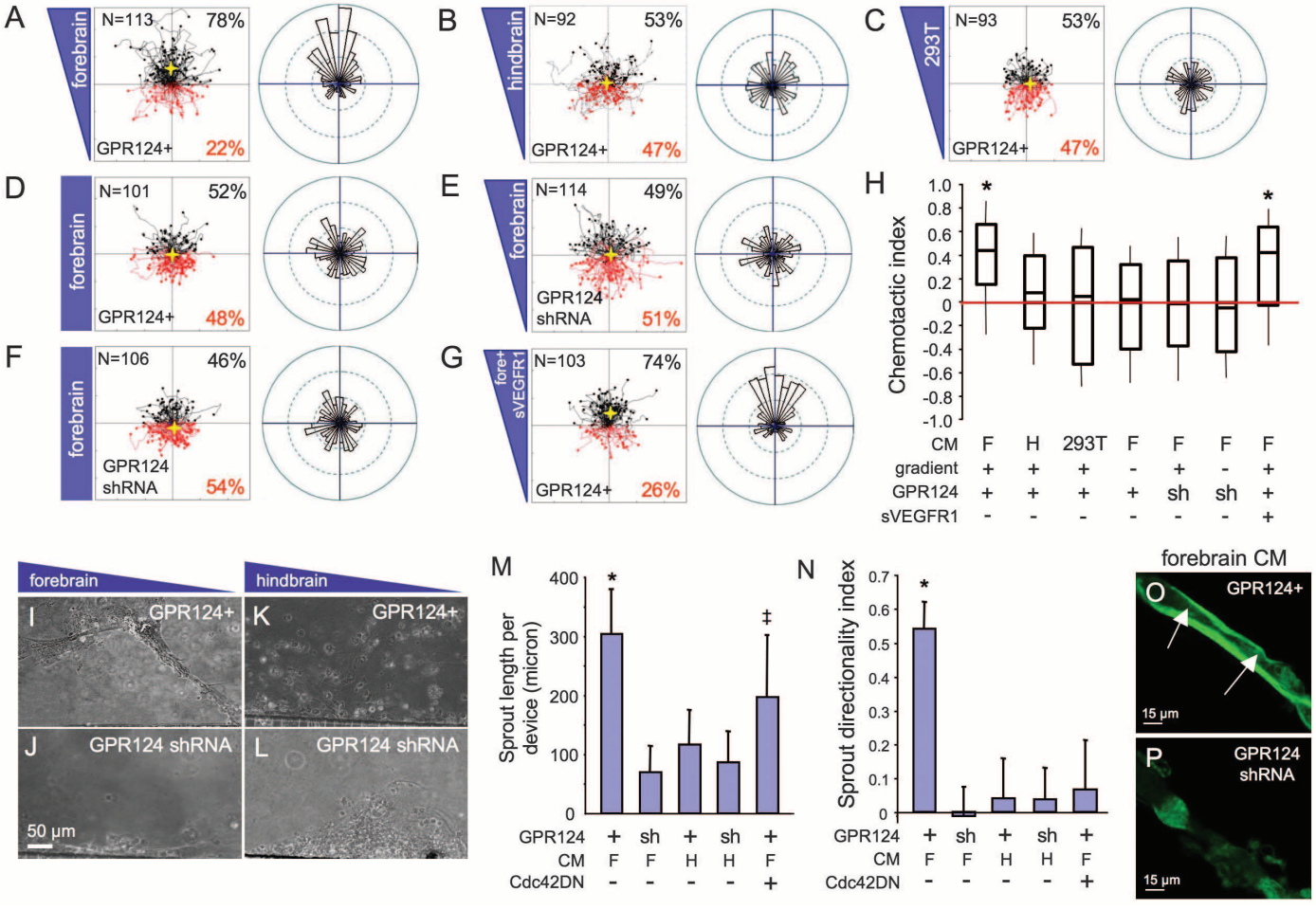

Fig. 4. GPR124 regulates CNS endothelial migration and sprout formation in vitro. Motility of the GPR124-expressing brain endothelial line bEND3 was monitored with real-time video microscopy in a microfluidic migration chamber, allowing extremely stable, shear-minimized linear chemoattractant gradients. (**A** to **C**) GPR124-overexpressing bEND3 cells ($GPR124^{+}$) exhibited directed migration toward gradients of conditioned medium (CM) from cultured E12.5 forebrain cortical cells but migrated randomly to equivalent hindbrain or HEK293T CM [tracks of individual cells (left) and angular histograms (right) are shown]. (**D** to **F**) No directed migration was observed with even distribution of forebrain CM across the microfluidic chamber (no gradient), or GPR124 shRNA; (**G**) migration was further insensitive to a recombinant soluble VEGFR1 ectodomain (400 ng/ml), indicating VEGF-independence. (**H**) Box plot of chemotactic indices of bEND3 migration (center line, median; boxes, upper and lower quartiles, $*P < 0.001$). (**I** to **L**) In a sprout formation assay, $GPR124^{+}$ bEND3 displayed collective cell migration and robust formation of stable sprouts toward forebrain CM gradients, but not to hindbrain CM nor upon GPR124 shRNA knockdown. (**M** and **N**) Dominant-negative Cdc42N17 inhibited sprout directionality but not elongation ($*P < 0.05$; ‡ indicates not significant). $GPR124^{+}$ sprouts toward forebrain CM–contained stable, contiguous lumens, whereas rare GPR124 shRNA sprouts were unstable and failed to lumenize. (**O** and **P**) Confocal microscopy. F, forebrain CM; H, hindbrain CM. Error bars are ± 1 SE. $*P < 0.05$; $n = 3$ to 5 chambers per condition.

Downloaded from www.sciencemag.org on November 11, 2010

GPR124$^{-/-}$ embryos displayed angiogenic phenotypes highly restricted to the CNS vasculature.

The angiogenic defects in GPR124$^{-/-}$ forebrain but not mid- or hindbrain suggested that GPR124 could mediate endothelial migration toward forebrain-enriched regional guidance cues within the embryonic CNS. The GPR124-expressing brain endothelial cell line bEND3 was used in a microfluidic migration chamber, allowing extremely stable, shear-minimized linear chemoattractant gradients and real-time video microscopy of cellular motility (fig. S16A) (*16*). GPR124-overexpressing bEND3 cells (GPR124^{+}) (fig. S16B) exhibited directed migration in microfluidic chambers toward gradients of conditioned medium from cultured E12.5 forebrain cortical cells (F) but migrated randomly when presented with equivalent hindbrain preparations (H) or with human embryonic kidney (HEK) 293T–conditioned medium (chemotactic indices of 0.44, 0.08, and 0.02, respectively) (Fig. 4, A to C and H, and fig. S17). Further, directed migration was not observed when forebrain-conditioned medium was evenly distributed across the microfluidic chamber (no gradient), or upon GPR124^{-} short hairpin RNA (shRNA) knockdown (Fig. 4, D to F and H, and fig. S17). GPR124^{+} bEND3 migration to the forebrain CM gradient was insensitive to a recombinant soluble VEGFR1 ectodomain, which is consistent with VEGF-independence. (Fig. 4, G and H, and fig. S17).

We also used a second microfluidic assay in which bEND3 cells sprouted through microcapillaries into an acellular chamber that contained a transverse gradient of chemoattractant (fig. S18). This revealed multicellular endothelial sprout elongation and directional migration toward forebrain- but not hindbrain-conditioned medium gradients that was ablated with GPR124 shRNA (Fig. 4, I to N). Cdc42 was required for GPR124-dependent directional migration but not sprout elongation, as revealed by a dominant-negative Cdc42 allele (Cdc42N17) (Fig. 4, M to N). GPR124^{+} sprouts to forebrain-conditioned medium demonstrated contiguous lumen formation upon three-dimensional confocal reconstruction, which was not observed with GPR124 shRNA (Fig. 4, O and P), paralleling lumen enlargement in Tie2-GPR124 transgenics (Fig. 3, H and J). Thus, GPR124 mediates cell-autonomous and VEGF-independent regulation of endothelial migration in response to factor (or factors) secreted from embryonic forebrain neuroepithelium.

Our studies demonstrate that GPR124 (TEM5) is a previously unknown proangiogenic, endothelial receptor with pronounced functional tropism for the CNS vasculature in both loss-of-function and gain-of-function settings. Although GPR124 was initially described as up-regulated in neoplastic (versus resting) endothelium (*11*, *12*), our work establishes its function in normal tissues as a previously unsuspected and essential regulator of CNS angiogenesis, via an endothelial cell-autonomous pathway regulating Cdc42-dependent angiogenic migration and sprouting. Despite the atretic and misoriented filopodia in GPR124 knockout vasculature, GPR124-deficient endothelium can incorporate into "tip cell" positions upon mosaic analysis (fig. S19).

Because GPR124 is expressed at all levels of the CNS vasculature, the forebrain- and ventral neural tube–specific angiogenic deficits suggest a corresponding embryonic spatial restriction of either GPR124 ligand or signaling. Further, the GPR124 phenotype indicates substantial regional heterogeneity in embryonic CNS requirements for angiogenic signals, which could operate in the context of telencephalic angiogenic gradients, as have been proposed (*17*). The spatial restriction of GPR124$^{-/-}$ angiogenesis deficits is strongly paralleled by a VEGF-independent activity mediating GPR124- and Cdc42-dependent migration to forebrain- but not hindbrain-conditioned medium. In principle, this activity could represent ligand or render competence to respond to ligand. However, this by no means excludes GPR124 interactions with nonsoluble factors such as extracellular matrix (*18*) or transmembrane proteins, or distinct mechanisms for nonangiogenic receptor functions. The progressive nature of Tie2-GPR124 vascular malformations indicates a continued sensitivity of brain endothelium to GPR124 during adulthood, with the adult temporal window possibly reflecting either moderate gain-of-function with receptor overexpression or differential sensitivity to receptor in adulthood.

Wnt/β-catenin (*8*, *9*), VEGF/Nrp1 (*19*, *20*), integrins α_v and β_8 (*21*–*23*), and Id1/Id3 (*24*) mutations impair CNS angiogenesis, often with knockout glomeruloid malformations that resemble the GPR124 phenotype (*25*). Regional regulation of angiogenesis has been reported in CXCL12/CXCR4 mutants although not in the CNS (*26*, *27*). However, as opposed to GPR124, none of these loci encode endothelial receptors with CNS functional tropism, and instead manifest vascular deficits globally or in subsets of non-CNS organs (*28*–*30*). Despite marked phenotypic overlap, GPR124 does not appear to exhibit epistasis with β-catenin (fig. S20), and we cannot exclude GPR124 function in a parallel pathway, coupling embryonic CNS angiogenesis to developmental Glut1 expression. Similar epistasis studies with Id1 and integrin β8 have also been negative (fig. S20).

The CNS enrichment of endothelial GPR124 expression, as well as the GPR124 gain- and loss-of-function angiogenesis phenotypes, suggest the potential relevance of this receptor to various CNS-related vascular pathologies, including stroke and malignancy. Certainly, the determination of potential causal relations between GPR124 and CNS vascular malformations or germinal matrix hemorrhage (*31*) in human and mouse should be worthwhile. The current analyses also provide insight into the poorly understood functions of the adhesion receptor class of GPCRs (*13*) and show how control of angiogenesis can be managed in different ways by specific organ systems, in this case with insight into angiogenesis in the CNS and development of the BBB. Similar signaling pathways may be deployed among vascular beds specific to other organ systems.

References and Notes

1. P. Carmeliet, *Nature* **438**, 932 (2005).
2. W. C. Aird, *Circ. Res.* **100**, 174 (2007).
3. P. Ballabh, A. Braun, M. Nedergaard, *Neurobiol. Dis.* **16**, 1 (2004).
4. W. M. Pardridge, *Methods Mol. Med.* **89**, 385 (2003).
5. Q. Shen *et al.*, *Science* **304**, 1338 (2004).
6. K. A. Hogan, C. A. Ambler, D. L. Chapman, V. L. Bautch, *Development* **131**, 1503 (2004).
7. R. Herken, W. Götz, K. H. Wattjes, *J. Anat.* **164**, 85 (1989).
8. J. M. Stenman *et al.*, *Science* **322**, 1247 (2008).
9. R. Daneman *et al.*, *Proc. Natl. Acad. Sci. U.S.A.* **106**, 641 (2009).
10. Materials and methods are available as supporting material on *Science* Online.
11. B. St Croix *et al.*, *Science* **289**, 1197 (2000).
12. E. B. Carson-Walter *et al.*, *Cancer Res.* **61**, 6649 (2001).
13. R. Fredriksson, D. E. Gloriam, P. J. Höglund, M. C. Lagerström, H. B. Schiöth, *Biochem. Biophys. Res. Commun.* **301**, 725 (2003).
14. S. Claxton *et al.*, *Genesis* **46**, 74 (2008).
15. T. M. Schlaeger *et al.*, *Proc. Natl. Acad. Sci. U.S.A.* **94**, 3058 (1997).
16. A. Shamloo, N. Ma, M. M. Poo, L. L. Sohn, S. C. Heilshorn, *Lab Chip* **8**, 1292 (2008).
17. A. Vasudevan, J. E. Long, J. E. Crandall, J. L. Rubenstein, P. G. Bhide, *Nat. Neurosci.* **11**, 429 (2008).
18. M. Vallon, M. Essler, *J. Biol. Chem.* **281**, 34179 (2006).
19. H. Gerhardt *et al.*, *Dev. Dyn.* **231**, 503 (2004).
20. S. Raab *et al.*, *Thromb. Haemost.* **91**, 595 (2004).
21. J. H. McCarty *et al.*, *Development* **132**, 165 (2005).
22. J. Zhu *et al.*, *Development* **129**, 2891 (2002).
23. B. L. Bader, H. Rayburn, D. Crowley, R. O. Hynes, *Cell* **95**, 507 (1998).
24. D. Lyden *et al.*, *Nature* **401**, 670 (1999).
25. M. R. Mancuso, F. Kuhnert, C. J. Kuo, *Lymphat. Res. Biol.* **6**, 173 (2008).
26. T. Ara, K. Tokoyoda, R. Okamoto, P. A. Koni, T. Nagasawa, *Blood* **105**, 3155 (2005).
27. A. F. Siekmann, C. Standley, K. E. Fogarty, S. A. Wolfe, N. D. Lawson, *Genes Dev.* **23**, 2272 (2009).
28. P. Carmeliet *et al.*, *Nature* **380**, 435 (1996).
29. N. Ferrara *et al.*, *Nature* **380**, 439 (1996).
30. A. Cattelino *et al.*, *J. Cell Biol.* **162**, 1111 (2003).
31. P. Ballabh, *Pediatr. Res.* **67**, 1 (2010).

32. We are indebted to R. Daneman, B. Barres, C. Chartier, and the Kuo laboratory for comments; J. Yuan and J. Hampton for animal husbandry and genotyping; and A. Connolly and H. Vogel for neuropathology. F.K. was supported by an American Heart Association (AHA) Postdoctoral Fellowship and M.R.M. by AHA Predoctoral Fellowship AHA09PRE2110036 and the Stanford Medical Scientist Training Program Program (National Institute of General Medical Science, NIH, GM07365). This work was also supported by NIH R21 NS070153 and AHA 10GRNT3130004 (H.S.); NIH R01NS27713 (W.L.Y.); P01NS44155 (W.L.Y. and H.S.); U.K. Medical Research Council G0501711 (M.F.); NIH 1DP2 OD006477, 1R21 NS058600, and National Academies Keck Futures Initiative CS10 grants (S.C.H.); and NIH 1R01NS052830, 1R01NS064517, 1R01HL074267, Brain Tumor Society, Goldhirsh Foundation, and the Stanford Center for Children's Brain Tumors grants (C.J.K.). F.K., H.W., and C.J.K. have a patent pending regarding vascular applications of GPR124.

Supporting Online Material

www.sciencemag.org/cgi/content/full/330/6006/985/DC1
Materials and Methods
Figs. S1 to S20
References

16 August 2010; accepted 4 October 2010
10.1126/science.1196554

Downloaded from www.sciencemag.org on November 11, 2010

NEW PRODUCTS

UV-VIS SPECTROSCOPY

The Evolution 200 series of next generation UV-Visible spectrophotometers includes three instruments which satisfy specific applications from standard quantitative analysis to research life science assays. This series features the new INSIGHT software with customized user environment scripting capabilities. Designed for routine QA/QC analyses in the life science, food and beverage, and material science industries as well as offering fast data collection rates for kinetics measurements (up to 100 data points/sec), these instruments combine high performance and straightforward software, enabling personalized operation for greater productivity. The Evolution 200 series instruments feature high quality accessories and application specific technology to meet a wide range of sampling needs. Innovative Smart accessories enable accurate, cost-effective sample handling with automated software recognition and programmable control. Adding temperature control and fiber optic accessories can increase the instrument's productivity and extend sampling options.

Thermo Fisher Scientific

For info: 1-800-532-4752 | www.thermoscientific.com/evo200

MITOCHONDRIAL DNA ISOLATION

The XIT Mitochondrial DNA kit combines FOCUS Mitochondria technology with the XIT DNA isolation technology in a single kit. The kit supplies Subcell buffers to lyse cell and animal tissue in order to remove cellular proteins and nuclei from the highly enriched, intact, and active mitochondrial fraction. The mitochondria are then lysed with the included lysis buffer and treated with LongLife Proteinase K to degrade the proteins. Subsequently, mitochondrial DNA can be isolated using alcohol precipitation. The kit is designed for around 100 preparations consisting of $20x10^6$ mammalian cells/prep. The XIT Mitochondrial DNA kit also contains protocols for isolation of mitochondria from soft (i.e. brain and liver) and hard (i.e. cardiac and skeletal muscle) tissue.

G-Biosciences

For info: 800-628-7730 | www.gbiosciences.com

FRAGMENT LIBRARY

The new Maybridge Ro3 Diversity Library has been computationally engineered to build on the key customer-driven features of the original Maybridge Ro3 Library, such as "Rule of Three" (Ro3) compliance, pharmacophoric enrichment, and quality assurance of at least 95 percent. The Maybridge Ro3 Diversity Library offers both an improved structural diversity profile and experimental solubility data for every one of the 1,500 member compounds. Full Ro3 compliance means that all 1,500 fragments have the physicochemical properties that increase the probability of successful "hits." The broad portfolio also provides access to analogues for fragment hopping, as well as reactive analogues for rapid hit evolution and derivatization. Consequently, these Maybridge Fragments provide an ideal starting point for a lead-optimization, structure-based drug discovery program, and the ultimate evolution of a new molecule in the drug discovery process. Every fragment in the new Maybridge library has been experimentally triaged to assure solubility in both dimethyl sulfoxide (200 mM) and aqueous phosphate buffer (1 mM).

Maybridge

For info: +44-(0)-1840-770567 | www.maybridge.com

MICROSCOPY IMAGE DECONVOLUTION

Designed to offer control and processing for microscope-based experimental systems, the cellSens Dimensions software package allows users to conduct a range of complex and highly sophisticated experiments, from extended focal imaging to multiple image alignment and multiple position imaging. The cellSens deconvolution solution module employs a constrained iterative algorithm to remove out-of-focus blur in advanced life science imaging. This high-speed operation provides extremely sharp images, as well as near confocal quality, with the ability to correct for any spherical aberrations. Integrating seamlessly with the cellSens Dimensions software, outstanding performance and quality are guaranteed. The resulting high-quality image stacks can be visualized in three dimensions, using the powerful VoxelViewer that shows structures, iso-surfaces, and projections. A broad range of image types can be deconvolved using the Olympus deconvolution solution module, including fluorescence, confocal, and brightfield.

Olympus

For info: +44-(0)-1702-616333 | www.microscopy.olympus.eu

GEL DOCUMENTATION

The GENi is an affordable, fully motorized gel documentation system. This innovative system generates true 16-bit publication quality images of fluorescent and colored DNA and protein gels. Designed for simple, quick detection, the GENi gel documentation system is fitted with a fully motorized camera and zoom lens, providing a two megapixel resolution, as well as a six position motorized filter wheel, ensuring safe, hands-off imaging in seconds. GENi features a compact darkroom and built-in computer with a large touch screen, which means the system takes up minimal bench space while still offering users complete control of the camera, optics, and filters. The system's powerful integral processor allows users to generate, print, and save perfect gel and blot images every time.

Syngene

For info: 800-686-4407 | www.syngene.com

Electronically submit your new product description or product literature information! Go to **www.sciencemag.org/products/newproducts.dtl** for more information.

Newly offered instrumentation, apparatus, and laboratory materials of interest to researchers in all disciplines in academic, industrial, and governmental organizations are featured in this space. Emphasis is given to purpose, chief characteristics, and availability of products and materials. Endorsement by *Science* or AAAS of any products or materials mentioned is not implied. Additional information may be obtained from the manufacturer or supplier.

Downloaded from www.sciencemag.org on November 11, 2010

Multiply The Power of Science

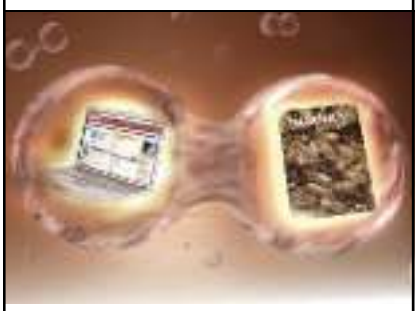

***Science* Careers**
Classified Advertising

For full advertising details, go to ScienceCareers.org and click For Employers, or call one of our representatives.

Tracy Holmes
Worldwide Associate Director
Science Careers
Phone: +44 (0) 1223 326525

UNITED STATES & CANADA

E-mail: advertise@sciencecareers.org
Fax: 202-289-6742

Tina Burks
Midwest/West Coast/
South Central/Canada
Phone: 202-326-6577

Elizabeth Early
East Coast & Industry
Phone: 202-326-6578

Marci Gallun
Sales Administrator
Phone: 202-326-6582

Online Job Posting Questions
Phone: 202-326-6577

EUROPE & REST OF WORLD

E-mail: ads@science-int.co.uk
Fax: +44 (0) 1223 326532

Alex Palmer
Phone: +44 (0) 1223 326527

Susanne Kharraz Tavakol
Phone: +44 (0) 1223 326529

Dan Pennington
Phone: +44 (0) 1223 326517

Lisa Patterson
Phone: +44 (0) 1223 326528

JAPAN

ASCA Corporation
Jie Chin
Phone: +81-3-6802-4616
Fax: +81-3-6802-4615
E-mail: careerads@sciencemag.jp

To subscribe to *Science*:
In United States call 866-434-2227
In the rest of the world call +1 202-326-6417

All ads submitted for publication must comply with applicable U.S. and non-U.S. laws. *Science* reserves the right to refuse any advertisement at its sole discretion for any reason, including without limitation for offensive language or inappropriate content, and all advertising is subject to publisher approval. *Science* encourages our readers to alert us to any ads that they feel may be discriminatory or offensive.

Science Careers
From the journal *Science* AAAS

POSITIONS OPEN

TEXAS A&M UNIVERSITY

The Department of Biochemistry and Biophysics at Texas A&M University (**website: http://biochemistry.tamu.edu**) invites applications for **TENURE-TRACK FACULTY POSITIONS** in an open search with an emphasis on areas related to chemical genetics, metabolomics, drug discovery, and imaging diagnostics. Faculty rank is open and applications from candidates at all levels are encouraged. In addition to establishing vigorous independent research programs, the successful candidates will fully participate in our undergraduate and graduate educational programs.

Candidates should submit curriculum vitae, up to three reprints, a description of research plans of up to three pages, and arrange for three professional reference letters to be submitted. All documents can be submitted electronically to **e-mail: sacsecy2@gmail.com** or in paper format to:

Biochemistry Search Committee
Texas A&M University
Department of
Biochemistry and Biophysics
3474 TAMU
College Station, TX 77843-3474

Review of applicants will begin November 15, 2010, and continue until the positions are filled.

Texas A&M University is an Equal Opportunity/Affirmative Action Employer that is committed to improving diversity.

MICROBIOLOGIST

The Department of Biological Sciences at Bowling Green State University (BGSU) invites applications for a tenure-track Microbiologist position beginning August 2011. Preference given to candidates who combine experimental and bioinformatic approaches. Possible areas of expertise include pathogenesis, biodiversity, microbial ecology, or microbial genetics. Applicants expected to develop productive research programs, actively seek extramural funding, and contribute to undergraduate and graduate teaching.

Applications should include a cover letter, curriculum vitae, statements of research plans and teaching plans/experience, representative publications and three reference letters, and should be submitted to: **Microbiologist Search Committee, Department of Biological Sciences, BGSU, Bowling Green, OH 43403-0208** by December 17, 2010. Further information about our department can be found at **website: http://www.bgsu.edu/departments/biology** or send to **e-mail: pmorris@bgsu.edu.**

BGSU is an Affirmative Action/Equal Opportunity Employer/Educator and encourages applications from women, minorities, veterans and persons with disabilities.

STAFF ASSOCIATE
Division of Immunogenetics
Department of Pathology & Cell Biology
Columbia University

Columbia University's Department of Pathology & Cell Biology, Division of Immunogenetics, invites applications for a Staff Associate position to perform flow cytometric analysis of human hematopoietic cells, report results to physicians and participate in the development of new laboratory protocols. Minimum requirements are: B.S. degree and four years experience in cellular immunology and/or molecular genetics. Experience in flow cytometry and computer skills is essential. The candidate should be certified by the New York State Department of Health as a laboratory technician or technologist. This position requires working evenings and/or weekend hours.

Interested applicants should apply online at **website: http://academicjobs.columbia.edu/applicants/Central?quickFind=53893.** *Columbia University is an Equal Opportunity/Affirmative Action Employer.*

POSITIONS OPEN

UT SOUTHWESTERN MEDICAL CENTER

TENURE-TRACK POSITIONS
The University of Texas
Southwestern Medical Center

ASSISTANT PROFESSORS. The Department of Physiology invites outstanding scientists with Ph.D., M.D., or equivalent degrees to apply for tenure-track Assistant Professor positions. Candidates who use innovative optical, mechanical, electrical, molecular, biological, or computational methods with important applications to physiological systems, ranging from individual genes and proteins to cells and organs are encouraged to apply. However, the scientific excellence of the candidates is more important than the specific area of research.

These positions are part of the continuing growth of the Department at one of the country's leading academic medical centers and will be supported by significant laboratory space on our new campus, competitive salaries, and exceptional start-up packages. The University of Texas Southwestern Medical Center is the scientific home to four Nobel Prize laureates, 18 members of the National Academy of Sciences, and 18 members of the Institute of Medicine. UT Southwestern conducts more than 3,500 research projects annually totaling more than $400 million.

Applicants should submit curriculum vitae, a brief statement of research plans, and arrange to have three letters of reference sent to: **James Stull, Ph.D., c/o Ronald Doris, Department of Physiology, The University of Texas Southwestern Medical Center, 5323 Harry Hines Boulevard, Dallas, TX 75390-9040.** *UT Southwestern strongly encourages applications from women, minorities, and people with physical challenges. An Equal Opportunity Employer.*

FACULTY POSITIONS

Eppley Institute, home of the NCI-designated University of Nebraska Medical Center Eppley Cancer Center, seeks candidates for full-time, tenure-track faculty positions. Candidates are expected to develop an independent extramurally funded research program in basic/translational cancer research complementary to existing strengths and allied with the overall directions of the Center, participate in graduate-level teaching in the Cancer Research Graduate Program and/or other UNMC graduate programs and engage in institutional service based on their expertise. Areas of particular interest include chemical biology with the objective of (a) identifying novel therapeutic agents using high throughput/systems biology, (b) targeted cancer therapies, (c) experimental cancer models, and (d) biological evaluation of nanomedicine cancer therapies. Eppley currently has 30 tenured and tenure-track faculty and the Cancer Center has over 100 primary members that focus on externally funded research. Faculty rank and compensation depend on qualifications. Start date is July 1, 2011. To apply, visit **website: https://jobs.unmc.edu** and search reference **requisition 3421.** Additional information at **website: http://www.unmc.edu/cancercenter/.** Submit a summary of research experience and future plan with a current curriculum vitae and three letters of reference electronically by December 31, 2010, to: **Matt Winfrey,** at **e-mail: winfreym@unmc.edu** or mail him at **Eppley Institute, 985950 Nebraska Medical Center, Omaha, NE 68198-5950.** *Equal Employment Opportunity/Affirmative Action; individuals from diverse backgrounds are encouraged to apply.*

THE AMERICAN UNIVERSITY OF BEIRUT
Department of Biology

The Biology Department at the American University of Beirut is seeking to fill an **ASSISTANT PROFESSORSHIP** in the field of Population Genetics with experience in Bioinformatics to begin September 15, 2011. Appointments at higher rank will be considered. Applications will be accepted until January 15, 2011. For more information on this position, please visit **website: http://www.aub.edu.lb/fas/.** *The American University of Beirut is an Affirmative Action/Equal Opportunity Employer.*

National Eye Institute

Associate Director for Science Policy and Legislation

The National Eye Institute (NEI), a major component of the National Institutes of Health (NIH) and the Department of Health and Human Services (DHHS), is seeking exceptional candidates for the challenging position of Associate Director for Science Policy and Legislation, NEI. The NEI is responsible for a national and international program to conduct and support research, training, health information dissemination, and other programs with respect to blinding eye diseases, visual disorders, mechanisms of visual function, preservation of sight, and the special health problems and requirements of individuals who are visually impaired.

The Associate Director for Science Policy and Legislation is located within the NEI Office of the Director and reports directly to the NEI Director. This position exercises the full range of supervisory authority and directs a staff consisting of Health Science Program Managers, Program Analysts, Technical Writer-Editors and Program Assistants. This is a scientific position at the highest level within the NEI that includes a significantly expanded scope of activities, including advising the NEI Director, setting scientific and programmatic priorities, developing scientific policy and determining resource allocation. The incumbent, as the Director of the Office of Program Planning and Analysis, serves as the NEI's delegate on scientific matters with Congressional staff, OMB, the extramural vision research community, and the National Advisory Eye Council with respect to planning and trans-NIH activities. The incumbent serves as the NIH Roadmap Nanomedicine Initiative (RNI) Project Team Leader and provides guidance to a trans-NIH team of senior extramural and intramural scientists.

NOTE: This is a time-limited appointment not to exceed five (5) years.

Applicants must possess a Ph.D., M.D., or equivalent doctorate degree in the biomedical sciences, with broad senior-level research experience and experience in direct administration of a research program. Applicants should be known and respected within their profession, both nationally and internationally, as distinguished individuals of outstanding scientific competence and administrative capability. Candidates should have demonstrated leadership; serving as a spokesperson; planning, program assessment, and analysis of program objectives; resolution of operational problems and issues; and the ability to manage financial and human resources including building, motivating, and maintaining a culturally diverse staff. Experience with NIH administrative policies, procedures and operations are highly desirable but not essential.

Salary is commensurate with experience and qualifications. Full Federal benefits are available including leave, health and life insurance, long-term care insurance, retirement, and retirement savings plan (401k equivalent).

Interested candidates should send a letter of interest, including a brief description of research and administrative experience, curriculum vitae and bibliography, and the names of at least three references to: **Chair, Search Committee at NEISearch@nei.nih.gov or 31 Center Drive, Room 6A03, MSC 2510, Bethesda, MD**. Applications should be received by December 15, 2010. For questions contact **Dr. Paul A Sieving, Director, NEI at paul.sieving@nih.gov**. For more information about NEI visit **http://www.nei.nih.gov/**

Department of Health and Human Services
National Institutes of Health

Clinical Director
National Institute of Arthritis and Musculoskeletal and Skin Diseases

The Intramural Research Program of the National Institute of Arthritis and Musculoskeletal and Skin Diseases (NIAMS) is seeking a physician-scientist to serve as Clinical Director. This individual will direct the NIAMS Program in Translational Research, which includes training and clinical care branches as well as multiple investigative laboratories and branches. Investigators in the Clinical Program conduct studies in natural history and treatment as well as basic investigations into the etiology and/or pathophysiology of disease. The candidate should have the ability to manage this diverse clinical research enterprise and to provide the leadership to maintain the outstanding track record of the NIAMS Clinical Program. The ideal candidate for this position is an M.D. or M.D.-Ph.D. who is board-certified or board-eligible in either Pediatrics, Internal Medicine and Rheumatology or Allergy/Immunology. Potential areas of concentration would include rheumatoid arthritis, systemic lupus erythematosus, ankylosing spondylitis, vasculitis, scleroderma, myositis, osteoarthritis, or other inflammatory/rheumatic diseases. The candidate should have experience in conducting clinical or translational research and in immunology, cell biology, genetics, or other areas of research relevant to rheumatic or autoimmune disease. The candidate will also be provided generous independent resources to develop his/her own clinical or translational research program as a tenured investigator within NIAMS.

The NIAMS Clinical Program is part of the NIH Intramural Research Program, located in Bethesda, Maryland. Investigators in this program have full privileges to admit their research subjects, free of charge to the patient, to the new Mark O. Hatfield Clinical Research Center, a state-of-the-art 230-bed hospital fully devoted to clinical and translational studies. Ample resources will be provided to the successful applicant to establish a first-rate Clinical Program and their own research program in his or her area of concentration. The NIAMS Intramural Research Program, headed by its Scientific Director, Dr. John O'Shea, comprises several outstanding programs in cytokine biology, signaling, genetics, and structural biology, and the broader NIH Bethesda campus provides a rich and highly interactive environment within a wide range of basic and translational research disciplines that relate directly to rheumatology.

Salary will be commensurate with experience. A full package of benefits, including retirement, health, life, and long-term care insurance, and a Thrift Savings Plan, is available. Qualified international applicants who have passed the ECFMG or USMLE examinations or have comparable qualifications are welcome to apply.

Interested applicants should send a curriculum vitae, a one-page summary of research interests, and the names of three referees to **Ms. Linda Peterson, 31 Center Drive, MSC 2350, Building 31, Room 4C12, Bethesda, MD 20892-2350, e-mail petersonl@arb.niams.nih.gov**. If you need additional information, please call **Dr. John O'Shea at 301-496-2612**. Review of applications will begin on or about **January 3, 2011**, but applications will be accepted until the position is filled.

WWW.NIH.GOV

Tenure/Tenure Track Investigator Position
Laboratory of Immunology

The Laboratory of Immunology (LI), Division of Intramural Research, National Institute of Allergy and Infectious Diseases, National Institutes of Health, invites applications for a tenure/tenure-track investigator position in immunology. Applicants should have a Ph.D., M.D., or equivalent degree; an outstanding record of postdoctoral accomplishment; and an interest in any area of biomedical research related to immunology.

Specifically, we seek a highly creative individual who will establish an independent, world-class research program that takes full advantage of the special opportunities afforded by the stable, long-term funding of the intramural research program at NIH. Applicants should be interested in developing and applying novel approaches to the study of problems of major biological and/or medical importance, which could include a significant clinical or translational effort in addition to bench research. The successful candidate would have access to the NIH Clinical Center, a state-of-the-art research hospital on the NIH campus in Bethesda, MD, and would have ample opportunity to participate in the activities of the Center for Human Immunology and other trans-NIH initiatives involving technology development, translational investigation, and multidisciplinary science.

Generous ongoing support for salary, technical personnel, postdoctoral fellows, equipment, and research supplies will be provided. Available cores or collaborative facilities include flow cytometry, advanced optical imaging, microarray generation and analysis, high throughput sequencing, computational biology, production of transgenic and gene-manipulated mice, biosafety level (BSL)-3 facilities, chemical genomics, and support for projects involving RNAi screening. In addition to an outstanding, international postdoctoral community, a superior pool of graduate and undergraduate students is available to the successful applicant.

NIAID's Laboratory of Immunology has a distinguished history of accomplishment in immunology. We strongly encourage application by outstanding investigators who can continue and enhance this record of achievement. Current LI investigators are Ronald Germain, Michael Lenardo, David Margulies, Stefan Muljo, William Paul, Ethan Shevach, and Tsan Xiao.

To apply, e-mail your curriculum vitae, bibliography, and an outline of a proposed research program (no more than two pages) in PDF format to Ms. Bao-Hanh Ngo at **LIT-TTSearch@niaid.nih.gov**. In addition, three letters of reference must be sent directly from the referee to Drs. Giorgio Trinchieri and Dan Kastner, Co-Chairs, NIAID Search Committee, c/o Ms. Bao-Hanh Ngo at **LIT-TTSearch@niaid.nih.gov** or 10 Center Drive, MSC 1356, Building 10, Room 4A22, Bethesda, MD 20892-1356. E-mail is preferred.

Applications will be reviewed starting **December 13, 2010**, and will be accepted until the position is filled. For further information about this position, contact Dr. William Paul at 301-496-5046 or **wpaul@niaid.nih.gov**.

A full package of benefits (including retirement and health, life, and long-term care insurance) is available. Women and minorities are especially encouraged to apply. U.S. citizenship is not required.

Further information on working at NIAID is available on our Web site at **www.niaid.nih.gov/careers/LIS**.

NIAID

National Institute of Allergy and Infectious Diseases

NATIONAL INSTITUTES OF HEALTH

Okinawa Institute of Science and Technology
New Faculty Positions in Mathematics

The Okinawa Institute of Science and Technology (OIST **http:// www.oist.jp**) invites applications for new faculty positions as it enters a period of growth in preparation for transition to an international graduate university in 2012. Approximately 15 faculty positions in several areas will be filled during this search. OIST provides a world-class research environment in newly completed facilities in an area of distinctive culture, unique ecology, and outstanding natural beauty.

Prof. Jonathan Dorfan, an internationally recognized experimental physicist, has been selected as the President of the graduate university. As the former Director of SLAC at Stanford, he has extensive experience supporting research in particle physics and the broad range of physical, chemical and life sciences that form the diverse program of the X-ray science carried out at SLAC's synchrotron source and its new X-ray laser.

The current OIST program is strongly focused in the Life Sciences and includes genomics, developmental biology, mathematical and computational biology, molecular & cell sciences and neuroscience. Furthermore, OIST is in the process of establishing the foundations of a complementary program focused in the physical sciences with several new appointments. We seek mathematicians, statisticians or logicians with a demonstrated ability to collaborate and contribute to interdisciplinary research in the natural sciences, and the intention to become an integrated member in the OIST research community. Applicants' areas of research do not necessarily need to be restricted to fields typically considered to belong to applied mathematics, and we welcome proposals which suggest new forms of interaction between mathematics and the natural sciences.

The nature of the physical plant and the non-departmental academic structure of OIST are specifically designed to foster inter- and cross-disciplinary research, thus facilitating research in new areas that could stimulate and enhance the existing areas of focus. Applicants with exceptional skills in the development of novel research tools and instrumentation, particularly approaches that will further revolutionize visualization and labeling and/or the manipulation of bio- and nano-systems and/or single molecule or atom probes, are strongly encouraged to apply.

Successful candidates will be given the opportunity to excel in their chosen area of research, and will be expected to contribute to graduate teaching, research supervision and other academic activities. Applicants should have a PhD or equivalent degree, and demonstrate excellence in research.

The initial appointment will be as Principal Investigator (PI) or Independent New Investigator (INI) for a term of five years. When the transition to a graduate university is completed in 2012, it is planned that PI and INI positions will change to a tenure track system with Assistant Professors, Associate Professors, and Professors. Some appointments will be made on a joint or part-time basis. Substantial internal funding will be provided to support the faculty member's research based on a 5-year research plan that is renewable after scientific review.

At a time when worldwide support for research is increasingly risk-averse and obtaining funding places an ever-growing burden on faculty, OIST promotes innovative research in a highly facilitating and supportive environment. This is achievable because OIST has internal research funding, offers outstanding central research facilities, and consults faculty on the design of new laboratory space. Central research facilities at OIST include core facilities for high performance computing, mass spectrometry, X-ray crystallography, confocal microscopy, radioisotope use, electron microscopy, sequencing and genomic analysis, genetic recombination facilities, and vivarium.

OIST is committed to being international with more than 50% of faculty, researchers, and students from outside Japan. The official language of OIST is English. OIST is an equal opportunity, affirmative action employer and encourages applications from women.

More details regarding the aims of the search and advantages of working at OIST are available in the Information for Applicants in the application package that is downloadable from the website (**http://www.oist.jp/en/newsevent/careers/683-faculty-positions-in-mathematics.html**). Applications should be submitted in accordance with the instructions in the application package. Applications for the current search close **15 December 2010**. Interviews will take place in late January, with a view to making appointments early in 2011.

STANFORD SCHOOL OF MEDICINE

Stanford University Medical Center

The Department of Genetics and the Center for Genomics and Personalized Medicine invites applications to fill **MULTIPLE TENURE-TRACK POSITIONS** at the **ASSISTANT, ASSOCIATE, and/or FULL PROFESSOR** level.

We are interested in outstanding scientists with innovative research programs in any area of genetics and/or genomics. Candidates should have a Ph.D. and/or M.D. degree and a clear record of creative achievement. The predominant criteria for appointment in the University Tenure Line are a major commitment to research and teaching.

The Department of Genetics and The Center for Genomics and Personalized Medicine at the Stanford University School of Medicine offer a highly collegial and interdisciplinary environment that spans clinical medicine, human genetics, model-organism genetics, and genome-scale approaches. For more information, see **http://genetics.stanford.edu**.

Candidates are encouraged to apply electronically before **December 7, 2010**, with curriculum vitae and a statement of research and teaching interests, in one pdf file, with your last name in the subject line, to: **genetics-search@stanford.edu**. Applicants for the position at the Assistant Professor rank should also arrange to have three letters of evaluation sent to:

Michael Snyder, Chair
Department of Genetics
300 Pasteur Drive, Alway M344
Stanford, CA 94305-5120
genetics-search@stanford.edu

Stanford University is an Equal Opportunity Employer and is committed to increasing the diversity of its faculty. It welcomes nominations of and applications from women and members of minority groups, as well as others who would bring additional dimensions to the University's research, teaching, and clinical missions.

University of Idaho
A LEGACY OF LEADING

Assistant Professor in Biological Sciences, Mathematics and/or Statistics

We seek an outstanding scientist who will conduct research and develop a nationally competitive externally funded research program at the University of Idaho. Preference will be given to candidates able to contribute to the Initiative for Bioinformatics and Evolutionary Studies (IBEST). IBEST is an interdisciplinary research group at the University of Idaho who study patterns and processes of evolution that occur over comparatively short periods of time. We investigate the relative importance and consequences of mutagenic processes, work to understand patterns of evolutionary change that emerge during the course of evolution, develop and test models of evolutionary processes, and devise means to analyze large sets of genetic data. The hallmarks of IBEST research are the coupling of empirical and theoretical research. We place a high value on interdisciplinary collaborations that blend the expertise of biologists, biochemists, ecologists, evolutionary biologists, mathematicians, statisticians, and computer scientists to examine the underpinnings of evolutionary biology.

The successful candidate will have a Doctorate degree in mathematics, statistics, biology, bioinformatics or a related field; at least one year of postdoctoral experience; knowledge and interest in fundamental aspects of evolutionary ecology and/or population genetics; a demonstrated ability to teach college-level courses; and evidence of an active research agenda.

For more information and to apply online please visit:
www.hr.uidaho.edu

Science Careers online @sciencecareers.org

WORCESTER POLYTECHNIC INSTITUTE

SEVEN FACULTY POSITIONS

Worcester Polytechnic Institute (WPI) in Worcester, Mass., continues to invest in the life sciences. In 2007 the university opened the WPI Life Sciences and Bioengineering Center (LSBC), which houses the life sciences-related graduate research programs of five academic departments and the WPI Bioengineering Institute (BEI). Since that time, WPI has recruited 16 new full-time faculty members in the life sciences and bioengineering, bringing to 34 the number of faculty working in interdisciplinary clusters within a strongly collaborative environment in the LSBC. As a result of this investment, graduate research and external research funding have increased considerably, with faculty awarded major funding from the NIH, NSF, DARPA, and other agencies.

In 2010–11 we are seeking to fill seven tenure-track positions in five deparments, including a new head for the Chemistry and Biochemistry Department. The ideal candidates for these positions will have research interests and expertise that are complementary to our current research areas, and be committed to collaboration among multidisciplinary teams and to securing external funding.

Applicants for the department head will be recognized leaders in their field and have a strong record of securing extramural funding. Applicants at the assistant professor level must have postdoctoral research experience with extramural support, or strong promise to obtain funding. All applicants must hold the PhD and have a strong commitment to teaching at the undergraduate and graduate levels. For more on the WPI Life Sciences Initiative, visit www.wpi.edu/+lsi.

Founded in 1865, WPI is one of the nation's oldest and most innovative technological universities. *U. S. News and World Report* consistently ranks WPI among the top national universities and recently placed WPI in its top 30 for faculty resources. WPI's 14 academic departments offer more than 50 undergraduate and graduate degree programs, including the PhD, in science, engineering, management, and the liberal arts. WPI offers a smoke-free environment, competitive compensation, and an excellent benefits package. To enrich education through diversity, WPI is an affirmative action, equal opportunity employer. It is a member of the Colleges of Worcester Consortium.

Life Sciences Initiative

Chemistry and Biochemistry • Head WPI invites applications and nominations for Head of the Department of Chemistry and Biochemistry. The new head will have a clear and creative vision for building and sustaining ambitious departmental research programs while maintaining a focus on excellence in teaching and have the skills necessary for the day-to-day management of the department activities and administrative staff. The Chemistry and Biochemistry head is responsible for coordinating with the other academic department heads across the wider WPI community in the development of interdisciplinary research teams for the purpose of securing external funding. Our vision for the new Head includes enhancing the department's role in the natural sciences at all levels and providing strategic positioning for new faculty appointments as we grow. **Contact:** Applications and nominations should be sent to cbcheadsearch@wpi.edu. Further inquiries may be directed to the Office of the Dean of Arts and Sciences, 508-831-4678 or dofcarcik@wpi.edu.

Chemistry and Biochemistry • Assistant Professor The department seeks candidates with expertise in synthesis with an application focus that complements research in our Life Science areas. An ability to teach inorganic chemistry is required. **Contact:** Professor Kris Wobbe at faculty-searchCBC@wpi.edu.

Biology and Biotechnology • Assistant Professor The department seeks candidates with significant research experience in neuroscience, with preference given to individuals studying mechanisms of neural degeneration and regeneration. **Contact:** Professor J. B. Duffy at Faculty-searchBBT@wpi.edu.

Biology and Biotechnology, and Mathematical Sciences • Assistant Professor The departments seeks candidates for cross-disciplinary work in bioinformatics and computational biology. **Contact:** Chairs of either the Biology and Biotechnology or Mathematical Sciences search committees at Bioinformaticsfaculty-search@wpi.edu.

Biomedical Engineering • Assistant Professor The department seeks candidates in the following areas: cellular and tissue engineering, biomechanics, biomaterials, bioinstrumentation, biosignal processing, physiological systems modeling, and biomedical imaging. **Contact:** Professor Ki H. Chon at kichon@wpi.edu.

Mathematical Sciences • Assistant Professor The department seeks candidates who both enhance existing departmental strengths in pure and applied analysis, computational mathematics, applied statistics, and discrete mathematics and contribute to our goals for growth in biological sciences, environmental sciences and climate, and energy research. **Contact:** Applications accepted through www.mathjobs.org.

Physics • Assistant Professor The department seeks candidates with an interest in optical imaging and spectroscopic microscopy as applied but not limited to single-molecule biophysics, cellular biophysics, and/or biomaterials. Preference will be given to applicants who can interact with one or more areas of Soft-Condensed Matter. **Contact:** PH search committee, ph-search@wpi.edu.

WORCESTER POLYTECHNIC INSTITUTE 1865 WPI

The University *of* Vermont

Engaging minds that change the world

Create the Future at the University of Vermont

To help create the new knowledge that the 21st century will require, the University of Vermont (UVM) is launching an innovative new program called the Transdisciplinary Research Initiative, or TRI. UVM is investing in developing three new world-class Spires of Excellence:

- **Complex Systems**
- **Food Systems**
- **Neuroscience, Behavior and Health**

We are seeking outstanding applicants with demonstrated potential for imaginative research, a clear vision for the future, a sense of innovation and entrepreneurship, and a strong desire to join transformational, multidisciplinary studies in one or more of these three Spires.

Candidates are expected to develop an internationally recognized program of scholarly and collaborative research and to excel in teaching at both the undergraduate and graduate levels.

UVM will be making up to thirty (30) tenured and tenure-track appointments for 2011-12, with specific attention to Spire-aligned hires. Please visit our TRI website to learn more about the UVM Spires of Excellence, or the UVM employment website to learn about multiple faculty openings across UVM.

Founded in 1791, the University of Vermont is one of the nation's oldest universities and is consistently ranked as one of the top public universities in the United States. The university comprises nine colleges and schools including a college of medicine and is located in Burlington, Vt., often rated one of the best small cities in America. The greater Burlington area has a population of approximately 150,000 and enjoys a panoramic setting on the shores of Lake Champlain bordered by the Adirondack and Green Mountains. There are ample opportunities for interactions with local industries. We are strongly committed to diversity and especially welcome applications from underrepresented groups including women and minority group members.

For further information about UVM, TRI positions currently available, or to apply on-line, please visit our websites at: **www.uvm.edu, www.uvm.edu/~tri, or www.uvmjobs.com**, respectively; **Job Hotline #802-656-2248; telephone #802-656-3150.** Applicants must apply for positions electronically. Paper resumes are not accepted. Job positions are updated daily.

The University of Vermont is an Equal Opportunity/Affirmative Action Employer. Applications from women and people from diverse racial, ethnic, and cultural backgrounds are encouraged.

VANDERBILT School of Medicine

FACULTY POSITION IN BIOCHEMISTRY/ X-RAY CRYSTALLOGRAPHY/ STRUCTURAL BIOLOGY BIOCHEMISTRY

The Department of Biochemistry at Vanderbilt University School of Medicine (**https!://medschool.vanderbilt.edu/biochemistry**) seeks candidates to fill a faculty position in macromolecular X-ray crystallography at the level of Assistant Professor (tenure-track) or Associate Professor (tenure). Vanderbilt University has been undergoing a transformation in recent years to further advance and lead in biomedical research, with structural biology as one of the key target areas. Major investments have also been made in bioinformatics, mass spectrometry/proteomics, cryo-EM, photonics, and chemical biology. In addition to in-house diffraction instrumentation and state-of-the-art crystallization robotics, biomolecular crystallographers at Vanderbilt have significant synchrotron beam time via the LS-CAT (sector 21) at the Advanced Photon Source. The successful candidate will be an active participant in the Center for Structural Biology, an established organizational structure for research training, and instrumentation (**http://www.structbio.vanderbilt.edu/**).

Please forward an electronic cover letter, curriculum vitae, contact information for three references, and description of research program as a single PDF file to **marlene.jayne@Vanderbilt.edu**. Alternatively, mail hard copies of these materials to:

Crystallography Search Committee
Vanderbilt University School of Medicine
c/o Marlene Jayne
607 Light Hall
Nashville, TN 37232

The application deadline is **December 31, 2010**, but applications will be evaluated as they arrive.

Women and minority candidates are especially encouraged to apply.

Bar-Ilan University

Academic Research Positions Faculty of Medicine, Bar-Ilan University

Bar-Ilan University is seeking outstanding senior and young scientists for tenure-track faculty positions to teach and lead research groups in Biomedical Sciences at the new Faculty of Medicine in Safed, Galilee region of Israel.

Suitable candidates should submit:

1. CV with essential information regarding research achievements (including a summary of current and future research goals), teaching abilities, and courses which can be taught by the candidate.
2. List of publications. Please indicate the impact factor for each journal and number of citations per article.
3. Three letters of recommendation from known scientists from three different institutes.

Please respond within 14 days to
Prof. Haim Breitbart (breith@mail.biu.ac.il) and
Dr. Edith Kahana (kmalag@mail.biu.ac.il).

UNIVERSITY of WISCONSIN
UWMILWAUKEE

Founding Dean of The School of Freshwater Sciences

(http://www4.uwm.edu/freshwater/)

The University of Wisconsin-Milwaukee (UWM) invites applications and nominations for the position of Founding Dean of the School of Freshwater Sciences (SFS). A major research university and Wisconsin's premier public urban institution, UWM (**www.uwm.edu**) enrolls more than 30,000 students.

SFS (**http://www4.uwm.edu/freshwater/**) is the first graduate school in the U.S. dedicated solely to the study of freshwater and was established in 2009 to maximize existing resources, identify emerging opportunities, and create a collaborative, interdisciplinary regional and global hub for environmentally balanced economic development. SFS has 14 faculty and scientists and 11 permanent support staff, along with additional project staff on funded projects. SFS confers degrees at the doctoral and masters level, with an inaugural class in fall 2010 of five doctoral and seven masters students.

In addition to academic, research, and service programs, the Dean is responsible for the Great Lakes Research Facility (GLRF), home to SFS and used as a base for UWM research vessels and collaboration with scientists from other campuses. The Wisconsin legislature appropriated $50 million for an 80,000 sq. ft. addition to and renovation of existing SFS facilities.

The Search Committee seeks candidates with a strong record of professional accomplishment, commitment to excellence in research and teaching, outstanding management and leadership skills, and experience building public/private partnerships. (See **http://www4.uwm.edu/secu/SFSDean/** for expanded description). The Dean must be an educational leader with the following qualifications or an equivalent combination thereof:

- Professional and scholarly achievements sufficient to be tenured as a full professor;
- A record of creating and disseminating knowledge on the subject of water; and
- Experience managing an academic/research unit or equivalent, including budget, grants and other external funds development, personnel, and communications management.

Applications and nominations will remain confidential. Candidate screening will begin January 10, 2011, but review will continue until the position is filled. Applicants should provide a letter describing relevant experiences and interest in the position; curriculum vitae; names of five references with titles, addresses and e-mail addresses. Individuals who wish to nominate a candidate should submit a letter of nomination, including name, position, address, telephone number and email address of the nominee.

Applications and nominations should be electronically submitted via PDF or MS Word to **UWMSFSDean@academic-search.com**.

The search is assisted by:

John B. Hicks, Senior Consultant
Academic Search, Inc.
John.hicks@academic-search.com
205-345-7221

The University of Wisconsin-Milwaukee is an Affirmative Action, Equal Employment Opportunity Employer.

STEP
PRINCETON UNIVERSITY

Program in Science Technology and Environmental Policy at Princeton University - 2011–2012 Research Fellowship Program

The Program in Science, Technology and Environmental Policy (**STEP**) at Princeton University's Woodrow Wilson School of Public and International Affairs (Michael Oppenheimer, Director) announces its 2011–2012 Fellowship Program. STEP will award one-year research positions (with the possibility of renewal for a second year) to eligible, talented researchers. These appointments, at the postdoctoral or more senior research level, are designed to promote basic policy-relevant research under the supervision of one or more STEP faculty members. STEP faculty is soliciting fellowship applications in the following areas of interest:

- **Michael Oppenheimer:** PHYSICAL SCIENCE OF EARTH SYSTEM: (1) Modeling of dynamic properties of ice sheets on a variety of geographic scales (in collaboration with colleagues at the Geophysical Fluid Dynamics Laboratory, GFDL). (2) Analysis of paleoclimate proxy data for sea level, ice extent, and temperature to improve the use of analogs in forecasting future sea level rise. This project focuses particularly, but not exclusively, on proxies from the Last Interglacial; see **http://www.nature.com/nature/journal/v462/n7275/full/nature08686.html**. DECISION THEORY and POLICY: Modeling the role of learning in decisions where structural model error is a key concern. This work will be coordinated with ongoing case studies of actual scientific learning coupled to policy decisions; see **http://www.springerlink.com/content/7uw8150573197707/fulltext.pdf**. CLIMATE IMPACTS: Econometric and other quantitative methods applied to human migration under climate change; see **www.pnas.org/cgi/doi/10.1073/pnas.1002632107**.
- **Denise Mauzerall:** (1) GLOBAL CHEMISTRY-CLIMATE AND ADJOINT MODELING (in collaboration with GFDL) of the sources, transport, radiative and climate impacts of black carbon including impacts on glacier melting. A key objective is the identification of mitigation strategies with co-benefits for climate and health. Experience with emission inventories, large data sets and /or with global chemistry and climate models is desired. See: **http://www.atmos-chem-phys-discuss.net/10/21615/2010/acpd-10-21615-2010.pdf**. (2) MITIGATION STRATEGIES: examination of potential climate benefits of fast-action mitigation strategies for non-CO_2 climate forcing agents. (3) GLOBAL AGRICULTURE: comparison of impacts of air pollution and climate change on yields.
- **Frank von Hippel:** New initiatives to further the goals of nuclear disarmament, nonproliferation and the prevention of nuclear terrorism by reducing global stocks of highly-enriched uranium and plutonium, the number of locations where they can be found, and the number of national facilities where they can be produced. (**www.fissilematerials.org**)
- **David Wilcove:** Identification and assessment of degraded lands in Southeast Asia for restoration or agricultural use (requires expertise in remote sensing); impact of bird and reptile trade on wild populations in Asia (modeling and field work); land-use changes and associated impacts on birds, mammals, and other taxa in East Africa or Asia. (field work)
- **Alexander Glaser:** Nuclear energy in the context of nonproliferation and climate change, with a focus on (1) exploring nuclear-energy options and constraints in developing countries or (2) on incorporating uncertainties in the treatment of nuclear power in integrated assessment models. (3) Technical and policy analysis of the nuclear fuel cycle, including approaches to strengthening international oversight and safeguards of nuclear facilities; for details, see **http://nuclearfutures.princeton.edu**.

The Research Fellows Program is open to all regardless of citizenship, but requires a completed Doctorate and does not support work towards the completion of a degree. STEP fellows will be eligible for salary and full employee benefits in accordance with University guidelines.

Applicants should send a CV and a cover letter indicating faculty they wish to apply with, describing their areas of expertise and interest via **https://jobs.princeton.edu** (use requisition number **1000839**) The review process will commence immediately and continue until positions are filled, although not all slots may be filled.

For more information about applying to Princeton please link to:
http://web.princeton.edu/sites/dof/ApplicantsInfo.htm

Princeton University is an Equal Opportunity Employer and complies with applicable EEO and affirmative action regulations.

Science Careers online @sciencecareers.org

Jiangsu Academy of Agricultural Sciences

Seeking Distinguished Scientists in Various Agriculture Areas

Jiangsu Academy of Agricultural Sciences (JAAS) is a professional agricultural research and extension institution that has been established since 1932. JAAS ranks at the top of provincial agricultural academies in China in terms of the comprehensive strength in agriculture. JAAS's headquarter and main research facilities are located in Nanjing, Jiangsu, China.

Currently, there are 3 distinguished full professor positions available for application in the following areas: breeding, food processing, bioenergy, facility agriculture, and large-scale farming for modern animal husbandry. Applicants should have a faculty position already beyond the assistant professor level in a university or the equivalent position in a research institution. In addition, all candidates should demonstrate excellent records of research accomplishment and have a command of bilingual language for English and Chinese, both in spoken and written.

Successful applicants will be offered a competitive package, including sufficient laboratory space, startup funding, relocation fee and competitive salary commensurate with experience, in addition to a housing allowance, and other employee benefit. Applicants can go to www.jaas.ac.cn for application details.

In addition, more information for other regular faculty positions from JAAS relevant to a variety of disciplines in agriculture is also available at www.jaas.ac.cn.

Contact information

E-mail: rsc-gbk@jaas.ac.cn; Tel: 086-25-84390037

MICHIGAN STATE UNIVERSITY

MSU-DOE PLANT RESEARCH LABORATORY
http://www.prl.msu.edu

Faculty Position in Plant Biology

The MSU-DOE Plant Research Laboratory (PRL) has a **twelve-month tenure-track faculty position** available at the Assistant, Associate or in exceptional cases Full Professor level. We seek to identify individuals who investigate fundamental questions in plant biology relevant to energy flow in the continuum between photon capture and the deposition of energy-rich molecules. Examples of such research include mechanisms of light harvesting, CO_2 fixation, energy regulatory networks, enzymes and metabolites involved in energy conversion, and computational approaches to model biological networks.

The PRL, with core funding from the U.S. Department of Energy, provides an excellent environment for creative research in plant biology. Michigan State University provides a stimulating atmosphere with world class colleagues and facilities, and exceptional breadth and depth in the plant sciences. PRL faculty members are jointly appointed in an appropriate academic department and are full members of the MSU tenure-stream faculty.

Applicants should have postdoctoral research experience with demonstrated productivity and evidence of potential for independent research. To assure consideration, applications should be submitted electronically to **prlsrch@msu.edu** by **December 15, 2010**. Applications should include curriculum vitae, a summary of research accomplishments, and a brief description of future plans. **Candidates at the assistant level should arrange to have three letters of reference submitted; senior candidates should include names and contact information for three referees.** Questions regarding this position should be directed to **prlsrch@msu.edu**.

Michigan State University is an Affirmative Action, Equal Opportunity Employer. MSU is committed to achieving excellence through cultural diversity. The university actively encourages applications and/or nominations of women, persons of color, veterans, and persons with disabilities.

Professor of Plant Diversity and Evolution and Director, Harvard University Herbaria

The Harvard University Herbaria (HUH; **http://www.huh.harvard.edu**) house one of the largest and most comprehensive collections of dried plant and fungal specimens in the world. These specimens are the key to our knowledge of plants and serve as a permanent reference to the diversity of life on earth. During the last three years the HUH has embarked on an ambitious plan to enhance its scientific mission through a series of key improvements in its laboratories, bioinformatics and collections infrastructure, and environmental controls. As part of this broader initiative, the Department of Organismic and Evolutionary Biology and the HUH now invite applications for a tenured faculty member in the Department of Organismic and Evolutionary Biology (OEB; **http://www.oeb.harvard.edu/**) who will also serve as Director. We seek an outstanding scientist who will teach at both undergraduate and graduate levels and who is engaged in an innovative research program. We are especially interested in individuals who undertake field and laboratory research in plant phylogenetics, genetics, speciation, biogeography, or ecology.

Please submit applications online at: **https://webapps.sciences.fas.harvard.edu/apply/oeb-huh-2010/**. Required materials include a curriculum vitae; a statement of research and teaching interests; four representative publications; and the names, institutional affiliations, and e-mail addresses of three references. Letters of nomination from third parties are also welcome and should be sent by e-mail to **Plant_Biodiversity_Search@oeb.harvard.edu**. Review of applications and nominations will begin on December 1st and conclude when the position is filled. Further information about OEB and HUH are available at **http://www.oeb.harvard.edu** and **http://www.huh.harvard.edu**. Address questions about the position to Professor Donald H. Pfister **dpfister@oeb.harvard.edu** and about the application/nomination process to Ms. Jeannette Everritt in OEB **jeverritt@oeb.harvard.edu**.

Harvard University is an Affirmative Action/Equal Opportunity Employer. Applications from women and minority candidates are strongly encouraged.

中国科学院

Faculty Positions

The Institute of Genetics and Developmental Biology (IGDB), Chinese Academy of Sciences (CAS), the neighborhood of Beijing Olympic Village, has several openings for group leaders to join the Key Laboratory of Molecular & Developmental Biology of CAS.

IGDB is a leading institution of life sciences in China. IGDB currently hosts 63 research groups, of which 18 groups are actively involved in addressing fundamental questions in animal development using model organisms such as C. elegans, Drosophila, Xenopus, zebra fish and mouse. IGDB seeks dynamic individuals with innovative research programs dedicated to vertebrate development in developmental neurobiology, stem cell biology, systems biology, animal cloning (cattle, sheep) and transgenic animal research. Candidates with experience in transgenic or knockout mouse are preferred to direct the mouse facility of IGDB. The appointment will be at Principal Investigator (full professor) level. Candidates are expected to hold a Ph.D. degree and a minimal four-year postdoctoral experience. Startup package will be accompanied by either the "One-Hundred Talents Program of CAS" or the "One-Thousand Talents Program of China". Salary and benefit will be provided based on their qualification. More information about IGDB can be found at **http://www.genetics.ac.cn** or **http://english.genetics.cas.cn/ .**

Interested candidates should submit a cover letter, curriculum vitae, representative publications, a statement of research experiences and interests as well as the names and contact information of three referees to:

Dr. Weicai Yang, Chair of the Search Committee
Institute of Genetics and Developmental Biology
Chinese Academy of Sciences
Beijing 100101, China
E-mail: wcyang@genetics.ac.cn

SOOCHOW UNIVERSITY

Faculty Positions at School of Radiation Medicine and Public Health

The School of Radiation Medicine and Public Health (SRMPH) of Soochow University in Suzhou, Jiangsu, China, is seeking outstanding candidates for **Associate and Full Professors** in the broad areas of Radiation Medicine, a National Key Discipline, which includes **radiation biology, radiation oncology, radiation protection, radiation chemistry, and nuclear science and technology.**

Candidates for the Associate Professor positions should have a PhD with at least 3 years of postdoctoral experience in the related fields and a scholarly publication record, while candidates for the Full Professor positions should have demonstrated the strong ability to develop an original and externally funded research program. All candidates should have a command of spoken and written English.

Successful applicants will be offered an excellent package including sufficient laboratory space, startup funding, relocation expense and competitive salary commensurate with experience, in addition to an apartment/condo rental allowance and other benefits.

The Search Committee will review applications immediately and the search will continue until all positions are filled. Applicants should submit (i) a cover letter summarizing current research projects and future plans, (ii) a curriculum vitae, and (iii) names and contact details of three professional referees to: **Search Committee, School of Radiation Medicine and Public Health (SRMPH). Dushu Lake Campus, Soochow University, 199 Ren-Ai Road, Industrial Park, Suzhou 215123, China; Fax: 86-512-65884830; E-mail: hlzhong@suda.edu.cn or jpcao@suda.edu.cn**.

SOOCHOW UNIVERSITY

Faculty Positions at Stem Cell Research Key Lab of Jiangsu Province

The Stem Cell Research Key Lab at Soochow University in Suzhou, China, is a newly created research center by Jiangsu Province and the Ministry of Education. We are seeking outstanding scientists for **Associate** or **Full Professor** positions in the broad areas of **Stem Cell Biology, Cancer Stem Cells** and **Stem Cell Immunology**.

Candidates for the Associate Professor positions should have a PhD with at least 3 years of postdoctoral experience in the related fields and a scholarly publication record, while candidates for the Full Professor positions should have demonstrated the strong ability to develop an original and externally funded research program. All candidates should have a command of spoken and written English.

Successful applicants will be offered an excellent package including sufficient laboratory space, startup funding, relocation expense and competitive salary commensurate with experience, in addition to an apartment/condo rental allowance and other benefits.

The Search Committee will review applications immediately and the search will continue until all positions are filled. Applicants should submit (i) a cover letter summarizing current research projects and future plans, (ii) a curriculum vitae, and (iii) names and contact details of three professional referees to: **Search Committee, Stem Cell Research Key Lab of Jiangsu Province; Building 17, Soochow University South Campus, 178 Ren-Ming Road, Suzhou 215007, China; Tel: 86-512-65732002; Fax: 86-512-65104908; E-mail: xueguangzh@yahoo.com.cn**.

DEAN
THE HENRY SAMUELI SCHOOL OF ENGINEERING

The University of California, Irvine invites applications and nominations for the position of Dean, The Henry Samueli School of Engineering. The university seeks an independent thinker with skills to navigate within a complex/multi-constituent organization, and who is decisive while fair, and strategically focused. The successful applicant will have a keen intellectual capacity and creativity, be an open and persuasive communicator and problem solver who leads from values, and be a candidate with energy and vision to head and continue the mission of the school. Key selection criteria will include:

- **Recognized leader in the latest intellectual advances in engineering**
- **Dedicated to establishing a culture that promotes the growth and continuing recruitment of world-class faculty**
- **Proven experience in faculty leadership, academic process, team building, and advancing diversity**
- **Demonstrated ability to work effectively with the community and other constituents in resource development, fund raising, and advancement of the School**
- **Established success as an administrator, including staff development, facility management, and fiscal leadership**

The Henry Samueli School of Engineering is one of ten schools at the University of California, Irvine. The School has more than 100 full-time faculty members, and an enrollment of approximately 2,600 undergraduate and 750 graduate students. The School represents a premier center for education and research with five departments: Biomedical Engineering, Chemical Engineering and Materials Science, Civil and Environmental Engineering, Electrical Engineering and Computer Science, and Mechanical and Aerospace Engineering. The School is equipped with excellent experimental facilities, major research centers, and state-of-the-art infrastructure, occupying nearly 295,000 square feet. Further information about the School can be found at this website: **http://www.eng.uci.edu/**.

Celebrating 45 years of innovation, the University of California, Irvine is a top-ranked public university dedicated to teaching, scholarship and community service. Founded in 1965, UCI is among the fastest-growing campuses in the University of California system, with more than 27,000 students, 1,500 faculty members and 9,000 staff. The second-largest employer in dynamic Orange County, home to more than 500 high-tech and medical device companies, UCI contributes an annual economic impact estimated at $3.3 billion. It is located on a 1,500-acre site three miles from the Pacific Ocean.

The successful candidate will join a dynamic community at UCI, and provide leadership in advancing the diversity of the school's faculty, staff, students and programs. UCI will continue to grow over the next decade and is currently engaged in a major capital campaign. As the leader of the School at this pivotal moment, the dean will work with the faculty to build on current strengths, to foster creativity and innovation, and to help secure the resources that will move the school forward. In addition, the dean will collaborate with faculty and administrators across the campus to expand the School's support of interdisciplinary research and education.

Review of applications will begin on **December 6, 2010** and the position will remain open until filled. Paper and electronic applications may be sent to the address below:

The Henry Samueli School of Engineering
Dean Search Committee
C/O JiWon Kim, jiwon@uci.edu
509 Aldrich Hall
University of California, Irvine
Irvine, CA 92697-1000
OR email: engrsrch@uci.edu

UCI is an Equal Opportunity Employer committed to excellence through diversity and strongly encourages applications from all qualified applicants, including women and minorities. UCI is responsive to the needs of dual career couples, is dedicated to work-life balance through an array of family-friendly policies, and is the recipient of an NSF ADVANCE Award for gender equity.

Science Careers online @sciencecareers.org

UCIrvine The Henry Samueli School of Engineering

TENURE-TRACK FACULTY POSITIONS

THE HENRY SAMUELI SCHOOL OF ENGINEERING AT THE UNIVERSITY OF CALIFORNIA, IRVINE invites qualified applicants for a faculty position beginning July 1, 2011. The position is at the rank of Assistant Professor (tenure track) and will be formally associated with *The Edwards Lifesciences Center for Advanced Cardiovascular Technology*. Applicants must hold a Ph.D. degree in biomedical engineering or related field, and will be expected to maintain a broad-based extramurally funded research program. Research areas of interest include broadly the application of engineering technologies to address structural defects or disease in the cardiovascular systems including, but not limited to, regenerative medicine (tissue engineering), photonic imaging and treatment, multiscale modeling, wireless communication systems, and biomedical micro- and nanoscale systems. In addition, the successful candidate will be expected to advise students and teach undergraduate and graduate courses as well as develop collaborative programs with other faculty members and programs at UCI. The University of California, Irvine is situated in Orange County's rapidly growing high technology sector that includes more than 310 biomedical companies which are actively involved in our program.

APPLY NOW - submit your application to our online recruitment program.

For full consideration, candidates should upload applications electronically, please refer to the following website for instructions: **http://www.eng.uci.edu/employment/applicationinstructions**. Applications should include a curriculum vitae, a brief (no more than 2 pages) description of current and future research and teaching interests, and names of at least three references. Questions regarding these positions may be addressed to Ms. Ruth M. Gratzer, **rmgratze@uci.edu**. For more information about *The Edwards Lifesciences Center for Advanced Cardiovascular Technology* or the Department of Biomedical Engineering please visit our websites at **http://cardiovascular.eng.uci.edu** or **http://www.bme.uci.edu**. Selection will begin **December 1, 2010**, and continue until the position is filled.

UCI is an Equal Opportunity Employer committed to excellence through diversity and strongly encourages applications from all qualified applicants, including women and minorities. UCI is responsive to the needs of dual career couples, is dedicated to work-life balance through an array of family-friendly policies, and is the recipient of an NSF ADVANCE Award for gender equity.

Neutron Scattering Instrument Scientist

Real Science. Real Life.

Neutron Sciences Directorate at Oak Ridge National Laboratory invites applications for an Extended Q-Range Small-Angle Neutron Scattering (EQ-SANS) Instrument Scientist.

The successful candidate will be a team member providing operational support for the new EQ-SANS instrument at the Spallation Neutron Source and developing a vigorous scientific program associated with the instrument.

An extensive record of research accomplishments using small angle neutron and/or x-ray scattering is required. A Ph.D. and a minimum of two years of experience as a Research Scientist in material science, physics, chemistry, or related fields(or equivalent combination of training and experience) are also required.

For more information about the position or to apply visit:
http://jobs.ornl.gov/neutron_science.shtml

neutrons.ornl.gov

10-G00055/Agim

Neutron Sciences · Oak Ridge · U.S. Department of Energy, Office of Science

USDA ARS Agricultural Research Service
www.ars.usda.gov

Research Plant Biologist/Res. Molecular Biologist/ Res. Geneticist (Plants)
Plant Gene Expression Center
Albany CA

Salary Range of $81,460 - $148,806
Announcement Open: September 20, 2010 to November 15, 2010

Applicants are invited to apply for a permanent, full-time position as a research scientist at the Plant Gene Expression Center (PGEC) of the United States Department of Agriculture (USDA), Agricultural Research Service (ARS). PGEC research is conducted through a close collaborative partnership with the University of California, Berkeley. The successful candidate is expected to develop an independent program to carry out innovative research that enhances our knowledge of plant processes, such as development and environmental response. The successful candidate's program should complement ongoing research at the PGEC, which concerns genetic and molecular analysis of disease resistance, circadian rhythms, light signaling, reproduction and development. The successful applicant will be considered for an Adjunct Faculty appointment in the Department of Plant and Microbial Biology, University of California, Berkeley. The position will be filled at the GS-12/13/14 level (Assistant/ Associate Professor equivalent, salary commensurate with experience).

To apply, print a copy of vacancy announcement **ARS-X10W-0257** from the ARS Careers Website at **www.ars.usda.gov/careers** and follow the application directions provided. For information about the position, please e-mail **Dr. Jennifer Fletcher**, **Jennifer.Fletcher@ars.usda.gov**. U.S. citizenship is required. Applications must be received by the closing date of the announcement.

USDA/ARS is an Equal Opportunity Employer and Provider.

Cell PRESS

Scientific Editors

Cell Press seeks to appoint multiple Scientific Editors with opportunities covering both scientific manuscripts and review material. Applicants with expertise in any relevant area of biomedical research will be considered. Working closely with the research community, your primary responsibilities will focus on acquiring, managing and developing new editorial content for the Cell Press research titles. These positions will also involve close interaction with other aspects of the business, including production and new product development, and therefore provide an excellent entry opportunity to scientific publishing. You will work in the Cell Press Cambridge, MA office as part of a growing editorial group that is highly dynamic and collaborative. These positions are an exciting opportunity to stay at the forefront of the latest scientific advances while developing a new career in a stimulating publishing environment.

The minimum qualification is a doctoral degree in a relevant life science discipline; additional postdoctoral or other experience is an advantage. Ideal candidates would have a strong scientific background and broad research interests, excellent writing and communication skills, strong organizational and interpersonal skills, plus creative energy and enthusiasm for science and science communication. Prior publishing or editorial experience is beneficial but not required.

To learn more about the available positions, visit careers.cell.com and search on key words "Cell Press". Alternatively, type this URL into your browser: **http://bit.ly/9o15ec**.

To apply for individual positions, please use the link within the posting to submit a CV and cover letter explaining your interest in the position and describing your qualifications, research interests and reasons for pursuing a career in scientific publishing.

No phone inquiries, please.

Cell Press is an Equal Opportunity Employer.

PICTURE YOURSELF AS A AAAS SCIENCE & TECHNOLOGY POLICY FELLOW

Make a Difference.
Help give science a greater voice in Washington, DC! Since 1973, AAAS Fellows have applied their skills to federal decision-making processes that affect people in the U.S. and around the world, while learning first-hand about the government and policymaking.

Join the Network.
Year-long fellowships are available in the U.S. Congress and federal agencies. Applicants must hold a PhD or equivalent doctoral-level degree in any behavioral/ social, biological, computational/ mathematical, earth, medical/health, or physical science, or any engineering discipline. Individuals with a master's degree in engineering and three years of post-degree professional experience also may apply. Federal employees are not eligible and U.S. citizenship is required.

Apply.
The application deadline for the 2011-2012 AAAS Fellowships is 5 December 2010. Fellowships are awarded in the spring and begin in September. Stipends range from $74,000 to $97,000.

Note: Additional fellowships are available through approximately 30 scientific society partners. Individuals are encouraged to apply with AAAS as well as with any scientific societies for which they qualify.

Enhancing Public Policy, Advancing Science Careers

Matthew Schmolesky, PhD

Neuroscience,
University of Utah

AAAS Fellow at the U.S. Department of State, Office of the Science and Technology Adviser to the Secretary (2005-06) and the Office of International Religious Freedom (2004-05)

Now a professor in the Department of Psychology at Weber State University

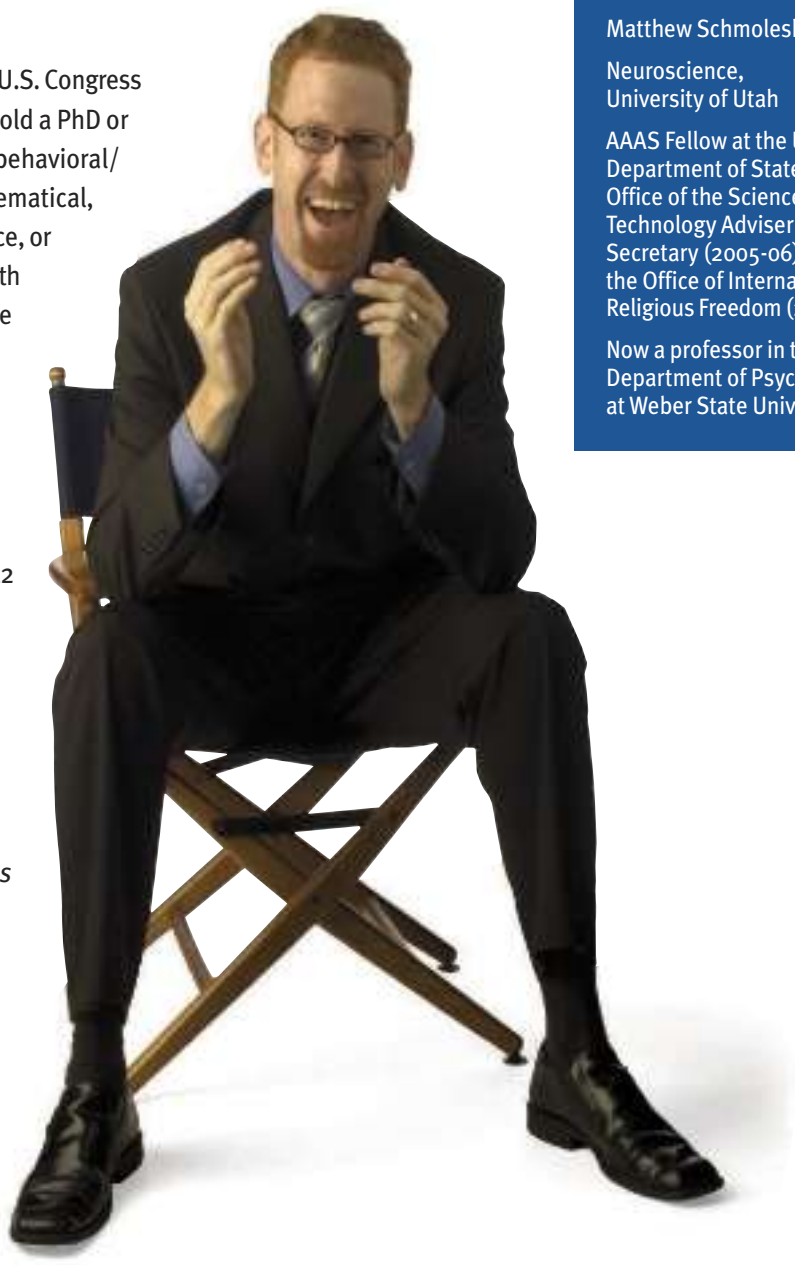

Full details at: **fellowships.aaas.org**

AAAS
ADVANCING SCIENCE, SERVING SOCIETY

Science Careers online @sciencecareers.org

BOWES RESEARCH FELLOWS
UNIVERSITY OF CALIFORNIA BERKELEY

The Bowes Research Fellows Program at the University of California, Berkeley, is seeking nominations of outstanding recent or imminent Ph.D. and M.D. graduates to be given the freedom to establish an independent research program as an alternative to the traditional postdoctoral experience. Bowes Fellows must have demonstrated exceptional promise and maturity in their graduate careers and be eager to engage the frontiers of biomedical and life sciences. Fellows will receive funding and space sufficient to maintain a laboratory of two to three members for a term of up to five years, free from the need to obtain grant support or the distractions of classroom teaching. Fellows will have principal investigator status, making them eligible to obtain outside funding from grants or other sources as their research programs expand.

Bowes Fellows benefit from the mentorship of our faculty, as well as from the exceptional breadth of our scientific resources and the highly interactive nature of the Berkeley community. In turn, our community benefits from the creative approaches Bowes Fellows take to solving important problems. Because interdisciplinary interactions are key to innovation, we seek to attract individuals who have broad interests in the life sciences and who have diverse expertise in experimental, theoretical and/or computational approaches.

Candidates must be nominated by their current mentor or by another senior investigator who can provide an in-depth analysis of their accomplishments and future potential. Refer potential reviewers to the UC Berkeley Statement of Confidentiality found at: **http://apo.chance.berkeley.edu/evalltr.html.**

Selected candidates will be asked to submit a brief research plan and to arrange for additional letters of recommendation. Finalists will be invited to interview on the UC Berkeley campus. Nominations must be received by **December 15, 2010** and should be sent to (e-mail submissions are preferred):

Michael Eisen, Chair, Bowes Research Fellows Selection Committee, Department of Molecular & Cell Biology, University of California, Berkeley, Stanley Hall, 304B, Berkeley CA, 94720-3220, mbeisen@berkeley.edu

The University of California is an Affirmative Action, Equal Opportunity Employer.

FACULTY POSITION IN CANCER RESEARCH

The Department of Molecular Carcinogenesis at The University of Texas MD Anderson Cancer Center, Science Park, **http://sciencepark.mdanderson.org**, seeks applications for a tenure-track position at the Assistant Professor level. Research in the department focuses on cellular, molecular, and genetic mechanisms of carcinogenesis and cancer prevention. We seek individuals working on mechanisms of carcinogenesis, in areas including genetic susceptibility, epigenetic reprogramming, genomic instability, inflammation/immune responses, signal transduction, transcriptional regulation and cancer stem cells. Preference will be given to candidates committed to working in a highly collaborative, interdisciplinary environment. The successful candidate will be expected to develop and maintain an internationally recognized and competitively funded research program, and to participate in graduate training. The department is well-funded with many outstanding core support services, including subsidized facilities for analysis of genetically engineered mouse models. Our Division is located in a pine-oak forest near the city of Austin, TX. MD Anderson offers outstanding research facilities, startup packages, and faculty benefits. Required qualifications include a Ph.D. (or equivalent), postdoctoral or independent scholarly research experience, and a strong publication record.

Candidates should submit a statement of research interest and a CV to the email address below by **January 15, 2011**. Applicants should also request that three letters of recommendation be sent to:

Richard D. Wood, Ph.D., Department of Molecular Carcinogenesis
Chair, Search Committee, email: mfendley@mdanderson.org

THE UNIVERSITY OF TEXAS
MD Anderson Cancer Center

MD Anderson Cancer Center is an equal opportunity employer and does not discriminate on the basis of race, color, national origin, gender, sexual orientation, age, religion, disability or veteran status except where such distinction is required by law. All positions are security sensitive and subject to examination of criminal history record information. MD Anderson Cancer Center is a smoke-free and drug-free environment.

Massachusetts Institute of Technology

FACULTY POSITIONS
in Mechanical Engineering
Massachusetts Institute of Technology

The Department of Mechanical Engineering at the Massachusetts Institute of Technology seeks outstanding candidates for tenure-track faculty positions in the following fields to begin July 1, 2011 or thereafter:

- **Bioengineering**
- **Design**
- **Ocean Science and Engineering**

A detailed description for each position is provided at: **http://search-meche.mit.edu.** Applicants should hold an earned Ph.D. in mechanical engineering or a relevant field by the beginning of the appointment. Faculty duties include teaching at the graduate and undergraduate levels, research, and supervision of student research.

We seek candidates who will provide inspiration and leadership in research and actively contribute to core mechanical engineering undergraduate and graduate level teaching. New faculty hires are expected to have a research focus in one of the disciplinary fields listed above. Applicants must have demonstrated: (1) outstanding research strength; (2) a strong disciplinary background; (3) strong experimental and/or theoretical skills; and (4) the potential to work across disciplinary boundaries. Appointment would be at the assistant or untenured associate professor level. In exceptional cases, a senior faculty appointment may be possible.

Applicants should send a curriculum vitae, a research statement, a teaching statement, and copies of not more than three publications. They should also arrange for four individuals to submit letters of recommendation on their behalf. This information must be entered electronically at the following site: **http://search-meche.mit.edu.** Full consideration will be given to applications submitted by **December 31, 2010.**

MIT is an Equal Opportunity/Affirmative Action Employer. Women and under-represented minorities are especially encouraged to apply.

DCU

Biomedical Diagnostics Institute

The Biomedical Diagnostics Institute (BDI) is a multidisciplinary research institute focused on the development of next generation diagnostic devices. A Science Foundation Ireland (SFI)-funded Centre for Science, Engineering and Technology (CSET), the BDI has developed a cutting-edge collaborative research programme involving leading researchers from partner academic institutions, companies and the clinical environment to create an integrated and cohesive partnership. Having pioneered advances in fundamental diagnostic technologies from our established core competencies in our first five years, BDI will now utilise these capabilities to focus on new research fields. This involves the development of diagnostic platform technologies in the areas of oncology, cardiovascular disease and infectious disease.

We are currently seeking applications from world-class research scientists at all levels (predoctoral, postdoctoral, and research technicians) to join our team with expertise in the following areas:

- **Assay Development (ref. AD1)**
- **Microfluidics (ref. MF1)**
- **Luminescent Dye Synthesis (Synthetic Chemistry) (ref. LD1)**
- **Surface Chemistry (ref.SC1)**
- **Bioinformatics & Pattern Recognition (ref. BP1)**
- **Platelet Biology (ref. PB1)**
- **Tumour Cell Biology (ref.TB1)**
- **Haemorheology/Acoustic wave transducers (ref. AW1)**

For informal queries:
E-mail **bdi@dcu.ie** stating the research area of interest and any queries you may have.

Application Procedure
Please submit your CV and Cover Letter by e-mail, **quoting in the subject line the reference number of the area in which you are interested**, to: **hr.applications@dcu.ie Closing Date: 26 November 2010.**

Human Resources Department, Dublin City University, Dublin 9, Ireland. Tel: +353 (0)1 700 5149 Fax: +353 (0)1 700 5500 E-mail: hr.applications@dcu.ie. For more information on the BDI, **visit www.bdi.ie.**

DCU is an equal opportunities employer.

NATIONAL ECOLOGICAL OBSERVATORY NETWORK

DATA PRODUCTS TEAM LEAD

The National Ecological Observatory Network (NEON, Inc.) is a nonprofit science corporation dedicated to understanding how changes in climate, land use and invasive species impact ecology.

The Data Products Team Lead will be responsible for leading the development and publishing the NEON Observatory High Level Data Product algorithms, including defining, documenting and implementing the models and algorithms used to convert NEON's environmental data into information that can be used by the scientific community and the general public.

Applicants should possess a Ph.D. in ecology, bioinformatics or a related environmental science field, preferably with a broad understanding of the present state of ecological research and modeling technologies, including bioinformatics. We seek a scientist with a very broad experience in quantitative environmental science with a profound knowledge of at least one of the major NEON subject areas: modeling/analysis of biodiversity, biogeochemistry, invasive species, infectious disease, ecohydrology, climate and land use. The incumbent will represent NEON nationally and internationally in ecological and eco-informatics, and should be an effective speaker and writer.

For complete details and to apply go to **www.neoninc.org**.

NEON is an Equal Opportunity Employer encouraging women, Minorities, to apply.

PURDUE UNIVERSITY

The Department of Chemistry and Department of Medicinal Chemistry and Molecular Pharmacology at Purdue University are pleased to announce the availability of an endowed Chair faculty position in drug discovery and development.

We seek an exceptional scientist with an outstanding track record of creativity in any area related to the science of drug discovery. Candidates seeking to advance their own discoveries through early stages of clinical trials and those with an established track record of leadership and/or advancement of drug candidates to the clinic are particularly encouraged to apply. Purdue University offers a thriving interdisciplinary research and education environment, with excellent faculty and exceptional support services associated with drug discovery and preclinical testing. More details about the departments involved in this search at Purdue can be found at: **www.chem.purdue.edu** or **www.mcmp.purdue.edu**.

Applicants should send curriculum vitae, a summary of planned research and the names of three references to: **Professor Paul B. Shepson, Department Head, Department of Chemistry, Purdue University, 560 Oval Drive, West Lafayette, IN 47907-2084**. Review of application material is currently ongoing and will continue until the position is filled.

Purdue University is an Equal Opportunity/ Equal Access/Affirmative Action Employer fully committed to achieving a diverse work force.

FELLOWSHIPS

Science Scholarships and Fellowships

UNCF/MERCK SCIENCE INITIATIVE

The UNCF/Merck Science Initiative is an innovative approach that creates opportunities in the biological, chemical and engineering sciences for African American students throughout the country.

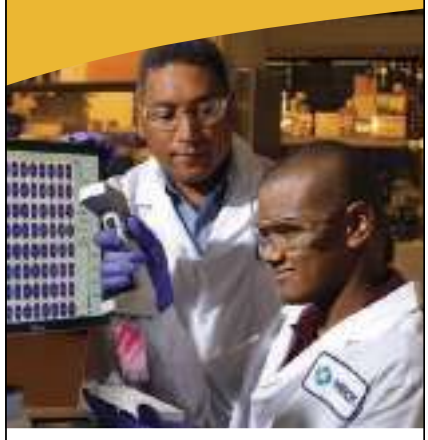

UNDERGRADUATE
Science Research Scholarship Awards
- Scholarships up to $25,000
- A paid summer internship at a Merck facility with stipend totaling more than $5,000
- Mentoring and networking opportunities
- Eligibility: College juniors, science or engineering majors, 3.3 GPA

GRADUATE
Science Research Dissertation Fellowships
- Fellowships up to $53,500
- Mentoring and networking opportunities
- Eligibility: Ph.D. or equivalent degree candidates engaged in dissertation research in the biological, chemical or engineering fields

POSTDOCTORAL
Science Research Fellowships
- Fellowships up to $92,000
- Mentoring and networking opportunities
- Eligibility: Ph.D. or equivalent degree recipients in the biological or chemical research fields

APPLY ON-LINE
http://umsi.uncf.org
Submit by December 1, 2010

T 703 205 3400
F 703 205 3550
E uncfmerck@uncf.org

UNCF MERCK MERCK COMPANY FOUNDATION

GENERAL ELIGIBILITY REQUIREMENTS:
Must be African American and a U.S. citizen or a permanent resident

Donnelly Centre — University of Toronto

Charles H. Best Postdoctoral Fellowships are available for qualified Ph.D. graduates (2 years or less postgraduate) in the field of molecular, genetic and genomic research. Applicants must address their applications to members of the Banting and Best Department of Medical Research at the University of Toronto.

Individual research programs include studies on gene expression, signal transduction, development, membrane transport and functional genomics, and are carried out in the new, state of the art Donnelly Centre **(http://www.thedonnellycentre.utoronto.ca/)**. Applications should be addressed to one or two of the BBDMR department members (listed at: **http://www.thedonnellycentre.utoronto.ca/positions/bpf.html**), whose interests match their own. Upon agreement of sponsorship, the applicant must send a curriculum vitae, transcripts and three letters of reference to their sponsoring Faculty mentor.

The deadline for completed applications is **December 17, 2010.** Successful applicants will be supported for two years with a generous stipend.

GRANTS

SEEKING THE WORLD'S BEST POST-DOCS

Academic freedom for up to five years
APPLY NOW!
www.society-in-science.org

society in science
The Branco Weiss Fellowship

POSITIONS OPEN

RESEARCH ZOOLOGIST
Department of Invertebrate Zoology

The Smithsonian's National Museum of Natural History seeks a zoologist to conduct an integrative, specimen- or collection-based research program in invertebrate evolution and biodiversity (exclusive of hexapods, myriapods, and arachnids). The successful candidate is expected to develop an internationally recognized research program that makes important contributions to understanding invertebrate evolution and biodiversity through synthetic research involving phylogenetics, genetics, anatomy, development, genomics, biogeography, conservation, informatics, or related fields. Frequent publication of highly regarded papers in competitive, peer-reviewed journals, curation of collections in specialty area, service to the scientific community in leadership capacities, acquisition of external funding, engagement in outreach activities, and mentorship of students are expected. Fit with existing strengths of the department's collections is desirable but not essential.

Full-time, four-year term appointment with full Government benefits to be filled at the GS-12 level; *U.S. citizenship required*. The museum's authorized salary range for this position at this time is $74,872 to $79,864 per annum. For complete requirements and application procedures, go to **website: http://www.sihr.si.edu** and refer to **Announcement 11A-RB-296421-DEU-NMNH** or contact **Robinette Burrell** at **telephone: 202-633-6318.** The announcement opens October 29, 2010. Applications must be received online by December 10, 2010, and must reference the announcement number. All applicants will be notified by e-mail when their application is received. *The Smithsonian Institution is an Equal Opportunity Employer.*

COGNITIVE PSYCHOLOGIST
Department of Psychology
University of California, Riverside

The Department of Psychology, University of California, Riverside, invites applications for a tenure-track **ASSISTANT PROFESSOR** position in Cognitive Psychology to start July 1, 2011. We seek applicants whose research examines experience-dependent changes in human cognitive and/or perceptual systems. Applicants should demonstrate a record of research excellence using methodological approaches involving human behavior, cognitive neuroscience, and/or computational modeling. Applicants should be committed to excellence in undergraduate and graduate education and interest in teaching quantitative methods at the graduate level is preferable. The Ph.D. is required and salary is commensurate with education and experience. Review of applicants will begin on December 15, 2010, and continue until the position is filled. Interested candidates should send their curriculum vitae, reprints if available, a cover letter describing research and teaching interests, and arrange to have three letters of recommendation sent to:

Professor Larry Rosenblum, Chair
Cognitive Search Committee
Department of Psychology
University of California, Riverside
Riverside, CA 92521

The University of California, Riverside is an Equal Opportunity/Affirmative Action Employer.

POSTDOCTORAL and JUNIOR FACULTY POSITIONS in T Cell Gene Therapy for Cancer and HIV/AIDS

Join integrated program of laboratory and clinical studies of designer T cells for cancer (brain, breast, other) and infectious disease (HIV, PML). Expertise sought in cell signaling, cytokines, transcription, cell trafficking, in vitro/in vivo imaging, molecular engineering, animal cancer models, and HIV. Contact **Dr. R. Junghans/Dr. P. Sampath** at **e-mail: ejuckett@rwmc.org.** Provide curriculum vitae, research interests, and names of three references. Roger Williams Medical Center is a major teaching hospital of the Boston University School of Medicine.

POSITIONS OPEN

SPRINGER LAB POSTDOCTORAL FELLOW

Structural Biology of Malaria Vaccines. Sporozoite sheath components; gametocyte surface recognition; and fusion proteins in fertilization.

Single Molecule Studies of Mechanobiology. Force-sensing in von Willebrand factor (VWF), flex-bonds, force in allostery and adhesion.

Structural Biology. TGF-b superfamily, VWF, Integrin activation, ligand binding, and therapeutics.

Cell Biology of Integrin Activation. Transmembrane Receptor Signaling.

Timothy A. Springer, Immune Disease Institute, Harvard Medical School, **website: http://labs.idi.harvard.edu/springer/.**

FACULTY POSITIONS in Regenerative Medicine and Stem Cell Biology
University of California, Irvine

The University of California, Irvine is planning a major expansion of research in the broad areas of regenerative medicine and stem cell biology. We seek outstanding candidates with a demonstrated track record in any of several key areas important to regenerative medicine, such as niche biology, asymmetric cell division, cancer stem cells, tissue engineering, cell matrix interactions, developmental potency/epigenetics, cell signaling, regeneration, organogenesis, and more, including pharmaceutical applications. Regenerative medicine and stem cell research have long histories of achievement at UC Irvine and the university has received significant research funding, as well as funding for a major research building from the California Institute of Regenerative Medicine. Core facilities within the Stem Cell Research Center provide laboratory space for carrying out work that is currently ineligible for federal funding.

Appointments will be made at the **ASSISTANT, ASSOCIATE,** or **FULL PROFESSOR** level, as supported by the qualifications and experience of the successful applicants.

Applicants should submit a letter of application, curriculum vitae, bibliography, three letters of reference, and statements of research and teaching interests using the online recruitment system (see instructions at **website: https://recruit.ap.uci.edu**).

Review of applications will begin December 1, 2010, and the recruitment will remain open until the positions are filled.

The University of California, Irvine is an Equal Opportunity Employer committed to excellence through diversity, and strongly encourages applications from all qualified applicants, including women and minorities. UCI is responsive to the needs of dual career couples, is dedicated to work-life balance through an array of family friendly policies, and is the recipient of an NSF ADVANCE Award for gender equity.

MARINE BIOLOGY-FISHERIES FACULTY POSITION

The Hawaii Institute of Marine Biology at the University of Hawaii at Manoa, SOEST, invites applications for non-tenure track, 11-month faculty **ASSISTANT RESEARCHER.** We seek a faculty member whose research interests include marine population dynamics and stock assessment, management strategy evaluation, climate effects, or ecosystem and food web modeling. The successful candidate is expected to train future practitioners in population assessment sciences and develop innovative assessment approaches to environmental variability, food web linkages, and spatial heterogeneity. A Ph.D. degree is required in marine biology, oceanography, zoology, fisheries science, mathematics/statistics, or related discipline. Postdoctoral and/or work experience in an appropriate/related discipline is desirable. Submit cover letter with (1) curriculum vitae, (2) statement of research accomplishments, future goals as related to HIMB, (3) three representative publications, and (4) the names and addresses of three references to: **Dr. Jo-Ann Leong, Director, e-mail: joannleo@hawaii.edu, HIMB, PO Box 1346, Kaneohe, HI 96744; website: http://worktuh.hawaii.edu.** *The University of Hawai'i is an Equal Opportunity/Affirmative Action Institution.*

POSITIONS OPEN

Smithsonian

SMITHSONIAN INSTITUTION FELLOWSHIP PROGRAM

GRADUATE STUDENT, PREDOCTORAL, POSTDOCTORAL, and **SENIOR FELLOWSHIPS** in animal behavior, ecology, and environmental science; including an emphasis on the tropics; Earth sciences and paleobiology; Evolutionary and systematic biology; History of science and technology. Tenable in residence at the Smithsonian facilities. Stipends and tenure vary. Awards are contingent upon the availability of funds.

Deadline: January 15 annually. Contact: **Office of Fellowships, Smithsonian Institution, Desk S, P.O. Box 37012, L'Enfant 7102 MRC 902, Washington, D.C. 20013-7012, telephone: 202-633-7070, e-mail: siofg@si.edu, website: http://www.si.edu/research+study.** *An Equal Opportunity Employer.*

PROFESSOR, BEHAVIORAL AND SOCIAL SCIENCES
Department of Community Health
Program in Public Health
Alpert Medical School of Brown University

The Department of Community Health in the Brown University Program in Public Health is searching for a **FULL PROFESSOR** (tenured) to serve as head of its Behavioral and Social Sciences Section. This position is part of a multi-year expansion plan for Public Health at Brown and is available as early as July 1, 2011. Academic leadership experience is desired and applications are encouraged from individuals with expertise in child and/or adolescent health, obesity, addictive behaviors, exercise, health disparities, and/or community-based intervention research. A Doctoral degree in a Behavioral and/or Social Science (or equivalent) is required.

All applicants should send a letter of application and curriculum vitae to: **Peter M. Monti, Ph.D., Chair of Behavioral and Social Sciences Search Committee, Brown University, Department of Community Health, Box G-S121-5, Providence RI 02912;** or send electronically to **e-mail: peter_monti@brown.edu.**

Review of applications will begin on December 1, 2010. Full consideration will be given to all applications received by February 1, 2011. Applications received after the priority deadline may be reviewed until the position is filled or the search is closed.

Brown University is an Equal Opportunity/Affirmative Action Employer, and actively solicits applications from women and minorities.

FACULTY, Department of Cancer Biology: Mayo Clinic in Florida and the Mayo Clinic Comprehensive Cancer Center seek an outstanding investigator in basic cancer research (Ph.D., M.D., or M.D.-Ph.D.) to join the Department of Cancer Biology at the rank of **ASSISTANT, ASSOCIATE,** or **FULL PROFESSOR.** Established in 2003 in Mayo Clinic Jacksonville, Florida, the department currently consists of a highly interactive core of NIH-funded faculty working on various aspects of basic and translational tumor biology. Current strengths include expertise in oncogenic signaling mechanisms, molecular mechanisms of carcinogenesis, cancer genomics, oxidative stress signaling in cancer, the tumor microenvironment in cancer development, and molecular mechanisms of invasion and metastasis. The ideal candidate would have an NCI-funded, established research program in a basic cancer research discipline with a national/international reputation. The Griffin Cancer Research Building is a state-of-the-art facility dedicated to cancer research and provides ample space for future growth. The Mayo Clinic's NCI-designated multi-site Comprehensive Cancer Center facilitates collaborations across all Mayo Clinic sites and provides potential interactions with several associated SPOREs. Interested parties should send a cover letter, curriculum vitae, contact information for three references, and a research program description to **Dr. Panos Z. Anastasiadis** (**e-mail: mcffaculty.recruitment@mayo.edu**), Chair of the Cancer Biology Search Committee. *Mayo Clinic is an Equal Opportunity Employer.*

Organized by: Alexander von Gabain and Thomas Decker

Scientific Advisory Board: Franz-Xaver Heinz, Hans Wigzell, Rafi Ahmed, Thomas Decker and Noel Barrett

For more information and registration please visit: **www.viennavaccines.com**

World Immune Regulation Meeting -V

special focus on ''Innate and Adaptive Immune Response and Role of Tissues in Immune Regulation''

WIR

24 - 27 March 2011

Congress Center Davos, Switzerland

Early Registration and Abstract Submission open until 01 December 2010

10 travel grants including free registration

www.wirm.ch

Confirmed speakers: A. Akbar - D. Artis - Y. Belkaid - D. Busch - A. Cerutti - A. Chervonsky - M. Cooper - D. Cua - G. De Libero - M. Edinger - M. Gilliet - H. Levitsky - D. Littman - Y.-J. Liu - Ch. MacKay - R. Maizels - M. Manz -C. Mauri - A. McKenzie - R. Mebius - L. Meyaard - A. O'Garra - E. Pamer - H. Ploegh - B. Pulendran - P. Romero - M. G. Roncarolo - T. Saito - E. Shevach - H. Spits - T. Stappenbeck - L. Steinman - M. Swartz - M. Taniguchi - Y. van Kooyk - A.-. Ziegler and more ...

SWEDISH FOUNDATION *for* STRATEGIC RESEARCH

Announces a call for proposals for the 2010

INGVAR CARLSSON AWARD

The aim of the programme is to identify and support young, well-qualified postdocs who intend to start independent, lasting and creative research careers on their return to Sweden.

The Foundation has set aside a maximum amount of SEK 36 million to fund up to twelve (12) three-year grants of SEK 3 million each (including overhead). The grants include a personal scholarship of SEK 50,000 that will be awarded each recipient.
A leadership training programme will be arranged for the grantees. Participation in this leadership programme is mandatory.
This announcement covers research in the natural sciences, engineering and medicine.

The following criteria apply for eligibility:

- The applicant must have received his or her PhD at a Swedish university not earlier than 1 January 2007 (adjusted for documented parental leave and, in the case of MDs, any clinical internship/residency period (AT).
- The applicant must have conducted continuous postdoctoral studies outside Sweden for at least 12 months prior to the application deadline.
- The applicant must become permanently active at a university in Sweden. His or her work in Sweden should have started not earlier than 1 January 2010, and not later than 31 March 2012.

The following criteria will be applied in the selection process:

- Scientific quality and potential, reflected in previous research as well as in the proposed research
- Originality and innovativeness of the proposed research
- Description of how the proposed research can be implemented in Sweden, as well as its strategic relevance and importance for Sweden's future competitiveness
- Applicant's international experience and network.

The application process takes place in one step; full proposals only are accepted.

The proposals must be written in English and submitted via the electronic application system (portal) of the Foundation at http://apply.stratresearch.se.

The submission period opens on 11 November 2010. All applications must be submitted by **3 February 2011 at 14:00 (2 pm CET) at the latest.**

Detailed instructions will be found at the electronic portal.

www.stratresearch.se

POSITIONS OPEN

PROTEOMICS AND BIOMARKERS
Faculty Appointments in Pharmacology

The Medical University of South Carolina seeks to recruit two outstanding scientists as part of the South Carolina Center of Economic Excellence and Endowed Chair Program in Proteomics. Individuals will be expected to establish outstanding individual research programs in proteomics and assist in the further development and application of proteomics research for diagnostics and biomarker identification in the areas of cancer, cardiovascular science, and/or neuroscience. Candidates must have demonstrated ability to secure peer reviewed research funding and will be expected to lead broader programmatic development on campus in this area of work. Appointment level will be commensurate with experience.

Extramural research funding awards to MUSC in fiscal year 2009 exceeded $217 million, reflecting tremendous continued growth in the research enterprise, including most recently a National Cancer Institute (NCI)-designated cancer center, an NIH Clinical and Translational Science Award and major regional and national partnerships. Two new research buildings dedicated to interdisciplinary work in Drug Discovery, Bioengineering, and Cancer Genomics will open in 2011.

This is an exceptional opportunity for talented, experienced and committed individuals to exert a major impact on the next phase of development and growth of the research and translational sciences programs at MUSC.

Located on the Atlantic coast in South Carolina, Charleston boasts one of the nation's most historic downtown areas, beaches and other outdoor recreational resources, and international cultural events such as the Spoleto Festival USA.

Interested candidates should submit their curriculum vitae, a summary of future research plans, and names of three references to apply. Nominations are also welcomed. Submit materials to:

Kenneth D. Tew, Ph.D., D.Sc.
John C. West Professor of Cancer Research and Chairman
Department of Cell and Molecular Pharmacology
Medical University of South Carolina
173 Ashley Avenue
Charleston, SC 29425

MUSC is an Equal Opportunity Employer supporting workplace diversity with minorities, females, veterans, and persons with disabilities.

ASSISTANT PROFESSOR OF BIOLOGY
Department of Biology

The Department of Biology at Arcadia University invites applications for a full-time, tenure-track Assistant Professor position for an organismal biologist with expertise in vertebrae biology beginning in the fall of 2011. Ranked among the top tier of comprehensive universities in the northern region of the United States, Arcadia University is a coeducational institution located in suburban Philadelphia that offers undergraduate and graduate study to more than 3,500 students annually. The successful candidate will teach required courses in the major including, but not limited to, the introductory biology sequence as well as an upper-level course in his or her area of expertise. Applicants are expected to engage undergraduate students in research projects, so postdoctoral research experience is desired. Candidates must have an earned Doctorate, a dedication to teaching biology majors and non-majors, and teaching experience at the university level.

For additional information, please visit **website: http://www.arcadia.edu.**

For full consideration, submit a letter of intent, a statement of teaching philosophy, a statement of research goals, curriculum vitae, and three letters of recommendation by December 15, 2010 to: **Dr. Archie J. Vomachka, Department of Biology, Arcadia University, 450 S. Easton Road, Glenside, PA 19038. Telephone: 215-572-2199; fax: 215-881-8758; e-mail: vomachka@arcadia.edu.**

Arcadia University seeks candidates of diverse cultural backgrounds and abilities. As an Affirmative Action/Equal Opportunity Employer, Arcadia University encourages members of underrepresented groups to apply.

POSITIONS OPEN

ASSISTANT PROFESSOR

The Department of Molecular and Cell Biology of The University of Texas at Dallas invites applications for tenure-track/tenured **ASSISTANT PROFESSOR, ASSOCIATE PROFESSOR, FULL PROFESSOR,** and **ENDOWED PROFESSOR** positions in emerging areas of biological sciences. Preference will be for investigators whose expertise complements existing strengths in the department.

We are looking for geneticists, molecular and cell biologists investigating diverse model organisms and pathogenic organisms.

The Schools of Natural Sciences & Mathematics, Behavioral & Brain Sciences, and Engineering & Computer Sciences are expanding, with an emphasis on recruiting faculty who can foster interdisciplinary interactions.

The minimum requirement is a Ph.D. in an appropriate discipline with at least two years of postdoctoral experience. Applicants should show evidence of a vigorous and independent research program that is or will be externally supported. Applicants for senior faculty positions should have a demonstrated record of external funding. Applicants should also show a strong interest in teaching at both the undergraduate and graduate levels.

Review of applications will begin immediately and will continue until all positions are filled.

Submit applications via the following **website: http://provost.utdallas.edu/facultyjobs/pnj101013#apply_now.**

The University of Texas at Dallas is an Equal Opportunity/Affirmative Action Employer.

ASSISTANT PROFESSOR
ANIMAL PHYSIOLOGY

The Department of Biological Sciences, California State University, Los Angeles, seeks to fill a tenure-track position in Animal Physiology beginning fall, 2011. A Ph.D. in Physiology or related field is required, with a minimum of one year related postdoctoral experience. The candidate is expected to teach undergraduate and graduate courses and participate in course and program development. The applicant must be committed to establishing an externally funded research program in an area of animal physiology and involving undergraduate and Master's students in the research. Submit curriculum vitae, statement of research plans, statement of teaching philosophy, official transcripts, three letters of recommendation, and the University's Application for Academic Employment from **website: http://www.calstatela.edu/univ/hrm/docs/forms/Empl_applic_academic.pdf** to: **Search Committee—Animal Physiology, Department of Biological Sciences, California State University, Los Angeles, 5151 State University Drive, Los Angeles, CA 90032** (**e-mail: nmcquee.calstatela.edu**). Review of completed applications will begin December 1, 2010, and continue until position is filled. *Equal Opportunity/Title IX/ADA Employer.*

TENURE-TRACK ASSISTANT PROFESSOR
Analytical Chemistry
Georgetown University

Georgetown University wishes to recruit a tenure-track Assistant Professor in Analytical Chemistry to begin fall 2011. Areas of research are open and should be complementary to existing research directions in the department. Candidates must have a Ph.D. degree in chemistry or a closely related field and postdoctoral training or equivalent is desirable. Development of an internationally recognized research program and teaching at the undergraduate and graduate levels are expected. Please send curriculum vitae, description of research plans, statement of teaching philosophy, and arrange for three letters of recommendation to be sent to: **Faculty Search Committee, Department of Chemistry, Georgetown University, Box 571227, Washington, DC 20057-1227.** For full consideration, complete applications should arrive before January 15, 2011. *Georgetown University is an Affirmative Action/Equal Opportunity Employer; applications from qualified women and minority candidates are encouraged.*

POSITIONS OPEN

The Department of Pharmacology at Tulane University School of Medicine is currently recruiting faculty members with a Ph.D. or equivalent degree for tenure-track positions at the level of **ASSISTANT** or **ASSOCIATE PROFESSOR.** Areas of preferred expertise included Vascular Biology or Mitochondrial Biology. These positions are being filled as part of a major expansion of the research program in the department with a new chairperson at Tulane University. These positions will be supported by significant laboratory space, competitive salaries, and excellent startup packages. The requirements for Assistant Professor include a minimum of two years of postdoctoral research experience and for Associate Professor a minimum of three years of experience at the level of Assistant Professor. The successful candidates are expected to have a distinguished record of scholarly activity including teaching experience in Pharmacology or other basic science area. For the Associate Professor level, NIH R01 or other significant extramural funding is expected.

Please submit application with full curriculum vitae and names of three references via e-mail to: **Dr. David Busija** (in care of **e-mail: dsanders@tulane.edu**), **Regents Professor and Chairman, Department of Pharmacology, Tulane University School of Medicine, New Orleans, LA 70112.** Please also include a letter that summarizes the future research plans. Review of applications will begin immediately and will continue until the positions are filled.

Tulane University is an Affirmative Action and Equal Opportunity Employer. We invite Women and Minorities to apply.

THE DEPARTMENT OF CHEMISTRY of The University of California, Irvine, invites applications for a **SENIOR FACULTY** position in synthetic chemistry broadly defined, including inorganic and organic chemistry. Applicants must have an international reputation for research excellence. The successful applicant will be expected to assume responsibility for undergraduate and graduate teaching in inorganic and/or organic chemistry, and to maintain a position of research leadership. Submit a complete curriculum vitae and publication record electronically via **website: https://recruit.ap.uci.edu**. Applicants should also submit the names of three references whom the Search Committee may contact. Applications will be accepted until the position is filled. *The University of California, Irvine is an Equal Opportunity Employer committed to excellence through diversity and strongly encourages applications from all qualified applicants, including women and minorities. UCI is responsive to the needs of dual career couples, is dedicated to work-life balance through an array of family-friendly policies, and is the recipient of an NSF ADVANCE Award for gender equity.*

POSTDOCTORAL POSITIONS available to study the unusual mechanisms of cytokinesis in Trypanosoma brucei. Research experience in molecular biology and cell biology is required. The candidate must have a recent Ph.D. degree. Send an updated curriculum vitae and names and addresses of three references to: **Professor C. C. Wang, Department of Pharmaceutical Chemistry, University of California, San Francisco, CA 94158-2280. Fax: 415-476-3382; e-mail: ccwang@cgl.ucsf.edu.**

☑ More scientists agree —we are the most useful website.
www.ScienceCareers.org

MARKETPLACE

Promab Biotechnologie. Inc.
Ascites Production
$20/ mouse
Recombinant Antibody
1-866-339-0871
www.promab.com info@promab.com